RARE EARTH ELEMENTS

PROCESSING, CATALYTIC APPLICATIONS AND ENVIRONMENTAL IMPACT

Edited by Basudeb Basu and Bubun Banerjee
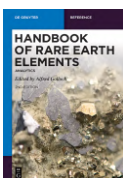
Basudeb Basu and Bubun Banerjee (Eds.)
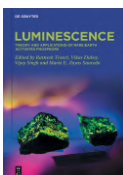**Rare Earth Elements**

Also of Interest

Handbook of Rare Earth Elements.
Analytics
Alfred Golloch (Ed.), 2022
ISBN 978-3-11-069636-3, e-ISBN 978-3-11-069645-5

Luminescence.
Theory and Applications of Rare Earth Activated Phosphors
Ratnesh Tiwari, Vikas Dubey, Vijay Singh and María Elena Zayas Saucedo
(Eds.), 2022
ISBN 978-3-11-067641-9, e-ISBN 978-3-11-067645-7

Rare Earth Chemistry
Rainer Pöttgen, Thomas Jüstel and Cristian A. Strassert, 2020
ISBN 978-3-11-065360-1, e-ISBN 978-3-11-065492-9
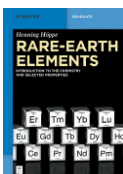
Rare-Earth Elements.
Introduction to the Chemistry and Selected Properties
Henning Höppe, planned 2024
ISBN 978-3-11-068081-2, e-ISBN 978-3-11-068082-9

Rare Earth Elements

Processing, Catalytic Applications and Environmental Impact

Edited by
Basudeb Basu and Bubun Banerjee

DE GRUYTER

Editors
Prof. Basudeb Basu
Former Professor
North Bengal University
Department of Chemistry
P.O.North Bengal University
Darjeeling-734013
West Bengal
India
e-mail: basudeb.basu@gmail.com

Dr. Bubun Banerjee
Department of Chemistry
Akal University
Talwandi Sabo, Bathinda 151302
Punjab
India
e-mail: banerjeebubun@gmail.com

Foreword

Rare earth metal salts are often found difficult to handle due to their strong oxophilicity, which makes them hygroscopic and reactive toward oxygen. However, this problem can be overcome by using specified lab equipments such as vacuum lines, glove boxes, etc. The catalytic applications of rare earth metals and salts have been extensively studied in C–H and C–F bond activation reactions, photocatalysis, lanthanide–halide exchange reactions, dinitrogen conversion, and most importantly for the synthesis of biologically promising carbocyclic and heterocyclic scaffolds. Many new transformations have been reported using rare earth metal salts as the catalyst. These applications have opened up the way to several new transformations in organic synthesis using rare earth metals in various oxidations states either in catalytic or in stoichiometric amounts.

Under this purview, I personally believe that this book entitled *Rare Earth Elements: Occurrence, Catalytic Applications and Environmental Impact*, edited by Prof. Basudeb Basu and Dr. Bubun Banerjee, is going to be a valuable resource for the researchers working in the fascinating fields of rare earth metals. The main aim of this book is to showcase the versatile applications of rare earth metals in various organic transformations. Moreover, bio-applicability, industrial applications, and environmental impact of rare earth metal salts have also covered in this book.

The first chapter describes the occurrence, environmental impact, and catalytic applications of various yttrium complexes for diverse organic transformations. Chapter 2 deals with the uses of half-sandwich organo rare earth metal–alkyl complexes as catalyst for the formation of various C–C bonds via C–H bond functionalization while the Chapter 3 demonstrates various rare earth metal-catalyzed one-pot multicomponent reactions. Chapter 4 focuses on the preparation and catalytic applications of light-weight rare earth metals in combination with *N*-heterocyclic carbine complexes. Chapter 5 summarizes the recent applications of lanthanum triflate as catalyst for various organic transformations. Catalytic role of various actinide complexes for useful organic transformations is described in Chapter 6. Chapters 7 and 8 provide elaborative literatures related to the catalytic applications of samarium and erbium-based compounds, respectively, in organic transformations. Chapters 9 and 10 summarize the catalytic applications of various rare earth metal trfilates, namely, gadolinium, scandium, and lanthanum triflates. The cerium(IV) ammonium nitrate (CAN)-catalyzed

synthesis of structurally diverse *O* and *S*-heterocycles is described in Chapter 11. Chapter 12 specially deals with the uses of rare earth metal complexes as efficient photocatalysts in organic synthesis. Chapter 13 focuses on updates about the various innovative as well as environmentally benign techniques utilized for bioremediation of rare earth elements to protect our mother Nature. Chapter 14 provides an up-to-date literature related to the biomedical applications of various rare earth elements. The final chapter shows the ways to the recovery of rare earth elements from electronic waste.

Prof. Asit K. Chakraborti, FRSC, LFICS, FASc, FNA
Raja Ramanna Fellow, School of Chemical Sciences,
Indian Association for the Cultivation of Science (IACS),
Kolkata, West Bengal, India
e-mail: asitkumarchakraborti@gmail.com;
ocakc@iacs.res.in

About Professor Asit K. Chakraborti

Professor Asit K. Chakraborti has been a founder faculty of National Institute of Pharmaceutical Education and Research (NIPER), S. A. S. Nagar, Mohali, Punjab, India, and had been intimately associated with the development of this pioneering institute of the country in the fields of pharmaceutical education and research. He is currently Raja Ramanna Fellow in the School of Chemical Sciences, Indian Association for the Cultivation of Science (IACS), Kolkata. He superannuated as Professor and Head of the Department of Medicinal Chemistry from NIPER in August 2019 and thereafter was Visiting Professor in the Department of Chemistry, IIT Ropar, Punjab, before joining IACS as Emeritus Fellow.

Prof. Chakraborti obtained an M.Sc. degree in Organic Chemistry from the University of Burdwan, Burdwan, West Bengal, India, in 1977 being placed first in the first class and a Ph.D. degree in Synthetic Organic Chemistry from IACS, Kolkata, India, in 1985.

He received post-doctoral research training in the Department of Chemistry, Clemson University, South Carolina, USA, during 1985–1987 and in Medicinal Chemistry at Purdue University, West Lafayette, Indiana, USA, during 1987–1989. After that he joined the Department of Chemistry at Burdwan University as a faculty in January 1990. He moved to the Department of Medicinal Chemistry at NIPER as Assistant Professor in November 1994, was elevated to Associate Professor in 1999 and Professor and Head in 2001. He has also been the Dean of NIPER.

Prof. Chakraborti has guided 41 Ph.D. and 130 Master's students, published 181 research papers with >12,000 citations with an *h* index of 65. He filed 42 patents of which 27 have been granted. He is among the top 2% Indian scientists (in the field of Organic Chemistry) in the World Ranking 2022 (Indian rank: 25; world rank: 1,326) and is one of the Top Chemistry Scientists 2022 (world rank: 3,713; national rank: 31).

His research interest in Organic Chemistry involved the development of new synthetic methodologies (transition-metal-based catalysis and organo-catalysis, C–H activation, etc.) in compliance with the green chemistry principles and deriving novel concepts (such as understanding the molecular-level role of acceleration of organic reactions in water and fluorous alcohols, the origin of the organo-catalytic potential of ionic liquids, etc.); development of green or sustainable chemistry for greener synthetic routes to bioactive natural products, cardiovascular drugs, and other biologically active molecules; and development of methodologies for solid/solution phase synthesis of small molecular libraries.

He is also a passionate medicinal chemist having focus on the target-based design and synthesis of new chemical entities in various therapeutic areas of tropical communicable and neglected diseases like tuberculosis, leishmaniasis; non-communicable diseases like inflammation, rheumatoid arthritis, asthma, and COPD; and diabetes.

Prof. Chakraborti has received several awards and recognition such as University Gold Medal, Bardhaman Sammilani Gold Medal, ISMAS Eminent Mass-Spectroscopist Award, Ranbaxy Research Award (Pharmaceutical Sciences), Chemical Research Society of India Silver and Bronze Medals, Indian Chemical Society's Professor P. K. Bose Memorial Award 2019, and Dr. Nitya Anand Endowment Lecture 2021 of INSA. He also received the Rajnibhai V. Patel PharmInnova Best Research Guide Awards for the most "innovative Ph.D. thesis" during 2017–2018 and 2016–2017, and the most "innovative MS thesis" during 2015–2016 and 2014–2015 in "pharmaceutical chemistry"; Certificate of Appreciation for Ph.D. Thesis Advisor of Eli Lilly and Company Asia Outstanding Thesis First Prize Awardee in 2013, 2012, and 2009 and Second Prize Award in 2009. He is Fellow of the Royal Society of Chemistry, has been elected Life Fellow of the Indian Chemical Society, Fellow of Indian Academy of Sciences, Bangalore, and Fellow of Indian National Science Academy, New Delhi.

Contents

List of authors

Hosam M. Saleh
Radioisotope Department
Nuclear Research Center
Egyptian Atomic Energy Authority
Cairo
Egypt
e-mail: hosam.saleh@eaea.org.eg

Amal I. Hassan
Radioisotope Department
Nuclear Research Center
Egyptian Atomic Energy Authority
Cairo
Egypt

Yadavalli Venkata Durga Nageswar
Retired Chief Scientist
Indian Institute of Chemical Technology
Tarnaka
Hyderabad
India
e-mail: dryvdnageswar@gmail.com

Katla Ramesh
Foreign Visiting Professor
Organic Chemistry Laboratory – 4
School of Chemistry and Food
Federal University of Rio Grande (FURG)
Rio Grande
RS-Brazil

Katla Rakhi
Organic Catalysis and Biocatalysis Laboratory
(LACOB)
Federal University of Grande Dourados (UFGD)
Dourados/MS
Brazil

Puja Basak
Department of Chemistry
University of North Bengal
Darjeeling
West Bengal
India

Pranab Ghosh
Department of Chemistry
University of North Bengal
Darjeeling
West Bengal
India
e-mail: pizy12@yahoo.com

Mohit Maingle
Department of Medicinal Chemistry
National Institute of Pharmaceutical Education
and Research (NIPER), Guwahati
Sila Katamur
Changsari
Kamrup 781101
Assam
India

Steeva Sunny
Department of Medicinal Chemistry
National Institute of Pharmaceutical Education
and Research (NIPER), Guwahati
Sila Katamur
Changsari, Kamrup 781101
Assam
India

Kate Ashru Ajinath
Department of Medicinal Chemistry
National Institute of Pharmaceutical Education
and Research (NIPER), Guwahati
Sila Katamur
Changsari, Kamrup 781101
Assam
India

Amrutha Cica Tomy
Department of Medicinal Chemistry
National Institute of Pharmaceutical Education
and Research (NIPER), Guwahati
Sila Katamur
Changsari, Kamrup 781101
Assam
India

Wagh Kanchan Madanrao
Department of Medicinal Chemistry
National Institute of Pharmaceutical Education
and Research (NIPER), Guwahati
Sila Katamur
Changsari, Kamrup 781101
Assam
India

Pathlavath Teja Sree
Department of Medicinal Chemistry
National Institute of Pharmaceutical Education
and Research (NIPER), Guwahati
Sila Katamur
Changsari, Kamrup 781101
Assam
India

Kapileswar Seth
Department of Medicinal Chemistry
National Institute of Pharmaceutical Education
and Research (NIPER), Guwahati
Sila Katamur
Changsari, Kamrup 781101
Assam
India
e-mail: kapileswar@niperguwahati.in

Asish Kumar Dey
Triveni Devi Bhalotia College
Kazi Nazrul University
Raniganj 713347, West Bengal
India

Sasadhar Majhi
Department of Chemistry (UG & PG)
Triveni Devi Bhalotia College
Kazi Nazrul University
Raniganj 713347, West Bengal
India
e-mail: sasadharmajhi@gmail.com

Khushboo Sharma
Department of Chemistry
University of Rajasthan
Jaipur 302004
Rajasthan
India

Naveen Sharma
Department of Chemistry
University of Rajasthan
Jaipur 302004
Rajasthan
India

Harshita Sachdeva
Department of Chemistry
University of Rajasthan
Jaipur 302004
Rajasthan
India
e-mail: drhmsachdevaster@gmail.com

Debasree Saha
Department of Chemistry
Raidighi College
24 Parganas (South)
Raidighi 743383
West Bengal
India

Chhanda Mukhopadhyay
Department of Chemistry
University of Calcutta
Kolkata 700009
West Bengal
India
e-mail: cmukhop@yahoo.co.in

Kantharaju Kamanna
School of Basic Sciences
Department of Chemistry
Rani Channamma University
Vidyasangama
Belagavi 591156
Karnataka
India
e-mail: kk@rcub.ac.in

Yamanappagouda Amaregouda
School of Basic Sciences
Department of Chemistry
Rani Channamma University
Vidyasangama
Belagavi 591156
Karnataka
India

Sabbasani Rajasekhara Reddy
School of Advanced Sciences
Department of Chemistry
Vellore Institute of Technology (VIT)
Vellore 632014
Tamil Nadu
India
e-mail: sekharareddy@vit.ac.in

Paranimuthu Panjacharam
School of Advanced Sciences
Department of Chemistry
Vellore Institute of Technology (VIT)
Vellore 632014
Tamil Nadu
India

K. Ganesh Kadiyala
Depatment of Chemistry
Shri Vishnu Engineering College for Women
Bhimavaram
Andhra Pradesh
India

Vanipenta Yamini
Sri A. S. N. M. Govt. College (A)
Palakollu
Andhra Pradesh
India

Kommuru Goutham
Indian Institute of Chemical Technology
Hyderabad
Telangana
India

Naresh Kumar Katari
Department of Chemistry
School of Science
GITAM Deemed to be University
Hyderabad
India
e-mail: nkatari@gitam.edu

Manish Taunk
Department of Physics
Maharaja Agrasen University
Baddi 174103
Himachal Pradesh
India
e-mail: manishphy@gmail.com

Gyan Chandra Pariyar
Department of Food Technology
University of North Bengal
Darjeeling
West Bengal
India

Bijeta Mitra
Department of Chemistry
University of North Bengal
Darjeeling
West Bengal
India

Suvodip Mukherjee
Department of Chemistry
University of North Bengal
Darjeeling
West Bengal
India

Pranab Ghosh
Department of Chemistry
University of North Bengal
Darjeeling
West Bengal
India
e-mail: pizy12@yahoo.com

Mausumi Ganguly
Department of Chemistry
Cotton University
Guwahati 781001
Assam
India
e-mail: ganguly_mausumi@rediffmail.com

Sangeeta Agarwal
Department of Chemistry
Cotton University
Guwahati 781001
Assam
India
e-mail: agarwalsangee@gmail.com

Bubun Banerjee
Department of Chemistry
Akal University
Talwandi Sabo
Bathinda 151302
Punjab
India
e-mail: banerjeebubun@gmail.com

Anu Priya
Department of Chemistry
Akal University
Talwandi Sabo
Bathinda 151302
Punjab
India

Aditi Sharma
Department of Chemistry
Akal University
Talwandi Sabo
Bathinda 151302
Punjab
India

Manmeet Kaur
Department of Chemistry
Akal University
Talwandi Sabo
Bathinda 151302
Punjab
India

Arvind Singh
Department of Chemistry
Akal University
Talwandi Sabo
Bathinda 151302
Punjab
India

Khushboo Sharma, Naveen Sharma and Harshita Sachdeva*

1 Occurrence, catalytic applications, and environmental impact of yttrium

1.1 Introduction

Rare earth elements (REEs) have a wide range of industrial applications, namely, in the production of catalysts and strong permanent magnets, glass additives, petroleum refining, wind turbines, renewable energy, fluorescent lights, fuel cells, laser technology, medical X-rays, MRI scanning, and also have defense-related applications and many more [1–4]. Fifteen lanthanide metallic elements including atomic numbers 57 to 71 and also scandium and yttrium comprise the Rare Earth Group. Yttrium and the heavy REEs with atomic numbers 64 to 71 are found together in the nature due to similar physical and chemical properties. The first rare earth element discovered was yttrium (Y). It is one of the heavy REE of Group-3 of the periodic table. It is the second most abundant REE on the Earth's crust after cerium. The average concentration of yttrium on the Earth's crust is 33 ppm. Johan Gadolin discovered yttria, metallic oxide, as a new earth and its story of discovery started in 1787 when coal like mineral was found by Carl Arrhenius in a feldspar/quartz mine near Ytterby, Sweden [5]. Yttria was suggested by Ekeberg for the name of this new earth metal. Yttrium metal was first obtained as a gray powder in 1828 by Friedrich Wohler by heating yttrium (III) chloride with potassium. Frank Spedding produced high pure metal in 1953 at Ames laboratory, in Iowa, using ion-exchange techniques. Yttrium is lustrous silvery soft and ductile metal which exists as trivalent ion and its compounds. The stability is due to the presence of oxide film formed on its surface. Yttrium hydroxide and hydrogen gas are formed when yttrium reacts with water. It formed clear colorless glass on treatment with borax. Yttrium causes dissolution of oxygen gas at relatively high concentrations. It is stable towards air but start to oxidize above 450 °C (840 °F), resulting in the formation of Y_2O_3. It reacts with dilute acids except HF with which it will form a protective layer YF_3 which prevents further reaction.

*Corresponding author: Harshita Sachdeva, Department of Chemistry, University of Rajasthan, Jaipur 302004, Rajasthan, India, e-mail: drhmsachdevaster@gmail.com
Khushboo Sharma, Naveen Sharma, Department of Chemistry, University of Rajasthan, Jaipur 302004, Rajasthan, India

1.2 Occurrence

Uranium ores contain yttrium and most of the "rare earth" minerals contain yttrium. Yttrium is refined commercially from bastnasite and monazite sands containing 0.2% and 3%, respectively. Commercial production is done by reduction of fluoride with calcium metal. It has 25 isotopes with 79–103 mass numbers. Naturally occurring yttrium has one isotope, Yttrium 89, which is stable. It does not occur as a free element in the earth's crust which makes it 28th among most abundant elements. Yttria was found to be a mixture of oxides from which nine elements, namely yttrium, scandium, and Lanthanide elements from terbium to lutetium were separated. Heavy rare earth ores, namely, Gadolinite, laterite clays, euxenite, xentine, contain yttrium. It is found in a large amount in the igneous rocks of earth crust. The hydrogenetic marine ferromanganese (Fe–Mn) crusts are mineral resources which contain number of critical elements like Ni, Co, Cu, Nb, V, Pt, Te, REEs, and yttrium. Fe–Mn crust deposit reserves are found in the north-equatorial Pacific Ocean, Atlantic Ocean, Indian Ocean, and Arctic Ocean [6]. Some Fe–Mn crust deposits were also found nearby Baltic Sea, continental margin, the South China Sea (SCS), and the California continental margin. The Pacific and Indian Oceans contain deep-sea sediments which are rich sources of REY (REY-rich mud). Mud layers which contain greater than 5000 ppm total concentrations of total Rare Earth Yttrium with ~ 1000 ppm of heavy REEs exist within the exclusive economic zone of Japan surrounding Marcus Island, northwestern Pacific Ocean [7]. In order to prevent REY resource depletion calamities, many nations, notably India and the USA, are now paying attention to the rare metals found in coal and coal ash. Additionally, coal seams typically have significant levels of REY. Eastern USA coal, Southwestern Chinese coal, and Far Eastern Russian coal all contain significant amounts of REY. Since 2014, there have been numerous publications in the literature about the extraction of RRY from coal combustion byproducts [8]. From a geology point of view, REEs chiefly originated from four sources, namely, carbonatites, clay deposits, igneous systems, and monazite-xenotime placer. RE mineral xenotime, YPO_4, is the yttrium's richest source [9]. China contains one-third of the world's REE deposits, and the total REY concentration in the Xinhua phosphorite deposit, Guizhou Province, China, is up to 45% than any other REE [10].

1.3 Catalytic applications of yttrium

1.3.1 Yttrium-based Lewis acids/bases as catalysts

Heterogeneous catalytic system based on yttrium halide surface complex have been used as powerful, simple, efficient, and recyclable Lewis acid catalyst for the cycloaddition of CO_2 to epoxides under atmospheric pressure. The catalyst

[($\equiv$SiO–)YCl(–OCH(CH$_3$)CH$_2$Cl)] is prepared by applying SOMC (surface organometallic chemistry) by grafting highly dehydroxylated silica on YCl$_3$/TBAB. Additionally, yttrium complexes have been used as versatile Lewis acid catalyst for reductive etherification of 5-hydroxymethyl furfural [11]. Further, some mono- and bis-amides of yttrium containing (N-isopropyl-2-(isopropylamino) troponiminato) group, namely, [(iPr)$_2$ATI]Y[N(SiMe$_3$)$_2$]$_2$ and [(iPr)$_2$ATI]$_2$Y[N(SiMe$_3$)$_2$], are described as precatalysts for the aminoalkynes hydroamination/cyclization reactions [12]. Furthermore, heterogeneous catalysts based on yttrium act as a Brønsted base and can be recycled without loss of its catalytic activity and selectivity. These diverse layered yttrium hydroxides (C$_{n-1}$H$_{2n-1}$COO$^-$/Y-layered REH, n = 1–10) act as catalysts for the formation of α,β-unsaturated nitriles in aqueous medium via Knoevenagel condensation of different kinds of substrates [13]. In yet another investigation, hydroboration of ketones and aldehydes is carried out by applying yttrium-based complex, namely [LSi(BH$_3$)(C$_5$Me$_4$)Y(CH$_2$SiMe$_3$)$_2$]$_2$, with L = PhC(NtBu)$_2$ as the catalyst. Y-based catalyst is found to be highly efficient and chemoselective, and it is prepared by the treatment of tetramethylcyclopentadiene LSi(BH$_3$)-(C$_5$HMe$_4$) with Y(CH$_2$SiMe$_3$)$_3$(THF) [14].

1.3.2 Yttrium-based nanocomposites as catalysts

Y$_2$O$_3$ nanocomposites have been successfully utilized for their photocatalytic activity in the degradation of synthetic dye, Rhodamine B. Yttrium nitrate is used as a precursor to prepare catalyst by hydrothermal method utilizing NaOH as a reducing agent [15]. Yttrium-doped CeO$_2$ exhibits high photocatalytic activity for degrading rhodamine B under the illumination of visible light. Synthesis of the pure cerium dioxide and Y-doped cerium dioxide nanopowders is carried out by the self-sustained reaction between nitrate and fuel followed by calcination at 700 °C for 2 h [16]. Further, hybrid hetero-structured nanoparticles, namely, Y-doped ZrO$_2$ functionalized with g-C$_3$N$_4$ (g-YZr), have been investigated for excellent photocatalytic Cr(VI) reduction activity and also for electrochemical energy storage applications. The photocatalytic activity may be attributed to their high surface area [17]. There is a report in the literature regarding a Y-based nanocomposite, namely, polypyrrole coupled with yttrium molybdate(YMoO$_4$/PPy), which shows high photocatalytic activity under light-emitting diode (LED) irradiation for the removal of nitrofuran-based antibiotic, nitrofurantoin (NFT) from water. YMoO$_4$ was prepared by hydrothermal method while template-driven growth of PPy nanorods was employed and finally preparation of YMoO$_4$/PPy composite was facilitated by ultrasonication [18]. Moreover, Eu, Y, and Lu-doped CeO$_2$ nanoparticle's photocatalytic effect for the reduction of organic pollutant, para-nitrophenol, under the irradiation of visible light has also been studied. It is established that the addition of photocatalyst causes enhancement in the reduction of p-nitrophenol to p-aminophenol. The synthesized nanomaterials have been utilized successfully as photocatalyst for the photoreduction of p-nitrophenolin the presence of reducing agent,NaBH$_4$. Further, it is observed that the addition of the photocatalyst

causes improvement in the reduction ability of $NaBH_4$ and the catalytic activity of $Lu_{0.05}CeO_2$ is found to be superior as compared to the other RE doped photocatalysts [19].

1.3.3 Yttrium-catalyzed enantioselective transformations

Pellissier [20] published a review article in 2016 citing enantioselective transformations catalyzed by chiral yttrium catalysts. These reactions include aldol reaction, Michael addition, epoxidation, Friedal-Crafts reaction, and ring-opening reactions. It is further reported that yttrium–based benzyl compounds possessing chiral iminophosphonamide ligands work under mild reaction conditions and are found to be highly reactive and selective for the catalytic asymmetric cross-dehydrogenative coupling of amines with prochiral silanes. By using this catalyst, catalytic kinetic resolution of an axially chiral silane and further in situ allylation can be achieved in good yields [21].

1.3.4 Yttrium-based MOFs as catalysts

A porous 3D MOF $[Y_5L_6(OH)_3(DMF)_3] \cdot 5H_2O$ (**1**) (where L = 3-amino-4-hydroxybenzoate) consisting of clusters formed by Y(III) and OH-ions joined by ligand is prepared by solvothermal process. MOF possesses good catalytic activity and also recyclability towards cyanosilylation of carbonyl compounds. Other advantages include solvent-free conditions and lower catalyst loading as compared with other related reported MOFs [22]. Furthermore, formation of a new Y-based metal-organic framework (MOF) GR-MOF-6, namely, $\{[YL(DMF)_2] \cdot (DMF)\}_n$ {H_3L = 5-[(4-carboxyphenyl)ethynyl] isophthalic acid; DMF = *N*,*N*-dimethylformamide}, is reported by a solvothermal route. This material proves to be an effective catalyst in the cyanosilylation of carbonyl compounds. It ranks second in the catalytic activity among the reported REM-based MOFs with the requirement of lowest catalyst loading [23].

1.3.5 Yttrium-based bimetal catalysts

An efficient bimetallic catalytic system, namely, Co–Y for the hydrogenolysis of aryl ethers originated from lignin-based biomass or aromatic plastics with ether bonds, has been developed by Wang et al. [24] (Figure 1.1). The bimetallic catalytic system was synthesized by co-precipitation method, and it shows good performance with a Co/Y, 12/1 molar ratio under mild reaction conditions even without using any promoter. It was further established that high activity results when Co interacts with Y species.
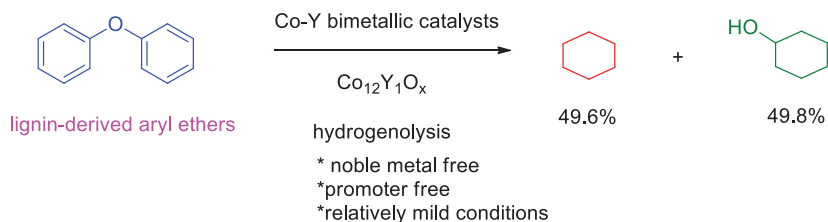
Figure 1.1: Co–Y catalytic system for the hydrogenolysis of aryl ethers.

1.3.6 Yttrium-based salts as catalysts

Aliphatic polyesters exhibit important property of biodegradability and recyclability and constitute significant group of plastics that can be easily synthesized from inexhaustible sources. The ring-opening copolymerization (ROCOP) of cyclic anhydrides and epoxides is a favorable route to sustainable polyesters with a broad variety of physical properties. The catalyst/co-catalyst pair of $YCl_3THF_{3.5}$ and *bis*(triphenylphosphoranylidene)ammonium chloride ([PPN]Cl) is reported as highly active, efficient, and controlled pair for the ROCOP of a variety of cyclic anhydrides and epoxides (Figure 1.2). This catalyst/co-catalyst pair exhibits good turn-over frequencies as compared to past literature reports [25].
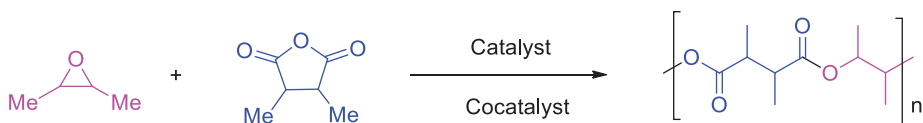
Figure 1.2: ROCOP of epoxides and cyclic anhydrides.

It is well established that cobalt-yttrium binary oxide (CYBO) can be applied in controlling organophosphorus pollution and reducing water eutrophication. CYBO possess a remarkable catalytic activity in activating peroxymonosulfate (PMS) and also higher capacity of phosphate adsorption. It is demonstrated that phenylphosphonic acid (PPOA) degraded completely within 30 min, further removing phosphate product within 60 min. In addition, CYBO possessed outstanding reusability and stability. Moreover, it does not cause decline in the degradation of PPOA and removal of phosphate occurred in five cycles at initial pH 7 [26].

1.3.7 Yttrium-based complexes as catalysts

The synthesis of well-defined, highly stable, and tunable phosphate ligated dialkyl yttrium complexes (PYR_2) is reported which on treatment with the borate reagent exhibit high selectivity and activity in the *cis*-1,4-polymerization of isoprene. Moreover, by using additive $AlMe_3$, switch in the stereoselectivity from *cis*-1,4-polymerization to *trans*-1,4-polymerization is observed [27]. Yttrium-based complexes, namely, amino-alkoxy-*bis*(phenolate) yttrium, complexes act as highly active and stereoselective catalyst for the polymerization of *rac*-lactide and *rac*-β-butyrolactone. A very small amount of catalyst is required for the manufacture of enormous amounts of polymer, and it also leads to the formation of polymer with functional end groups, which find applications in macromolecular engineering [28]. Amido-imino complexes of yttrium act as catalysts for hydroamination or cyclization of 2,2-dimethyl-4-pentenylamineintramolecularlyat room temperature [29]. There is a report in the literature regarding the synthesis of cyclohexyl-bridged complexes, namely, [{(*R*,*R*)-Cy(BDI^{Mes})$_2$}YN(SiMe$_3$)$_2$] ((*R*,*R*)-**3**), [{(*R*,*R*)-Cy-(BDI^{Mes})$_2$}LaN(SiMe$_3$)$_2$] ((*R*,*R*)-**4**), and [{(*R*,*R*)-Cy(BDI^{DIPP})$_2$}LaN(SiMe$_3$)$_2$] ((*R*,*R*)-**5**) of yttrium and lanthanum. The complexes are obtained in enantiomerically pure form and show good catalytic activity in the asymmetric hydroamination or cyclization of aminoalkenes. It is observed that the bulkiness of the aryl substituents and ionic radius of the metal highly influenced the catalytic activity of the complexes. The smaller yttrium metal center in complex (*R*,*R*)-**3** led to reduced activity as well as a reversal in enantio-selectivity [30]. In yet another investigation, it is observed that yttrium (amidate) complexes are used as highly active precatalysts for the mild amidation of aldehydes with amines. Reactions occur rapidly at room temperature within 5 min resulting up to 98% yield of the product. Further, reaction takes place without using any additional base, heat, light, or oxidant. Functionalized amines and/or aldehydes undergo this reaction [31].

1.4 Environmental impact of yttrium

The demand for REE is growing worldwide due to their range of applications from agriculture to medicine and petroleum industry. Hence, water systems are contaminated at a faster rate due to disposal of these elements into water bodies. Their extraction and use is growing rapidly resulting in REY complexes being released into the atmosphere including aquatic systems which is a matter of great concern about their probable effects on aquatic plants and animals.

1.4.1 Role of yttrium on the tolerance of *Potamogeton crispus* to acute nickel toxicity

Nickel is a toxic pollutant which acutely affects the aquatic species of plants and animals. Aquatic plants are recommended as phyto-remediating agents which remove heavy metals from water. Though nickel is known for its toxicity on aquatic plants, the further investigations on increasing nickel tolerance is still required. REEs' role in resisting heavy-metal pollution in plants is receiving great interest recently. There is a report in the literature which indicates that Y in low doses cause positive regulation of polyamine transformation, inhibition of oxidative stress, stimulation of photosynthesis, and finally cause promotion of the resist ability of curly-leaf pondweed (*Potamogeton crispus*) to nickel stress. Thus, REEs have application in the regulation of submerged plant tolerance to aquatic heavy-metal pollution [32].

1.4.2 Effect of yttrium on photosynthetic responses of young maize plants

In one more study, examination of the effects of diverse concentrations of yttrium on its distribution and accumulation, response to photosynthesis, concentration of free-proline and growth of young maize (*Zea mays* L., hybrid NS-640) plants is described. It is observed that yttrium (Y) reduced the growth of maize plant and also photosynthetic performance when present in higher concentrations. Further, there is decrease in the dimensions of stomata while significant increase in the density on abaxial and adaxial epidermis is observed. Further, reduction is caused in the root length, plant height, and dry mass and total leaf area. There is decrease in the concentration of chlorophyll *a,* chlorophyll *b*, free-proline, and carotenoids. Moreover, intensities of photosynthesis and transpiration were also reduced in the presence of yttrium. It is further observed that yttrium reduces conductance of water vapor to stomata, photosynthetic water use efficiency (WUE) and water content. Experimental results indicated that yttrium produced unfavorable effects on the physiological processes and hence plant growth in higher concentrations [33].

1.4.3 Effects of yttrium on the toxicity of *Nymphoides peltata*

There is a report regarding the evaluation of effects of yttrium on the subcellular distribution, bioaccumulation, and its acute toxicity on *Nymphoides peltata*. The effects of 1–5 mg/L of yttrium concentrations were evaluated by measuring changes in nutrient contents, photosynthetic pigments, ultrastructure, and non-enzymatic and enzymatic antioxidants. It is observed that there is decrease in the accumulation of yttrium in subcellular fractions in the order of cell wall > organelle > soluble fraction.

Yttrium is present in higher concentrations in cellulose and pectin as compared to other biomacromolecules. The content of P and K reduced while increase in the contents of Mg, Ca, Fe, Mn, and Mo is observed. Additionally, it was noticed that for all concentrations of yttrium in *N. peltata*, ascorbate and catalase activity reduced considerably. Furthermore, chlorosis and injury to chloroplasts and mitochondria are observed even at the lowest concentration of yttrium. Content of pigment further decreased with increase in the yttrium concentration. The results showed that exogenous yttrium was present in extremely high concentration in water bodies that might produce injurious effects on aquatic organisms. *N. peltata* is proposed as a biomonitor for the assessment of metal pollution in aquatic ecosystems [34].

1.4.4 Effects of yttrium on bioaccumulation in coastal species from Maluan Bay, China

There are large numbers of reports on the impact of REEs as environmental pollutant while there are little reports on their distribution and accumulation in coastal species. There is a recent report indicating the effect of concentrations of 15 naturally occurring RREs, including yttriumon bioaccumulation patterns of species. It was observed that bioaccumulation patterns seemed to be element- and species-dependent even in the same taxa or phylum, while limited possibility is observed for bio-magnification. Furthermore, there is notably higher concentration of REEs in molluscs as compared to other species [35].

1.4.5 Bioaccumulation of yttria NPs in Brassicaceae, *Brassica oleracea*

Nowadays, there is increasing interest in the use of engineered nanoparticles (ENPs) due to their wide range of applications. It is a matter of great concern that their exposure to environment may lead to their probable entry into food chains and hence may cause deleterious health effects. In this context, plants play a major role in the uptake and transport of these nanoparticles in the food chain. A report on yttria NP absorption, translocation, and bioaccumulation in edible cabbage (Brassicaceae, *Brassica oleracea*) can be found in the literature [36]. The yttria ENPs were said to be taken up by the root but not by the cabbage shoot. On the other hand, both the cabbage root and the shoot contained various non-yttria minerals. The buildup of yttria NPs at primary-lateral-root junctions was discovered to be the principal cause of their obstruction.

1.5 Conclusions

Yttrium-based nanocomposites, halide complexes, metal organic frameworks, bimetals, and yttrium-based salts/complexes can be used as efficient catalysts for chemical transformations. Yttrium in low concentrations improves photosynthesis, reduces oxidative stress, and favorably controls polyamine transformation. They also assist *Potamogeton crispus*, a kind of curly-leaf pondweed, in surviving nickel stress. In the subcellular fractions of *Nymphoides peltata*, accumulation of yttrium is seen to decrease in the following order: cell wall > organelle > soluble fraction. Yttrium is present in higher concentrations in cellulose and pectin in *N. peltata* as compared to other biomacromolecules. A decrease in the P and K content and a rise in the Mg, Ca, Fe, Mn, and Mo content are both seen. For all yttrium concentrations in *N. peltata*, ascorbate and catalase activity also experienced considerable declines. Even at the lowest yttrium concentrations, *N. peltata* exhibits morphological signs of senescence, including chlorosis and damage to the chloroplasts and mitochondria.

References

[1]   Mallmann, EJJ, Sombra, AS, Goes, JC, Fechine, PB. Yttrium iron garnet: Properties and applications review. Solid State Phenom, 2013, 202, 65–96.

[2]   Tickner, BJ, Stasiuk, GJ, Duckett, SB, Angelovski, G. The use of yttrium in medical imaging and therapy: Historical background and future perspectives. Chem Soc Rev, 2020, 49, 6169–6185.

[3]   Murali, N, Mouli, SK, Riaz, A, Lewandowski, RJ, Salem, R. Extrahepatic applications of yttrium-90 radioembolization. Semin Interv Radiol, 2021, 38, 479–481.

[4]   Chandekar, KV, Shkir, M, Khan, A, Sayed, MA, Alotaibi, N, Alshahrani, T, Algarni, H, AlFaify, S. Significant and systematic impact of yttrium doping on physical properties of nickel oxide nanoparticles for optoelectronics applications. J Mater Res Technol, 2021, 15, 2584–2600.

[5]   Strauss, ML. The Recovery of Rare Earth Oxides Fromwaste Fluorescent Lamps, Colorado School of Mines, 2016.

[6]   Ren, Y, Sun, X, Guan, Y, Xiao, Z, Liu, Y, Liao, J, Guo, Z. Distribution of rare earth elements plus yttrium among major mineral phases of marine Fe–Mn crusts from the South China Sea and Western Pacific Ocean: A comparative study. Minerals, 2018, 9, 8.

[7]   Tanaka, E, Nakamura, K, Yasukawa, K, Mimura, K, Fujinaga, K, Iijima, K, Nozaki, T, Kato, Y. Chemostratigraphy of deep-sea sediments in the western North Pacific Ocean: Implications for genesis of mud highly enriched in rare-earth elements and yttrium. Ore Geol Rev, 2020, 119, 103392.

[8]   Fu, B, Hower, JC, Zhang, W, Luo, G, Hu, H, Yao, H. A review of rare earth elements and yttrium in coal ash: Content, modes of occurrences, combustion behavior, and extraction methods. Prog Energy Combust Sci, 2022, 88, 100954.

[9]   Balaram, V. Rare earth elements: A review of applications, occurrence, exploration, analysis, recycling, and environmental impact. Geosci Front, 2019, 10, 1285–1303.

[10] Chen, J, Yang, R, Zhang, J, Chao, J. Occurrence of yttrium in the Zhijin phosphorus deposit in Guizhou Province, China. Open Geosci, 2022, 14, 776–784.

[11] Sodpiban, O, Del, GS, Barman, S, Aomchad, V, Kidkhunthod, P, Ould-Chikh, S, Poater, A, D'Elia, V, Basset, JM. Synthesis of well-defined yttrium-based Lewis acids by capturing a reaction intermediate

and catalytic application for cycloaddition of CO_2 to epoxides under atmospheric pressure. Catal Sci Tech, 2019, 9, 6152–6165.

[12] Bürgstein, MR, Berberich, H, Roesky, PW. (Aminotroponiminato) yttrium amides as catalysts in alkyne hydroamination. Organometallics, 1998, 17, 1452–1454.

[13] Hara, T, Habe, M, Nakanishi, H, Fujimura, T, Sasai, R, Moriyoshi, C, Kawaguchi, S, Ichikuni, N, Shimazu, S. Specific lift-up behaviour of acetate-intercalated layered yttrium hydroxide interlayer in water: Application for heterogeneous Brønsted base catalysts toward Knoevenagel reactions. Catal Sci Tech, 2022, 12, 2061–2070.

[14] Lou, K, Zu, F, Yi, J, Cui, C. Synthesis and structure of a dimeric yttrium complex [LSi (BH$_3$)(C$_5$Me$_4$) Y (CH$_2$SiMe$_3$)$_2$]$_2$ (L= PhC (NtBu)$_2$) and Its catalytic application for Hydroboration of Ketones and Aldehydes. Organometallics, 2021, 40, 4092–4097.

[15] Magdalane, CM, Kaviyarasu, K, Vijaya, JJ, Siddhardha, B, Jeyaraj, B. Facile synthesis of heterostructured cerium oxide/yttrium oxide nanocomposite in UV light induced photocatalytic degradation and catalytic reduction: Synergistic effect of antimicrobial studies. J Photochem Photobiol B: Biol, 2017, 173, 23–34.

[16] Akbari, FA, Saravanan, R, Jamshidijam, M, Mangalaraja, RV, Gracia, MA. Preparation of nanosized yttrium doped CeO2 catalyst used for photocatalytic application. J Saudi Chem Soc, 2015, 19, 505–510.

[17] Reddy, CV, Reddy, KR, Zairov, RR, Cheolho, B, Shim, J, Aminabhavi, TM. g-C$_3$N$_4$ nanosheets functionalized yttrium-doped ZrO$_2$ nanoparticles for efficient photocatalytic Cr (VI) reduction and energy storage applications. J Environ Manage, 2022, 315, 115120.

[18] Yashas, SR, Shivaraju, HP, Sandeep, S, Swamy, NK, Gurupadayya, B. Application of yttrium molybdate tethered polypyrrolenanocomposite for the photocatalytic remediation of nitrofurantoin in water. Surf Interfaces, 2022, 32, 102102.

[19] Keerthana, M, Pushpa, MT, Sangavi, R, Arockia, SJP, Arthanareeswari, M. Effect of europium, yttrium and lutetium doping on the photocatalytic property of CeO$_2$ nanoparticles in the reduction of p-nitrophenol under visible light. Chem Select, 2022, 7, 202103610.

[20] Pellissier, H. Recent developments in enantioselective yttrium-catalyzed transformations. Coord Chem Rev, 2016, 324, 17–38.

[21] Li, N, Guan, BT. Yttrium–benzyl complexes bearing chiral iminophosphonamide ligands: synthesis and application in catalytic asymmetric amine-silanedehydrocoupling reactions. Adv Synth Catal, 2017, 359, 3526–3531.

[22] Echenique, EE, Pérez, JM, Rojas, S, Cepeda, J, Seco, JM, Fernández, I, Rodríguez, DA. A novel yttrium-based metal–organic framework for the efficient solvent-free catalytic synthesis of cyanohydrin silyl ethers. Dalton Trans, 2021, 50, 11720–11724.

[23] Pérez, JM, Rojas, S, García, GA, Montes, AH, Ruiz, MC, Romero, CMS, Choquesillo, LD, Abdelkader, FVK, Pérez, MM, Cepeda, J, Rodríguez, DA. Catalytic performance and electrophoretic behavior of an yttrium–organic framework based on a tricarboxylic asymmetric alkyne. InorgChem, 2022, 61, 1377–1384.

[24] Wang, SW, He, ZH, Chen, JG, Yang, SY, Wei, YY, Wang, K, Wang, W, Ma, X, Liu, ZT. Cobalt-yttrium bimetal catalyzed hydrogenolysis of aryl ethers. Biomass Bioenergy, 2022, 164, 106565.

[25] Wood, ZA, Assefa, MK, Fieser, ME. Simple yttrium salts as highly active and controlled catalysts for the atom-efficient synthesis of high molecular weight polyesters. Chem Sci, 2022, 13, 10437–10447.

[26] Chen, C, Pang, Y, Li, Y, Li, W, Lan, Y, Shen, W. Dual functional cobalt-yttrium binary oxide activation of peroxymonosulfate for degradation of phenylphosphonic acid and simultaneous adsorption of phosphate product. J Chem Eng, 2022, 429, 132185.

[27] Yang, P, Du, HZ, Zhang, XY, Xia, YL, Sun, JT, Peng, Q, Guan, BT. Well-defined phosphate yttrium dialkyl complexes for catalytic stereo-controllable 1, 4-polymerization of isoprene. Chin Chem Lett, 2022, 33, 2402–2406.

[28] Amgoune, A, Thomas, CM, Carpentier, JF. Yttrium complexes as catalysts for living and immortal polymerization of lactide to highly heterotacticPLA. Macromol Rapid Commun, 2007, 28, 693–697.

[29] Kaneko, H, Tsurugi, H, Panda, TK, Mashima, K. Intramolecular alkylation of α-diimine ligands giving amidoimino and diamido scandium and yttrium complexes as catalysts for intramolecularhydroamination/cyclization. Organometallics, 2010, 29, 3463–3466.

[30] Vitanova, DV, Hampel, F, Hultzsch, KC. Linked bis (β-diketiminato) yttrium and lanthanum complexes as catalysts in asymmetric hydroamination/cyclization of aminoalkenes (AHA). J Organomet Chem, 2011, 696, 321–330.

[31] Thomson, JA, Schafer, LL. Yttrium (amidate) complexes for catalytic C–N bond formation. Rapid, room temperature amidation of aldehydes. Dalton Trans, 2012, 41, 7897–7904.

[32] Lyu, K, Wang, X, Wang, L, Wang, G. Rare-earth element yttrium enhances the tolerance of curly-leaf pondweed (Potamogetoncrispus) to acute nickel toxicity. Environ Pollut, 2019, 248, 114–120.

[33] Maksimovic, I, Kastori, R, Putnik, DM, Borišev, M. Effect of yttrium on photosynthesis and water relations in young maize plants.J. Rare Earths, 2014, 32, 372–378.

[34] Fu, Y, Li, F, Xu, T, Cai, S, Chu, W, Qiu, H, Sha, S, Cheng, G, Xu, Q. Bioaccumulation, subcellular, and molecular localization and damage to physiology and ultrastructure in Nymphoidespeltata (Gmel.) O. Kuntze exposed to yttrium. Environ Sci Pollut Res, 2014, 21, 2935–2942.

[35] Wang, Z, Yin, L, Xiang, H, Qin, X, Wang, S. Accumulation patterns and species-specific characteristics of yttrium and rare earth elements (YREEs) in biological matrices from Maluan Bay, China: Implications for biomonitoring. Environ Res, 2019, 179, 108804.

[36] Chen, Y, Sanchez, C, Yue, Y, de, AM, González, JM, Parkinson, DY, Liang, H. Observation of yttrium oxide nanoparticles in cabbage (Brassica oleracea) through dual energy K-edge subtraction imaging. J Nano Biotechnol, 2016, 14(1), 1–10.

Mohit Maingle, Steeva Sunny, Kate Ashru Ajinath, Amrutha Cica Tomy, Wagh Kanchan Madanrao, Pathlavath Teja Sree and Kapileswar Seth[*]

2 Half-sandwich organo-group-3 metal-catalyzed C–C bond formation via sp² C–H bond functionalization

2.1 Introduction

The C–H bonds are ubiquitously present in various organic molecules as well as natural resources [1]. They have emerged as an increasingly powerful component of C–H bond activation/functionalization strategy. The strategic evolution of C–H bond activation has set the stage for step-, atom- and cost-effective pathways for sustainable growth [2] synchronizing "green" chemistry aspects [3]. Contrary to traditional cross-coupling reactions, the C–H bond activations do not require pre-functionalization of both starting materials. Thus, following C–H bond activation/functionalization, the lengthy synthetic procedures, and additional unwanted by-products, which are typically associated with classical cross-coupling reactions, can be avoided. In the last few decades, this transformative tool has offered easy access to fine chemicals and other common/complex molecular scaffolds relevant to medicinal chemistry, agrochemicals, materials science, and late-stage derivatization of bioactive entities and natural products [4–8].

The C–H bonds possess low reactivity and high bond dissociation energy and lack polarity. These attributes make the C–H bonds chemically inert and thermodynamically stable [9] and render the bond breaking and making process during C–H bond activation a challenging subject with high activation energy demand ($\Delta G^{\neq}$) [10]. Selective breakage of a particular C–H bond needs to overcome the kinetic energy demand of the bond [11] and productively takes place by means of internal and

Note: Mohit Maingle and Steeva Sunny contributed equally.

[*]**Corresponding author: Kapileswar Seth,** Department of Medicinal Chemistry, National Institute of Pharmaceutical Education and Research (NIPER), Guwahati, Sila Katamur, Changsari, Kamrup 781101, Assam, India, e-mail: kapileswar@niperguwahati.in
Mohit Maingle, Steeva Sunny, Kate Ashru Ajinath, Amrutha Cica Tomy, Wagh Kanchan Madanrao, Pathlavath Teja Sree, Department of Medicinal Chemistry, National Institute of Pharmaceutical Education and Research (NIPER), Guwahati, Sila Katamur, Changsari, Kamrup 781101, Assam, India

external factors [12, 13], which involve reframing critical reaction components and parameters [14–17].

The almost indistinguishable difference in reactivity among analogous multiple C–H bonds of a substrate results in a mixture of regioisomeric products [18]. Thus, introducing desired functional groups in a highly siteselective and chemoselective manner is one of the challenging features of C–H bond activation/functionalization [19]. To solve this problem, the Lewis basic heteroatom(s) or functional group(s) that act(s) as directing group(s) (DGs) has/have been explored successfully to determine the reaction trajectory [20–26]. The control of all aspects of siteselectivity involves the coordination of DGs to corresponding Lewis acidic metal center paving the metal center to the vicinity of the selected C–H bond. This enforces intramolecular C–H bond activation via cyclometallation leading to carbometalated species [27–29] and the net result is preferential siteselectivity [30, 31].

In the past couple of years, transition metal-catalyzed reactions have contributed appreciably to the field of C–H bond functionalization extending from valuable noble metals to cheap abundant non-noble-type metals [32, 33]. The catalytic transition metal center governs facile selective breakage of a C–H bond either by donation of electron (nucleophilic activation) or through removing an electron from concerned C–H bond (electrophilic activation) via highly ordered transition state (TS) and depending on the substrate structure and type of reaction environment [34]. In principle, a transition metal is inserted into a less polar C–H bond, resulting in a highly polarized organometallic M–C σ-bond with an enhanced reactivity [29, 35], and fulfils the kinetic energy barrier of concerned C–H bond activation. The overall result indicates selective cleavage of the concerned C–H bond.

Since the metal center is directly engaged in the intermediate M–C σ-bond formation, the character, valence electron types, and oxidation number of concerned metal atom primarily guide the chosen C–H bond functionalization mode under a particular reaction condition [36, 37]. In general, the f-block elements exhibit the following characteristics, (i) lack valence electrons in d^n-shell, and allow one electron oxidation process with f^n-configuration [38], (ii) restricted oxidation states [39], (iii) f-orbitals exhibit poor shielding on peripheral electrons from effective nuclear charge [40] which may make donation of valence electrons relatively difficult. These features of f-block elements discriminate them from the late transition metals in a mode of mechanism of C–H bond activation. The late transition metals prefer C–H bond activation via oxidative addition displaying two-electron redox chemistry possessing varied oxidation states [36, 37]. Typically, high electropositive nature of f-block elements induces a high degree of polarization to M–X bond (X = C, N) along with p-block elements. Thus, the M–X bond stays in polarized form ($^{\delta+}M - X^{\delta-}$) and follows a σ-bond metathesis route (2σ–2σ process) [41–43] for selective cleavage of the less polar C–H bond. The σ-bond metathesis pathway could be lower energy demanding process even if oxidative addition is feasible [44].

In general, auxiliary ligands hold a remarkable place in promoting homogenous transition metal-catalyzed C–H bond functionalization chemistry through modulation of the activation energy demand of underlying mechanistic steps of the process. The change in structural and reactivity patterns of the respective metal center in a catalytic cycle is attributed to the σ-donor and π-acceptor type coordination ability of the associated ligands [45]. These changes in transition metal center are defined with respect to kinetic reactivity and, thereby, extend the possibility of substrate scope exploration of the reaction. In contrast to d-block metal chemistry, the f-block metal complexes demonstrate unique reactivity profiles by virtue of their different electronic, structural, and energetic properties. The high electropositive character and commonly observed + 3 oxidation state of rare-earth metal centers make their chemistry considerably ionic, inducing specific reactivity [46, 47]. Here, the electrostatic interaction is balanced by a stable anionic strong σ-donor and weak π-acceptor ligand, e.g., N- or C-based donor group, and thereby stabilizes the metal center. For example, anionic aliphatic carbon and di-alkyl-substituted nitrogen-based ligands ($-CH_2Ph$-*ortho*-NMe_2) have mostly been used with lanthanide metal complexes. The rare-earth metal centers typically require sterically bulky ligands to satisfy high coordination numbers (12–26) around large ions to stabilize the coordination status of the metal center obviating thermal decomposition. Meanwhile, the absence of β-hydrogen atom in anionic ligand prevents the decomposition of Ln–alkyl complex by β-hydrogen elimination route. In addition, the cyclopentadienyl monoanions and cyclooctatetraenyl dianions are commonly participated ligands to stabilize the coordination environment of lanthanide complexes through electrostatic and steric adjustment [46–49]. Simultaneously, in lanthanide chemistry, steric crowding may play a critical role in ligand-directed cyclometalative C–H bond activation step guided by favorable entropy parameter (ΔS) and change in Gibbs free energy (ΔG) at high temperature [50, 51]. Among carbocylic ligands, such as η^5-C_5H_5 (Cp), and η^5-C_5Me_5 (Cp*), Cp* is widely accepted for its potential to stabilize the coordination sphere of large rare-earth metal center on account of its bigger size as well as improved solubility [52]. In a constrained geometrical environment, the bulky ligands display specific reactivity patterns with a rare-earth metal center in a predictable and reliable fashion by giving access to metal center through a highly ordered channel [53]. In addition to the profound impact of ligand structure and electronics on stereo-, regio-, and chemoselective outcomes, other notable accomplishments of ligands include enhanced solubility in organic solvents, prevention of degradation of the concerned metal complex and extension of catalyst life span [35]. Thus, the performance of a metal catalyst concerning reactivity, such as turnover number/frequency, substrate capacity, selectivity, and other reaction parameters (e.g., temperature, pressure, time, and sensitivity to oxygen/moisture), is unambiguously repurposed by the electronic as well as steric properties of the associated ligands. Therefore, the design and development of an appropriate ligand is the prima facie objective in performing known metal-catalyzed chemistry to achieve improved catalytic performance and application of new reactions [54, 55].

The C–H bond activation catalyzed by rare-earth metals has garnered paramount attention for more than four decades. A pioneering report on rare-earth metal-catalyzed C–H bond functionalization by Dr. Patricia Watson could be found dated back to 1980s, which involves sp^2 C–H bond activation of benzene and pyridine mediated by Lu–alkyl and Lu–H complexes in intramolecular and intermolecular reactions, and sp^3 C–H bond activation of methyl group of SiMe$_4$ functionality [56]. The end products were organolutetium complexes characterized by new Lu–C bonds as distinct stoichiometric 1:1 metal-ligand complex. Since the foremost example of C–H bond activation catalyzed by rare-earth metal, which was reported from Prof. Watson, the scope of this strategy has been dramatically expanded. In fact, the development of elegant C–H activation techniques by Prof. William J. Evans, Prof. Peter Junk, Prof. Alexander Trifonov, Prof. Reiner Anwander, to name a few, shed light on the potential of f-element-catalyzed C–H bond functionalization strategies [57–63].

In the past few years, detailed investigations have been done on the relatively underexplored area of f-element-catalyzed construction of C–C bonds via C–H bond activation/functionalization approach. The developments and contributions in this field have been summarized in the forms of reviews, accounts, and perspective [64–68]. In this chapter, we have briefly outlined the state of art in the arena of half-sandwich organo-group-3 metal-catalyzed sp^2 C–H bond activation/functionalization furnishing C–C bonds. In particular, attention has been paid on functionalization of sp^2 C–H bonds of small molecule scaffolds for their derivatization through C–C bond formation.

2.2 Group-3 metal-catalyzed sp^2 C–H bond functionalization

2.2.1 C–H bond addition to alkenes for alkylation

The conventional Friedel–Crafts (FC) alkylation reaction of electron rich aromatic compounds, namely anisole, under Lewis acid catalysis provides a route to derivatize the aromatics with new C–C bonds. However, electronic as well as steric control of aromatic rings dominate the ratio of regioisomeric products, and in general, the reactions typically suffer from limitations of a mixture of *ortho* and *para* regioisomeric products [69]. The use of late transition metals as Lewis acidic centers [37] controlling regioselectivity at *ortho*-position by activating the alkylation agents could not serve the purpose owing to poor coordination ability of the metals with weak coordinating [70, 71] ether functionality. In addition, oxygen center is weak σ-donating atom and fails to target correct *ortho* C–H bond, which results in the formation of highly strained four-membered cyclometalated species. In addition to the type of transition metal, reaction environments, and nature of reactions largely dictate the coordination capability of DGs [72]. On the contrary, a high degree of *para*-selectivity has been

observed during FC acylation reaction of electronically populated aromatics with Ac_2O catalyzed by rare-earth complex, $Yb(OTf)_3$ [73]. In this report, high regioselectivity has been achieved with Yb^{3+} center and further enabled excellent recyclability of the catalyst system, as $Yb(OTf)_3$ is highly stable in water.

Typically, the f-block metal centers possess high oxophilicity [74–76] and high π-electron affinity for unsaturated C–C bonds [39, 77], encompassing challenging reaction partners, e.g., unactivated olefins [78–80]. Envisioning these understandings, Hou et al. described *ortho*-selective C–H bond alkylation of anisole analogues (**1**) with varied range of unsaturated unactivated olefins (**2**), such as aliphatic alkenes and biased olefins, such as styrene analogues (**3**) (Figure 2.1-i) [81]. The half-sandwich Sc–dialkyl complex Sc-**1** plus an equivalent molar quantity of co-catalyst $[Ph_3C][B(C_6F_5)_4]$ were used as catalytic condition and afforded 1:1 addition product **4a** (R = H, Ar = Ph) plus minor 1:2 product **5a** (R = H, Ar = Ph). Studies with yttrium (Y-**1**) or gadolinium (Gd-**1**) derivative of the dialkyl complex were also compatible producing almost quantitative yields of **4a**, which could be accounted to lower efficacy of Y-**1** and Gd-**1** toward polymerization or constant insertion of styrene (**3a**) [82, 83]. Investigation into the scope of olefins revealed **2** to produce branched alkylation, whereas biased **3** delivered linear derivatives. High chemoselectivity was observed for C–H bond with Y-**1** over sensitive C–halogen bonds on aromatic system. In case of 2-methoxynaphthalene, C3–H bond rendered higher reactivity than C1–H site, perhaps due to steric impact of *peri*-H at C8-position. Moreover, the steric control allowed C–C bond construction at more accessible *ortho*-C–H position of *meta*-methylanisole. The steric demand generally induces a sluggish rate of reaction on internal alkenes in carbometallation step relative to terminal alkenes [84–93]. Satisfyingly, productive yields were obtained for *ortho* sp^2 C–H bond alkylation of nonflexible 2,3-dihydrobenzofuran and anisole with norbornene (**2a**) as bulky coupling partner catalyzed by Y-**1** and Sc-**1**. The easiness of σ-bond metathesis step on relatively acidic sp^2 C–H bond [41–43] ensured unique selectivity at sp^2 C–H position over sp^3 C–H or benzylic site of 2,3-dihydrobenzofuran. In the case of *para*-allyl-4-methoxyanisole, the *ortho* C–H alkylation has been observed over olefin polymerization with Y-**1** catalytic system and allyl-/vinyl-trimethylsilane as alkylating agent retained the -SiMe₃ group on final alkylation products during Sc-**1** catalysis. These results highlight the robustness of Sc-**1** and Y-**1** catalytic systems. The plausible mechanistic pathway (Figure 2.1-ii) of the transformation involves *in situ* formation of a species **I** (cationic) from neutral precursor M-**1** with activator $[Ph_3C][B(C_6F_5)_4]$, followed by coordination of vacant location on **I** to anisole oxygen center and concurrent, *ortho*-selective sp^2 C–H bond activation by σ-bond metathesis operation forming a four-membered species **III**. The large size rare-earth metal center, along with the strong Lewis acidic character or oxophilicity of the rare-earth metal element [74–76] stabilizing **III**. Subsequently, steric hindrance at C1-center of aliphatic alkenes leads to the insertion of other part through 2,1-manner on M–C(aryl) σ-bond generating species **IIIa**. However, the insertion of C1-site of styrenes to M–C(aryl) σ-bond through 1,2-manner is directed by benzallylic coordination and stabilization to generate species

IIIb. Thus, the different modes of addition of aliphatic alkenes and styrenes account for branched and linear alkylation products, respectively.
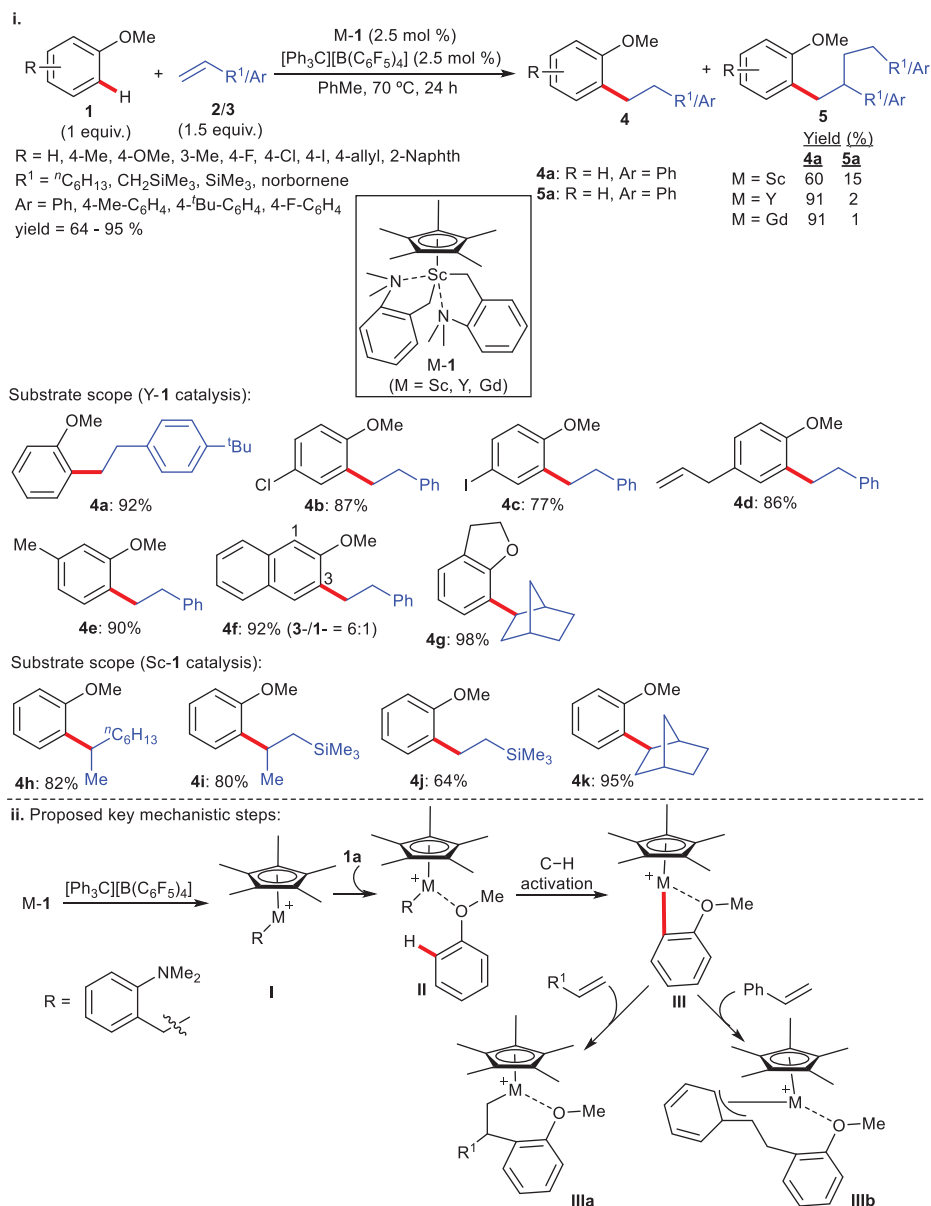

Figure 2.1: (i) A few selected examples of *ortho*-selective C–H bond alkylation of anisole analogues catalyzed by half-sandwich Sc-**1**/Y-**1** complex, and (ii) proposed mechanism.

Emboldened by the efficiency of Y–alkyl complex in catalytic cycle to endorse arene *ortho*-sp^2 C–H bond activation [81], Hou and Lou described Y-**2**-catalyzed *ortho*-sp^2 C–H bond alkylation of *N,N*-dimethylanilines (**6**) along **2** (Figure 2.2-i) [94]. An enumerated study of the substrate scope of both **6** and **2** revealed a high degree of regioselectivity at *ortho*-site delivering respective branched mono-alkylation products (**7**) in synthetically useful yields. Moreover, no *ortho*-di-alkylated product was formed, which could be due to huge steric congestion in TS, composed of mono-alkylated derivative and cationic Y–alkyl complex. Further extension of substrate scope studies to *meta*-substituted **6** leads to alkylation at *ortho* C–H site with less steric hindrance. The quantitative yield was obtained upon incorporation of bulky **2a** at *ortho* C–H bond of **6**, whereas 1,1-disubstituted alkenes, namely, 2-methylstyrene and internal acyclic olefins, like 2-octene were incompetent on account of steric bias of olefin moieties. The steric control on aryl ring also played a vital role in the reactivity. The reaction proceeded well with *N*-ethyl-*N*-methyl aniline, whereas sterically inevitable *N,N*-dimethyl-*ortho*-toluidine, *N,N*-diethyl aniline, and *N*-phenylpiperidine remained futile in the standard reaction environment. However, biased styrene system or conjugated cyclic diene, for example, 1,3-cyclohexadiene furnished oligomer products, can be ascribed to the increased reactivity of Y-**2** for polymerization [82, 83]. Highly activated olefin analogues having enone motifs failed to afford the desired products and led to the prediction of a mechanistically different pathway rather than conventional FC reactions. The density functional theory (DFT) computation reflected σ-bond metathesis mechanism (Figure 2.2-ii). The catalytic process begins through the coordination of nitrogen atom of **6a** to Y$^+$ center [76, 95] of cationic **IV**, generated in situ from equimolar neutral precursor Y-**2** and activator [Ph$_3$C][B(C$_6$F$_5$)$_4$]. Subsequently, C–H activation by σ-bond metathesis afforded cyclometalated **VII** via TS **VI**. Finally, the addition of less congested β-site of olefin on **VII** furnished branched alkylation products, whereby the steric repulsion between C$_5$Me$_4$SiMe$_3$ ligand and α-substituent could be avoided in TS-**VIII**.

In search of better, cheap, and ample source of alkyl group for C–H alkylation catalyzed by rare-earth element, the ethylene motif could be an interesting substitute. However, the unactivated ethylene unit prefers oligomerization to C–H bond alkylation, particularly with electron-demanding pyridine moiety. The previous literature report on *ortho*-selective C–H bond alkylation of pyridine along ethylene moiety catalyzed by neutral Y–metallocene complex raised concerns, such as high temperature (100 °C), pressure of ethylene (40 bar), and a narrow substrate space (applicable to ethylene only) [96]. Apart from these, incorporating higher olefins remained futile to provide the desired products with a slow reaction rate and catalytically unachievable. Later Hou and co-workers seeded the concept of *ortho*-selective C–H bond addition of pyridine analogues (**8**) with ethylene (**2b**) utilizing cationic Sc–alkyl/Y–alkyl complex (Figure 2.3-i) [97]. The strong coordinating ability of pyridyl nitrogen center to a di-cationic Y-atom plus the efficacy of Y-atom toward selective activation of the targeted C–H bond [98] and better activation of olefinic unit by a cationic Sc–alkyl/Y–alkyl complex through high π-electron affinity [39, 77] have been the driving force. The reaction held ample
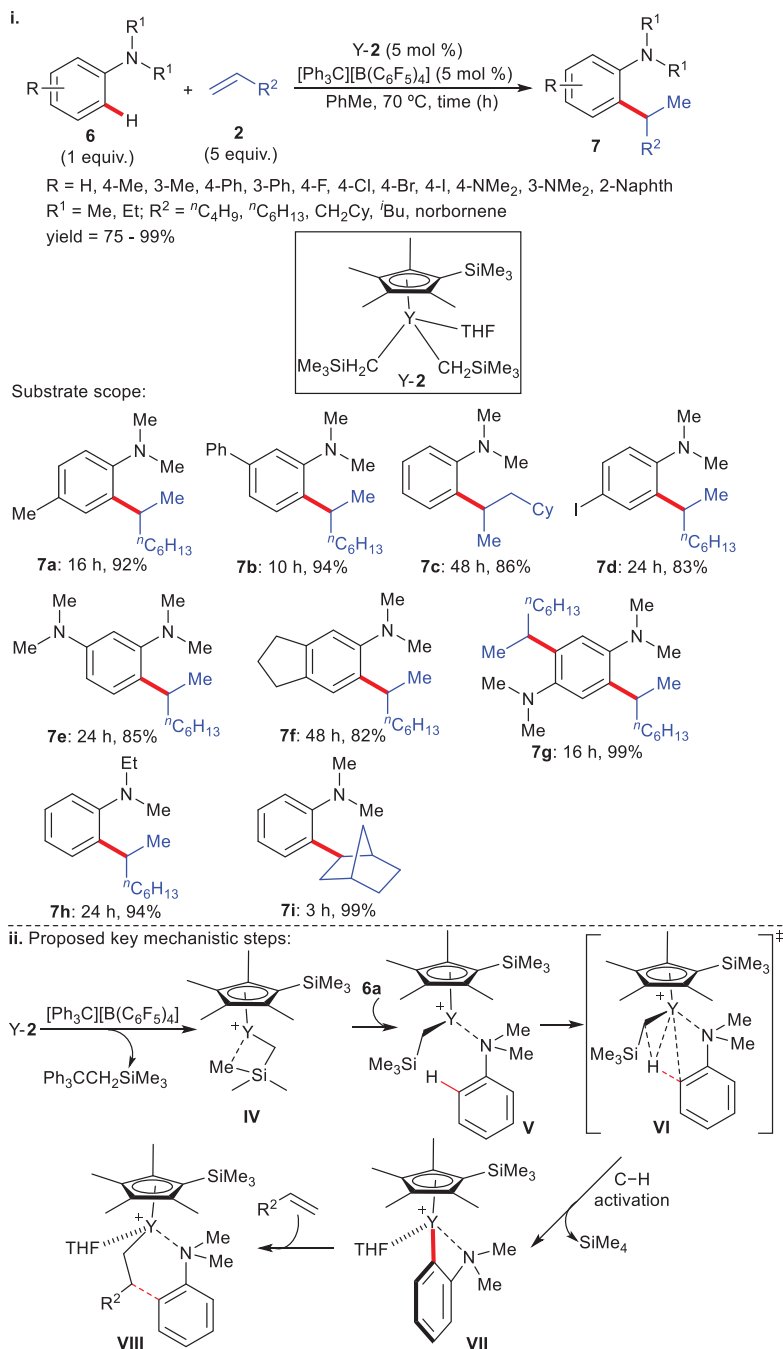
Figure 2.2: (i) A few selected examples of *ortho*-selective C–H bond alkylation of *N,N*-dimethyl anilines catalyzed by half-sandwich Y-**2** complex, and (ii) proposed mechanism.

substrate scope in the presence of Sc-**1** plus equimolar activator B(C$_6$F$_5$)$_3$ as catalytic system and used a variety of pyridine scaffolds and olefins, such as α-alkenes, sterically congested alkenes, styrenes, and conjugated dienes. The reaction was also applicable to bulky 2-*tert*-butyl pyridine derivative affording *ortho*-C–H alkylation aided by catalytic Y-**1** and remained totally ineffective with Sc-**1** catalyst. Perhaps, the strong coordinating ability of larger Y ion to pyridyl N-atom as well as ease of *ortho*-C–H deprotonation in a subsequent step leading to efficient C–H metalation are responsible factors. The catalyst Sc-**1** favored olefin polymerization as Sc ion is small in size and was unreachable to *ortho*-C–H bond of bulky 2-*tert*-Bu group delaying C–H metalation. This approach has opened a new avenue to incorporate alkyl group selectively at the targeted pyridyl *ortho*-C–H bond in case of 2-phenylpyridine moiety, rather than at *ortho*-C–H bond of pendant phenyl unit, observed under pyridine directed C–H bond functionalization catalyzed by transition metal [20–26]. This result indicated favorable σ-bond metathesis by a f-element with a highly reactive acidic *ortho*-C–H bond in pyridine core [41–43]. The unbiased/unactivated aliphatic α-alkenes, namely, 1-hexene and 1-octene had a propensity to generate branched alkylated products solely with 2-ethylpyridine motif, which followed easy insertion of M–C(aryl) σ-bond through 2,1-manner in order to reduce steric hindrance between ligand Cp* and substituents on C1-site of olefins in the corresponding TSs (similar to **IIIa/VIII**). Furthermore, biased **3** underwent C–H bond alkylation with 2-ethylpyridines only in the presence of a larger ion Y-**1** catalyst to give exclusive linear products, whereas the same reaction failed with Sc-**1** catalyst. This anomalous behavior of **3** suggested an increased rate of styrene polymerization under Sc-catalyst over Y-catalyst [82, 83]. Linear alkylation products were obtained through M–C(aryl) σ-bond addition to **3** following 1,2-manner manifested by the stabilization via benzallylic mode of Y$^+$ center in the respective TS (resemble to **IIIb**). Regarding the scope of transformation, the alkylation of pyridine with **3** and **2** generated branched and linear isomeric products, respectively, employing a Ni-based catalyst system [99]. The sharp contradiction with respect to regioselectivity highlights that character, population of valence electron, oxidation status, and ancillary ligands attached to metal ion exhibit a profound effect on the electronic as well as steric features of a typical organometallic M–C σ-bond and introduce a well-defined reactivity pattern [36, 37]. The high kinetic isotopic effect (KIE) value ($k_H/k_D = 4.9$) obtained from intermolecular competition between pyridine (**8a**) and **8a-d_5** with **2a** has proved C–H bond activation as rate-limiting step (Figure 2.3-ii). Plausible mechanistic steps comprise in situ generation of species **IX** through pyridyl nitrogen atom chelation to Sc$^+$-/Y$^+$-ion [98].

Transition metal-catalyzed asymmetric induction at a prochiral center following a C–H bond activation/functionalization route with the assistance of chiral auxiliary/components has attracted much attention in the synthetic organic chemistry community [100]. This inspired Hou and co-workers to disclose chiral Sc–alkyl complex, (Sc-**2**) catalyzed *ortho*-C–H bond addition of **8** along **2** through an enantioselective manner (Figure 2.4) [101]. The chirality was induced by a sterically heavy chiral binaphthyl
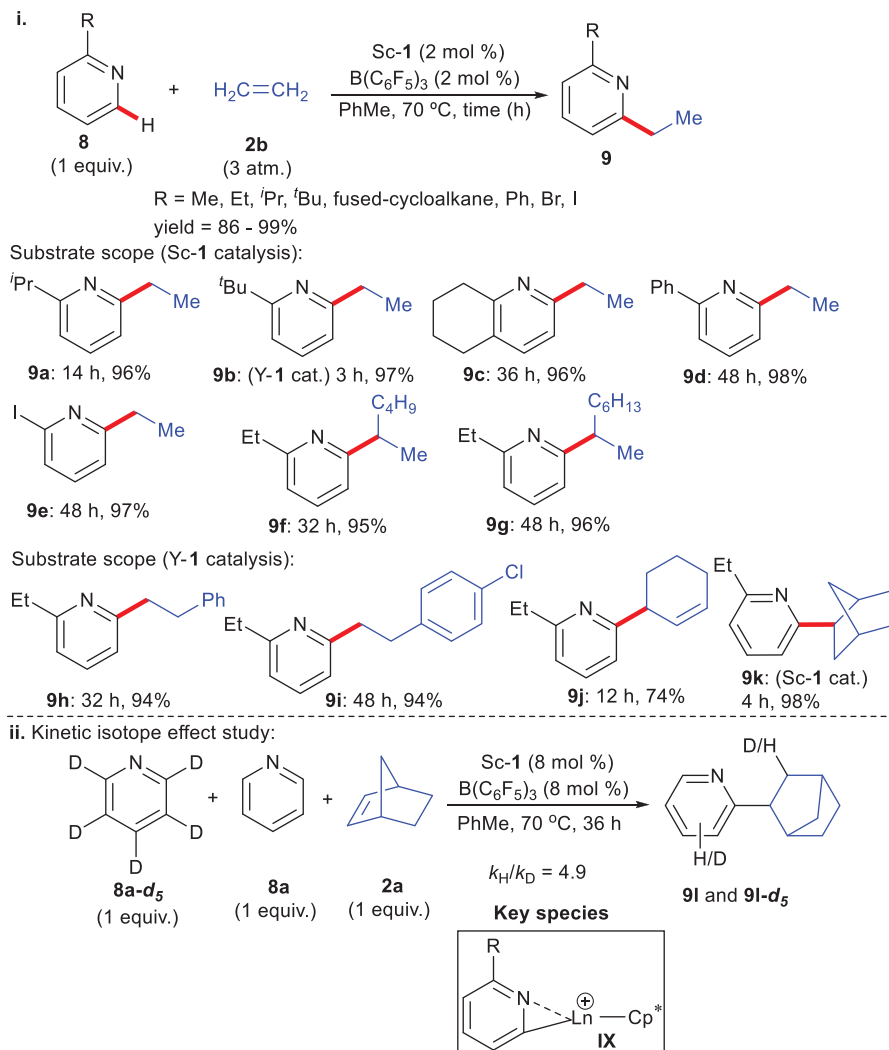
Figure 2.3: (i) A few selected examples *ortho*-selective C–H bond alkylation of pyridines catalyzed by Sc-**1**/Y-**1** complex, and (ii) related study of kinetic isotope effect.

group-attached cyclopentadiene ligand associated with the Sc-**2** catalyst, and the N-chelation of pyridine ring to cationic Sc center guided the desired *ortho*-C–H bond activation. The pyridine derivatives gave respective alkylated compounds in good to excellent yields and high enantioselectivity. In addition, sterically encumbered 2-*tert*-butyl pyridine scaffolds were precisely functionalized at *ortho*-C–H bond with a smaller Sc ion (Sc-**2**), contrary to the previous approach, which demanded a larger Y ion [97]. However, this ambiguous behavior remains unclear. Noticeably, the reaction condition failed to incorporate unsubstituted pyridine or

quinoline moiety, where unproductive strong coordination of pyridyl nitrogen to Sc atom may be the reason in absence of steric influence at *ortho*-site. Consequently, it deactivates the metal center and inhibits easy access to olefin unit. The high degree of enantioselectivity was primarily determined by factors such as steric crowding of Cp unit, α-substituent on olefin and *ortho*-substituent on pyridine ring. All these combining factors favored TS-**XI** over TS-**X** furnishing (*R*)-isomer as a major product. Perhaps, this finding represents the foremost report of asymmetric C–H bond activation strategy catalyzed by chiral Sc–alkyl complex.
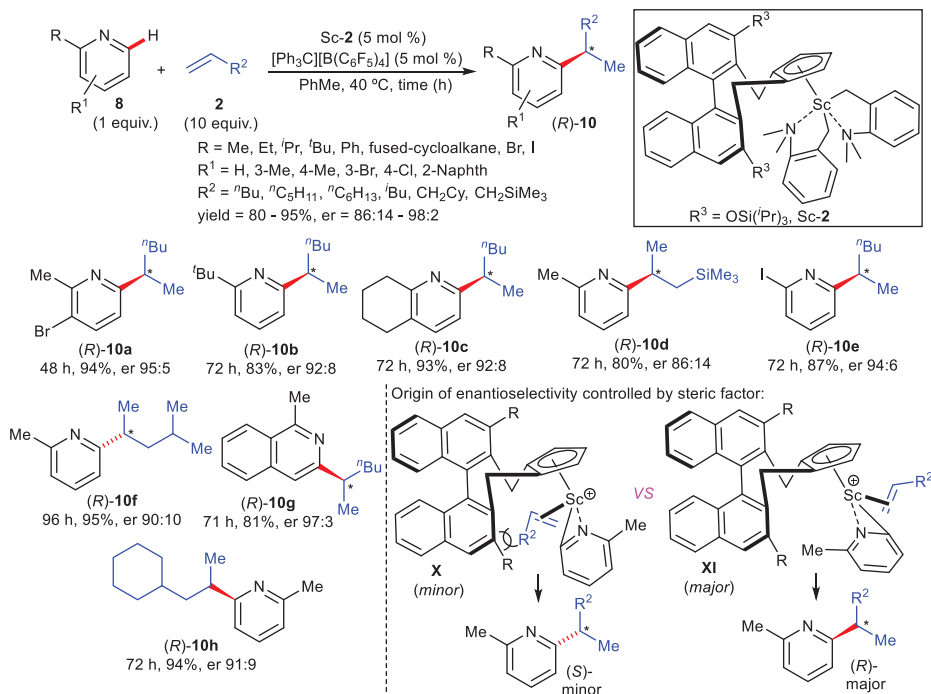
Figure 2.4: A few selected enantioselective *ortho*-C–H bond alkylation of pyridine analogues catalyzed by chiral Sc-**2** complex.

Over the past decade, great effort has been devoted to the generation of all-carbon quaternary stereocenters in bioactive scaffolds because of the possibility of structural rigidification enforcing remarkable biological properties [102–105]. In an attempt, Hou achieved C–H cycloaddition of C2-center of imidazole (**11**) to N1-corded-1,1-disubstituted olefins catalyzed by Sc-**1** furnishing β-all-carbon quaternary stereocenters in an *exo*-selective fashion (Figure 2.5-i) [106]. Excellent yields were obtained upon *exo*-selective Markovnikov-type addition of a wide range of **11** and **2/3** to deliver fused 5-/6-membered bicyclic imidazole ring system (**12**). This result is diametrically opposed to transition metal-catalyzed *endo*-selective cyclization avoiding the generation of a quaternary stereocenter [107].

Notably, the chiral Sc-**3** catalyst afforded chiral fused 5-/6-membered bicyclic 4,5-diaryl-substituted-imidazole derivatives (**12′**) having β-all-carbon quaternary stereocenters in excellent yields and high enantioselectivity (Figure 2.5-ii). Presumably, bulky arene rings at C4- and C5-positions on imidazole unit endow steric congestion in the TS, leading to high degree of enantioselectivity. Excellent enantioselectivity was achieved in the presence of O-/S-atom in the side chain. The coordinating ability of O-/S-atom did not hamper enantioselectivity, thereby endorsing better coordination ability between basic nitrogen atoms of imidazole unit with Sc$^+$ ion [74–76].

The plausible mechanistic cycle (Figure 2.5-iii) starts with the in situ formation of cationic Sc-complex **I** and coordination of Sc$^+$ ion to N3-center of **11a** (R = H, R^1 = ^{n}Bu, n = 1), followed by activation of either imidazole C2–H bond or C4–H bond. However, the species **XII** is generated over **XIIa**, which accounts for favored σ-bond metathesis operation at reactive C2–H bond of imidazole unit which is highly acidic [41–43]. Intramolecular addition of a tethered olefinic unit on **XII** to Sc–C bond under steric and electronic influence delivers species **XIV** via **XIII**. The hydrogen abstraction from **11a** by **XIV** furnishes **12a** with subsequent regeneration of **XII** to complete the catalytic cycle. The higher reactivity of imidazole C2–H of **11′** toward σ-bond metathesis is the prime cause for its selective deprotonative metalation than that at *ortho*-C–H site of pendant aryl unit at C4 position.

The regio-/site-selective C–H bond functionalization has brought in new opportunities to access regiodivergent products by repurposing proper combination of metal/ligand, steric as well as electronic properties of catalyst, ligands, reagents, and ring strain related to intermediates [108–115]. The growing interest in this area has led to the development of C–H bond alkylation of 2-phenylquinolines (**13**) along **2** and **3** either at C(C8)–H or *ortho*-C–H site of 2-phenyl ring under the catalytic influence of Sc–alkyl and Y–alkyl complex following delicate adjustment of metal center and associated ligand steric demand (Figure 2.6-i) [116]. The combination of Sc-containing catalyst Sc-**1** (smaller in size) with a larger ligand (Cp*) afforded C(C8)–H alkylated product along **3a** in decent yield having excellent regioselectivity (**14a/15a** > 20:1). Respective decrease in regioselectivity or yield was observed with increase or decrease of steric congestion on Cp ligand via substituting –Me group with respective –SiMe$_3$ group or H atom. On the other hand, a combination of Y-containing catalyst, Y-**3** (larger in size) with comparatively smaller ligand (C$_5$HMe$_4$) favored *ortho*-selective C(Ph)–H alkylation along **3a** (**14a/15a** = 1/9). Likewise, to Sc-analogue the Y-**3** system exhibited similar regioselective results with an enhanced or reduced steric crowding of the associated ligand. Other than the type of f-element metal center and steric features of attached ligand, the electronic and/or steric status of the olefins were also crucial for regioselectivity. For example, the **2** exhibited high regioselectivity for *ortho*-C(Ph)–H alkylation leading to **16** and C8–H alkylation leading to **17** catalyzed by Sc-**1** and Y-**3**, respectively. In a sharp contrast, **3** demonstrated high regioselectivity for *ortho*-C(Ph)–H and C8–H alkylation with Y-**3** and Sc-**1**, respectively. An enumerated study through DFT calculations highlighted the potential of Sc-**1** and Y-**3** to catalyze both the C8–H bond and *ortho*-C(Ph)–H bond functionalization each (Figure 2.6-ii). Nevertheless,

i. Substrate scope of *exo*-selective C–H cycloaddition:

R = H, 5,6-Me$_2$, 5,6-Cl$_2$, 5,6-Ar$_2$, 5-Br, 6-Br, 2-naphth
R^1 = H, Me, ^{n}Bu, C$_7$H$_{15}$, Bn, CH$_2$OAr, CH$_2$SAr, fused-cycloalkane, Ar, styryl, alkyne
n = 0, 1; yield = 91 - 96%

12a, 96%   **12b**, 95%   **12c**, 93%   **12d**, 96%
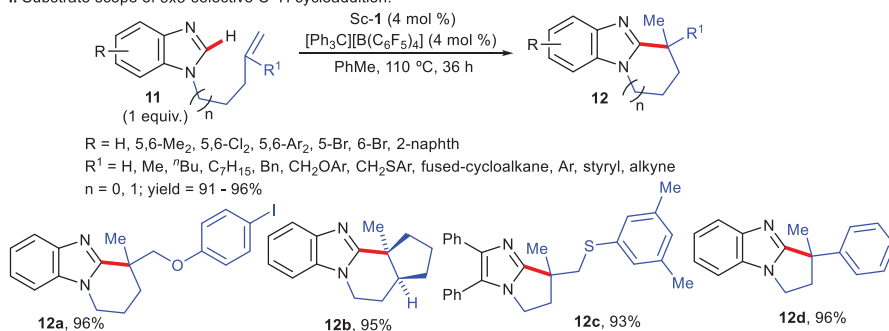
ii. Substrate scope of asymmetric *exo*-selective C–H cycloaddition:

Ar = Ph, 4-Me-C$_6$H$_4$, 4-OMe-C$_6$H$_4$, 4-F-C$_6$H$_4$, 4-Br-C$_6$H$_4$
R^1 = H, Me, ^{n}Bu, C$_7$H$_{15}$, Bn, CH$_2$OAr, CH$_2$SAr, fused-cycloalkane, Ar, styryl, alkyne
n = 0, 1; yield = 92 - 96%, er = 84:16 - 97:3

(R)-**12a′**, 93%   (R)-**12b′**, 94%   (S)-**12c′**, 95%   (R)-**12d′**, 95%
er 92:8   er 94:6   er 88:12   er 94:6
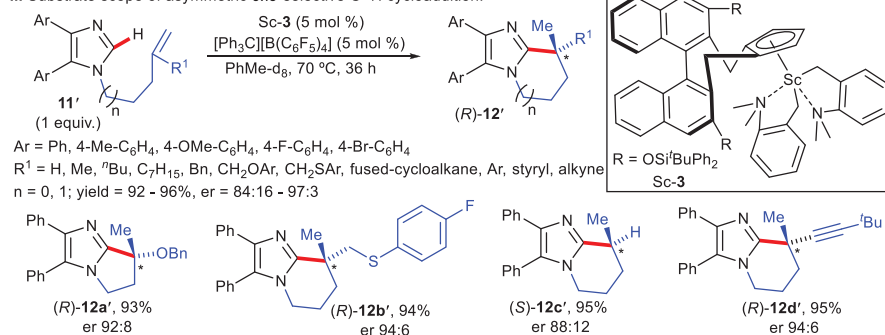
iii. Probable mechanism:
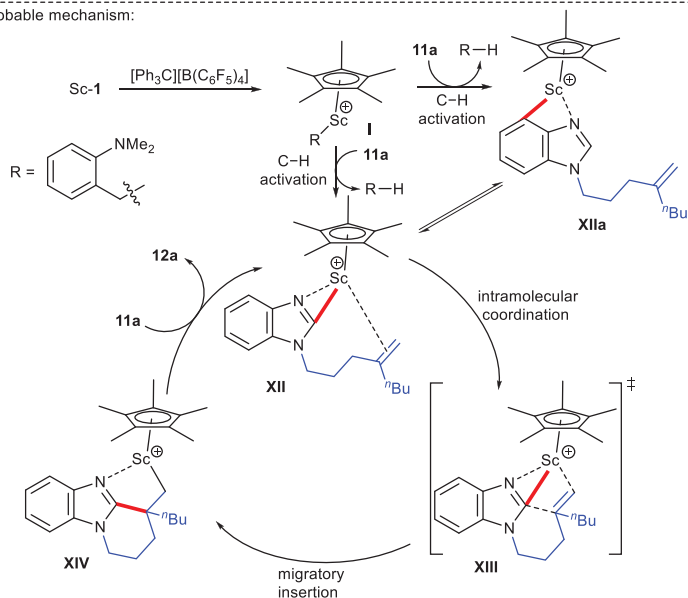
Figure 2.5: A few selected examples of cyclization of imidazole analogues to fused bicyclic imidazole derivatives intramolecularly following, (i) achiral strategy catalyzed by half-sandwich Sc-**1** complex, (ii) an asymmetric approach catalyzed by half-sandwich chiral Sc-**3** complex, and (iii) probable mechanistic cycle.

lower $\Delta G^{\neq}$ value of C8–Sc bond construction over C8–Y bond (species **XV**, $\Delta G^{\neq}$ = 22.5 *vs* 26.4 kcal/mol) and lower $\Delta G^{\neq}$ value of *ortho*-C(Ph)–Y bond over *ortho*-C(Ph)–Sc bond (species **XVI**, $\Delta G^{\neq}$ = 23.8 vs 29.7 kcal/mol), concluded selective C8–H bond and *ortho*-C(Ph)–H bond activation by Sc-**1** and Y-**3** catalysts, respectively. It is proposed that the steric repulsion among quinolyl unit and the sterically crowded Cp* group of Sc-**1** was the detrimental factor for *ortho*-C(Ph)–H alkylation. The activation of C8–H catalyzed by Sc-**1** proceeded well, devoid of such strong steric demand. Moreover, such steric hindrance had a marginal effect on Y-**3**-catalyzed *ortho*-C(Ph)–H bond activation attributed to relatively large size of Y atom over Sc center and attached smaller ligand C_5HMe_4 than Cp* on Sc-**1**. The addition of **3a** to species **XV** under catalytic influence of Sc-**1** ($\Delta G^{\neq}$ = 23.8 kcal/mol) furnished **XVa** and addition to species **XVI** by catalytic influence of Y-**3** ($\Delta G^{\neq}$ = 25.5 kcal/mol) provided **XVIa**. The stabilization via benzallylic mode in both species **XVa** and **XVIa** triggered M–C σ-bond addition through 1,2-fashion affording linear alkylated products. Although this transformation gave precise siteselectivity with **3a**, poor reactivity limited the use of unactivated **2** [78–80]. Higher value of $\Delta G^{\neq}$ (25.7 kcal/mol) was necessary for Sc-**1**-catalyzed incorporation of **2** to **XV** over the transformation of **XV** to **XVII** ($\Delta G^{\neq}$ = 24.1 kcal/mol). Consequently, under Sc-**1** catalysis, the **2** was added up to **XVII** following *ortho*-C(Ph)–H alkylation resulting in **XVc**. In parallel, under Y-**3** catalysis, lower value of $\Delta G^{\neq}$ (28.7 kcal/mol) for the conversion of **XVI** to **XVII** over the insertion of **2** to **XVI** ($\Delta G^{\neq}$ = 31.8 kcal/mol) was calculated. This was extremely proficient to afford C8–H alkylation product under the catalytic influence of Y-**3**. The insertion of M–C σ-bond to **2** through 2,1-fashion catalyzed by Sc-**1** and Y-**3** complex delivered branched alkylated products circumventing the steric repulsion between Cp* or C_5HMe_4 moieties and substituent on C1-site on **2**. Therefore, this protocol offers a prudent way to access structurally diverse quinoline derivatives and is judiciously governed by an energy barrier for the interconversion of preliminary C–H metalated species.

Immense progress has been made in the arena of stereodivergent catalysis to construct novel organic scaffolds possessing multiple stereocenters from the same reactant allowing access of all possible stereocenters [117–121]. Early reports on siteselective C–H bond activation governed by comparative size of group-3 metal ion and bulkiness of attached ligands [116] enabled the chemists investigating a new route to synthesize diastereodivergent 1-aminoindanes catalyzed by half-sandwich Sc-**4** or Y-**3** complex (Figure 2.7-i) [122]. The reaction of aromatic aldimines (**18**) with unactivated **2** and **3** has been accomplished via a [3 + 2] annulation pathway. The steric demand of the attached ligands of Sc-**4** or Y-**3** played a vital role in the generation of diastereomerically organized products without any external chiral contribution by means of chiral ligand-metal combination [101, 106]. Excellent *trans*-diastereoselective 1-aminoindanes (**19a/20a**, dr < 1:19) have been successfully obtained in the presence of bulky ligand $C_5Me_4SiMe_3$ on Sc-**4** during the reaction of **18a** with **3a**. However, replacing –$SiMe_3$ group with a smaller H atom resulted in either loss or complete reversal of *trans*-diastereoselectivity. In the case of Y-**3** catalysis, productive *cis*-diastereoselectivity (**19a/20a**, dr > 1:19) and decent yield were observed with relatively small ligand C_5HMe_4 and larger Y atom. The increased steric hindrance
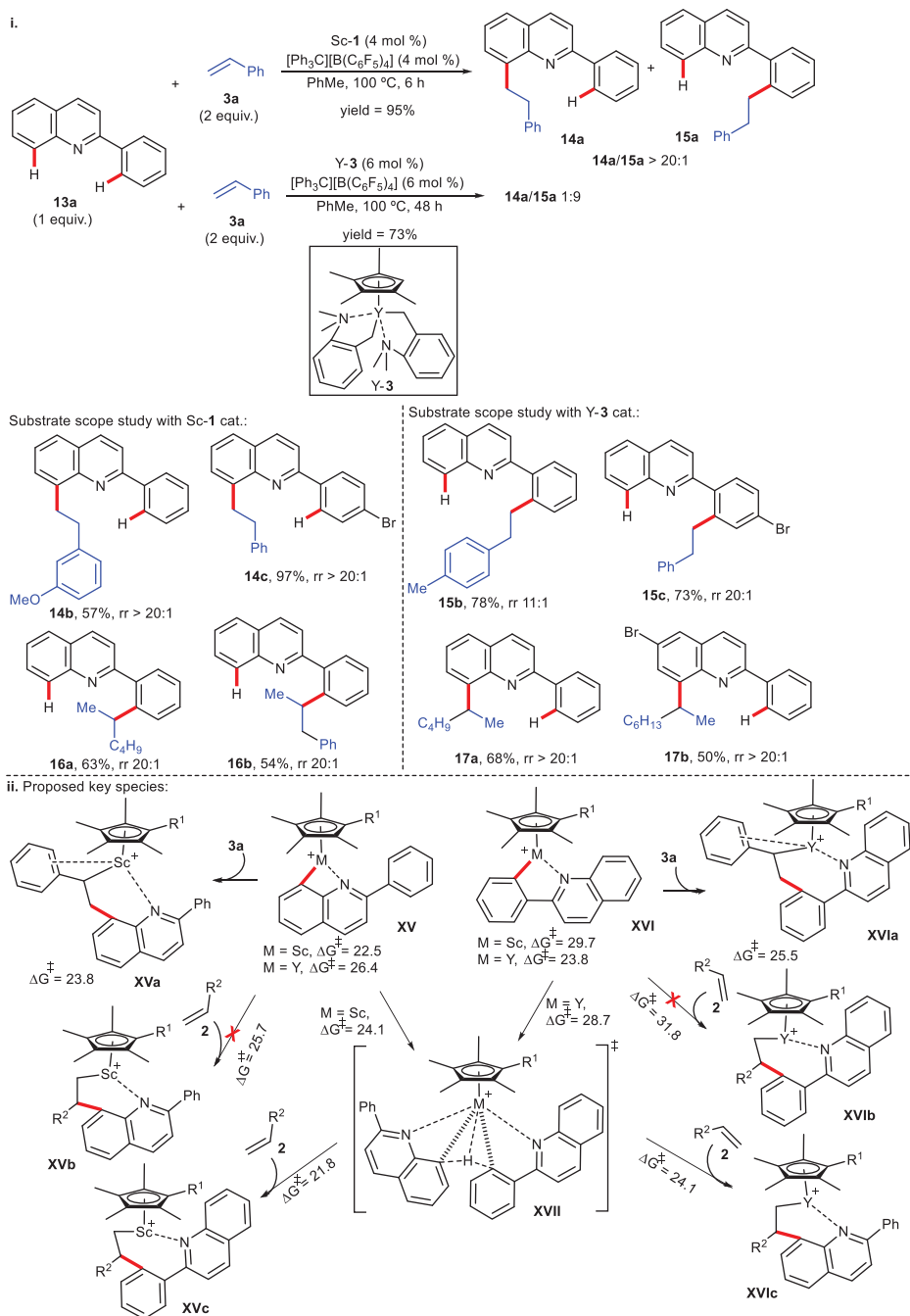
Figure 2.6: (i) A few selected examples of regiodivergent C–H bond alkylation of 2-arylquinolines catalyzed by half-sandwich Sc-**1**/Y-**3** complex, and (ii) probable crucial species.

around the ligand by substituting H atom with –Me/–SiMe$_3$ functionality and decrease in steric hindrance by substituting –Me groups with H atoms resulted in either low yield or poor diastereoselectivity. This strategy has enlightened a new way to synthesize diverse 1-aminoindanes in *trans*- and *cis*-diastereoselective manner catalyzed by respective Sc-**4** and Y-**3** complex. The presence of *tert*-Bu group at *para*-position of **3a** had a negligible effect on *trans*-diastereoselectivity in the case of Sc-**4** catalysis, but it reduced the *cis*-diastereoselectivity (dr = 3:1) in the case of Y-**3** catalysis. Perhaps, an increased steric hindrance in *cis*-oriented TS under Y-**3** catalysis is responsible. The catalytic reactions of **18** with *meta*-substitution on arene ring allowed siteselectivity at the *para*-C–H bond due to steric impact. On the other hand, the **2** formed *trans*-diastereoselective 1,3-isomers (**21**) via [3 + 2] annulation in the presence of catalytic Sc-**4**. However, in these cases, the *trans*-diastereoselectivity was low, which might be attributed to the preferred 2,1-insertion of less congested C2-site of **2** to Sc–C σ-bond and possibility of flexible rotation of linear alkane side arms, thereby increasing steric crowding in TS. On the contrary, **2** failed completely under Y-**3** catalysis, which could be attributed to preferable olefin polymerization over [3 + 2] annulation [65]. Notably, a regioisomeric mixture (C2/C6 = 4:1) was obtained with *meta*–SMe group on arene ring of **18** in high *cis*-diastereoselectivity. Presumably, the Y$^+$ center interacts with –SMe group in the TS and is liable for the observed regioisomeric mixture. It is postulated that steric hindrance of bulky C$_5$Me$_4$SiMe$_3$ ligand around small Sc$^+$ center disfavored this type of interaction in case of Sc-**4** catalysis. Steric tuning in the proposed TS **XVIII** and **XIX** could be the cause of observed diastereoselectivity (Figure 2.7-ii). In the content of further investigation, it was found that the steric repulsion between bulky C$_5$Me$_4$SiMe$_3$ ligand and N-^{t}Bu group was the underlining basis of poor interaction of smaller Sc ion with π-electron cloud of phenyl ring on **3a**, which then restricts proper spatial orientation in species **XVIII**. The Sc–C σ-bond nucleophilically attacks the C=N unit giving rise to major *trans*-isomer **20a**, minimizing steric crowding in **XVIIIa**. The interaction among Y$^+$ center and π-electron cloud of phenyl unit of **3a** is feasible in **XIX** owing to larger size of Y center and associated smaller ligand, C$_5$HMe$_4$. The interaction of Y··· phenyl type plus concerted coordination of N → Y led to an attack nucleophilically in *cis*-fashion via Sc–C σ-bond in C=N unit of species **XIXa** to afford *cis*-product, **19a** as predominant one. On the other hand, steric demand in TS was affirmed by the bulky *tert*-butyl group on N-center of **18**, which has been noteworthy for the observed diastereoselectivity.

Luo carried out an elaborate mechanistic study on [3 + 2] annulation of **18** with **3a** by DFT calculations to depict the mechanistic pathway of catalyst guided inversion of stereoselectivity and analyze the cause of diastereoselectivity [123]. The stabilization of crucial TSs or intermediates was predominantly characterized by noncovalent type interactions, namely, π··· H–C and π··· metal interactions, along with steric plus electronic factors to control the observed diastereoselectivity. The *cis*-diastereoselective product (**19a**) was exclusively formed as obvious from the small energy barrier to ensure coherent orbital
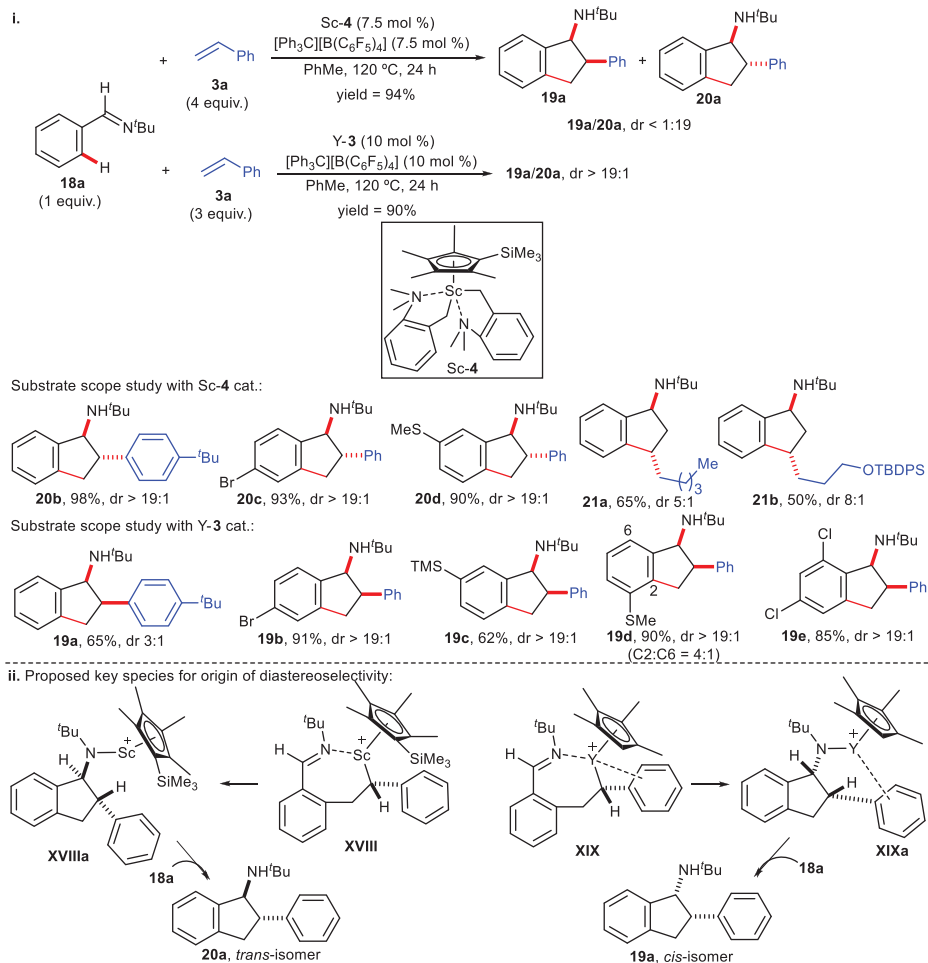
Figure 2.7: (i) A few selected examples of diastereodivergent access of 1-aminoindanes via [3 + 2] annulation catalyzed by half-sandwich Sc-**4**/Y-**3** complex, and (ii) proposed crucial species for observed diastereoselectivity.

interaction between catalytic Y-**3** and **3a** because of less steric congestion between C_5HMe_4 ligand and **18**. However, the change in orbital interaction efficiency of Sc-**4** with **3a** has been observed during π··H–C interaction among N^{t}Bu unit and π-electron density of benzene nucleus because of steric repulsion of heavy ligand, $C_5Me_4SiMe_3$ attached to small Sc$^+$ ion and aldimine motif. Henceforth, these interactions paved the way to generate *trans*-diastereoselective molecules (**20**). Thus, this approach keeps promise to revolutionize organic synthesis enabling stereospecific and stereoconvergent annulation governed by standardized metal/ligand combination of catalyst system.

2.2.2 C–H bond addition to alkynes for olefination

Apart from typical activation of olefinic moieties and stereochemical induction, the cationic Sc–alkyl complex can successfully activate an alkyne unit through π-interaction. Recently, Luo and Huo explored *ortho*-selective mono-C–H olefination of heteroaromatics corded metallocene framework (**22**) along alkynes (**23**) following an asymmetric approach by employing Sc-**5** as chiral catalyst (Figure 2.8-i) [124]. A library of new planar-chiral metallocene embedded with quinoline/pyridine moiety (**24**) was synthesized. A wide range of **22** and **23** was probed with the varied electronic effects, which resulted in satisfactory yield and excellent enantioselectivity.

A remarkable effect was observed with respect to **23**, in which the C–C bond construction specifically happened at C(alkyl)–end other than C(arene)–end of unsymmetrical **23**, owing to the dominant effect of steric hindrance over electronic factor. The incorporation of sterically hindered diphenylacetylene unit and benzo[*g*]quinoline motifs (fused system), 2,4-dimethylpyridine and *ortho*-methylpyridine moieties attached to metallocene as DG delivered low yields. Gratifyingly, a ruthenocene substrate was found applicable for the same transformation; although a slight reduction in enantioselectivity has been observed. The catalytic condition remained futile toward *ortho*-di-olefination, presumably, due to steric hindrance caused by the primary mono-alkenylated analogue. Among the possible dual C–H bond activation positions at the quinoline C8-site and *ortho*-position of Cp ring on metallocene motif, regioselective alkenylation was witnessed with metallocene moiety only.

The DFT studies (Figure 2.8-ii) suggested that activation of both C(C8)–H bond of quinoline (species **XXI**) as well as *ortho*-C–H bond of Cp (species (*R*)-**XXII**) have close values of $\Delta G^{\neq}$ 25.4 and 25.2 kcal/mol, respectively. However, (*R*)-**XXII** was selectively converted to (*S*)-**24k** by insertion of Sc–C(Cp) σ-bond to **23k** possessing $\Delta G^{\neq}$ value of 21.1 kcal/mol. On the other hand, the species **XXI** failed to generate C8-alkenylated product due to the requirement of larger $\Delta G^{\neq} = 25.8$ kcal/mol for the Sc–C(C8) σ-bond insertion to **23k**. Therefore, the **XXI** undergoes easy interconversion to (*R*)-**XXII** owing to less value of $\Delta G^{\neq} = 20.1$ kcal/mol. Direct conversion of species **XX** to enantiomeric species (*S*)-**XXII** by (Cp)C–H activation failed because of larger value of $\Delta G^{\neq} = 29.7$ kcal/mol. Further insertion of Sc–C(Cp) σ-bond to **23k** failed on account of higher value of $\Delta G^{\neq} = 27.4$ kcal/mol and thereby ruled out the generation of (*R*)-**24k**, albeit (*R*)-**XXII** can easily arrange to (*S*)-**XXII** with $\Delta G^{\neq} = 19.6$ kcal/mol.

The structurally rigid spiro-hydroquinoline scaffold containing a quaternary carbon stereocenter with a free N–H group constitutes a ubiquitous class of pharmacologically, biologically active molecules and important natural products [125–127]. The presence of an unprotected N–H group in the quaternary carbon stereocenter of spiro-hydroquinolines is of paramount importance on account of its drug-like physicochemical properties and high binding affinity with proteins [128, 129]. An easy and simple route to access chiral spiro-hydroquinolines is catalytic asymmetric dearomative annulation of substituted quinolines. Traditional synthetic procedures for the asymmetric
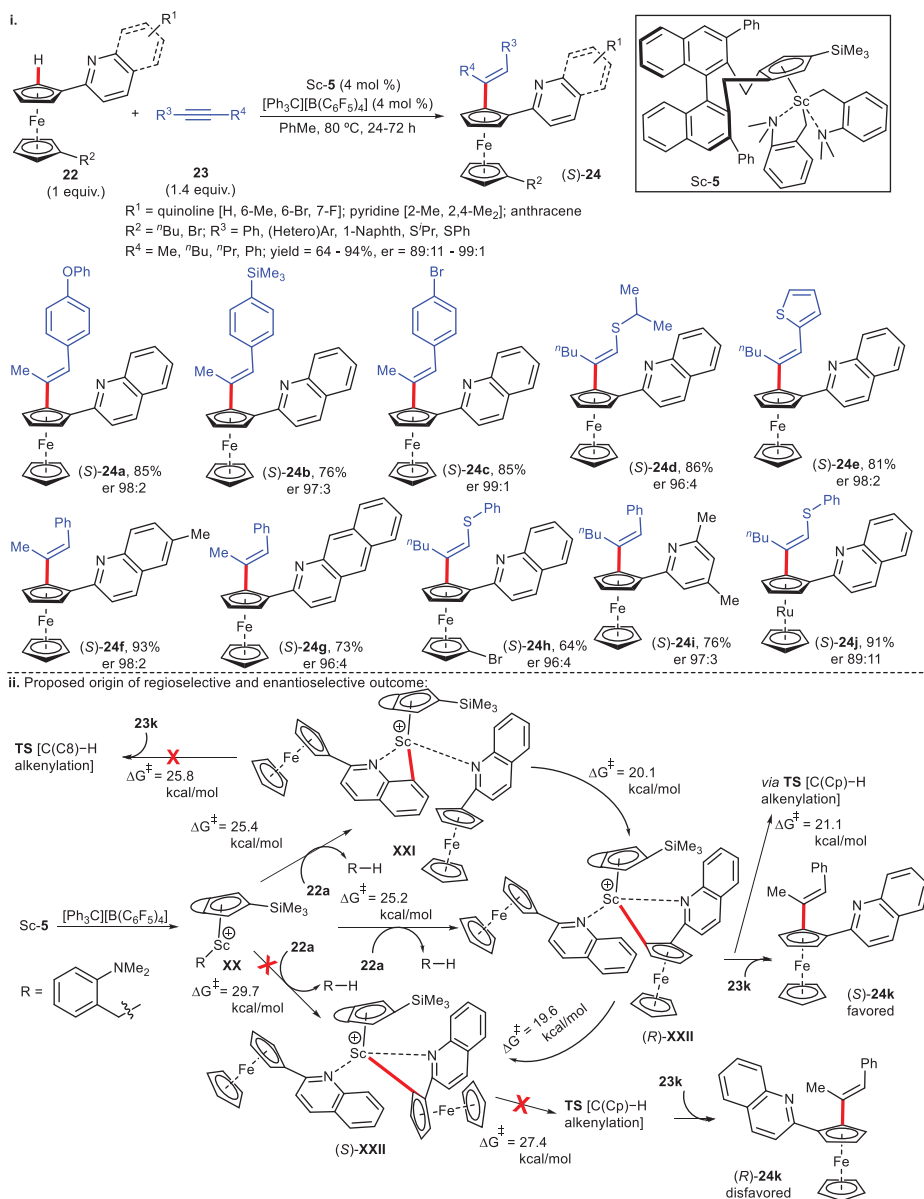
Figure 2.8: (i) A few selected examples of olefination of ferrocenes and ruthenocene with alkynes catalyzed by chiral Sc-**5** complex, and (ii) proposed crucial species for regio-/enantio-selectivity.

construction of N–H free spiro-hydroquinoline frameworks suffered from drawbacks owing to the difficulty in asymmetric addition to *ipso*-carbon center of the quinoline moiety [130–132]. Thus, inspired by the above-mentioned need, Hou and co-workers employed catalytic half-sandwich Sc-**4** in dearomative [3 + 2] spiro-annulation via C–H

bond activation of **13** with **23** for facile synthesis of spiro-dihydroquinoline derivatives (**25**) (Figure 2.9-i) [133]. This strategy represents an ingenious way following a cascade sequence of C–H bond olefination and intramolecular cyclization to afford a library of **25** in synthetically acceptable yields with high regioselectivity. The protocol gave straightforward access to spiro-dihydroquinoline product (**25a**) exclusively bearing a free N–H group, which upon further functionalization with benzyl bromide (**26**) in the presence of *n*-BuLi afforded *N*-benzylation derivative (**25a-Bz**). This transformation, in particular, provided direct evidence of the formation of **25a** following a dearomative [3 + 2] spiro-annulation mechanism rather than an expected C–H bond alkenylation end product only. The result is in sharp contrast to an early report on rhodium-catalyzed reactions of pyridines or quinolines with **23** where aromaticity of the *N*-heterocycle is retained and furnished isoquinolinium salts as end products [134]. Concerning the substrate scope of **13** for this transformation, *para*-substituted Ph, –F, –Cl, –I, –OPh, –SMe at the *ortho*-phenyl ring of **13** were all tolerated. A methyl group was compatible on the *ortho*-phenyl ring regardless of its position. Furthermore, methyl, phenyl, styrenyl, halide, and trimethylsilyl substituents at different positions of the *ortho*-phenyl ring also showed excellent reactivity. The reaction permitted **13** with substituent at the C3 or C4 position of pyridine moieties such as 4–Me, 4–Cl, 3–Me, and 3–Br, as well. Remarkably, vinyl halide moieties and benzo-fused quinoline derivatives were also tolerated the standard reaction conditions to afford desired products with free N–H group. The assessment of substrate scope with **23** revealed good functional group tolerance of alkynes bearing both aromatic and aliphatic substituents. Moreover, excellent regioselectivity has been obtained with **23** possessing both aromatic and aliphatic substituents. In these cases, the carbon atom bearing an aryl substituent preferably added up to C=N unit in **13** due to steric factor, whereas the carbon center bearing an aliphatic substituent preferably formed C–C bond via initial C–H bond activation. Apart from these substitution effects, the reaction also worked well with **23** at the carbon center bearing a silyl substituent which could be attributed to the electronic effect. In addition, phosphine and thiophene groups were also comfortably incorporated, conversely to late transition metal catalysis. Interestingly, in case of a conjugated eneyne system, excellent regioselectivity occurred at the C≡C unit, and the C=C was unreactive. Presumably, the high degree of unsaturation of C≡C unit induces better π-electron affinity to Sc ion. Thus, it is evident that the substrate space was quite broad through the variation of both **13** and **23**. The survival of sensitive functional moieties, such as halo, thio, silyl, reflects the robustness of the present catalytic system. The practical applicability of the protocol has been highlighted through a "gram scale" synthesis of **25a**.

Following the success of achiral dearomative spiro-annulation of **13** with **23**, the investigators developed a protocol for the enantioselective construction of spiro-hydroquinolines (**25′**) utilizing chiral Sc-**5** catalyst under the same reaction condition (Figure 2.9-ii). A wide range of **13** and **23** have proved to be useful substrates for this chiral transformation and afforded decent yields of **25′** along with high enantioselectivity. The absolute configuration of **25′** has been established as "*S*" unambiguously through single crystal XRD analysis.
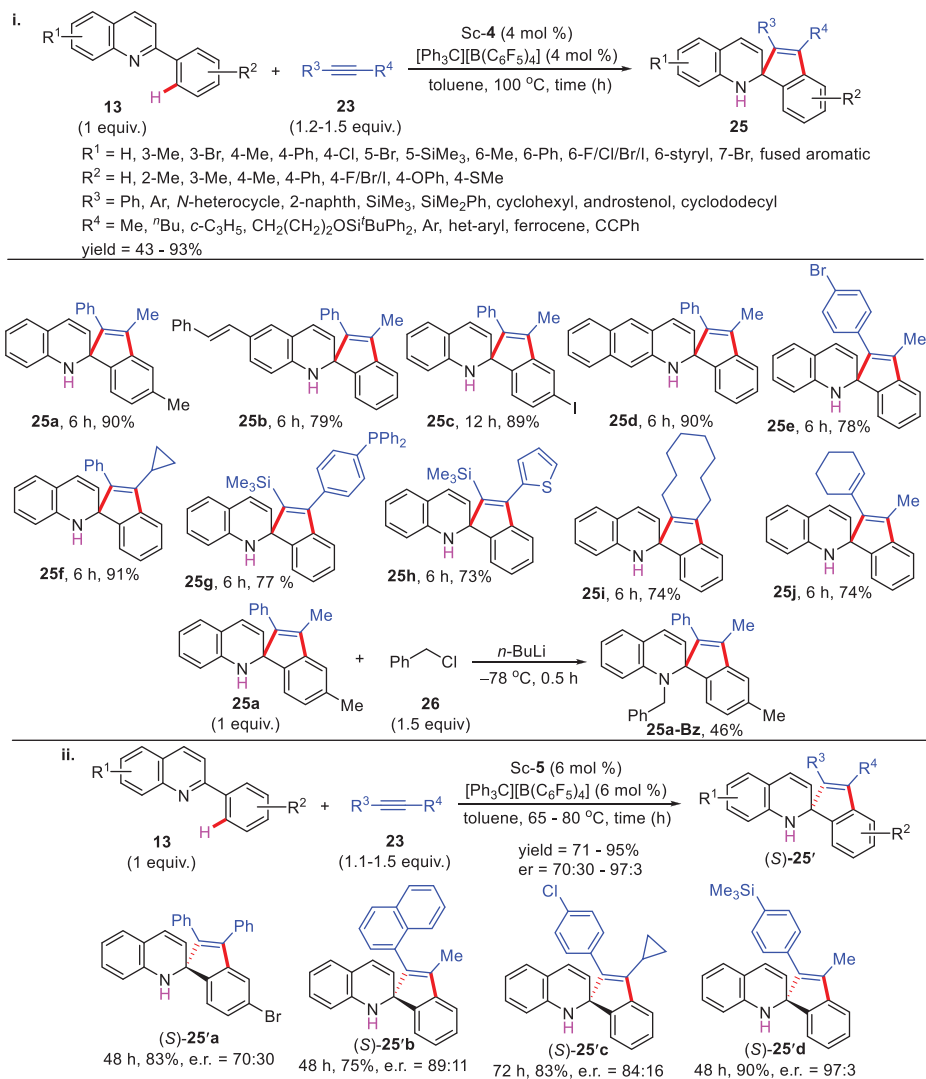
i.

R[1] = H, 3-Me, 3-Br, 4-Me, 4-Ph, 4-Cl, 5-Br, 5-SiMe$_3$, 6-Me, 6-Ph, 6-F/Cl/Br/I, 6-styryl, 7-Br, fused aromatic
R[2] = H, 2-Me, 3-Me, 4-Me, 4-Ph, 4-F/Br/I, 4-OPh, 4-SMe
R[3] = Ph, Ar, N-heterocycle, 2-naphth, SiMe$_3$, SiMe$_2$Ph, cyclohexyl, androstenol, cyclododecyl
R[4] = Me, ^{n}Bu, c-C$_3$H$_5$, CH$_2$(CH$_2$)$_2$OSi^{t}BuPh$_2$, Ar, het-aryl, ferrocene, CCPh
yield = 43 - 93%

25a, 6 h, 90%   **25b**, 6 h, 79%   **25c**, 12 h, 89%   **25d**, 6 h, 90%   **25e**, 6 h, 78%

25f, 6 h, 91%   **25g**, 6 h, 77 %   **25h**, 6 h, 73%   **25i**, 6 h, 74%   **25j**, 6 h, 74%

ii.

(S)-**25′a**
48 h, 83%, e.r. = 70:30

(S)-**25′b**
48 h, 75%, e.r. = 89:11

(S)-**25′c**
72 h, 83%, e.r. = 84:16

(S)-**25′d**
48 h, 90%, e.r. = 97:3

Figure 2.9: A few selected examples of cascade sequence of alkenylation and intramolecular cyclization catalyzed by half-sandwich Sc-**4** complex to afford spiro-dihydroquinoline in (i) racemic form, and (ii) enantiomerically enriched form.

2.2.3 C–H bond addition to allenes for olefination

Allenes have entered the circle of valuable coupling partners offering the same features as other π-electron rich entities, for example, alkyne/olefin, and displayed a high affection of π-bond to M–C nucleophiles in metal-catalyzed C–H bond olefinations [135]. The presence

of dual-orthogonal cumulative π-bonds in allenes reflected correlative reactivity to alkyne and alkene motifs, as evident from M–allyl or M–alkenyl intermediates [136]. As compared to alkene and alkyne the marginal reactivity difference in vicinal C=C bonds in the case of allene unit raises the regio- and stereo-selectivity concerns. The strong Lewis acidic nature [76] and high π-electron affinity [39, 77] of cationic group-3 metal catalysts can be exploited to surmount the difficulties associated with allene system. Emboldened by this concept, Hou reported *ortho*-selective C–H bond alkenylation of **8** along allenes (**27**) using Sc-**4** catalyst (5 mol%) along with equimolar [Ph$_3$C][B(C$_6$F$_5$)$_4$] as co-catalyst (Figure 2.10-i) [137]. In the case of unsymmetrical **27** branched olefinated products were delivered with excellent regio- and stereo-selectivity. The reaction outcome can be attributed to the incorporation of pyridyl moiety at middle C-center and H-atom attached to sterically less crowded terminal C-center of **27**. This result revealed a better regioselective outcome of Sc-**4** catalyst over Zr-catalyst, in which the latter furnished 1:1 regioisomeric mixture of allyl- and vinyl-azazirconacycle ultimately [138]. This strategy enabled construction of a library of vinyl pyridines (**28**) in decent yields with a diversified scope of **8** and **27** in *E*-selective manner. Importantly, regardless of the size of substituents, the electron-donating or withdrawing groups at *ortho*-position of **8** were found essential. Perhaps the coordination capacity of adjacent N-atom is regulated through the electronic influence of *ortho*-substituents. On the other hand, the presence of large substituents at *ortho*-position of **8**, e.g., phenyl ring or attached to allene unit, namely, menthylallene and phenylallene, reduced the catalytic efficiency of Sc-**4**, but the reaction rate enhanced more conveniently with Sc-**6** catalyst associated with smaller Cp ligand. The fundamental feature has been observed that the present catalytic system selectively activated pyridyl *ortho*-C–H bond solely, contrary to *ortho*-C–H bond activation of corded phenyl unit of 2-phenylpyridine moiety aided through pyridine unit as DG [20–26]. The σ-bond metathesis mechanism at more acidic and reactive *ortho*-C–H bond of pyridine motif [41–43], together with the positive impact of Cp ligand, probably is the reason of observed regioselectivity in case of 2-phenylpyridine moiety.

The mechanistic investigations highlighted C–H activation as the rate-determining step and have been evident from the high KIE value ($k_H/k_D = 5.6$) during intermolecular competition reaction of 2-methylpyridine (**8b**) and **8b-*d*$_4$** with cyclohexylallene (**27a**) (Figure 2.10-ii). The primary focal point of the mechanism has been proposed as σ-bond metathesis path with a pyridyl C–H bond, which is more acidic and reactive, aided by Cp ligand (Figure 2.10-iii). The mechanism initiates with the pyridyl (**8c**) nitrogen atom coordination to Sc–Cp complex (cationic), followed by *ortho*-C–H bond activation resulting in species **XXIII**. Subsequently, the **27a** attaches to **XXIII** via π-coordination to sterically less crowded terminal C=C bond forming species **XXIV**, whereupon the bulky cyclohexyl group should be positioned in distant from the pyridyne ring to minimize the steric demand. The Sc–C σ-bond incorporation to C=C (species **XXV**) and subsequent σ-bond metathesis operation of **XXV** with **8c** delivers **28j** via species **XXVI** and regenerates **XXIII** closing the catalytic cycle. The primary criteria for regio- and stereo-selectivity involve preference of coordination of allene system to cationic **XXIII** and migratory insertion to **XXV**. A second
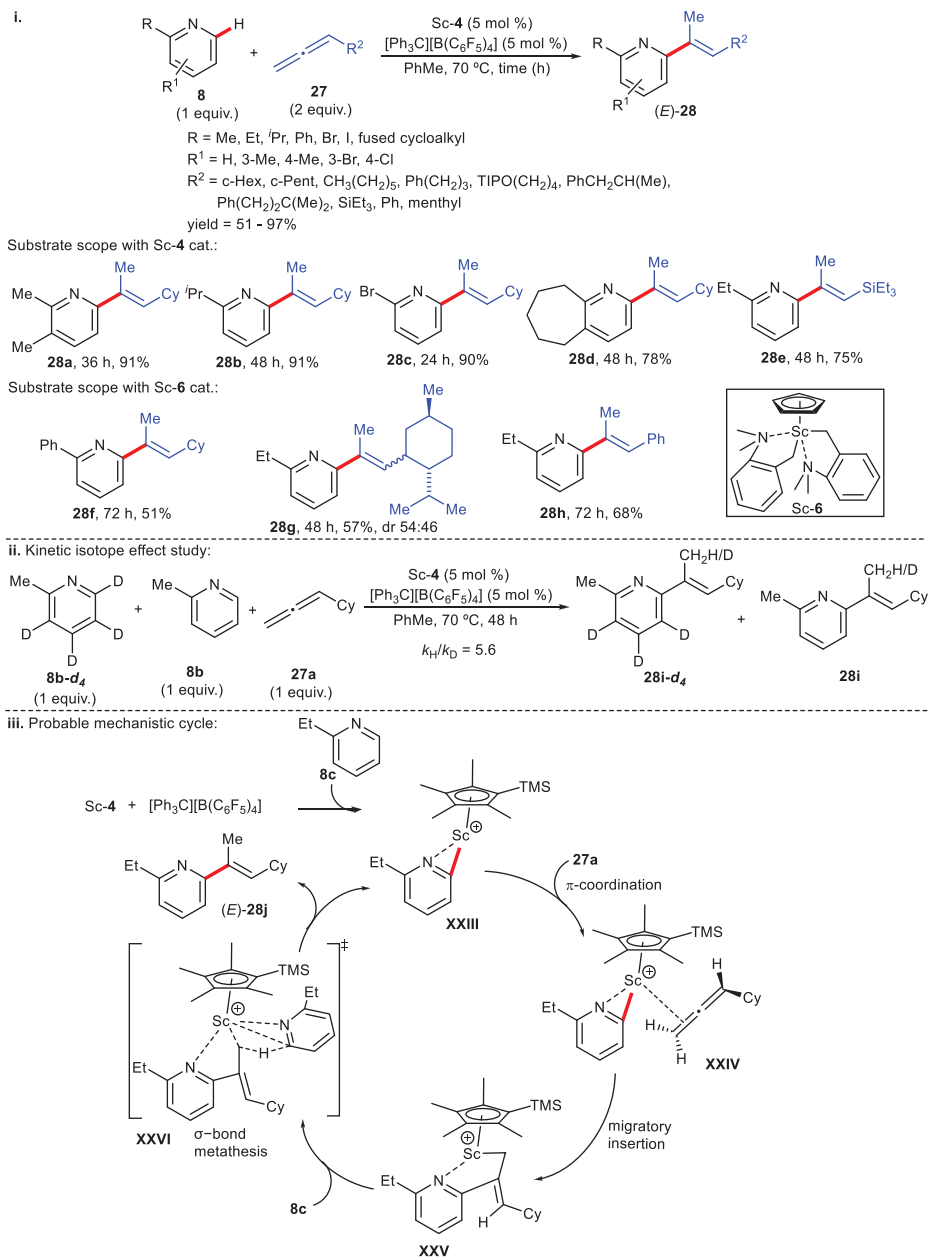
i.

R = Me, Et, ^{i}Pr, Ph, Br, I, fused cycloalkyl
R^1 = H, 3-Me, 4-Me, 3-Br, 4-Cl
R^2 = c-Hex, c-Pent, $CH_3(CH_2)_5$, TIPO$(CH_2)_4$, PhCH$_2$CH(Me),
    Ph$(CH_2)_2$C(Me)$_2$, SiEt$_3$, Ph, menthyl
yield = 51 – 97%

Substrate scope with Sc-**4** cat.:

28a, 36 h, 91%   **28b**, 48 h, 91%   **28c**, 24 h, 90%   **28d**, 48 h, 78%   **28e**, 48 h, 75%

Substrate scope with Sc-**6** cat.:

28f, 72 h, 51%   **28g**, 48 h, 57%, dr 54:46   **28h**, 72 h, 68%

ii. Kinetic isotope effect study:

k_H/k_D = 5.6

8b-d_4   **8b**   **27a**   **28i-d_4**   **28i**
(1 equiv.)   (1 equiv.)   (1 equiv.)

iii. Probable mechanistic cycle:

Figure 2.10: (i) A few selected examples of olefination of pyridine analogues with allenes catalyzed by Sc-**4**/Sc-**6** complex, and (ii) and (iii) mechanistic investigations relevant to plausible catalytic cycle.

deprotonation from *ortho*-C–H site of another **8c** has been reasoned as the detected deuterium atom inclusion at vinylic methyl terminals of **28i** and **28i-d_4**. This, in turn, has proven the transfer of proton from pyridyl *ortho*-C–H bond to allene methylenic site.

2.3 Conclusions

The catalytic C–H activation/functionalization presents a valuable synthetic route for the selective installation of functional groups to construct a vast class of compounds ranging from biologically relevant small molecular scaffolds to divergent polymeric frameworks. Therefore, the concept of C–H functionalization via C–H activation has extended the versatility of synthetic chemistry by rendering attractive features, such as atom-, step-, and economic feasibility as well as sustainability. Among the prevalent metal-catalyzed C–H bond activation/functionalization strategy, catalytic influence of half-sandwich organo rare-earth metal–alkyl complexes has become one of the efficient tactics in synthetic, medicinal, and materials chemistry.

The half-sandwich group-3 metal–dialkyl complexes with attached one monoanionic ligand, e.g., Cp/Cp*, enabled directed/(non)-directed C–H bond activation to several other organic transformations. This strategy also displayed precise site-/regioselectivity and a high degree of enantioselectivity as well as diastereoselectivity, adding elegance to the catalytic system. Insights into mechanistic studies concluded exclusion of one alkyl unit from neutral dialkyl precursors with an equimolar [Ph$_3$C][B(C$_6$F$_5$)$_4$] as activator accompanied by σ-bond metathesis path or 1,2-type addition leading to C–H bond activation. Reframing respective ancillary ligands and/or nature of metal center along with ligand steric demand regulating the congested environment exhibited a profound influence on the catalytic property as well as selectivity. The potential efficacy of the mechanistic pathway is also dependent on the Lewis acidity, strong electropositivity, the affinity of π-electron cloud and heteroatom, and stability in +3 oxidation number of the rare-earth metal center. DFT studies have been widely employed to depict the origin of site-/regio-selectivity, enantio-/diastereo-selectivity of C–H functionalization strategies.

Given the existing knowledge on the unique bonding features and reactivity pattern of rare-earth metal catalysis and huge potential to be explored in the near future, it is anticipated that these catalytic systems will allow transformations on a versatile and synthetically useful scale with beneficial physical, mechanical, and optical properties. Taken together, the broad opportunity and applications of these transformations suggest that C–H activation could deliver novel architectural frameworks which are of widespread utility to the synthetic community.

References

[1]   Godula, K, Sames, D. C–H bond functionalization in complex organic synthesis. Science, 2006, 312, 67–72.

[2]   Dalton, T, Faber, T, Glorius, F. C–H activation: Toward sustainability and applications. ACS Cent Sci, 2021, 7, 245–261.

[3]   Tundo, P, Anastas, P, Black, DS, Breen, J, Collins, T, Memoli, S, Miyamoto, J, Polyakoff, M, Tumas, W. Synthetic pathways and processes in green chemistry. Introductory overview. Pure Appl Chem, 2000, 72, 1207–1228.

[4]   McMurray, L, O'Hara, F, Gaunt, MJ. Recent developments in natural product synthesis using metal-catalysed C–H bond functionalisation. Chem Soc Rev, 2011, 40, 1885–1898.

[5]   Schönherr, H, Cernak, T. Profound methyl effects in drug discovery and a call for new C–H methylation reactions. Angew Chem Int Ed, 2013, 52, 12256–12267.

[6]   Cernak, T, Dykstra, KD, Tyagarajan, S, Vachal, P, Krska, SW. The medicinal chemist's toolbox for late stage functionalization of drug-like molecules. Chem Soc Rev, 2016, 45, 546–576.

[7]   Simonetti, M, Cannas, DM, Just-Baringo, X, Vitorica-Yrezabal, IJ, Larrosa, I. Cyclometallated ruthenium catalyst enables late-stage directed arylation of pharmaceuticals. Nat Chem, 2018, 10, 724–731.

[8]   Feng, K, Quevedo, RE, Kohrt, JT, Oderinde, MS, Reilly, U, White, MC. Late-stage oxidative C(sp^3)–H methylation. Nature, 2020, 580, 621–627.

[9]   Blanksby, SJ, Ellison, GB. Bond dissociation energies of organic molecules. Acc Chem Res, 2003, 36, 255–263.

[10]   Shilov, AE, Shul'pin, GB. Activation of C–H bonds by metal complexes. Chem Rev, 1997, 97, 2879–2932.

[11]   Xue, X-S, Ji, P, Zhou, B, Cheng, J-P. The essential role of bond energetics in C–H activation/functionalization. Chem Rev, 2017, 117, 8622–8648.

[12]   Hammett, LP. The effect of structure upon the reactions of organic compounds. Benzene derivatives. J Am Chem Soc, 1937, 59, 96–103.

[13]   Nandy, A, Kulik, HJ. Why conventional design rules for C–H activation fail for open-shell transition-metal. ACS Catal, 2020, 10, 15033–15047.

[14]   Hashiguchi, BG, Young, KJH, Yousufuddin, M, Goddard III, WA, Periana, RA. Acceleration of nucleophilic CH activation by strongly basic solvents. J Am Chem Soc, 2010, 132, 12542–12545.

[15]   Kuhl, N, Hopkinson, MN, Wencel-Delord, J, Glorius, F. Beyond directing groups: Transition-metal-catalyzed CH activation of simple arenes. Angew Chem Int Ed, 2012, 51, 10236–10254.

[16]   Gensch, T, James, MJ, Dalton, T, Glorius, F. Increasing catalyst efficiency in C–H activation catalysis. Angew Chem Int Ed, 2018, 57, 2296–2306.

[17]   Yu, C, Sanjosé-Orduna, J, Patureau, FW, Pérez-Temprano, MH. Emerging unconventional organic solvents for C–H bond and related functionalization reactions. Chem Soc Rev, 2020, 49, 1643–1652.

[18]   Newhouse, T, Baran, PS. If CH bonds could talk: Selective C–H bond oxidation. Angew Chem Int Ed, 2011, 50, 3362–3374.

[19]   Hartwig, JF, Larsen, MA. Undirected, homogeneous C–H bond functionalization: Challenges and opportunities. ACS Cent Sci, 2016, 2, 281–292.

[20]   Daugulis, O, Do, H-Q, Shabashov, D. Palladium- and copper-catalyzed arylation of carbonhydrogen bonds. Acc Chem Res, 2009, 42, 1074–1086.

[21]   Lyons, TW, Sanford, MS. Palladium-catalyzed ligand-directed C–H functionalization reactions. Chem Rev, 2010, 110, 1147–1169.

[22]   Zhang, M, Zhang, Y, Jie, X, Zhao, H, Li, G, Su, W. Recent advances in directed C–H functionalizations using monodentate nitrogen-based directing groups. Org Chem Front, 2014, 1, 843–895.

[23] Chen, Z, Wang, B, Zhang, J, Yu, W, Liu, Z, Zhang, Y. Transition metal-catalyzed C–H bond functionalizations by the use of diverse directing groups. Org Chem Front, 2015, 2, 1107–1295.

[24] Zhu, R-Y, Farmer, ME, Chen, Y-Q, Yu, J-Q. A Simple and versatile amide directing group for CH functionalizations. Angew Chem Int Ed, 2016, 55, 10578–10599.

[25] Iqbal, Z, Joshi, A, De, SR. Recent advancements on transition-metal-catalyzed, chelation-induced *ortho*-hydroxylation of arenes. Adv Synth Catal, 2020, 362, 5301–5351.

[26] Rej, S, Ano, Y, Chatani, N. Bidentate directing groups: An efficient tool in C–H bond functionalization chemistry for the expedient construction of CC bonds. Chem Rev, 2020, 120, 1788–1887.

[27] Kleiman, JP, Dubeck, M. The preparation of cyclopentadienyl [*o*-(phenylazo)phenyl]nickel. J Am Chem Soc, 1963, 85, 1544–1545.

[28] Cope, AC, Siekman, RW. Formation of covalent bonds from platinum or palladium to carbon by direct substitution. J Am Chem Soc, 1965, 87, 3272–3273.

[29] Albrecht, M. Cyclometalation using d-block transition metals: Fundamental aspects and recent trends. Chem Rev, 2010, 110, 576–623.

[30] Neufeldt, SR, Sanford, MS. Controlling site selectivity in palladiumcatalyzed C–H bond functionalization. Acc Chem Res, 2012, 45, 936–946.

[31] Hirano, K, Miura, M. A lesson for site-selective C–H functionalization on 2-pyridones: Radical, organometallic, directing group and steric controls. Chem Sci, 2018, 9, 22–32.

[32] Mousseau, JJ, Charette, AB. Direct functionalization processes: A journey from palladium to copper to iron to nickel to metal-free coupling reactions. Acc Chem Res, 2013, 46, 412–424.

[33] Gandeepan, P, Müller, T, Zell, D, Cera, G, Warratz, S, Ackermann, L. 3d transition metals for C–H activation. Chem Rev, 2019, 119, 2192–2452.

[34] Hashiguchi, BG, Bischof, SM, Konnick, MM, Periana, RA. Designing catalysts for functionalization of unactivated CH bonds based on the C–H activation reaction. Acc Chem Res, 2012, 45, 885–898.

[35] Arnold, PL, McMullon, MW, Rieb, J, Kühn, FE. C–H bond activation by f-block complexes. Angew Chem Int Ed, 2015, 54, 82–100.

[36] Ryabov, AD. Mechanisms of intramolecular activation of carbon-hydrogen bonds in transition-metal complexes. Chem Rev, 1990, 90, 403–424.

[37] Labinger, JA, Bercaw, JE. Understanding and exploiting C–H bond activation. Nature, 2002, 417, 507–514.

[38] Huang, W, Diaconescu, PL. C–H bond activation of hydrocarbons mediated by rare-earth metals and actinides: Beyond σ-bond metathesis and 1,2-addition. Adv Organomet Chem, 2015, 64, 41–75.

[39] Watson, PL. Ziegler-Natta polymerization: The lanthanide model. J Am Chem Soc, 1982, 104, 337–339.

[40] Huheey, JE, Keiter, EA, Keiter, RL. Inorganic Chemistry. Principles of Structure and Reactivity, 4th ed., Singapore: Pearson Education Inc., 2004, Chapter 2.

[41] Fendrick, CM, Marks, TJ. Actinacyclobutanes. Implementation of thermochemically based strategies for the ring-opening stoichiometric C–H functionalization of saturated and olefinic hydrocarbons. J Am Chem Soc, 1986, 108, 425–437.

[42] Thompson, ME, Baxter, SM, Bulls, AR, Burger, BJ, Nolan, MC, Santarsiero, BD, Schaefer, WP, Bercaw, JE. "σ bond metathesis" for C–H Bonds of hydrocarbons and Sc–R (R = H, alkyl, aryl) bonds of permethylscandocene derivatives. Evidence for noninvolvement of the π system in electrophilic activation of aromatic and vinylic C–H bonds. J Am Chem Soc, 1987, 109, 203–219.

[43] Waterman, R. σ-bond metathesis: A 30-year retrospective. Organometallics, 2013, 32, 7249–7263.

[44] Webster, CE, Fan, Y, Hall, MB, Kunz, D, Hartwig, JF. Experimental and computational evidence for a boron-assisted, σ-bond metathesis pathway for alkane borylation. J Am Chem Soc, 2003, 125, 858–859.

[45] Engle, KM, Yu, J-Q. Developing ligands for palladium(II)-catalyzed C–H functionalization: Intimate dialogue between ligand and substrate. J Org Chem, 2013, 78, 8927–8955.

[46] Morss, LR. Thermochemical properties of yttrium, lanthanum, and the lanthanide elements and ions. Chem Rev, 1976, 76, 827–841.

[47] Evans, WJ. Organometallic Lanthanide Chemistry. Adv Organomet Chem, 1985, 24, 131–177.

[48] Tilley, TD, Anderson, RA, Spencer, B, Ruben, H, Zalkin, A, Templeton, DH. Divalent lanthanide chemistry. Bis(pentamethylcyclopentadienyl)europium(II) and -ytterbium(II) derivatives: Crystal structure of bis(pentamethylcyclopentadienyl) (tetrahydrofuran)ytterbium(II)-hemitoluene at 176 K. Inorg Chem, 1980, 19, 2999–3003.

[49] Wayda, AL, Evans, WJ. Synthesis of a bis(pentamethylcyclopentadienyl) derivative of neodymium. Inorg Chem, 1980, 19, 2190–2191.

[50] Dias, AR, Salema, MS, Simões, JAM. Thermochemistry of the complexes Ti(η^5-C$_5$Me$_5$)(C$_5$Me$_4$CH$_2$) and Ti(η^5-C$_5$Me$_5$)[C$_5$Me$_3$(CH$_2$)$_2$]. J Organomet Chem, 1989, 364, 97–103.

[51] Johnson, KRD, Hayes, PG. Cyclometalative C–H bond activation in rare earth and actinide metal complexes. Chem Soc Rev, 2013, 42, 1947–1960.

[52] Evans, WJ, Davis, BL. Chemistry of tris(pentamethylcyclopentadienyl) f-element complexes, (C$_5$Me$_5$)$_3$M. Chem Rev, 2002, 102, 2119–2136.

[53] Evans, WJ, Gonzales, SL, Ziller, JW. Synthesis and X-ray crystal structure of the first tris (pentamethylcyclopentadienyl)metal complex: (η^5-C$_5$Me$_5$)$_3$Sm. J Am Chem Soc, 1991, 113, 7423–7424.

[54] Piers, WE, Emslie, DJH. Non-cyclopentadienyl ancillaries in organogroup 3 metal chemistry: A fine balance in ligand design. Coord Chem Rev, 2002, 233–234, 131–155.

[55] Mills, DP, Liddle, ST. Ligand Design in Modern Lanthanide Chemistry, Ligand Design in Metal Chemistry: Reactivity and Catalysis, 1st ed., Stradiotto, M, Lundgren, RJ, ed., John Wiley & Sons, Ltd., 2016; Chapter 12, 330–363 and references cited therein.

[56] Watson, PL. Facile C–H activation by lutetium–methyl and lutetium–hydride complexes. J Chem Soc, Chem Commun, 1983, 276–277.

[57] Jaroschik, F, Momin, A, Nief, F, Le Goff, X-F, Deacon, GB, Junk, PC. Dinitrogen reduction and C–H activation by the divalent organoneodymium complex [(C$_5$H$_2$tBu$_3$)$_2$Nd(μ-I)K([18]crown-6)]. Angew Chem Int Ed, 2009, 48, 1117–1121.

[58] Jende, LN, Maichle-Mössmer, C, Anwander, R. Rare-earth-metal alkylaluminates supported by N-donor-functionalized cyclopentadienyl ligands: C–H bond activation and performance in isoprene polymerization. Chem Eur J, 2013, 19, 16321–16333.

[59] Rong, W, He, D, Wang, M, Mou, Z, Cheng, J, Yao, C, Li, S, Trifonov, AA, Lyubov, DM, Cui, D. Neutral binuclear rare-earth metal complexes with four μ$_2$-bridging hydrides. Chem Commun, 2015, 51, 5063–5065.

[60] Corbey, JF, Woen, DH, Palumbo, CT, Fieser, ME, Ziller, JW, Furche, F, Evans, WJ. Ligand effects in the synthesis of Ln^{2+} complexes by reduction of tris (cyclopentadienyl) precursors including C–H bond activation of an indenyl anion. Organometallics, 2015, 34, 3909–3921.

[61] Palumbo, CT, Halter, DP, Voora, VK, Chen, GP, Ziller, JW, Gembicky, M, Rheingold, AL, Furche, F, Meyer, K, Evans, WJ. Using diamagnetic yttrium and lanthanum complexes to explore ligand reduction and C–H bond activation in a tris(aryloxide) mesitylene ligand system. Inorg Chem, 2018, 57, 12876–12884.

[62] Diether, D, Meermann-Zimmermann, M, Törnroos, KW, Maichle-Mössmer, C, Anwander, R. Rare-earth metal-promoted (double) C–H-bond activation of a lutidinyl-functionalized alkoxy ligand: Formation of [ONC] pincer-type ligands and implications for isoprene polymerization. Dalton Trans, 2020, 49, 2004–2013.

[63] Jenkins, TF, Bekoe, S, Ziller, JW, Furche, F, Evans, WJ. Synthesis of a heteroleptic pentamethylcyclopentadienyl yttrium(II) complex, [K (2.2.2-cryptand)]{(C$_5$Me$_5$)$_2$Y^{II}[N(SiMe$_3$)$_2$]}, and its C–H bond activated Y(III) derivative. Organometallics, 2021, 40, 3917–3925.

[64] Tsurugi, H, Yamamoto, K, Nagae, H, Kaneko, H, Mashima, K. Direct functionalization of unactivated C–H bonds catalyzed by group 3–5 metal alkyl complexes. Dalton Trans, 2014, 43, 2331–2343.

[65] Nishiura, M, Guo, F, Hou, Z. Half-sandwich rare-earth-catalyzed olefin polymerization, carbometalation, and hydroarylation. Acc Chem Res, 2015, 48, 2209–2220.

[66] Wu, Y-H, Zhang, L-Y, Wang, N-X, Xing, Y. Recent advances in the rare-earth metal triflates-catalyzed organic reactions. Catal Rev, 2022, 64, 679–715.

[67] Lyubov, DM, Trifonov, AA. Ln(II) alkyl complexes: From elusive exotics to catalytic applications. Inorg Chem Front, 2021, 8, 2965–2986.

[68] Seth, K. Recent progress in rare-earth metal-catalyzed sp^2 and sp^3 C–H functionalization to construct C–C and C–heteroelement bonds. Org Chem Front, 2022, 9, 3102–3141.

[69] Calloway, NO. The friedel-crafts syntheses. Chem Rev, 1935, 17, 327–392.

[70] Engle, KM, Mei, T-S, Wasa, M, Yu, J-Q. Weak coordination as a powerful means for developing broadly useful C–H functionalization reactions. Acc Chem Res, 2012, 45, 788–802.

[71] Mandal, R, Garai, B, Sundararaju, B. Weak-coordination in C–H bond functionalizations catalyzed by 3d metals. ACS Catal, 2022, 12, 3452–3506.

[72] De Sarkar, S, Liu, W, Kozhushkov, SI, Ackermann, L. Weakly coordinating directing groups for ruthenium(II)-catalyzed C–H activation. Adv Synth Catal, 2014, 356, 1461–1479.

[73] Kawada, A, Mitamura, S, Kobayashi, S. Lanthanide tri-fluoromethanesulfonates as reusable catalysts: Catalytic Friedel-Crafts acylation. J Chem Soc Chem Commun, 1993, 1157–1158.

[74] Watson, PL. Di- and tri-valent complexes of ytterbium via novel metal oxidation. J Chem Soc Chem Commun, 1980, 652–653.

[75] Deelman, B-J, Booij, M, Meetsma, A, Teuben, JH, Kooijman, H, Spek, AL. Activation of ethers and sulfides by organolanthanide hydrides. Molecular structures of (Cp$^*_2$Y)$_2$(μ-OCH$_2$CH$_2$O)(THF)$_2$ and (Cp$^*_2$Ce)$_2$(μ-O)(THF)$_2$. Organometallics, 1995, 14, 2306–2317.

[76] Booij, M, Deelman, B-J, Duchateau, R, Postma, DS, Meetsma, A, Teuben, JH. C–H activation of arenes and substituted arenes by the yttrium hydride (Cp$^*_2$YH)$_2$: Competition between Cp* ligand metalation, arene metalation, and H/D exchange. Molecular structures of Cp$^*_2$Y(μ-H)(μ-η^1,η^5-CH$_2$C$_5$Me$_4$)YCp* and Cp$^*_2$Y (o- C$_6$H$_4$PPh$_2$CH$_2$). Organometallics, 1993, 12, 3531–3540.

[77] Watson, PL, Parshall, GW. Organolanthanides in catalysis. Acc Chem Res, 1985, 18, 51–56.

[78] Deb, A, Bag, S, Kancherla, R, Maiti, D. Palladium-catalyzed aryl C–H olefination with unactivated, aliphatic alkenes. J Am Chem Soc, 2014, 136, 13602–13605.

[79] Seth, K, Bera, M, Brochetta, M, Agasti, S, Das, A, Gandini, A, Porta, A, Zanoni, G, Maiti, D. Incorporating unbiased, unactivated aliphatic alkenes in Pd(II)-catalyzed olefination of benzyl phosphonamide. ACS Catal, 2017, 7, 7732–7736.

[80] Ali, W, Prakash, G, Maiti, D. Recent development in transition metal-catalysed C–H olefination. Chem Sci, 2021, 12, 2735–2759.

[81] Oyamada, J, Hou, Z. Regioselective C–H alkylation of anisoles with olefins catalyzed by cationic half-sandwich rare earth alkyl complexes. Angew Chem Int Ed, 2012, 51, 12828–12832.

[82] Luo, Y, Baldamus, J, Hou, Z. Scandium half-metallocene-catalyzed syndiospecific styrene polymerization and styrene–ethylene copolymerization: Unprecedented incorporation of syndiotactic styrene–styrene sequences in styrene–ethylene copolymers. J Am Chem Soc, 2004, 126, 13910–13911.

[83] Nishiura, M, Hou, Z. Novel polymerization catalysts and hydride clusters from rare-earth metal dialkyls. Nat Chem, 2010, 2, 257–268.

[84] Ozawa, F, Kubo, A, Hayashi, T. Catalytic asymmetric arylation of 2,3-dihydrofuran with aryl triflates. J Am Chem Soc, 1991, 113, 1417–1419.

[85] Werner, EW, Mei, T-S, Burckle, AJ, Sigman, MS. Enantioselective Heck arylations of acyclic alkenyl alcohols using a redox-relay strategy. Science, 2012, 338, 1455–1458.

[86] Mei, T-S, Patel, HH, Sigman, MS. Enantioselective construction of remote quaternary stereocentres. Nature, 2014, 508, 340–344.

[87] Xu, L, Hilton, MJ, Zhang, X, Norrby, P-O, Wu, Y-D, Sigman, MS, Wiest, O. Mechanism, reactivity, and selectivity in palladium-catalyzed redox-relay Heck arylations of alkenyl alcohols. J Am Chem Soc, 2014, 136, 1960–1967.

[88] Faulkner, A, Race, NJ, Scott, JS, Bower, JF. Copper catalyzed Heck-like cyclizations of oxime esters. Chem Sci, 2014, 5, 2416–2421.

[89] Yue, G, Lei, K, Hirao, H, Zhou, J. Palladium-catalyzed asymmetric reductive Heck reaction of aryl halides. Angew Chem Int Ed, 2015, 54, 6531–6535.

[90] Patel, HH, Sigman, MS. Palladium-catalyzed enantioselective Heck alkenylation of acyclic alkenols using a redox-relay strategy. J Am Chem Soc, 2015, 137, 3462–3465.

[91] Hazelden, IR, Ma, X, Langer, T, Bower, JF. Diverse N-heterocyclic ring systems via aza-Heck cyclizations of N-(pentafluorobenzoyloxy)sulfonamides. Angew Chem Int Ed, 2016, 55, 11198–11202.

[92] Maity, S, Dolui, P, Kancherla, R, Maiti, D. Introducing unactivated acyclic internal aliphatic olefins into a cobalt catalyzed allylic selective dehydrogenative Heck reaction. Chem Sci, 2017, 8, 5181–5185.

[93] Xi, Y, Ma, S, Hartwig, JF. Catalytic asymmetric addition of an amine N–H bond across internal alkenes. Nature, 2020, 588, 254–260.

[94] Song, G, Luo, G, Oyamada, J, Luo, Y, Hou, Z. ortho-Selective CH addition of N,N-dimethyl anilines to alkenes by a yttrium catalyst. Chem Sci, 2016, 7, 5265–5270.

[95] Evans, WJ, Meadows, JH, Hunter, WE, Atwood, JL. Organolanthanide and organoyttrium hydride chemistry. 5. Improved synthesis of [(C5H4R)2YH(THF)]2 complexes and their reactivity with alkenes, alkynes, 1,2-propadiene, nitriles, and pyridine, including structural characterization of an alkylideneamido product. J Am Chem Soc, 1984, 106, 1291–1300.

[96] Deelman, B, Stevels, WM, Teuben, JH, Lakin, MT, Spek, AL. Insertion chemistry of Cp*2Y(2-pyridyl) and molecular structure of the unexpected CO insertion product (Cp*2Y)2(μ-η2:η2-OC(NC5H4)2). Organometallics, 1994, 13, 3881–3891.

[97] Guan, B-T, Hou, Z. Rare-earth-catalyzed C–H bond addition of pyridines to olefins. J Am Chem Soc, 2011, 133, 18086–18089.

[98] Arndt, S, Elvidge, BR, Zeimentz, PM, Spaniol, TP, Okuda, J. Formation of a dicationic yttrium η2-pyridyl complex from an yttrium methyl dication by C–H activation of pyridine. Organometallics, 2006, 25, 793–795.

[99] Nakao, Y, Yamada, Y, Kashihara, N, Hiyama, T. Selective C-4 alkylation of pyridine by nickel/Lewis acid catalysis. J Am Chem Soc, 2010, 132, 13666–13668.

[100] Giri, R, Shi, B-F, Engle, KM, Maugel, N, Yu, J-Q. Transition metal-catalyzed C–H activation reactions: Diastereoselectivity and enantioselectivity. Chem Soc Rev, 2009, 38, 3242–3272.

[101] Song, G, Wylie, WNO, Hou, Z. Enantioselective C–H bond addition of pyridines to alkenes catalyzed by chiral half-sandwich rare-earth complexes. J Am Chem Soc, 2014, 136, 12209–12212.

[102] Quasdorf, KW, Overman, LE. Catalytic enantioselective synthesis of quaternary carbon stereocenters. Nature, 2014, 516, 181–191.

[103] Marek, I, Minko, Y, Pasco, M, Mejuch, T, Gilboa, N, Chechik, H, Das, JP. All-carbon quaternary stereogenic centers in acyclic systems through the creation of several C–C bonds per chemical step. J Am Chem Soc, 2014, 136, 2682–2694.

[104] Liu, Y, Han, S-J, Liu, W-B, Stoltz, BM. Catalytic enantioselective construction of quaternary stereocenters: Assembly of key building blocks for the synthesis of biologically active molecules. Acc Chem Res, 2015, 48, 740–751.

[105] Wang, Z. Construction of all-carbon quaternary stereocenters by catalytic asymmetric conjugate addition to cyclic enones in natural product synthesis. Org Chem Front, 2020, 7, 3815–3841.

[106] Lou, S-J, Mo, Z, Nishiura, M, Hou, Z. Construction of all-carbon quaternary stereocenters by scandium-catalyzed intramolecular C–H alkylation of imidazoles with 1,1-disubstituted alkenes. J Am Chem Soc, 2020, 142, 1200–1205.

[107] Diesel, J, Grosheva, D, Kodama, S, Cramer, N. A bulky chiral N-heterocyclic carbene nickel catalyst enables enantioselective C–H functionalizations of indoles and pyrroles. Angew Chem Int Ed, 2019, 58, 11044–11048.

[108] Daugulis, O, Zaitsev, VG. Anilide *ortho*-arylation by using C–H activation methodology. Angew Chem Int Ed, 2005, 44, 4046–4048.

[109] Deprez, NR, Kalyani, D, Krause, A, Sanford, MS. Room temperature palladium-catalyzed 2-arylation of indoles. J Am Chem Soc, 2006, 128, 4972–4973.

[110] Phipps, RJ, Grimster, NP, Gaunt, MJ. Cu(II)-catalyzed direct and site-selective arylation of indoles under mild conditions. J Am Chem Soc, 2008, 130, 8172–8174.

[111] Phipps, RJ, Gaunt, MJ. A meta-selective copper-catalyzed C–H bond arylation. Science, 2009, 323, 1593–1597.

[112] Hickman, AJ, Sanford, MS. High-valent organometallic copper and palladium in catalysis. Nature, 2012, 484, 177–185.

[113] Yu, M-S, Lee, W-C, Chen, C-H, Tsai, F-Y, Ong, T-G. Controlled regiodivergent C–H bond activation of imidazo[1,5-*a*]pyridine via synergistic cooperation between aluminum and nickel. Org Lett, 2014, 16, 4826–4829.

[114] Usui, K, Haines, BE, Musaev, DG, Sarpong, R. Understanding regiodivergence in a Pd(II)-mediated site-selective C–H alkynylation. ACS Catal, 2018, 8, 4516–4527.

[115] Lin, W, Zhang, K-F, Baudoin, O. Regiodivergent enantioselective C–H functionalization of Boc-1,3-oxazinanes for the synthesis of β^2- and β^3-amino acids. Nat Catal, 2019, 2, 882–888.

[116] Lou, S-J, Zhang, L, Luo, Y, Nishiura, M, Luo, G, Luo, Y, Hou, Z. Regiodivergent C–H alkylation of quinolines with alkenes by half-sandwich rare-earth catalysts. J Am Chem Soc, 2020, 142, 18128–18137.

[117] Miller, LC, Sarpong, R. Divergent reactions on racemic mixtures. Chem Soc Rev, 2011, 40, 4550–4562.

[118] Krautwald, S, Carreira, EM. Stereodivergence in asymmetric catalysis. J Am Chem Soc, 2017, 139, 5627–5639.

[119] Kan, SBJ, Maruyama, H, Akakura, M, Kano, T, Maruoka, K. Catalyst-controlled, enantioselective, and diastereodivergent conjugate addition of aldehydes to electron-deficient olefins. Angew Chem Int Ed, 2017, 56, 9487–9491.

[120] Xiao, L, Wei, L, Wang, C-J. Stereodivergent synthesis of enantioenriched γ-butyrolactones bearing two vicinal stereocenters enabled by synergistic copper and iridium catalysis. Angew Chem Int Ed, 2021, 60, 24930–24940.

[121] Yang, S-Q, Wang, Y-F, Zhao, W-C, Lin, G-Q, He, Z-T. Stereodivergent synthesis of tertiary fluoride-tethered allenes via copper and palladium dual catalysis. J Am Chem Soc, 2021, 143, 7285–7291.

[122] Cong, X, Zhan, G, Mo, Z, Nishiura, M, Hou, Z. Diastereodivergent [3 + 2] annulation of aromatic aldimines with alkenes via C–H activation by half-sandwich rare-earth catalysts. J Am Chem Soc, 2020, 142, 5531–5537.

[123] Wang, P, Luo, G, Yang, J, Cong, X, Hou, Z, Luo, Y. Theoretical studies of rare-earth-catalyzed [3 + 2] annulation of aromatic aldimine with styrene: Mechanism and origin of diastereoselectivity. J Org Chem, 2021, 86, 4236–4244.

[124] Lou, S-J, Zhuo, Q, Nishiura, M, Luo, G, Hou, Z. Enantioselective C–H alkenylation of ferrocenes with alkynes by half-sandwich scandium catalyst. J Am Chem Soc, 2021, 143, 2470–2476.

[125] Fotie, J, Kaiser, M, Delfin, DA, Manley, J, Reid, CS, Paris, J-M, Wenzler, T, Maes, L, Mahasenan, KV, Li, C, Werbovetz, KA. Antitrypanosomal activity of 1,2-dihydroquinolin-6-ols and their ester derivatives. J Med Chem, 2010, 53, 966–982.

[126] Sridharan, V, Suryavanshi, PA, Menéndez, JC. Advances in the chemistry of tetrahydroquinolines. Chem Rev, 2011, 111, 7157–7259.

[127] Muthukrishnan, I, Sridharan, V, Menéndez, JC. Progress in the chemistry of tetrahydroquinolines. Chem Rev, 2019, 119, 5057–5191.

[128] Blakemore, DC, Castro, L, Churcher, I, Rees, DC, Thomas, AW, Wilson, DM, Wood, A. Organic synthesis provides opportunities to transform drug discovery. Nat Chem, 2018, 10, 383–394.

[129] Campos, KR, Coleman, PJ, Alvarez, JC, Dreher, SD, Garbaccio, RM, Terrett, NK, Tillyer, RD, Truppo, MD, Parmee, ER. The importance of synthetic chemistry in the pharmaceutical industry. Science, 2019, 363, eaat0805.

[130] Gilman, H, Gainer, GC. The reaction of aryllithium compounds with 2-arylquinolines. J Am Chem Soc, 1947, 69, 877–880.

[131] Wang, S-G, Zhang, W, You, S-L. Construction of *spiro*-tetrahydroquinolines via intramolecular dearomatization of quinolines: Free of a preinstalled activation group. Org Lett, 2013, 15, 1488–1491.

[132] Wang, Y, Liu, Y, Zhang, D, Wei, H, Shi, M, Wang, F. Enantioselective rhodium-catalyzed dearomative arylation or alkenylation of quinolinium salts. Angew Chem Int Ed, 2016, 55, 3776–3780.

[133] Lou, S-J, Luo, G, Yamaguchi, S, An, K, Nishiura, M, Hou, Z. Modular access to spiro-dihydroquinolines via scandium-catalyzed dearomative annulation of quinolines with alkynes. J Am Chem Soc, 2021, 143, 20462–20471.

[134] Zhang, G, Yang, L, Wang, Y, Xie, Y, Huang, H. An efficient Rh/O_2 catalytic system for oxidative C–H activation/annulation: Evidence for Rh(I) to Rh(III) oxidation by molecular oxygen. J Am Chem Soc, 2013, 135, 8850–8853.

[135] Ma, S. Electrophilic addition and cyclization reactions of allenes. Acc Chem Res, 2009, 42, 1679–1688.

[136] Santhoshkumar, R, Cheng, C-H. Fickle reactivity of allenes in transition metal-catalyzed C–H functionalizations. Asian J Org Chem, 2018, 7, 1151–1163.

[137] Song, G, Wang, B, Nishiura, M, Hou, Z. Catalytic C–H bond addition of pyridines to allenes by a rare-earth catalyst. Chem Eur J, 2015, 21, 8394–8398.

[138] Guram, AS, Jordan, RF. Alkene and alkyne insertion reactions of cationic $Cp_2Zr(\eta^2$-pyridyl)(L)$^+$ complexes. Zirconium-mediated functionalization of pyridines. Organometallics, 1991, 10, 3470–3479.

K. Ganesh Kadiyala, Vanipenta Yamini, Kommuru Goutham
and Naresh Kumar Katari*

3 Rare earth metal-catalyzed multicomponent reactions

3.1 Introduction

Multicomponent reactions (MCRs) are one-pot synthetic processes that involve at least three commercially available or easily accessible substrates that combine together to produce a single product through cascade reactions [1]. MCRs are advantageous and popular because of their atom-economy and step-efficiency, which reduce waste generation. In particular, their ease of use and their adaptability to experimental techniques reveal their entries to a broad array of synthetic compounds over the multiple combination opportunities of coupling reagents. The Strecker reaction was the first ever reported example of such an MCR reaction in which α-aminonitriles were synthesized from aldehydes. Following Strecker's synthesis, the chemical community rapidly progressed to further carbonyl-based MCRs. The well-known aldehyde-based MCR is the Mannich reaction, which yields an iminium intermediate, which is obtained from formaldehyde and amines, either primary or secondary, which reacts with carbonyl compound to afford β-aminocarbonyls [2]; and the Biginelli reaction converts an aldehyde, a *β*-ketoester, and urea into dihydropyrimidones [3]. Simultaneously, isocyanide-based MCRs are also developed. The first isocyanide-based MCRs report, Passerini reaction [4], was published in 1921 and rapidly attained prominence in the pharmaceutical sector. The Ugi condensation [5], another foremost isocyanide-based MCR that consists of an aldehyde, an amine, a carboxylic acid, and an isocyanide, allows for the hasty assembly of libraries of *α*-aminoacyl amide derivatives, making it useful for drug development.

Nowadays, the overall demand for practical and effective synthetic methods propels new research and encourages the creative rethinking of well-established ideas. The desire for sustainable energy and atom-efficient reactions are driving an increase in the demand for Lewis acid-catalyzed multicomponent reaction methods, which open up new avenues in synthetic organic chemistry. Rare earth metal-induced MCRs

*Corresponding author: Naresh Kumar Katari, Department of Chemistry, School of Science, GITAM Deemed to be University, Hyderabad, India, e-mail: nkatari@gitam.edu
K. Ganesh Kadiyala, Depatment of Chemistry, Shri Vishnu Engineering College for Women, Bhimavaram, Andhra Pradesh, India
Vanipenta Yamini, Sri A. S. N. M. Govt. College (A), Palakollu, Andhra Pradesh, India
Kommuru Gowtham, Indian Institute of Chemical Technology, Hyderabad, Telangana, India

are one of the Lewis acid catalysts that are currently developing, although significant advancements are anticipated in this area shortly.

3.2 Various organic synthesis using rare earth metals as catalysts

3.2.1 Synthesis of substituted pyrroles derivatives

Pyrrole is an important constituent of porphyrin, chlorophyll, and bile pigment. It is also a main scaffold of amino acids such as proline and hydroxyproline. In addition to these prevalent compounds, pyrrole structural fragments are particularly found in natural products of marine origin. The most prominent and well-known method for the preparation of pyrrole is Paal-Knorr synthesis [6, 7]. Depending on the importance of pyrrole moiety, several scientific communities have showcased various synthetic protocols [8, 9] for the preparation of pyrrole scaffold.

Shiraishi and co-workers [10] developed an efficient and mild MCR protocol for the synthesis of multi-substituted pyrrole compounds (**4**) (Figure 3.1). The protocol involves the reaction of rare earth metal SmI_2 or $SmCl_3$-catalyzed coupling of amines (**1**), aldehydes (**2**), and nitroalkane (**3**).
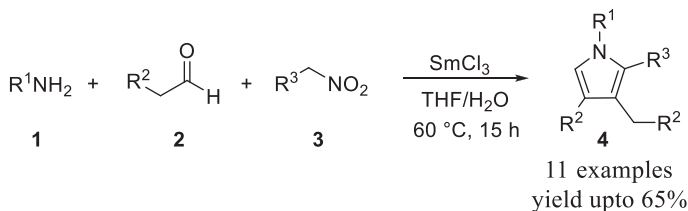
Figure 3.1: Synthesis of samarium catalyzed pyrroles through MCR.

This MCR sequence involves the reaction of amine (**1**) and aldehyde (**2**) to form imine (**A**), which undergoes aldol condensation with aldehyde (**2**) in the presence of samarium catalyst to give α, β-unsaturated imine (**B**). The obtained α, β-unsaturated imine (**B**) reacts with nitroalkane (**3**) under heating, following the Michael addition adduct (**C**), proton abstraction adduct (**D**), cyclization, and isomerization (**E**), giving multi-substituted pyrrole derivatives (**4**) (Figure 3.2). The present protocol is suitable for aldimines, but is a limitation for ketimines obtained from the condensation of ketones and amines.

Encouraged by the synthesis of samarium (III)-catalyzed pyrroles, the same group developed a diversified protocol for the regioselective construction of pyrroles (**7**) by the reaction of nitroalkenes (**6**) and imines (**8**) under samarium catalysis (Figure 3.3) [11]. In this protocol, a wide range of nitro alkenes (**6**) (obtained from amines (**1**) and
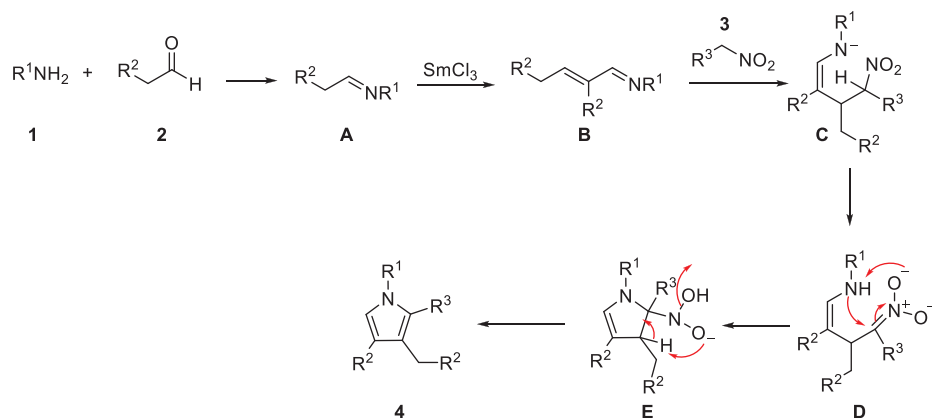
Figure 3.2: Reaction mechanism of samarium (III)-catalyzed pyrroles synthesis through MCR.

9 examples
yield upto 80%
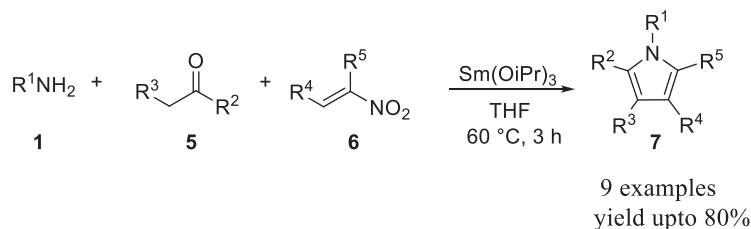
Figure 3.3: Synthesis of pyrroles via samarium-catalyzed MCRs.

an aldehyde or ketones (**5**)) (Figure 3.4) and imines (**8**) were combined to generate substituted pyrroles (**7**) as well as fused pyrrole derivatives in moderate to good yields. The yield of the pyrrole derivative was affected by the substituent alkyl group attached to the nitrogen atom of imines. As the bulkiness of the alkyl group increases, yield of the corresponding pyrrole derivative decreases.

3.2.2 Synthesis of functionalized dihydropyrimidine derivatives via Biginelli condensation

Dihydropyrimidines (DHPMs) are a class of nitrogen-containing complexes heterocyclic scaffolds that are present in several marine alkaloids (such as crambine and batzelladine) [12]. In addition, it has been found that they are effective HIV gp-120CD4 inhibitors [13]. Besides, a number of multi-functionalized dihydropyrimidines also reveal antitumor [14], antibacterial [15], antiviral [16], and anti-inflammatory properties [17] in addition to having exceptional pharmacological effectiveness. Despite many
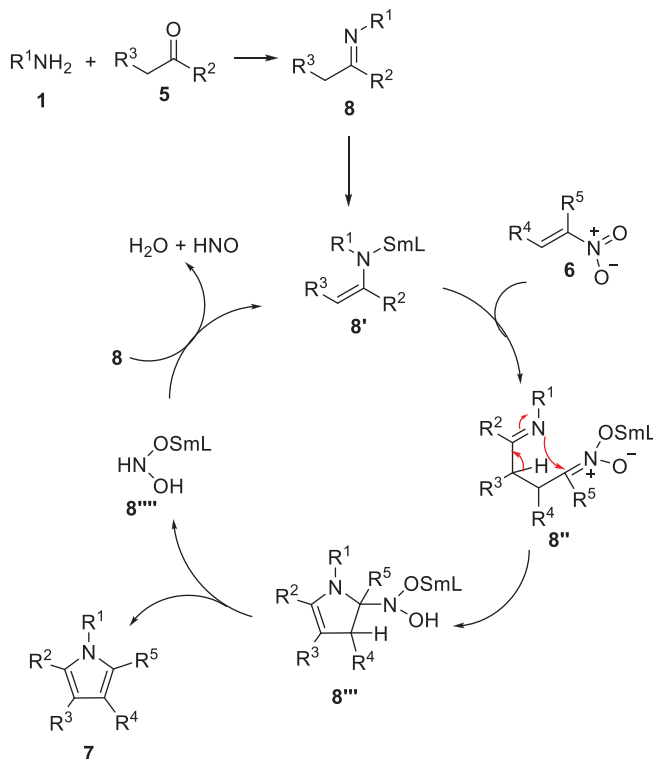
Figure 3.4: Reaction mechanism of samarium (III)-catalyzed pyrroles synthesis through MCR.

approaches that have materialized [18–26], still it requires mild protocols for the construction of dihydropyrimidine derivatives.

Ma and co-workers [27] reported an highly efficient Yb(OTf)$_3$-mediated multicomponent reaction of aldehydes (**9**), urea (**10**), and β-ketoesters (**11**), via the Biginelli reaction for the preparation of dihydropyrimidines (**12**) under a solvent-free environment at 100 °C (Figure 3.5). Replacing β-ketoesters with 1,3-diketones, the reaction proceeds smoothly, furnishing dihydropyrimidines.
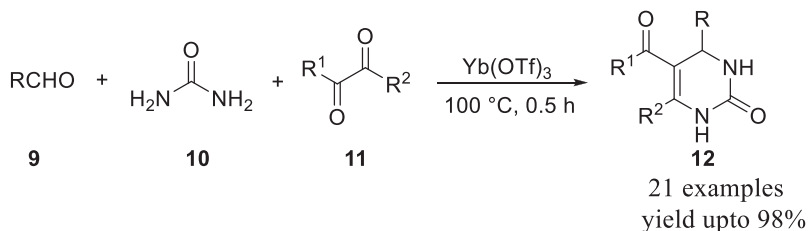
Figure 3.5: Synthesis of dihydropyrimidines via Yb(OTf)$_3$-catalyzed MCRs.

A representative procedure for the synthesis of pyrimidinones (**15**) was provided by Narasaiah et al. [28] via multicomponent reaction of urea (**10**), β-ketoesters(**13**), and aldehydes (**14**) under samarium catalysis (Figure 3.6). The present protocol involves the elimination of tedious work-up process for the purification of products. Purification of products encompasses the removal of the solvent under reduced pressure. The resulting residue was mixed with crushed ice for a while, filtered, dried, and purified by recrystallization from methanol.
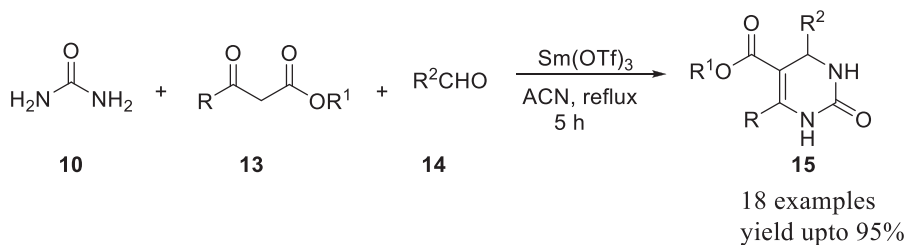
Figure 3.6: Synthesis of dihydropyrimidines via Sm(OTf)$_3$-catalyzed MCRs.

Complex optically active dihydropyrimidines (**17**) have been generated utilizing a highly enantioselective multicomponent reactions using Biginelli condensation, and employing a recyclable asymmetric Yb(OTf)$_3$ catalyst with a new hexadentate chiral ligand (**L**) (Figure 3.7) [29]. The reaction produces high yields of dihydropyrimidines with decent enantioselectivity (Figure 3.7–I). A suggested transition state model assigned the product's absolute configuration. The acylimine intermediate produced in situ might coordinate with the Yb atom. The pyridyl group shielded the coordinated acylimine's *si*-face, allowing the enol ester to attack as nucleophile from the re-face.
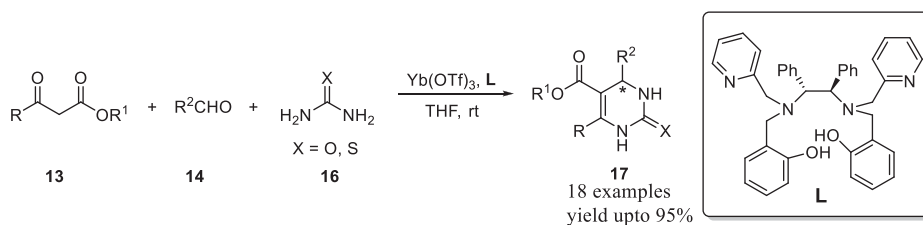
Figure 3.7: Asymmetric synthesis of dihydropyrimidines via Yb(OTf)$_3$-catalyzed MCRs.
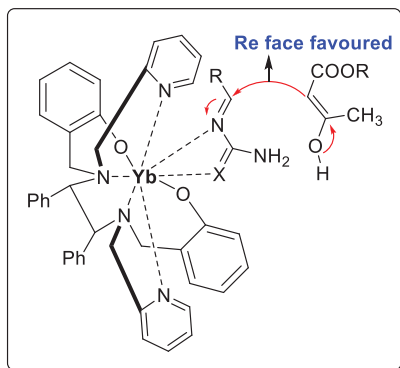
Figure 3.7-I: Transition state model showing *Re*-face attack of enol.

3.2.3 Synthesis of nitrogen containing compounds via Ugi reaction

Ugi reaction constitutes 4-component coupling (4CC) of amines, aldehydes, carboxylic acid, and isonitriles for the construction of libraries of nitrogen-containing compounds [30]. Keung and co-workers [31] have demonstrated scadium triflate-catalyzed variable Ugi three component coupling reaction for the synthesis of *α*-aminoamidine derivatives (Figure 3.8). This new method revealed a novel route for the preparation of imidopyrazine (**24**) (Figure 3.9) and hydantoin imide (**27**) (Figure 3.10).

Okandeji et al. [32] reported a high yielding multicomponent Ugi reaction using sub-stoichiometric amounts of ytterbium and scandium triflate catalysts for the production of α-acylamino carboxamide (**30** and **31**) (Figure 3.11). The activation of the imine intermediate of this multicomponent reaction is principally responsible for the
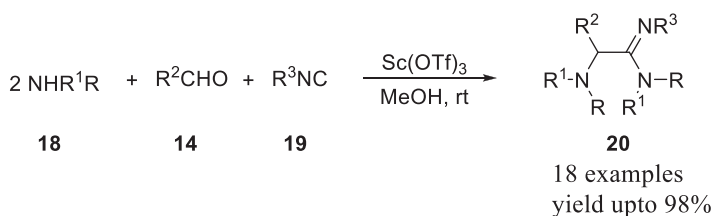
Figure 3.8: Sc(OTf)$_3$-mediated variable MCRs for constructing *α*-aminoamidine.
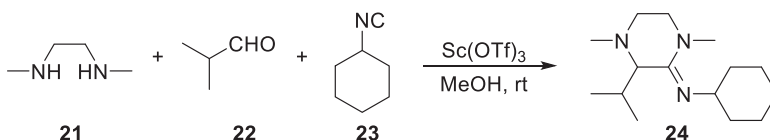
Figure 3.9: Sc(OTf)$_3$-mediated variable MCRs for assembling imidopyrazine.
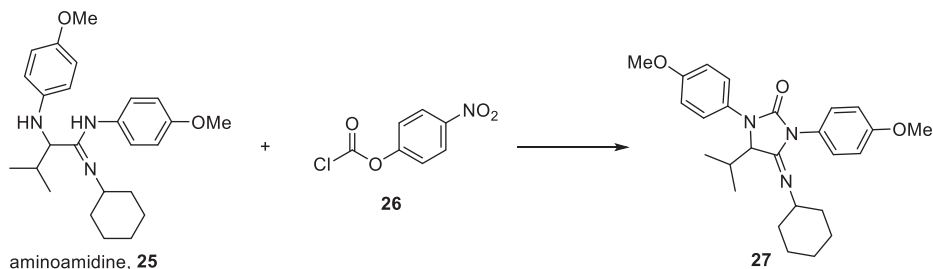
Figure 3.10: Sc(OTf)$_3$-mediatedhydantoin imide preparation via MCRs.
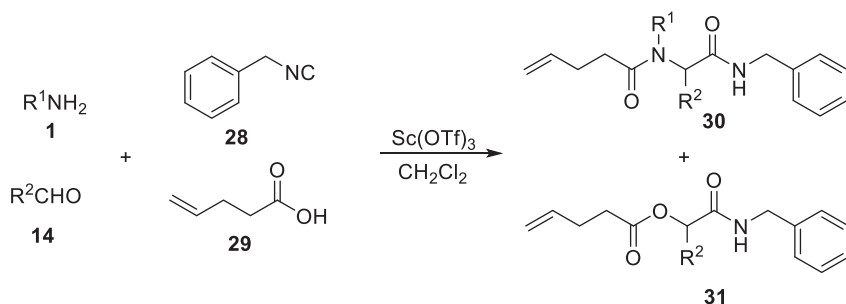
Figure 3.11: Sc(OTf)$_3$-catalyzed Ugi4CC for the synthesis of α-acylamino carboxamide.

improvement in product yield. The possibility of realizing catalytic asymmetric Ugi 4CC reactions is encouraged by the apparent mechanism of catalysis, the striking variations in yield between the catalyzed and uncatalyzed reactions, and the accessibility of chiral Sc(III) complexes.

3.2.4 Synthesis of oxazolidinones

In 2016, Xu et al. [33] reported a three component coupling of propylene oxide (PO) (**32**), carbon dioxide (**33**), and substituted anilines (**34**) for the synthesis of oxazolidinones (**35**) under rare earth metal catalyst stabilized by amine-bridged tri-(phenolato) ligands (**L1-L6**) (Figure 3.12). In this reaction, a series of rare earth metal catalyst stabilized by amine-bridged tri-(phenolato) ligands complexes were prepared and studied for their catalytic efficiency (Figure 3.13). Complexes with electron-withdrawing group attached to the aromatic ring increase the acidity of the rare earth metal, which in turn enhances the activity of substrates, leading to quantitative yields of oxazolidinones (**35**). Excess ratio of PO (**32**)-to-aniline (**34**) was essential for the significant increase in the yield of the product. Ortho-substituted, irrespective of electron-donation or withdrawing anilines, and aliphatic amines were unsuitable for this conversion.
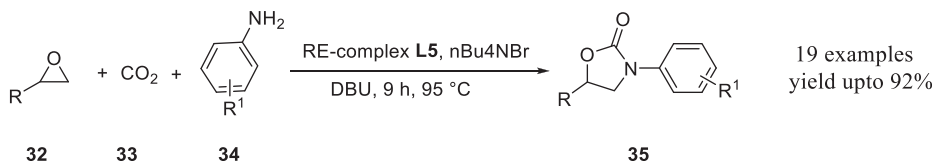
Figure 3.12: Nd-complex-catalyzed 3CC for the synthesis of oxazalidinones.

$R_1 = R_2 = Me$, RE = Y (**L1**), Sm (**L2**), Nd(**L3**), La(**L4**)
$R_1 = R_2 = Cl$, RE = Nd (**L5**), and
$R_1 = {}^{t}Bu$, $R_2 = Cl$, RE = Nd (**L6**),
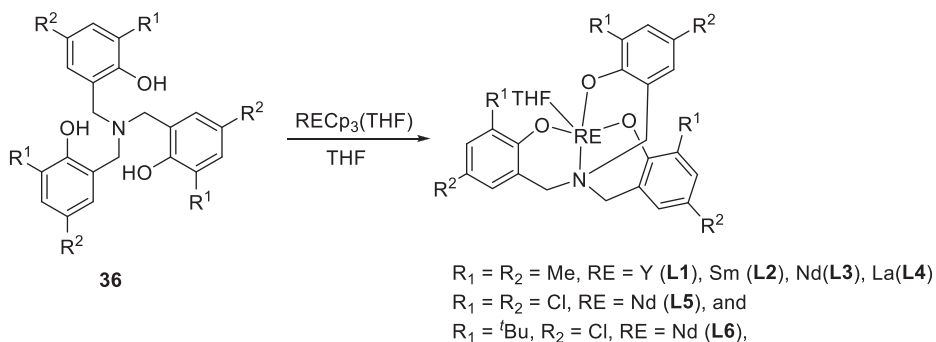
Figure 3.13: Synthesis of rare earth metal catalyst stabilized by amine-bridged tri-(phenolato) ligand complexes.

Pioneering work on 3 CC reactions for the synthesis of oxazolidinones provided the first report of 3-aryloxazolidinone (**35**) synthesis from easily available three component coupling of epoxide (**32**), aniline (**34**), and dialkyl carbonate (**37**) (ratio 2:1:2), under solvent-free rare earth metal amide catalysis (Figure 3.14) [34]. In addition, the reaction produces MeOH as the byproduct. The reaction is limited to monosubstituted epoxides, whereas in the reaction with vicinal disubstituted epoxides, the reaction is sluggish or does not takes place. Catalytic efficiency of metal amides decreases with decrease in ionic radii of rare earth metal ions.
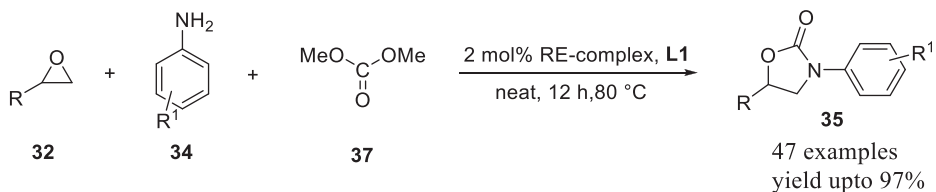
Figure 3.14: Synthesis of oxazolidinones, catalyzed by rare earth metal amide.

Cerric ammonium nitrate (CAN)-mediated synthesis of Betti bases (**40**) [35] from commercially available substrates *viz*. aryl and alkylamines (**34**), substituted benzaldehydes (**38**), and 2-naphthol (**39**), (1:1.2:1) was reported by Mekheimer et al. [36] (Figure 3.15).
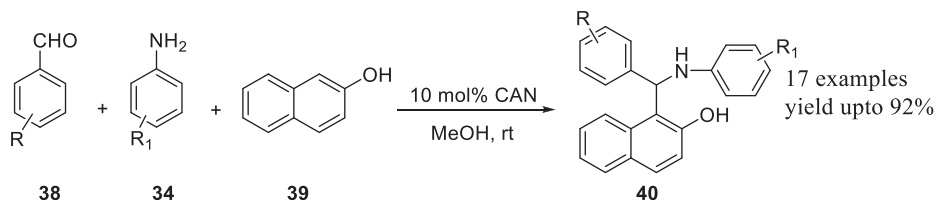
Figure 3.15: CAN-mediated synthesis of Betti base.

The reaction works well in ambient conditions with moderate-to-good yields in methanol. When the methanol was replaced by water, the reaction furnishes Schiff base, instead of betti base.

3.2.5 Synthesis of 3-aminoimidazoles

Rapid and efficient microwave-assisted 3 component coupling (3 CC) Ugi reaction of amidine (**41**), isocyanides (**19**), and aldehydes (**14**) for the synthesis of libraries of 3-aminoimidazoles (**42**), catalyzed by scandium triflate in methanol was described by Ireland and co-workers [37] (Figure 3.16). A variety of combinations of amidine (**41**), aldehydes (**14**), and isocyanides (**19**) undergo coupling to give a wide range of aminoimidazoles (**42**). The reaction was completed in a very short span of 10 min.
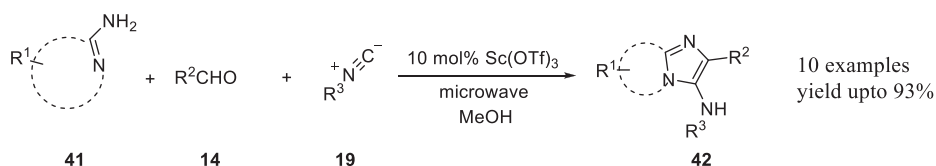
Figure 3.16: Microwave-assisted Sc(OTf)$_3$-catalyzed 3 CC Ugi reaction for the formation of 3-aminoimidazoles.

Hulme et al. [38] proposed a related 3 component coupling reaction for the synthesis of 3-aminoimidazopyridines (**45**) under microwave irradiation, catalyzed by scandium triflate using simply accessible reactants – 2-aminopyridine (**43**), trimethylsilylcyanide (**44**), (TMSCN, anisonitrile equivalent), and aldehyde (**14**) in methanol (Figure 3.17).
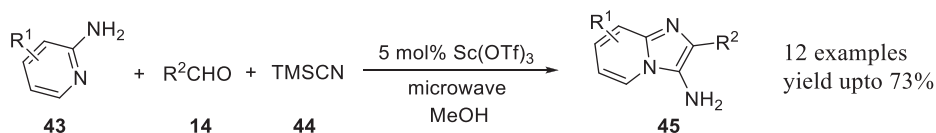
Figure 3.17: Sc(OTf)$_3$-catalyzed formation of 3-aminoimidazopyridines under microwave conditions.

3.2.6 Synthesis of quinoline derivatives via Pavarov reaction

In 2011, Vicente-García et al. [39] reported an effective Sc(OTf)$_3$-mediated domino Pavarov reaction [40] for the synthesis of diverse heterocycle tetrahydro-quinoline derivatives (**47**) by employing oxa-, thia-, and imidazolones as a novel class of electron-rich olefin partner (**46**) (dienophile) interaction with anilines (**34**) and aldehydes (**14**) (Figure 3.18). The use of a new class of olefin (dienophile) opens up a new direction for the construction of structural diversity of tetrahydroquinoline derivatives. The obtained MCR adducts were conveniently oxidized to yield the corresponding quinolones (**48**).
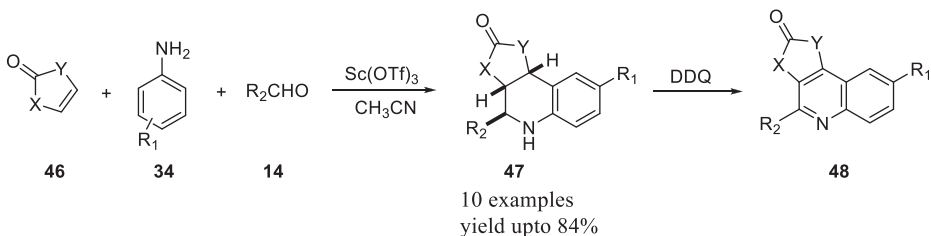
Figure 3.18: Sc(OTf)$_3$-catalyzed multicomponent Pavarov reaction toward the construction of quinolone derivatives.

Dhanapal et al. [41] reported scandium(III) triflate-catalyzed Povarov reaction between *para*-substituted anilines (**34**), vinyl pyrrolidone (**49**), and phenanthrene-9-carbaldehyde (**50**) for the synthesis of quinolines (**51**) as fluorescence probes for bacteria detection (Figure 3.19). The reaction was conducted at room temperature using Sc(OTf)$_3$ in acetonitrile to produce *cis*-2-(phenanthren-10-yl)-4-(2-oxopyrrolin-1-yl)tetrahydroquinoline intermediates that could then be further oxidized with DDQ in refluxing methylbenzene (toluene) to produce the corresponding quinoline derivatives (**51**).

Figure 3.19: Pavarov multicomponent assembly of quinolone catalyzed by Sc(OTf)$_3$.

3.3 Conclusions

In conclusion, we have showcased the synthetic utility of rare earth metal complexes toward the synthesis of carbon and nitrogen heterocyclic compounds. Albeit, rare earth metal complexes are expensive compared to standard transition metal complexes, they are frequently employed in sub-sub-stoichiometric amounts. It is significant to note that the rare earth metal complexes are active in aqueous environment, eliminating the need for laborious drying process of the reaction conditions. Despite great contributions made in multicomponent reaction by using rare earth metal complexes, there is still room for further development and applications of water-tolerant rare earth complexes in sustainable MCR methodologies. It is also important to encourage the research community to develop advanced methods for the recovery and recycling of rare earth metal complexes. Additionally, investigation on the sequential MCRs with rare earth complexes would permit chemists to construct heterocyclic scaffolds with great complexity and biological profiles.

References

[1]   Strecker, A. On the artificial formation of lactic acid and a new body homologous to glycocoll.Ann Chem Pharm, 1850, 75, 27–45.

[2]   Blicke, FF. The Mannich reaction. Org React, 1942, 1, 303–341.

[3]   Biginelli, P, Gazz, P. Synthesis of 3,4-Dihydropyrimidin-2(1*H*)-ones. Chim Ital, 1893, 23, 360–416.

[4]   Passerini, M, Simone, L. Composto del *p*-isonitril-azobenzoloconacetone ed acidoacetico. Gazz Chim Ital, 1921, 51, 126–129.

[5]   Ugi, I, Meyr, R, Fetzer, U, Steinbrückner, C. VersuchemitIsonitrilen. Angew Chem, 1959, 71, 386–386.

[6]   Paal, C. Ueber die derivate des acetophenonacetessigesters und des acetonylacetessigesters. Berichte der deutschenchemischen Gesellschaft, 1884, vol 17, 2756–2767.

[7]   Knorr, L. Synthese von furfuran derivatenaus dem diacetbernsteinsäureester. Berichtederdeutschenchemischen Gesellschaft, 1884, 17, 2863–2870.

[8]   Tzankova, D, Vladimirova, S, Peikova, L, Georgieva, MJ. Synthesis of pyrrole and substituted pyrroles. Chem Technol Metall, 2018, 53, 451–464.

[9]   Estévez, V, Villacampa, M, Menéndez, JC. Recent advances in the synthesis of pyrroles by multicomponent reactions. Chem Soc Rev, 2014, 43, 4633–4657.

[10]   Shiraishi, H, Nishitani, T, Sakaguchi, S, Ishii, Y. Preparation of substituted alkyl pyrroles via samarium-catalyzed three-component coupling reaction of aldehydes, amines, and nitroalkanes. J Org Chem, 1998, 63, 6234–6238.

[11]   Shiraishi, H, Nishitani, T, Nishihara, T, Sakaguchi, S, Ishii, Y. Regioselective synthesis of alkylpyrroles from imines and nitroalkenes by lanthanide compounds. Tetrahedron, 1999, 55, 13957–13964.

[12]   Hegedüs, A, Hell, Z, Vígh, I. Convenient one-pot heterogeneous catalytic method for the preparation of 3,4-Dihydropyrimidin-2(1*H*)-ones. Synth Commun, 2006, 36, 129–136.

[13]   Patil, AD, Kumar, NV, Kokke, WC, Bean, MF, Freyer, AF, De Brosse, C, Mai, S, Truneh, A, Faulkner, DJ, Carte, B, Breen, AL, Hertzberg, RP, Johnson, RK, Westley, JW, Potts, BCM. Novel alkaloids from the spongeBatzella sp.: Inhibitors of HIV gp120-Human CD4 binding. J Org Chem, 1995, 60, 1182–1188.

[14] Peters, T, Lindenmaier, H, Haefeli, W, Weiss, J. Interaction of the mitotic kinesin Eg5 inhibitor monastrol with P-glycoprotein. Naunyn Schmiedebergs Arch Pharmacol, 2006, 372, 291–299.

[15] Choi, SH, McCollum, D. A role for metaphase spindle elongation forces in correction of merotelic kinetochore attachments. Curr Biol, 2012, 22, 225–230.

[16] Cochran, JC, Gilbert, SP. ATPase mechanism of Eg5 in the absence of microtubules: Insight into microtubule activation and allosteric inhibition by monastrol. Bio chem, 2005, 44, 16633–16648.

[17] Tcherniuk, S, van Lis, R, Kozielski, F, Skoufias, DA. Mutations in the human kinesin Eg5 that confer resistance to monastrol and S-trityl-l-cysteine in tumor derived cell lines. Bio chem Pharmacol, 2010, 79, 864–872.

[18] Kappe, CO. Recent advances in the Biginelli dihydropyrimidine synthesis new tricks from an old dog. Acc Chem Res, 2000, 33, 879–888.

[19] Armstrong, RW, Combs, AP, Tempest, PA, Brown, SD, Keating, TA. Multiple-component condensation strategies for combinatorial library synthesis. Acc ChemRes, 1996, 29, 123–131.

[20] Ramarao, AV, Gurjar, MK, Vasudevan, J. An enantiospecific synthesis of the tricyclic guanidine segment of the anti-HIV marine alkaloid batzelladine A. ChemCommun, 1995, 1369–1370.

[21] Atwal, KS, Swanson, BN, Unger, SE, Floyd, DM, Merelandm, S, Hedberg, A, O'Reilly, BC. Dihydropyrimidine calcium channel blockers. 3. 3-Carbamoyl-4-aryl-1,2,3,4-tetrahydro-6-methyl-5-pyrimidinecarboxylic acid esters as orally effective antihypertensive agents. J Med Chem, 1991, 34, 806–811.

[22] Aron, ZD, Overman, LE. The tethered Biginelli condensation in natural product synthesis. Chem Commun, 2004, 253–265.

[23] Kaur, R, Chaudhary, S, Kumar, K, Gupta, MK, Rawal, RK. Recent synthetic and medicinal perspectives of dihydropyrimidinones: A review. Eur J Med Chem, 2017, 132, 108–134.

[24] Hu, EH, Sidler, DR, Dolling, UH. Unprecedented catalytic three component one-pot condensation reaction: An efficient synthesis of 5-Alkoxycarbonyl-4-aryl-3,4-dihydropyrimidin-2(1H)-ones. J Org Chem, 1998, 63, 3454–3457.

[25] Yadav, JS, Reddy, BVS, Reddy, KB, Raj, KS, Prasad, AR. Ultrasound-accelerated synthesis of 3,4-dihydropyrimidin-2(1H)-ones with ceric ammonium nitrate. Perkin Trans, 2001, 1, 1939–1941.

[26] Sun, Q, Wang, Y, Ge, Z, Cheng, T, Li, R. A highly efficient solvent-free synthesis of dihydropyrimidinones catalyzed by zinc chloride. Synthesis, 2004, 7, 1047–1051.

[27] Ma, Y, Qian, C, Wang, L, Yang, M. Lanthanide triflate catalyzed Biginelli reaction. One-pot synthesis of dihydropyrimidinones under solvent-free conditions. J Org Chem, 2000, 65, 3864–3868.

[28] Narsaiah, AV, Reddy, AR, Yadav, JS. Samarium triflate-catalyzed Biginelli condensation: An improved method for the synthesis of 3,4-Dihydropyrimidin-2(1H)-ones. SynthCommun, 2011, 41, 2794–2799.

[29] Huang, Y, Yang, F, Zhu, C. Highly enantioseletive Biginelli reaction using a new chiral ytterbium catalyst: asymmetric synthesis of dihydropyrimidines. J Am Chem Soc, 2005, 127, 16386–16387.

[30] Ugi, I, Werner, B, Dömling, A. The chemistry of isocyanides, their multi component reactions and their libraries. Molecules, 2003, 8, 53–66.

[31] Keung, W, Bakir, F, Patron, AP, Rogers, D, Priest, CD, Darmohusodo, V. Novel α-amino amidine synthesis via scandium(III) triflate mediated 3CC Ugi condensation reaction. Tetrahedron Lett, 2004, 45, 733–737.

[32] Okandeji, BO, Gordon, JR, Sello, JK. Catalysis of Ugi four component coupling reactions by rare earth metal triflates. J Org Chem, 2008, 73, 5595–5597.

[33] Xu, B, Wang, P, Lv, M, Yuan, D, Yao, Y. Transformation of carbon dioxide into oxazolidinones and cyclic carbonates catalyzed by rare-earth-metal phenolates. Chem Cat Chem, 2016, 8, 2466–2471.

[34] Zhou, M, Zheng, X, Wang, Y, Yuan, D, Ya, Y. A multicomponent approach to oxazolidinone synthesis catalyzed by rare-earth metal amides. Chem Cat Chem, 2019, 11, 5783–5787.

[35] Cardellicchio, C, Capozzi, MAM, Naso, F. The Betti base: The awakening of a sleeping beauty. Tetrahedron Asymm, 2010, 21, 507–517.

[36] Mekheimer, RA, Asiri, AM, Abdel Hameed, AM, Awed, RR, Sadek, KU. An efficient multicomponent, one-pot synthesis of Betti bases catalyzed by cerium (IV) ammonium nitrate (CAN) at ambient temperature. Green Process Synth, 2016, 5, 365–369.

[37] Ireland, SM, Tye, H, Whittaker, M. Microwave-assisted multi-component synthesis of fused 3-aminoimidazoles. Tetrahedron Lett, 2003, 44, 4369–4371.

[38] Schwerkoske, J, Masquelin, T, Perunb, T, Hulme, C. New multi-component reaction accessing 3-aminoimidazo[1,2-a]pyridines. Tetrahedron Lett, 2005, 46, 8355–8357.

[39] Vicente-García, E, Ramón, R, Lavilla, R. New heterocyclic inputs for the Povarov multicomponent reaction. Synthesis (Stuttg), 2011, 2237–2246.

[40] Forero, JSB, Junior, JJ, da Silva, FM. The Povarov reaction as a versatile strategy for the preparation of 1,2,3,4-tetrahydroquinoline derivatives: An overview. Curr Org Synth, 2014, 12, 102–107.

[41] Dhanapal, R, Perumal, PT, Damodiran, M, Ramprasath, C, Mathivanan, N. Synthesis of quinoline derivatives for fluorescent imaging certain bacteria. Bioorg Med Chem Lett, 2012, 22, 6494–6497.

Sabbasani Rajasekhara Reddy* and Paranimuthu Panjacharam

4 Synthesis and catalytic activity of light rare earth *N*-heterocyclic carbene (NHC) complexes

4.1 Introduction

N-Heterocyclic carbenes (NHCs) are auxiliary ligands with long half-lives and widely used in catalytic processes. Nucleophilic compounds are NHCs with a high electron density. Thus, they are more likely to turn as σ-donors and interact with a wide variety of metals and non-metals. When compared to phosphine ligands, NHCs have a very limited range of electron-donating ability. In the 1960s, Wanzlick et al. [1, 2] reported on the reactivity and stability of NHCs, as well as their use as ligands in metal complexes. Arduengo and coworkers [3] were the first to report the highly stable and sterically hindered crystalline carbene (**1**) 1,3-di-1-adamantyl-imidazol-2-ylidene (Figure 4.1). NHCs are more effective and efficient ligands in catalysis due to the resonance effect [4–6]. Because of its strong electron-donating ability and accepting ability and ease of modification with steric and electronic effects, the NHC ligand system has received a lot of attention in the catalytic process [7–10]. They have recently been used in the synthesis of biomass-derived ionic liquids from various sugars, and these sugar base ionic liquids have been investigated in organic synthesis and other societal applications [11–16].

Lanthanide elements, scandium, and yttrium make up rare earth elements (REEs), which are frequently found in the same ores and deposits and have similar physical properties. Light REEs include cerium (Ce), lanthanum (La), neodymium (Nd), praseodymium (Pr), promethium (Pm), and samarium (Sm), whereas heavy REEs include dysprosium (Dy), europium (Eu), erbium (Er), gadolinium (Gd), holmium (Ho), lutetium (Lu), terbium (Tb), thulium (Tm), scandium (Sc), ytterbium (Yb), and yttrium (Y).

Transition metal ligated NHC complexes play an important role in polymerization, olefin metathesis, cross coupling, and hydro functionalization reactions, and as

*Corresponding author: Sabbasani Rajasekhara Reddy,** Department of Chemistry, School of Advanced Sciences, Vellore Institute of Technology (VIT), Vellore 632014, Tamil Nadu, India, e-mail: sekharareddy@vit.ac.in

Paranimuthu Panjacharam, Department of Chemistry, School of Advanced Sciences, Vellore Institute of Technology (VIT), Vellore 632014, Tamil Nadu, India
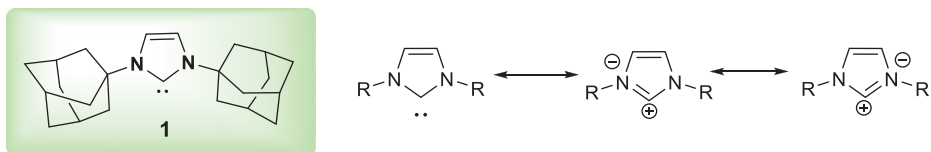
Figure 4.1: Highly stable N-heterocyclic carbene and resonance effect.

nucleophilic reagents for organic transformations in organometallic chemistry [17–21]. In recent decades, transition metal-NHC complexes have emerged as a powerful tool in organic transformation and catalysis [22]. NHC complexes with electropositive lanthanide metals have recently gained attention due to their excellent stabilizing properties, which can support unusually high oxidation states. Because of their strong attachment to the metal center, donor-functionalized polydentate NHC ligands in particular demonstrated increased stability. REEs with NHC complexes can expect chemical bond activation and ring-opening polymerization (ROP) due to their oxidation state, larger ionic radii of lanthanide metals with NHC ligands' stability.

Ln complexes are thought to have distinct advantages over transition metal catalysts in the coordination polymerization of conjugated dienes, styrene, and ROP of cyclic esters. Ln-NHCs are still underutilized in this field, though. Monodentate NHC ligands with Ln complexes were first developed by Schumann et al. [23]. Additionally, Arduengo et al. [24] reported Sm(II) complexes containing NHC ligands (Figure 4.2). The preparation of Ln complexes bearing LREEs with various mono- and bidentate NHC ligands is covered in this chapter due to the significance of NHC ligands with Ln metals. Additionally, the catalytic activity of ROP is examined, as well as the addition of carbodiimide and silane to amines, activation of CO_2 and heteroallenes, dihydrogen activation, and hydrophosphination reactions.

R= Me, ^{i}Pr
Ln= Yb(**2**), Sm(**3**)

n= 1(**4**), 2(**5**)
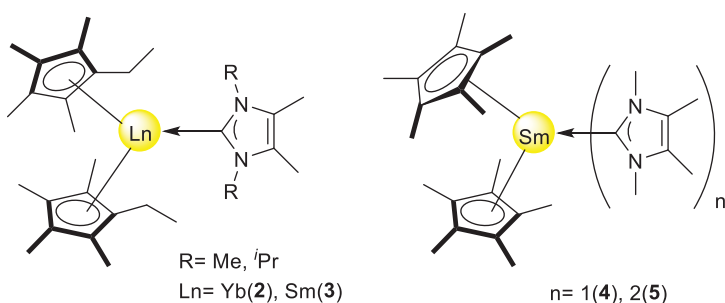
Figure 4.2: First reported Ln-NHC complexes.

4.2 Catalytic polymerization using LREE-NHC complexes

Cui and coworkers [25] investigated the *cis*-1, 4-polymerization of isoprene with complexes of lanthanide di bromides, which was mediated by the CCC-pincer 2,6-xylenyl bisphenol (carbene). By reacting $LnCl_2$ with (PBNHC-Br)$_3$.2 HBr [(2, 6-(2, 4, 6-Me$_3$C$_6$H$_2$-NCHCHNCCH$_2$)$_2$-1-Br-C$_6$H$_3$)$_3$.2HBr] in a THF solvent system at room temperature, the complexes were generated. Using three equivalents of n-BuLi, the mixture was vigorously stirred, producing moderate to good yields of complexes (Figure 4.3). Lanthanum complexes with organoborates and AlR_3 activate the isoprene precursor during the polymerization process. Highly selective *cis*-1,4-polyisoprene products were produced over a wide temperature range (20–80 °C), and the molecular structure of Ln/NHC complexes also enhances selectivity (Figure 4.4).

Ln = Sc(**6**), Y(**7**), La(**8**), Nd(**9**), Sm(**10**), Gd(**11**), Dy(**12**), Ho(**13**), Tm(**14**), Lu(**15**)
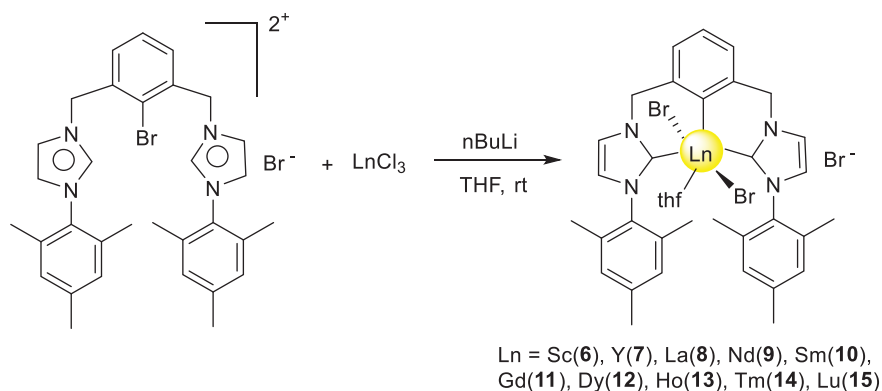
Figure 4.3: Synthesis of rare-earth metal dibromide NHC complexes using CCC-pincer bis-(NHC) ligand.
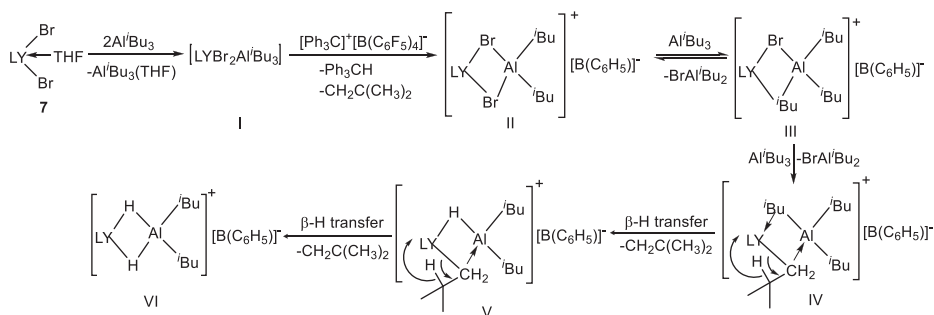
Figure 4.4: Catalytic pathway of polymerization.

It was found that Nd complexes with NHC ligation can act as conjugated dienes' pre-catalysts for polymerization. Using analogues of Nd–NHC complexes, Wu and coworkers [26] carried out highly selective *cis*-1,4-polymerization of butadiene and isoprene. The synthesis of Nd–NHC complexes **16–18** took place at 25 °C using NdCl₃. *x*THF and NHC ligands (Figure 4.5). The authors look into the *tri*-isobutylaluminum (TIBA) catalyzed coordination polymerization of **Nd-16** complexes and their binary catalytic system. With yields of up to 99% and 98%, respectively, high-molecular-weight polybutadienes (Mw = 250,780 kg/mol) and polyisoprene (Mw = 210,530 kg/mol) were formed from conjugated dienes. The molar ratios of the binary system, the ageing procedure, and the temperature all have an impact on the molecular weight and molecular weight dispersion of the polymerized products.
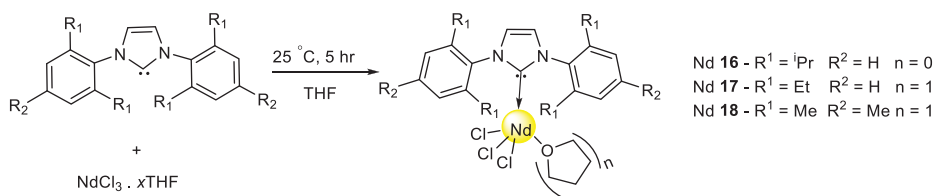
Figure 4.5: Synthesis of Nd–NHC complexes.

Ni et al. [27] investigated the ROP of ʟ-lactide using lanthanide compounds with bis(phenolate)NHC and imidazolinium-bridged bis(phenolate) ligands. Ln complexes were synthesized via metathesis and characterized using single crystal X-ray and spectroscopic techniques. In situ, the ligand was synthesized by reacting KN(SiMe₃)₂ (6 equiv) with NHC ligand (2 equiv). Lanthanide precursors react with the ligands generated to form bis(phenolate) NHC Lanthanide complexes. The catalytic activity of complexes was investigated. Bis(phenolate) NHC complexes are excellent initiators, whereas imidazolinium-bridged bis(phenolate) complexes had no catalytic activity. Lanthanide metal elements as well as radii work together to improve polymerization activity. The ʟ-lactide ROP was thought to have a coordination-insertion mechanism, and the NHC moiety was believed to be the polymerization catalyst (Figure 4.6).

The same group is investigating the catalytic activity of pyrimidinium bridging bis (phenolate)NHC with rare earth complexes for the polymerization of *n*-hexyl isocyanate. In situ, complexes were synthesized, by combining the ligand (L = 1,3-bis[*O*-4,6-di-tBu-C₆H₂-2-CH₂][C(NCH₂CH₂CH₂N)] with KN(SiMe₃)₂ and Ln[N(SiMe₃)₂](Ln = Nd, Y, Sm) (Figure 4.7). All of the complexes are characterized using single-crystal X-ray and NMR. However, these complexes were NMR inactive for the Nd complex due to its paramagnetic nature. As per polymerization studies, NHC ligands with rare earth complexes based on pyrimidinium and imidazolinium have higher catalytic activity than non-NHC rare earth complexes. Polymerization activity is enhanced by the metal radius, solvent system, reaction conditions, and ligand frame works. Polyisocyanates are high-molecular-weight
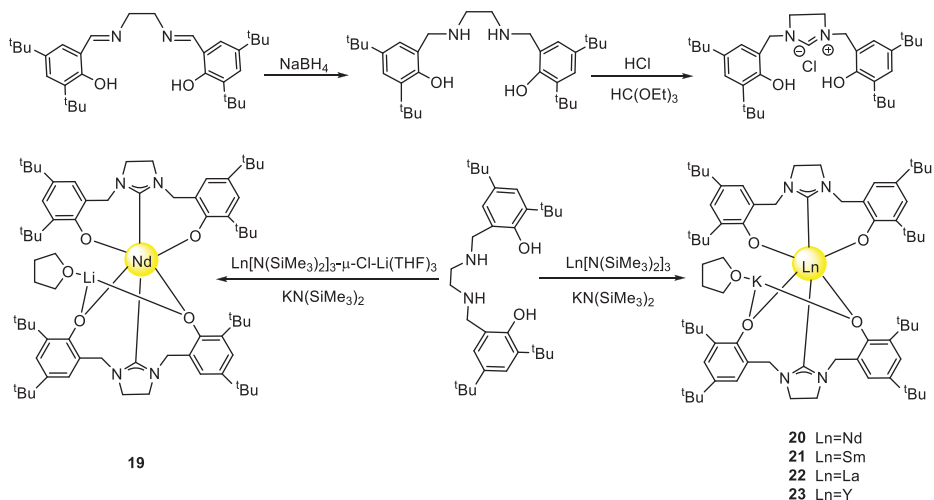
Figure 4.6: Synthesis of Ln-bis(phenolate)NHC complexes.

polymers (up to 10^6) with a narrow molecular weight distribution ($M_w/M_n = 1.7–2.3$). NMR analysis clearly shows that the complex's NHC moiety plays a crucial role in initiation of polymerization (Figure 4.8) [28].
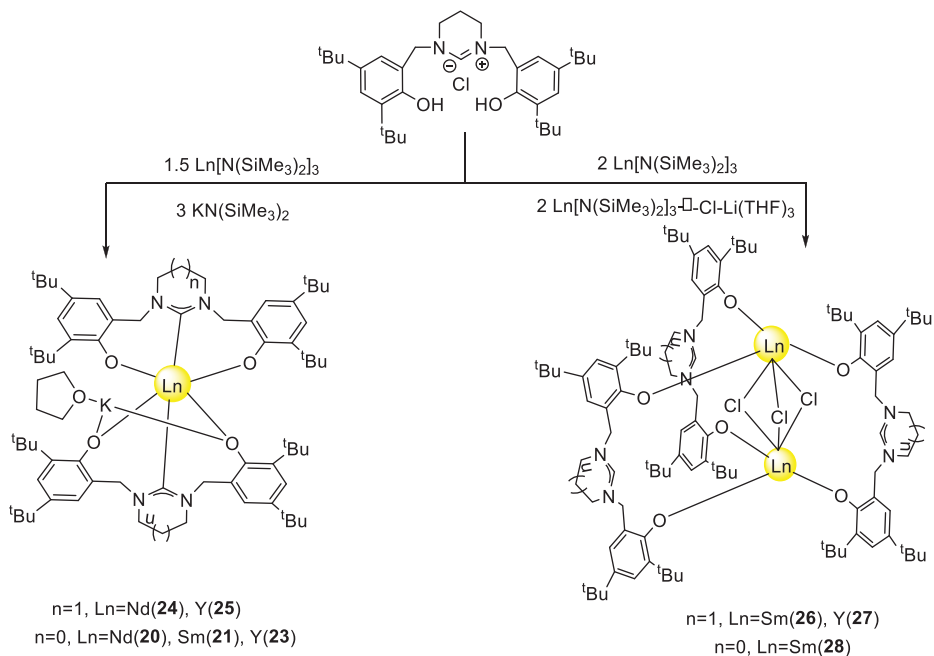
Figure 4.7: Synthesis of Ln-NHC complexes.
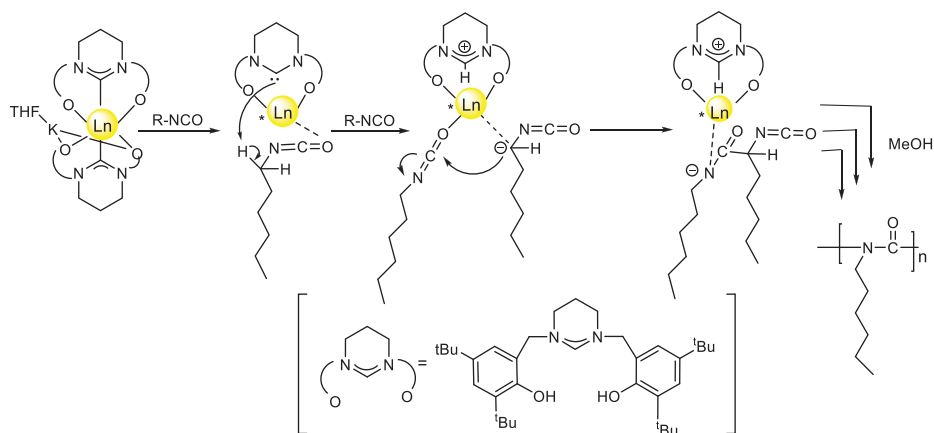
Figure 4.8: The mechanistic pathway of the initiation of Ln-NHC complexes.

High molar mass cyclic polylactide (cPLA) was synthesized by Arnold et al. [29] using a homogeneous, highly active Ce(III)-NHC catalyst with low loading. Both saturated and unsaturated NHC ligands have good activity in complexes of Ce(III), with saturated NHC being the most active. The cyclic polylactide (PLA) is constructed using exceptional activity, superb control, and selectivity due to the Lewis acidic and basic nature of the Ce(III) ion and NHC ligand combination. This results in PLA with a high molar mass. The production of cyclic lactide and cyclic polyesters from rac-lactide, caprolactone, or butyrolactone has been outstanding. The lactide initially coordinates with Ce in the systematic pathway, lowering the barrier to nucleophilic attack and allowing the labile NHC moiety to open the ring. The propagation then produces a zwitterionic intermediate in which the anionic chain end is stabilized by coordination to Ce. Finally, the intramolecular *trans*-esterification step produced cyclic polymers with a high molar mass (Figure 4.9).

Cui and Li et al. [30] have synthesized and characterized divalent lanthanide bis (amido) complexes [Ln- Sm, Eu, Yb] and their skeleton was confirmed by X-ray diffraction method. Comparatively all other NHC adducts of Ln(II) complexes, the ROP of rac-LA achieved effectively using three coordinated Samarium complex. The highly active Sm(II) complex synthesized by the treatment of NHC ligand with $(THF)_2Sm[N-(SiMe_3)_2]_2$. The larger radius of the Sm metal ion in low coordinated complex effectively interacts the lactide, and the ROP was initiated by the catalyst via coordination-insertion pathway. The Lewis acidic behavior of Sm ion activates the electrophilic center of the monomer. Subsequently, nucleophilic attacks take place at amido group on the activated monomer delivered ROP product (Figure 4.10).
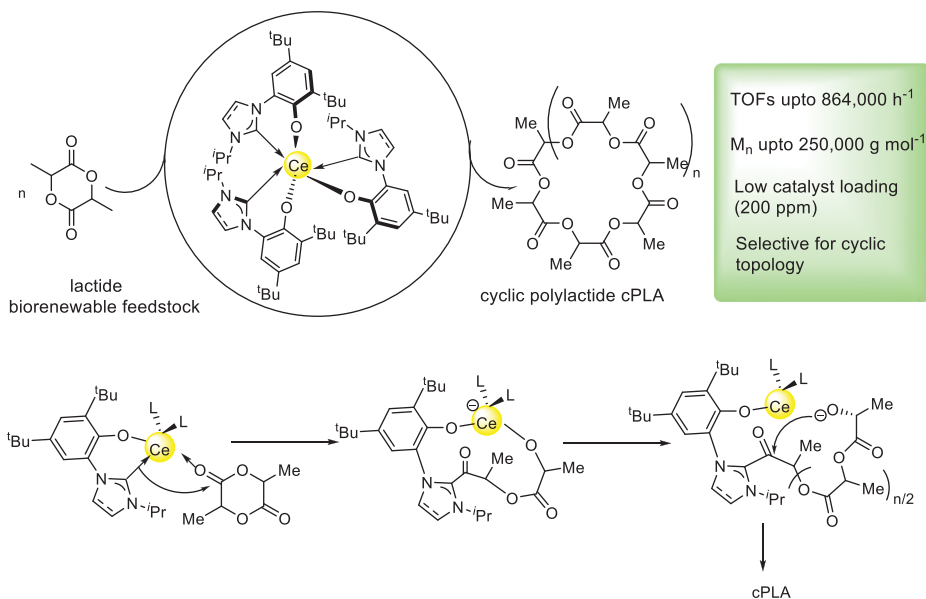
Figure 4.9: Synthesis and catalytic pathway of Ce-NHC complexes for cyclic PLA formation.
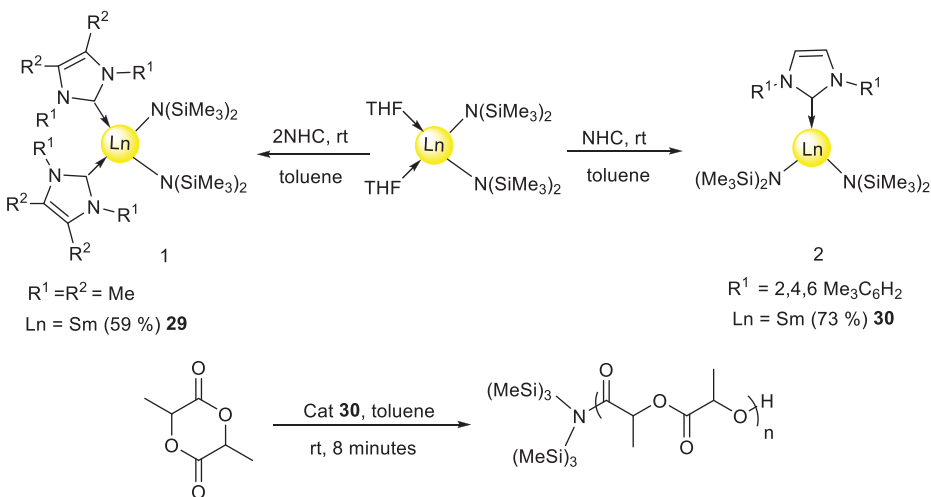
Figure 4.10: Synthesis of NHC-Ln(II) bis(amido) complexes and their catalytic ROP of rac-LA.

4.3 Addition of amines to carbodiimide using LREE-NHC complexes

Shen et al. [31] reported lanthanide amide complexes with enol functionalized NHC ligands. Enol-functionalized NHC-ligated rare earth complexes are developed at room temperature by combining a 1:4:1 molar ratio of rare earth halide (Ln = Y, Nd, Sm, and Yb) with enol functionalized imidazolium salt and NaN(TMS)$_2$. The molecular structure of the synthesized complexes was determined using X-ray diffraction analysis. The majority of the five coordinated metal complexes with monomeric form adopt distorted trigonal bipyramid geometry. The Yb complex exhibits excellent activity when amines are added to carbodiimides with synthesized complexes (Figure 4.11). Wang et al. [32] synthesized rare earth metal complexes with CNC-Pincer diarylamido bis(NHC). At room temperature, the reaction of H$_3$LCl$_3$ and [(Me$_3$Si)$_2$ N]$_3$RE(-Cl)Li (THF)$_3$ with two equivalents of nBuLi in THF yields moderate yields of CNC-Pincer ligated rare earth amido complexes (RE = Y, Eu and Sm). The catalytic activity of synthesized complexes, carbodiimides formed by the addition of terminal alkyne C-H bonds, was first reported. Metal ions also improve the catalytic activity of highly active rare earth metal complexes (RE = Er(**35**), Y(**36**), Sm(**37**), Eu(**38**)) (Figure 4.12).
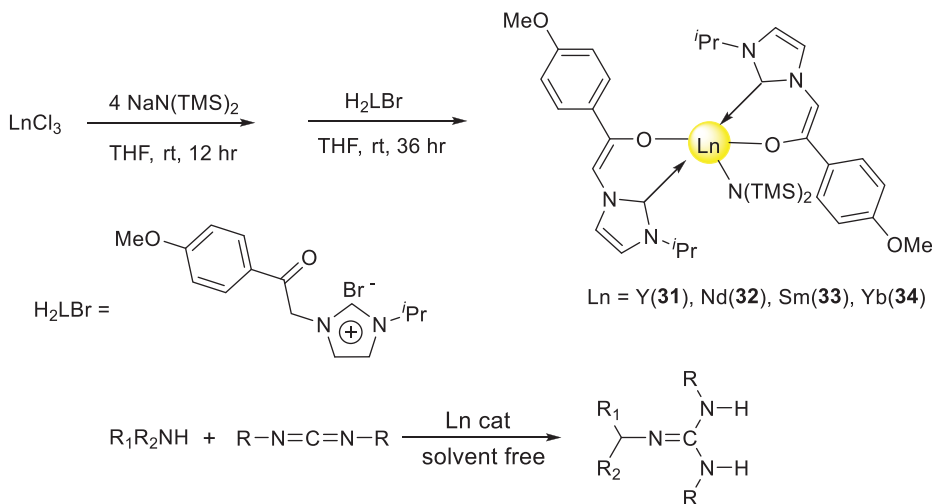
Figure 4.11: Synthesis of enol functionalized NHC-Ln amide complexes.
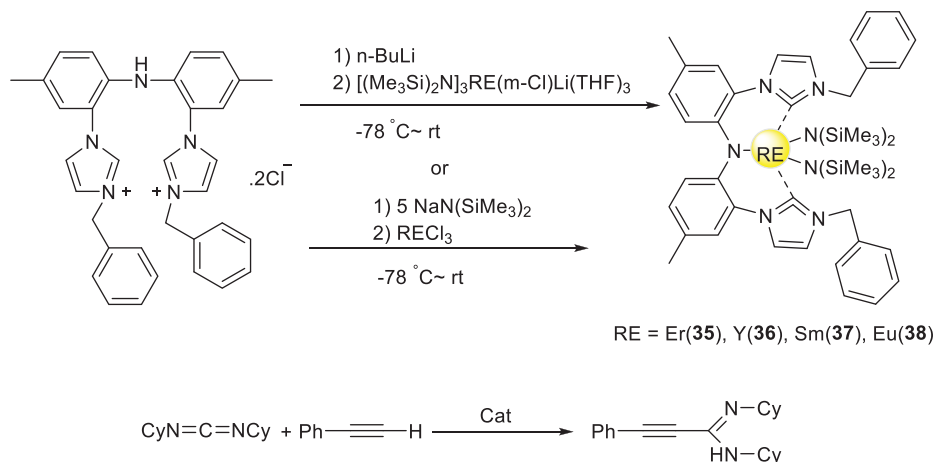
Figure 4.12: Synthesis of diarylamido-linked bis(NHC) rare earth metal amides.

4.4 Silane-amine addition using LREE-NHC complexes

Sadow et al. [33] successfully synthesized the divalent dialkyl ligated Sm and Yb complexes. The homoleptic Sm complexes achieved by the treatment of samarium (II) iodine with $KC(SiHMe_2)_3$(2 equiv) in THF solvent system over 12 hr at rt. Under this condition diamagnetic Yb complexes were formed. The paramagnetic center of Sm(II) confirmed by the NMR and IR spectroscopic analysis at the same time the Sm(II) with B $(C_6F_5)_3$(1 or 2 equiv) provided the zwitterionic hydridoborate compounds. The changes observed in the IR, ^{11}B and ^{19}F NMR spectra evidence the paramagnetic behavior of Sm II complexes. The cross-dehydrocoupling reactions of organo silane and amines are examined by the distinct structure of three coordinated Sm and Yb dialkyl complexes. The complexes are prepared by the reaction of **39** and **40** precursors with NHC ligands (1,3-di-tert-butylimidazol-2-ylidene(Im^{t}Bu) produced monoadducts of Yb and Sm (4a and 4b) complexes by the displacement of THF ligands. In the samarium complexes, both alkyl ligands contain 3c–2e Sm←H−Si structures versus alkyl ligands of ytterbium compounds that contain diagnostic and secondary interactions (Figure 4.13).

4.5 Carbon dioxide and heteroallene activation using LREE-NHC complexes

Arnold et al. [34] described the well-known bidentate *ortho*-aryloxide-NHC ligand with lanthanum complexes. The reactions of *ortho*-aryloxide NHC pro-ligand with $KN(SiMe_3)_2$
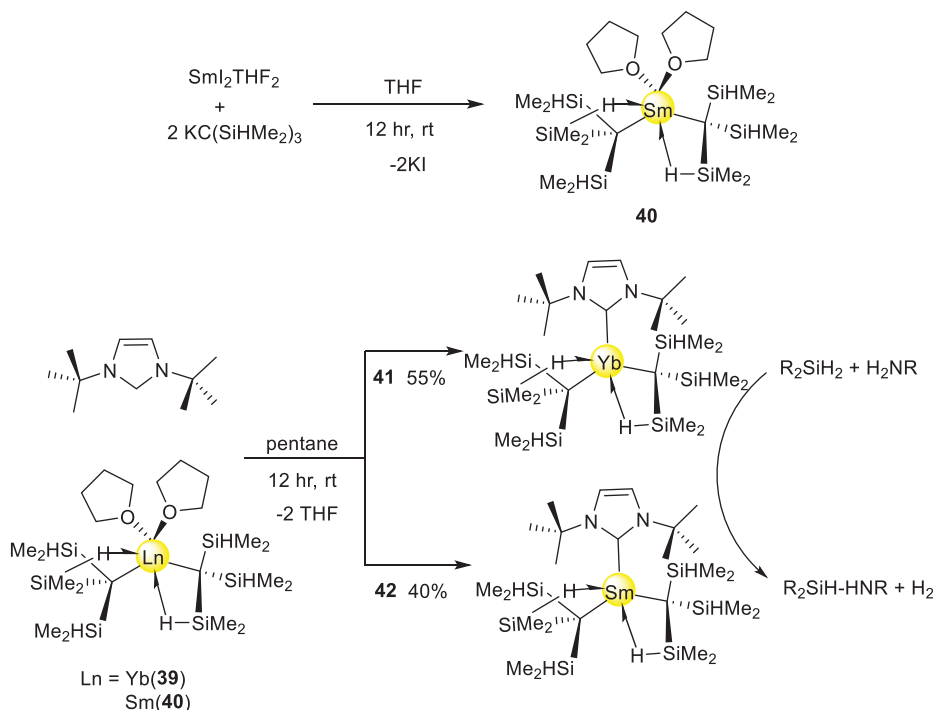
Figure 4.13: Synthesis of rare earth bis(alkyl) compounds.

and $LnCl_3(THF)_n$ (Ln = Ce, Sm, Eu) resulted in the formation of complexes. Cerium complexes react quantitatively with carbon dioxide to produce $Ce(LR.CO_2)_3$ complexes. CO insertion occurs solely through three cerium carbene bonds. The CO_2-insertion products are formed at room temperature, but only the mesityl substituted $Ce(LMes)_3$ complex is reversible due to the steric environment. $Ce(LMes.CO_2)_3$ is an active catalyst in the transformation of propylene oxide to propylene carbonate. A study of $Ce(LR)_3$'s ability to insert a CO_2 isoelectronic species of heteroallenes revealed that selectivity is affected by solvent and ligand size. Finally, the authors reported that this catalysis requires the combination of Lewis base–acid type of NHC-CO and Ce-epoxide activation (Figure 4.14).

4.6 Dihydrogen activation using LREE-NHC complexes

Using homoleptic rare earth aryl hydroxides with NHCs, Xu et al. [35] investigated cooperative hydrogen activation and catalytic hydrogenation. Under the 1 bar of H_2, the Lewis pairs of RE/NHC are converted to aminals via reductive hydrogenation. Further, they also investigated the catalytic hydrogenation with a frustrated Lewis pair of La/NHC
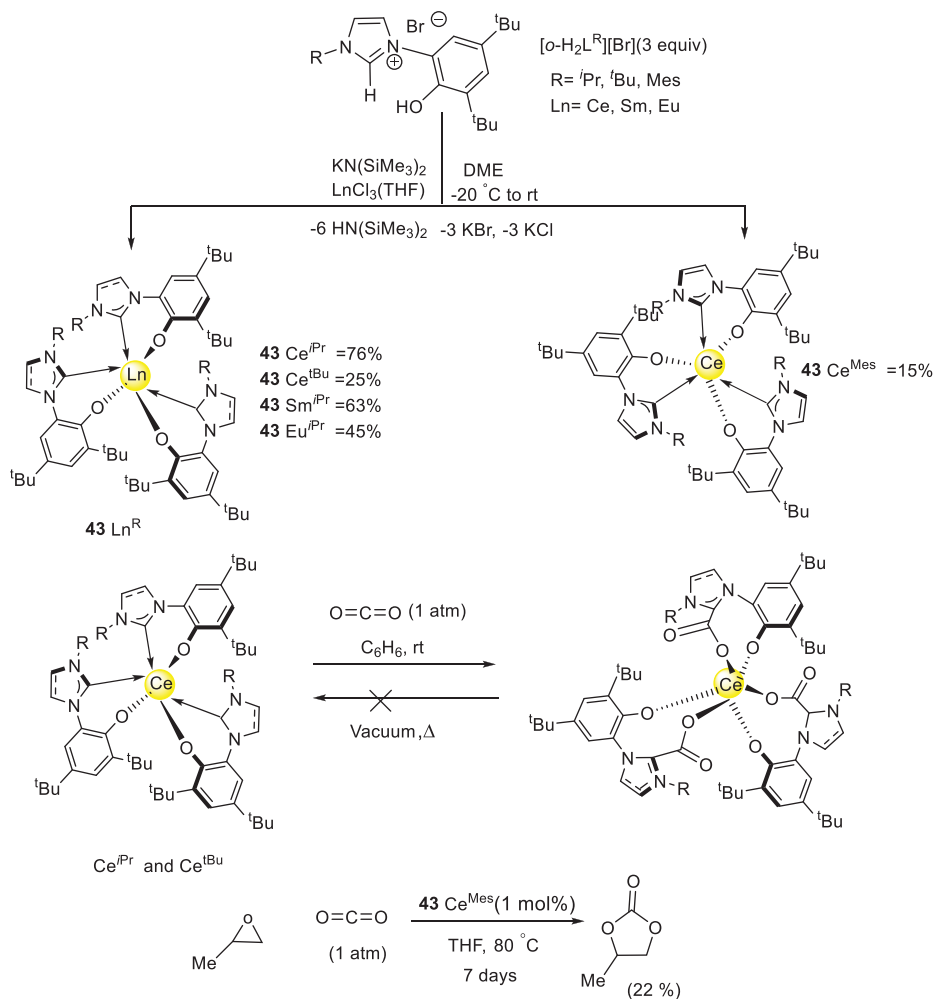
Figure 4.14: Synthesis of Ce-NHC complexes and their catalytic activity.

the products of 1, 2 addition and deprotonation from carbon monoxide and phenyl acety-lene (Figure 4.15).

4.7 Hydrophosphination using LREE-NHC complexes

Trifonov et al. [36] reported metal bis(amido) analogues of complexes ligated by NHC ligands [M = Ca, Yb, Sm]. Complexes were thus synthesized by reacting $[(Me_3Si)_2 N]_2 M$ $(NHC)_2$ with NHC ligands (2 equiv) at room temperature. Stable bis(amido) complexes with NHCs, as well as complexes of 4,5 M, were discovered to be active catalysts for

the intermolecular hydrophosphination of PH_3 with styrene, 2-vinyl pyridine, and phenyl acetylene. Styrene addition to PH_3 in various ratios produced selectively regio and chemo products of primary, secondary, and tertiary phosphines with high yields. At the same time, the catalytic activity of the pre catalyst is excellent due to metal ion Lewis base coordination. The hydrophosphination of 2-vinyl pyridine and phenyl acetylene with PH_3 catalyzed by metal complexes yields *tris*(2-(pyridin-2-yl)ethyl)phosphine and tertiary *tris*-(*Z*-styryl)phosphine (Figure 4.16).
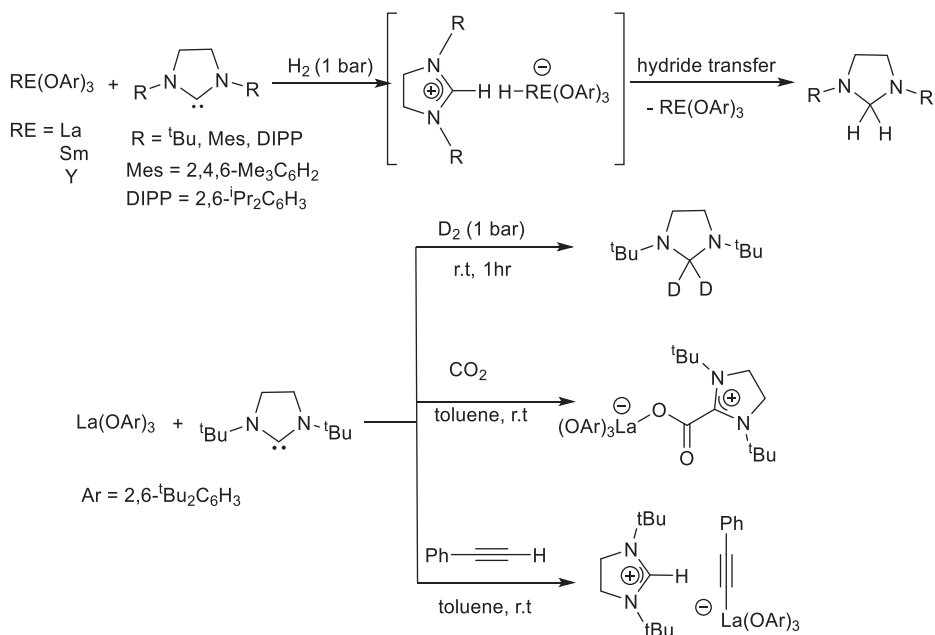
Figure 4.15: Reactions of La-NHC FLP with various substituents.
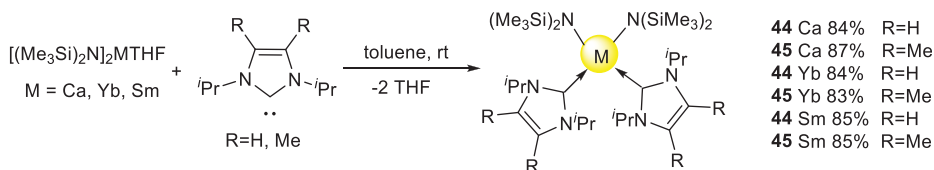
Figure 4.16: Synthesis of metal bis(amido) complexes ligated by NHC ligands.

Trifonov and coworkers [37] are the pioneers for synthesis of expanded ring *N*-heterocyclic carbene with Ln(II) amido complexes. Authors reported the synthetic way of Sm and Yb complexes and the catalytic activity of olefin hydrophosphination. The reaction of six-membered NHC ligand with $Ln[N(SiMe_3)_2]_2$ (Ln = Sm, Yb) in toluene at rt delivered the Ln(II) bis-amido complexes. Hydrophosphination of alkenes, especially styrene
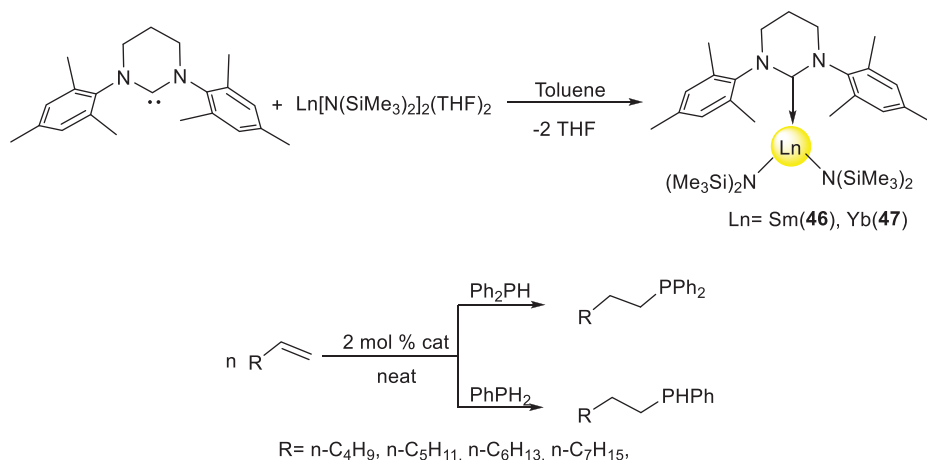
Figure 4.17: Synthesis of Ln(II) amido-NHC complexes and their activity of hydrophosphination.

with $PhPH_2$ and Ph_2PH, produced high regioselective anti-Markovniko addition products and chemo selective secondary and tertiary phosphines quantitatively. Under mild condition, Sm(II) complex act as pre-catalyst and leads to the intermolecular hydrophosphination products of 1-alkene, cyclohexene, and norbornene in an excellent manner (Figure 4.17).

Trifonov et al. [38] synthesized several NHC-stabilized amido compounds and demonstrated the NHCs' catalytic activity as a function of σ-donor capacity. The author investigated the hydrophosphination of $PhPH_2$ and PH_3 with alkenes in low catalyst loading under mild reaction conditions. In addition to PH_3 and styrene, complexes with electron-donating NHCs are the most efficient pre catalysts (Figure 4.18). When compared to other Ln(II) and Ca(II) complexes, excellent activity was achieved using three coordinated complexes $(NHC)_2Sm[N(SiMe_3)_2]$ [NHC-1,3-diisopropyl-2H-imidazol-2-ylidene] (**52Sm)**. Chemoselectively, anti-Markovnikov addition products with 98% conversion from $PhPH_2$ to *cis*-stilbene and norborene were obtained. The rate equation for hydrophosphination described by the kinetic study of the (**52Sm)** complex is rate = k[styrene]^1[52 Sm]^1 (Figure 4.19).

4.8 Conclusions

In conclusion, we discussed current developments in the synthesis of N-heterocyclic carbene fused light rare earth metal complexes as well as the effectiveness of these complexes as catalysts. Transition metal complexes with the NHC ligand system have many well-documented applications in catalysis. LREE-based NHC complexes are less studied in catalytic applications than transition metal complexes with NHC ligand

nNHC	Complex	Yield
n = 1	**48** Yb	87%
	48 Sm	88%
	49 Yb	86%
	49 Sm	87%
	50 Yb	85%
	50 Sm	84%
	51 Yb	79%
	51 Sm	81%
n = 2	**52** Yb	83%
	52 Sm	85%
	52 Ca	84%
	53 Yb	84%
	53 Sm	85%
	53 Ca	87%

dmp = 2,6-$Me_2C_6H_3$
dipp = 2,6-$^iPr_2C_6H_3$
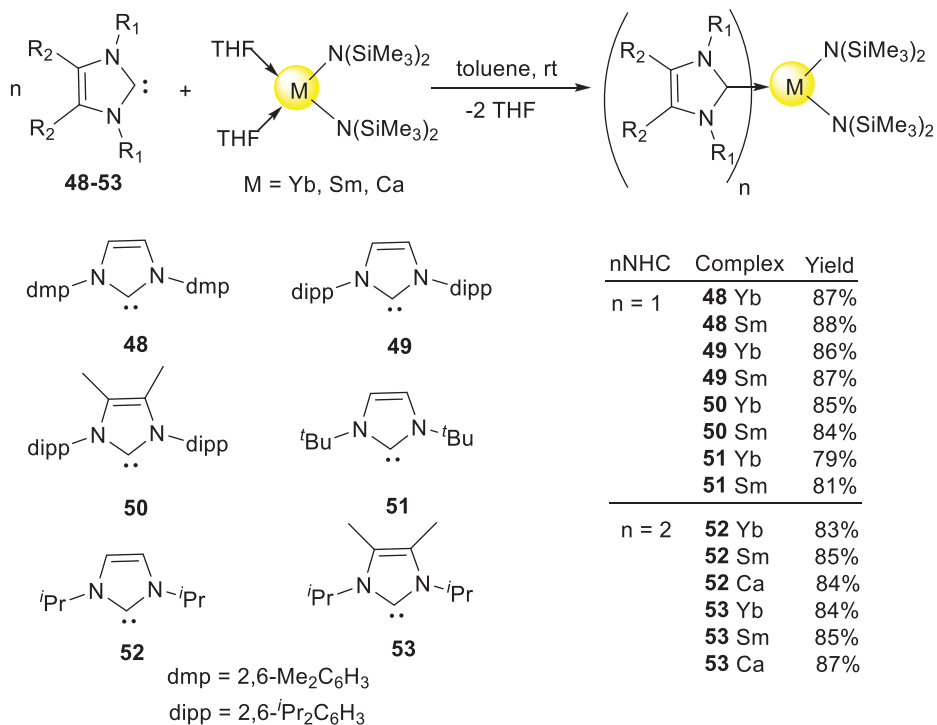
Figure 4.18: Synthesis of various NHC-stabilized amido compounds.
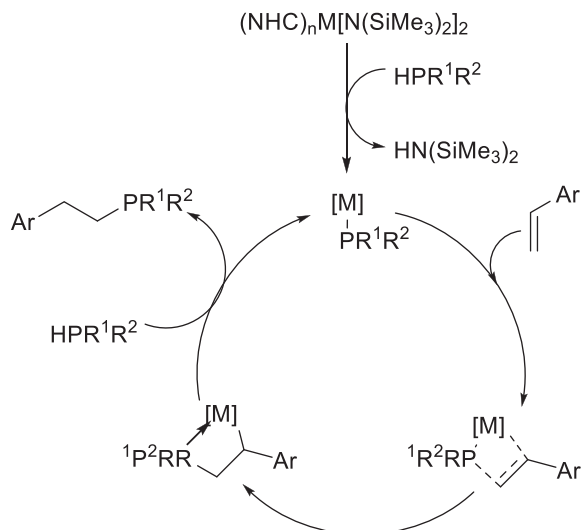
Figure 4.19: The proposed mechanism of hydrophosphination.

systems. Thus, N-heterocyclic carbene ligated light rare earth metal complexes have gained significant importance in the field of catalysis with various organic transformations in recent years. The metal ion–NHC ligand combination exhibits Lewis acid–base behavior, which promotes a number of functional group transitions. The activity of complexes is improved by the more electropositive character of the metal, lanthanide contraction, ionic radii, metal oxidation states, and highly substituted NHC ligand system. In particular, Ce(III)-NHC complexes effectively produce cyclic lactides and cyclic polyesters from rac-lactide, caprolactone, or butyrolactones; additionally various LRRE-NHC complexes produce various functionalized polymers using ROP technique. Further, catalytic activity of LREE NHC complexes was widely explored for the dihydrogen activation, addition reactions between the carbodiimide with amine, silane with amine, activation of CO_2, and hydrophosphination reactions. Except for praseodymium (Pr) and promethium (Pm), the synthesis and catalytic activity of LREE with various NHC ligands have been judiciously investigated. There is therefore room for these underutilized metals with NHC-based ligands in contemporary organic synthesis and environmentally friendly catalysis.

References

[1]   Wanzlick, HW. Aspects of nucleophilic carbene chemistry. Angew Chem Internat Edit, 1962, 1, 75–80.
[2]   Wanzlick, HW, Schonherr, HJ. Direct synthesis of a mercury salt-carbene complex. Angew Chem Internat Edit, 1968, 7, 141–142.
[3]   Arduengo, AJ, Harlow, RL, Kline, M. A stable crystalline carbene. J Am Chem SOC, 1991, 113, 361–363.
[4]   Hahn, FE, Jahnke, MC. Heterocyclic carbenes: Synthesis and coordination chemistry. Angew Chem Internat Edit, 2008, 47, 3122–3172.
[5]   Díez-gonzález, S, Marion, N, Nolan, SP. N-heterocyclic carbenes in late transition metal catalysis. Cheme Rev, 2009, 109, 3612–3676.
[6]   Hopkinson, MN, Richter, C, Schedler, M, Glorius, F. An overview of N-heterocyclic carbenes. Nature, 2014, 510, 485–496.
[7]   Jacobsen, H, Correa, A, Poater, A, Costabile, C, Cavallo, L. Understanding the M (NHC) (NHC = N-heterocyclic carbene) bond. Coord. Cheme Rev, 2009, 253, 687–703.
[8]   Nelson, DJ, Nolan, SP. Quantifying and understanding the electronic properties of N-heterocyclic carbenes. Chem Soc Rev, 2013, 42, 6723–6753.
[9]   Nair, V, Bindu, S, Sreekumar, V. N-Heterocyclic carbenes: reagents, not just ligands. Angew Chem Internat Edit, 2004, 43, 5130–5135.
[10] Smith, CA, Narouz, MR, Lummis, PA, Singh, I, Nazemi, A, Li, CH, Crudden, CM. N-Heterocyclic carbenes in materials chemistry. Cheme Rev, 2019, 119, 4986–5056.
[11] Rayadurgam, J, Reddy, SR. Synthesis of D-ribose and D-galactose derived chiral ionic liquids as recyclable chiral solvent for michael addition reaction. Trends Carbohydr Res, 2015, 7, 60–67.
[12] Jayachandra, R, Reddy, SR. A remarkable chiral recognition of racemic Mosher's acid salt by naturally derived chiral ionic liquids using ^{19}F NMR spectroscopy. RSC Adv, 2016, 6, 39758–39761.
[13] Muthukuru, P, Krishnaraj, P, Rayadurgam, J, Reddy, SR. Naturally derived sugar-based ionic liquids: An emerging tool for sustainable organic synthesis and chiral recognition. New J Chem, 2021, 45, 20075–20090.

[14] Jayachandra, R, Reddy, SR, Lakshmipathy, R. D-Galactose based hydrophobic ionic liquid: A new adsorbent for the removal of Cd^{2+} ions from aqueous solution. Environ Prog Sustain Energy, 2019, 38, S139–S145.

[15] Jayachandra, R, Lakshmipathy, R, Reddy, SR. Hydrophobic D-galactose based ionic liquid for the sequestration of Pb^{2+} ions from aqueous solution. J Mol Liq, 2016, 219, 1172–1178.

[16] Garg, P, Reddy, SR. Biomass-derived sugar ionic liquid as a sustainable organocatalyst: An efficient synthesis of functionalized dihydropyrano coumarins. Asian J Org Chem, 2022, 11, e202200322.

[17] Ogba, OM, Warner, NC, O'Leary, DJ, Grubbs, RH. Recent advances in ruthenium-based olefin metathesis. Chem Soc Rev, 2018, 47, 4510–4544.

[18] Fortman, GC, Nolan, SP. N-Heterocyclic carbene (NHC) ligands and palladium in homogeneous cross-coupling catalysis: A perfect union. Chem Soc Rev, 2011, 40, 5151–5169.

[19] Gao, P, Sipos, G, Foster, D, Dorta, R. Developing NHC-iridium catalysts for the highly efficient enantioselective intramolecular hydroamination reaction. ACS Catal, 2017, 7, 6060–6064.

[20] Wang, N, Xu, J, Lee, JK. The importance of N-heterocyclic carbene basicity in organo catalysis. Org Biomol Chem, 2018, 16, 8230–8244.

[21] Doddi, A, Peters, M, Tamm, M. N-heterocyclic carbene adducts of main group elements and their use as ligands in transition metal chemistry. Cheme Rev, 2019, 119, 6994–7112.

[22] Montgomery, TP, Johns, AM, Grubbs, RH. Recent advancements in stereoselective olefin metathesis using ruthenium catalysts. Catalysts, 2017, 7, 87.

[23] Schumann, H, Glanz, M, Winterfeld, J, Hemling, H, Kuhn, N, Kratz, T. Organo lanthanoid-carbene-adducts. Angew Chem Int Ed Engl, 1994, 33, 1733–1734.

[24] Arduengo, AJ, Tamm, M, McLain, SJ, Calabrese, JC, Davidson, F, Marshall, WJ. Carbene-lanthanide complexes. J Am Chem Soc, 1994, 116, 7927–7928.

[25] Lv, K, Cui, D. CCC-Pincer Bis(carbene) lanthanide dibromides. Catalysis on Highly cis-1,4-selective polymerization of isoprene and active species. Organometallics, 2010, 29, 2987–2993.

[26] Zhang, S, Wu, N, Wu, Y. Highly Cis-1,4 selective polymerization of conjugated dienes catalyzed by N-heterocyclic carbene-ligated neodymium complexes. Chinese J Polym Sci, 2020, 38, 1305–1312.

[27] Zhang, M, Ni, X, Shen, Z. Synthesis of bimetallic Bis(phenolate) N-Heterocyclic carbene lanthanide complexes and their applications in the ring-opening polymerization of L-lactide. Organometallics, 2014, 33, 6861–6867.

[28] Zhang, M, Zhang, J, Ni, X, Shen, Z. Bis(phenolate) N-heterocyclic carbene rare earth metal complexes: Synthesis, characterization and applications in the polymerization of n-hexyl isocyanate. RSC Adv, 2015, 5, 83295–83303.

[29] Kerr, RWF, Ewing, PMDA, Raman, SK, Smith, AD, Williams, CK, Arnold, PL. Ultrarapid cerium(III)−NHC catalysts for high molar mass cyclic polylactide. ACS Catal, 2021, 11, 1563–1569.

[30] Pan, Z, Gao, D, Zhang, C, Guo, L, Li, J, Cui, C. Synthesis and reactivity of N-heterocyclic carbene stabilized lanthanide(II) Bis(amido) complexes. Organometallics, 2021, 40, 1728–1734.

[31] Li, Z, Xue, M, Yao, H, Sun, H, Zhang, Y, Shen, Q. Enol-functionalized N-heterocyclic carbene lanthanide amide complexes: Synthesis, molecular structures and catalytic activity for addition of amines to carbodiimides. J Organomet Chem, 2012, 713, 27–34.

[32] Gu, X, Zhu, X, Wei, Y, Wang, S, Zhou, S, Zhang, G, Mu, X. CNC-pincer rare-earth metal amido complexes with a diarylamido linked biscarbene ligand: synthesis, characterization, and catalytic activity. Organometallics, 2014, 33, 2372–2379.

[33] Pindwal, A, Ellern, A, Sadow, AD. Homoleptic divalent dialkyl lanthanide-catalyzed cross-dehydrocoupling of silanes and amines. Organometallics, 2016, 35, 1674–1683.

[34] Arnold, PL, Kerr, RWF, Weetman, C, Docherty, SR, Rieb, J, Wang, K, Jandl, C, McMullon, MW, Pothig, A, Kuhn, FE, Smith, AD. Selective and catalytic carbon dioxide and heteroallene activation mediated by cerium N-heterocyclic carbene complexes. Chem Sci, 2018, 9, 8035–8045.

[35] Chang, K, Dong, Y, Xu, X. Dihydrogen activation by intermolecular rare-earth aryloxide/N-heterocyclic carbene Lewis pairs. Chem Commun, 2019, 55, 12777–12780.

[36] Trifonov, A, Lapshin, I, Basalov, I, Lyssenko, K, Cherkasov, A. Ca(II), Yb(II) and Sm(II) bis(Amido) complexes coordinated by NHC ligands – efficient catalysts for highly regio and chemoselective consecutive hydrophosphinations with PH_3. Chem Eur J, 2019, 25, 459–463.

[37] Lapshin, IV, Cherkasov, AV, Asachenko, AF, Trifonov, A. Ln(II) amido complexes coordinated by ring expanded N-heterocyclic carbenes – Promising catalysts for olefin hydrophosphination. Chem Commun, 2020, 56, 12913–12916.

[38] Lapshin, IV, Cherkasov, AV, Lyssenko, KA, Fukin, GK, Trifonov, A. N-Heterocyclic carbene-coordinated M(II) (M = Yb, Sm, Ca) Bisamides: Expanding the limits of intermolecular alkene hydrophosphination. Inorg Chem, 2022, 61, 9147–9161.

Yadavalli Venkata Durga Nageswar*, Katla Ramesh and Katla Rakhi

5 Lanthanum triflate–assisted organic transformations: a decade update

5.1 Introduction

The last two decades have witnessed faster growth in the application of rare earth metal triflouromethane sulfonates (triflates) [RE(OTf)$_3$] for a wide range of organic transformations. Lanthanides, scandium, and yttrium are in combination called rare earth elements. Due to the unique properties exhibited by lanthanide triflates (Ln(OTf)$_3$), these have attracted widespread attention among researchers across the world. Ln(OTf)$_3$ (Ln = La, Ce, Pr, Nd, Sm, Eu, Gd, Tb, Dy, Ho, Er, Tm, Yb, Lu) have proved to be promising, powerful, mild, and selective Lewis acid catalysts and have been employed in a number of synthetic reactions. Moreover, these Lewis acid catalysts often displayed high chemo- and regio-selectivity in many difficult protocols. Lanthanide triflates are cost-effective, less toxic, recyclable, and water-tolerant. Stability and oxophilicity are the salient features of these eco-friendly catalysts. Compared to conventional Lewis acids such as AlCl$_3$, BF$_3$, and SnCl$_4$, which are decomposed or deactivated in the presence of water, lanthanide triflates have been employed safely even in aqueous medium for a variety of organic reactions with a significant functional group tolerance. These new type of triflate catalysts can be easily prepared from the corresponding metal oxides or chlorides by heating in aqueous trifluoromethanesulfonic acid solutions.

In 1987, Forsberg and co-researchers employed lanthanide(III) ions as efficient catalysts in the reaction between nitriles and amines [1]. Pioneering research work of Kobayashi's research group [2–4] on lanthanide triflates as potential Lewis acid catalysts is significant, and has attracted widespread attention. Many research groups are fostering their applications in a number of chemical processes in aqueous as well as other protic media. Lanthanide triflates have been used as Lewis acid catalysts successfully in several reactions like allylation [5–8], Friedel Crafts [9–11], Diels Alder [12–14], Michael [15], and Mukaiyama aldol reactions [16, 17]. Furthermore, these have been efficiently used as catalysts even for biomass conversions [18–20]. Hitherto, many reviews have

*__Corresponding author: Yadavalli Venkata Durga Nageswar__, Retired Chief Scientist, Indian Institute of Chemical Technology-IICT, Tarnaka, Hyderabad, India, e-mail: dryvdnageswar@gmail.com
Katla Ramesh, Organic Chemistry Laboratory-4, School of Chemistry and Food, Federal University of Rio Grande-FURG, Rio Grande, RS, Brazil
Katla Rakhi, Organic Catalysis and Biocatalysis Laboratory – LACOB, Federal University of Grande Dourados-UFGD, Dourados/MS, Brazil

been published on the catalytic applications of lanthanide triflates [21–25]. This review on lanthanum triflate–assisted organic reactions showcases the important research works reported during the last ten years.

5.2 Lanthanum triflate–assisted organic transformations

5.2.1 Mukaiyama aldol reaction

Meshram and co-authors [26] communicated an efficient diastereoselective Mukaiyama aldol reaction of 2-(trimethylsilyloxy) furan (**2**) with various (*N*-alkyl)isatins (**1**) promoted by 5 mol% lanthanumtriflate providing 3-hydroxy-(5-oxo-2,5-dihydro-furan-2yl)-indolin-2-ones (**3/3a**) in encouraging yields (Figure 5.1).

R = H, Me, Et, Ph, CH$_2$Ph
R^1 = F, Cl, Br, CH$_3$, OCH$_3$, NO$_2$

19 entries, 80-93%
(Threo:Erythro) up to <95:5
Unseparable diastereomers
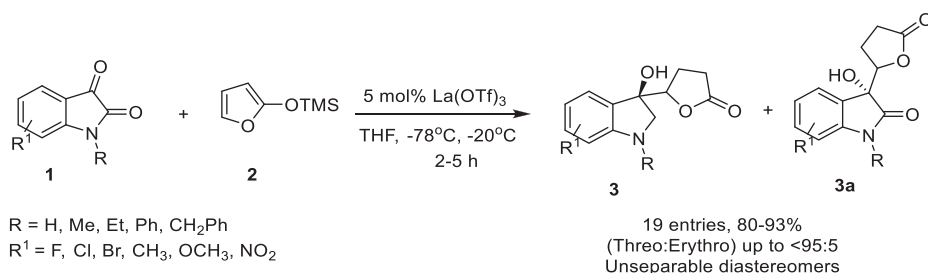
Figure 5.1: La(OTf)$_3$-assisted vinylogous Mukaiyama aldol reactions.

5.2.2 Synthesis of pyrrolo[3,2*f*]- and pyrrolo[2,3*h*]quinoline derivatives

Nagarajan and Ramesh [27] prepared a wide range of pyrrolo[3,2 *f*]- and pyrrolo[2,3*h*]quinoline (**4**) derivatives in high yields from substituted 5-aminoindoles (**5**), benzaldehydes (**6**) and phenylacetylenes (**7**) by an efficient simple one-pot process through an unexpected mechanistic pathway (Figure 5.2a–c). Lanthanum triflate was employed as a catalyst. During optimization PdCl$_2$, Pd(OAC)$_2$, CuI, AgOTf, Ag$_2$CO$_3$, InCl$_3$, In(OTf)$_3$, Cu(OTf)$_2$, TEMPO, AIBN, and La(OTf)$_3$ were screened as catalysts to check for their efficiencies. Solvents like EtOH, CH$_2$Cl$_2$, THF, DMF, DMSO, and toluene as well as solvent-free conditions were examined. Scope of the reaction was extended to include various aromatic aldehydes (**6**), phenyl acetylenes (**7**), and 5-aminoindoles (**5**). Ionic liquid [Bmim][BF$_4$] provided the best results.

(a)

5

7

6

10 mol% La(OTf)$_3$

[Bmim] BF$_4$

R^1 = H, Me
R^2,R^3,R^4 = Me
R^2, R^4 = H. R^3 = Cl
R^4 = H, F, Cl, Br, Me, OMe

4

A
8 entries, 42-50%

4a

B
8 entries, 23-28%

(b)

5

7

6

PhCHO

10 mol% La(OTf)$_3$

[Bmim] BF$_4$

R^1 = H, Me
R^2 = H,Me, OMe

8

A
4 entries, 46-52%

8a

B
4 entries, 26-27%

(c)

5

6

7

PhCHO

10 mol% La(OTf)$_3$

[Bmim] BF$_4$

R^1, R^2, R^3 = Me, R^4 = H
R^1 = Et, R^2/ R^3 = Me, R^4 = H
R^1 = Bn, R^2/ R^3 = Me, R^4 = H
R^1 = H, R^2/ R^3 = Me, R^4 = H
R^1 = SO$_2$Ph, R^2/ R^3 = Me, R^4 = H
R^1 = H, R^2/ R^3 = Me, R^4 = Cl

9

A
6 entries, 42-50%

9a

B
6 entries, 22-27%
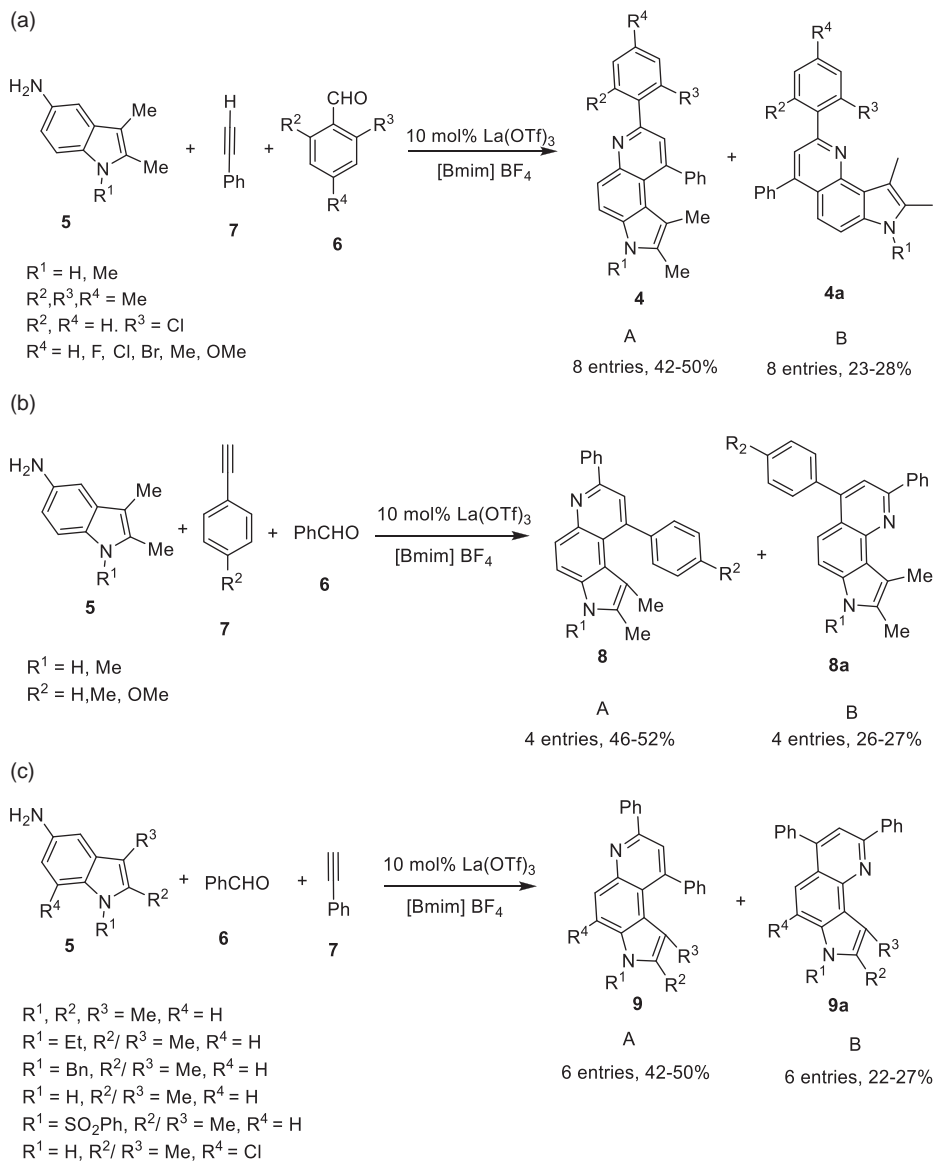
Figure 5.2: (a) Reactions with various aldehydes in the presence of [Bmim][BF$_4$]. (b) Reactions with different phenyl acetylenes in the presence of [Bmim][BF$_4$]. (c) Reactions with various amino indoles in the presence of [Bmim][BF$_4$].

5.2.3 Synthesis of cis-1,4-benzoxazines and 1,2,3,4-tetrahydroquinoxaline derivatives

Liu and co-researchers [28] established a novel, concise, and economical Domino synthetic process for benzo-1,4-heterocycle derivatives from 2-furyl carbinols and *o*-amino phenols via a Piancatelli/C–N-coupling/Michael addition protocol, having a broad substrate scope, assisted by La(OTf)$_3$ (Figure 5.3a and b). In the initial investigation the authors examined the catalytic efficiencies of a number of Lewis acids and Bronsted acids such as Sc(OTf)$_3$, Yb(OTf)$_3$, La(OTf)$_3$, TsOH, pentaflourobenzoic acid, Cu(OTf)$_3$, FeCl$_3$, TiCl$_4$, La(Pfb)$_3$, Yb(Pfb)$_3$, and Sc(Pfb)$_3$. Among all, the rare earth salts, FeCl$_3$, TsOH, exhibited good activity, but the rare earth pentafluorobenzoates proved to be less effective. It was observed that 5 mol% La(OTf)$_3$ in CH$_3$CN at 80 °C was ideal for the methodology. A large library of biologically relevant 1,4-benzoxazine (**10**) and 1,2,3,4-tetrahydroquinoxaline (**11**) compounds were prepared utilizing the process.

(a)

R^1 = Ph, 4-OMe-C$_6$H$_4$, 4-CF$_3$-C$_6$H$_4$
4-F-C$_6$H$_4$, Et, n-bn, R^2 = H, Cl, Me, tBu, NO$_2$

23 entries, 10–92%

(b)

R^1 = H, Ph, Et, 4-OMe-C$_6$H$_4$,
4-F-C$_6$H$_4$, R^2 = Ac, Ts, Ms

8 entries, 45–88%.
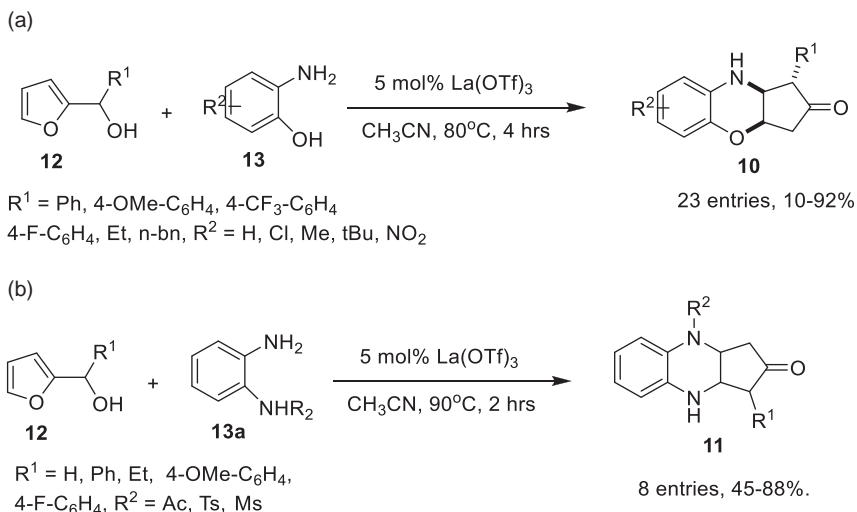
Figure 5.3: (a) Domino synthesis of *cis*-1,4-benzoxazine derivatives. (b) Domino synthesis of 1,2,3,4-tetrahydroquinoxaline derivatives.

5.2.4 Synthesis of tetrahydroquinazolinones

Jardosh and Patel [29] established a one-pot synthesis of tetrahydroquinazolinone (**14**) derivatives by the cyclo-condensation of cyclic β-diketones (**15**), *N*-allylquinolones (**16**), and thiourea/*N*-phenylthiourea (**17/17a**) catalyzed by lanthanum triflate at room temperature in the presence of ethanol (Figure 5.4). These compounds were screened for antimicrobial activity.
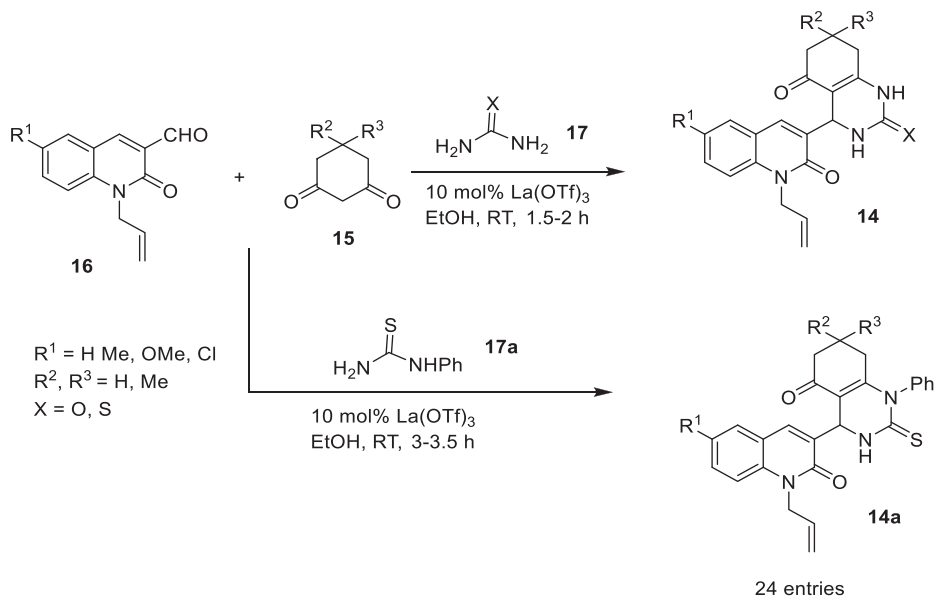
Figure 5.4: Preparation of tetrahydroquinazolinones.

5.2.5 Synthesis of β-phosphonomalonates

Sobhani and Pakdin-Parizi [30] developed easily separable, new magnetically recyclable heterogeneous Lewis acid-lanthanum(III)triflate supported on nanomagnetic γ-Fe$_2$O$_3$ and characterized using XRD, FT-IR, ICP, TGA, VSM, and HRTEM. This was successfully applied for an eco-friendly one-pot synthesis of β-phosphonomalonates (**18**), from aliphatic/aromatic/heterocyclic aldehydes (**6**), malononitrile (**19**), and triethyl phosphite (**20**) under solvent-free conditions at room temperature. The protocol proceeds via tandem Knoevenagel-phospha-Michael reaction (Figure 5.5). The authors prepared Schiff base supported γ-Fe$_2$O$_3$@SiO$_2$ from γ-Fe$_2$Co$_3$ MNPS, which were synthesized by the chemical co-precipitation technique. γ-Fe$_2$O$_3$ MNPS was reacted with tetraethyl orthosilicate (**21**) to provide γ-Fe$_2$O$_3$@SiO$_2$. It was further functionalized on the surface with 3-aminopropyltriethoxysilane (**22**) followed by the condensation with salicylaldehyde (**6a**) resulting in γ-Fe$_2$O$_3$@SiO$_2$-L which was allowed to react with La(OTf)$_3$ to obtain[γ-Fe$_2$O$_3$@SiO$_2$La(OTf)$_3$]-the final newly developed catalyst. During optimization studies various catalysts like γ-Fe$_2$O$_3$, La(OTf)$_3$, γ-Fe$_2$O$_3$@SiO$_2$-La(OTf)$_2$, and aminopropylated γ-Fe$_2$O$_3$@SiO$_2$ were examined for their efficacies. Solvents such as H$_2$O, EtOH, CHCl$_3$, toluene, and solvent-free conditions were investigated for best results. The authors have used alkyl, aryl, and heteroarylaldehydes (**6**) in the protocol with success. Significant loss of catalytic activity was not observed even after five runs. The catalyst was easily isolated with the assistance of an external magnet.

R^1 = H, 2-Cl, 3-Cl, 4-Cl, 3Br, 4-Br, 4-Me, 3-OMe, 4-OMe, 4-OH,

R = CH_3-$(CH_2)_2$-, CH_3-$(CH_2)_5$,
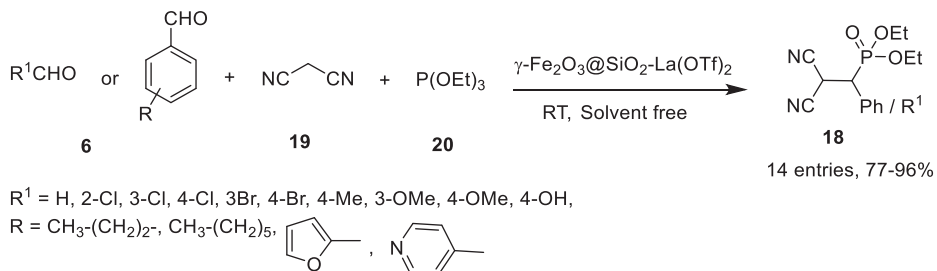
Figure 5.5: γ-Fe_2O_3@SiO_2-La(OTf)$_2$-assisted preparation of β-phosphonomalonates.

5.2.6 Sommelet reaction

Xu and Su [31] disclosed an improved Sommelet reaction from benzyl halides (**23**) and hexamethylenetetramine (HMT) (**24**) yielding aryl aldehydes (**25**) employing La(OTf)$_3$ as catalyst in aqueous medium with sodium dodecyl sulfate (SDS) as solubilizer (Figure 5.6a–c). During optimization studies the authors examined the efficiencies of different catalysts like Zn(OTf)$_2$, Mg(OTf)$_2$, Cu(OTf)$_2$, Bi(OTf)$_3$, Yb(OTf)$_3$, Y(OTf)$_3$, and La (OTf)$_3$. Several surfactants such as PEG-400, CTAB, CAB-35, Triton-X-100, and SDS were investigated for their suitability protocol. The authors observed that HMT (0.5 mol), La(OTf)$_3$ (0.03 mmol), and SDS (2 wt%) in water medium at 100 °C are ideal conditions for 1 mmol of benzylhalide (**23**) derivative. The methodology was extended to a wide range of benzyl halides (**23**). It was noted that the compounds with electron-donating groups provided better yields than those with electron-withdrawing groups. Various biphenyl-4-carboxaldehydes (**26**) were also made from the corresponding diphenyl-4-methyl bromides (**27**) following this protocol.

5.2.7 Aldol reaction

Sasaki and co-authors [32] described the preparation of α,α-difluoro-β-OH-ketones (**29**) by the aldol reaction between carbonyl compounds (**30**) and difluoroenol-*o*-Boc (tertiary butyloxy carbonyl)esters (**31**) catalyzed by La(OTf)$_3$ (Figure 5.7–c). In the initial studies, Cu(OTf)$_2$, TiCl$_4$, Sn(OTf)$_2$, and La(OTf)$_3$ were examined for their efficiencies as catalysts. DCM and DCE were tested for their suitability as solvents for the reaction. The scope of the methodology was extended to include different difluoroenol-*o*-Boc esters (**31**) and several aliphatic/aromatic/heterocyclic aldehydes/ketones (**6**) in the reactions.

(a)
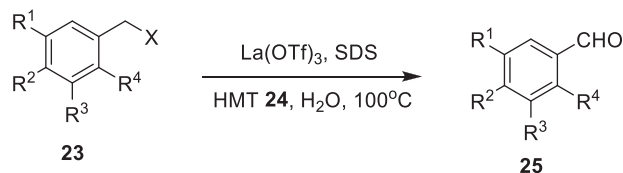
R^1 = H, Me, R^2 = H, Me, OMe, Br,
I, NO_2, CO_2H, R^3 = H, Me, R^4 = H, NO_2
X = Cl, Br, I

14 entries, 72-92%

(b)

R= CN, CO_2Et, Ph_3C
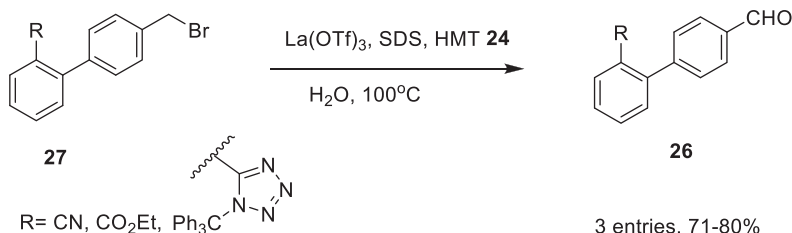
3 entries, 71-80%

(c)
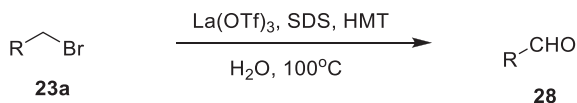
R = 2- napthyl, n-butyl, Allyl

3 entries, 10-94%

Figure 5.6: (a) Sommelet reaction of benzyl halides assisted by La(OTf)$_3$/SDS. (b) Sommelet reaction assisted by La(OTf)$_3$/SDS. (c) Sommelet reaction promoted by La(OTf)$_3$/SDS.

5.2.8 Petasisborono-Mannich reaction

Reddy et al. [33] unveiled a new one-pot three-component Petasisborono-Mannich re-action producing a broad range of tertiary amine (**36**) derivatives from two different salicylaldehydes (**6**), 2-formyl pyridine (**37**), arylboronic acids (**38**), and substituted morpholines/piperidines (**39/39a**) catalyzed by reusable La(OTf)$_3$ under microwave ir-radiation conditions(Figure 5.8). The protocol was also checked under normal conven-tional method by conducting the reaction at 60 °C for 10–26 min in oil both. Several catalysts such as CuI, AgF, InF$_3$, FeCl$_3$, SiO$_2$, Pd(PPh$_3$)$_4$, PdCl$_2$, Pd(OAc)$_2$, Y(OAc)$_3$.H$_2$O, Yb(OAc)$_2$, Yb(OTf)$_3$,AgOTf, Sc(OTf)$_3$, and La(OTf)$_3$ were assessed for their efficiencies, for a model reaction between 3-formyl-4-OH benzoate (**40**), morpholine (**39**), and 2-chlorophenyl

(a)

R^1 = 4-OMe-C$_6$H$_4$, 4-Me-C$_6$H$_4$, 4-Cl-C$_6$H$_4$,
4-F-C$_6$H$_4$, 4-*c*-C$_6$H$_{11}$, 1-adamantyl, 2-furyl
R^2 = 2-OMe-C$_6$H$_4$, 3-OMe-C$_6$H$_4$, 4-OMe-C$_6$H$_4$,
2-NO$_2$-C$_6$H$_4$, 3-NO$_2$-C$_6$H$_4$, 4-NO$_2$-C$_6$H$_4$, 2-furyl,
2-Thienyl, n-C$_6$H$_{13}$, n-C$_5$H$_9$, n-C$_6$H$_{11}$

(b)

(c)

Ph/Me, Ph/Et, Me/Me, -(CH$_2$)$_5$-
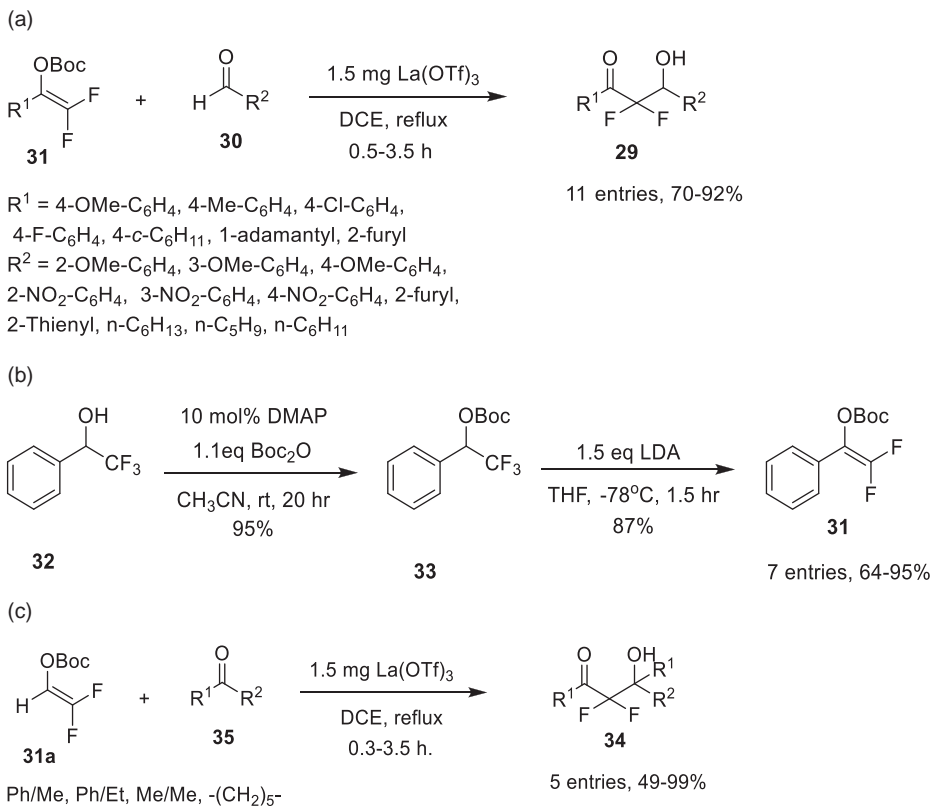
Figure 5.7: (a) Synthesis of α,α-difluoro-β-OH-ketones mediated by La(OTf)$_3$. (b) Preparation of difluoroenol *O*-Boc ester. (c) Synthesis of α,α-difluoro-β-OH-ketones.

benzoic acid (**41**). 1,4-Dioxane, EtOH, THF, toluene, MeOH, DCM, and CCl$_4$ were tested for a suitable solvent medium for the protocol. La(OTf)$_3$ was checked for the recyclability and observed that there is no significant loss of activity up to five consecutive cycles.

5.2.9 Synthesis of spiro[-indolo-3,10'-indeno[(1,2-*b*) quinolin]-2,4,11'-triones

Kumari and co-authors [34] developed an eco-friendly one-pot three-component methodology for the preparation of spiro[indolo-3,10-indeno[1,2-*b*]quinolin]-2,4,11′-triones (**43**) from isatins (**1**), enaminones (**44**), and 1,3-indanediones (**45**) in PEG-400 assisted by recyclable La(OTf)$_3$ catalyst in both conventional conditions and ultrasonic irradiation conditions (Figure 5.9). Reaction involves unusual ring opening of isatin (**1**) moiety followed by the recyclization.

R[1] = Me, Pr-n, Me, Ph,

R[2] = n-Bu, Ph,

R[1]/R[2] = 39, 39A

R[3] = C$_6$H$_5$, 2-Cl-C$_6$H$_4$ (**41**), 2-Me-C$_6$H$_4$, 3,4(OMe)$_2$ C$_6$H$_3$, 4-OMe-C$_6$H$_4$, 2-naphthyl, 2-thienyl

R =

40

37
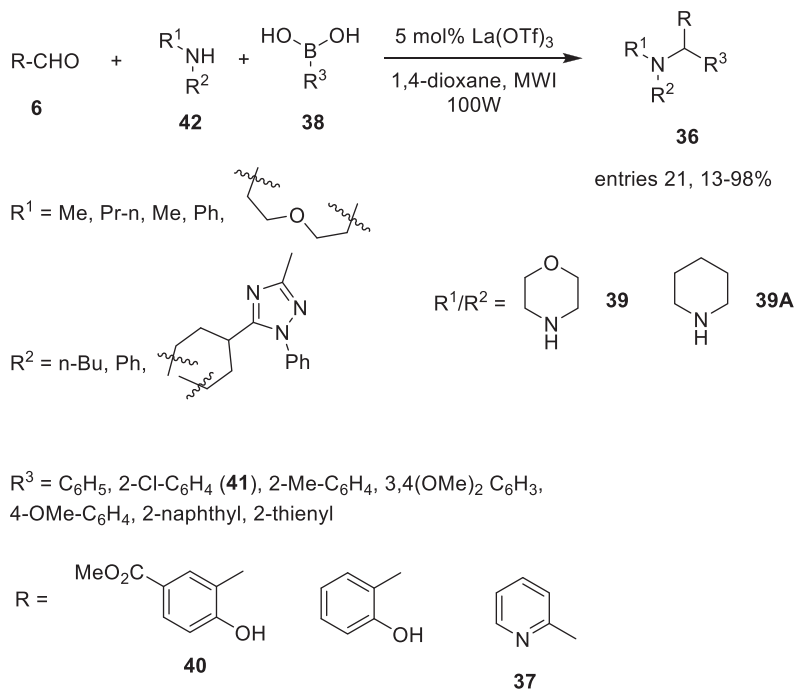
Figure 5.8: La(OTf)$_3$-catalyzed petasisborono-Mannich reaction.

R[1] = H, NO$_2$, R[2] = H, Me,
R[3] = Ph, Ph-CH$_2$, 4-Cl-C$_6$H$_4$, 4-Br-C$_6$H$_4$, 4-Me-C$_6$H$_4$,
4-OMe-C$_6$H$_4$, C$_4$H$_9$

Method A conventional
22 entries, 85-96%
Method B Ultrasonication
87-95%
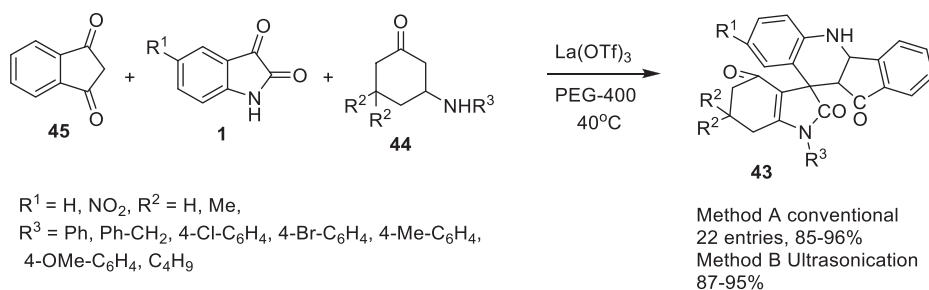
Figure 5.9: Synthesis of spiro[-indolo-3,10′-indeno[(1,2-b) quinolin]-2,4,11′-triones.

During optimization EtOH, MeOH, ethylene glycol, CH$_3$CN, PEG-400, and PEG-600 were tested for a facilitating medium. CAN, FeCl$_3$, and La(OTf)$_3$ were examined for their catalytic activity toward the protocol. The recyclability of La(OTf)$_3$, PEG-400 system was observed to be ideal and is reusable up to six runs.

5.2.10 Construction of C-hydroxy diketopiperazine scaffolds

Wang et al. [35] discussed in their research paper a convenient and efficient construction of C-hydroxydiketopiperazine (**46**) scaffolds, under microwave conditions, catalyzed by reusable La(OTf)$_3$ (Figure 5.10). Several Lewis acids such as MgBr$_2$, Et$_2$O, MgCl$_2$, CaCl$_2$, as well as lanthanide triflates like La(OTf)$_3$, Ce(OTf)$_3$, Pr(OTf)$_3$, Nd(OTf)$_3$, Sm(OTf)$_3$, Eu(OTf)$_3$, Gd(OTf)$_3$, Tb(OTf)$_3$, Dy(OTf)$_3$, Ho(OTf)$_3$, Er(OTf)$_3$, Tm(OTf)$_3$, Yb(OTf)$_3$, and Lu (OTf)$_3$ were screened for their efficiencies. Among these La(OTf)$_3$ drastically reduced the reaction time. Authors concluded that diketone (**47**) scaffold binds to La(OTf)$_3$ under *Z*-configuration, followed by the nucleophilic attack of amide (**48**) under the TEA activation, affording the title products.
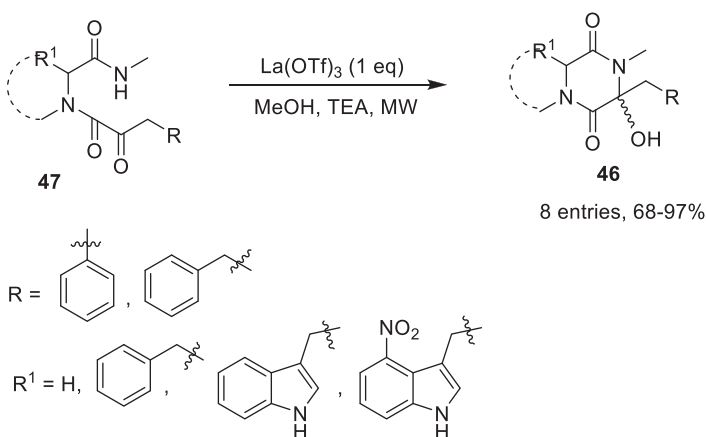
Figure 5.10: C-hydroxydiketopiperazine scaffolds.

5.2.11 Synthesis of 5-substituted-1 *H*-tetrazoles

Meshram and co-researchers [36] prepared 5-substituted-1 *H*-tetrazoles (**49**) by a facile and straight forward approach via (3 + 2) cycloaddition between aromatic/heterocyclic nitriles (**50**) and sodium azide (**51**) (Figure 5.11). Heterogeneous recyclable silica-supported lanthanum triflate [La(OTf)$_3$-SiO$_2$] was employed as a catalyst. In the initial studies, several silica supported Lewis acids like BiCl$_3$.SiO$_2$, SbCl$_3$.SiO$_2$, and Ln(OTf)$_3$.SiO$_2$ were examined, and it was observed that Ln(OTf)$_3$.SiO$_2$ in DMF-MeOH (4:1) at 100 °C was the most favorable reaction condition for the protocol producing title compounds in high yields. The catalyst retained the activity up to four cycles.
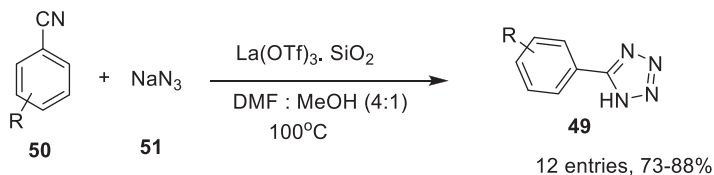
R = H, 4-Cl, 4-Br, 4-Me, 2-Me, 4-NO$_2$, 4-CHO, 4-OH, 2-OH,
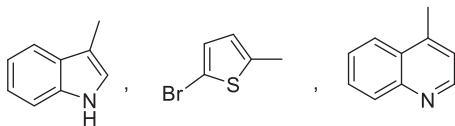
Figure 5.11: La(OTf)$_3$.SiO$_2$-promoted preparation of 5-substituted-1H-tetrazoles.

5.2.12 Synthesis of quaternary α-triflouromethyl-3-oxo-ester derivatives

Granados et al. [37] reported an efficient and highly enantioselective approach for the synthesis of quaternary α-triflouromethyl-3-oxo-ester (**52**) derivatives employing La(OTf)$_3$ and chiral Py-box-type-C$_2$-symmetrical ligands (Figure 5.12a–c). 5-(Triflouro-methyl) dibenzothio-pheniumtetraflouroborate (**53**) (Umemoto's reagent) and 1-triflouro methyl-1,2-benziodoxol-3(1H)-one(**54**) (Togni's reagent) were screened for their efficiencies. Togni's reagent afforded higher yields. Indanyl-Py-box ligand improved the reaction performance. The authors proposed the formation of reactive cationic iodonium species (**55**). The versatility of the process is its applicability to a broad range of cyclic β-ketoesters (**56**). It was observed that the size of the ester group strongly influenced the enantio control.

5.2.13 Nitration of alkyl aromatics

Ketike et al. [38] reported nitration of alkyl aromatics (**61**) promoted by lanthanum triflate anchored SBA-15 as an efficient eco-friendly recyclable catalyst under solvent-free conditions at 90 °C (Figure 5.13). The authors prepared diamine functionalized microporous silica (SBA-ED) by treating microporous silica (SBA-15) with *N*-[3-(trimethoxysilyl) propyl]-ethylene diamine (TPED) and then anchored it with La(OTf)$_3$ to obtain the catalyst SBA-ED-LT. It was characterized by XRD, FTIR, and TGA. Utilizing N$_2$-sorption data textural and structural parameters of the functionalized SBA-15 samples like SB-15, SBA-ED, SBA-EHD-LT were examined for their efficiencies. Reaction parameters like aromatic compound to HNO$_3$ ratio, amount of catalyst, reaction temperatures, and reaction times were optimized. No significant loss of activity was observed till five runs.

(a)

10 mol% La(OTf)$_3$

L$_3$ (12 mol%), -35°C
CH$_3$CN, 4 A°Ms
54 (1.2 equiv.)

57
n = 1, 2

52

14 entries, 65-85%
ee (53-99%)

R = CH$_3$, tBu, Bz, -CH (C(CH$_3$)$_2$, -CH (CH$_2$(CH$_3$)$_2$
R^1 = H, F, CF$_3$, OCH$_3$, C(CH$_3$)$_3$
R^2 = H, C(CH$_3$)$_3$, F, Br

(b)

58

L1

59

L2

60

L3

53

54

(c)

55
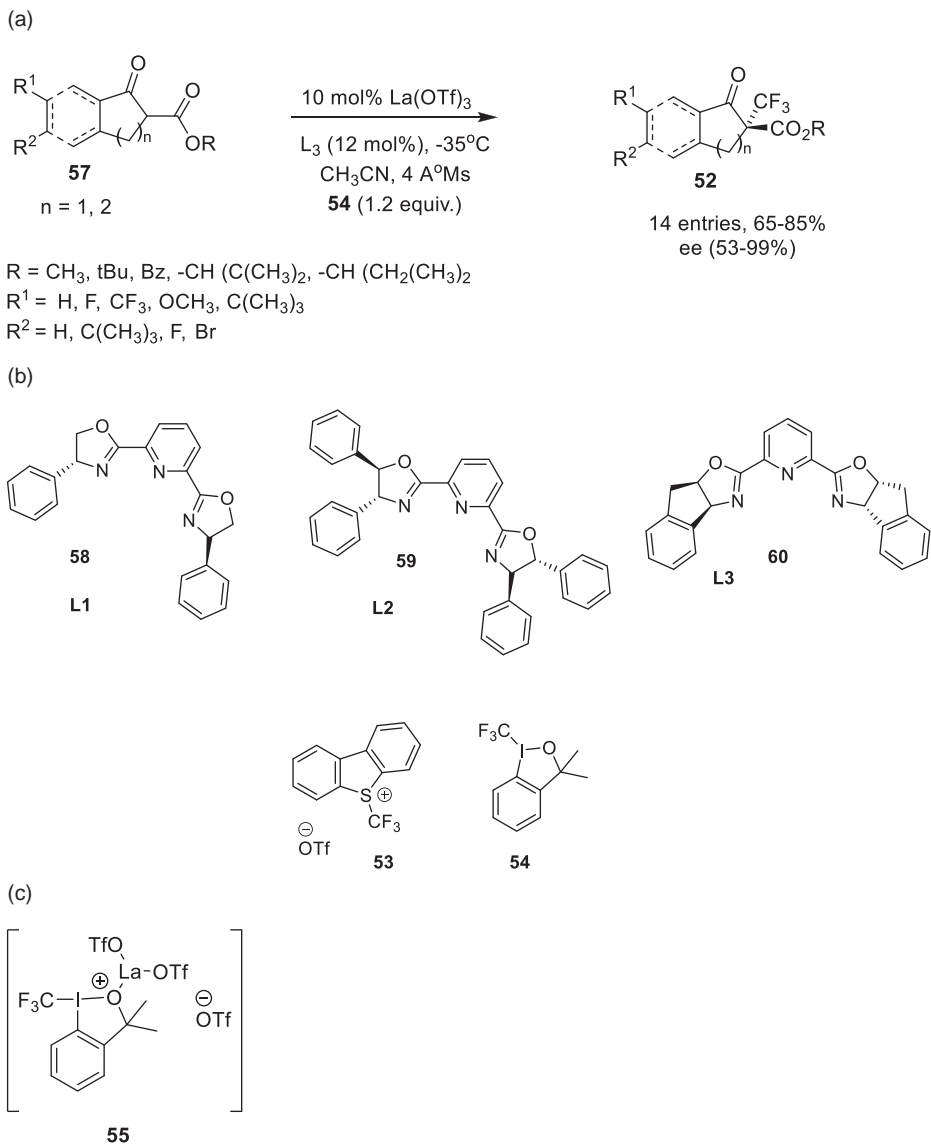
Figure 5.12: (a) Formation of quaternary α-triflouromethyl-3-oxo-ester derivatives. (b) Structures of **L1**, **L2**, **L3**,**53**,**54**. (c) *Iodonium* species intermediate.
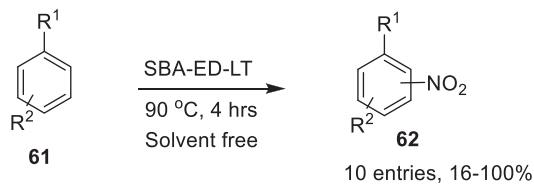
R^1 = R^2 = H, CH$_3$; CH$_3$, 2-CH$_3$; CH$_3$, 4-CH$_3$; H, F; H, Cl; H, Br; H, I; H, OMe; H, OH

Figure 5.13: Nitration assisted by SBA-ED-LT.

5.2.14 Preparation of malonamides

Jennings and co-researchers [39] designed and developed a three-component reaction providing indolyl malonamides (**63**), with interesting photo physical properties from coumarin-3-carboxylates (**64**), indole derivatives (**65**) and primary amines (**66**) catalyzed by La(OTf)$_3$ at room temperature (Figure 5.14a and b). Initially, the authors examined the scope of indole additions (**65**) to coumarin-3-carboxylates (**64**), while screening different catalysts for their efficiencies. During the course of study catalysts like ScCl$_3$, Y(OTf)$_3$, TiCl$_4$, La(OTf)$_3$, and Sc(OTf)$_3$ were analyzed. It was observed that 10 mol% Sc(OTf)$_3$ in toluene at 50 °C yielded *trans*-indolylchromanone derivatives (**67**). After developing the general methodology for about nine addition products in the range of 82–98%, the authors studied the applicability of the process to indolylmalonamides (**63**).

During optimization, different solvents and catalysts were examined and 10 mol% of La(OTf)$_3$ in CH$_2$Cl$_2$ at room temperature provided the malonamides (**63**) in encouraging yields.

5.2.15 Synthesis of tetrasubstituted pyrroles

Tan et al. [40] unveiled microwave-assisted preparation of tetra substituted pyrroles (**70**) by the condensation/alkyne-aza-cyclization/isomerization (**71**) sequence, catalyzed by La(OTf)$_3$ (Figure 5.15). During initial studies the authors examined the efficiencies of various catalysts such as Ni(OTf)$_3$, Yb(OTf)$_3$, Sc(OTf)$_3$, Cu(OTf)$_2$, CuBr, and La(OTf)$_3$ and also investigated the role of different additives like PPh$_3$, TMEDA, DPPP, and DPPE. The authors utilized several propargylated-ketoesters (**72**) and a wide range of aliphatic amines (**66**) as reactants in the (4 + 1) annulation approach. During the course of development of the process, solvents such as toluene, dioxane, PhCF$_3$ and DMF were tested for suitability. The authors demonstrated the utility of these end products in the construction of fully functionalized pyrroles through simple chemical transformations.

(a)

X = H, F, OMe, Y = Br, H, OMe, R = Me, ^{t}Bu
R^1 = H, Me
R^2 = H, Me

67

9 entries, 82–98%

(b)

(i)

X = H, F, OMe, Y = H, OMe, R = H, Me, R^1 = H, Me,
R^2 = p-methoxyphenyl, morpholinyl, pyrrolinyl

63

11 entries, 35–90%

(ii)

63

27%

+

68

34%

69

25%
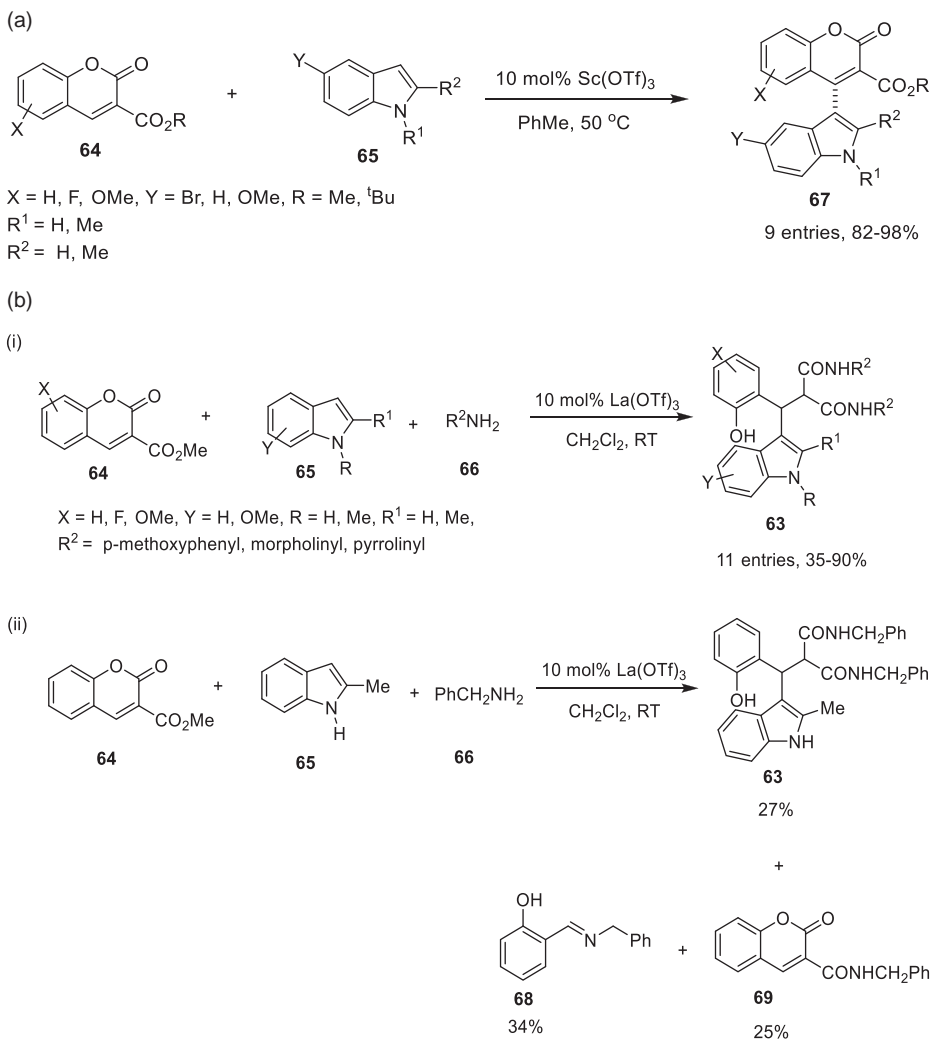
Figure 5.14: (a) Indole addition to coumarine-3-carboxylates. (b) Preparation of malonamides.

5.2.16 Preparation of 1,4-butanediol diacetates

Zhu et al. [41] conducted successfully a novel multistep tandem one-pot process for 1,4-butanediol diacetates (**73**) by the conversion of furan carboxylic acid (**74**) to BDA promoted by Pd/C and La(OTf)$_3$ catalytic system (Figure 5.16). The authors claim that the method provides a promising way for broadening the application of common biomass substrates. In the initial studies the effect of many lanthanide triflates on the protocol was investigated and observed that highest BDA (**73**) was obtained with La(OTf)$_3$. The
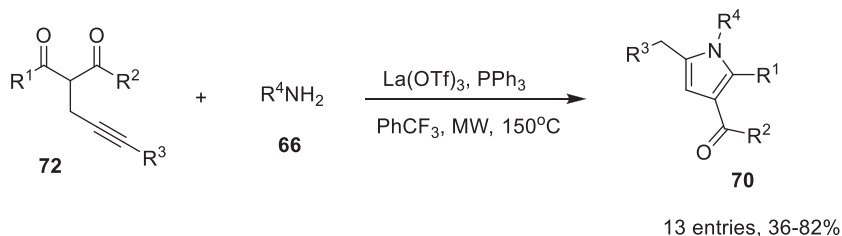
R^1 = Me, Ph, 2-furyl, 4-Br-C$_6$H$_4$, 4-OMe-C$_6$H$_4$, 2-OMe-C$_6$H$_4$,
3-Me-C$_6$H$_4$, 4-Me-C$_6$H$_4$, R^2 = OMe, OEt, R^3 = H, Me, R^4 = CH$_2$CHMe$_2$,
-CH$_2$- 2-furyl, 4-Me-C$_6$H$_4$-CH$_2$-, Ph, -CH$_2$-CH$_2$-OMe, -CH$_2$-CH$_2$-3-indolyl,
4-OMe-C$_6$H$_4$,
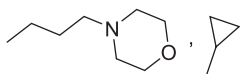
Figure 5.15: Preparation of α-aryl tetrasubstituted pyrroles.
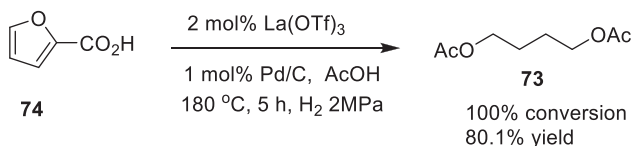
Figure 5.16: Preparation of 1,4-butanediol diacetates.

temperature has a major role in this continuous multi-step transformation of FCA to BDA (**74/73**). A series of experiments were conducted to fix hydrogen pressure. Effect of reaction times as well as effective substrate concentrations to gain maximum yield was also studied. The role of various reaction intermediates as substrates was examined.

5.2.17 Synthesis of 2,5-diformylfurans

Nguyen et al. [42] reported a one-step, direct, and facile preparation of 2,5-diformylfuran (**75**) from glucose (**76**) and fructose (**77**) using a combination of sulfur (**78**), La(OTf)$_3$, and dimethylsulfoxide system, by a dehydration/oxidation process(Figure 5.17). In the initial studies, the efficacies of various catalysts like H$_2$SO$_4$, H$_3$PO$_4$, HO(OTf)$_3$, Bi(OTf)$_3$, and La (OTf)$_3$ were verified. DMF, DMSO, dioxane, and nitrobenzene were tested as solvents for their suitability for carrying out the process.
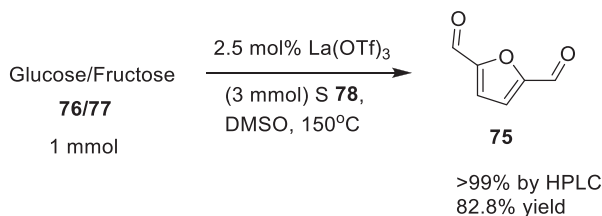
Figure 5.17: Preparation of 2,5-diformyl furan assisted by La(OTf)$_3$/S.

5.2.18 Synthesis of pyrazole-tethered imidazo[1,2-*a*]azine derivatives

Sharma and co-authors [43] described a one-pot multi-component diversity-oriented synthesis of pyrazole tethered imidazo[1,2-*a*]azine (**79**) derivatives, involving 2-amino azines (**66a**), isonitriles (**80**), and pyrazol carbaldehydes (**81**) as reactants, catalyzed by La(OTf)$_3$ (Figure 5.18a and b). As claimed, the protocol has the advantages such as low catalyst loadings, shorter reaction times, atom economy, functional group tolerance, scalability, and multiple bond formations in single step. Initially, the efficiencies of different catalysts like I$_2$, Sc(OTf)$_3$, Cu(OTf)$_2$, and La(OTf)$_3$ were assessed. Toluene, methanol, water, DMF, DMSO, and ethanol were tested for suitability as solvents. The protocol was extended to the preparation of pyrazol-C-5-tethered imidazo[1,2-a] pyridines (**79**) and 4-iodopyrazole-C-3-tethered imidazo[1,2-a]pyridine derivatives (**82**). Scalability of the approach was established employing 2-amino pyridine (**66b**), tert. butyl isocyanide (**80a**), and pyrazole-3-carbaldehyde (**81**) derivatives as reactants.

5.2.19 Direct amidation reaction

Morimoto et al. [44] reported La(OTf)$_3$ as an efficient simple component catalyst for the preparation of variety of amides (**85**) from amines (**42**) and esters(**86**) under mild reaction conditions (Figure 5.19a and b). The reaction between benzyl amine (**42**)and ethyl-3-phenylpropionate (**87**) was selected as a model reaction for initial studies. La (OTf)$_3$ was chosen as a catalyst of choice among other acidic catalysts, as it afforded 98% yield of the title compound after 24 h of reaction time at 50 °C. The process was extended to include aliphatic, α, β-unsaturated and aromatic/heterocyclic esters (**86/86a**) as well as primary/secondary amines (**66**). As a part of research study the authors conducted experiments on the catalyst controlled amidation of esters and applied the methodology for the synthesis of some important compounds. The suitability of the catalytic system was established in the selective amidation of some esters and amines in the presence of similar functionalities with excellent yields.

(a)

R[1] = F, Cl,
R[2] = Ph, CH$_3$

R[3] = tert.butyl, CH$_2$-CO$_2$Et,
R[4] = H, 3-Me, 4-Me, 5-Me, 6-Me, 5-F,
5-Cl, 3,5-Cl$_2$, 3-Br, 5-Br

21 entries, 16-81%

(b)

R[2] = Ph, Me

58%

86%
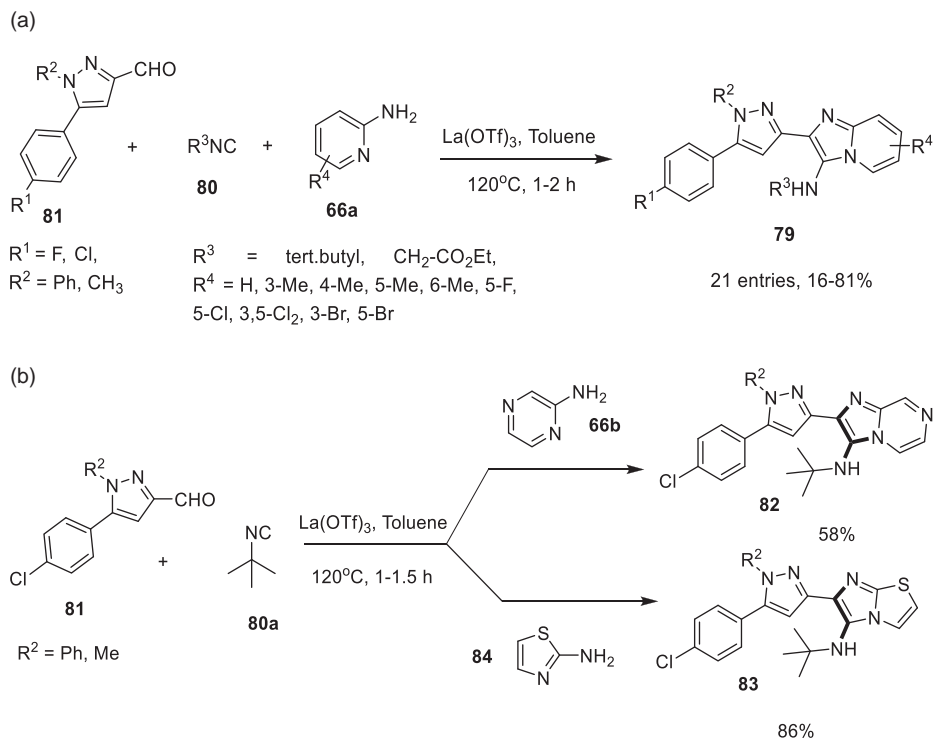
Figure 5.18: (a) Preparation of pyrazole-C-3-tethered imidazo[1,2-*a*] pyridine derivatives. (b) Pyrazole-C-3-substituted imidazo [1,2-a] pyrazine and imidazo [2,1-b] thiazole derivatives.

5.2.20 Asymmetric cyclopropanation

Zhang and co-authors [45] designed and developed asymmetric cyclopropanation of 2-cyano-3-aryl acrylates (**89**) employing 2-bromomalonates (**90**) catalyzed by La(OTf)$_3$ and chiral N, N[1]-dioxide system (Figure 5.20a–c). Initially, several metal triflates like Mg(OTf)$_2$, Sc(OTf)$_3$, Ni(OTf)$_2$, and La(OTf)$_3$ were assessed for their efficiencies for the present protocol and noted that La(OTf)$_3$ provided better results than others. Among the ligands chiral N, N[1]-dioxide L$_2$-RaEt$_2$ (**91**) with small steric hindrance contributed for enhanced enantioselectivities up to 89% *ee*. Several organic and inorganic bases such as K$_2$CO$_3$, K$_3$O$_4$.6H$_2$O, NEt$_3$, and ipr$_2$NEt were screened and ipr$_2$NEt provided the best results. Reactions employing diverse range of 2-cyano acrylates (**92**) were conducted. It was reported that enantioselectivity decreased with increase in substituent size. Highly functionalized chiral cyclopropanes (**89**) were prepared in yields (up to 93%) with good ee values (up to 91% ee) and excellent d.r. (>95:5 dr). The present catalytic system was applied to the three-component tandem halogenation/asymmetric MIRC reaction of ethyl-2-cyano-3-phenyl acrylate (**92**), diethylmalonate (**90**) and NBS (**93**).

(a)
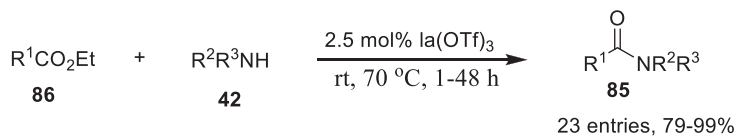
R^1 = H, Me, CF$_3$, Ph, Ph-CH$_2$, CH$_2$CN, Ph-CH$_2$-CH$_2$, Ph-CH=CH, 4-I-C$_6$H$_4$, 4-Me-C$_6$H$_4$
CH$_2$-NH-Bz, Ph-CH$_2$-CH-NHBoC,
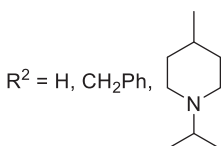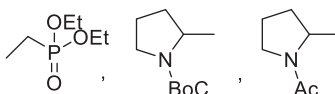
R^2 = H, CH$_2$Ph,

R^3 = H, n-C$_5$H$_9$, CH$_2$Ph, 4-OMe-C$_6$H$_4$, (CH$_2$)$_6$-OTBS

R^2/R^3 =
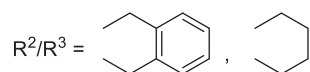
(b)
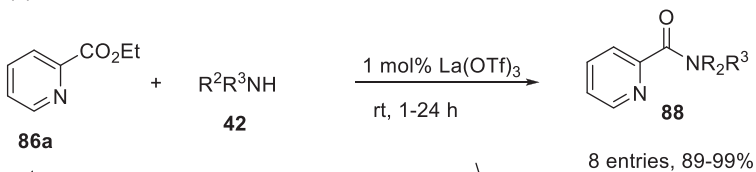
R^1 = H, Me

R^3 = CH$_2$Ph, -CH$_2$-CH$_2$-CH$_3$, -CH$_2$-CH$_2$-Ph,

R^2/R^3 =
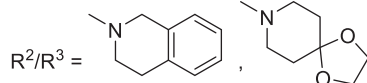
Figure 5.19: (a) Direct amidation promoted by La(OTf)$_3$. (b) Direct amidation of ethyl-2-pyridine carboxylate.

5.2.21 Synthesis of poly-substituted dihydropyran derivatives

Zhang et al. [46] developed and studied extremely novel Rh(I)/La(III) co-catalytic three-component strategy for the convergent synthesis of poly-substituted dihydropyran derivatives (**95**), obtained by the reaction of vinyl cyclopropanes (**96**), diazo esters (**97**), and diphenylsulfoxide (**98**). Vinyl cyclopropanes (**96**) undergo isomerization resulting in conjugated dienes followed by their [4 + 2] cycloaddition with vicinal

(a)

21 entries, 30-98%
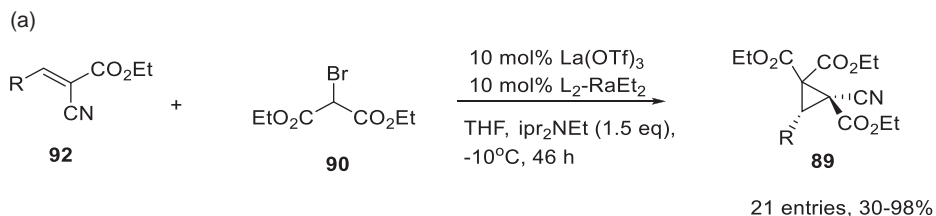
R = Ph, 2-Me-C$_6$H$_4$,3-Me-C$_6$H$_4$,4-OMe-C$_6$H$_4$, 3-OPh-C$_6$H$_4$, 3,4-Me$_2$-C$_6$H$_3$,4-F-C$_6$H$_4$, 2-Cl-C$_6$H$_4$,
3-Cl-C$_6$H$_4$, 4-Br-C$_6$H$_4$, 3-F$_3$C-C$_6$H$_4$, 3-NO$_2$-C$_6$H$_4$, 2-naphthyl, 3-pyridyl, 2-thienyl,
C$_6$H$_5$-CH=CH, Ph-CH$_2$CH$_2$

(b)

(c)
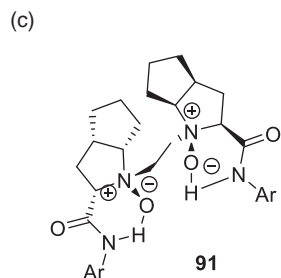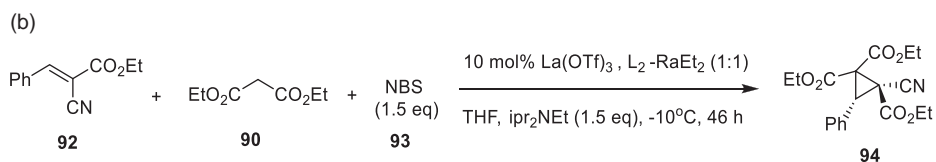
L$_2$RaEt$_2$; Ar = 2,6-Et$_2$C$_6$H$_3$

Figure 5.20: (a) Synthesis of highly functionalized chiral cyclopropanes. (b) Tandem halogenation/
asymmetric MIRC reaction. (c) L$_2$-RaEt$_2$.

tricarbonyl compounds (**99**) (Figure 5.21a–c). In the process diphenyl sulfoxide (**98**) trans-
fers oxygen atom to diazo esters (**97**) forming tricarbonyl compounds (**100**). Different
Lewis acids like AgOTf, Cu(OTf)$_2$, Sc(OTf)$_3$, Yb(OTf)$_3$, TMSOTf, and La(OTf)$_3$ were screened
for their efficiencies in the initial optimization studies. La(OTf)$_3$ was reported to have
given the best results. The authors obtained the isomerization products in these reactions
where in olefin unit migrates to the adjacent carbon. Substrates with electron-donating
groups produced more such isomers.

The versatility of this scalable process was demonstrated with differently substi-
tuted vinyl cyclopropanes (**96**) and diazo esters (**97**).

(a)

R = Ph, 4-BrC$_6$H$_4$, 4-PhC$_6$H$_4$, 4-OMeC$_6$H$_4$, 4-CF$_3$C$_6$H$_4$, 4-CO$_2$MeC$_6$H$_4$, 3,5-Me$_2$C$_6$H$_3$,3,4-OMe$_2$C$_6$H$_3$, 2-F,3-ClC$_6$H$_3$, 4-tBuC$_6$H$_4$, 2-Naphthyl, 2-Thienyl, -(CH$_2$)$_3$-Ph

(b)

(c)
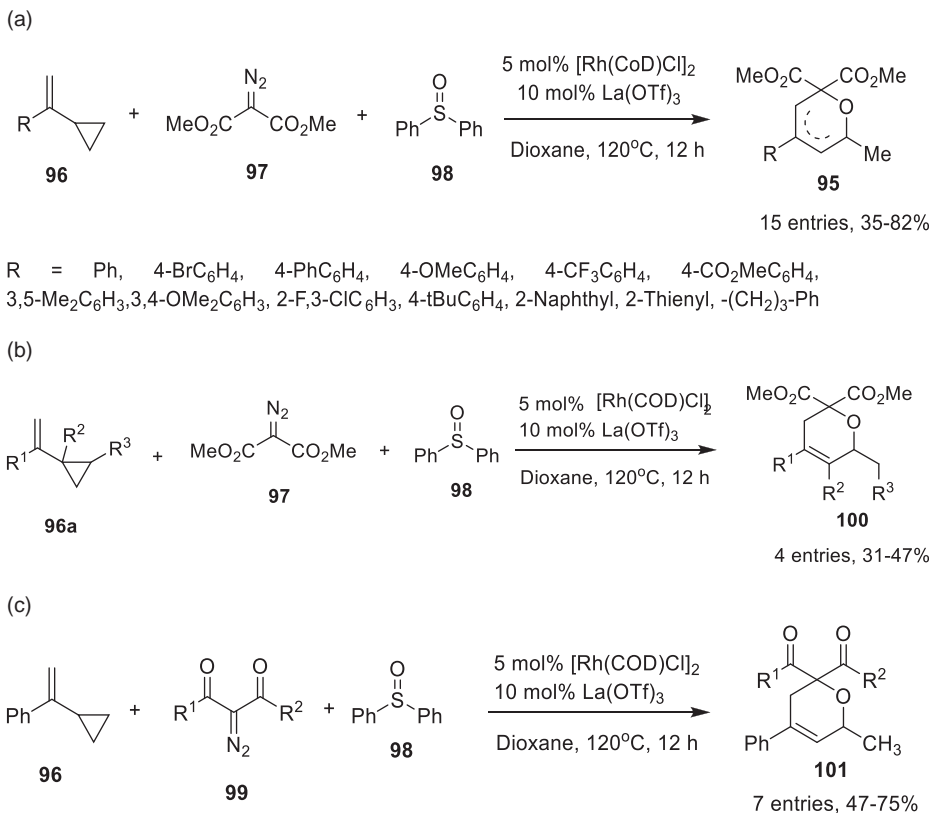
Figure 5.21: (a) Reactions with different vinyl cyclopropanes. (b) Reaction of vinyl cyclopropanes with substituents at other locations. (c) Reactions with varied diazoesters.

5.2.22 Preparation of nonsymmetric urea derivatives

Bui and Kim [47] prepared nonsymmetric urea derivatives (**102/104/105**) successfully from *N*-benzyloxy carbonyl, *N*-allyloxy carbonyl and *N*-2,2,2-trichloroethoxy carbonyl-protected amines (**103**) assisted by La(OTf)$_3$ (Figure 5.22a–c). During optimization studies the authors conducted experiments to validate the efficacies of various catalysts such as LaCl$_3$, La(OAc)$_3$, La(OTf)$_3$, Sm(OTf)$_3$, Nd(OTf)$_3$, Sc(OTf)$_3$, Zn(OTf)$_2$, Mg(OTf)$_2$, and Al(OTf)$_3$. Several solvents were examined for their suitability and PhCF$_3$ gave best results. The broader applicability of this novel process was demonstrated by preparing a large library of the title compounds from diversely substituted *N*-Cbz/*N*-Troc/*N*-Alloc protected amines as well as aliphatic/aromatic/alicyclic/heterocyclic amines (**42/66**). Scale up studies was also conducted by the authors.

(a)

10 entries, 75-94%
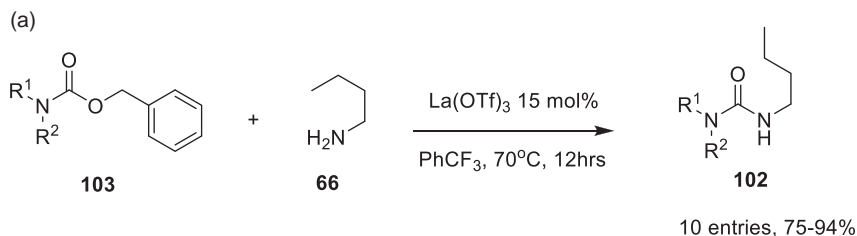
R^1/R^2 = H, Ph; 4-CH$_3$C$_6$H$_4$, H; 2,4-(CH$_3$)$_2$-C$_6$H$_3$, H; O-Me-4-C$_6$H$_4$, H; 4-Cl-C$_6$H$_4$, H; 2,4-Cl$_2$-C$_6$H$_3$, H; 4-NO$_2$-C$_6$H$_4$, H; C$_6$H$_{13}$, H, C$_5$H$_9$; H, C$_3$H$_3$

(b)

12 entries, 78-96%
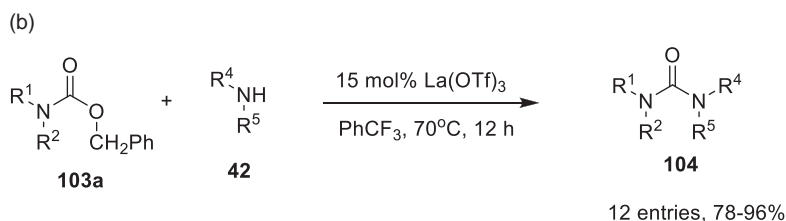
R^1, R^2 = H, Ph; H, C$_4$H$_9$, C$_4$H$_9$;
R^4/R^5 = H, C$_4$H$_9$; H, CH$_2$-C$_6$H$_5$; H, C$_6$H$_{11}$; C$_5$H$_{10}$, (C$_3$H$_7$)$_2$-,C$_4$H$_8$; C$_4$H$_8$O

(c)

22 entries, 78-96%
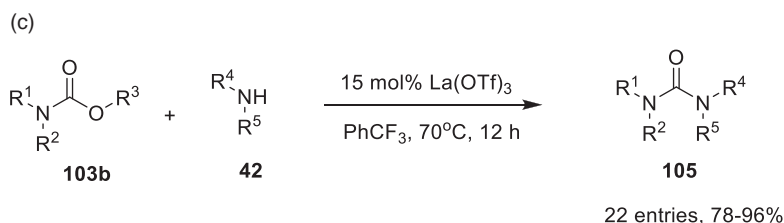
R^1, R^2 = H, Ph, C$_4$H$_9$, H, C$_4$H$_9$
R^4/R^5 = H, C$_4$H$_9$, H, CH$_2$-C$_6$H$_5$, H, C$_6$H$_{11}$, C$_5$H$_{10}$, (C$_3$H$_7$)$_2$-,C$_4$H$_8$; C$_4$H$_8$O

Figure 5.22: (a) La(OTf)$_3$ promoted preparation of nonsymmetrical urea derivatives from butyl amines. (b) La(OTf)$_3$-assisted preparation of non-symmetrical urea derivatives from *N*-Cbz amines and different amines. (c) Reaction of *N*-allocor *N*-Troc-protected amines.

5.2.23 Synthesis of chromenopyrazolones

Hariprasad et al. [48] explored a facile method to obtain chromenopyrazolones(**106**) by the reaction of salicylaldehyde phenylhydrazones(**107**) with β-ketoesters(**108**) and activated alkynes (**109**) assisted by La(OTf)$_3$ at 30 °C under solvent-free conditions (Figure 5.23a–d). The scope of the process was investigated using several salicylalde-hyde phenylhydrazones (**107**) and ethyl-3-oxobutanoate (**110**). During optimization process AcOH, P-TsOH, AlCl$_3$, FeCl$_3$, InCl$_3$, SnCl$_2$, H$_2$SO$_4$, Cu(OAc)$_2$, ZrOCl$_2$.8H$_2$O, Sc(OTf)$_3$, Bi(OTf)$_3$ and La(OTf)$_3$ were examined as catalysts. Toluene, DCM, EtOH, and CH$_3$CN were tested as solvents. Conventional heating at 130 °C in the absence of any solvent

(a)
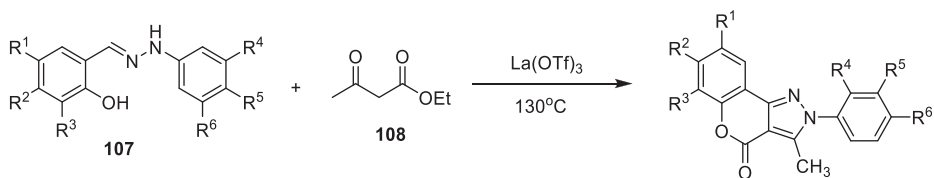
R^1 = H, CH$_3$, F, Cl, Br, R^2 = H, OCH$_3$
R^3 = H, Cl, Br, R^4 = H, CH3, R^5 = H, CH$_3$, Cl
R^6 = H, CH$_3$, OCH$_3$, Cl

15 entries, 46-79%

(b)
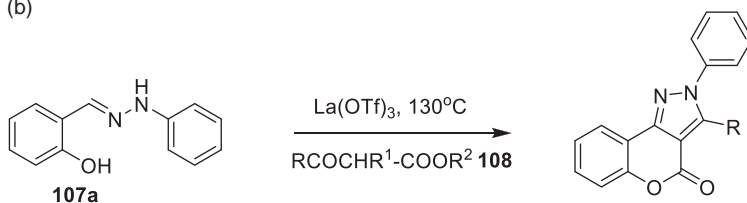
R = Ph, CF$_3$, CCl$_3$, CH$_2$Cl, CH$_3$, OEt
R^1 = H, Cl
R^2 = Et, CH$_2$CH$_2$OMe

8 entries, 62-76%

(c)
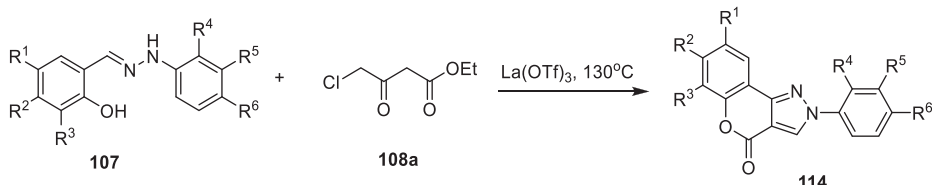
R^1 = H, CH$_3$, R^2 = H, R^3 = H,
R^4 = H, CH$_3$, R^5 = H, R^6 = H, OCH$_3$, Cl.

5 entries, 50-67%

(d)
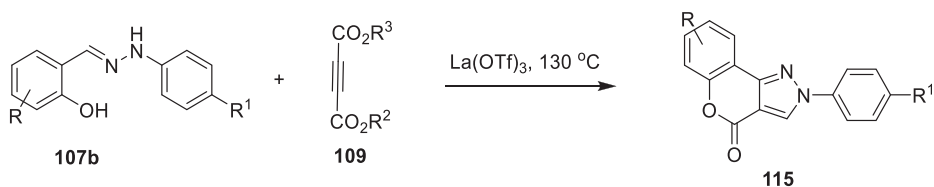
R = H, 4-OCH$_3$, 5-CH$_3$, 5-Br, 5-Cl
R^1 = H, Cl, CH$_3$, R^2 = CH$_3$, Et
R^3 = H, CH$_3$, Ph, CO$_2$Et, CO$_2$CH$_3$

11 entries; 51-77%

Figure 5.23: (a) Preparation of chromenopyrazolones. (b) Reaction with β-ketoesters: preparation of chromenopyrazolones. (c) Cyclization and reductive dechlorination with ethyl-4-chloro-3-oxobutanoate. (d) Synthesis of chromenopyrazolone-3-carboxylates.

provided better results. The scope of the method was expanded to include various substituted salicylaldehyde phenyl hydrazones (**107**). The research work was also extended to synthesize chromenopyrazolones (**111**) from β-ketoesters (**108**), activated alkynes (**109**) and salicylaldehyde phenylhydrazones (**107**). Phenyl, triflouro, trichloro oxobutanoates (**112**) and diethyl malonate (**113**) did not yield the product.

5.3 Conclusions

This review highlights the superior catalytic activity of La(OTf)$_3$ toward various organic transformations, particularly reported in the last ten years. The authors wish that the present review stimulates further research and application of La(OTf)$_3$ to a diverse range of synthetic applications, resulting in the discovery of new and improved methodologies. The authors of this review sincerely appreciate and acknowledge the research groups of the publications cited herein. All the figures are redrawn and are representative. The scholars are advised to go through the original research articles for detailed information and learning.

References

[1]   Forsberg, JH, Spaziano, VT, Balasubramanian, TM, Liu, GK, Kinsley, SA, Duckworth, CA, Poteruca, JJ, Brown, PS, Miller, JL. Use of lanthanide(III) ions as catalysts for the reactions of amines with nitriles. J Org Chem, 1987, 52, 1017–1021.
[2]   Kobayashi, S. Lanthanide Trifluoromethanesulfonates as stable Lewis acids in aqueous media. Yb (OTf)$_3$ Catalyzed hydroxymethylation reaction of silyl enol ethers with commercial formaldehyde solution. Chem Lett, 1991, 2187–2190.
[3]   Kobayashi, S, Hachiya, I. The aldol reaction of silyl enol ethers with aldehydes in aqueous media. Tetrahedron Lett, 1992, 33, 1625–1628.
[4]   Kobayashi S.Hachiya I. Lanthanide triflates as water-tolerant Lewis acids. Activation of commercial formaldehyde solution and use in the aldol reaction of silyl enol ethers with aldehydes in aqueous media. J Org Chem, 1994;59:3590–3596.
[5]   Aggarwal, VK, Vennall, GP. Scandium trifluoromethanesulfonate, a novel catalyst for the addition of allyltrimethylsilane to aldehydes. Tetrahedron Lett, 1996, 37, 3745–3746.
[6]   Belluci, C, Cozzi, PG, Umanironchi, A. Catalytic allylation of imines promoted by lanthanide triflates. Tetrahedron Lett, 1995, 36, 7289–7292.
[7]   Aspinall, HC, Browning, AF, Greeves, N, Ravenscroft, P. Ytterbium trifluoromethanesulfonate [Yb(OTf)$_3$] as a novel catalyst for the allylation of aldehydes. Tetrahedron Lett, 1994, 35, 4639–4640.
[8]   Hachiya, I, Kobayshi, S. Aqueous reactions with a Lewis acid and an organometallic reagent. The scandium trifluoromethanesulfonate-catalyzed allylation reaction of carbonyl compounds with tetraallyltin. J Org Chem, 1993, 58, 6958–6960.

[9]   Tsuchimoto, T, Tobita, K, Hiyama, T, Fukuzawa, SI. Scandium(III) triflate catalyzed friedel-crafts alkylation with benzyl and allyl alcohols. Synlett, 1996, 1996, 557–559.

[10] Hachiya, I, Moriwaki, M, Kobayashi, S. Hafnium(IV) Trifluoromethanesulfonate, an efficient catalyst for the friedel-crafts acylation and alkylation reactions. Bull Chem Soc Jpn, 1995, 68, 2053–2060.

[11] Kawada, A, Mitamura, S, Kobayashi, S. Ln(OTf)3-LiClO4 as reusable catalyst system for Friedel-Crafts acylation. Chem Commun, 1996, 183–184.

[12] Kobayashi, S, Ishitani, H, Hachiya, I, Araki, M. Asymmetric Diels-Alder reactions catalyzed by chiral lanthanide(III) trifluoromethanesulfonates. Unique structure of the triflate and stereoselective synthesis of both enantiomers using a single chiral source and a choice of achiral ligands. Tetrahedron, 1994, 50, 11623–11636.

[13] Kobayashi, S, Araki, M, Hachiya, I. A chiral scandium catalyst for enantioselective diels-alder reactions. J Org Chem, 1994, 59, 3758–3759.

[14] Yu, LB, Chen, DP, Wang, PG. Aqueous aza Diels-Alder reactions catalyzed by lanthanide(III) trifluoromethanesulfonates. Tetrahedron Lett, 1996, 37, 2169–2172.

[15] Marko, E, Evans, GR. Catalytic, enantioselective, inverse electron-demand diels-alder (IEDDA) reactions of 3-carbomethoxy-2-pyrone (3-CMP). Tetrahedron Lett, 1994, 35, 2771–2774.

[16] Kobayashi, S, Hachiya, I, Yasuda, M. Aldol reactions on solid phase. Sc(OTf)3-Catalyzed aldol reactions of polymer-supported silyl enol ethers with aldehydes providing convenient methods for the preparation of 1,3-diol, β-hydroxy carboxylic acid, and β-hydroxy aldehyde libraries. Tetrahedron Lett, 1996, 37, 5569–5572.

[17] Kobayashi, S, Hachiya, I. Lanthanide triflates as water-tolerant Lewis acids. Activation of commercial formaldehyde solution and use in the aldol reaction of silyl enol ethers with aldehydes in aqueous media. J Org Chem, 1994, 59, 3590–3596.

[18] Barrett, AGM, Braddock, DC. Scandium(III) or lanthanide(III) triflates as recyclable catalysts for the direct acetylation of alcohols with acetic acid. Chem Commun, 1997, 351–352.

[19] Tsuchimoto, T, Tobita, K, Hiyama, T, Fukuzawa, S. Scandium(III) triflate-catalyzed friedel-crafts alkylation reactions. J Org Chem, 1997, 62, 6997–7005.

[20] Kobayashi, S, Hamada, T, Nagayama, S, Manabe, K. Lanthanide Trifluoromethanesulfonate-catalyzed asymmetric aldol reactions in aqueous media. Org Lett, 2001, 3, 165–167.

[21] Kobayashi, S. Rare earth metal trifluoromethanesulfonates as water-tolerant Lewis acid catalysts in organic synthesis. Synlett, 1994, 1994, 689–701.

[22] Steel, PG. Recent developments in lanthanide mediated organic synthesis. J Chem Soc Perkin Trans, 2001, 1, 2727–2751.

[23] Kobayashi, S, Manabe, K. Development of novel Lewis acid catalysts for selective organic reactions in aqueous media. Acc Chem Res, 2002, 35, 209–217.

[24] Kobayashi, S, Sugimura, M, Kitagawa, H, Hidetoshi, L, Lam, WW-L. Rare-earth metal triflates in organic synthesis. Chem Rev, 2002, 102, 2227–2302.

[25] Luo, S, Lizhi, Z, Talukdar, A, Zhang, G, Xueling, M, Cheng, J-P, Wang, PG. Recent advances in rare earth-metal triflate catalyzed organic synthesis in green media. Mini Rev Org Chem, 2005, 2, 177–202.

[26] Meshram, HM, Ramesh, P, Reddy, BC, Sridhar, B, Yadav, JS. Diastereoselective Mukaiyama aldol reaction of (N-alkyl) isatins with 2-(trimethylsilyloxy)furan by using lanthanum triflate. Tetrahedron, 2011, 67, 3150–3155.

[27] Nagarajan, R, Ramesh, S. One-pot synthesis of pyrrolo[3,2-f]- and Pyrrolo[2,3-h]quinoline derivatives: Observation of an unexpected mechanistic pathway. Synlett, 2012, 2012, 717–722.

[28] Liu, J, Shen, Q, Yu, J, Zhu, M, Han, J, Wang, L. A concise domino synthesis of benzo-1,4-heterocycle compounds via a piancatelli/C-N Coupling/Michael addition process promoted by La(OTf)$_3$. EurJ Org Chem, 2012, 35, 6933–6939.

[29] Jardosh, H, Patel, M. Lanthanum triflate triggered synthesis of tetrahydroquinazolinone derivatives of N-allyl quinolone and their biological assessment. J Serbian Chem Soc, 2012, 77, 1561–1570.

[30] Sobhani, S, Pakdin-Parizi, Z. Lanthanum(III) triflate supported on nanomagnetic γ-Fe_2O_3: A new magnetically recyclable heterogeneous Lewis acid for the one-pot synthesis of β-phosphonomalonates. RSC Adv, 2014, 4, 13071–13077.

[31] Wenhao, X, Weike, S. Improved sommelet reaction catalyzed by lanthanum triflate. J Chem Res, 2014, 38, 710–714.

[32] Sasaki, S, Suzuki, T, Uchiya, T, Toyota, S, Hirano, A, Tanemura, M, Teramoto, H, Yamauchi, T, Higashiyama, K. Synthesis of α,α-difluoro-β-hydroxy ketone via the La(OTf)$_3$-catalyzed aldol reaction of carbonyl compounds with difluoroenol O-Boc esters. J Fluor Chem, 2016, 192, 78–85.

[33] Reddy, BN, Rani, CR, Reddy, SM, Pathak, M. An efficient and green La(OTf)$_3$ catalyzed petasisborono-mannich reaction for the synthesis of tertiary amines. Res Chem Intermed, 2016, 42, 7533–7549.

[34] Kumari, S, Rajeswari, M, Khurana, JM. La(OTf)$_3$-catalyzed, three-component synthesis of spiro [Indolo-3,10′-indeno[1,2-b]quinolin]-2,4,11′-triones in PEG-400 under conventional heating and ultrasonic irradiation. Synth Commun, 2016, 46, 387–394.

[35] Wang, Q-P, Zhang, H-B, Ning, X, Hang, H, Huang, Z-L, Song, H-R, Wang, X, Wang, PG. Microwave-assisted construction of C-Hydroxydiketopiperazines using lanthanum(III) Triflate. Asian J Org Chem, 2015, 4, 132–136.

[36] Meshram, GA, Deshpande, SS, Wagh, PA, Vala, VA. Silica supported lanthanum triflate mediated synthesis of 5-substituted-1H tetrazoles. Tetrahedron Lett, 2014, 55, 3557–3560.

[37] Granados, A, Rivilla, I, Cossío, FP, Vallribera, A. Lanthanum-catalyzed enantioselective trifluoromethylation by using an electrophilic hypervalent iodine reagent. Eur J Chem, 2019, 25, 8214–8218.

[38] Ketike, T, Muppala, A, Ganjala, VSP, Kamaraju, SR, Burri, DR, Ganji, G. Lanthanum triflate anchored SBA-15 is an effective catalyst for the nitration of alkyl aromatics. J Appl Chem, 2020, 9, 628–637.

[39] Jennings, JJ, Bhatt, CP, Franz, AK. Lanthanum(III)-catalyzed three-component reaction of coumarin-3-carboxylates for the synthesis of indolylmalonamides and analysis of their photophysical properties. JOrg Chem, 2016, 81, 6211–6222.

[40] Tan, X-M, Lai, Q-M, Yang, Z-W, Long, X, Zhou, H-L, You, X-L, Jiang, X-J, Cui, H-L. La(OTf)$_3$ catalyzed synthesis of α-aryl tetrasubstituted pyrroles through [4+1] annulation under microwave irradiation. Tetrahedron Lett, 2015, 58, 163–167.

[41] Zhu, R, Zhou, G, Gong, B, Deng, J, Fu, Y. Cascade conversion of furancarboxylic acid to butanediol diacetate over Pd/C and La(OTf)$_3$ catalytic system. Appl Catal A-Gen, 2020, 608, 117888–117889.

[42] Nguyen, QNB, Le, HAN, Ly, PD, Phan, HB, Tran, PH. One-step synthesis of 2,5-diformylfuran from monosaccharides by using lanthanum(iii) triflate, sulfur, and DMSO. Chem Commun, 2020, 56, 13005–13008.

[43] Sharma, S, Paul, AK, Singh, V. La(OTf)$_3$Catalysed one-pot synthesis of pyrazole tethered imidazo[1,2-a]azine derivatives and evaluation of their light emitting properties. New J Chem, 2020, 44, 684–694.

[44] Morimoto, H, Fujiwara, R, Shimizu, Y, Morisaki, K, Ohshima, T. Lanthanum(III) triflate catalyzed direct amidation of esters. Org Lett, 2014, 16, 2018–2021.

[45] Zhang, Y, Lin, L, Chen, Y, Liu, X, Feng, X N, N′ -dioxide-lanthanum(III)-catalyzed asymmetric cyclopropanation of 2-cyano-3-arylacrylates with 2-bromomalonates. Adv Synth Catal, 2017, 359, 1831–1836.

[46] Zhang, Y-L, Guo, R-T, Luo, H, Liang, X-S, Wang, X-C. Convergent synthesis of dihydropyrans from catalytic three-component reactions of vinylcyclopropanes, diazoesters, and diphenyl sulfoxide. Org Lett, 2020, 22, 5627–5632.

[47] Bui, TT, Kim, H-K. Lanthanum(III) trifluoromethanesulfonate catalyzed direct synthesis of ureas from N-benzyloxycarbonyl-, N-allyloxycarbonyl-, and N-2,2,2-trichloroethoxycarbonyl-protected amines. Synlett, 2020, 31, 997–1002.

[48] Hariprasad, KS, Prasad, KV, Raju, BC. La(OTf)$_3$ catalyzed reaction of salicylaldehyde phenylhydrazones with β-ketoesters and activated alkynes: Facile approach for the preparation of chromenopyrazolones. RSC Adv, 2016, 6, 108654–108661.

Debasree Saha and Chhanda Mukhopadhyay*

6 Current advances in the application of actinide complexes for useful organic transformations

6.1 Introduction

The role of actinide complexes in organometallic catalysis has not been explored much until the last couple of decades due to difficulty in handling actinides, most of which are unstable and radioactive in nature. Only the first four actinides, namely, actinium, thorium, protactinium and uranium, are found in nature. Neptunium and plutonium are found in uranium minerals in very minute quantities. Rest are all man-made. Moreover, since all the actinide members are radioactive in nature, it is really hazardous and difficult to involve actinides in catalyzing organic reactions. However, with the development of newer technologies in radioactive chemistry, it has now become relatively easier to handle actinides especially the earlier ones. Thus, researchers all over the world have started exploring the unique properties of actinides which include high ionic radii, availability of 5 f valence orbitals, and existence of range of coordination numbers, all of which make them quite suitable as competent catalytic agents.

A few reviews covering the synthesis and unique reactivities of actinide complexes are available in literature [1–34]. In this chapter, we aim to highlight a few types of organic reactions that are suitably catalyzed by actinide complexes. This chapter will thus have 12 subheadings, namely, hydroamination of terminal alkynes, hydrosilylation of terminal alkynes, dehydrocoupling reaction of amines with silanes, hydrothiolation of terminal alkynes, Tischenko reaction, coupling reaction of terminal alkynes and isonitriles, addition of alcohols to carbodiimides, oligomerization of alkynes, hydroxyalkylation/cyclization of alkynyl alcohols, ring-opening polymerization of cyclic esters, ring-opening polymerization of epoxides and catalytic insertion of protic nucleophiles to heterocumulenes. We would highlight the scope of actinide catalysis in each of the above reactions with the hope of inspiring future research in actinide catalysis so that the world may see greater use and application of actinides.

*Corresponding author: Chhanda Mukhopadhyay, Department of Chemistry, University of Calcutta, Kolkata 700009, West Bengal, India, e-mail: cmukhop@yahoo.co.in
Debasree Saha, Department of Chemistry, Raidighi College, 24 Parganas (South), Raidighi 743383, West Bengal, India

6.2 Hydroamination of terminal alkynes

Hydroamination, as the name suggests, involves addition of N–H bond to alkene or alkyne. This is a fundamental reaction in organic synthesis. However, there are not many references of actinide complexes catalyzing this reaction.

Eisen and his group [35] developed a methodology where cyclopentadienyl complexes of actinides catalyze hydroamination of terminal alkynes (**1**) with aliphatic amines (**2**) leading to the formation of imines (**3, 4**) (Figures 6.1 and 6.2). The reaction generated trace amounts of alkyne oligomerization products as by-products. Uranium and thorium cyclopentadienyl complexes successfully catalyze the hydroamination reaction. The regioselectivity of the methodology could be controlled by the choice of alkyne and actinide metal catalyst.
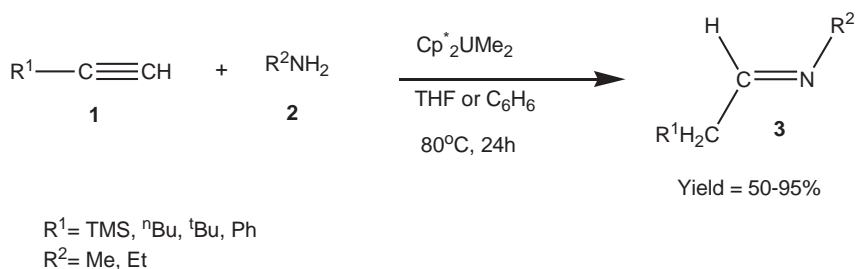
Figure 6.1: Uranium-catalyzed hydroamination of terminal alkynes with aliphatic amines.
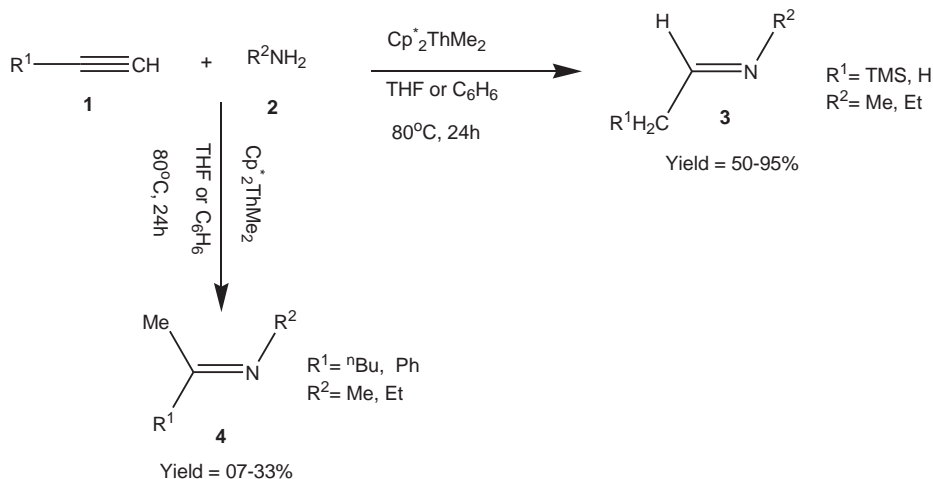
Figure 6.2: Thorium-catalyzed hydroamination of terminal alkynes with aliphatic amines.

Uranium complexes resulted in the formation of terminal imines (**3**). With uranium catalysis, in case of trimethyl silyl-substituted acetylene, the product imine underwent 1,3 shift of the silyl group leading to the formation of enamine. Thorium-catalyzed hydroamination resulted in two types of imines namely terminal imine (**3**) and nonterminal imine (**4**). With trimethyl-substituted acetylene, the product is terminal imine while with butyl- or phenyl-substituted acetylene, the product is the unexpected non terminal imine.

6.3 Hydrosilylation of terminal alkynes

Addition of Si–H bond to terminal alkyne plays a very important role in organosilicon chemistry. After hydroamination reaction, Eisen and his group [36] employed organo-actinide complexes for successful hydrosilylation of terminal alkynes. The regiospecificity and chemoselectivity of the methodology could be controlled by factors such as the type of alkyne used, type of metal and catalyst used, substituent on the silane skeleton, ratio between silane and alkyne, solvent and reaction temperature.

When the reaction was carried out at room temperature, *trans*-vinylsilane (**7**) was obtained as the major product with silylalkyne (**8**) and alkene (**9**) as minor products (Figure 6.3). As reaction temperature was increased, *cis*-vinylsilane and double-hydrosilylated alkene were obtained as products.
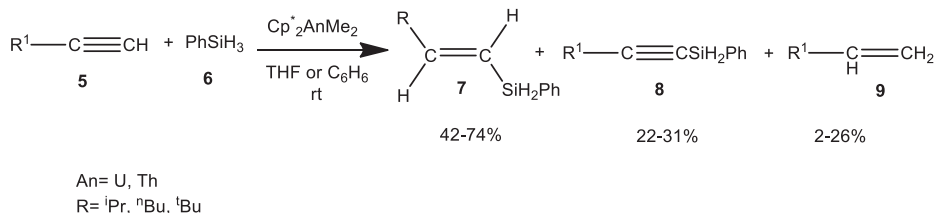
Figure 6.3: Uranium/thorium-catalyzed hydrosilylation of terminal alkynes.

6.4 Dehydrocoupling reaction of amines with silanes

Eisen and his group [37] synthesized aminosilanes (**12, 13, 14**) by dehydrogenative coupling of silanes (**10**) and amines (**11**) catalyzed by [(Et$_2$N)$_3$ U][BPh$_4$] (Figure 6.4). The method provided a successful alternative for the synthesis of aminosilanes thereby eliminating the formation of toxic ammonium halides that are generated during ammonolysis, which by far had been the conventional method of synthesis of silazanes.

It was observed that for a particular silane reacting with a primary amine RNH$_2$, the reactivity depended on the steric hindrance of the R group. The order of reactivity was found to be primary > secondary > tertiary with respect to the R group of the

primary amine. As compared to primary amines and silanes, secondary silanes and secondary amines were less reactive towards this kind of dehydrogenative coupling leading to the formation of aminosilanes.
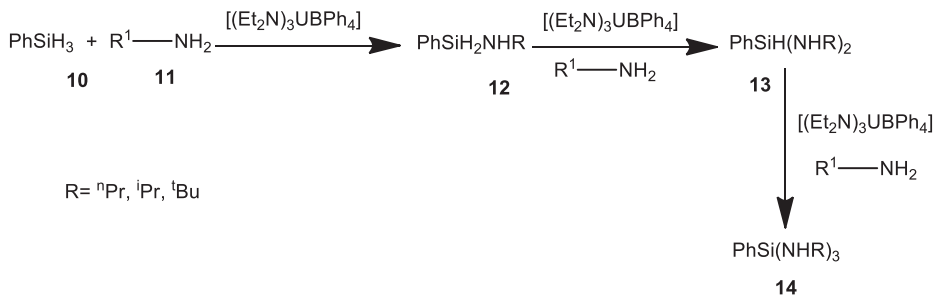
Figure 6.4: Uranium-catalyzed dehydrocoupling reaction of silanes and amines.

6.5 Hydrothiolation of terminal alkynes

Hydrothiolation of alkene/alkyne is an important reaction in organic synthesis as it helps to install sulfur as a heteroatom in the carbon skeleton. In 2009, Marks et al. [38] reported a highly efficient method of hydrothiolation of terminal alkynes (**15**) with thiols (**16**) mediated by organoactinides producing a range of vinyl sulfides (**17**) (Figure 6.5). This reaction was previously found to be catalyzed by a few late transition metals. However, aliphatic thiols were sluggish towards the reaction and the previously reported protocols failed to achieve hydrothiolation of alkynes with aliphatic thiols. Marks and his group successfully involved aliphatic thiols to produce the corresponding hydrothiolated product with alkynes thus making the methodology versatile.

Although several U(IV) and Th(IV) complexes were found to mediate hydrothiolation, the authors studied and reported the activity of $Me_2SiCp''_2Th[CH_2TMS]_2$ complex in details. Several aliphatic, aromatic and benzylic thiols participated in the reaction. However,
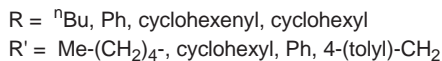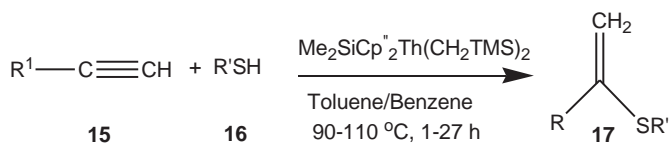
Figure 6.5: Thorium-catalyzed hydrothiolation of terminal alkynes.

primary aliphaticthiols were found to be more reactive than their secondary counterparts due to steric reason. On the alkyne front, aromatic, aliphatic as well as alicyclic alkynes produced the desired hydrothiolation product.

6.6 Tischenko reaction

The Tischenko reaction is a green atom efficient method for the synthesis of esters by coupling of aldehydes. In 2018, Eisen and co-researchers [39] synthesized and characterized a series of benzimdazolin-2-iminato actinide(IV) complexes with actinium metal as uranium and thorium. These complexes were used for the catalysis of homo- and cross-coupling of aldehydes (**18**, **20**) leading to the formation of esters (**19, 21, 22, 23, 24**) via Tischenko reaction (Figure 6.6).

 Substrates containing electron-withdrawing groups gave better results as compared to those with electron-donating groups. In case of cross-coupling of two aldehydes, a mixture of the homo-coupled and cross-coupled products (**21, 22, 23, 24**) was obtained

An = U, Th

R = C_6H_5, 4-CN-C_6H_4, 4-NO_2-C_6H_4, 3-NO_2-C_6H_4,
4-Me-C_6H_4, 4-CF_3-C_6H_4, 4-MeO-C_6H_4, 1-naphthyl,
2-naphthyl, 2-furyl, 2-pyridyl, 2-thienyl, ^{i}Pr, cyclohexyl
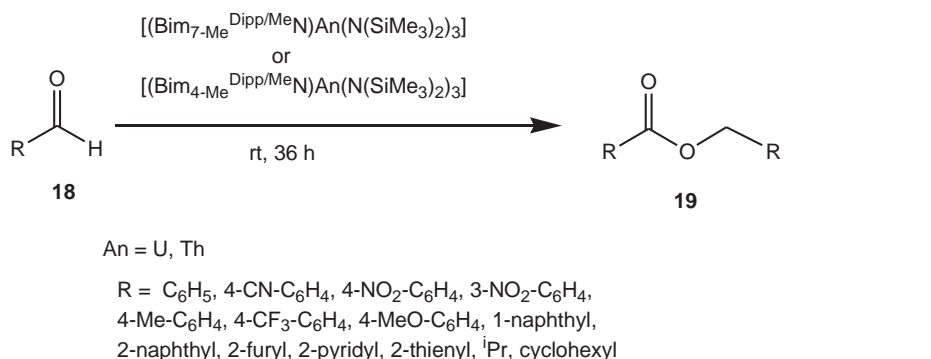
Figure 6.6: Uranium-/thorium-catalyzed homocoupling of aldehydes.

An = U, Th

R = C_6H_5
R' = 2-naphthyl, 2-pyridyl, 3-NO_2-C_6H_4, ^{i}Pr, cyclohexyl
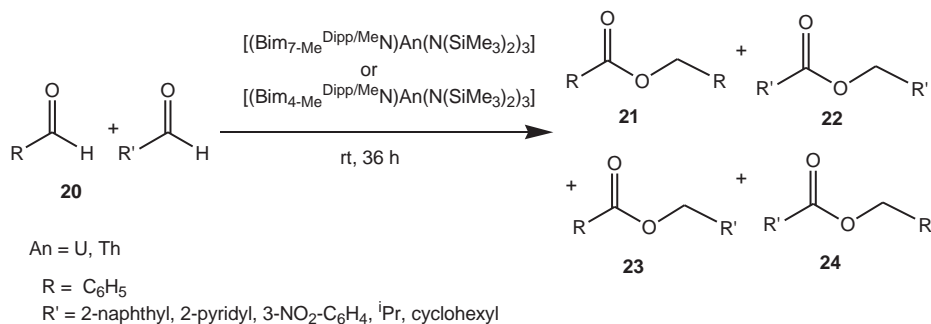
Figure 6.7: Uranium/thorium-catalyzed cross-coupling of aldehydes.

(Figure 6.7). The thorium catalysts were also employed for coupling between aldehydes and alcohols and cross-coupling between aldehydes and trifluoromethylketones.

6.7 Coupling reaction of terminal alkynes and isonitriles

Insertion of isonitriles into metal-acetylide bonds of transition metals is known to happen under stoichiometric conditions [40–42]. However, actinides have not been commonly involved in such reactions.

In 2004, Eisen and his group [43] reported a method where terminal alkynes (**25**) underwent coupling reaction with tert-butylisonitrile (**26**) under the catalysis of [(Et$_2$N)$_3$ U] [BPh$_4$] and Cp*$_2$AnMe$_2$ where the actinides involved were thorium and uranium (Figure 6.8). The reaction occurred via 1,1 insertion of the terminal carbon atom of isonitrile into a metal-imine or metal-acetylide bond. The product distribution was dependent on the nature of catalyst and alkyne/isonitrile ratio (Figure 6.9).
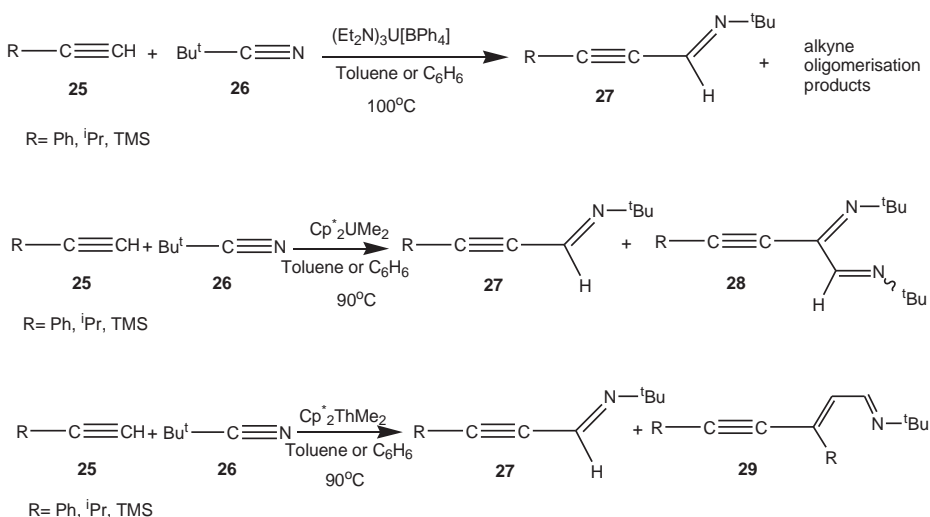
Figure 6.8: Uranium/thorium-catalyzed coupling reaction of terminal alkynes and isonitriles.

entry	catalyst	R	catalyst/^{t}BuNC/ R-C≡CH	time	27(%)	28(%)	29(%)
1	A	Ph	1:50:50	48	81		
2	A	^{i}Pr	1:40:55	48	81		
3	A	TMS	1:40:50	48	80		
4	A	TMS	1:50:30	6	56	13	
				24	81	19	
5	B	Ph	1:40:60	48	90	10	
6	B	^{i}Pr	1:50:20	48	50	50	
7	B	^{i}Pr	1:40:70	48	75	25	
8	B	^{i}Pr	1:100:100	18	90		
9	B	^{i}Pr	1:100:200	2	19		
				17	95		5
				64	60		40
				210	47		53
10	C	^{t}Bu	1:100:100	18	80		
11	C	^{t}Bu	1:100:100	18	90		
12	C	TMS	1:100:100	23	90		
13	C	TMS	1:100:180	18	85		

A = [(Et$_2$N)$_3$U][BPh$_4$] ; B = Cp*$_2$UMe$_2$; C = Cp*$_2$ThMe$_2$

Figure 6.9: Product distribution for uranium/thorium-catalyzed coupling reaction of terminal alkynes and isonitriles.

6.8 Addition of alcohols to carbodiimides

Amido actinide complexes were successfully used for the catalysis of alcohol (**28**) addition to carbodiimides (**29**) (Figure 6.10) by Eisen and his group [44]. The reaction yielded isoureas (**30**) with excellent yields and high stereoselectivities. Isoureas have potent application in synthesis of drugs and other biologically active molecules. This methodology has resulted in an alternative method for synthesis of isourea derivatives. In addition to this the method also provides a novel utility of actinides in catalysis. Based on computational studies and relevant experimental kinetic and thermodynamic data, the authors proposed a plausible mechanism for the reaction.

6.9 Oligomerization of alkynes

Earlier, mainly organolanthanides and transition metals were employed for alkyne polymerization. However, in 1995, Eisen and his group [45] used Cp*$_2$AcMe$_2$ (Ac = U, Th) as an effective catalyst for oligomerization of terminal alkynes (Figure 6.11).
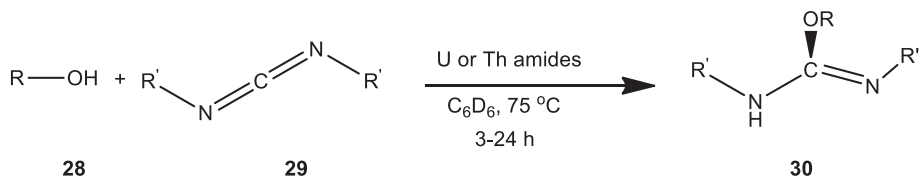
R= Me, Et, ^{i}Pr, ^{t}Bu, Ph

R'= ^{i}Pr, p-tolyl

Figure 6.10: Uranium/thorium-mediated addition of alcohols to carbodiimides.
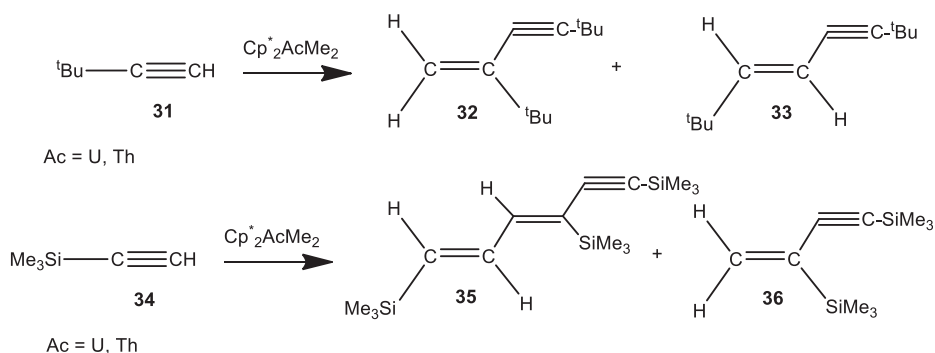
Figure 6.11: Uranium/thorium-catalyzed oligomerization of alkynes.

Cp*$_2$AcMe$_2$ reacted with an excess of tert-butylacetylene (**31**) in a regioselective fashion to yield the head-to-tail dimer 2,4-di-tert-butyl-l-buten-3-yne (**32**) as the main product. The head-to-head dimer (*E*)-1,4-di-tert-butyl-l-buten-3-yne (**33**) was formed in trace amount. However, with trimethyl-silyl-acetylene, mainly catalytic trimerization (**35**) occurs along with small amounts of head-to-tail dimer 2,4-bis(trimethylsilyl)-1-buten-3-yne (**36**).

The authors gave a plausible mechanism for the oligomerization of alkynes (Figure 6.12). The first step involves alkyne C–H bond activation leading to the formation of organo-actinide bisacetylide complex (**38**) along with methane. This is followed by the insertion of the alkyne (in a head to tail fashion) into the alkyne C–H bond, thus resulting in the formation of alkenylactinidecomplex (**39**). This complex then participates in two kinds of reactions; one is σ bond metathesis with an alkyne to produce the dimer (**40**), and the other is insertion of alkyne (tail to head fashion) into (**39**), thus yielding complex bis(dienyny1) organoactinide complex (**41**). This bis(dienyny1) organoactinide complex then participates in σ bond metathesis with another alkyne yielding the dienyne (**42**) and regenerating the bisacetylide complex (**38**).
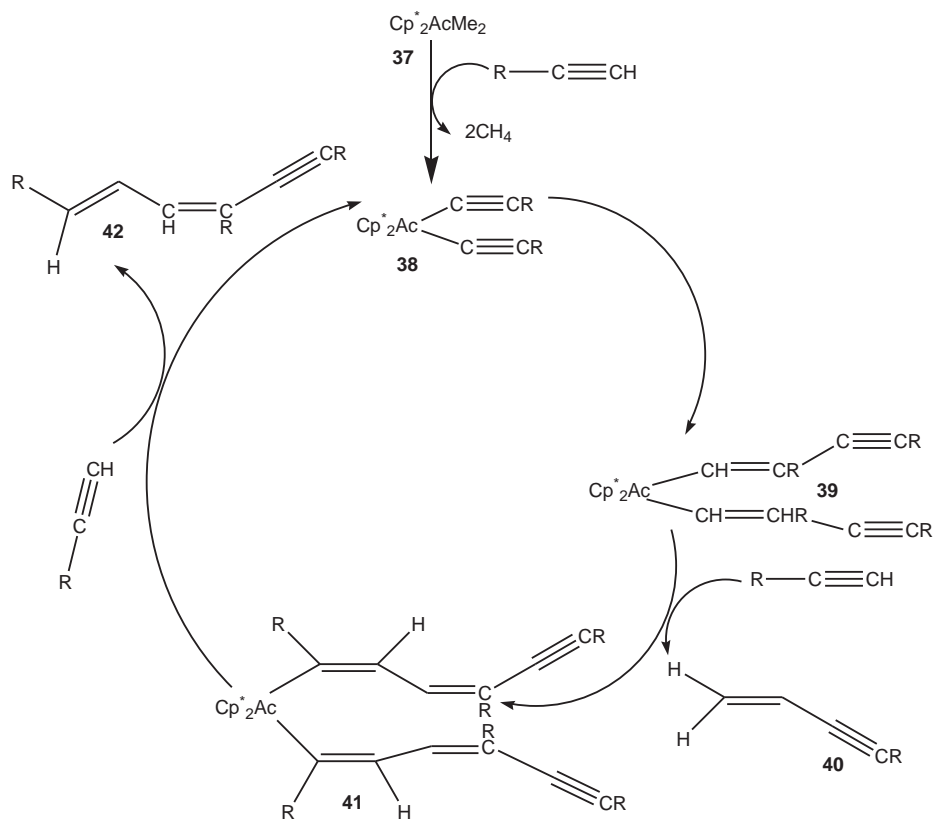
Figure 6.12: Plausible mechanism of uranium/thorium-catalyzed oligomerization of alkynes.

6.10 Hydroxyalkylation/cyclization of alkynyl alcohols

Hydroxyalkylation is a method of addition of an O–H bond across a carbon-carbon double or triple bond. In 2013, Marks and his group [46] reported a highly selective methodology for the hydroxyalkylation/cyclization of alkynyl alcohols (**43**) catalyzed by organothorium complexes (Figure 6.13). Three different thorium catalysts were studied for the reaction, out of which (CGC)Th(NMe$_2$)$_2$ (where CGC = Me$_2$Si(η^5-Me$_4$C$_5$)(^{t}BuN)) showed the best catalytic activity. Several primary and secondary alcohols as well as terminal and internal alkynes were compatible with the reaction. However, primary alcohols and terminal alkynes gave better results as compared to secondary alcohols and internal alkynes thus showing that steric effect has a dominant role in the reaction.

The reaction when monitored via 1H-NMR spectroscopy showed the rate law to be zero order with respect to substrate and first order with respect to catalyst. Based on

reactivity patterns, activation data, and kinetic study, the authors proposed a mechanism involving insertion of alkyne into Th–O bond followed by fast Th–C protonolysis resulting in the formation of product and regeneration of the starting Th–OR species.
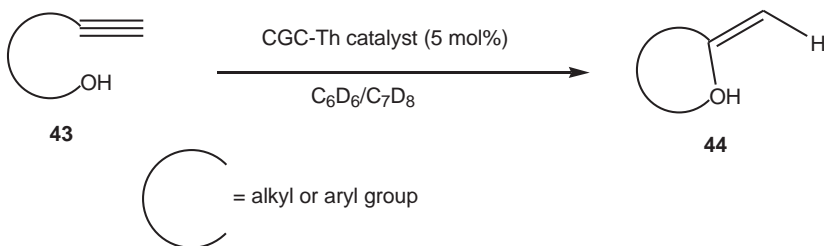
Figure 6.13: Thorium-catalyzed hydroxyalkylation/cyclization of alkynyl alcohols.

6.11 Ring-opening polymerization of cyclic esters

Polymers of cyclic esters like ε-caprolactone and L-lactide, being biodegradable in nature, have high importance as sustainable polymers in industries. It was commonly believed that presence of oxygen containing substrates would decrease the catalytic activity of actinides as early actinides are known to be oxophilic in nature. However, Eisen and his coworkers [47] successfully employed actinide complexes (**45, 46, 47**) (Figure 6.14) for the ring-opening polymerization of ε-caprolactone and L-lactide (Figure 6.15).

Out of the three complexes employed as catalysts, thorium complex (**47**) was found to exhibit highest catalytic activity. This might be attributed to the lower oxophilic nature of thorium as compared to uranium. Temperature had a dominant role in the conversion rate and catalytic activity. It was observed that as temperature was increased, reactions proceeded in less time with higher conversion.
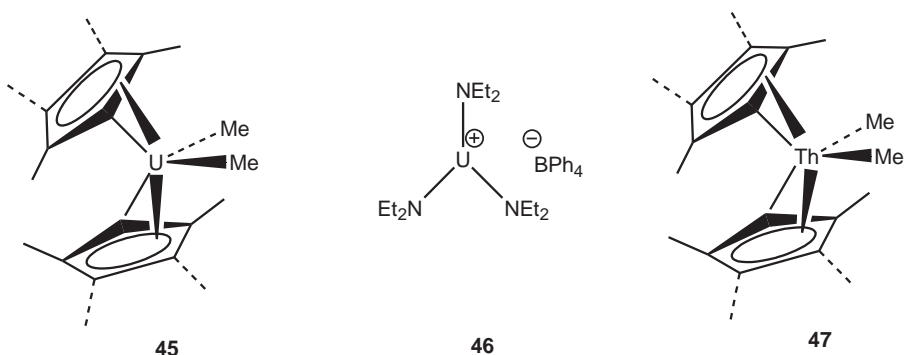
Figure 6.14: Actinide complexes employed as catalysts for ring-opening polymerization of ε-caprolactone.
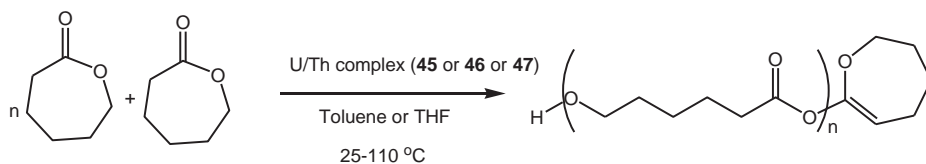
Figure 6.15: Actinide complexes catalyzed ring-opening polymerization of ε-caprolactone.

6.12 Ring-opening polymerization of epoxides

Walshe and his group [48] used uranium complexes (Figure 6.16) as precatalysts for the ring-opening polymerization of propylene oxide and cyclohexene oxide. The polymerization reactions occur at room temperature with only 1 mol% of the catalyst.

Based on spectroscopic and kinetic and thermodynamic evidences, the authors suggested a bimetallic mechanism for the polymerization reaction where the epoxide coordinated to a uranium center is attacked by aryloxide or halide attached to another uranium center [49].
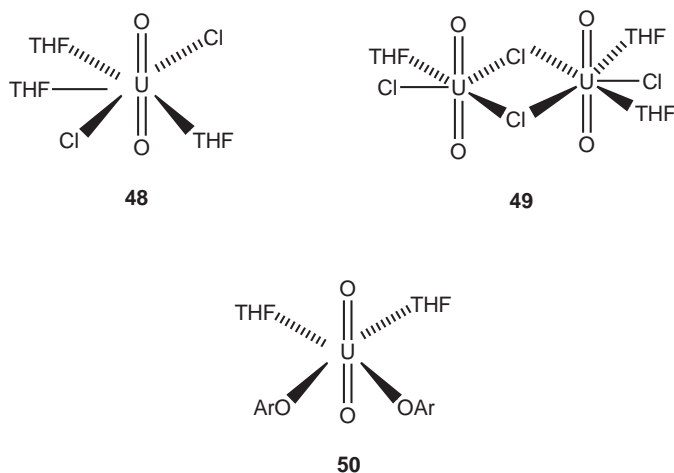
Figure 6.16: Actinide complexes employed for ring-opening polymerization of epoxides.

6.13 Catalytic insertion of protic nucleophiles to heterocumulenes

In 2015, Eisen and his group [50] prepared actinide pre-catalysts (**51, 52, 53)** (Figure 6.17) and used them in the catalytic insertion of C–H/N–H/P–H/S–H bonds to heterocumulenes (Figure 6.18). High reaction rates and good functional group tolerances were observed in the case of insertion into carbodiimides. However, insertion into phenylisothiocyanateand phenylisocyanate exhibited less reactivity.

A variety of protic nucleophilic substrates like amines, phosphines, thiols, and even alkynes successfully participated in the reaction thus bringing out the versatility of the methodology. Based on deuterium labeling studies for the reaction of N,N'-diisopropylcarbodiimide and $PhND_2$, the authors proposed a mechanism involving protolytic cleavage of guanidinate as the rate determining step.
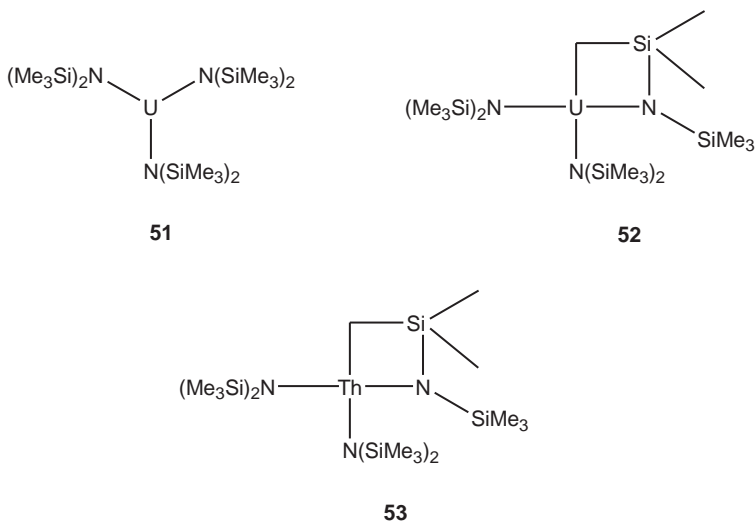
Figure 6.17: Actinide complexes employed for catalytic insertion of protic nucleophiles into heterocumulenes.

Figure 6.18: Actinide complexes catalyzed insertion of protic nucleophiles into heterocumulenes.
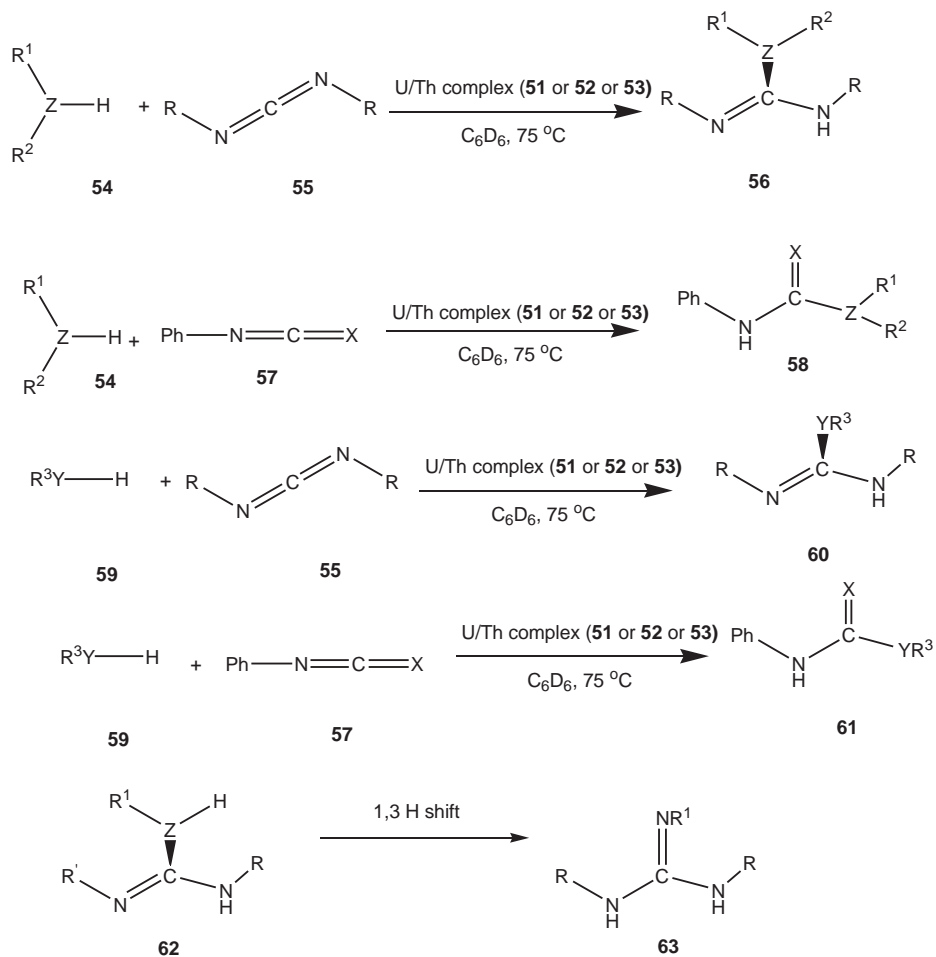
R= ^{i}Pr, p-tolyl

R^1= Et, ^{i}Pr, Ph, 4-MeO-Ph,4-Me-Ph, 4-Cl-Ph

R^2= H, Et, Ph

Z= N, P

X= O,S

R^{3}Y = PhCH$_2$S-, TMS—C≡C— , Ph—C≡C—

6.14 Conclusions

In spite of the hazards related to the handling of actinides, research on actinides, especially uranium and thorium, is steadily progressing. The potential of these actinides in organometallic chemistry is gradually being exploited, and this in turn will lead to more research on other actinide members as well, thus exploring their full strength as organometallic agents. In this chapter, we tried to assemble a few areas where actinides have been successfully employed as catalysts in organic synthesis. We sincerely hope that this chapter will prove to be useful in the future growth of research on actinides.

References

[1]   Ephritikhine, M. Synthesis, structure, and reactions of hydride, borohydride, and aluminohydride compounds of the f-elements. Chem Rev, 1997, 97, 2193–2242.

[2]   Berthet, JC, Ephritikhine, M. New advances in the chemistry of uranium amide compounds. Coord Chem Rev, 1998, 178–180, 83–116.

[3]   Edelmann, FT, Lorenz, V. Lanthanides and actinides: Annual survey of their organometallic chemistry covering the year 1996. Coord Chem Rev, 2000, 209, 99–160.

[4]   Edelmann, FT, Gun'ko, Y. Lanthanides and actinides: Annual survey of their organometallic chemistry covering the year 1995. Coord Chem Rev, 1997, 165, 163–237.

[5]   Blake, PC, Edelman, MA, Hitchcock, PB, Hu, J, Lappert, MF, Tian, S, Müller, G, Atwood, JL, Zhang, H. Organometallic chemistry of the actinides. J Organomet Chem, 1998, 551, 261–270.

[6]   Hitchcock, PB, Hu, J, Lappert, MF, Tian, S. Organometallic chemistry of the actinides. Part 3 novel 1-aza-allyl- and β-diketiminatothorium chlorides; X-ray structures of [{Th(L¯L')2(μ3-Cl)(μ-Cl)2K (OEt2)}∞] and [Th(L¯L)2Cl2] [LL′ = N(SiMe3)C(But)C(H)SiMe3; LL = N(SiMe3)C(Ph)2CH]. J Organomet Chem, 1997, 536–537, 473–480.

[7]   Hitchcock, PB, Holmes, SA, Lappert, MF, Tian, S. Synthesis, structures and reactions of ytterbium(II) alkyls. J Chem Soc Chem Commun, 1994, 2691–2692.

[8]   Marks, TJ, Abel, EW, Stone, FGA, Wilkinson, G, eds.,Comprehensive Organometallic Chemistry I, Oxford: Pergamon Press, 1982, (Chapter 21).

[9]   Edelmann, FT. In: Comprehensive Organometallic Chemistry II. Abel, EW, Stone, FGA, Wilkinson, G, eds., Elsevier Science, Oxford, 1995, 12.

[10]   Barnea, E, Eisen, MS. Organoactinides in catalysis. Coord Chem Rev, 2006, 250, 855–899.

[11]   MacNeil, CS, Dickie, TKK, Hayes, PG. In: Pincer Compounds: Chemistry and Applications. Morales, DM, ed., Elsevier, 2018.

[12]   Andrea, T, Barnea, E, Wang, J, Eisen, MS. Catalysis vs. Oxophilicity: Breaking the myth of inactive actinide-oxo complexes. IOP Con Ser Mater Sci Eng, 2010, 9, 012027–012036.

[13]   Batrice, RJ, Karmel, ISR, Eisen, MS. In: Encyclopedia of Inorganic and Bioinorganic Chemistry, John Wiley & Sons, Ltd., 2018.

[14]   Leduc, J, Frank, M, Jürgensen, L, Graf, D, Raauf, A, Mathur, S. Chemistry of actinide centers in heterogeneous catalytic transformations of small molecules. ACS Catal. 2019, 9(6), 4719–4741.

[15]   Karmel, ISR, Batrice, RJ, Eisen, MS. Catalytic organic transformations mediated by actinide complexes. Inorganics, 2015, 3, 392–428.

[16]   Bart, SC, Meyer, K. Highlights in uranium coordination chemistry. Struct Bond, 2008, 127, 119–176.

[17]   Fox, AR, Bart, SC, Meyer, K, Cummins, CC. Towards uranium catalysts. Nature, 2008, 455, 341–349.

[18] Arnold, PL, Turner, ZR. Carbon oxygenate transformations by actinide compounds and catalysts. Nat Rev Chem, 2017, 1, 0002.

[19] Su, J, Windorff, CJ, Batista, ER, Evans, WJ, Gaunt, AJ, Janicke, MT, Kozimor, SA, Scott, BL, Woen, DH, Yang, P. Identification of the formal+2 oxidation state of neptunium: Synthesis and structural characterization of {Np-II[C$_5$H$_3$(SiMe$_3$)$_2$]$_3$}$^{1-}$. J Am Chem Soc, 2018, 140, 7425–7428.

[20] Ward, AL, Lukens, WW, Lu, CC, Arnold, J. Photochemical route to actinidetransition metal bonds: synthesis, characterization and reactivity of a series of thorium and uranium heterobimetallic complexes. J Am Chem Soc, 2014, 136, 3647–3654.

[21] Falcone, M, Poon, LN, Tirani, FF, Mazzanti, M. Reversible dihydrogen activation and hydride transfer by a uranium nitride complex. Angew Chem Int Ed, 2018, 57, 3697–3700.

[22] Falcone, M, Barluzzi, L, Andrez, J, FadaeiTirani, F, Zivkovic, I, Fabrizio, A, Corminboeuf, C, Severin, K, Mazzanti, M. The role of bridging ligands in dinitrogen reduction and functionalization by uranium multimetallic complexes. Nat Chem, 2018, 11, 154–160.

[23] Gardner, BM, Stewart, JC, Davis, AL, McMaster, J, Lewis, W, Blake, AJ, Liddle, ST. Homologation and functionalization of carbon monoxide by a recyclable uranium complex. Proc Natl Acad Sci U S A, 2012, 109, 9265–9270.

[24] Gardner, BM, Liddle, ST. Small-molecule activation at uranium(III). Eur J Inorg Chem, 2013, 2013, 3753–3770.

[25] Liu, H, Ghatak, T, Eisen, MS. Organoactinides in catalytic transformations: Scope, mechanisms and Quo Vadis. Chem Commun, 2017, 53, 11278–11297.

[26] Weiss, CJ, Wobser, SD, Marks, TJ. Organoactinide-mediated hydrothiolation of terminal alkynes with aliphatic, aromatic, and benzylic thiols. J Am Chem Soc, 2009, 131, 2062–2063.

[27] Dalodière, E, Virot, M, Morosini, V, Chave, T, Dumas, T, Hennig, C, Wiss, T, Dieste Blanco, O, Shuh, DK, Tyliszcak, T, Venault, L, Moisy, P, Nikitenko, SI. Insights into the sonochemical synthesis and properties of salt-free intrinsic plutonium colloids. Sci Rep, 2017, 7, 43514–43523.

[28] Hudry, D, Apostolidis, C, Walter, O, Janßen, A, Manara, D, Griveau, J-C, Colineau, E, Vitova, T, Prüßmann, T, Wang, D, Kübel, C, Meyer, D. Ultra-small plutonium oxide nanocrystals: An innovative material in plutonium science. Chem Eur J, 2014, 20, 10431–10438.

[29] Fang, B, Ren, W, Hou, G, Zi, G, Fang, D-C, Maron, L, Walter, MD. An actinide metallacyclopropene complex: synthesis, structure, reactivity, and computational studies. J Am Chem Soc, 2014, 136, 17249–17261.

[30] Matson, EM, Breshears, AT, Kiernicki, JJ, Newell, BS, Fanwick, PE, Shores, MP, Walensky, JR, Bart, SC. Trivalent uranium phenylchalcogenide complexes: exploring the bonding and reactivity with CS$_2$ in the Tp*$_2$UEPh series (E = O, S, Se, Te). Inorg Chem, 2014, 53, 12977–12985.

[31] Zhou, E, Ren, W, Hou, G, Zi, G, Fang, D-C, Walter, MD. Small molecule activation mediated by a thorium terminal imido metallocene. Organometallics, 2015, 34, 3637–3647.

[32] Ren, W, Zhou, E, Fang, B, Hou, G, Zi, G, Fang, D-C, Walter, MD. Experimental and computational studies on the reactivity of a terminal thorium imidometallocene towards organic azides and diazoalkanes. Angew Chem Int Ed, 2014, 53, 11310–11314.

[33] Liddle, ST. The renaissance of non-aqueous uranium chemistry. Angew Chem Int Ed, 2015, 54, 8604–8641.

[34] Burns, CJ, Eisen, MS. The Chemistry of the Actinide and Transactinide Elements, 3rd ed., Morss, LR, Edelstein, N, Fuger, J, eds.,Springer, 2006, 2911–3012.

[35] Haskel, A, Straub, T, Eisen, MS. Organoactinide-catalyzed intermolecular hydroaminationof terminal alkynes. Organometallics, 1996, 15, 3773–3775.

[36] Dash, AK, Wang, JQ, Eisen, MS. CatalyticHydrosilylation of terminal alkynes promoted by organoactinides. Organometallics, 1999, 18, 4724–4741.

[37] Wang, JX, Dash, AK, Berthet, JC, Ephritikhine, M, Eisen, MS. Dehydrocoupling reactions of amines with silanes catalyzed by[(Et$_2$N)$_3$U][BPh$_4$]. J Organomet Chem, 2000, 610, 49–57.

[38]   Weiss, CJ, Wobser, SD, Marks, TJ. Organoactinide-mediated hydrothiolation of terminal alkynes with aliphatic, aromatic, and benzylic thiols. J Am Chem Soc, 2009, 131, 2062–2063.

[39]   Liu, H, Khononov, M, Fridman, N, Tamm, M, Eisen, MS. Synthesis, characterization and catalytic performances of benzimidazolin-2-iminato actinide (IV) complexes in the tishchenko reactions for symmetrical and unsymmetrical esters. J Organomet Chem, 2018, 857, 123–137.

[40]   Martins, AM, Ascenso, JR, De-Azevedo, CG, Dias, AR, Duarte, MT, Da-Silva, JF, Veiros, LF, Rodrigues, SS. Insertion of isocyanides into group 4 metal−carbon and metal−nitrogen bonds. Syntheses and DFT calculations. Organometallics, 2003, 22, 4218–4228.

[41]   Takei, F, Yanai, K, Onitsuka, K, Takahashi, S. Screw-sense-selective polymerization of aryl isocyanides initiated by a Pd-Pt μ-EthynedylDinuclear complex: a novel method for the synthesis of single-handed helical poly(isocyanide)s with the block copolymerization technique. Chem Eur J, 2000, 6, 983–993.

[42]   Ahlers, W, Erker, G, Frohlich, R. Reaction of (σ-alkynyl) Group 4 metallocene cation complexes with alkyl- and arylisocyanides. J Organomet Chem, 1998, 571, 83–89.

[43]   Barnea, E, Andrea, T, Kapon, M, Berthet, J-C, Ephritikhine, M, Eisen, MS. Catalytic coupling of terminal alkynes with isonitriles promoted by organoactinide complexes. J Am Chem Soc, 2004, 126, 10860–10861.

[44]   Batrice, RJ, Kefalidis, CE, Maron, L, Eisen, MS. Actinide-catalyzed intermolecular addition of alcohols to carbodiimides. J Am Chem Soc. 2016, 138(7), 2114–2117.

[45]   Straub, T, Haskel, A, Eisen, MS. Organoactinide-catalyzed oligomerization of terminal acetylenes. J Am Chem Soc, 1995, 117, 6364–6365.

[46]   Wobser, SD, Marks, TJ. Organothorium-catalyzed hydroalkoxylation/cyclization of alkynylalcohols. Scope, mechanism, and ancillary ligand effects. Organometallics, 2013, 32, 2517–2528.

[47]   Barnea, E, Moradove, D, Berthet, J-C, Ephritikhine, M, Eisen, MS. Surprising activity of organoactinide complexes in the polymerization of cyclic mono- and diesters. Organometallics, 2006, 25, 320–322.

[48]   Baker, RJ, Walshe, A. New reactivity of the uranyl ion: Ring opening polymerisation of epoxides. Chem Commun, 2012, 48, 985–987.

[49]   Braune, W, Okuda, J. An efficient method for controlled propylene oxide polymerization: the significance of bimetallic activation in aluminum lewis acids. Angew Chem Int Ed, 2003, 42, 64–68.

[50]   Batrice, RJ, Eisen, MS. Catalytic insertion of E-H bonds (E=C, N, P, S) into heterocumulenes by amido-actinide complexes. Chem Sci, 2016, 7, 939–944.

Asish Kumar Dey and Sasadhar Majhi*

7 Role of samarium in organic synthesis

7.1 Introduction

Organic synthesis is a particular branch of chemical synthesis which has led to a magnificent host of benefits for society involving useful products ranging from pharmaceuticals and agricultural chemicals to diagnostics and high-technology materials [1]. The organic synthetic community has shown interest in the applications of lanthanide derivatives in catalysis because of their potent Lewis acid characters along with their nontoxicity [2]. Several organic transformations, including aza-Henry reaction, Mukaiyama aldol, [4 + 2] cycloaddition, Reformatsky reaction, stereoselective β-elimination, Michael reaction, multicomponent reaction, Michael-iminoaldol tandem reaction, Tishchenko reaction, and more, were carried out by Kagan's reagent, samarium diiodide (SmI_2) efficiently [3, 4]. Henri Kagan invented samarium(II) iodide (SmI_2) as a potent single-electron reducing agent in 1977 which has found increasing uses in organic synthesis [5]. SmI_2 also catalyzes the ring opening of epoxides successfully at room temperature and it can be applied in the total synthesis of bioactive natural products [6–14]. Various chemical transformations include the utilization of expensive and stoichiometric amounts of reagents that suffer from poor regioselectivity [15, 16]. Moreover, these chemical syntheses need more reaction times. So, the development of novel and efficient methodologies for organic synthesis is still demanding. In this context, samarium diiodide and metallic samarium exhibit widespread applications as powerful reducing agents [2–5]. Currently, metallic samarium has attracted attention as a reducing agent as it is cheap, stable in the air, and can be employed directly as a reductant instead of samarium diiodide [16, 17]. The present article focuses on the applications of samarium diiodide and metallic samarium in organic synthesis.

***Corresponding author: Sasadhar Majhi,** Department of Chemistry (UG and PG), Triveni Devi Bhalotia College, Kazi Nazrul University, Raniganj 713347, West Bengal, India. e-mail: sasadharmajhi@gmail.com
Asish Kumar Dey, Triveni Devi Bhalotia College, Kazi Nazrul University, Raniganj 713347, West Bengal, India

7.2 Applications of samarium diiodide and metallic samarium in organic synthesis

This section deals with the applications of samarium diiodide and metallic samarium in chemical synthesis since the primary goal of this article is to represent the brilliant applications of lanthanide derivatives for syntheses of valuable organic compounds. In 2002, B. K. Banik published a graceful and stylish review regarding samarium metal in chemical synthesis [17]. So, this chapter aims to cover the uses of samarium diiodide mainly and metallic samarium also in organic transformations from 2002 to 2021.

7.2.1 Multicomponent reaction

Multicomponent reactions are convergent transformations that generate a single product from three or more starting materials through a one-pot fashion, where it preserves all or most of the atoms of the reactants and it furnishes high yields, and atom/step economy [18]. Organic compounds comprising diarylmethanol skeletons have broad applications in the areas of medicine and materials [19]; they can also be used as intermediates in the synthesis of several anti-inflammatory and anticancer drugs [20]. Diphenhydramine (DPH) containing diarylmethanol scaffold is employed to treat a variety of allergic diseases [20, 21] and a benzhydrol diacetate derivative displays moderate HL-60 cell-growth-inhibitory activity with a half-maximal inhibitory concentration (IC$_{50}$) value of 3.5 μM [22]. Recently, Liu et al. [23] reported the synthesis of promising organic compounds including diarylmethanol skeletons under the Sm–CuI catalyst system through the three-component C–H functionalization reaction from commercially available halobenzenes **1**, esters **2**, and *N,N*-dimethylformamide **3** in 2021 (Figure 7.1). This novel one-pot strategy took place under mild conditions to furnish desired products **4** in moderate to good yields (43–83%, bromobenzene as a substrate) which demonstrates an encouraging perspective for the exploitation of samarium metal in organic reactions.

7.2.2 Reductions

The reduction reaction plays central importance in organic chemistry along with biochemistry [24]. Hence, this section deals with the reduction reaction in chemical synthesis.
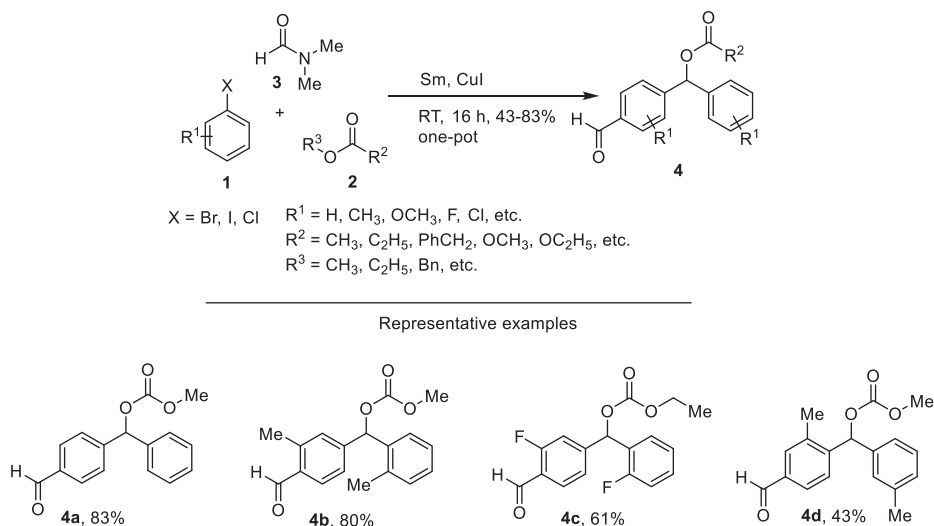
Figure 7.1: Three-component reaction for the synthesis of diarylmethanol skeletons in the Sm–CuI system.

7.2.2.1 Allylic benzoate reduction

O'Neil et al. [25] carried out SmI$_2$-assisted allylic benzoate reductions to offer a novel route to access asymmetric carbon atoms in 2020. It has been investigated that stereospecificity in these transformations is solely dependent on the nature of the alkene substituents; the reaction is stereospecific for substrates bearing alkyl-substituted alkenes (*trans*-**5** to **6**, *cis*-**5** to **7**) whereas the transformation becomes nonstereospecific for the insertion of a phenyl substituent (*trans*-**8** or *cis*-**8** to **9**) (Figure 7.2). The results indicated that the stereochemistry of the main product from these transformations is compatible with a mechanism including the construction of a chelated organosamarium intermediate, thereafter the intramolecular protonation from water molecule that is likely tied to the Sm^{3+} (**10** to **10a** to **11**) [26]. The strong rationale is introduced based on the stabilization of a suggested organosamarium intermediate by the phenyl ring [27].

7.2.2.2 Bis-benzoyl ester reduction

W. O'Neil and coworkers [28] accomplished the total synthesis of the biologically relevant biphenolic phytochemical honokiol (**18**) involving the samarium-promoted bis-benzoyl ester reduction in 2016. Neolignan honokiol (**18**) exhibits powerful antioxidative, antiangiogenic, anticancer, and anti-inflammatory activities [29]. 5-Bromo-2-methoxybenzaldehyde
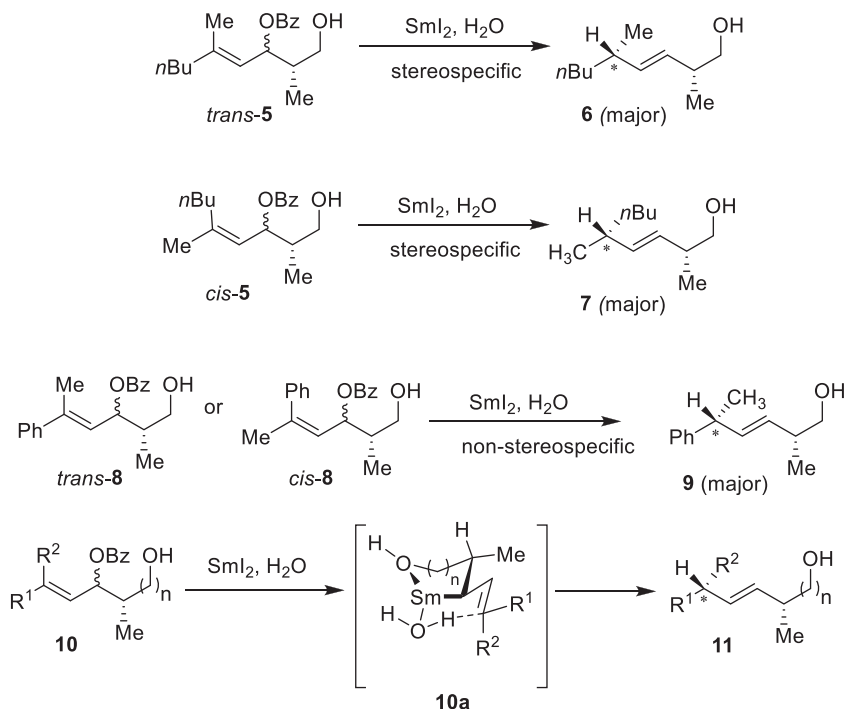
Figure 7.2: Regio- along with diastereoselective allylic benzoate reductions by $SmI_2(H_2O)_n$ through organosamarium intermediate.

(**12**) produced boronate ester (**13**); the biphenyl core (**15**) was constructed by the reaction of 3-bromo-4-methoxybenzaldehyde (**14**) with boronate ester (**13**) through a Suzuki coupling in excellent yield on the multi-gram scale (Figure 7.3). The dialdehyde (**15**) was treated with vinylmagnesium bromide to furnish the intermediate diol (**16**); the diol (**16**) underwent acylation with benzoyl chloride followed by treatment with SmI_2/MeOH delivered dimethylhonokiol (**17**) in 98% yield as a vital step. The natural bioactive honokiol (**18**) was obtained from dimethylhonokiol (**17**) in the presence of the tris(pentafluorophenyl)borane/Et_3SiH system in 42% overall yield from readily available aldehydes (**14**) and (**12**) [28].

7.2.2.3 Reduction of phenacyl azide

In heterocyclic chemistry, the synthesis of pyrroles plays an important role as various pyrroles are subunits of secondary metabolites, pharmaceutical agents along with polymers [30]. Zhang et al. [31] provided an efficient protocol for the synthesis of 2,4-diarylpyrroles **20** from easily accessible starting materials phenacyl azides **19** using Kagan's reagent, samarium(II) iodide under mild and neutral conditions with good

yields for the first time (Figure 7.4). It has been investigated that samarium(II) iodide can effectively stimulate the reduction of starting materials **19** at room temperature as a green methodology.
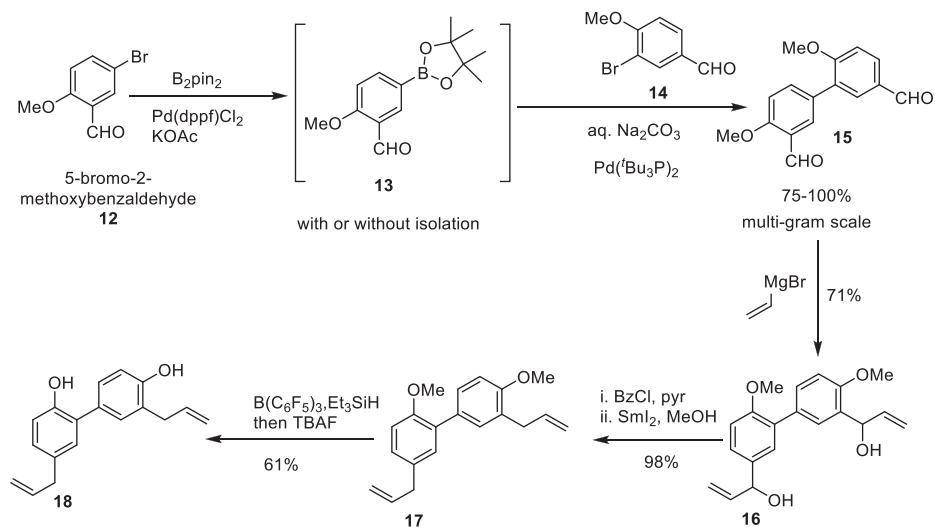
Figure 7.3: Total synthesis of natural bioactive honokiol utilizing the samarium-promoted bis-benzoyl ester reduction.
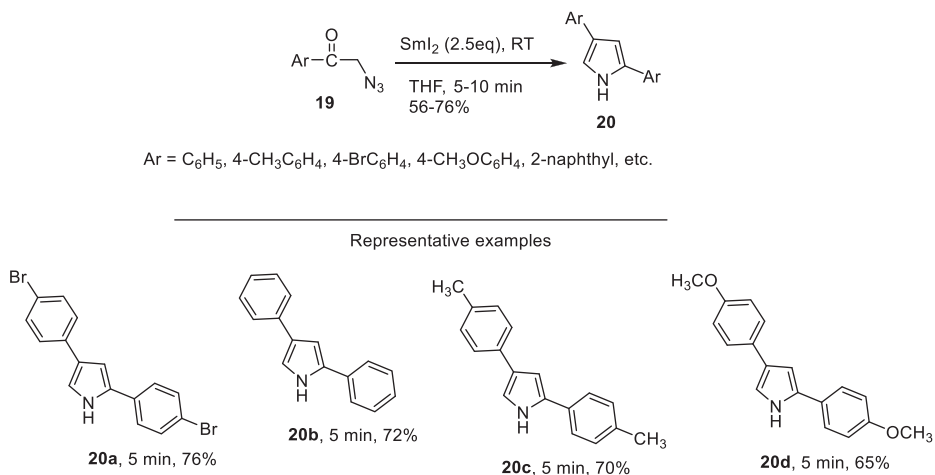
Figure 7.4: Reduction of phenacyl azides promoted by samarium(II) iodide.

7.2.3 Reformatsky reaction

The β-hydroxy-γ-alkenyl-ketones (esters or acids, amides) are of great interest due to their applications as synthetic intermediates and they are also subunits of secondary metabolites such as eremofortin F [32], mohangic acids [33], largazole [34] and more. Laschat and coworkers [35] executed an asymmetric SmI$_2$-assisted Reformatsky reaction involving terpene-derived enals as rarely electrophilic substrates in 2019. This methodology provided stereochemically well-developed 3-hydroxy-4-alkenyl- along with 3-hydroxy-2-methyl-4-alkenyl imides from 3-(2-haloacyl)-2-oxazolidinones. 3-(2-Haloacyl)-2-oxazolidinones **21a**, **b** and **24** were treated with enals geranial (*E*)-**22** and neral (*Z*)-**22** to furnish the desired imides (**23**, **25**) in the presence of the SmI$_2$ in THF for 1 h (Figure 7.5). The results indicated that geranial (*E*)-**22** delivered the diastereomers (3′*R*,4′*E*)-**23a** and (3′*S*,4′*E*)-**23a** in 73 and 6% yield (dr 92:8) whereas (3′*R*,4′*Z*)-**23a** and (3′*S*,4′*Z*)-**23a** were obtained from neral (*Z*)-**22** yielded in 71 and 7% yield (dr 91:9). It is interesting to note that the configuration of the enal C = C double bond does not influence both yields and diastereoselectivities.

7.2.4 Stereoselective β-elimination

Halovinyl carbohydrate derivatives act as valuable synthetic intermediates; they are employed as intermediates in the synthesis of natural products [36], nucleosides [37], and *C*-glycosides [38]. Rodríguez-Solla and coworkers [39] developed a novel methodology for the synthesis of carbohydrate-derived (*Z*)-vinyl halides and silanes in 2018. Galactose-derived aldehyde (**26**) was treated with lithium diisopropylamide (LDA) in THF at −78 °C to produce derivatives (**27a-d**) in good yield (64–86%) with moderate selectivity. Initially, organolithium reagents furnished the diiodomethylcarbinol intermediate (**27a**) in good yield (28–86%), but these reagents are not stable even at low temperatures (Figure 7.6). However, base LDA provided the best results for the synthesis of the corresponding addition products (**27a–d**) in terms of yield and selectivity (Table 7.1) [39]. Next, compounds **27** were converted in the corresponding acetates **28** in the presence of the acetic anhydride (Ac$_2$O) in pyridine and 4-dimethylaminopyridine (DMAP) in excellent yields (93–98%). Finally, halocarbinol acetates **28** (as a mixture of D-/L-*glycero* stereoisomers) delivered the targeted (*Z*)-vinyl halides (**29a-c**) and the vinylsilane **29d** using 2.5 equiv. of SmI$_2$ in THF under reflux through β-elimination reaction as a key step (Table 7.2). This transformation took place in a stereoselective manner but not in a stereospecific fashion as the diastereoisomeric ratio arises from compounds **28** to **29**.

A plausible mechanism was also provided for the synthesis of (*Z*)-vinyl halides (**29a-c**) and the vinylsilane **29d**. Halocarbinol acetates **28** reacted with the first equivalent of samarium diiodide to furnish a radical intermediate **30** (Figure 7.7). Next, the radical specie **30** was transformed into the anionic intermediate **31** by the second
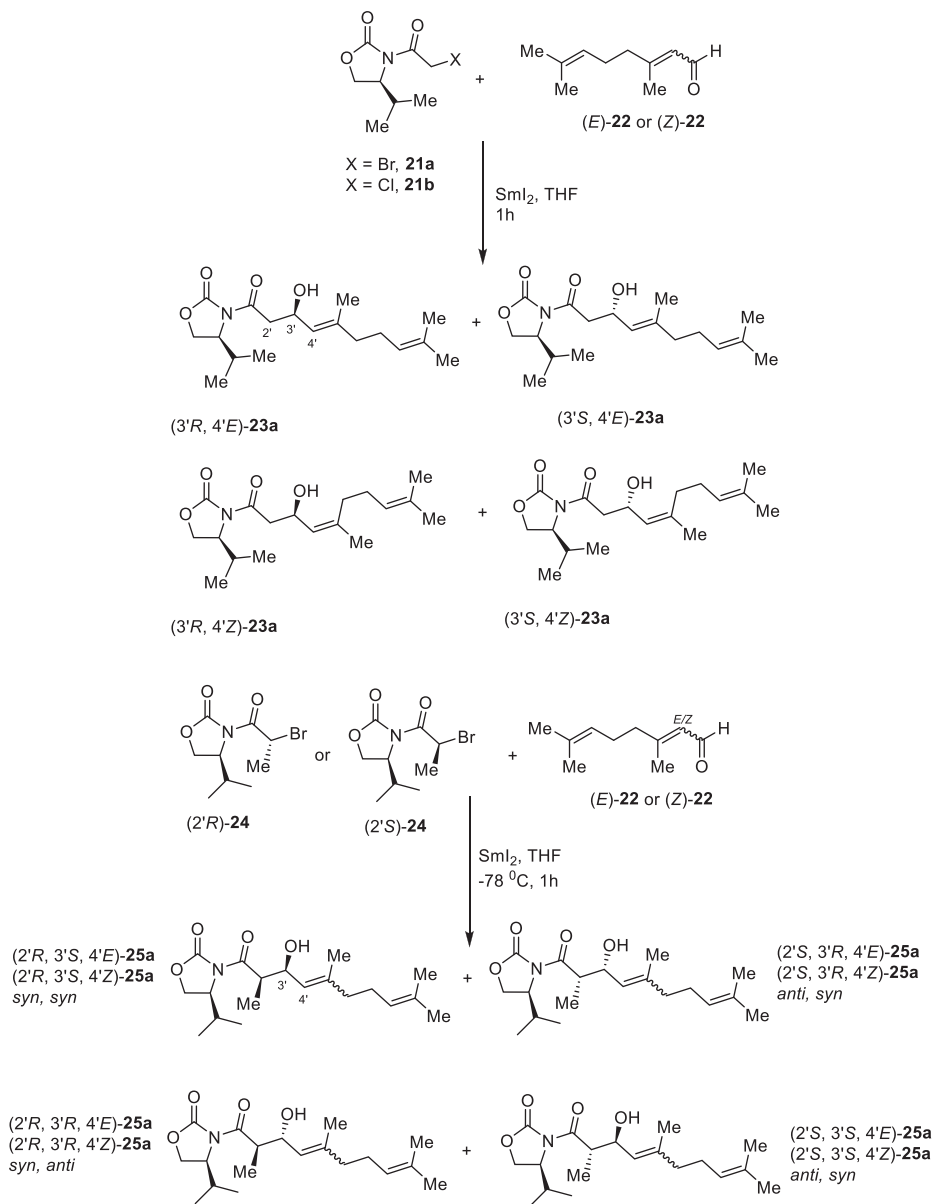
Figure 7.5: SmI$_2$-promoted Reformatsky reaction of 3-(haloacetyl)oxazolidinones and 3-(2-bromopropanoyl)oxazolidinone with terpene-derived enals.

equivalent of samarium diiodide. The anionic intermediate **31** was effective to generate (*Z*)-vinyl compound **29** through 1,2-elimination [39]. A six-membered ring **31** was obtained by the chelation of Sm(III) center with the oxygen atom of the acetyl group. The

(*Z*)-selectivity in this transformation was interpreted by the chelation-control model; chair-like structure **I–II** was accepted in which the X^1 and R occupy an axial and equatorial position, respectively.
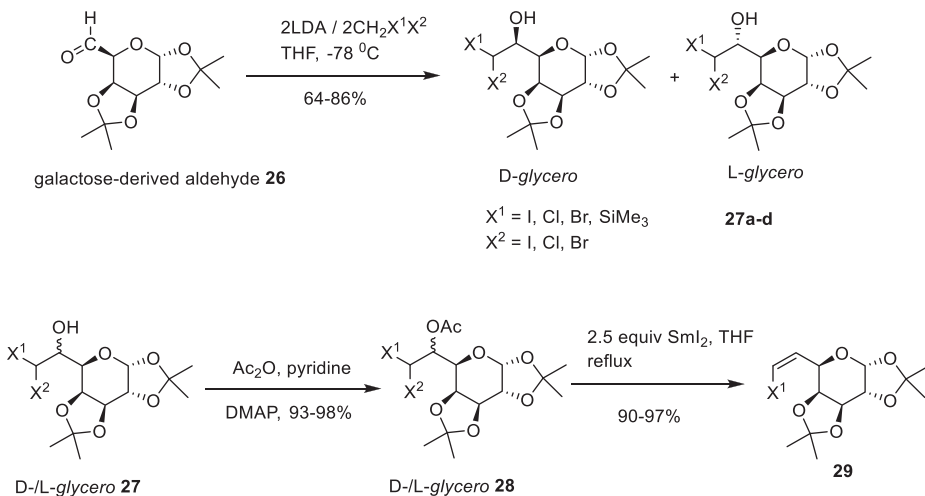
Figure 7.6: Synthesis of (*Z*)-vinyl halides and the vinylsilane.

Table 7.1: Preparation of halomethyl carbinols **27a-d.**

Entry	X^1	X^2	Intermediate (27)	D-/L-*glycero*	Yield (%)
1	I	I	**27a**	82/18	86
2	Cl	I	**27b**	66/34	64
3	Br	Br	**26c**	84/16	79
4	SiMe₃	Cl	**27d**	67/33	70
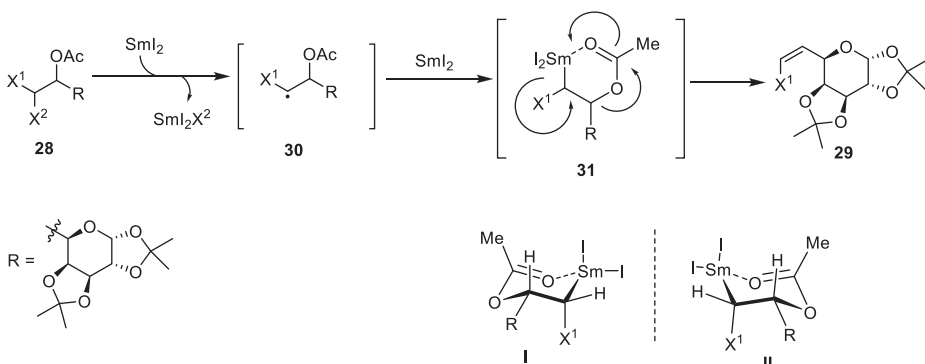
Figure 7.7: A plausible mechanism for the synthesis of (*Z*)-vinyl halides and the vinylsilane.

Table 7.2: Synthesis of targeted (Z)-vinyl halides **29a-c** and silane **29d.**

Entry	X^1	X^2	Desired product (29)	Z/E	Yield (%)
1	I	I	**29a**	95/5	90
2	Cl	I	**29b**	96/4	97
3	Br	Br	**29c**	94/6	95
4	SiMe$_3$	Cl	**29d**	81/19	97

7.2.5 Aza-Henry reaction

The aza-Henry reaction, also known as nitro-Mannich reaction, includes the nucleophilic addition of nitroalkanes to imines to furnish C–X or C–C bonds in better yield and stereocontrol of the method usually; it is considered as one of the most efficient synthetic tools for the syntheses of intermediates for valuable pharmaceutical targets as well as of chiral auxiliaries for asymmetric catalysis [40]. Rodríguez-Solla et al. [41] developed a new protocol for the preparation of nitroamines **34** by the aza-Henry reaction of bromonitromethane **33** with different imines **32** in the presence of the SmI$_2$ under very mild conditions (Table 7.3 and Figure 7.8). When these transformations were carried out on sugar-based imines **35** with bromonitromethane **33**, the corresponding nitroamines **36** were derived in high yields with moderate to good stereoselectivities promoted by SmI$_2$ in THF (Table 7.4 and Figure 7.9). Synthetic prospects of nitroamines were also obtained by their reduction in the presence of SmI$_2$/H$_2$O at room temperature using pyrrolidine in THF (Figure 7.10) with a 77–89% yield.
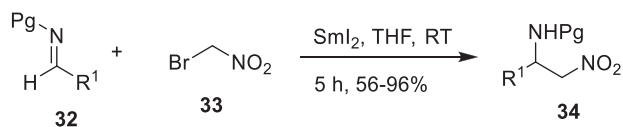
R^1 = n-C$_7$H$_{15}$, s-Bu, Ph, PhCH$_2$CH$_2$, p-CNC$_6$H$_4$, p-MeOC$_6$H$_4$, etc.
Pg = Ts, PMP, BOC

Figure 7.8: Synthesis of 2-amino-1-nitroalkanes.

7.2.6 Intramolecular reductive cyclization

Synthetic chemists are attracted to constructing spiro core through the novel and efficient strategies due to the biological importance of this scaffold in nature [42]. Currently, cyclization reactions including the use of SmI$_2$ as a powerful one-electron reducing agent have been proved to be important tools for the synthesis of molecules of natural
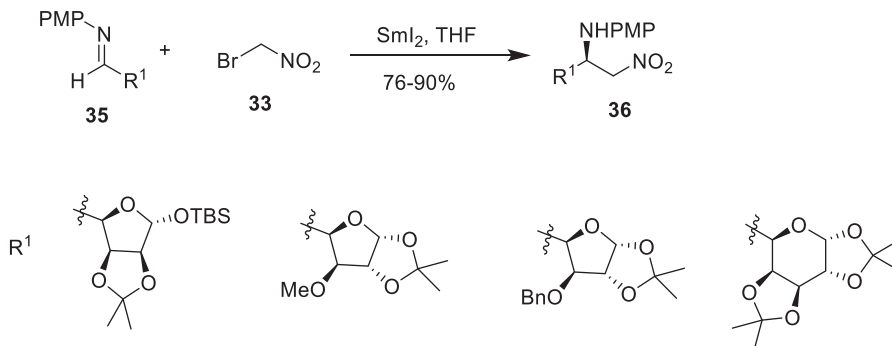
Figure 7.9: Synthesis of carbohydrate-obtained aminonitroalkanes.
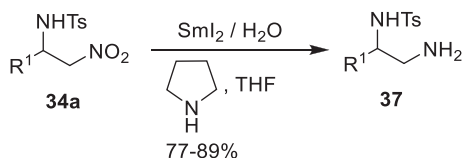
$R^1 = n\text{-}C_7H_{15}, PhCH_2CH_2, c\text{-}C_7H_{15}$
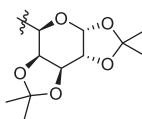
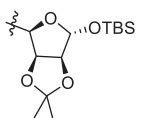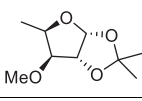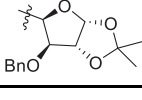**Figure 7.10:** Synthesis of 1,2-diaminoalkanes.

Table 7.3: Preparation of 2-amino-1-nitroalkanes.

Entry	32	R^1	Pg	34	SmI$_2$ (%)
1	**32a**	$n\text{-}C_7H_{15}$	Ts	**34a**	96
2	**32b**	s-Bu	Ts	**34b**	95
3	**32c**	$PhCH_2CH_2$	Ts	**34c**	89
4	**32d**	$c\text{-}C_6H_{11}$	Ts	**34d**	88
5	**32e**	Ph	Ts	**34e**	56
6	**32 f**	$n\text{-}C_7H_{15}$	PMP	**34 f**	92
7	**32 g**	i-Pr	PMP	**34 g**	90
8	**32 h**	s-Bu	PMP	**34 h**	87
9	**32i**	$C_{10}H_{19}$	PMP	**34i**	84
10	**32 j**	Ph	PMP	**34 j**	64
11	**32k**	$p\text{-}CNC_6H_4$	PMP	**34k**	61
12	**32 l**	$p\text{-}MeOC_6H_4$	BOC	**34 l**	67
13	**32 m**	Ph	BOC	**34 m**	65
14	**32 n**	$p\text{-}CNC_6H_4$	BOC	**34 n**	60

origin [43]. Hence, Hsu et al. [44] demonstrated a methodology for synthesizing spiranes that focuses on the intramolecular cyclization transformations of enone-aldehydes onto various spirocyclic γ-hydroxyketones under mild conditions in the presence of the SmI$_2$ as a key step. Initially, enone–aldehydes **38**–**41** were obtained from 3-alkoxyenones as

Table 7.4: Preparation of carbohydrate-obtained aminonitroalkanes.

Entry	35	R^1	36	dr	Yield (%)
1	**35a**		**36a**	2/1	76
2	**35b**		**36b**	2.5/1	81
3	**35c**		**36c**	4/1	86
4	**35d**		**36d**	5/1	90

spirane precursors. Next, the targeted spirocyclic γ-hydroxyketones **42**–**45** were synthesized from enone–aldehydes **38**–**41** as inseparable diastereoisomers in moderate to good yields utilizing 2 equiv. of SmI$_2$ in MeOH and THF at 0 °C for 10–30 min instead of 4 equiv. of it as the ketone was converted to alcohol due to an excess of the reducing agent (Figure 7.11). Finally, compounds **46**–**49** were also prepared from γ-hydroxyketones **42**–**45** in the presence of the pyridinium chlorochromate (PCC) in DCM at room temperature through an oxidation reaction.

7.2.7 Intramolecular alkene-ketyl radical cyclization

Yang et al. [45] achieved a stereoselective total synthesis of secondary metabolite pseudolaric acid A (**54**) involving a samarium diiodide-promoted intramolecular alkene-ketyl radical cyclization as a central step from readily available starting material allyl bromide (**50**). The total synthesis was initiated through an alkylation reaction of a ketoester (**51**) with allyl bromide (**50**) to afford an intermediate (**52**) over three steps. The intermediate (**52**) underwent an intramolecular alkene-ketyl radical cyclization to furnish a cyclic product (**53**) in the presence of the SmI$_2$ as vital steps with a 78% yield (Figure 7.12). The cross-coupling provided the target intermediate with an excellent yield on a gram scale, creating three novel stereocenters with 91:9 diastereoselectivity [46, 47]. Finally, cyclic product (**53**) delivered natural product pseudolaric acid A (**54**) efficiently; the total synthesis was completed in 16 steps from starting material ultimately.

enone-aldehydes **38–41**

R = H, CH₃, etc.

γ-hydroxyketones **42-45**

46-49

Representative examples

42a + **42a'**

10 min, 75%, dr = 1:5:1

42b + **42b'**

25 min, 70%, dr = 5:1

45a + **45a'**

10 min, 33 + 52%
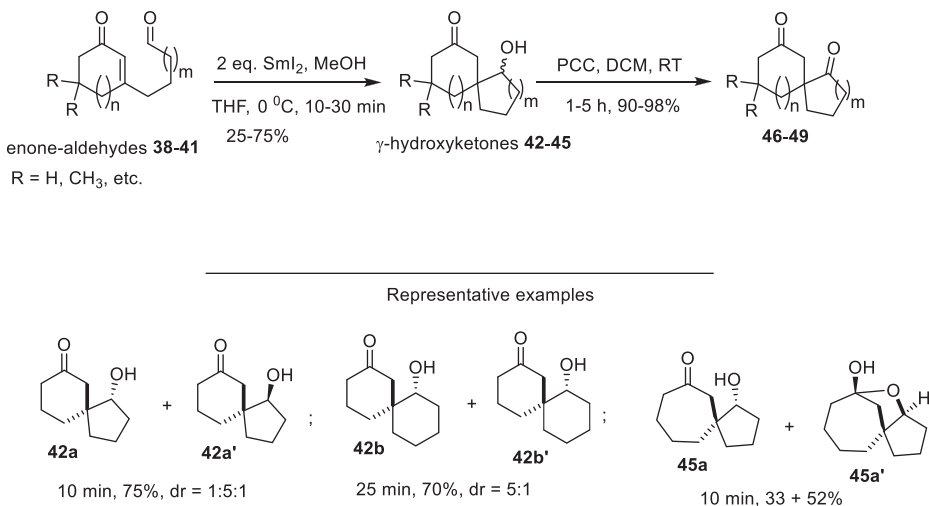
Figure 7.11: Synthesis of spirocyclic γ-hydroxyketones **42–45** through intramolecular reductive cyclization.

allyl bromide **50**

+

ketoester **51**

a) SmI₂ (2,5 equiv), HMPA (10 equiv) THF, RT
b) TMSOTf, lutidine, DCM
(78%, 2 steps)
1.93 g scale

11 steps

pseudolaric acid A (**54**)
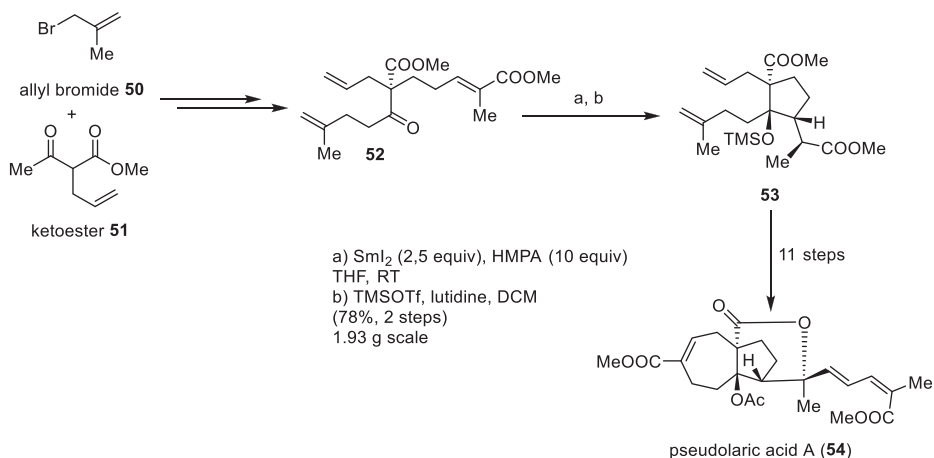
Figure 7.12: A stereoselective total synthesis of pseudolaric acid A applying an intramolecular alkene-ketyl radical cyclization by samarium diiodide.

7.2.8 Substitution reaction

Jia et al. [48] described a simple and straightforward protocol for the construction of amide bonds in the presence of the samarium metal under mild and neutral reaction conditions. Acyl chlorides **55** were treated with amines **56** to provide the targeted amides **57** utilizing samarium metal instead of tertiary amines in high yield (82–99%) as a promoter; the application of tertiary amines make a significant problem in the synthesis of

peptides (Figure 7.13) [49]. Table 7.5 summarized the results and the reactivity of acyl chlorides under the present situations was also investigated; these chlorides reacted with aliphatic primary along with secondary amines and aromatic amines to deliver the desired amides smoothly. It has been observed that aromatic acyl chlorides carrying both electron-donating and electron-withdrawing groups produced amides in excellent yields. It has been also examined that aliphatic acyl chlorides also afforded higher yields of the targeted amides compared to aromatic acyl chlorides.
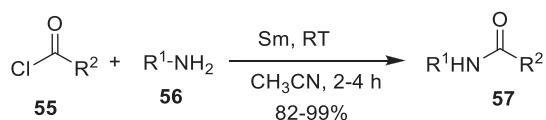
R^1 = Ph, p-ClC$_6$H$_4$, p-MeC$_6$H$_4$, p-MeOC$_6$H$_4$, tBu, morpholine, c-hexylamine, etc.
R^2 = Ph, p-ClC$_6$H$_4$, p-NO$_2$C$_6$H$_4$, p-MeOC$_6$H$_4$, tBu, etc.

Figure 7.13: The synthesis of several amides using samarium metal as a promoter.

Table 7.5: The synthesis of several amides using samarium metal as a promoter at room temperature.

Entry	Time (h)	Acyl chloride (55)	Amine (56)	Yield (%)
1	3	PhCH$_2$COCl	PhNH$_2$	99
2	2	tBuCOCl	PhNH$_2$	97
3	2	tBuCOCl	tBuNH$_2$	96
4	2	PhCH = CHCOCl	c-Hexylamine	96
5	2	p-ClC$_6$H$_4$COCl	PhNH$_2$	95
6	4	p-ClC$_6$H$_4$COCl	p-MeOC$_6$H$_4$NH$_2$	95
7	3	PhCOCl	c-Hexylamine	94
8	2	PhCOCl	PhNH$_2$	93
9	2	p-MeC$_6$H$_4$COCl	c-Hexylamine	92
10	3	tBuCOCl	Morpholine	85
11	4	PhCOCl	Morpholine	82

7.2.9 Stereoselective synthesis of *cis*-β-alkoxy-γ-alkyl-γ-lactones

Lactones specially γ-lactones make them attractive lead structures for the improvement of novel drugs owing to their various biological activities such as antitumor, anti-inflammatory, antiviral, antibiotic, and more [50]. Padrón et al. [51] demonstrated a SmI$_2$-assisted methodology for the preparation of *cis*-β-alkoxy-γ-alkyl-γ-lactones from linear precursors. At first, appropriate alcohol (**58**) was treated with an equimolar amount of methyl propyolate (**59**) in the presence of half an equivalent of tri-*n*-butyl phosphine in THF to afford the β-alkoxyacrylate (**60**) in good yields (69–72%). Next, the

corresponding γ-lactone (**62**) was obtained by the reaction of the β-alkoxyacrylate (**60**) with *n*-octanal (**61**) using SmI_2 as a promoter (Figure 7.14). It is interesting to note that the stereochemistry of the substituents on the ring is *cis* instead of *trans*. It has been also observed that synthesized *cis*-β-alkoxy-γ-alkyl-γ-lactones display antiproliferative activities in vitro [51].
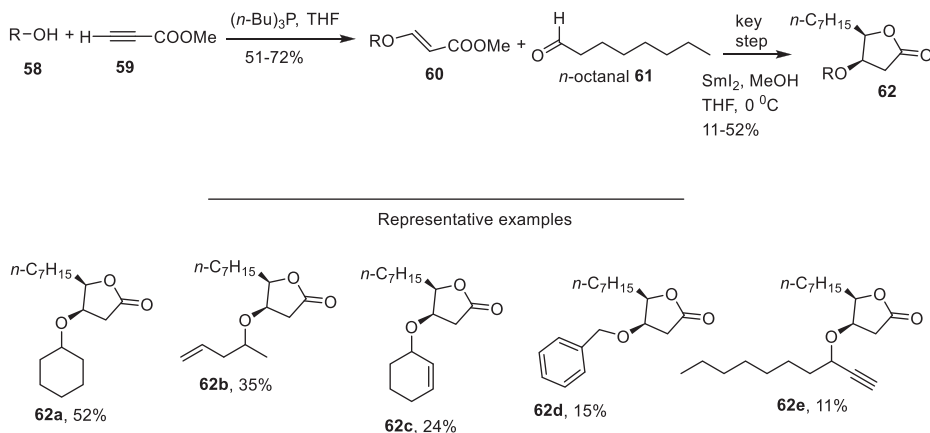
Figure 7.14: Preparation of *cis*-β-alkoxy-γ-alkyl-γ-lactones through a SmI_2-assisted methodology.

7.2.10 Regioselective ring opening of epoxides

2-Amino alcohols, versatile intermediates, are used for the synthesis of many biologically potent natural products, unnatural amino acids, and β-blockers [52]. The regioselective ring opening was accomplished by Yadav and coworkers [53] in which ring opening of various oxiranes **63** with different amines **64** occurred regioselectively in the presence of the catalyst samarium triflate (10 mol%) to afford β-amino alcohols **65** and **66** in excellent yields at below room temperature (Figure 7.15). For example, styrene oxide was treated with isopropyl amine to provide β-amino alcohol as a single isomer through ring-opening reactions, progressing from the terminal attack of the nucleophile. However, sterically hindered alicyclic amine namely *N*-phenyl piperazine was treated with styrene oxide to afford a mixture of regioisomers in a ratio of 3:2 through the attack of the nucleophile at benzylic and at the terminal position. β-Blockers, namely atenolol (**71**) through Willgerodt reaction, propranolol (**66a**), and β-adrenoceptor agonist RO363 (**78**), via the same methodology were also performed by the same investigators (Figures 7.16 and 7.17) [53, 54]. The drug atenolol (**71**) is employed for the remedy of hypertension and angina pectoris [53].

R^1 = alkyl, aryl, aryloxy, cycloalkyl
R^2 = alkyl, aryl, heterocyclic

Representative examples

65a, 1h, 96%

65b, 1.5h, 93%

66a, 2h, 89%

66b, 2h, 87%
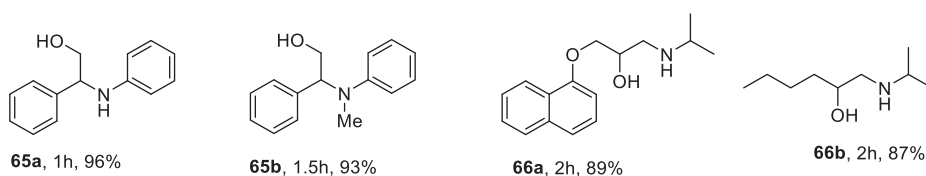
Figure 7.15: Regioselective ring opening of several oxiranes with different amines.

4-hydroxy acetophenone **67**
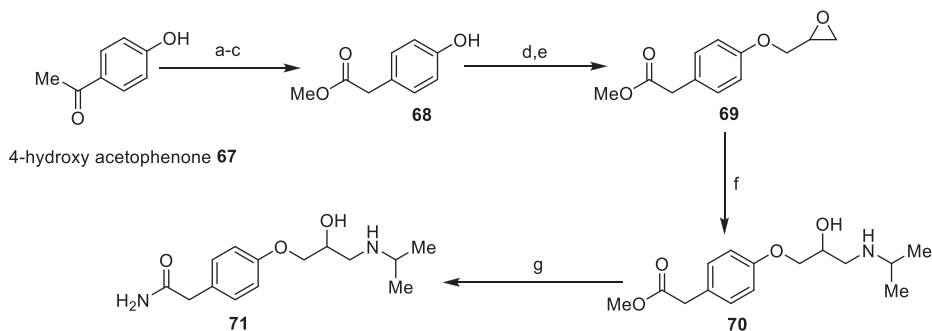
Reagents and conditions a) sulphur, morpholine b) NaOH-EtOH c) SOCl$_2$, MeOH
d) allyl bromide e) m-CPBA f) isopropyl amine, Sm(OTf)$_3$ g) liquid ammonia

Figure 7.16: Synthesis of β-blocker atenolol.

7.2.11 Tishchenko reaction

The Tishchenko reaction is an efficient tool for the synthesis of various secondary metabolites including macrolides, polyketides, as well as coalescing agents in the paint industry [55, 56]. Pohmakotr and coworkers [57] executed the aldol-Tishchenko reaction for the stereoselective synthesis of *anti*-1,3-diol monoesters from the samarium dienolate with different aldehydes for the first time (Figure 7.18). The phenylsulfonyl activated cyclopropyl ketone (**79**) underwent a regioselective reductive cleavage in the presence of the samarium(II) iodide to generate the samarium dienolate (**81**) through the formation of intermediate (**80**). Next, the samarium dienolate (**81**) was treated with various aldehydes **82** including aliphatic and aromatic aldehydes to deliver the desired

2-substituted *anti*-1,3-diol monoester derivatives **83**, **84**, and more. Besides, the stereoselective formation of optically active polyoxygenated organic compounds was carried out by the tandem aldol-Tishchenko reaction in the presence of the samarium dienolate (**81**) [57].

Reagents and conditions a) HBr, AcOH
b) benzylbromide, K$_2$CO$_3$, acetone
c) *m*-CPBA
d) NaOH-EtOH
e) epichlorohydrin, K$_2$CO$_3$, acetone
f) 3',4'-dimethoxyphenylethyl amine, Sm(OTf)$_3$, RT
g) Pd/C

Figure 7.17: Synthesis of β-adrenoceptor agonist RO363.

R = ethyl, n-butyl, n-heptyl, phenyl
4-ClC$_6$H$_4$, 4-CH$_3$C$_6$H$_4$, etc.
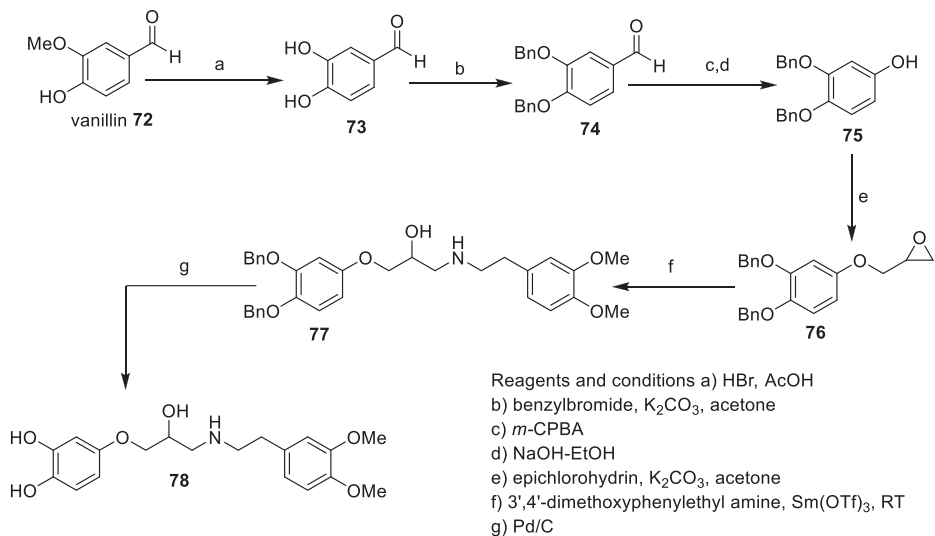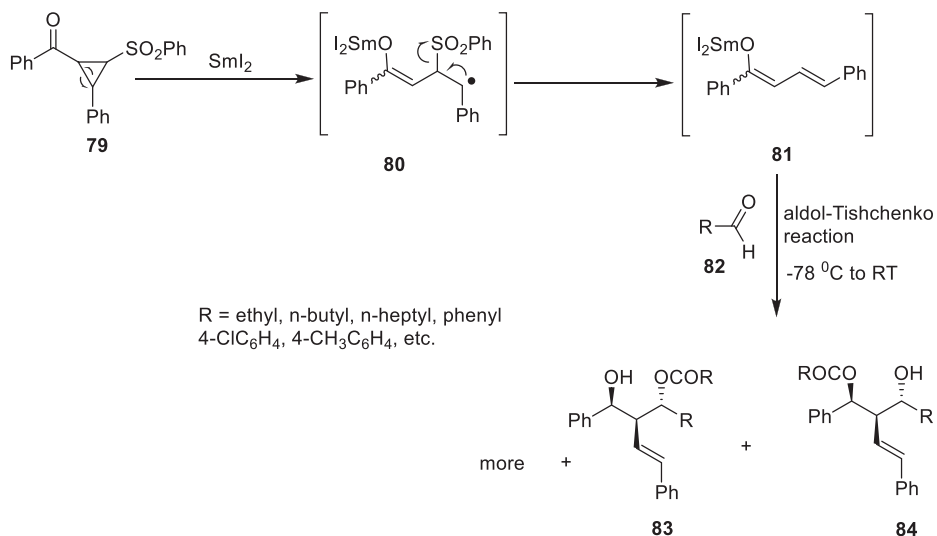
Figure 7.18: Aldol-Tishchenko reaction for the stereoselective synthesis of *anti*-1,3-diol monoesters.

7.2.12 Reductive elimination

In organic synthesis, the Baylis–Hillman reaction is a popular reaction in constructing carbon-carbon bonds by the reaction of the α-position of an activated alkene with a carbon electrophile, namely an aldehyde [58]. Adducts of the Baylis–Hillman reaction are valuable precursors for the stereoselective synthesis of several multifunctional compounds [59]. Zhang and coworkers [60] described a convenient and efficient protocol for the syntheses of (E)-methylcinnamic ester derivatives **86** utilizing the acetate of Baylis-Hillman adduct as substrate (**85**) through the reductive elimination, assisted by samarium metal employing a catalytic amount of iodine in THF for 1–4.5 h with 65–95% yield (Figure 7.19). The same authors also accomplished the stereospecific syntheses of (2Z)-2-(iodomethyl)alk-2-enoates **88** involving iodine in a 1:1 ratio with metallic samarium (2 mmol Sm power and 2 mmol I_2) under reflux in 87–97% yield within 25 min from the Baylis–Hillman adducts **87** (Figure 7.20).
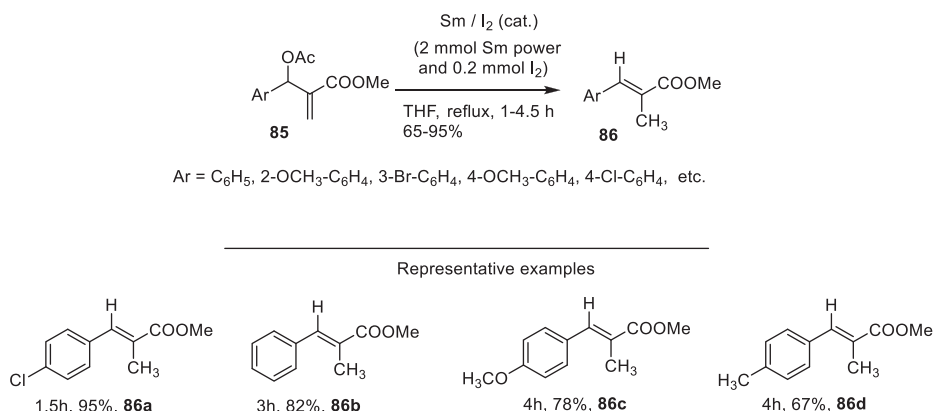
Figure 7.19: Synthesis of (E)-methylcinnamic ester derivatives by samarium metal and a catalytic amount of iodine.

7.2.13 Cleavage of the N–O bond

Brandi et al. [61] developed a general protocol that is particularly effective for the reaction of 5-spirocyclopropane isoxazolidines **89** to the corresponding β-aminocyclopropanols **90** in the presence of the SmI_2 as a selective and mild reagent (Figure 7.21). For the N–O bond cleavage in isoxazolidines, a saturated five-membered ring having adjacent nitrogen and oxygen atoms, SmI_2 was employed as a reducing agent. It is interesting to note that the preparation of compound **90c** (90%) revealed the stability of a four-membered cyclic ring adjacent to the oxygen atom. Besides, the comparatively low yield for compound **90d** (55%) was attributed to partial hydrolysis of the ester group in the basic work-up.

Ar = C$_6$H$_5$, 2-OCH$_3$-C$_6$H$_4$, 2-Cl-C$_6$H$_4$, 4-OCH$_3$-C$_6$H$_4$, 4-Cl-C$_6$H$_4$, etc.
R = CH$_3$, C$_2$H$_5$

Representative examples

97%, **88a**   95%, **88b**   90%, **88c**   87%, **88d**
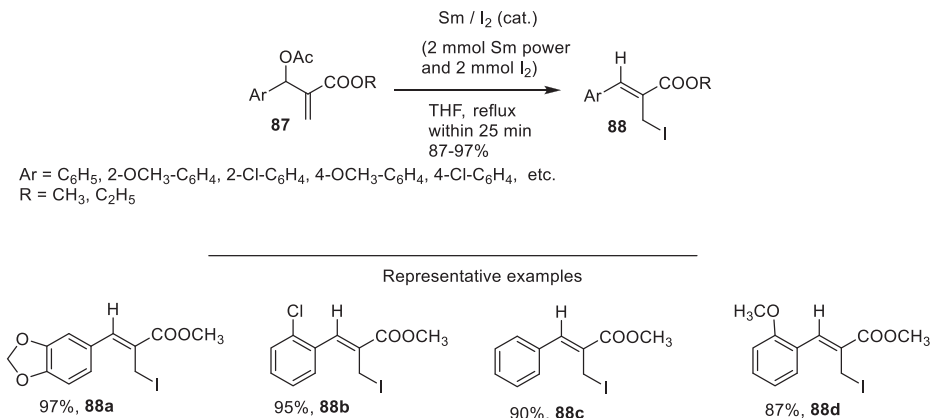
Figure 7.20: Synthesis of (2Z)-2-(iodomethyl)alk-2-enoates by samarium metal and a iodine in a 1:1 ratio.

R^2-R^3 = -CH$_2$-CH$_2$-

Representative examples

90a, 98%   **90b**, 95%   **90c**, 90%   **90d**, 55%
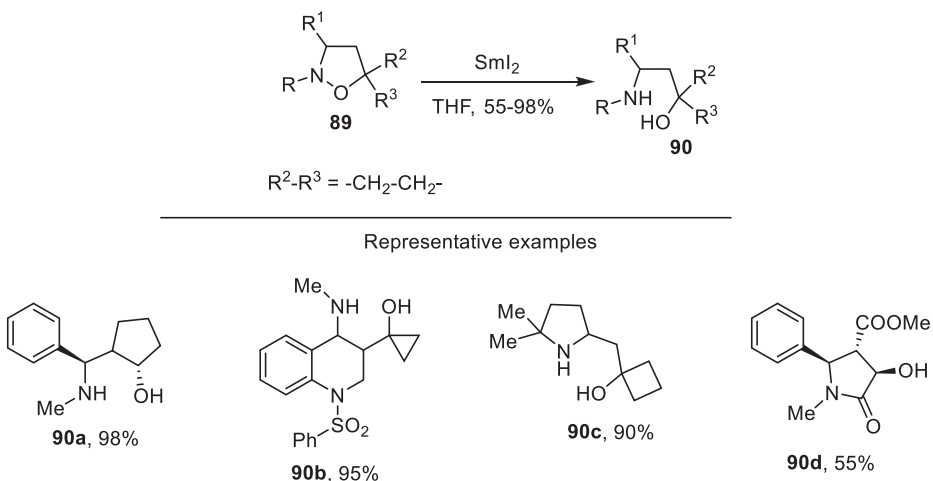
Figure 7.21: Reduction of isoxazolidines through the N–O bond cleavage in the presence of the SmI$_2$.

7.3 Conclusions

In 1977, Kagan introduced samarium(II) iodide (SmI$_2$) to organic synthesis; it acts as one of the most multitalented single-electron transfer reagents. It is an extremely powerful reductant, yet it is chemoselective reagent; its selectivity toward functional groups in organic synthesis is refined by the application of suitable ligands and additives. Chemical reactions assisted by SmI$_2$ are carried out under user-friendly as well as operationally simple reaction conditions. It has been successfully utilized in both academic and industrial settings as a single-electron reduction. There is enhancing

attention to carrying out organic transformation with the help of the direct reaction of metals. The direct application of lanthanide samarium metal in synthetic transformation has gained the attention of the organic community since it consists of a powerful reducing ability, it is a cheap metal, and it is stable in the air. So, the present chapter wishes to concentrate the attention on the applications of samarium diiodide and metallic samarium in organic synthesis from 2002 to 2021.

References

[1]   Nicolaou, KC. Organic synthesis: The art and science of replicating the molecules of living nature and creating others like them in the laboratory. Proc R Soc A, 2014, 470, 20130690.

[2]   Kobayashi, S, Sugiara, M, Kitagawa, H, Lam, WWL. Rare-earth metal triflates in organic synthesis. Chem Rev, 2002, 102, 2227–2302.

[3]   Collin, J, Giuseppone, N, Van de Weghe, P. Lanthanide iodides, a new family of efficient Lewis acid catalysts. Coord Chem Rev, 1998, 178–180, 117–144.

[4]   Giuseppone, N, Collin, J. Tandem Mukaiyama Michael–aldol reactions catalysed by samarium diiodide. Tetrahedron, 2001, 57, 8989–8998.

[5]   Namy, JL, Girard, P, Kagan, HB. A new preparation of some divalent lanthanide iodides and their usefulness in organic synthesis. Nouv J Chim, 1977, 1, 5–7.

[6]   Mahji, S. Diterpenoids: Natural distribution, semisynthesis at room temperature and pharmacological aspects-a decade update. ChemistrySelect, 2020, 5, 12450–12464.

[7]   Majhi, S. Synthesis of bioactive natural products and their analogs at room temperature–an update. Phys Sci Rev, 2022; doi.org/: 10.1515/psr-2021-0094.

[8]   Majhi, S. Applications of ultrasound in total synthesis of bioactive natural products: A promising green tool. Ultrason Sonochem, 2021, 77, 105665.

[9]   Majhi, S. Applications of Norrish type I and II reactions in the total synthesis of natural products: A review. Photochem Photobiol Sci, 2021, 20, 1357–1378.

[10]   Majhi, S. Discovery, development, and design of anthocyanins-inspired anticancer agents-a comprehensive review. Anticancer Agents Med Chem, 2022; DOI: 10.2174/1871520621666211015142310.

[11]   Majhi, S, Das, D. Chemical derivatization of natural products: Semisynthesis and pharmacological aspects-A decade update. Tetrahedron, 2021, 78, 131801.

[12]   Majhi, S. The art of total synthesis of bioactive natural products via microwaves. Curr Org Chem, 2021, 25, 1047–1069.

[13]   Majhi, S. Applications of Yamaguchi method to esterification and macrolactonization in total synthesis of bioactive natural products. ChemistrySelect, 2021, 6, 4178–4206.

[14]   Majhi, S. Recent developments in the synthesis and anti-cancer activity of acridine and xanthine-based molecules. Phys Sci Rev, 2022; doi.org/: 10.1515/psr-2021-0216.

[15]   Chang, GX, Lowary, TL. A glycosylation protocol based on activation of glycosyl 2-pyridyl sulfones with samarium triflate. Org Lett, 2000, 2, 1505–1508.

[16]   Wang, L, Li, P, Zhou, L. A novel reduction of sodium alkyl thiosulfates using samarium metal without an activating agent in water. Tetrahedron Lett, 2002, 43, 8141–8143.

[17]   Banik, BK. Samarium metal in organic synthesis. Eur J Org Chem, 2002, 2431–2444.

[18]   John, SE, Gulati, S, Shankaraiah, N. Recent advances in multi-component reactions and their mechanistic insights: A triennium review. Org Chem Front, 2021, 8, 4237–4287.

[19] Abdelwahab, NS, Edrees, FH, Alsaadi, MT, Amin, NH, Saad, AS. Simultaneous estimation of dimenhydrinate, cinnarizine and their toxic impurities benzophenone and diphenylmethylpiperazine; in silico toxicity profiling of impurities. RSC Adv, 2020, 10, 37439–37448.

[20] Kirkpatrick, D, Momot, M, Anthony, C. Development and validation of assay and impurities methods for acetaminophen and diphenhydramine tablets. Sep Sci Plus, 2020, 3, 267–275.

[21] Zhu, N, Su, M, Wan, W-M, Li, Y, Bao, H. Practical method for reductive deuteration of ketones with magnesium and D_2O. Org Lett, 2020, 22, 991–996.

[22] Misawa, T, Aoyama, H, Furuyama, T, Dodo, K, Sagawa, M, Miyachi, H, et al. Structural development of benzhydrol-type 1'-acetoxychavicol acetate (ACA) analogs as human leukemia cell-growth inhibitors based on quantitative structure-activity relationship (QSAR) analysis. Chem Pharm Bull, 2008, 56, 1490–1495.

[23] Song, B, Zhang, D, Xiao, S, Liu, C, Chen, H, Yan, Q. Access to diarylmethanol skeletons via a samarium/copper-mediated sequential three-component C−H functionalization reaction. J Org Chem, 2021, 86, 9854–9860.

[24] Heravi, M, Vazinfard, M, Faghihi, Z. Recent applications of birch reduction in total synthesis of natural products. Curr Org Chem, 2015, 19, 1491–1525.

[25] Leitch, MA, O'Neil, GW. Substrate-dependent stereospecificity in samarium-mediated allylic benzoate reductions. Tetrahedron, 2020, 76, 131707.

[26] Ramír ez-solís, A, Amaro-Estrada, JI, Hernandez-Cobos, J, Maron, L. Aqueous solvation of SmI_2: A born-oppenheimer molecular dynamics density functional theory cluster approach. J Phys Chem A, 2017, 121, 2293–2297.

[27] Chciuk, TV, Anderson Jr, WR, Flowers, RA. Proton-coupled electron transfer in the reduction of carbonyls by samarium diiodide–water complexes. J Am Chem Soc, 2016, 138, 8738–8741.

[28] Wright, AM, O'Neil, GW. Total synthesis of honokiol by selective samarium-mediated allylic benzoate reduction. Tetrahedron Lett, 2016, 57, 3441–3443.

[29] Cheng, C, Zhang, QW, Yang, Y, Li-Gen, L. Honokiol: A naturally occurring lignan with pleiotropic bioactivities. Chin J Nat Med, 2021, 19, 481–490.

[30] Gilchrist, TL. Synthesis of aromatic heterocycles. J Chem Soc Perkin Trans, 1999, 1, 2849–2866.

[31] Fana, X, Zhang, Y. SmI_2-mediated synthesis of 2,4-diarylpyrroles from phenacyl azides. Tetrahedron Lett, 2002, 43, 1863–1865.

[32] Mandavid, H, Rodrigues, AMS, Espindola, LS, Eparvier, V, Stien, D. Secondary metabolites isolated from the amazonian endophytic fungus diaporthe sp. SNB-GSS10. J Nat Prod, 2015, 78, 1735–1739.

[33] Bae, M, Moon, K, Kim, J, Park, HJ, Lee, SK, Shin, J, Oh, D-C. Mohangic acids A-E, *p*-Aminoacetophenonic acids from a marine-mudflat-derived *Streptomyces* sp. J Nat Prod, 2016, 79, 332–339.

[34] Taori, K, Paul, VJ, Luesch, H. Structure and activity of largazole, a potent antiproliferative agent from the floridian marine cyanobacterium *symploca* sp. J Am Chem Soc, 2008, 130, 1806–1807.

[35] Sinast, M, Zuccolo, M, Wischnat, J, Sube, T, Hasnik, F, Baro, A, Dallavalle, S, Laschat, S. Samarium iodide-promoted asymmetric reformatsky reaction of 3–(2-Haloacyl)-2-oxazolidinones with Enals. J Org Chem, 2019, 84, 10050–10064.

[36] Dixon, DJ, Ley, SV, Gracza, T, Szolcsany, P. Total synthesis of the polyenoyltetramic acid mycotoxin erythroskyrine. J Chem Soc Perkin Trans, 1999, 1, 839–841.

[37] Wnuk, SF, Sacasa, PR, Lewandowska, E, Andrei, D, Cai, S, Borchardt, RT. Synthesis of 5'-functionalized nucleosides: *S*-Adenosylhomocysteine analogues with the carbon-5' and sulfur atoms replaced by a vinyl or halovinyl unit. Bioorg Med Chem, 2008, 16, 5424–5433.

[38] Goekjian, PG, Wu, T, Kang, H, Kishi, Y. Preferred conformation of C-glycosides. 7. Preferred conformation of carbon analogs of isomaltose and gentiobiose. J Org Chem, 1991, 56, 6422–6434.

[39] Soto, M, Soengas, RG, Silva, AMS, Gotor-Fernandez, V, Rodríguez-Solla, H. Synthesis of carbohydrate-derived (*Z*)-vinyl halides and silanes: Samarium-promoted stereoselective 1,2-elimination on sugar-derived α-halomethylcarbinol acetates. Tetrahedron, 2018, 74, 5475–5480.

[40] Marques-Lopez, E, Merino, P, Tejero, T, Herrera, RP. Catalytic enantioselective aza-henry reactions. Eur J Org Chem, 2009, 2401–2420.

[41] Rodríguez-Solla, H, Concellon, C, Alvaredo, N, Soengas, RG. The use of samarium or sodium iodide salts as an alternative for the aza-Henry reaction. Tetrahedron, 2012, 68, 1736–1744.

[42] Pradhan, R, Patra, M, Behera, AK, Mishra, BK, Behera, RK. A synthon approach to spiro compounds. Tetrahedron, 2006, 62, 779–828.

[43] Nakata, T. SmI$_2$-induced reductive cyclizations for the synthesis of cyclic ethers and applications in natural product synthesis. Chem Soc Rev, 2010, 39, 1955–1972.

[44] Hsu, D-S, Hsu, C-W. Spiranes synthesis based on samarium diiodide-mediated reductive cyclization. Tetrahedron Lett, 2012, 53, 2185–2188.

[45] Xu, T, Li, C-C, Yang, Z. A concise approach for the total synthesis of pseudolaric acid A. Org Lett, 2011, 13, 2630–2633.

[46] Szostak, M, Fazakerley, NJ, Parmar, D, Procter, DJ. Cross-coupling reactions using samarium(II) iodide. Chem Rev, 2014, 114, 5959–6039.

[47] Nicolaou, KC, Ellery, SP, Chen, JS. Samarium diiodide-mediated reactions in total synthesis. Angew Chem Int Ed, 2009, 48, 7140–7165.

[48] Shi, F, Li, J, Li, C, Xueshun, J. Samarium-mediated mild and facile method for the synthesis of amides. Tetrahedron Lett, 2010, 51, 6049–6051.

[49] Cho, DH, Jang, DO. Indium-mediated mild and facile method for the synthesis of amides. Tetrahedron Lett, 2004, 45, 2285–2287.

[50] Rodríguez, AD, Piña, IC, Barness, CL. Synthesis and biological evaluation of cembranolide analogs containing cyclic ethers. J Org Chem, 1995, 60, 8096–8100.

[51] Donadel, OJ, Martín, T, Martín, VS, Padrón, JM. Samarium(II) promoted stereoselective synthesis of antiproliferative *cis*-β-alkoxy-γ-alkyl-γ-lactones. Bioorg Med Chem Lett, 2007, 17, 18–21.

[52] Corey, EJ, Zhang, F. *re* – and *si* -face-selective nitroaldol reactions catalyzed by a rigid chiral quaternary ammonium salt: A highly stereoselective synthesis of the HIV Protease Inhibitor amprenavir (Vertex 478). Angew Chem Int Ed, 1999, 38, 1931–1934.

[53] Yadav, JS, Ramesh Reddy, A, Venkat Narsaiah, A, Reddy, BVS. An efficient protocol for regioselective ring opening of epoxides using samarium triflate: Synthesis of propranolol, atenolol and RO363. J Mol Catal A Chem, 2007, 261, 207–212.

[54] Bose, DS, Narsaiah, AV. An efficient asymmetric synthesis of (*S*)-atenolol: Using hydrolytic kinetic resolution. Bioorg Med Chem, 2005, 3, 627–630.

[55] Paterson, I, Davies, RDM, Marquez, R. Total synthesis of the callipeltoside aglycon. Angew Chem Int Ed, 2001, 40, 603–607.

[56] Törmäkangas, OP, Koskinen, AMP. Fast aldol-tishchenko reaction utilizing 1,3-diol monoalcoholates as the catalysts. Org Process Res Dev, 2001, 5, 421–425.

[57] Reutrakul, V, Jaratjaroonphong, J, Tuchinda, P, Kuhakarn, C, Kongsaeree, P, Prabpai, S, Pohmakotr, M. Samarium dienolate mediated stereoselective synthesis of *anti*-1,3-diol monoesters via aldol-Tishchenko reaction. Tetrahedron Lett, 2006, 47, 4753–4757.

[58] Basavaiah, D, Rao, AJ, Satyanarayana, T. Recent advances in the baylis−hillman reaction and applications. Chem Rev, 2003, 103, 811–892.

[59] Kabalka, GW, Venkataiah, B, Dong, G. Preparation of substituted allyl acetates and sulfones from Baylis–Hillman adducts in ionic liquid media. Tetrahedron Lett, 2003, 44, 4673–4675.

[60] Li, J, Hua, X, Zhang, Y. Metallic samarium and iodine promoted facile and efficient syntheses of trisubstituted alkenes from the acetates of Baylis–Hillman adducts. Tetrahedron Lett, 2005, 46, 1931–1934.

[61] Revuelta, J, Cicchi, S, Brandi, A. Samarium(II) iodide reduction of isoxazolidines. Tetrahedron Lett, 2004, 45, 8375–8377.

Kantharaju Kamanna* and Yamanappagouda Amaregouda

8 Role of erbium-based compounds in organic transformations

8.1 Introduction

Erbium (Er) is a chemical element, comes under lanthanide rare earth metal series, and appears in the periodic table, with symbol of "Er," atomic number 68 and mass number 167.259 Da [1]. The pure erbium is found in silvery white color with reasonably good stability in air, but slowly reacts with water and dissolves in diluted mineral acids rapidly [2]. Erbium showed strong paramagnetic properties at above 815 K temperature [3] discovered first by Carl Gustaf Mosander in 1842, and named "Terbia" [4]. Due to the confusion arising from the similar properties of the rare earth metals, the name of the terbium and erbium was interchanged later [4]. Erbium (Er) is abundant in many rare earth minerals; among its important sources are xenotime, laterite ionic clays, and euxenite, also generated during nuclear fission and in the earth crust abundant as tungsten and tantalum [5]. Scientists demonstrated that the natural erbium mainly occurs in stable six isotopic forms that are tabulated in Table 8.1 [6]. These radioactive isotopes found to be relatively unstable, and their half-life ranges from 1 s to 9.4 days [7]. The bulk metal purification is preferred in industries by employing liquid-liquid solvent extraction and ion-exchange techniques [8].

Table 8.1: Various isotopic forms of "Er" abundant in nature.

S. no.	Isotope	% Abundant
1	Er-166	33.5
2	Er-168	26.98
3	Er-167	22.87
4	Er-170	14.91
5	Er-164	1.6
6	Er-162	0.14

*Corresponding author: Kantharaju Kamanna,** Department of Chemistry, School of Basic Sciences, Rani Channamma University, Vidyasangama, P-B, NH-4, Belagavi 591156, Karnataka, India, e-mail: kk@rcub.ac.in
Yamanappagouda Amaregouda, Department of Chemistry, School of Basic Sciences, Rani Channamma University, Vidyasangama, P-B, NH-4, Belagavi 591156, Karnataka

The metallic "Er" element showed only one preferred structural form (allotropic) that is well known, and adopts a close packed hexagonal structure with $\alpha = 3.5592$ Å at room temperature [9]. The optical properties of the Er(III) ion showed characteristic raising high-energy state by absorption of IR radiation and emit wavelength of 1.55 mm, which is commonly found application in fiber optic signal transmission [10]. Hence, this element is majorly used in fiber optic communications as a signal amplifier for long-distance telephone and data cables [11]. The composed compounds of Er are extensively used in laser source, pink coloring agent for glasses, and intermetallic compounds [12]. The lanthanide series along the row elements are exhibiting many interesting properties with discontinuity between Eu and Gd. In comparison to conventional catalysts employed, due to their extra stability toward water, lanthanide salts have emerged as alternative Lewis acids (LA) that are employed in various organic transformations [13]. Moreover, these erbium-based salts are found to be inexpensive, with not much toxicity to the environment as well as reaction [14, 15]. Therefore, lanthanide-derived salts contribute in green chemistry protocol development as an LA catalyst for numerous organic transformations [16, 17]. Using mass spectrometry techniques, competitive ligand dissociation and respective complex monitored tendency relative to the LA properties of the series of rare earth metal triflates have been evaluated [18, 19]. Er(III)triflates compound are most active species in the Lanthanide(III) derivatives series that are examined for their LA tendency [20–22]. The Er(III) salt Lewis acid strength was determined by correlation of hydrolysis constants (pK_a) and WERC experiments are well documented (water exchange rate constant) [23, 24]. According to Kobayashis parameters metal compounds that exhibit pK_a values ranging from 4.3 to 1.08 and WERC values higher than 3.2×10^6 M^{-1} S^{-1} are believed to be having higher acidic strength [25, 26]. Er (III) ions showed pK_a = 7–9, and WERC = 1.4×10^8 M^{-1} S^{-1}, which is in the accordance with Kobayashis concept [27, 28] and excelled Er(III) ion as a better LA catalyst properties [29]. The intrinsic properties of the LA nature of the lanthanide series ions are observed in experiments as their principal properties [30], by the prediction of rate of the reaction catalyzed measured agreement with other lanthanide series salts, and erbium salts emerged superior in the reaction rate and gave excellent yield of the product [31]. Despite these interesting LA properties of the Er(III) salts evaluated experimentally suggest that [32] Er(III) ion is directly involved in the process of transition than simple proton in the case of acid-catalyzed reaction [33–35]. Herein, we are excited to bring to interesting properties and Lanthanide series behavior of the Er(III) based salts employed in the various organic transformations by various research groups across the globe reported as a compiled book chapter. This chapter summarizes fundamental facts, properties and derivative of rare earth metal Er(III) application in numerous organic transformation documented in the literature as homogeneous and heterogeneous catalysts is discussed (Figure 8.1).
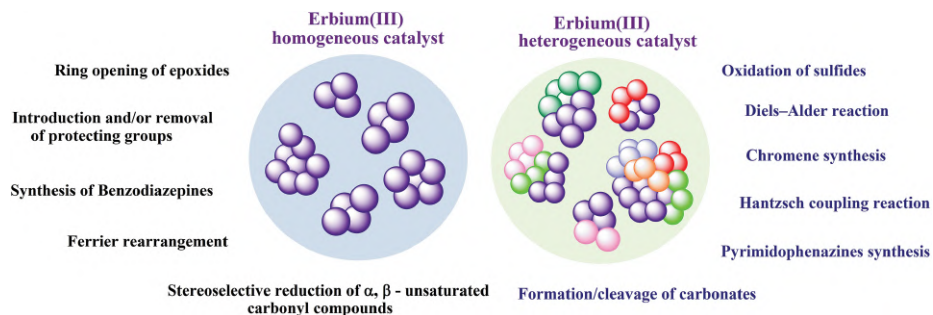
Figure 8.1: Various organic transformations reported using Er salts catalyzed both in homogeneous and heterogeneous system.

8.2 Erbium-based derivatives used as a homogeneous catalyst

Rajaguru et al. [36] reported erbium triflate-catalyzed synthesis of highly substituted imidazole derivatives (**4**) by the reaction of variety of aryl aldehydes (**2**), substituted aniline (**3**), and α-azido chalcone (**1**) in acetonitrile under reflux temperature via multicomponent approach isolated imidazole derivative product in good yield. Authors also screened various Lewis acid catalytic properties and solvent systems and concluded that to achieve outstanding yields of the bioactive imidazole molecules, Er (OTf)$_3$ and acetonitrile are best suited catalyst and solvent, respectively (Figure 8.2).

$$R^1 = R^2 = H$$
$$R^3 = 4\text{-methyl}$$
$$R^4 = 4\text{-bromo}$$
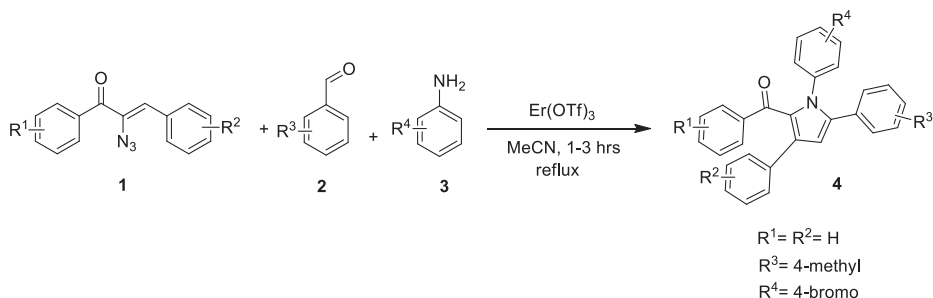
Figure 8.2: Synthesis of highly substituted imidazole derivatives.

The selective synthesis of enaminones (**7**), aldimines (**7a**), and ketimines (**7b**) via aromatic imine is demonstrated by Er(OTf)$_3$ catalysis, and compared to CeCl$_3$/NaI catalyzed reaction gave Michael reaction, but this Er-based catalysts reported observed no Michael adduct formation during the reaction, and authors claimed added advantages of the Er(OTf)$_3$ catalysis compared to other catalysts screened by them. The derivative of

ketimines (**7**) can be obtained under erbium-based catalysis by the reaction of 1,3-diketone (**5**) and aromatic amine (**6**) gave ketimine product (**7**). The same authors also utilized this catalysts for the aldimine and ketimine derivative synthesis by the reaction of aldehydes and ketones respectively with amine followed in the second step reduction using LiBH$_4$ gave respective imine product reported [37] (Figure 8.3).
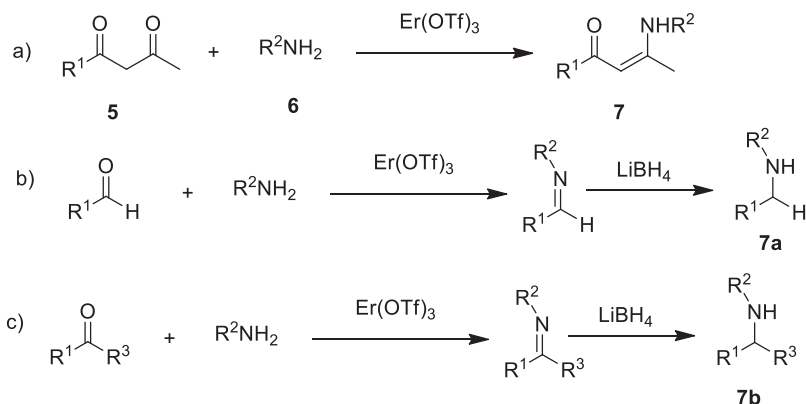
Figure 8.3: Synthesis of enaminones (**7**), aldimines (**7a**), and ketimines (**7b**).

Procopio et al. [38, 39] described that α-azido alcohols are given with TMSN$_3$ and TMSCN by stereoselective ring opening of epoxide (**10, 11**) and β-hydroxynitriles (**12, 13**) products are the convenient intermediates employed for various valuable organic molecule syntheses (Figure 8.4).

The authors also studied kinetics of the rate of the reaction based on reagent used for the reaction. Due to strong nucleophilic nature of the CN$^-$, TMSCN was showed to be more reactive than TMSN$_3$ in the Er(OTf)$_3$-catalyzed ring opening of the epoxide reaction compared to other nucleophiles, thus validating the use of Er(OTf)$_3$ as a Lewis acid when coordinated with the oxygen atom. Authors were able to explain the mechanistic pathways of the ring opening by two different kinds of nucleophiles attack on the asymmetrical epoxide (**8**). In an early transition state the attack of strong nucleophile (–CN) occurred faster as the intact arrangement of the epoxide is noticed and the attacking nucleophile profoundly influences the attached groups. The best stabilization of the positive charge, on the other hand, is noticed by reduced nucleophilic nature (-N$_3$) which inadvertently takes longer time to add transition state during ring opening involving cleavage of C–O bond. Therefore authors concluded that a suitable nucleophilic attack (-CN and -N$_3$) on the benzylic position is favored.

Chemists majorly focused research on the protection of functional group phenol and alcohol protection into tert-butyl ethers is challenging. It is observed that under the commonly used basic conditions tert-butyl ether is one of the stable ethers.
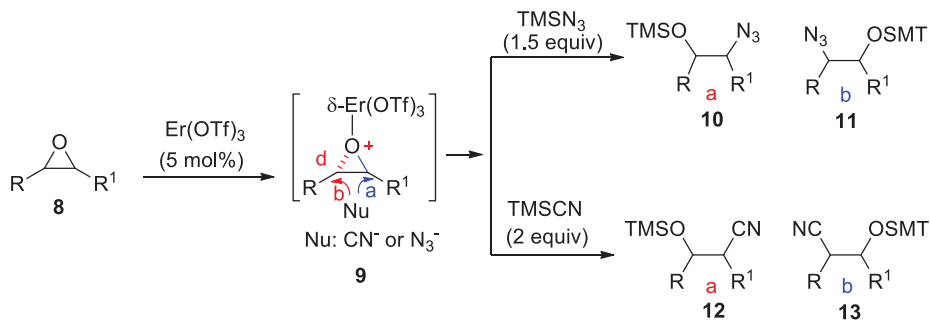
Figure 8.4: Regio- and stereoselective epoxide ring opening.

But for the formation and cleavage involved the organic synthesis, its use is scarce, due to requirement of harsh reaction conditions. $Er(OTf)_3$ acting as mild Lewis acid catalyst exhibiting a dual function of protecting the –OH group of phenol and alcohol by tert-butyl ether formation has been described by Procopio et al. [40]. The authors studied an optimized amount of $Er(OTf)_3$ required for 1 mmol of the reaction 5 mol% with Boc-anhydride as a tert-butyl group source, and showed expedient conversion of phenol [example: 4-(2-hydroxyethyl)-2-methoxyphenol (**14**)] to tert-butyl ether derivatives (**15**) in excellent product isolation (Figure 8.5). Further, authors optimized a solvent system required for the reaction, and claimed solvent-free condition works efficiently in isolation of the product quantitatively with a simple workup step. Since, the excess Boc-anhydride present in the reaction quickly degraded into isobutene and CO_2, hence, the end product separation was pure, and in many case not required chromatographic purification.
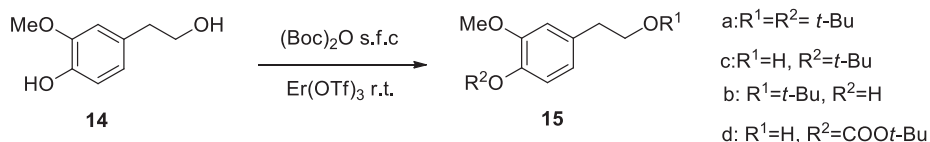
Figure 8.5: $Er(OTf)_3$-catalyzed alcoholic and phenolic protection using Boc-anhydride.

Furthermore, the same authors described $Er(OTf)_3$ is capable of deprotection of the acid-labile tert-butyl ether group noticed efficiently. The ether cleavage remains part of the functional group conversion to achieve free hydroxyl group after temporarily blocked. The authors reported tert-butyl ether (**16**) protected phenolic derivative gets cleaved immediately into 4-methoxyphenol (**17**) and 2-methylprop-1-ene (**18**) in a methanol solvent using 10 mol% catalyst in MW irradiation condition reported (Figure 8.6) [40].

Acylation is another major functional group protection route used in organic transformation, and especially used in amine and hydroxyl group protection. The regioselective acetylation is again challenging for chemists due to multiple hydroxyl groups in
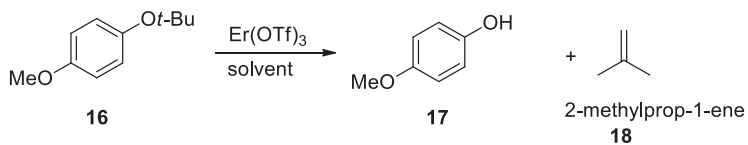
Figure 8.6: Deprotection of tert-butyl ether.

polyols and carbohydrates. Nonetheless, various synthetic routes have been reported with environmentally hazardous or expensive catalysts involving tedious reaction condition [41–55]. Nardi et al., reported that in the presence of Er(OTf)$_3$, an efficient selective acetylation to bioactive molecules, due to unique properties of the erbium(III) salts stability and catalytic performance in water. In the presence of catalytic amount of Er(OTf)$_3$, researchers tested 1-acetylimidazole for the acetylation of carbohydrates (**19**) in an aqueous medium under MW and it gave excellent product isolation (**21**) (Figure 8.7). A variety of multifunctional natural products, namely phenyl D-pyranosides, methyl D-pyranosides, phenolic antioxidant compounds, nucleosides, and aliphatic alcohols, are successfully acetylated by development of newer protocols by the authors.
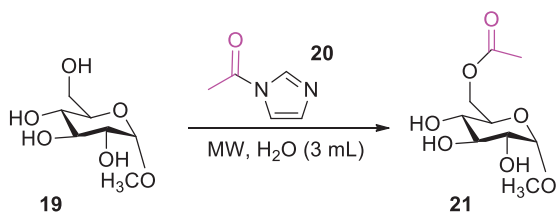
Figure 8.7: Acetyl group protection.

The Lewis acid catalytic properties of the Er salts further extended to synthesize functionalized benzodiazepines, whose structure is built by the fusion of benzene with diazepine ring. Benzodiazepines (BZDs) have showed many pharmacological applications; consequently, wide synthetic methods have been demonstrated for expedient synthesis to access new BZD scaffolds [56–58]. Further, researchers revealed highly therapeutic applications and low side effects noticed for the 1,5-BZDs compared to 1,4-BZDs. Er(OTf)$_3$ has emerged as a better choice catalyst in combination with MW-assisted condensation reaction of o-phenylenediamine or *o*-aminophenol or *o*-aminothiophenol (**22**) with carbonyl compounds (**23**) gave functionalized 1,5-benzodiazepines/1,5-benzoxazepines/1,5-benzothiazepines (**24**) (Figure 8.8). Furthermore, authors studied optimized catalytic amount 5 mmol% in acetonitrile solvent system gave quantitative product isolation, and authors tested these synthesized derivatives for hepatitis C virus NS$_5$B pharmacological applications.

Amblard et al. [59] reported one-pot reaction involved 1,2-phenylendiamine (**25**) with dimedone (**26**) in Er(OTf)$_3$ (5 mol%) and ACN solvent room temperature stirring
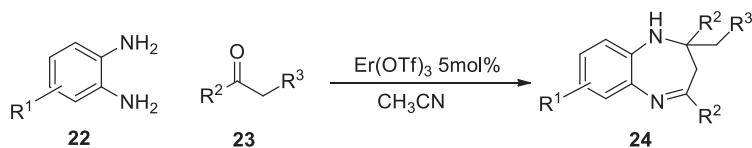
Figure 8.8: Synthesis of 1,5-benzoheterodiazepines.

gave 3-(2-aminobenzyl)-5,5-dimethylcyclohex-2-en-1-one (**27**), followed by an equivalent of acyl or aryl chloride (**28**) gave 1,5-benzodiazepine-type product (**29**) in excellent yields with faster rate of formation of the product (Figure 8.9). Further, authors examined the biological utility of these molecules synthesized in polymerase inhibitors.
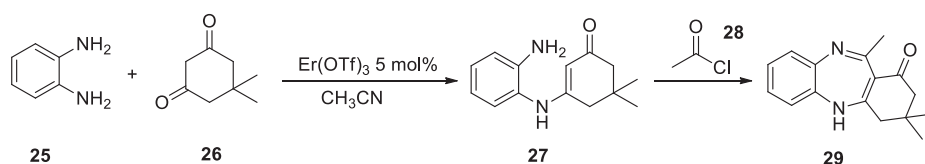
Figure 8.9: One-pot synthesis of 1,5-benzodiazepine.

Herrera et al. [60, 61] reported the selective benzimidazole product formation (**31**) by the reaction of *o*-phenylenediamine (**25**) with a wide range of aryl aldehyde derivatives (**30**) at 1–2 °C cold condition, or at reflux temperature (80 °C) for the electron-deficient aryl aldehydes (Figure 8.10). The authors claimed 2-substituted benzimidazole derivatives exclusively obtained in this catalyzed reaction, and also explained charge density located on carbonyl group attributed the formation of the other *N*-alkylated product (**32**).
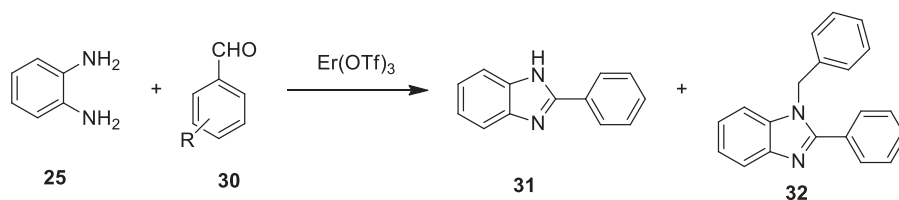
Figure 8.10: Benzimidazole synthesis.

The importance of Er(III)-catalyzed carbonyl of ketone was further studied on Luche reaction. This reaction is a conversion of α,β-unsaturated ketone into allylic alcohol, the previous researcher reported use of other lanthanide salts for the reaction, and these reagents are sensitive to quantity used and reaction required solvents are the major limitation for the Luche protocol noticed. Thus, researchers discovered Er(OTf)$_3$ as an alternative LA catalysts for the eco-friendly, and simple protocol synthesis in 5 mol% of Er(OTf)$_3$ in 1 equiv. NaBH$_4$ enabled reduction of the formed carbonyl product (**33**).

Authors used a green solvent for reactions such as 2-MeTHF; this solvent allowed final product isolation directly, and not required extraction steps are the major advantages reported (Figure 8.11). The method was examined on chiral natural α,β-unsaturated substrates, like 3,5-dimethylcyclohex-2-enone, (*R*)-pulegone and (*R*)-carvone resulted diastereoselectivity toward the product allyl alcohol formation observed (**34** & **35**) products with *cis* configuration [62, 63].

R = alkyl, aryl
R^1 = alkyl, aryl, H
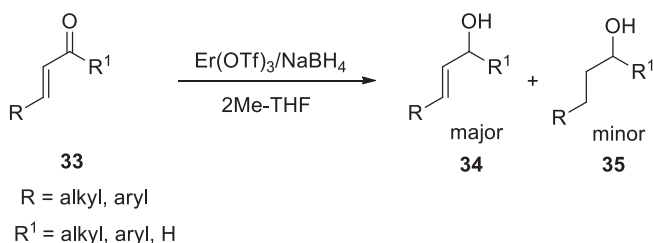
Figure 8.11: Er(OTf)$_3$ catalyzed for selective Luche reduction.

Another exciting use of Erbium triflate in various chemical transformations developed is also extended to natural compound conversion in the concept of semisynthetic protocol. The conversion made on natural product is directly labeled under natural product–based drug discovery. Procopio et al. reported use of Er(OTf)$_3$ in manipulation of a oleuropein skeleton, a natural product. Authors developed, and then patented, a very mild protocol for the oleuropein hydrolysis catalyzed by Lewis acid. This protocol developed is found very challenging, because of the oleuropein containing other functional groups competing with it. In this work, oleuropein (**36**) in aqueous acetonitrile with erbium triflate (10 mol%) under reflux temperature gave intermediate product (**37**), and this intern equilibrate with many broken complex products (**38**, **39**, **40**, and **41**) were identified in LC-MS and 1H-NMR analysis by the authors reported (Figure 8.12) [64, 65].
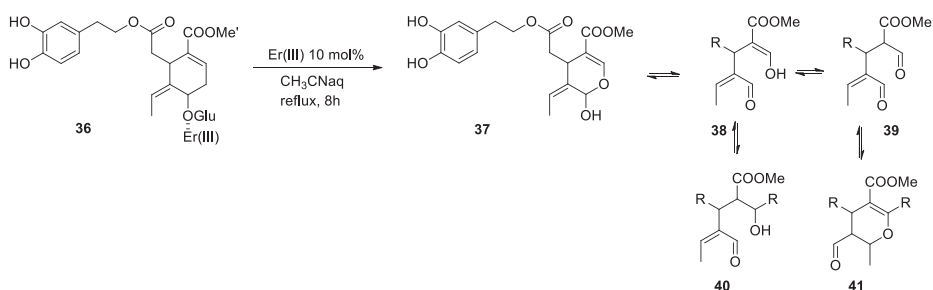
Figure 8.12: Synthesis of aglycones of oleuropein.

In continuation of modification of the above product, Procopio et al. [64, 65] demonstrated simple acetylation to achieve oleuropein 4-(2-acetoxyethyl)-1,2-phenylene

diacetate (**41**) from 4-(2-hydroxyethyl)benzene-1,2-diol (**42**) derivatives (Figure 8.13). Further, authors evaluated biological and molecular modeling data for this semisynthetic oleuropein natural derivative. The pharmacological studies showed anti-inflammatory activity; antioxidant and anti-proliferative effects on breast cancer cells, as well as anti-growth action were evaluated and revealed that these derivatives have significant pharmacological applications.
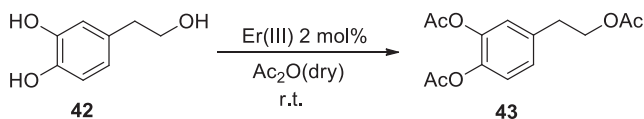
Figure 8.13: Acetylation of oleuropein derivatives.

In another piece of work reported by the same group extended this semisynthetic protocol for the hydroxytyrosol (**42**) acylation using fatty acid chloride (**44**) gave product of 4-(2-acetoxyethyl)-1,2-phenylene diacetate (**45**) (Figure 8.14). Butyryl, decanoyl, elaidyl, stearyl, oleyl, linoleyl, and palmitoyl groups were conjugated to hydroxytyrosol, and permeation through in vitro in Franz diffusion cells model was studied [66–68]. In an in vitro Franz cell model, these derivatives showed potential as topical therapeutic agents for the cutaneous diseases' treatment as they permeated efficiently through the stratum corneum epidermis (SCE) membrane.
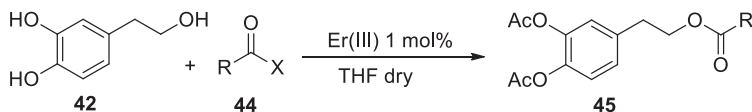
a: R= $CH_3(CH_2)_{14}$; b: R=$CH_3(CH_2)_2$;c:R= $CH_3(CH_2)_8$;d: R=$CH_3(CH_2)_{16}$;
e: R= $CH_3(CH_2)_7$=$(CH_2)_7$(*cis*);e: R= $CH_3(CH_2)_7$=$(CH_2)_7$(*trans*);
e: R= $CH_3(CH_2)_4$CH=CHCH$_2$CH=CH$(CH_2)_7$(*cis*)X = RCO or Cl

Figure 8.14: Synthesis of hydroxytyrosol fatty acid esters.

A dialdehyde moiety conjugated with 2-(3,4-hydroxyphenyl) ethyl (3S,4E)-4-formyl-3-(2-oxoethyl)hex-4-enoate(3,4-DHPEA-EDA) and 2-(3,4-hydroxyphenyl) 4-formyl-3-(2-oxoethyl)hex-4-enoate(p-HPEA-EDA), present in virgin olive oil and other oils of two active principles, has been exhaustively worked upon in recent years has shown very good health and peculiar sensory properties. These modified derivatives endorsed various health benefits in humans and its quantity in oil and waste olive water contains few tens to some hundreds of mg/kg. Nonetheless, further exploration of the antioxidant and other physiological benefits of this compound has been hindered, due to difficulties in isolation to pure compound in sufficient quantity for the investigation [69]. Considering these exciting

pharmacological behaviors of 3,4-DHPEA-EDA, subsequent research work demonstrated a synthetic protocol based on erbium triflate as a catalysts produced these derivatives in high yield and purity (Figure 8.15) [70]. The reaction of 3,4-dihydroxyphenethyl (Z)-3,4-diformylhex-4-enoate (**46**) in 10 mol% of Er(III) under aqueous medium in reflux condition gave (Z)-4-((S)-4-carboxy-1-oxobutan-2-yl)amino)oxy)-6-(2-(3,4-dihydroxyphenethoxy)-2-oxoethyl)-5-ethylidenecyclohex-1-ene-1-carboxylic acid (**47**).
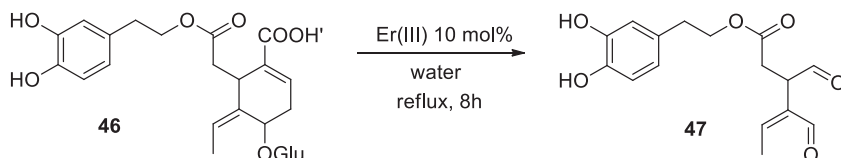

Figure 8.15: Synthesis of 3,4-DHPEA-EDA.

Procopio and his co-workers described dihydropyrimidinone derivatives (DHPMs) (**50**) of libraries synthesis via Biginelli condensation of ethyl acetoacetate (**5**), benzaldehyde (**48**), and urea (**49**) in solvent-free-catalyzed Er(III)chloride (5 mol%) in a Q-tube reactor or microwave irradiation (Figure 8.16) [71–77]. The authors claimed the use of catalysts found some added advantages for the protocol like mild reaction condition, eco-friendly nature, and isolation of product in high yield.
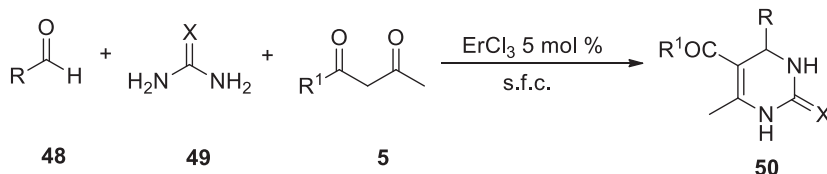
Figure 8.16: Synthesis of 4-aryl-3,4-dihydropyrimidin-2(1 H)-ones.

Procopio et al. demonstrated that for the acylation of alcohols and phenols $Er(OTf)_3$ emerged as a mild and efficient catalyst (**53**) achieved by the reaction of respective alcohol and phenol (**51**) with different acid anhydrides (**52**) (Figure 8.17). A large number of functionalized substrates of the acidic anhydrides {Ac_2O, $[(CH_3)_3CO]_2O$, Bz_2O, $(EtCO)_2O$, and $(CF_3CO)_2O$} has been employed by the authors and isomerization of chiral centers of the alcohols and phenols is not observed. Moreover recycling and reuse of the catalyst for many cycle of the reaction without loss of its catalytic activity have been claimed by the authors [71–77].

Agnihotri et al. [78] reported that in mild deprotection protocol of benzylidene derivatives cleavage $Er(OTf)_3$ acts as an efficient Lewis acid catalyst. A modified procedure for simultaneous cleavage of the benzylidene acetal (**54**) and peracetylation of
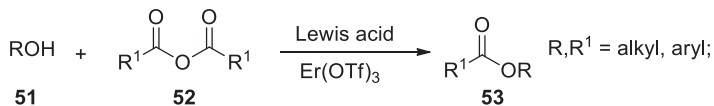
Figure 8.17: Acylation of alcohols and phenols with different acid anhydrides.

the substrates to give quantitative yields of propane-1,2,3-triol (**55**) in a short reaction time has been developed authors (Figure 8.18).
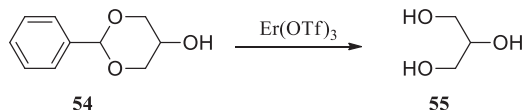
Figure 8.18: Deprotection of *cis*-1,3-O-benzylidene glycerol.

Dalpozzo et al. [79] described that for the acylation of alcohols and phenols (**53**) by the reaction of OH group of alcohol or phenol (**51**) with a wide range of functionalized substrates with various acidic anhydrides (**52**), namely (Ac$_2$O, (EtCO)$_2$O, (ButCO)$_2$O, (PriCO)$_2$O, and (CF$_3$CO)$_2$), catalyzed by a powerful catalyst ErCl$_3$ yielded isomerization free of chiral centers product (**53**). Authors claimed that the catalyst used in this reaction can be recycled and reused for several times and it is an added advantage (Figure 8.19).
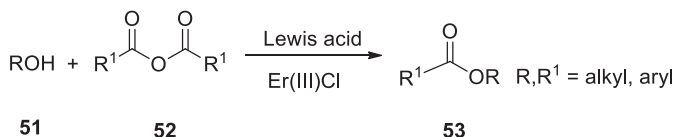
Figure 8.19: Acylation of alcohols from anhydrides.

Eco-friendly method of both protection and deprotection of tert-butyl ethers on alcohols and phenols has been described Procopio et al. [80]. The protection step involved solvent-free reaction rt in Er(OTf)$_3$, catalyst, and recovered in water phase and reused several times reported. The tert-butyl group gets detached faster from the phenols and alcohols in methanol under MW irradiation system making the deprotection step eco-friendly. In a typical example, author gave attention to phenol protection with optimized reaction condition of catalyst and reaction time for the tert-butyl ether (**16**) formation from 4-methoxyphenol (**17**). Surprisingly, authors noticed by-product (*t*-Butyl carbonate) formation can be avoided when the reaction is carried out in reflux temperature (**56**), but furnished considerably low yield of (**16**) (Figure 8.20).

Procopio et al. reported mechanistic pathway of tert-butyl cation involved in the conversion of tert-butyl (4-methoxyphenyl)carbonate (**56**) formed during the reaction
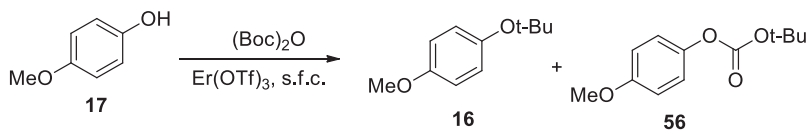
Figure 8.20: Protection of 4-methoxyphenol.

as by-product to 1-(tert-butoxy)-4-methoxybenzene (**16**) catalyzed by Er(OTf)$_3$ at high temperature (Figure 8.21) [80].
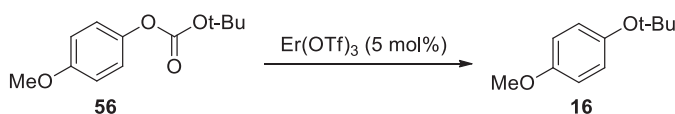

Figure 8.21: Transformation of tert-butyl carbonate into tert-butyl ether.

Quick and efficient conversion of a wide range of functional phenols and alcohols simultaneously gave very good yields of tert-butyl ether product with purity as reported by Procopio et al. [80]. One of the model reactions carried out presented the reaction of 4-(2-hydroxyethyl)-2-methoxyphenol (**59**) in the presence of Boc-anhydride and Er(OTf)$_3$ gave tert-butyl ether derivatives (**60**) (Figure 8.22).

a: $R^1 = R^2 =$ t-Bu
b: $R^1 =$ t-Bu, $R^2 =$ H
c: $R^1 =$ H, $R^2 =$ t-Bu
d: $R^1 =$ H, $R^2 =$ C(O)Ot-Bu
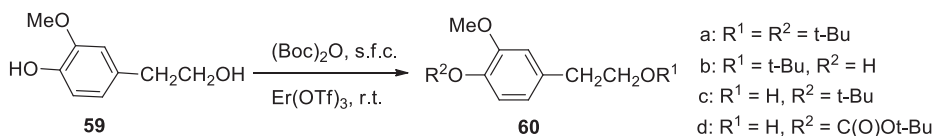
Figure 8.22: Differentiation between alcoholic and phenolic functionalities protection.

Procopio et al. [80] reported ErCl$_3$ in EL solvent emerged green solvent medium for the reaction of furfural (**61**) with amine (**62**) gave *N,N*-substituted-*trans*-4,5-diaminocyclopent-2-enones (**63**). The protocol gave diastereoselective versatile synthetic intermediates with functionalized complex derivatives in excellent yield with enantiomeric pure isolated (Figure 8.23).
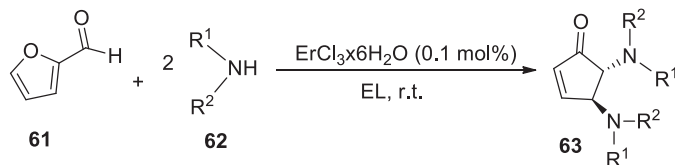
Figure 8.23: Synthesis of N,N'-substituted *trans*-4,5-diaminocyclopent-2-enones.

The synthesis of a series of anti-Markovnikov alcohols (**65**) from terminal and internal epoxides (**64**) using low catalyst loading, permitted by an efficient and mild isomerization – transfer hydrogenation reaction based on a cobalt pincer catalyst, has been studied by Liu et al. [81] (Figure 8.24). The reaction catalyzed by Lewis acid (3 mol%) Er(OTf)$_3$-catalyzed epoxide isomerization, and subsequent cobalt-catalyzed transfer of hydrogenation using ammonia borane as a hydrogen source found best suitable protocol for the formation of product (**65**) isolation in good yield and purity.
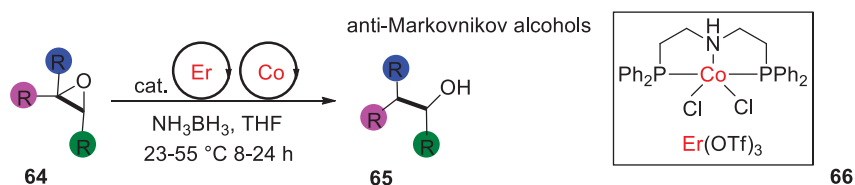
Figure 8.24: Synthesis of anti-Markovnikov products.

The application of erbium triflate into regio- and stereoselective epoxide ring opening in the presence of trimethylsilylazide (TMSN$_3$) and trimethylsilylcyanide (TMSCN) is described on 2-(phenoxymethyl)oxirane (**67**) model reactant to form a ((1-azido-3-phenoxy-propan-2-yl)oxy)trimethylsilane (**68**) in good yield isolated (Figure 8.25).
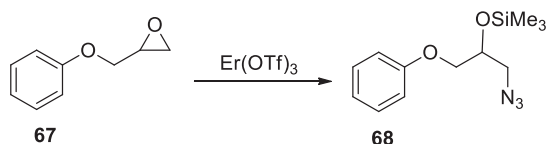
Figure 8.25: Epoxide ring opening with TMS-N$_3$ and TMS-CN.

Zhu et al. [82] described methyl (*E*)-2-oxo-4-phenylbut-3-enoate (**69**) with 2,3-dihydrofuran (**70**) reaction gave methyl-(3a*S*,4*S*,7a*R*)-4-phenyl-2,3,3a,7a-tetrahydro-4H-furo[2,3-b]pyran-6-carboxylate (**71**)-catalyzed ligand-Er(OTf)$_3$ (Figure 8.26) [82].
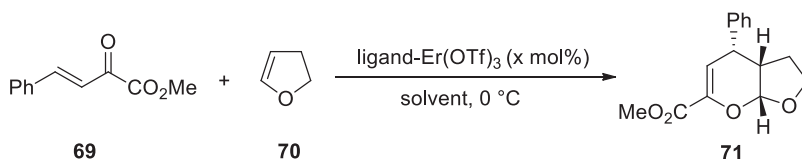
Figure 8.26: α,β-Unsaturated-ketoester with 2,3-dihydrofuran HAD reaction.

Further, authors also examined the methyl (*E*)-2-oxo-4-phenylbut-3-enoate (**69**) reaction with 3,4-dihydro-2H-pyran (**72**) in ligand-Er(OTf)$_3$ catalysts to form a product methyl (4a*S*,5*S*,8a*R*)-5-phenyl-3,4,4a,8a-tetrahydro-2H,5H-pyrano[2,3-*b*]pyran-7-carboxylate (**73**) (Figure 8.27) [82].
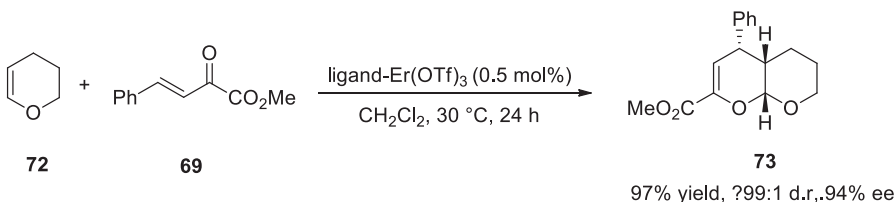

Figure 8.27: Cycloaddition of 3,4-dihydro-2H-pyran.

Furthermore, authors' extended reaction of methyl (*E*)-2-oxo-4-phenylbut-3-enoate (**69**) with alkene (**74**) reaction accelerated above catalyst in dichloromethane (DCM) solvent gave pyran (**75**) derivate in good yield isolation reported (Figure 8.28) [82].
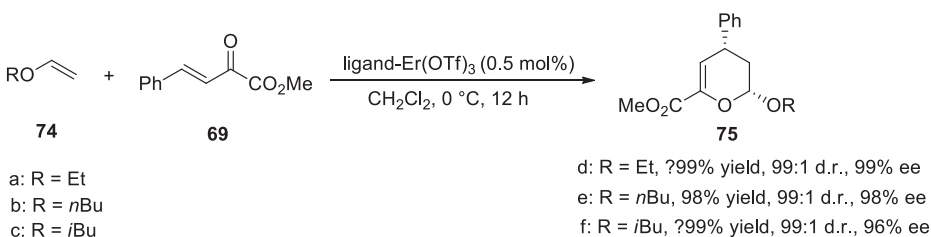
Figure 8.28: Synthesis of pyran derivatives.

Moreover authors' extended work to β,γ-unsaturated α-ketoesters (**69**) reaction with cyclopentadiene (**76**) isolated good product yield of 77 [82]. In their optimization of the catalysts, authors used L5/Er(OTf)$_3$ and L5/Cu(OTf)$_2$ catalysts and showed both catalysts gave moderate chemoselectivity and excellent enantioselective synthesis of methyl (4*R*,4a*S*,7a*S*)-4-phenyl-4,4a,5,7a-tetrahydrocyclopenta[b]pyran-2-carboxylate (**77**) and methyl 2-oxo-2-((1*S*,2*R*,3*R*,4*R*)-3-phenylbicyclo[2.2.1]hept-5-en-2-yl)acetate (**78**) products (Figure 8.29).
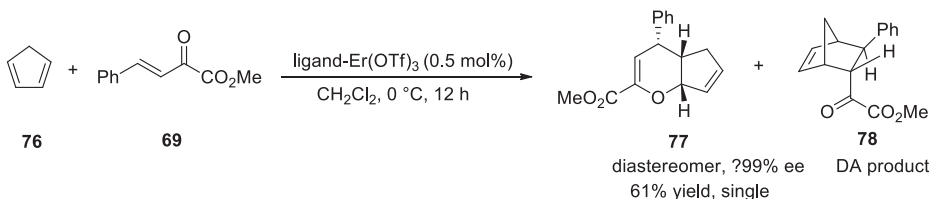

Figure 8.29: Enantioselective synthesis of pyran derivatives.

The same authors demonstrated sterically hindered alkene (**79**) reaction to unsaturated α,β-ketoesters (**69**) afforded methyl 2-methoxy-2-methyl-4-phenyl-3,4-dihydro-2H-pyran-6-carboxylate (**80**) having quaternary carbon gave >99% yield, >99% d.r, and >99% ee (Figure 8.30) [82].
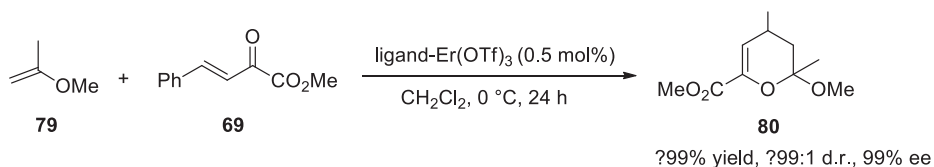

Figure 8.30: Pyran derivates synthesized from sterically hindered alkene.

The same authors reported vinyl sulfide (**81**) reaction with unsaturated α-ketoesters (**69**) gave pyran derivatives (**82**) stereoselectively. However, phenyl(vinyl)sulfane (**81**) reactivity slower than electron-rich alkenes was noticed (**69**) (Figure 8.31) [82].
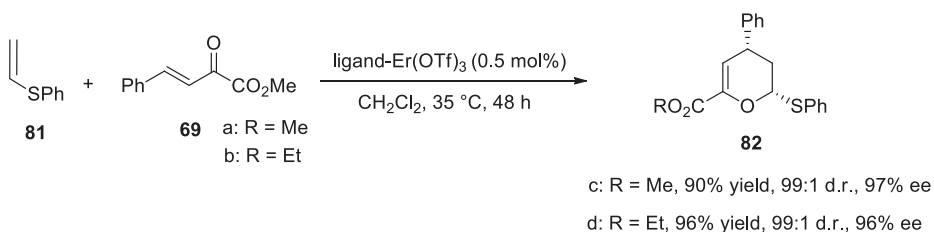
Figure 8.31: Pyran derivatives synthesized from vinyl sulfides.

Further the authors extended the reaction of ethyl(vinyl)sulfane (**83**) with unsaturated α,β-ketoesters (**69**) in the same catalysts under DCM solvent and that gave pyran derivate in excellent yield and purity (**84**) (Figure 8.32) [82].
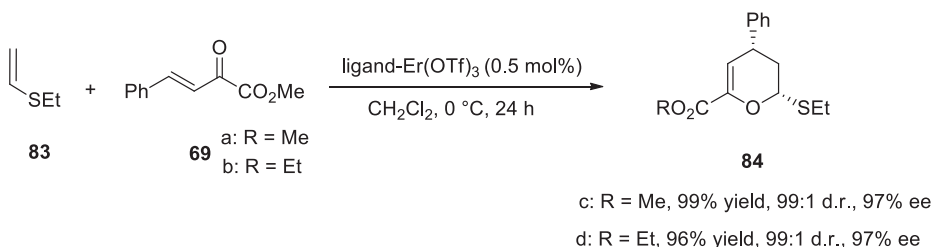

Figure 8.32: Pyran derivatives synthesized from ethyl(vinyl)sulfane.

Erbium trifluoromethanesulfonate is a derivative of erbium that has also emerged as a suitable catalyst for the Friedel–Crafts acylation of arenes (**85**) containing electron-donating group and aromatic carboxylic acids (**86**) (electron-withdrawing group) as an acylating agent accelerated by microwave irradiation. Authors studied several factors involved for the reaction condition, and revealed the developed method is efficient, faster, and less waste producing, thus allowing the method to be used it in a wide range of aryl ketones (**87**) synthesis in good yields (Figure 8.33) [83].
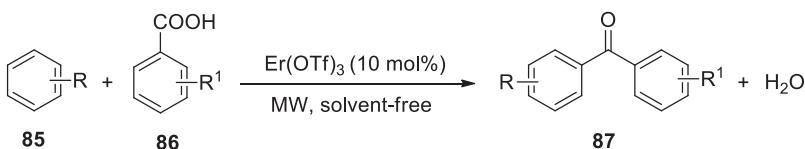
Figure 8.33: Acylation of aromatic compounds with benzoic acids.

Bortolini et al. [84] described 1,3-dipolar cycloaddition of nitrone (**88**) with alkene (**89**) afforded isoxazolidines (**90**) in the presence of Er(OTf)$_3$ and ionic liquids. Authors claimed catalyst and ionic liquids solvent medium is recycled, and reused up to five times (Figure 8.34).
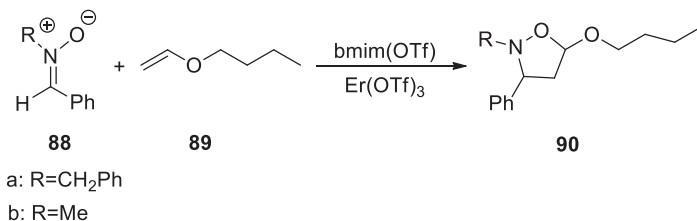

a: R=CH$_2$Ph
b: R=Me

Figure 8.34: Cycloaddition of nitrone with alkene.

Dalpozzo et al. [85] described the synthesis of 1,5-benzodiazepine (**91**) in high yield after optimized solvent and catalyst condition for OPD (**25**) with acetone act as a reactant under solvent-free in 5 mol% catalyst gave 2,2,4-trimethyl-2,3-dihydro-1H-1,5-benzodiazepine (**91**). Author also studied the role of the catalyst in the reaction, and noticed no progress of the reaction, even after prolonged reaction time without catalyst (Figure 8.35).
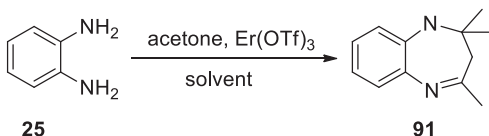

Figure 8.35: Er(OTf)$_3$ catalyzed reaction of o-phenylendiamine and acetone.

Further, the same authors extended OPD/*o*-aminothiophenol/*o*-aminophenol (**22**) derivatives with aryl- or alkyl-ketone derivatives (acetone derivative) (**92**) catalyzed Er(OTf)$_3$ at room temperature gave 1,5-benzodiazepine (**93**). Authors optimized reaction and tolerance of the substitution on the benzene ring gave product isolation in excellent yields (Figure 8.36) [85].
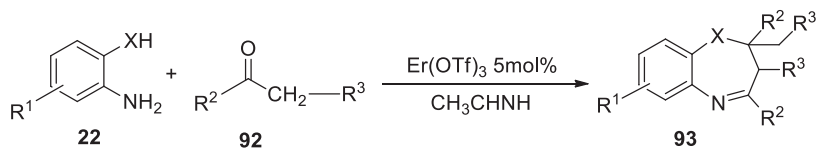

Figure 8.36: 1,5-Benzoheteroazipenes synthesis.

Dalpozzo et al. [85] reported the reaction of *o*-anilino derivatives (**94**) and chalcone (**95**) gave 1,5-benzodiazepine derivative (**96**) in good yield isolation. Further, authors are able to do SAR on chalcone substituents and showed crucial hydroxyl group at 2-position of chalcone presence give positive effect on the rate of formation of the expected product in good yield (Figure 8.37).
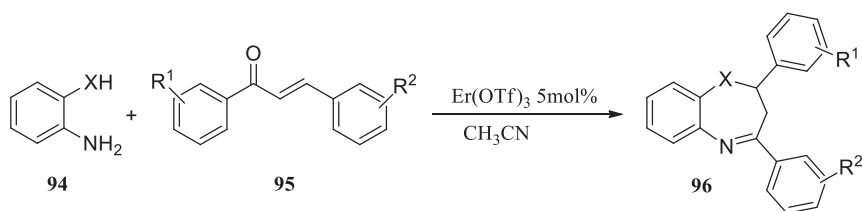

Figure 8.37: Synthesis of benzoheterodiazepines from *o*-phenylendiamine and chalcones.

Dalpozzo et al. [85] demonstrated Er(OTf)$_3$ catalyzed *vic*-diacetates (**97**) from epoxide (**8**) ring opening in the presence of acetic anhydride (Figure 8.38). Further, authors are able to explained the mechanistic route of *vic*-diacetate formation involving two coordination sites for the erbium ion, the oxygen atom of epoxide or carbonyl group of acetic anhydride giving rise to complexes
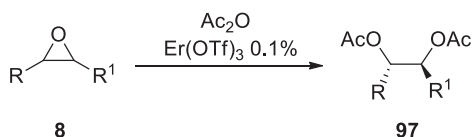

Figure 8.38: Synthesis of *vic*-diacetates from epoxides.

A and B, respectively, resulting in catalytic loop formation; finally, the coupling between C and D leads to the catalyst regeneration and product formation explained (Figure 8.39).
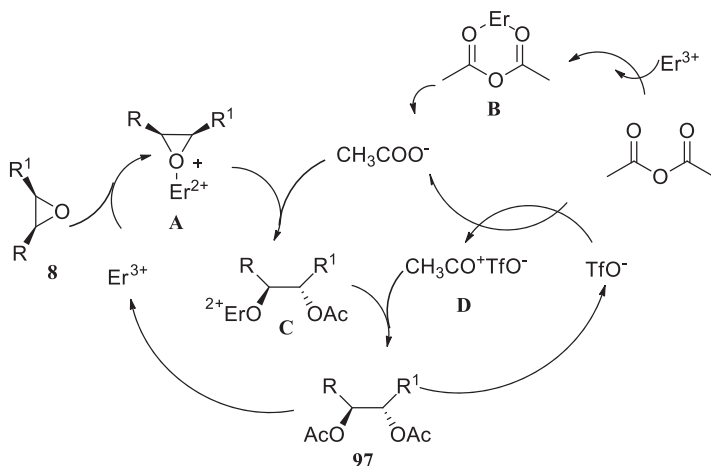

Figure 8.39: Probable pathway of formation of *vic*-diacetates.

Dalpozzo et al. [86] reported the 1,1-diethoxy cyclohexane (**98**) deprotection in the presence of $Er(OTf)_3$ in polar solvent. Authors noticed the catalysts activity more efficient in solvent CH_3NO_2, and CH_3CN in water, and less efficient showed in diethyl ether, $CHCl_3$, THF, and CH_2Cl_2 in water medium noticed. Furthermore, authors optimized the catalyst amount and found 1 mol% catalysts found better, and also revealed water is crucial in the reaction. Further, authors performed reaction in a dry solvent, but isolated very low yields of the product reported (Figure 8.40).
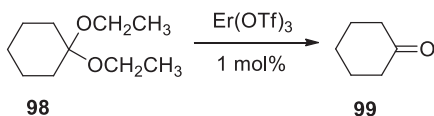

Figure 8.40: Deprotection of 1,1-diethoxy cyclohexanone.

Procopio et al. [87] reported that allylation of 3,4,6-tri-*O*-acetyl-D-glucal (**100**) with allyltrimethylsilane (**101**) (1.5 equiv.) derivative in a optimized solvent and catalyst at room temperature gave 95% of the product allyl 2,3-unsaturated acetyl C-glycoside (**102**). Surprisingly, authors noticed no reaction in solvent THF, Et_2O, and $CHCl_3$ used even after longer reaction time extension (Figure 8.41).

The product 2-(3,4-hydroxyphenyl)ethyl(3*S*,4*E*)-4-formyl-3-(2-oxoethyl)hex-4-enoate (3,4-DHPEA-EDA) obtained by natural demethyloleuropein-2 formed from oleuropein-1 present in the olive oil hydrolysis by Lewis acid. The catalyzed reaction removed sugar moiety and biological pathway mimic deglycosylation gave isomeric pure form after
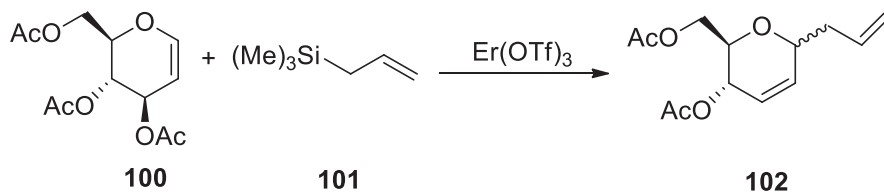
Figure 8.41: Allylation of 3,4,6-tri-*O*-acetyl-D-glucal.

solid product extraction process. Authors revealed that the biomimetic synthetic method showed more convenient route than classical multistep approach employed for the oleocanthal preparation reported. The reaction of (*E*)-4-(2-(3,4-dihydroxyphenethoxy)-2-oxoethyl)-3-ethylidene-2-methyl-3,4-dihydro-2H-pyran-5-carboxylic acid (**103**) in Er(OTf)$_3$/H$_2$ presence gives 3,4-dihydroxyphenethyl (*E*)-4-formyl-3-(2-oxoethyl)hex-4-enoate (**104**), and the reaction of reactant **103** in Er(OTf)$_3$/D$_2$ presence gives 3,4-dihydroxyphenethyl (*E*)-4-formyl-3-(2-oxoethyl-1,1-d2)hex-4-enoate (**105**) (Figure 8.42) [88]. Further, authors screened the transformed product for anti-tumor and anti-inflammatory studies and are comparable activities.
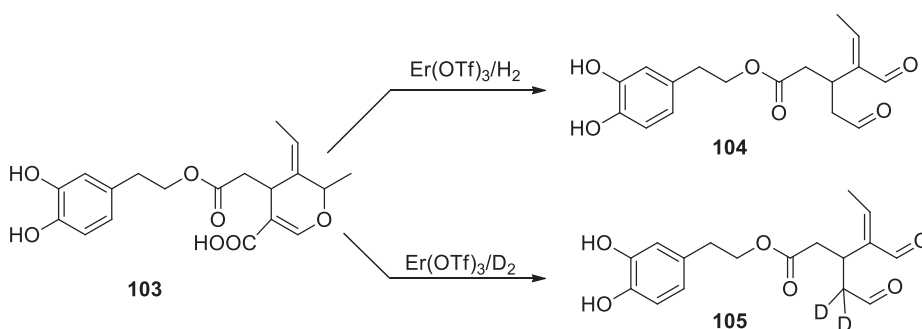

Figure 8.42: Synthesis of 3,4-DHPEA-EDA and its deuterated analogue.

Paonessa et al. [88] studied the eco-friendly strategy of functional group protection/deprotection, and concerning phenols and alcohol acylation using Er(OTf)$_3$. The conversion of epigallocatechin gallate (EGCG) (**106**) to EGCG fatty acid esters (**107**) in the presence of 2-MeTHF and Er(OTf)$_3$ described. Authors claimed developed protocol had advantages of simple reaction condition and eco-friendly method of EGCG acetylated using acetic anhydride in solvent-less at room temperature (Figure 8.43). Further, authors examined synthesized EGCG fatty acid esters for antioxidant properties.

A new *trans*-acetalization in the presence of alcohol as an nucleophile catalyzed Er(OTf)$_3$ gave a new class of lipophilic oleuropein aglycone derivatives (**109**) as reported by Nardi et al. [89]. Thus, authors revealed success in the first attempt for the
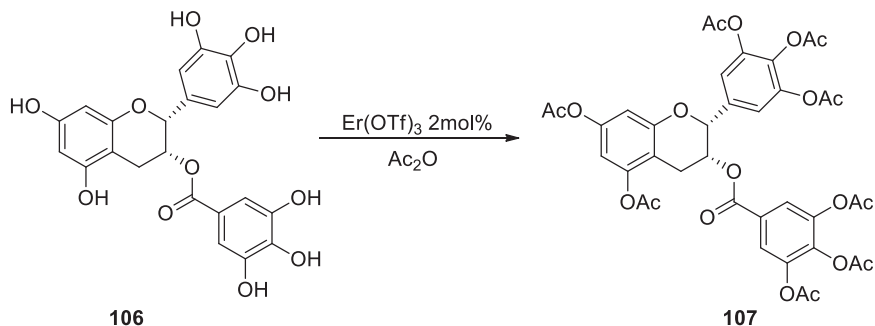
Figure 8.43: Synthesis of EGCG per-acetated.

exchange of the glycosidic moiety of the oleuropein (**108**) molecule with a less lipo-philic entity, and methanol used as a nucleophile source as well as solvent. Er is able to coordinate acetal oxygen to form the oxonium ion and subsequent attack of the nucleophilic alcohol (Figure 8.44). The authors claimed the development of method is robust and efficient *trans*-acetalization of oleuropein (**108**) giving a recent class of li-pophilic oleuropein aglycones (**109**).
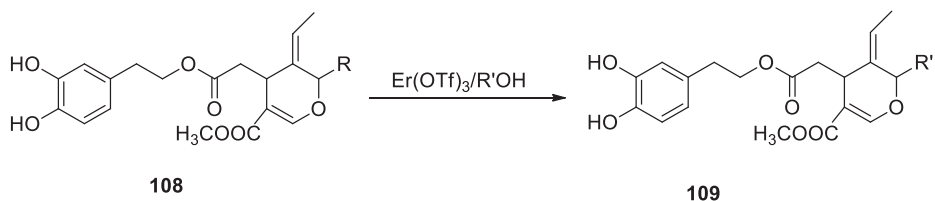
Figure 8.44: Synthesis of 3,4-DHPEA using Er(OTf)$_3$.

The reaction of *o*-phenylenediamine (**25**) and benzaldehyde (**110**) derivatives catalyzed by Erbium nitrate gave 1,2-disubstituted benzimidazole derivatives in excellent yield re-ported for the synthesis of disubstituted benzimidazoles (**111**) (Figure 8.45) [90].

Figure 8.45: Synthesis of disubstituted benzimidazoles.

The synthesis of 2,3-unsaturated C-glycosides (**114**) via Ferrier rearrangement using the reaction of 3,4,6-tri-*O*-acetyl-D-glucal (**112**) with protected trimethylsilyl thymine (**113**)

generated in situ using HMDS, using of Er(OTf)$_3$ as a Lewis acid catalyst for gave good product isolation (Figure 8.46) has been reported [91].
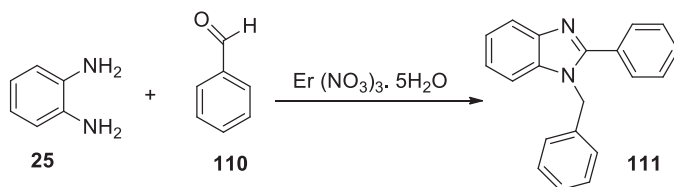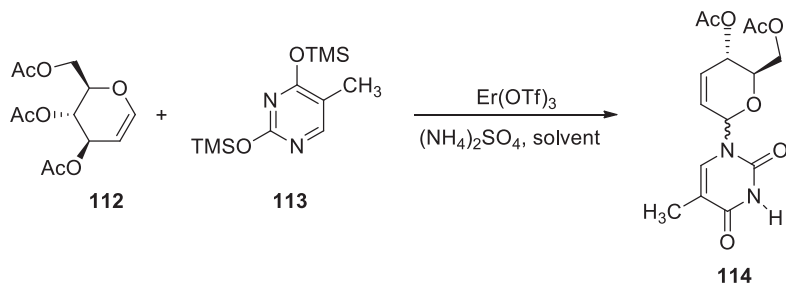

Figure 8.46: Synthesis of 2,3-unsaturated C-glycosides.

Sashidhara et al. [92] described elegant MCRs of phenylimidazoquinoxalines (**118**) synthesis from phenylglyoxaldehydes (**115**), *O-N*-Boc-phenylenediamines (**116**), azido ketones (**117**), and substituted TOSMICs via MW irradiation. Authors found developed method had several advantages for developing complex fused heterocycles due to, simplicity of the method, molecular diversity, and atom economy readily available starting materials is desirable for the new drug discovery (Figure 8.47).
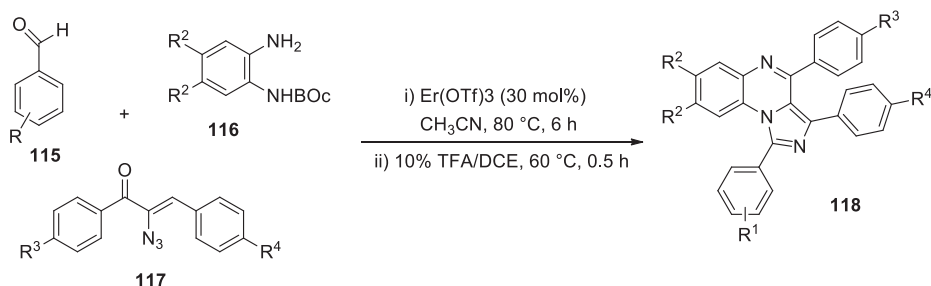
Figure 8.47: Synthesis of imidazo[1,5-a] quinoxalines.

8.3 Erbium-based heterogeneous catalyst

Due to the present increasing concerns on the environmental and economic protocol development, researchers are more interested to develop the homogeneous catalytic method into a heterogeneous system of safe and inexpensive alternative route. Heterogeneous catalysts showed many added advantages compared to homogeneous, majorly due to the recovery and recycling of the catalyst several times is often easier and isolated product showed more selectivity and high yield product isolation. Compared to more research work on

homogeneous phase of Er-based salt catalysts, very less research work is reported on the heterogeneous catalysts. There are essentially two different routes reported to convert homogeneous catalysts in to a heterogeneous catalyst. Successful demonstration of both the strategies is done wherein Er salts include metal-organic frameworks (MOFs) or large-surface-area inorganic carriers supported on soluble catalysts [93–95]. Herein, authors compiled recent work reported on Er derived heterogeneous catalysts developed and described application in various organic transformations.

Procopio et al. [96] reported reaction of *p*-methoxy phenol (**119**) and BoC$_2$O in the presence of heterogeneous Er-MCM-41 metal organic frameworks as Lewis catalysts condition free of solvent, at room temperature gave tert-butyl ethers (**121**) and/or Boc protected derivatives (**120**), the formation of product can be controlled based on choice and amount of the Lewis acid catalyst used reported (Figure 8.48).
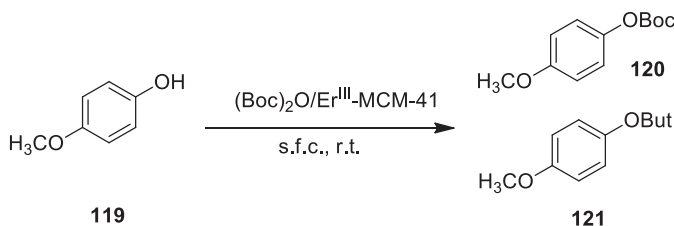
Figure 8.48: The reaction between 4-methoxyphenol and Boc$_2$O.

Hajiashrafi et al. [97] described three component reactions of ammonium acetate, benzaldehyde derivative (**115**), and ethyl acetoacetate (**122**) in ethanol with an suitable amount of Er-MOF as a catalyst (20 mg) at 70 °C gave 1,4-dihydropyridine dicarboxylate (**123**) product in good yield. Author claimed the separation of the catalyst by simple centrifuge, and obtained unrefined product which was purified by chromatography to give target product **123** (Figure 8.49). It is also noticed that the Er-MOF catalyst is recovered and reused five times without considerable loss of the catalytic activity studied.
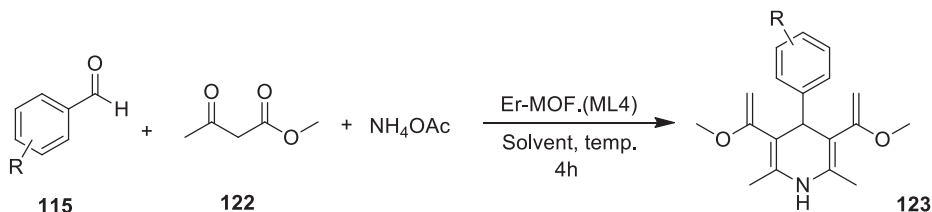
Figure 8.49: Three-component Hantzsch reaction catalyzed by Er-MOF.

Authors studied the effect of the quantity of the catalyst loaded and reaction temperature for the formation of dihydropyridines (**123**).The probable mechanistic pathway of

formation of dihydropyridines (**123**) by the reaction of ethyl acetoacetate (**122**) and aromatic aldehyde (**115**) is outlined in Figure 8.50 [96].
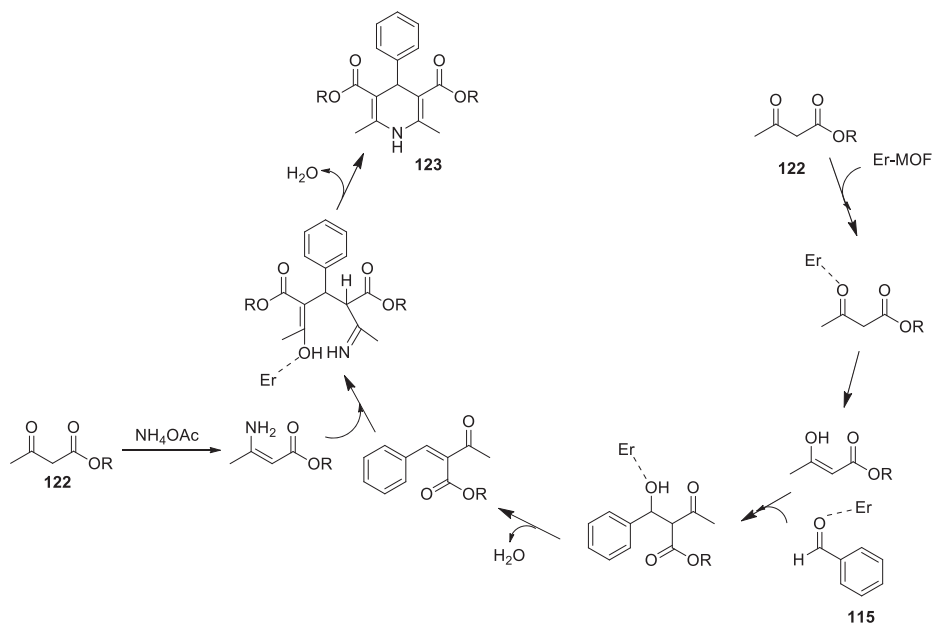
Figure 8.50: Proposed mechanisms for the formation of dihydropyridine.

Hajiashrafi et al. [97] reported the MCRs of arylaldehyde (**115**), malononitrile (**124**) and dimedone (**26**) in a catalytic quantity of Er-MOF (40 mg) at 70 °C in ethanol gave chromene derivative (**125**) (Figure 8.51). After completion of the reaction, the product was dissolved in DCM, and the catalyst removed by centrifugation at 6000 rpm for 10 min, solvent evaporated, obtained precipitate recrystallized in ethanol gave product **125**. The catalyst can be recycled up to four times without any measurable loss of its activity as claimed by the Authors.
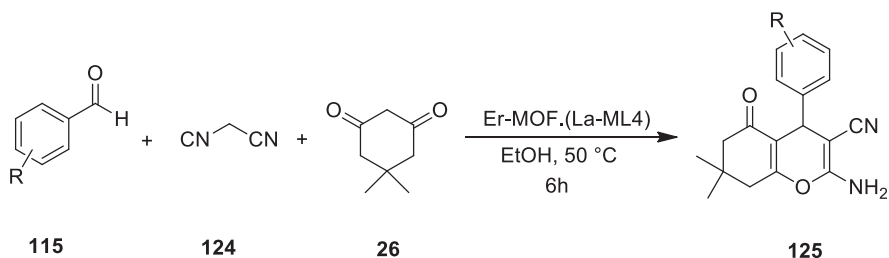
Figure 8.51: Er-MOF-catalyzed synthesis of tetrahydro-4H-chromenes.

Further, authors screened A wide range of solvent system suitable and amount of catalyst for the synthesis of chromenes studied (**125**). Authors claimed the reaction not proceeded in the absence of catalysts, suggesting reaction required catalysts to forward the reaction. The proposed mechanistic route of tetrahydro-4H-chromenes (**125**) formation under the influence of Er-MOF is showed in Figure 8.52 [97]. It is predicted that by accepting the lone pair of electron on the oxygen atom, Er(III) species acts as a Lewis acid to activate the carbonyl group of the dimedone in tetrahydro-4H-chromene synthesis.
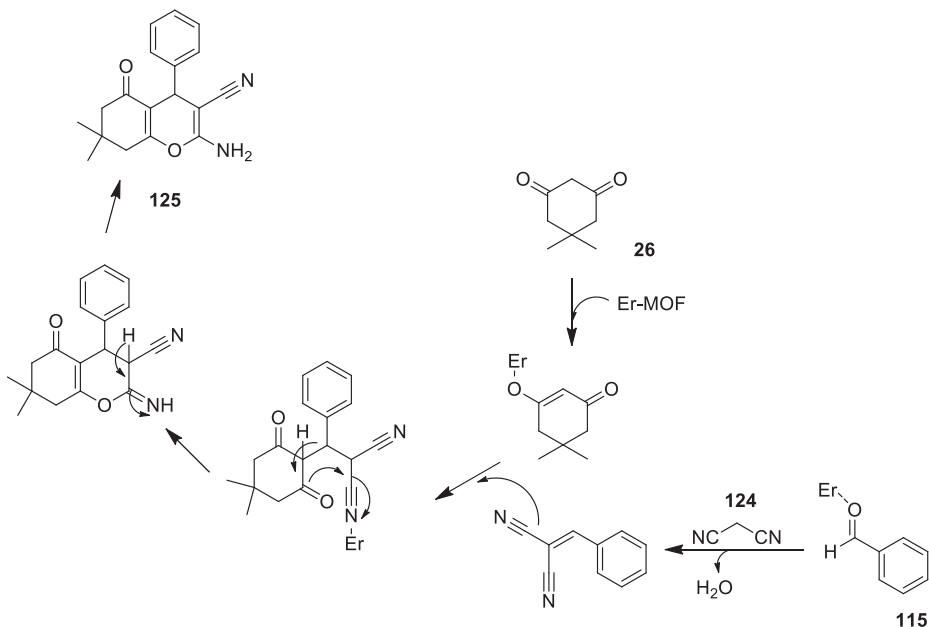
**Figure 8.52:** Proposed mechanism of tetrahydro-4H-chromene formation.

Verma et al. [98] described four-component reaction between 2-hydroxynaphthalene-1,4-dione (**126**), benzene-1,2-diamine (**25**), N-methyl-4-piperidone (**127**) and 2-aminopyridine (**128**) for structurally diverse spiroannulated pyrimidophenazines (**129**) synthesis under optimized Erbium doped TiO_2 NP reaction condition (Figure 8.53). It has been observed by the authors that the catalysts can be recyclable up to five times without change in its catalytic activity. Further, the developed method found added advantages like mild condition, excellent yield with high purity, faster reaction rate, and high atom economy with the use of a recyclable environmentally sustainable heterogeneous catalyst.

The immobilization of a novel functional material on iminodiacetic acid–erbium (Er) complex onto the surface of $CoFe_2O_4$ NPs has been demonstrated by Tamoradi et al. [99]. The synthesis of 1,8-naphthyridine derivatives (**130**) via a three-component reaction involving 2-aminopyridine (**128**), malononitrile (**124**) and various aryl aldehydes (**129**) using

Figure 8.53: Synthesis of spiroannulated pyrimidophenazines.

the catalytic activity of novel prepared material was showed by the authors. The recovery and recycling of the catalyst up to seven times without appreciable loss activity has been noticed (Figure 8.54).
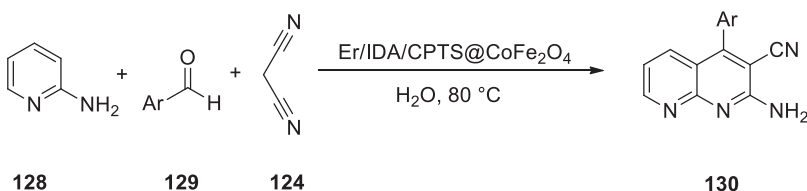
Figure 8.54: 1,8-Naphthyridine derivative synthesis.

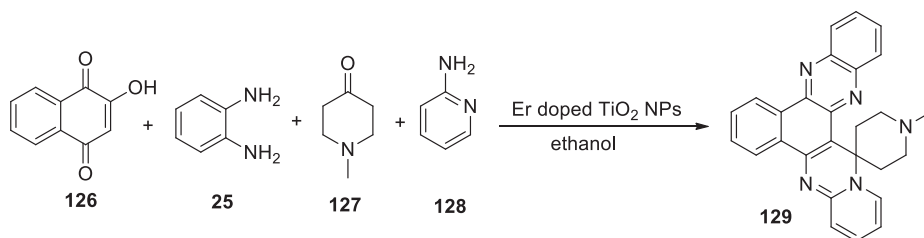Furthermore, authors demonstrated probable mechanistic pathways for the initial condensation reaction of 2-aminopyridine (**128**) with activated aromatic aldehyde (**131**). The pyridine nucleus gets aromatized by the formation of Er-enolate of malononitrile (**124**) in addition to the iminium intermediate via Michael-type pathway. The cyclo-condensation of the free α-amine by addition to the flanked nitrile gives the desired 4-aryl-2-amino-3-cyano-1,8-naphthyridine derivatives (**132**) in good yield and purity (Figure 8.55) [99].

The influence of Er(OTf)$_3$ in the Diels–Alder reactions between different dienes and dienophiles in ionic liquids have been reported by Bortolini et al. [100]. The cyclo-addition undertaken in the usual solvent and the present method has been compared by the authors who observed that the present method takes shorter reaction time and gave excellent yields of final product. An enhancement of regio- and endo- exo selectivity was also observed in most cases. The product formed is readily separated from the ILs containing catalyst and recovered in very high purity for the direct reuse up to six cycles has been reported. The reaction of cyclopentadiene (**76**) with acyclic dienes (**133**) afforded corresponding cycloaddition products (**134**) and (**135**) giving high yields and in methyl pyridinium triflate an optimal endo:exo ratio of 86:14 has been reported (Figure 8.56).

Further, authors extended reaction to 1,3-cyclohexadiene (**136**) with acyclic dienes (**133**) and it gave products **134** and **135** with exceptional endo selectivity up to 98:2.
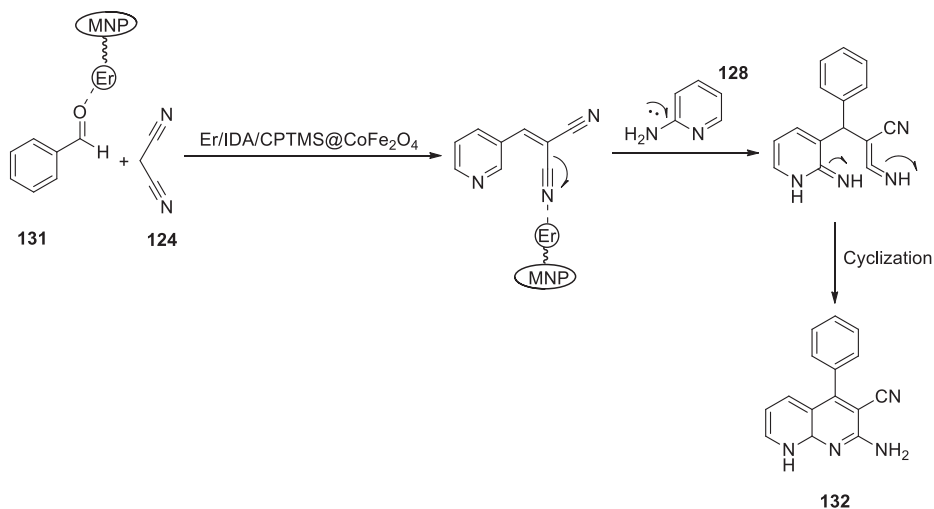
Figure 8.55: Plausible reaction mechanism of naphthyridine synthesis.
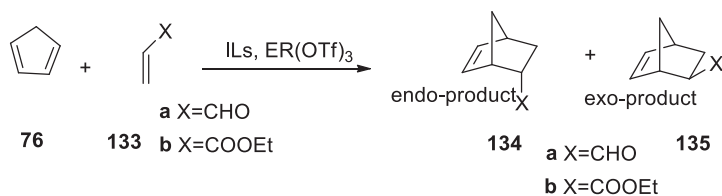
Figure 8.56: Diels–Alder reactions of cyclopentadiene.

Authors also examined other set of acyclic dienes, that is, 2-methylbutadiene, butadiene, and butadiene acetate, that gave a very good yield. Surprisingly authors noticed Diels–Alder cycloaddition reactions were not given when the dienophile was changed from acrolein to ethyl acrylate (Figure 8.57) [100]. Furthermore, the yield of highly regioselective products (**138**) from the reaction of 2-methyl butadiene (**137**) with acrolein (**133a**) or ethyl acrylate (**133b**) has been reported by the same authors (Figure 8.58).
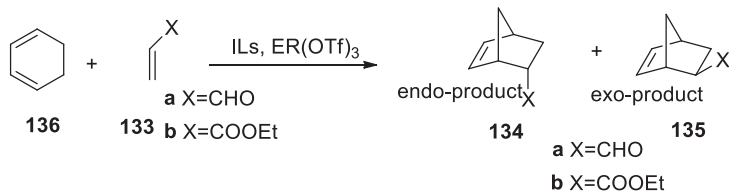
Figure 8.57: Diels–Alder reactions of cyclohexadiene.
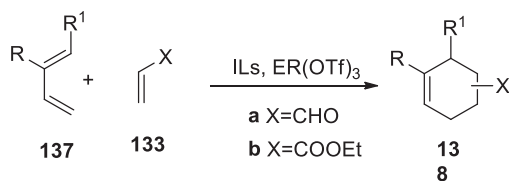
Figure 8.58: Diels–Alder reactions of acyclic dienes.

The role of Er-based heterogeneous catalyst was successfully tested for direct tetrazole derivative (**140**) synthesis from substituted benzonitrile (**139**). The optimization of the needed quantity of the catalyst to obtain excellent product isolation was done by the authors, and it was found that 50 mg of catalyst is ideal for the complete reaction, and also the reaction temperature monitored and found at 120 °C temperature gave product isolation high yield. Finally, the study of the substrate scope of the MCM 41@Serine/Ce and MCM-41@Serine/Er catalytic preparation of tetrazole derivatives was undertaken, and the reaction catalyzed gave an excellent yield of product in a short time (Figure 8.59) [101].
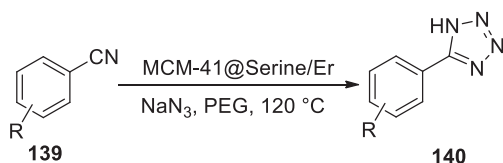
Figure 8.59: Synthesis of tetrazole derivatives.

Only one of the two or more identical competing functional groups, present in the molecule selectively reacted during the reaction and this kind of selectivity, is termed ad homo selectivity as explained by the same author. It is notable to observe that,2,2'-disulfanediyldibenzoic acid (**141**) without further oxidation to disulfoxides or sulfones are converted to monosulfoxide derivative (**142**, **143**, and **144**) and isolated (Figure 8.60) [101].
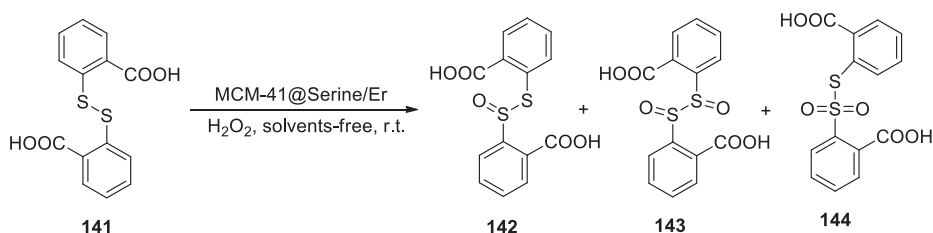
Figure 8.60: Homoselective oxidation of 2,2'-disulfanediyldibenzoic acid.

Sorkhabi et al. [102] described MCR of aromatic aldehyde (**110**), malononitrile (**124**), and barbituric acid (**145**) in CoFe$_2$O$_4$@FA-Er as a heterogeneous catalysts at 100 °C solvent-free condition under sonication in aqueous medium gave excellent product of pyrano[2,3-*d*]pyrimidinone (**146**). Authors claim that the usage of a physical method like using an external magnet to separate the catalyst from the reaction mixture and isolation of the product by solvent extraction gave excellent yield and purity (Figure 8.61).
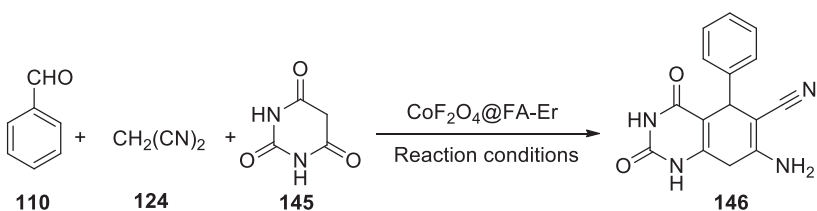
Figure 8.61: Pyrano[2,3-*d*]pyrimidinone derivative synthesis.

Further, the same authors described another scheme of MCRs of aryl aldehyde (**110**), malononitrile (**124**), and 4-hydroxycoumarin (**147**) in CoFe2O4@FA-Er (40 mg) at 80 °C under solvent-free sonication gave excellent product 3,4-dihydropyrano[c]chromene (**148**) isolation (Figure 8.62) [102]. Again author described easy separation of catalysts from reaction mixture by physical external magnetic method, isolation product and recrystallized.
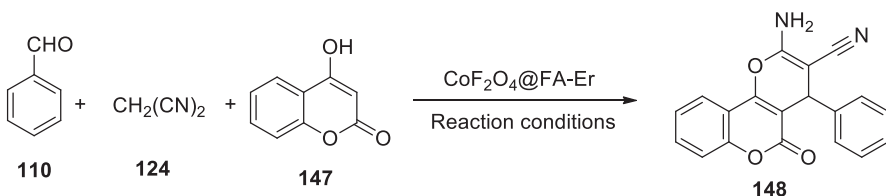
Figure 8.62: Amino-4-aryl-3-cyano-5-oxo-4H,5H-pyrano[3,2-c]chromene synthesis.

The mesoporous silica supported Er(III) catalyzed cyanosilylation of a wide variety of aromatic as well as aliphatic aldehydes or ketones has been demonstrated by Procopio et al. [103]. All the aliphatic as well as aromatic aldehydes (**149**) gave corresponding cyanohydrins products (**150** and **151**), a good to excellent yield of trimethylsilyl-protected and deprotected cyanohydrins are reported (Figure 8.63). No drastic effect on the reaction rates has been reported by authors by studying the substituent effect on the aromatic ring. But, the reaction in aromatic ketones required forceful condition and long reaction time afforded poor product isolation, but significantly high yield of the product isolated for the aliphatic ketone.
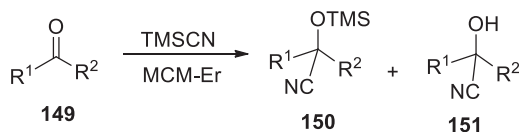
Figure 8.63: Cyanosilylation reaction of aldehydes and ketones.

8.4 Conclusions

Erbium(III)-derived salts showed characteristic green catalysts development concept such as inexpensive, abundant, good LA properties, mild reaction condition, and stable in aqueous or organic solvent systems, and easily retrieved and recycled numerous times without significant change of its efficacy. The catalytic activity of the Er-based salts has emerged as a Lewis acid behavior and found remarkable applications in a number of organic reactions involving C–C and C–X heteroatom containing functional molecule synthesis by various synthetic conditions. Researchers have described that the Er salts are tolerable to various solvent system and mild reaction condition making them the choice of the catalyst for various complex natural molecule synthesis. The versatility and unique nature of the catalysis with efficiency of erbium(III) has been aptly demonstrated by some interesting organic reactions performed using homogeneous, heterogeneous, and multifunctional catalysis. Nevertheless, still Er(III)-based heterogeneous catalysts reaction is not much explored, compared to homogeneous counterpart. Thus in future direction, researchers can discover more and more utility of these Er-based heterogeneous catalysts for complex organic molecule construction. In erbium salt catalysis, using zeolites as an application in multifunctional solid support along with usage of chiral ligand anchoring for the asymmetric synthesis remains a largely unexplored area of research.

List of abbreviations

Er(III)	Erbium triflate
WERC	Water exchange rate constant
PPS	Principal properties
LA	Lanthanide
TMSN$_3$	Trimethylsilylazide
TMSCN	Trimethylsilylcyanide
Er(OTf)$_3$	Erbium(III) trifluoromethanesulfonate
MWI	Microwave irradiation
US	Ultrasound
PBDs	Pyrrolo[1, 4]benzodiazepines
CH$_3$CN	Acetonitrile

NaBH$_4$	Sodium borohydride
2-MeTHF	2-Methyltetrahydrofuran
DHPMs	4-Aryl-3,4-dihydropyrimidin-2(1H)-ones
Ac$_2$O	Acetic anhydride
(EtCO)$_2$O	Propionic anhydride
(CF$_3$CO)$_2$	Trifluoroacetic anhydride
MCRs	Multicomponent reactions
EGCG	Epigallocatechin gallate

References

[1]   Laveuf, C, Cornu, S. A review on the potentiality of rare earth elements to trace pedogenetic processes. Geoderma, 2009, 154, 1–12.

[2]   Patnaik, P. Handbook of Inorganic Chemicals, New York: McGraw-Hill, 2003.

[3]   Babailov, SP, Stabnikov, PA, Zapolotsky, EN. et al. Lanthanides as NMR probes of fast molecular dynamics at high magnetic fields and temperature sensors: Conformational interconversion of erbium ethylenediaminetetraacetate complexes. Inorg Chem, 2013, 52, 5564–5569.

[4]   Mosander, CG. Terbium, 65 Tb General properties Name, symbol. History, 7440, 27–29.

[5]   Long, KR, Gosen Van, BS, Foley, F. et al. The principal rare earth elements deposits of the United States: A summary of domestic deposits and a global perspective. In: Non-renewable Resource Issues, Springer, 2012, 131–155.

[6]   Fetter, S, Cheng, ET, Mann, FM. Long-term radioactivity in fusion reactors. Fusion Eng Des, 1988, 6, 123–130.

[7]   Kiss, GG, Rauscher, T, Szücs, T. et al. Determining reaction cross sections via characteristic X-ray detection: α-induced reactions on 169Tm for the astrophysical γ-process. Phys Lett B, 2011, 695, 419–423.

[8]   Woller, N, Subklew, G, Schwuger, MJ. Reactive liquid-liquid extraction of heavy metals from leachate with oil-soluble complexing surfactants. Colloids Surf A Physicochem Eng Asp, 1996, 117, 189–200.

[9]   Buckley, DH, Johnson, RL. The influence of crystal structure and some properties of hexagonal metals on friction and adhesion. Wear, 1968, 11, 405–419.

[10]   Al-Hadeethi, Y, Sayyed, MI, Raffah, BM. et al. Optical properties and radiation shielding features of Er^{3+} ions doped B$_2$O$_3$–SiO$_2$–Gd$_2$O$_3$–CaO glasses. Ceram Int, 2021, 47, 3421–3429.

[11]   Conway, E. Optical fiber communications principles and practice. Scie-Resour, 2019.

[12]   Neary, CR, Highley, DE. The Economic Importance of the Rare Earth elements.Developments in Geochemistry, Elsevier, 1984, 423–466.

[13]   Caravan, P, Ellison, JJ, McMurry, TJ. et al. Gadolinium (III) chelates as MRI contrast agents: Structure, dynamics, and applications. Chem Rev, 1999, 99, 2293–2352.

[14]   Mao, Y, Park, T, Zhang, F. et al. Environmentally friendly methodologies of nanostructure synthesis. Small, 2007, 3, 1122–1139.

[15]   Nasrollahzadeh, M, Mahmoudi-gomyek, S, Motahharifar, N. et al. Recent developments in the plant-mediated green synthesis of Ag-based nanoparticles for environmental and catalytic applications. Chem Rec, 2019, 19, 2436–2479.

[16]   De Clercq, R, Dusselier, M, Sels, BF. Heterogeneous catalysis for bio-based polyester monomers from cellulosic biomass: Advances, challenges and prospects. Green Chem, 2017, 19, 5012–5040.

[17]   Chaturvedi, K, Malvi, D, Dhangar, M. et al. Recent advances in the green synthesis of lanthanide-based organic compounds for broad application spectrum in different sectors. Rev, 2022.

[18]   Sugiura, M, Kitagawa, H, Lam, WW. et al. Rare-earth metal triflates in organic synthesis, 2002.

[19] Hartwig, JF. Transition metal catalyzed synthesis of arylamines and aryl ethers from aryl halides and triflates: Scope and mechanism. AngewChemie Int Edn, 1998, 37, 2046–2067.

[20] Edelmann, FT. Lanthanide amidinates and guanidinates: From laboratory curiosities to efficient homogeneous catalysts and precursors for rare-earth oxide thin films. Chem Soc Rev, 2009, 38, 2253–2268.

[21] Gerus, A, Ślepokura, K, Lisowski, J. Carbonate-bridged dinuclear lanthanide (III) complexes of chiral macrocycle. Polyhedron, 2019, 170, 115–121.

[22] Chow, CY, Bolvin, H, Campbell, VE. et al. Assessing the exchange coupling in binuclear lanthanide (iii) complexes and the slow relaxation of the magnetization in the antiferromagnetically coupled Dy 2 derivative. Chem Sci, 2015, 6, 4148–4159.

[23] Lawton, MC. Metal Triflatecatalysed Organic Transformations, University of Johannesburg (South Africa), 2010.

[24] Galan, E. Catalysis of Phosphoryl Transfer Reactions by Metal Complexes, Ottawa: National Library of Canad, Bibliothèquenationale du Canada, 2001.

[25] Reis, NV. Homogeneous Catalysts for the ROCOP of CO_2 and Epoxides, University of Oxford, 2020.

[26] Xu, W, Thierry, O, Freddy, K. et al. Iron-modified mesoporous silica as an efficient solid lewis acid catalyst for the mukaiyama aldol reaction. ACS Catal, 2018, 1932–1944.

[27] Ishikawa, A, Takata, T, Matsumura, T. et al. Oxysulfides $Ln_2Ti_2S_2O_5$ as stable photocatalysts for water oxidation and reduction under visible-light irradiation. J Phys Chem B, 2004, 108, 2637–2642.

[28] Imanaka, N, Kobayashi, Y, Fujiwara, K. et al. Trivalent rare earth ion conduction in the rare earth tungstates with the Sc2 (WO4) 3-type structure. Chem Mater, 1998, 10, 2006–2012.

[29] Seri, K, Inoue, Y, Ishida, H. Catalytic activity of lanthanide (III) ions for the dehydration of hexose to 5-hydroxymethyl-2-furaldehyde in water. Bull Chem Soc Jpn, 2001, 74, 1145–1150.

[30] Fortuna, CG, Musumarra, G, Nardi, M. et al. Principal properties (PPs) for lanthanide t riflates as Lewis-acid catalysts. J Chemom, 2006, 20, 418–424.

[31] Yan, C, Zhao, H, Perepichka, DF. et al. Lanthanide ion doped upconverting nanoparticles: Synthesis, structure and properties. Small, 2016, 12, 3888–3907.

[32] Friesen, S, Krickl, S, Luger, M. et al. Hydration and ion association of La 3+ and Eu 3+ salts in aqueous solution. Phys Chem Chem Phys, 2018, 20, 8812–8821.

[33] Aschauer, S, Schilder, L, Korth, W. et al. Liquid-phase isobutane/butene-alkylation using promoted lewis-acidic IL-catalysts. Catal Lett, 2011, 141, 1405–1419.

[34] Binnemans, K. Lanthanides and actinides in ionic liquids. Chem Rev, 2007, 107, 2592–2614.

[35] Schneider, H-J, Yatsimirsky, AK. Lanthanide-catalyzed hydrolysis of phosphate esters and nucleic acids. Metal Ions Biol Syst, 2003, 40, 369–462.

[36] Rajaguru, K, Suresh, R, Mariappan, A. et al. Erbium triflate promoted multicomponent synthesis of highly substituted imidazoles. Org Lett, 2014, 16, 744–747.

[37] Dalpozzo, R, De Nino, A, Nardi, M. et al. Erbium(III) triflate: A valuable catalyst for the synthesis of aldimines, ketimines, and enaminones. Synthesis, 2006, 1127–1132.

[38] Oliverio, M, Nardi, M, Costanzo, P. et al. Erbium salts as non-toxic catalysts compatible with alternative reaction media. Sustainability (Switzerland), 2018, 10, 1–20.

[39] Procopio, A, Costanzo, P, Dalpozzo, R. et al. Efficient ring opening of epoxides with trimethylsilylazide and cyanide catalyzed by erbium(III) triflate. Tetrahedron Lett, 2010, 51(39), 5150–5153.

[40] Procopio, A, Costanzo, P, Curini, M. et al. An eco-sustainable erbium(III) triflate catalyzed formation and cleavage of tert -butyl ethers. Synthesis, 2011, 73–78.

[41] Procopio, A, Dalpozzo, R, De Nino, A. et al. Erbium(III) triflate as an extremely active acylation catalyst. Adv Synth Catal, 2004, 346, 1465–1470.

[42] Dalpozzo, R, De Nino, A, Maiuolo, L. et al. Erbium triflate riA valuable and non-toxic catalyst for the synthesis of acylals and enol esters. Arkivoc. 2006, 2006, 181–189.

[43] Ballini, R, Boscia, G, Carloni, S, et al Zeolite HSZ-360 as a new reusable catalyst for the direct acetylation of alcohols and phenols under solventless conditions. 1998;

[44] Giuseppe, A, Rinaldi, S. Mg (ClO$_4$)$_2$ as a powerful catalyst for the acylation of alcohols under solvent-free conditions. Synlett, 2003, 2003, 39–42.

[45] Bartoli, G, Bosco, M, Dalpozzo, R. et al. Zn (ClO$_4$)$_2$· 6H$_2$O as a powerful catalyst for a practical acylation of alcohols with acid anhydrides. Eur JOC, 2003, 4611–4617.

[46] Chandra, KL, Saravanan, P, Singh, RK. et al. Lewis acid catalyzed acylation reactions: Scope and limitations. Tetrahedron, 2002, 58, 2–7.

[47] Dalpozzo, R, De Nino, A, Maiuolo, L. et al. Highly efficient and versatile acetylation of alcohols catalyzed by cerium (III) triflate. Tetrahedron Lett, 2003, 44, 5621–5624.

[48] Danieli, B, Luisetti, M, Sampognaro, G, et al. organic solvents. 1997, 177.

[49] Sugahara, K, Satake, N, Kamata, K. et al. A basic germanodecatungstate with a À 7 charge: Efficient chemoselective acylation of primary alcohols. Angew Chem, 2014, 13464–13468.

[50] Muramatsu, W, William, JM, Wataru Muramatsu, OO, William, JM, Onomura, O. J of Org Chem, 2012.

[51] Nardi, M, Di Gioia, ML, Costanzo, P. et al. Selective acetylation of small biomolecules and their derivatives catalyzed by Er(OTf)$_3$. Catalysts, 2017, 7.

[52] Nagayama, S, Busujima, T. Lewis acid catalysts stable in water. correlation between catalytic activity in water and hydrolysis constants and exchange rate constants for substitution of inner-sphere water ligands. J Am Chem Soc, 1998, 7863, 8287–8288.

[53] Manabe, KEI. Development of novel lewis acid catalysts for selective organic reactions in aqueous media. Acc Chem Res, 2002, 35, 209–217.

[54] Tsuruta, H, Imamoto, T. Evaluation of the relative Lewis acidities of lanthanoid (iii) compounds by tandem mass spectrometry. Chem Comm, 1999, 2, 1703–1704.

[55] Nardi, M, Cozza, A, Maiuolo, L. et al. 1, 5-Benzoheteroazepines through eco-friendly general condensation reactions. Tetrahedron Lett, 2011, 52, 4827–4834. Available from: http://dx.doi.org/10.1016/j.tetlet.2011.06.029.

[56] Schlitz, H. Rechtsmedizin modern screening strategies in analytical toxicology with special regard to new benzodiazepines. Zeit Fur Recht, 1988, 19–37.

[57] Cannon, JG, Boger, DL. Stereochemistry and Biological Activity of Drugs, Edited by, 1985, vol. 74, 1985.

[58] Kuo, C, Wang, C, Kavala, V. et al. Efficient TCT-catalyzed synthesis of 1,5-benzodiazepine derivatives under mild conditions. Molecules, 2008, 2313–2325.

[59] Amblard, M, Daffix, I, Bedos, P. et al. Design and synthesis of potent bradykinin agonists containing a benzothiazepine moiety. J Med Chem, 1999, 4185–4192.

[60] Synthesi, O, Cozza, A, De Nino, A. et al. One-pot synthesis of dibenzo. Synthesis, 2011, 800–804.

[61] Herrera Cano, N, Uranga, JG, Nardi, M. et al. Selective and eco-friendly procedures for the synthesis of benzimidazole derivatives. The role of the Er(OTf)$_3$ catalyst in the reaction selectivity. Beilstein J Org Chem, 2016, 12, 2410–2419.

[62] Tzani, MA, Gabriel, C, Lykakis, IN. Selective synthesis of benzimidazoles from o-phenylenediamine and aldehydes promoted by supported gold nanoparticles. Nanomaterials, 2020, 10, 2405.

[63] Gemal, AL, Luche, J. Lanthanoids in organic synthesis. 6. The reduction of a-enones by sodium borohydride in the presence of lanthanoid chlorides: Synthetic and mechanistic aspects. J Am Chem Soc, 1981, 5454–5459.

[64] Nardi, M, Sindona, G, Costanzo, P. et al. Eco-friendly stereoselective reduction of a, b -unsaturated carbonyl compounds by Er (OTf) 3 / NaBH 4 in 2-MeTHF. Tetrahedron, 2015, 71, 1132–1135.

[65] Procopio, A, Alcaro, S, Nardi, M. et al. Synthesis, biological evaluation, and molecular modeling of oleuropein and its semisynthetic derivatives as cyclooxygenase inhibitors. J Agric Food Chem, 2009, 57, 11161–11167.

[66] Bulotta, S, Corradino, R, Celano, M. et al. Antiproliferative and antioxidant effects on breast cancer cells of oleuropein and its semisynthetic peracetylated derivatives. Food Chem, 2011, 127, 1609–1614.

[67] Bulotta, S, Corradino, R, Celano, M. et al. Antioxidant and antigrowth action of peracetylatedoleuropein in thyroid cancer cells. J Mol Endocrinol, 2013, 1.

[68] Procopio, A, Celia, C, Nardi, M. et al. Lipophilic hydroxytyrosol esters: Fatty acid conjugates for potential topical administration, 2011.

[69] Ho, CHO, Ndga, II. Ibuprofen-like activity in extra-virgin olive oil. Nature, 2005, 437, 45–46.

[70] Servili, M. Contribution of phenolic compounds to virgin olive oil quality. Eur J Lipid Sci Technol, 2002, 104, 602–613.

[71] Os, Ä, Ey, ÄMEZ. Main polyphenols in the bitter taste of virgin olive oil. structural confirmation by on-line high-performance liquid. J Agric Food Chem, 2003, 6021–6025.

[72] Montedoro, G, Servili, M, Baldioli, M. Simple and hydrolyzable phenolic compounds in virgin olive oil. 2. Initial characterization of the hydrolyzable fraction. J Agric Food Chem, 1992, 1577–1580.

[73] Sindona, G, Caruso, A, Cozza, A. et al. 4-Formyl-3- (2-Oxoethyl) Hex-4-Enoate] on primary human vascular endothelial cells. Curr Med Chem, 2012, 4006–4013.

[74] Nardi, M, Bonacci, S, De Luca, G. et al. Biomimetic synthesis and antioxidant evaluation of 3,4-DHPEA-EDA [2-(3,4-hydroxyphenyl) ethyl (3S,4E)-4-formyl-3-(2-oxoethyl)hex-4-enoate]. Food Chem, 2014, 162, 89–93. http://dx.doi.org/10.1016/j.foodchem.2014.04.015.

[75] Di, DL, Benabdelkamel, H, Mazzotti, F. et al. High-throughput assay of oleopentanedialdheydes in extra virgin olive oil by the UHPLC – ESI-MS/MS and isotope dilution methods. Analy Chem, 2011, 1990–1995.

[76] Biginelli, CP. Aldehyde-urea derivatives of aceto-and oxaloacetic acids. Gazzchim Ital, 1893, 23, 360–413.

[77] Oliverio, M, Costanzo, P, Nardi, M. et al. Facile ecofriendly synthesis of monastrol and its structural isomers via biginelli reaction. ACS Sustain Chem Eng, 2014, 2, 1228–1233.

[78] Agnihotri, G, Misra, AK. Mild and efficient method for the cleavage of benzylidene acetals using HClO4-SiO2 and direct conversion of acetals to acetates. Tetrahedron Lett, 2006, 47, 3653–3658.

[79] Dalpozzo, R, De Nino, A, Maiuolo, L. et al. Erbium(III) chloride: A very active acylation catalyst. Aust J Chem, 2007, 60, 75–79.

[80] Procopio, A, Costanzo, P, Curini, M. et al. Erbium (III) chloride in ethyl lactate as a smart ecofriendly system for efficient and rapid stereoselective synthesis of trans-4, 5-diaminocyclopent-2-enones. ACS Sustain Chem Eng, 2013, 1, 541–544.

[81] Liu, X, Longwitz, L, Spiegelberg, B. et al. Erbium-catalyzed regioselective isomerization-cobalt-catalyzed transfer hydrogenation sequence for the synthesis of anti-markovnikov alcohols from epoxides under mild conditions. ACS Catal, 2020, 10, 13659–13667.

[82] Zhu, Y, Xie, M, Dong, S. et al. Asymmetric cycloaddition of β,γ-unsaturated α-ketoesters with electron-rich alkenes catalyzed by a chiral Er(OTf)3/N,N'- dioxide complex: Highly enantioselective synthesis of 3,4-dihydro-2H-pyrans. Eur J Chem, 2011, 17, 8202–8208.

[83] Tran, PH, Hansen, PE, Nguyen, HT. et al. Erbium trifluoromethanesulfonate catalyzed friedel-crafts acylation using aromatic carboxylic acids as acylating agents under monomode-microwave irradiation. Tetrahedron Lett, 2015, 56, 612–618. Available from: http://dx.doi.org/10.1016/j.tetlet.2014.12.038.

[84] Bortolini, O, De Nino, A, Maiuolo, L. et al. 1,3-Cycloaddition of nitrones in ionic liquids catalyzed by Er(III): An easy access to isoxazolidines. Tetrahedron Lett, 2007, 48, 7125–7128.

[85] Dalpozzo, R, De Nino, A, Nardi, M. et al. 1,2-diacetates by epoxide ring opening promoted by erbium (III) triflate. Arkivoc, 2006, 2006, 67–73.

[86] Dalpozzo, R, De Nino, A, Maiuolo, L. et al. Er(OTf)$_3$ as a mild cleaving agents for acetals and ketals. Synthesis, 2004, 496–498.

[87] Procopio, A, Dalpozzo, R, De Nino, A. et al. Er(OTf)$_3$ as new efficient catalyst for the stereoselective synthesis of C-pseudoglycals. Synthesis, 2006, 332–338.

[88] Paonessa, R, Nardi, M, Di Gioia, ML. et al. Eco-friendly synthesis of lipophilic EGCG derivatives and antitumor and antioxidant evaluation. Nat Prod Commun, 2018, 13, 1117–1122.

[89] Nardi, M, Bonacci, S, Cariati, L. et al. Synthesis and antioxidant evaluation of lipophilic oleuropein aglycone derivatives†. Food Funct, 2017, 8.

[90] Sarkar, A, Jana, S, Nayek, HP. A pentanuclear Er (III) coordination cluster as a catalyst for selective synthesis of 1,2-disubstituted benzimidazoles. Appl Organomet Chem, 2021, 35, 1–9.

[91] Procopio, A, Dalpozzo, R, De Nino, A. et al. Er(OTf)$_3$ as a valuable catalyst in a short synthesis of 2′,3′-dideoxy pyranosyl nucleosides via Ferrier rearrangement. Synthesis, 2006, 2608–2612.

[92] Sashidhara, KV, Prasad Dodda, R, Upadhyay, A. et al. Synthesis of highly substituted imidazo[1,5-a]quinoxalines through a multicomponent reaction followed by deprotection–cyclization. Adv Synth Catal, 2016, 358, 2612–2618.

[93] Rawat, V, Das, A, Srivastava, CM, eds., Heterogeneous Catalysis in Organic Transformations. 2022.

[94] Chughtai, AH, Ahmad, N, Younus, HA, Laypkov, A, Verpoort, F. Metal–organic frameworks: Versatile heterogeneous catalysts for efficient catalytic organic transformations. Chem Soc Rev, 2015, 44(19), 6804–6849.

[95] Cho, H, Török, F, Béla, T. "Energy efficiency of heterogeneous catalytic microwave-assisted organic reactions.". Green Chem, 2014, 16(7), 3623–3634.

[96] Procopio, A, Cravotto, G, Oliverio, M. et al. An eco-sustainable erbium(III)-catalyzed method for formation/cleavage of O-tert-butoxy carbonates. Green Chem, 2011, 13, 436–443.

[97] Hajiashrafi, T, Karimi, M, Heydari, A. et al. Erbium-organic framework as heterogeneous lewis acid catalysis for hantzsch coupling and tetrahydro-4H-chromene synthesis. Catalysis Lett, 2017, 147, 453–462.

[98] Verma, K, Tailor, YK, Khandelwal, S. et al. An efficient and environmentally sustainable domino protocol for the synthesis of structurally diversespiroannulatedpyrimidophenazines using erbium doped TiO2 nanoparticles as a recyclable and reusable heterogeneous acid catalyst. RSC Adv, 2018, 8, 30430–30440.

[99] Tamoradi, T, Daraie, M, Heravi, MM. et al. Erbium anchored iminodiacetic acid (IDA) functionalized CoFe2O4nano particles: An efficient magnetically isolable nanocomposite for the facile synthesis of 1,8-naphthyridines. NJC, 2020, 44, 11049–11055.

[100] Bortolini, O, De Nino, A, Garofalo, A. et al. Erbium triflate in ionic liquids: A recyclable system of improving selectivity in diels-alder reactions. Appl Catal, 2010, 372, 124–129.

[101] Molaei, S, Ghadermazi, M. Immobilization of cerium (IV) and erbium (III) in mesoporous MCM-41: Two novel and highly active heterogeneous catalysts for the synthesis of 5-substituted tetrazoles, and chemo- and homoselective oxidation of sulfides. Applied J Organomet Chem, 2019, 33, 1–20.

[102] Sorkhabi, S, Mozafari, R, Ghadermazi, M. New advances in catalytic performance of erbium-folic acid-coated CoFe$_2$O$_4$ complexes for green one-pot three-component synthesis of pyrano[2,3-d]pyrimidinone and dihydropyrano[3,2-c]chromenes compounds in water. Appl Organomet Chem, 2021, 35, 1–22.

[103] Procopio, A, Das, G, Nardi, M. et al. A mesoporous ErIII-MCM-41 catalyst for the cyanosilylation of aldehydes and ketones under solvent-free conditions. Chem Sus Chem, 2008, 1, 916–919.

Bubun Banerjee*, Anu Priya, Aditi Sharma, Manmeet Kaur
and Arvind Singh

9 Gadolinium triflate-catalyzed various organic transformations

9.1 Introduction

Organic synthesis is considered as the back bone of drug discovery [1–2]. More than 90% commercially available drugs are either synthesized or semisynthesized in the laboratory by using various organic transformations. Catalysts play an important role in carrying out those transformations [3]. Among many other metal catalysts, the last decade has shown huge applications of various metal triflate salts as catalysts in diverse organic transformations [4–20]. Among various metal triflate salts, gadolinium (III) trifluoromethanesulfonate [$Gd(OTf)_3$, Gadolinium triflate] has gained significant attention as a Lewis acidic catalyst for various organic transformations. The electronic configuration of Gadolinium metal is $[Xe]4f^75d^16s^2$ and it was discovered in 1880 by Jean Charles Galissard de Marignac [21]. This was first isolated in 1886 by Lecoq de Bois-baudran [22]. The color of metallic gadolinium is silvery-white. It is paramagnetic at room temperature [23]. Gadolinium oxyorthosilicate salt has been used in X-ray radiometers [24]. It has been used in semiconductor fabrication and nuclear reactor shielding. Gd-EDTA complexes have been used as injectable contrast agent for MRIs. It is named after the Finnish chemist and geologist, Johan Gadolin [25, 26]. Among few other gadolinium salts, gadolinium triflate has been used majorly as the catalyst for various organic transformations. It was employed as an efficient catalyst for various organic name reactions such as Friedel-crafts acetylation [27], Diels-Alder reactions [28], electrophilic nitration [29], Michael addition [30], Aldol reaction [31–34], etc. Like other lanthanide-based metal triflates, strictly anhydrous conditions are not required for $Gd(OTf)_3$, as it is relatively more water-tolerant [35] and thus, it can be recycled after completion of the reaction. In addition, it is a commercially available and relatively inexpensive reagent.

*Corresponding author: Bubun Banerjee,** Department of Chemistry, Akal University, Talwandi Sabo, Bathinda 151302, Punjab, India, e-mail: banerjeebubun@gmail.com
Anu Priya, Aditi Sharma, Manmeet Kaur, Arvind Singh, Department of Chemistry, Akal University, Talwandi Sabo, Bathinda, 151302, Punjab, India

The present chapter focuses on the catalytic application of Gd(OTf)$_3$ or its complexes as a mild Lewis acidic catalyst in various organic synthesis reported during the last decade.

The following sections describe the catalytic role of gadolinium(III) triflate and its complexes in organic synthesis.

9.2 Gadolinium triflate-catalyzed synthesis of bioactive heterocycles

9.2.1 Synthesis of bioactive *N*-heterocycles

9.2.1.1 Synthesis of polyhydroquinoline derivatives

Polyhydroquinoline derivatives are found to possess significant biological activities including antibacterial, antimalarial, anti-asthmatic, anti-inflammatory, and tyrosine kinase-inhibitory efficiency [36, 37]. Due to this immense biological importance, a number of methods were reported for the synthesis of polyhydroquinoline derivatives involving a series of homogeneous as well as heterogeneous catalysts, under various reaction conditions [38–55]. These methods definitely have some merits but, at the same time, suffer from a number of drawbacks, such as use of acidic or basic catalysts, toxic solvents, longer reaction times, lesser yields, high temperatures, tedious work-up procedure, etc. In many occasions, it was not possible to recover and reuse the used catalyst. In 2017, Mansoor et al. [56] developed an efficient protocol for the synthesis of a series of polyhydroquinoline derivatives (**5**) in excellent yields via one-pot four-component reactions of substituted benzaldehydes (**1**), dimedone (**2**), ethyl acetoacetate (**3**), and ammonium acetate (**4**) in the presence of a catalytic amount of gadolinium(III) trifluoromethanesulfonate (Gd(OTf)$_3$) as catalyst in ethanol at room temperature (Figure 9.1). During optimization, a number of other solvents such as methanol, acetonitrile, tertiary-butanol, 1,4-dioxane, acetone, toluene, cyclohexane, and dichloromethane were tested but found less effective. The used catalyst was recovered and recycled for four further runs with almost equal efficiency. Under the same reaction conditions, other catalysts such as ZnCl$_2$, AlCl$_3$, FeCl$_3$, NdCl$_3$, La(OTf)$_3$, Nd(OTf)$_3$, and Yb(OTf)$_3$ afforded lesser products.

9.2.1.2 Synthesis of quinolines

In 2009, Wu et al. [57] reported a mild and efficient route for the synthesis of a series of structurally diverse quinoline derivatives (**8**) via Friedländer annulation reaction between *o*-aminobenzophenones (**6**) and various ketones (**2,3,7a-7d**), in the presence of
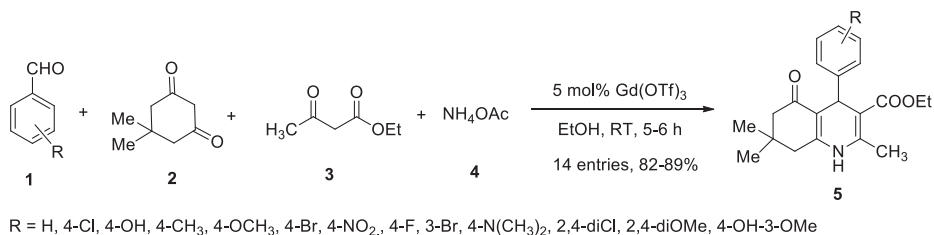
R = H, 4-Cl, 4-OH, 4-CH$_3$, 4-OCH$_3$, 4-Br, 4-NO$_2$., 4-F, 3-Br, 4-N(CH$_3$)$_2$, 2,4-diCl, 2,4-diOMe, 4-OH-3-OMe

Figure 9.1: Gadolinium triflate-catalyzed synthesis of polyhydroquinoline derivatives.

gadolinium triflate (Gd(OTf)$_3$) as catalyst in ionic liquid 1-n-butyl-3-methylimidazolium hexafluorophosphate ([Bmim][PF$_6$]) at 60 °C (Figure 9.2). All the reactions were completed within just 15 min and afforded excellent yields.
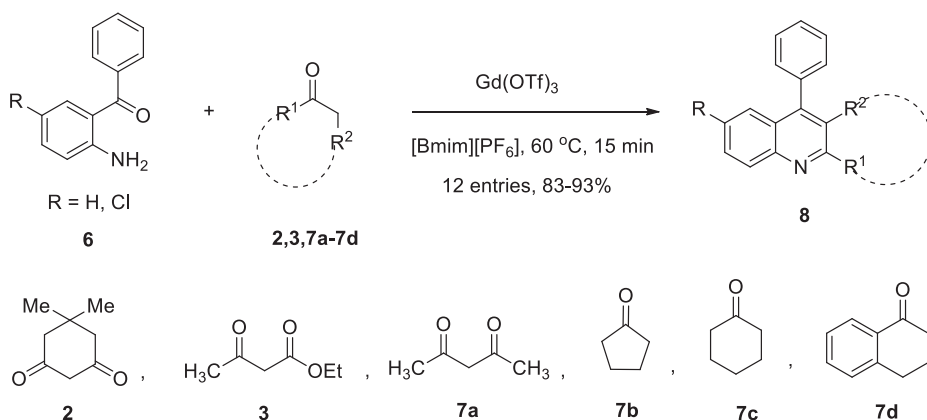
Figure 9.2: Gadolinium triflate-catalyzed synthesis of quinoline derivatives in ionic liquid.

9.2.1.3 Synthesis of tetrahydroquinolines

In 2009, by using gadolinium triflate as catalyst, Murarka et al. [58] prepared a series of polycyclic tetrahydroquinolines (**10**) from the tertiary anilines having appropriate acceptor group in the ortho position (**9**) (Figure 9.3). During optimization, gadolinium triflate as catalyst showed better efficiency than the other Lewis acidic catalysts employed, such as Mg(OTf)$_2$, Mg(ClO$_4$)$_2$, Mg(ClO$_4$)$_2$·6H$_2$O, InCl$_3$, Zn(OTf)$_2$, Cu(OTf)$_2$, Ni(ClO$_4$)$_2$·6H$_2$O, FeCl$_3$·6H$_2$O, Yb(OTf)$_3$, La(OTf)$_3$, and Sc(OTf)$_3$. It was proposed that the reaction proceeded through intramolecular, redox neutral C-H bond functionalization, followed by ring closure reaction (Figure 9.4).
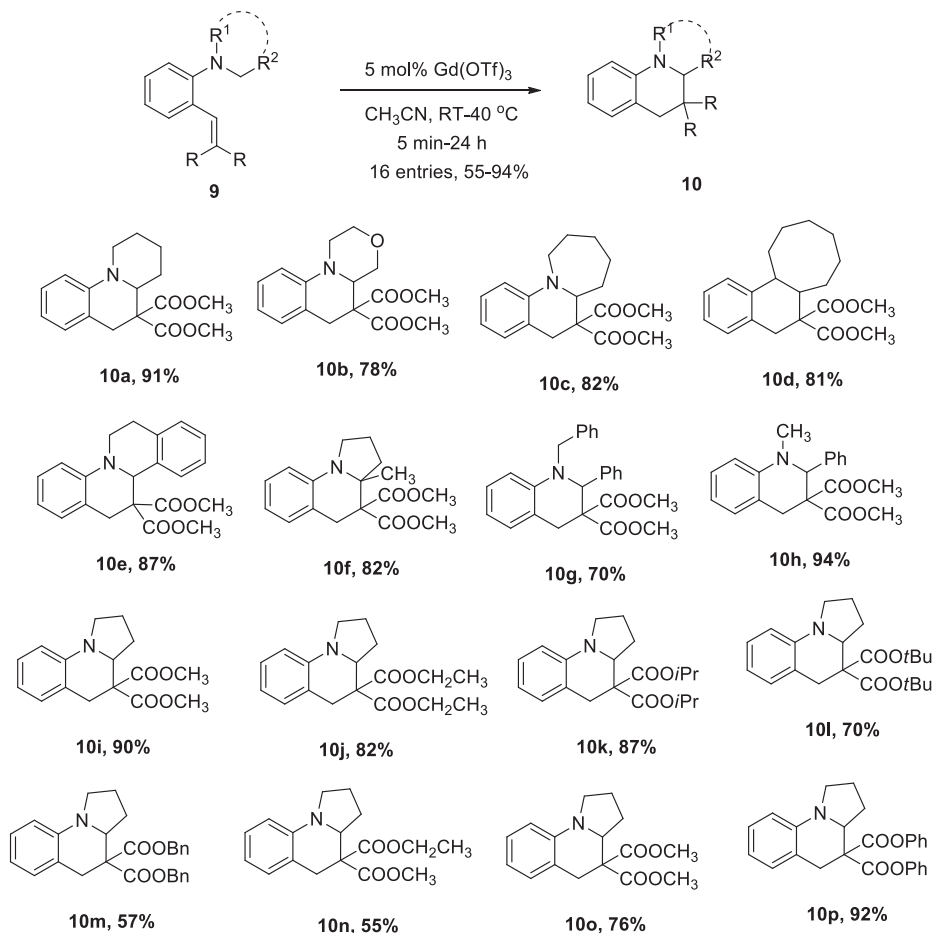
Figure 9.3: Gadolinium triflate-catalyzed synthesis of tetrahydroquinolines.
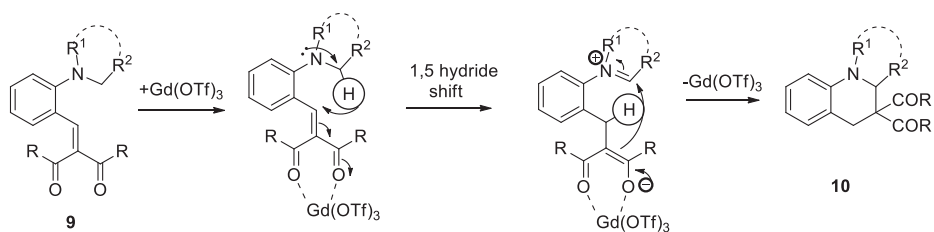
Figure 9.4: Plausible mechanism for the gadolinium triflate-catalyzed synthesis of tetrahydroquinolines.

9.2.1.4 Synthesis of 2-(1,3-diphenyl-1*H*-pyrazol-4-yl)-1*H*-benzo[d]imidazole

In 2020, Srinivas et al. [59] reported a mild, facile, and efficient method for the synthesis of 2-(1,3-diphenyl-1*H*-pyrazol-4-yl)-1*H*-benzo[*d*]imidazoles (**13**) in excellent yields from the reactions of 1*H*-benzo[*d*]imidazoles (**11**) and 1,3-diaryl-1*H*-pyrazole-4-carbaldehydes (**12**) in the presence of gadolinium(III)triflate as catalyst in ethanol, under refluxed conditions (Figure 9.5).
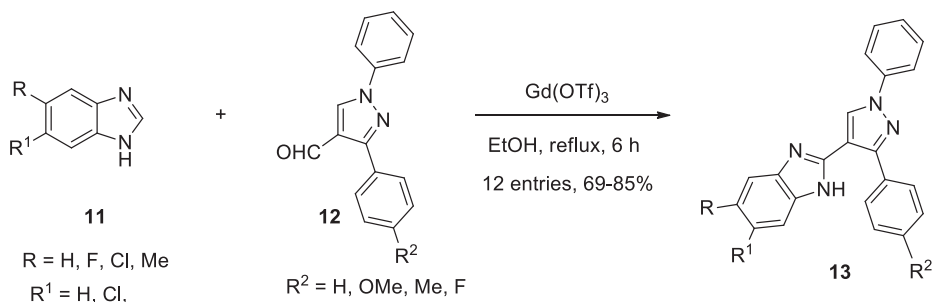
Figure 9.5: Gadolinium(III)triflate-catalyzed synthesis of 2-(1,3-diphenyl-1 *H*-pyrazol-4-yl)-1 *H*-benzo[*d*] imidazole.

9.3 Synthesis of bioactive *O*-heterocycles

9.3.1 Synthesis of chiral 1,3-dioxolanes

In 2014, Chen et al. [60] prepared a series of *N,N′*-dioxide–metal complexes and evaluated the catalytic activities of those synthesized complexes for the highly diastereo- and enantioselective [3 + 2] cycloaddition of aryl oxiranyl diketones (**14**) and aromatic aldehydes (**1**) (Figure 9.6). It was proposed that the reaction goes through the C–C bond cleavage of oxiranes followed by [3 + 2] cycloaddition with aromatic aldehydes. The corresponding chiral 1,3-dioxolanes (**15**) were obtained in excellent yields (up to 99%). It was proposed that gadolinium plays an important role in the transition state.

Ar = C₆H₅, 3-MeC₆H₄, 3-OMeC₆H₄, 3-OPhC₆H₄, 4-MeC₆H₄, 3-ClC₆H₄, 3-BrC₆H₄, 1-napthyl, 2-napthyl, 3-furyl, 3-thienyl, 4-ClC₆H₄, 4-BrC₆H₄, 3-OMeC₆H₄

Ar¹ = C₆H₅, 3-MeC₆H₄, 4-MeC₆H₄, 2-FC₆H₄, 3-FC₆H₄, 4-FC₆H₄, 4-ClC₆H₄, 2-furyl, 3-furyl, 2-thienyl, 3-thienyl
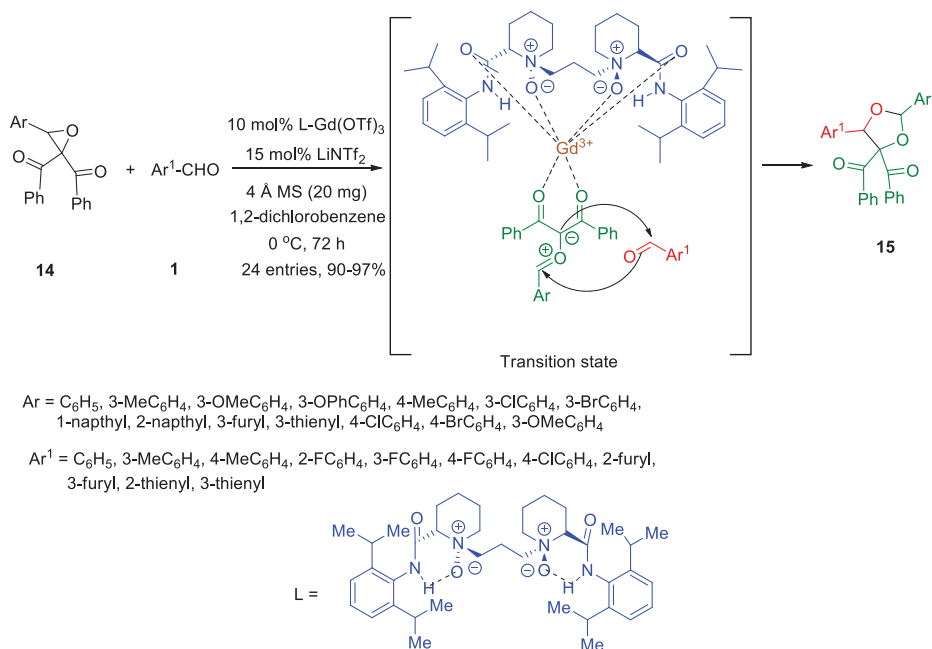
Figure 9.6: *N,N′*-dioxide–gadolinium complex-catalyzed synthesis of chiral 1,3-dioxolanes.

9.4 Gd(OTf)₃-catalyzed miscellaneous organic transformations

9.4.1 Acetylation of alcohols, amines, and phenols

In 2005, Alleti et al. [61] reported a facile method for the acetylation of alcohols or phenols (**17**) using acetic anhydride (**16**) as reagent, in the presence of a catalytic amount of gadolinium triflate (0.2–0.5 mol%) immobilized in the ionic liquid (1-butyl-3-methylimidazolium tetrafluoroborate ([bmim][BF₄]) at room temperature (Figure 9.7). The corresponding acetylated products were formed in excellent yields. It is noteworthy that they were able to recover the catalytic system Gd(OTf)₃/[bmim][BF₄] and be reused three times with almost equal efficiency. Under the same optimized conditions, a series of amines (**18**) also acetylated with excellent yields. The same group also achieved the acetylation of a series of structurally diverse alcohols, phenols, and amines using a catalytic amount (0.01–0.1 mol%) of gadolinium triflate as an efficient catalyst in acetonitrile at room temperature (Figure 9.8) [62].

Later on, in 2008, Yoon et al. [63] prepared chloromethyl polystyrene (CMPS) resin-supported gadolinium triflate (CMPS-IM-Gd(OTf)₃) as an efficient and reusable catalyst. Using 0.5 mol% of this heterogeneous catalyst, they achieved the acetylation
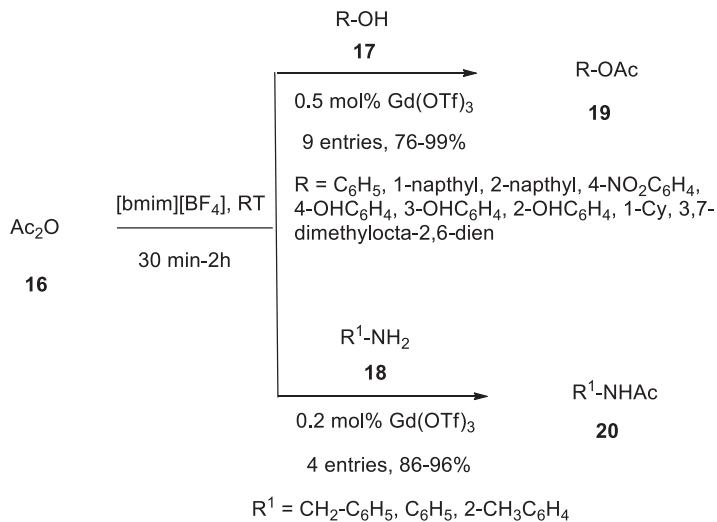
Figure 9.7: Gadolinium triflate-catalyzed acetylation of alcohols, phenols, and amines in ionic liquid.
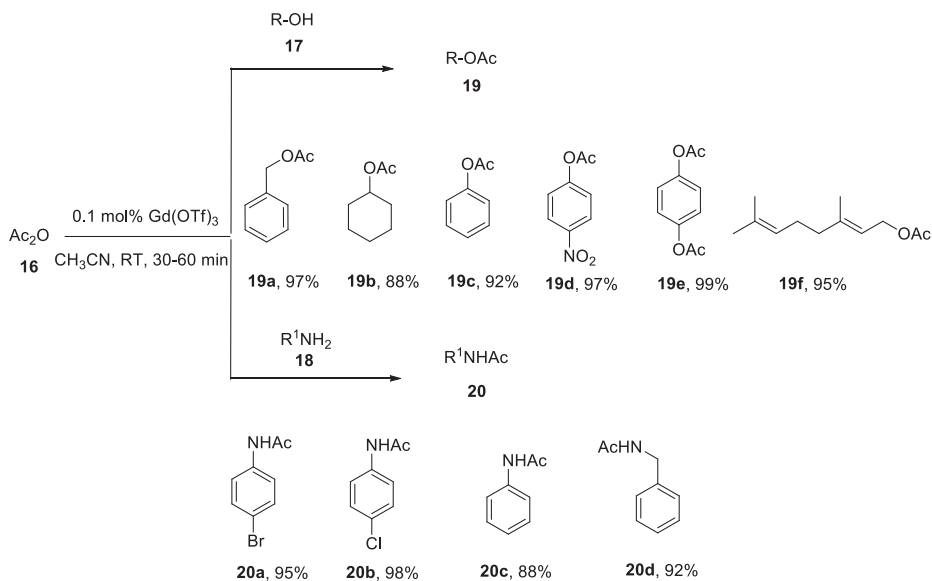
Figure 9.8: Gadolinium triflate-catalyzed acetylation of alcohols, phenols, and amines in acetonitrile.

of various alcohols and phenols with acetic anhydride as reagent in dimethyl sulfoxide, at room temperature (Figure 9.9). This polymer-supported heterogeneous catalyst was recovered successfully and recycled 10 times, without any significant loss of catalytic activity.
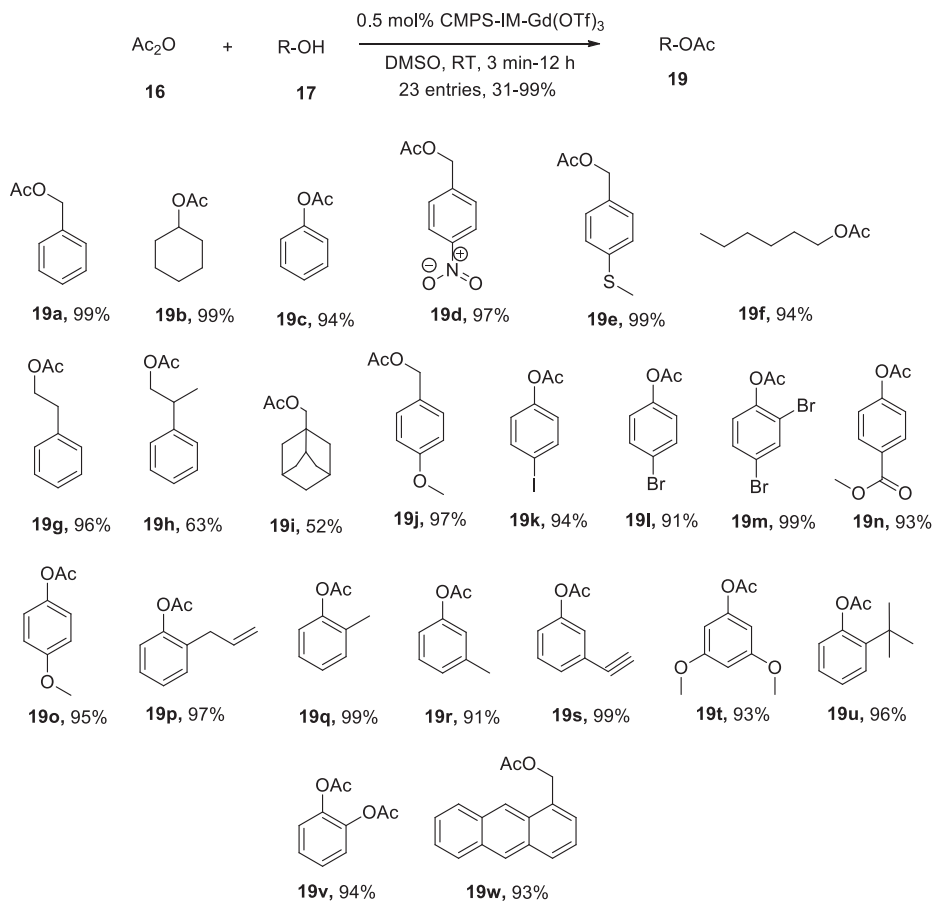
Figure 9.9: Polymer-supported Gadolinium triflate-catalyzed acetylation of alcohols and phenols.

9.4.2 Conjugate addition of cyanide to enones

In 2008, Tanaka et al. [64] developed an efficient method for the catalytic conjugate addition of *tert*-butyldimethylsilyl cyanide (TBSCN) (**21**) to various enones (**20**), by using cooperative catalysis of Ni(0)–cyclooctadiene complex and Gd(OTf)$_3$ (Figure 9.10). Further studies revealed that the presence of a catalytic amount of norbornadiene (nbd) as ligand accelerates the rate of the reaction. Under the optimized reaction conditions, a wide variety of structurally diverse enones (**20**) underwent the process smoothly and afforded the desired cyanide conjugates (**22**) in excellent yields. This reaction is regarded as a key step for the synthesis of Tamiflu, an important anti-influenza drug [65]. Earlier, this reaction was generally carried out without Gd(OTf)$_3$, which required harsh reaction conditions [66]. After use of a catalytic amount of Gd

(OTf)$_3$ as co-catalyst, this reaction was achieved at room temperature. The mechanism of this transformation is shown in Figure 9.11.
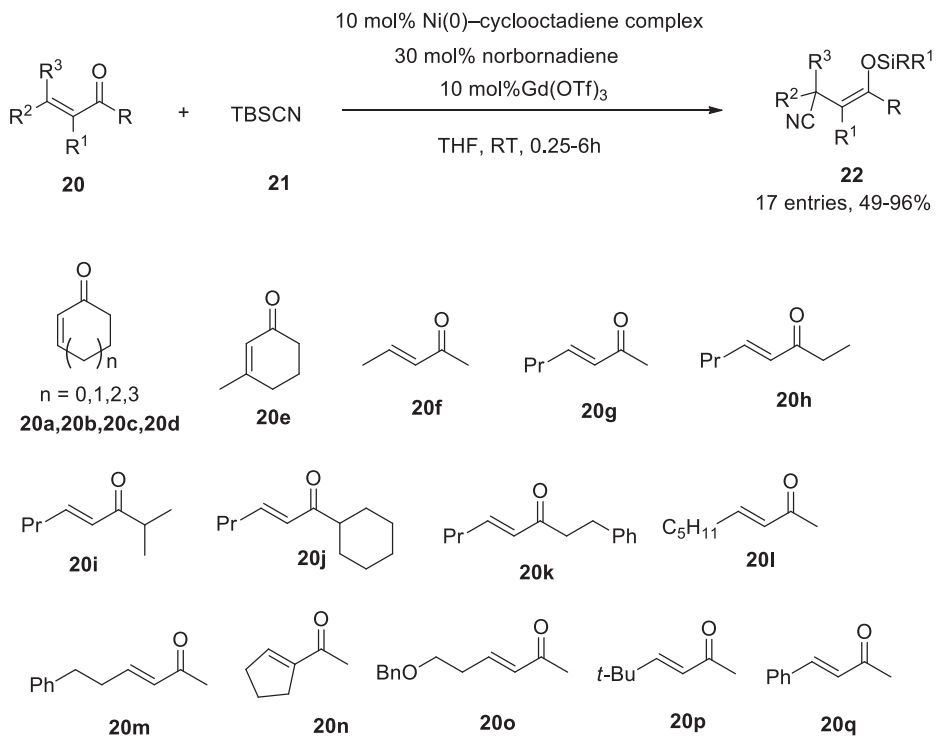
Figure 9.10: Gadolinium triflate-catalyzed conjugate addition of cyanide to enones.
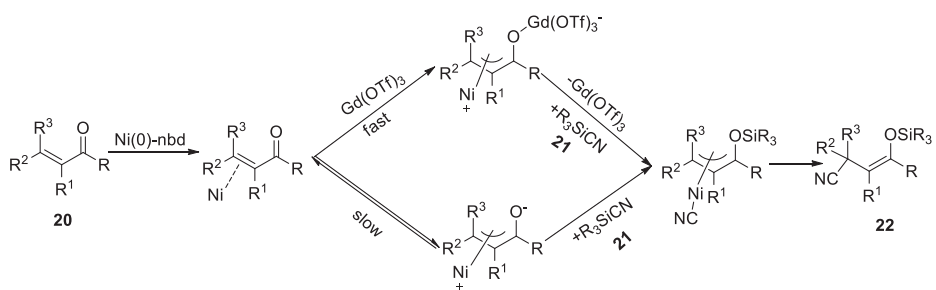
Figure 9.11: Plausible mechanism for the conjugate addition of cyanide to enones.

9.4.3 Regio- and enantioselective aminolysis of aromatic trans-2, 3-epoxy sulfonamides

Using the same Gd-*N,N'*-dioxide complex (reported by Chen et al. [60]) as catalyst, in 2015, Wang and Yamamoto [67] achieved the first enantioselective aminolysis of aromatic trans-2,3-epoxy sulfonamides (**24**) with the reactions of various primary or secondary amines (**23**) in chloroform, at ambient temperature (Figures 9.12). Under these catalytic conditions, ring opening reaction proceeded enantioselectively at the C-3 position and afforded the corresponding 3-amino-3-phenylpropan-2-olamines (**25**) in excellent yields. During optimization, a number of other metal triflates, such as La

25a, R^1 = C$_6$H$_5$, 98%
25b, R^1 = 4-BrC$_6$H$_4$, 97%
25c, R^1 = 4-FC$_6$H$_4$, 94%
25d, R^1 = 4-OMeC$_6$H$_4$, 98%
25e, R^1 = 4-PhC$_6$H$_4$, 97%
25f, R^1 = 3-ClC$_6$H$_4$, 97%
25g, R^1 = 3,5-OMe$_2$C$_6$H$_3$, 96%
25h, R^1 = 2-OMeC$_6$H$_4$, 96%
25i, R^1 = 2,4,6-C$_6$H$_2$, 96%
25j, R^1 = 1-napthyl, 93%
25k, R^1 =Bn, 98%
25l, R^1 = *n*-Oct, 95%
25m, R^1 = c-Hex, 94%
25n, R^1 = Ph$_2$CH, 95%

25o, **R^1 = Ph, 98%**
25p, **R^1 = Bn, 98%**

25q, 98%

25r, 96%

25s, 93%

25t, X = F, 98%
25u, X =Br, 97%

25v, 63%

25w, 96%

25x, 92%

25y, 98%

Figure 9.12: Gadolinium triflate-catalyzed regio- and enantioselective aminolysis of aromatic trans-2,3-epoxy sulfonamides.

(OTf)$_3$, Sc(OTf)$_3$, Y(OTf)$_3$, Ce(OTf)$_3$, Sm(OTf)$_3$, Yb(OTf)$_3$, Pr(OTf)$_3$, Eu(OTf)$_3$, and Te(OTf)$_3$ were also screened; among them, Gd(OTf)$_3$ showed highest catalytic efficiency.

9.4.4 Asymmetric α-amination of 4-substituted pyrazolones

In 2011, Yang et al. [68] employed another Gd-*N,N'*-dioxide complex in dichloromethane and accomplished the asymmetric *R*-amination of 4-substituted pyrazolone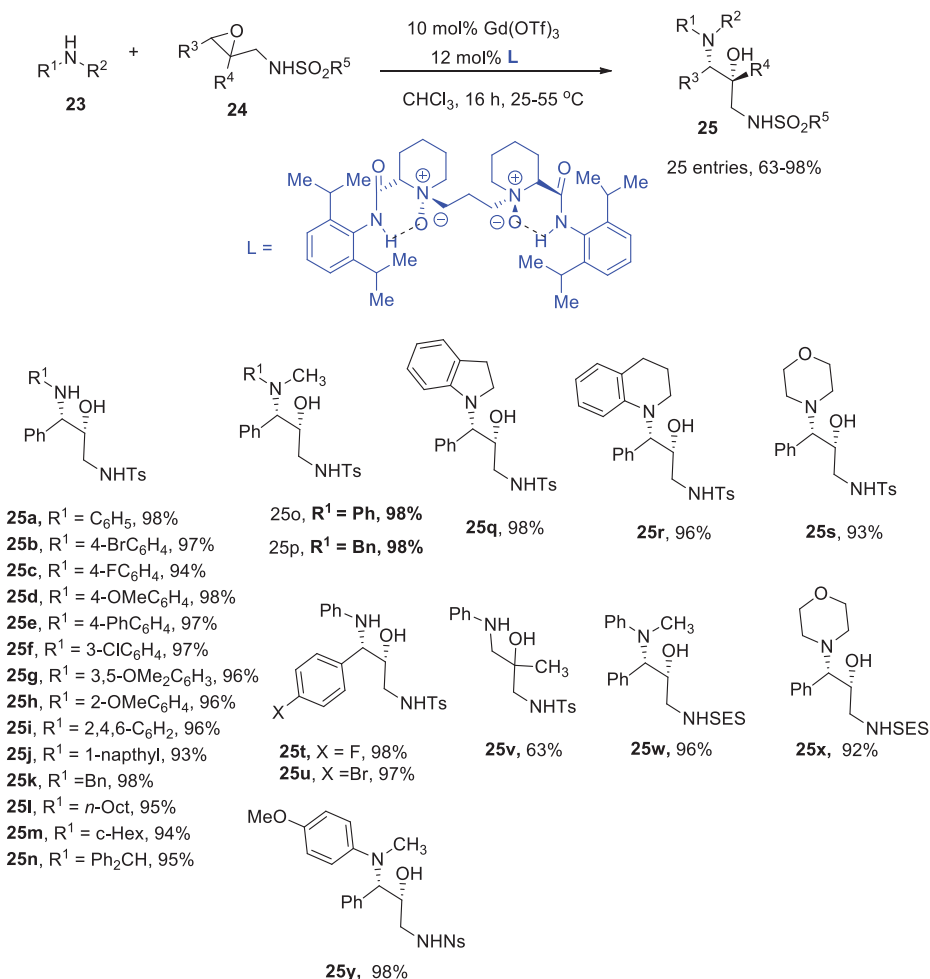s (**26**) with azodicarboxylates (**27**), which afforded the corresponding chiral 4-amino-5-pyrazolone derivatives (**28**) in excellent yields (up to 99%) and high enantioselectivities (90–97% ee) (Figure 9.13). A number of other triflate salts such as La(OTf)$_3$, Ce (OTf)$_3$, Pr(OTf)$_3$, Nd(OTf)$_3$, Sm(OTf)$_3$, Eu(OTf)$_3$, Tb(OTf)$_3$, Dy(OTf)$_3$, Ho(OTf)$_3$, Er(OTf)$_3$, Tm(OTf)$_3$, and Lu(OTf)$_3$ were also screened but found less effective as compared to Gd (OTf)$_3$ in terms of product yields and enantioselectivity.

R^1 = Bn, 2-MePhCH$_2$, 3-MePhCH$_2$, 4-MePhCH$_2$, 2-MeOPhCH$_2$, 3-MeOPhCH$_2$, 4-MeOPhCH$_2$, 2-ClPhCH$_2$, 3-ClPhCH$_2$, 4-ClPhCH$_2$, 4-BrPhCH$_2$, 2,4-Cl$_2$PhCH$_2$, 2-furanylmethyl, 2-thienylmethyl, 1-napthylmethyl, 2-napthylmethyl, n-Propyl, allyl, -(CH$_2$)$_4$-

R^2 = ^{i}Pr, Et, Bn
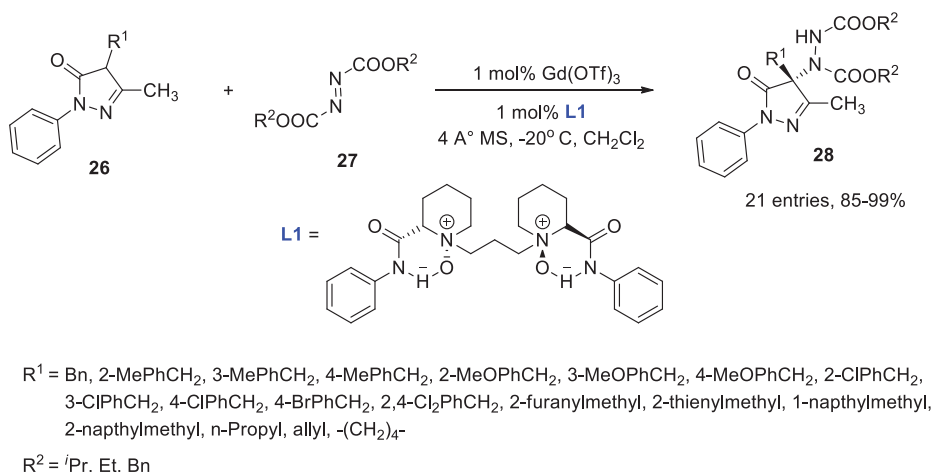
Figure 9.13: Gadolinium triflate-catalyzed asymmetric α-amination of 4-substituted pyrazolones.

9.4.5 Synthesis of γ-nitropyrazoleamides

In 2015, Yao et al. [69] used the same *N,N'*-dioxide/Gadolinium(III) complex (**L**) as catalyst for the synthesis of a series of γ-nitropyrazoleamides (**31**) from the reactions between nitroalkane (**29**) and pyrazoleamides (**30**) in dichloromethane as a solvent at 30 °C (Figure 9.14). Desired products were afforded in excellent yields (up to 99%) with excellent enantioselectivities (up to 99% ee) after 3 days of stirring.

R = H, CH$_3$, C$_6$H$_5$

R^1 = CH$_3$, C$_6$H$_5$

R^2 = 4-ClC$_6$H$_4$, 4-FC$_6$H$_4$, C$_6$H$_5$, 4-BrC$_6$H$_4$, 4-MeC$_6$H$_4$, 4-OMeC$_6$H$_4$, 3-BrC$_6$H$_4$, 3-MeC$_6$H$_4$, 2-BrC$_6$H$_4$, 2-MeOC$_6$H$_4$, 3,4-diClC$_6$H$_3$, 3,4-diOMeC$_6$H$_3$, 2-furyl, 2-thienyl, CH$_3$COO-, CH$_3$, C$_3$H$_7$

Figure 9.14: Gadolinium triflate-catalyzed synthesis of γ-nitropyrazoleamides.

9.4.6 Synthesis of 5-substituted dipyrromethanes

In 2006, Temelli and Unaleroglu [70] synthesized a series of dipyrromethanes (**34**) from the reactions of excess pyrrole (**32**) and *N*-Tosyl imine (**33**), in the presence of 10 mol% gadolinium triflate as catalyst at 100 °C (Figure 9.15). Under this condition, compounds (**35**) were also formed as by-products. When the same reactions were carried out at room temperature, compounds (**35**) formed as the major product in some cases.
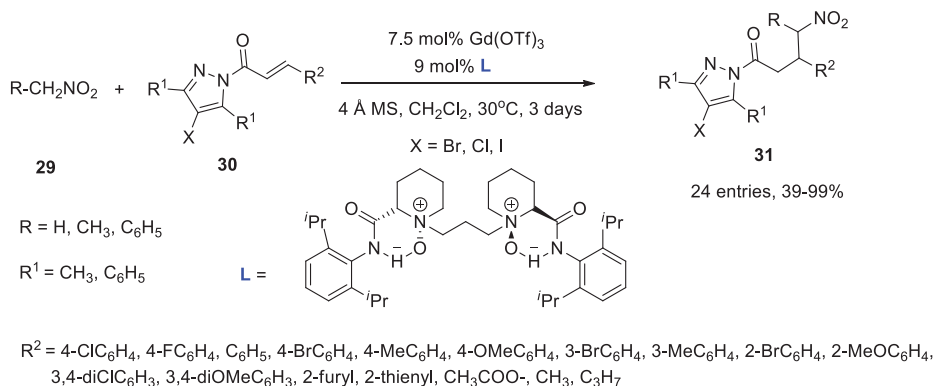

R = H, 4-OCH$_3$, 2-OCH$_3$, 4-CH$_3$, 2-OH,
4-NO$_2$, 4-CF$_3$, 4-F,4-Cl, 4-Br
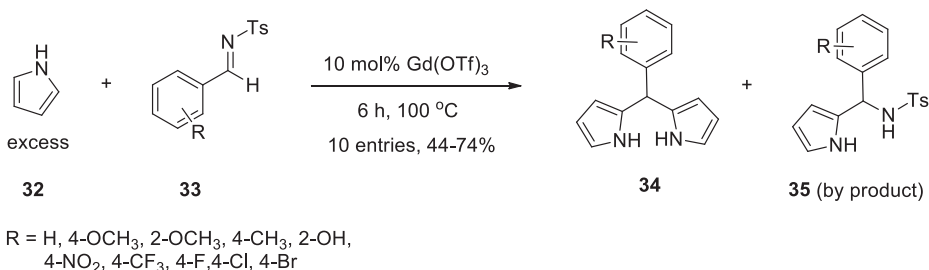
Figure 9.15: Gadolinium triflate-catalyzed synthesis of dipyrromethanes.

9.4.7 Synthesis of 2-alkylated pyrrole derivatives

Next year, the same group [71] developed another gadolinium triflate-catalyzed protocol for the synthesis of a series of novel 2-alkylated pyrrole derivatives (**37**) regioselectively, from the reactions of pyrrole (**32**) and substituted dimethyl 2-benzylidenemalonates (**36**) in THF at room temperature (Figure 9.16). Intramolecular cyclization of the synthesized 2-alkylated pyrrole derivatives (**37**) was used for the construction of new diastereoselective 3-oxo-2,3-dihydro-1 *H*-pyrrolizine derivatives (**38**) in good yields.

R = H, 4-OH, 4-CH$_3$, 4-OCH$_3$, 4-Br, 4-NO$_2$, 4-F, 4-CF$_3$, 2-OCH$_3$

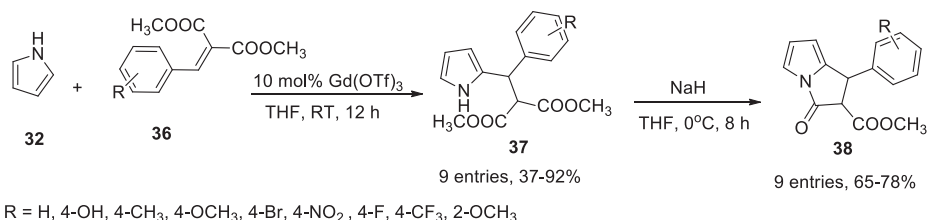**Figure 9.16:** Gadolinium triflate-catalyzed synthesis of novel 2-alkylated pyrrole derivatives.

9.5 Conclusions

Due to its unique beneficial nature, gadolinium triflate has gained significant attention as an efficient Lewis acidic catalyst. As a result, by using a catalytic amount of gadolinium triflate as catalyst, various organic transformations such as Friedel-crafts acetylation reaction, Diels-Alder reactions, Electrophilic nitration, Michael addition, Aldol reaction, and many others were achieved successfully. In this chapter, we have summarized applications of gadolinium triflate and its complexes as catalysts for various organic transformations. In some cases, the mechanism of the reaction and the role of gadolinium triflate as catalyst are also discussed.

References

[1] Banik, BK, Banerjee, B. Heterocyclic Anticancer Agents, Berlin, Boston, De Gruyter, 2022. https://doi.org/10.1515/9783110735772.

[2] Kiriiri, GK, Njogu, PM, Mwangi, AN. Exploring different approaches to improve the success of drug discovery and development projects: A review. Futur J Pharm Sci, 2020, 6, 27. https://doi.org/10.1186/s43094-020-00047-9.

[3] Brahmachari, G, Banerjee, B. Catalyst-free organic synthesis at room temperature in aqueous and non-aqueous media: An emerging field of green chemistry practice and sustainability. Curr Green Chem, 2015, 2, 274–305.

[4] Shi, M, Cui, SC, Li, QJ. Zirconium triflate-catalyzed reactions of indole, 1-methylindole, and pyrrole with α,β-unsaturated ketone. Tetrahedron, 2004, 60, 6679–6684.

[5] Srinivasulu, R, Satyanarayana, PVV, Kumar, KR. Zinc triflate: A mild and efficient catalyst for deprotection of tetrahydropyranyl ethers. Russ J Gen Chem, 2013, 83, 2419–2422.

[6] Coca, A, Turek, E. Synthesis of 5-substituted 1*H*-tetrazoles catalyzed by ytterbium triflate hydrate. Tetrahedron Lett, 2014, 55, 2718–2721.

[7] Verma, GK, Shukla, G, Nagaraju, A, Srivastava, A, Singh, MS. In(OTf)$_3$-mediated dehydrative annulation of β-ketothioamides with phenylglyoxal: One-pot access to diversely functionalized pyrrol-2-thiones. Tetrahedron Lett, 2014, 55, 5182–5185.

[8] Nishizawa, M, Imagawa, H, Yamamoto, H. A new catalyst for organic synthesis: Mercuric triflate. Org Biomol Chem, 2010, 8, 511–521.

[9] Nakamura, M, Niiyama, K, Yamakawa, T. Versatile method for the synthesis of 4-substituted 6-methyl-3-oxabicyclo[3.3.1]non-6-ene-1-methanol derivatives: Prins-type cyclization reaction catalyzed by hafnium triflate. Tetrahedron Lett, 2009, 50, 6462–6465.

[10] Huang, SG, Mao, HF, Zhou, SF, Zou, JP, Zhang, W. Recyclable gallium(III) triflate-catalyzed [4+3] cycloaddition for synthesis of 2,4-disubstituted-3H-benzo[*b*][1,4]diazepines. Tetrahedron Lett, 2013, 54, 6178–6180.

[11] Kundal, S, Jalal, S, Paul, K, Jana, U. Fe(OTf)$_3$-catalyzed aromatization of substituted 3-methyleneindoline and benzo-furan derivatives: A selective route to C-3-alkylated indoles and benzofurans. Eur J Org Chem, 2015, 2015, 5513–5517.

[12] Kumar, M, Sribalan, R, Padmini, V. Er(OTf)$_3$ assisted efficient synthesis of 3-hydroxynaphthalene-1,4-dione derivatives via pseudo four-component reactions and their biological evaluation. ChemistrySelect, 2017, 2, 489–493.

[13] Paraskar, AS, Sudalai, A. Cu (OTf)$_2$ or Et$_3$N-catalyzed three-component condensation of aldehydes, amines and cyanides: A high yielding synthesis of α-aminonitriles. Tetrahedron Lett, 2006, 47, 5759–5762.

[14] Chen, S, Li, L, Zhao, H, Li, B. Ce(OTf)$_3$-catalyzed multicomponent domino cyclization–aromatization of ferrocenylacetylene, aldehydes, and amines: A straightforward synthesis of ferrocene-containing quinolines. Tetrahedron, 2013, 69, 6223–6229.

[15] Khaksar, S, Vahdat, SM, Alipour, M. Cerium (IV) triflate-catalyzed domino annulation approaches to the synthesis of highly substituted piperidines. C R Chimie, 2013, 16, 1024–1028.

[16] Dhimane, H, Meunier, S, Vanucci-Bacqué, C, Lhommet, G. Construction of cis-azadecalone units via novel intermolecular Diels–Alder reaction. Tetrahedron Lett, 2002, 43, 1645–1648.

[17] Kumar, A, Rao, MS. An expeditious and greener one-pot synthesis of 4H-chromenes catalyzed by Ba (OTf)$_2$ in PEG-water. Green Chem Lett Rev, 2012, 5, 283–290.

[18] Bailey, JL, Sudini, RR. Synthesis of 2, 4- and 2, 5-substituted oxazoles via a silver triflate mediated cyclization. Tetrahedron Lett, 2014, 55, 3674–3677.

[19] Ladziata, V. Recent applications of rare-earth metal(III) triflates in cycloaddition and cyclization reactions. Arkivoc, 2014, 1, 307–336.

[20] Banerjee, B. Sc(OTf)$_3$ catalyzed carbon-carbon and carbon-heteroatom bond forming: A review. Arkivoc, 2017, 1, 1–25.

[21] Haynes, WM, ed., CRC Handbook of Chemistry and Physics. 95[th]ed., Boca Raton, FL: CRC Press/ Taylor and Francis, 2015, Weeks, Mary Elvira (1932).

[22] Donnelly, LF, Nelson, RC. Renal excretion of gadolinium mimicking calculi on non-contrast CT. Pediatr Radiol, 1998, 28, 417–417. https://doi.org/10.1007/s002470050374.

[23] Coey, JMD, Skumryev, V, Gallagher, K. Rare-earth metals: Is gadolinium really ferromagnetic? Nature, 1999, 401, 35–36.

[24] Ryzhikov, VD, Grinev, BV, Pirogov, EN, Onyshchenko, GM, Ivanov, AI, Bondar, VG, Katrunov, KA, Kostyukevich, SA. Use of gadolinium oxyorthosilicate scintillators in x-ray radiometers. Opt Eng, 2005, 44, 016403.

[25] Website: American Elements: The advanced materials manufacturer. https://www.americanele ments.com/gadolinium-trifluoromethanesulfonate-52093-29-5.

[26] Website: Wikipedia: The free encyclopedia. https://en.wikipedia.org/wiki/Gadolinium.

[27] Balaguer, A, Selhorst, R, Turnbull, K. Metal triflate–catalyzed friedel–crafts acetylation of 3-phenylsydnone. Synth Commun, 2013, 43, 1626–1632.

[28] Evans, DA, Wu, J. Enantioselective rare-earth catalyzed quinone Diels−Alder reactions. J Am Chem Soc, 2003, 125, 10162–10163.

[29] Waller, FJ, Barrett, AGM, Braddock, DC, McKinnell, RM, Ramprasad, D. Lanthanide(III) and Group IV metal triflate catalyzed electrophilic nitration: 'nitrate capture' and the rôle of the metal centre. J Chem Soc, 1999, 1, 867–871.

[30] Alleti, R, Oh, WS, Perambuduru, M, Ramana, CV, Reddy, VP. Imidazolium-based polymer supported gadolinium triflate as a heterogeneous recyclable Lewis acid catalyst for Michael additions. Tetrahedron Lett, 2008, 49, 3466–3470.

[31] Kobayashi, S, Hachiya, I. The aldol reaction of silylenol ethers with aldehydes in aqueous media. Tetrahedron Lett, 1992, 33, 1625–1628.

[32] Kobayashi, S, Nagayama, S, Busujima, T. Lewis acid catalysts stable in water. correlation between catalytic activity in water and hydrolysis constants and exchange rate constants for substitution of inner-sphere water ligands. J Am Chem Soc, 1998, 120, 8287–8288.

[33] Kobayashi, S, Hamada, T, Nagayama, S, Manabe, K. Lanthanide trifluoromethanesulfonate-catalyzed asymmetric aldol reactions in aqueous media. Org Lett, 2001, 3, 165–167.

[34] Kobayashi, S, Hachiya, I, Takahori, T. Lanthanide trifluoromethanesulfonates as reusable catalysts: Aldol reactions in organic solvents. Synthesis, 1993, 1993, 371–373.

[35] Kobayashi, S, Hachiya, I. Lanthanide triflates as water-tolerant Lewis acids. activation of commercial formaldehyde solution and use in the aldol reaction of silylenol ethers with aldehydes in aqueous media. J Org Chem, 1994, 59, 3590–3596.

[36] Chen, WY, Qin, SD, Jin, JR. HBF$_4$-catalyzed Biginelli reaction: One-pot synthesis of dihydropyrimidin-2 (1H)-ones under solvent-free conditions. Catal Commun, 2007, 8, 123–126.

[37] Roma, G, Braccio, MD, Grossi, G, Mattioli, F, Ghia, M. 1,8-Naphthyridines IV. 9-Substituted N,N-dialkyl -5-(alkylamino or cycloalkylamino) [1,2,4]triazolo[4,3-a][1,8]naphthyridine-6-carboxamides, new compounds with anti-aggressive and potent anti-inflammatory activities. Eur J Med Chem, 2000, 35, 1021–1035.

[38] Nagarapu, L, Kumari, MD, Kumari, NV, Kantevari, S. MCM-41 catalyzed rapid and efficient one-pot synthesis of polyhydroquinolines via the Hantzsch reaction under solvent-free conditions. Catal Commun, 2007, 8, 1871–1875.

[39] Tu, SJ, Zhou, JF, Deng, X, Cai, PJ, Wang, H, Feng, JC. One step synthesis of 4-arylpolyhydroquinoline derivatives using microwave irradiation. Chin J Org Chem, 2001, 21, 313–316.

[40] Sabitha, G, Reddy, GSKK, Reddy, CS, Yadav, JS. A novel TMSI-mediated synthesis of Hantzsch 1,4-dihydropyridines at ambient temperature. Tetrahedron Lett, 2003, 44, 4129–4131.

[41] Ji, SJ, Jiang, ZQ, Lu, J, Loh, TP. Facile ionic liquids-promoted one-pot synthesis of polyhydroquinoline derivatives under solvent free conditions. SynLett, 2004, 2004, 831–835.

[42] Heravi, MM, Bakhtiari, K, Javadi, NM, Bamoharram, FF, Saeedi, M, Oskooie, HO. K$_7$[PW$_{11}$CoO$_{40}$]-catalyzed one-pot synthesis of polyhydroquinoline derivatives via the Hantzsch three component condensation. J Mol Catal A: Chem, 2007, 264, 50–52.

[43] Wang, L-M, Sheng, J, Zhang, L, Han, J-W, Fan, Z-Y, Tian, H, Qian, C-T. Facile Yb(OTf)$_3$ promoted one-pot synthesis of polyhydroquinoline derivatives through Hantzsch reaction. Tetrahedron, 2005, 61, 1539–1543.

[44] Donelson, JL, Gibbs, RA, De, SK. An efficient one-pot synthesis of polyhydroquinoline derivatives through the Hantzsch four component condensation. J Mol Catal A: Chem, 2006, 256, 309–311.

[45] Ko, S, Sastry, MNV, Lin, C, Yao, CF. Molecular iodine-catalyzed one-pot synthesis of 4-substituted-1,4-dihydropyridine derivatives *via* Hantzsch reaction. Tetrahedron Lett, 2005, 46, 5771–5774.

[46] Maheswara, M, Siddaiah, V, Rao, YK, Tzeng, Y, Sridhar, C. A simple and efficient one-pot synthesis of 1,4-dihydropyridines using heterogeneous catalyst under solvent-free conditions. J Mol Catal A Chem, 2006, 17, 179–180.

[47] Gupta, R, Gupta, R, Paul, S, Loupy, A. Covalently anchored sulfonic acid on silica gel as an efficient and reusable heterogeneous catalyst for the one-pot synthesis of Hantzsch 1,4-Dihydropyridines under solvent-free conditions. Synthesis, 2007, 2007, 2835–2838.

[48] Ko, S, Yao, CF. Ceric ammonium nitrate (CAN) catalyzes the one-pot synthesis of polyhydroquinoline via the Hantzsch reaction. Tetrahedron, 2006, 62, 7293–7299.

[49] Reddy, CS, Raghu, M. Cerium(IV) ammonium nitrate catalysed facile and efficient synthesis of polyhydroquinoline derivatives through Hantzsch multicomponent condensation. Chin Chem Lett, 2008, 19, 775–779.

[50] Kumar, A, Maurya, RA. Efficient synthesis of Hantzsch Esters and Polyhydroquinoline derivatives in Aqueous Micelles. Synlett, 2008, 2008, 883–885.

[51] Chandrasekhar, S, Rao, YS, Sreelakshmi, L, Mahipal, B, Reddy, CR. Tris(pentafluorophenyl)borane-catalyzed three-component reaction for the synthesis of 1,8-dioxodecahydroacridines under solvent-free conditions. Synthesis, 2008, 2008, 1737–1740.

[52] Sridhar, R, Perumal, PT. A new protocol to synthesize 1,4-dihydropyridines by using 3,4,5-trifluorobenzeneboronic acid as a catalyst in ionic liquid: Synthesis of novel 4-(3-carboxyl-1H-pyrazol-4-yl)-1,4-dihydropyridines. Tetrahedron, 2005, 61, 2465–2470.

[53] Debache, A, Boulcina, R, Belfaitah, A, Rhouati, S, Carboni, B. One-Pot Synthesis of 1,4-dihydropyridines via a phenylboronic acid catalyzed Hantzsch three-component reaction. Synlett, 2008, 2008, 509–512.

[54] Kumar, S, Sharma, P, Kapoor, KK, Hundal, MS. An efficient, catalyst- and solvent-free, four-component, and one-pot synthesis of polyhydroquinolines on grinding. Tetrahedron, 2008, 64, 536–542.

[55] Kumar, A, Maurya, RA. Synthesis of polyhydroquinoline derivatives through unsymmetrical Hantzsch reaction using organocatalysts. Tetrahedron, 2007, 63, 1946–1952.

[56] Mansoor, SS, Aswin, K, Logaiya, K, Sudhan, SPN. An efficient one-pot multi component synthesis of polyhydroquinoline derivatives through Hantzsch reaction catalysed by Gadolinium triflate. Arab J Chem, 2017, 10, S546–S553.

[57] Wu, JL, Hou, RS, Wang, HM, Kang, IJ, Chen, LC. Gd(OTf)$_3$-[Bmim][PF$_6$]: A novel and recyclable catalytic system for the synthesis of quinolines. J Chin Chem Soc, 2009, 56, 867–872.

[58] Murarka, S, Zhang, C, Konieczynska, MD, Seidel, D. Lewis acid catalyzed formation of tetrahydroquinolines via an intramolecular redox process. Org Lett, 2009, 11, 129–132.

[59] Srinivas, B, Rao, KP. Design an Efficient Method for the Synthesis of 2-(1,3-diphenyl-1*H*-pyrazol-4-yl)-1*H*-benzo [d] imidazole. Mapana J Sci, 2020, 19, 21–31.

[60] Chen, W, Lin, L, Cai, Y, Xia, Y, Cao, W, Liu, X, Feng, X. Catalytic asymmetric [3+2] cycloaddition of aromatic aldehydes with oxiranes by C–C bond cleavage of epoxides: Highly efficient synthesis of chiral 1,3-dioxolanes. Chem Commun, 2014, 50, 2161–2163.

[61] Alleti, R, Oh, WS, Perambuduru, M, Afrasiabi, Z, Sinn, E, Reddy, VP. Gadolinium triflate immobilized in imidazolium based ionic liquids: A recyclable catalyst and green solvent for acetylation of alcohols and amines. Green Chem, 2005, 7, 203–206.

[62] Alleti, R, Perambuduru, M, Samantha, S, Reddy, VP. Gadolinium triflate: An efficient and convenient catalyst for acetylation of alcohols and amines. J Mol Catal A Chem, 2005, 226, 57–59.

[63] Yoon, HJ, Lee, SM, Kim, JH, Cho, HJ, Choi, JW, Lee, SH, Lee, YS. Polymer-supported gadolinium triflate as a convenient and efficient Lewis acid catalyst for acetylation of alcohols and phenols. Tetrahedron Lett, 2008, 49, 3165–3171.

[64] Tanaka, Y, Kanai, M, Shibasaki, M. Catalytic conjugate addition of cyanide to enones: Cooperative Catalysis of Ni(0) and Gd (OTf)$_3$. Synlett, 2008, 2008, 2295–2298.

[65] Fukuta, Y, Mita, T, Fukuda, N, Kanai, M, Shibasaki, M. De novo synthesis of Tamiflu via a catalytic asymmetric ring-opening of meso-aziridines with TMSN$_3$. J Am Chem Soc, 2006, 128, 6312–6313.

[66] Yamatsugu, K, Kamijo, S, Suto, Y, Kanai, M, Shibasaki, M. A concise synthesis of Tamiflu: Third generation route via the diels–alder reaction and the curtius rearrangement. Tetrahedron Lett, 2007, 48, 1403–1406.

[67] Wang, C, Yamamoto, H. Gadolinium-catalyzed regio- and enantioselective aminolysis of aromatic trans-2,3-epoxy sulfonamides. Angew Chem, 2015, 127, 8884–8887.

[68] Yang, Z, Wang, Z, Bai, S, Liu, X, Lin, L, Feng, X. Asymmetric α-amination of 4-substituted pyrazolones catalyzed by a chiral Gd(OTf)$_3$/N,N′-dioxide complex: Highly enantioselective synthesis of 4-amino-5-pyrazolone derivatives. Organic Lett, 2011, 13, 596–599.

[69] Yao, Q, Wang, Z, Zhang, Y, Liu, X, Lin, L, Feng, X. N,N′-Dioxide/Gadolinium(III)-catalyzed asymmetric conjugate addition of nitroalkanes to α,β-unsaturated pyrazolamides. J Org Chem, 2015, 80, 5704–5712.

[70] Temelli, B, Unaleroglu, C. A novel method for the synthesis of dipyrromethanes by metal triflate catalysis. Tetrahedron, 2006, 62, 10130–10135.

[71] Unaleroglu, C, Yazici, A. Gadolinium triflate-catalyzed alkylation of pyrroles: Efficient synthesis of 3-oxo-2, 3-dihydro-1*H*-pyrrolizine derivatives. Tetrahedron, 2007, 63, 5608–5613.

Puja Basak and Pranab Ghosh*

10 Scandium(III) and lanthanum(III) trifluoromethanesulfonate-catalyzed organic synthesis

10.1 Introduction

The triflate salts of lanthanides are known as lanthanide triflates. Due to their hard nature and strong attraction for the oxygen present in the carbonyl group, lanthanide compounds act as strong Lewis acids [1]. Lanthanide triflate was supposed to be among the strongest Lewis acids among the lanthanide compounds because they include the electron-withdrawing trifluoromethanesulfonyl group. In synthetic organic chemistry, lanthanides have begun to emerge as mild and selective reagents [2]. Trifluoromethanesulfonates (triflates) [3] of scandium(III) and lanthanide(III) have been used as Lewis acid catalysts in the Diels–Alder [4], allylation [5], Friedel-Crafts [6], and Mukaiyama aldol [7–8] reactions. Chemists have used lanthanide triflates as Lewis acids due to the high radius and distinct coordination number of lanthanide(III) [9]. The chemical compound scandium trifluoromethanesulfonate, often known as scandium triflate, has the formula $Sc(SO_3CF_3)$, and is a water-tolerant Lewis acid. In the course of our research to look for alternative metal triflates, we first focused on lanthanide triflates because they have different properties from metal halides [10]. $AlCl_3$, $SnCl_4$, BF_3, and other common Lewis acids are deactivated and broken down in the presence of water [11], while $Sc(OTf)_3$ is stable enough to work in aqueous media as a Lewis acid catalyst. Despite the fact that the same reaction requires stoichiometric concentrations of conventional Lewis acids, many reactions run without issue in presence of catalytic amounts of this reagent. Additionally, different imines and hydrazones (compounds containing N) can be successfully activated using catalytic amounts of $Sc(OTf)_3$ in both aqueous and organic solvents. Even though they both contain identical characteristics, $Sc(OTf)_3$ possesses catalytic activity frequently substantially higher than that of the analogous lanthanide triflates $Ln(OTf)_3$. After the reaction, $Sc(OTf)_3$ can be quantitatively recovered and used again. The Michael addition reaction can be catalyzed by $Sc(OTf)_3$ and subsequently converts silyl enol ethers to α,β-unsaturated ketones in high yields in DCM solvent at rt. The other lanthanide triflate, $La(OTf)_3$, also catalyzes the aldol condensations between silyl enol ethers and formaldehyde as a Lewis acid catalyst [12].

*Corresponding author: Pranab Ghosh, Department of Chemistry, University of North Bengal, Darjeeling, West Bengal, India, e-mail: pizy12@yahoo.com
Puja Basak, Department of Chemistry, University of North Bengal, Darjeeling, West Bengal, India

10.2 Preparation procedure

10.2.1 Scandium triflate preparation method

Scandium triflate $Sc(OTf)_3$ is available commercially. This is synthesized from the reaction of scandium oxide (Sc_2O_3) and aqueous trifluoromethanesulfonic acid (TfOH) at 100 °C for 1 h (Figure 10.1). The clear aqueous solution is then filtered and subsequently dried for 40 h in vacuum (<1 mmHg) at 200 °C to get the triflate in its anhydrous condition, which is finally stored over P_2O_5 [13].
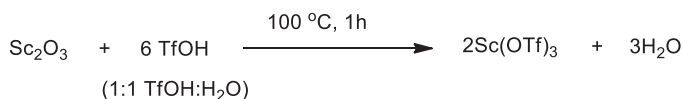
$$Sc_2O_3 \quad + \quad 6\ TfOH \quad \xrightarrow{100\ ^oC,\ 1h} \quad 2Sc(OTf)_3 \quad + \quad 3H_2O$$
$$(1{:}1\ TfOH{:}H_2O)$$

Figure 10.1: The synthesis of scandium triflate from Sc_2O_3.

10.2.2 Lanthanum triflate ($La(CF_3SO_3)_3$) preparation method

Lanthanum oxide (La_2O_3) is added in slight excess amount to the aqueous solution of triflic acid (50% v/v); after that the reaction mixture is stirred at room temperature for 15 min and the remaining part of the oxide is removed by filtration; the resultant filtrate is concentrated in vacuum at 60 °C and azeotropic distillation in vacuum with toluene is used to eliminate any remaining water; the hydrated product is put in a flask with a stirring bar, a stopcock with a glass wool stopper, and a NaOH trap; After that, it is heated for 16 h (at 140 °C/0.1 mmHg or 180 °C/1.0 mmHg) under vacuum condition. $La(OTf)_3$ in its anhydrous state is a white to gray-white solid [14–16].

10.3 Scandium triflate-catalyzed organic reactions

10.3.1 Aldol-type reactions

$Sc(OTf)_3$ performs well as a catalyst in aldol-type reactions involving the combination of silyl enol ethers (**1**) and aldehydes (**2**) (Figure 10.2). The reactions of 1-trimethylsiloxycyclohexene with benzaldehyde in DCM were studied to determine the activity of common rare earth triflates [Sc, Y, $Yb(OTf)_3$]. When $Yb(OTf)_3$ or $Y(OTf)_3$ are present, the reaction proceeds slowly at −78 °C, but an aldol-type adduct (**3**) is created with an 81% yield when $Sc(OTf)_3$ is present. It is obvious that $Sc(OTf)_3$ is more active in this scenario than $Y(OTf)_3$ or Yb(OTf) [17].
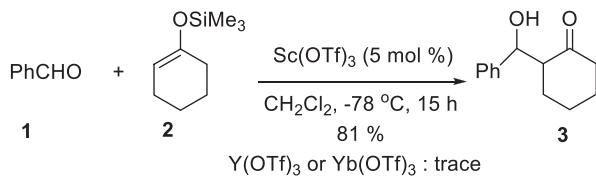
Figure 10.2: Sc(OTf)$_3$-catalyzed aldol-type reactions of silyl enol ethers and aldehydes.

When silyl enolates (**5**) and aldehydes (**4**) are combined in aqueous media (H$_2$O-THF), Sc(OTf)$_3$ is efficient in preventing the water-sensitive silyl enolates from decomposing significantly (Figure 10.3). Thus, aldehydes in aqueous solution, including formaldehyde and chloroacetaldehyde, can therefore be employed immediately to generate high yields of the corresponding aldol adduct (**6**) [11].
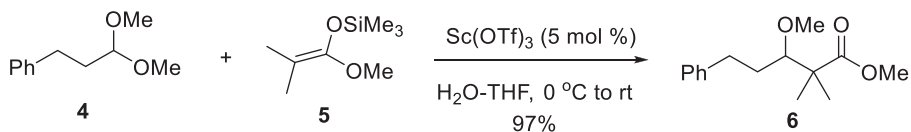

Figure 10.3: Aldol-type reaction of silyl enolates with aldehydes catalyzed by Sc(OTf)$_3$.

10.3.2 Michael reaction

When α,β-unsaturated carbonyl compounds (**6**) and silyl enol ethers or ketene silyl acetals (**7**) undergo a Michael reaction, Sc(OTf)$_3$ catalyzes the reaction, producing high yields of the related 1,5-dicarbonyl compounds (**8**) after acid workup. The valuable synthetic compound silyl enol ethers were isolated after working up the crude adducts without acid (Figure 10.4). The catalyst can be recovered and reused almost entirely. In the presence of 3 mol % Me$_2$Cu(CN)Li$_2$, Sc(OTf)$_3$ also catalyzes the 1,4-addition of PhMe$_2$Si-ZnMe$_2$Li to enones [18].
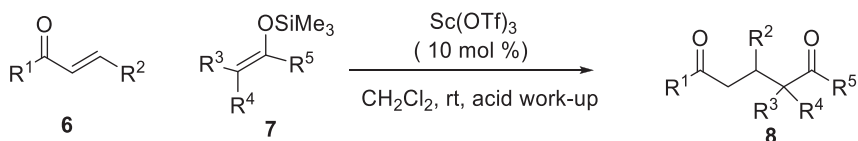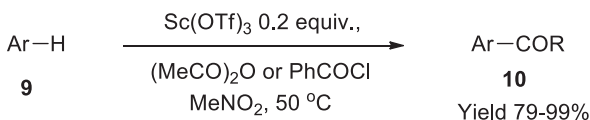

Figure 10.4: Sc(OTf)$_3$-catalyzed Michael reaction.

10.3.3 Friedel–crafts acylation, alkylation, and related reactions

Friedel-Crafts acylation needs a stoichiometric amount of $AlCl_3$, whereas the same reaction is smoothly catalyzed by a required amount of $Sc(OTf)_3$ (Figure 10.5) [19]. A single, highly yielding acetylated product (**10**) is produced by acetylating thioanisole with either *o*- or *m*-dimethoxybenzene (**9**). Anisole can be benzoylated with both benzoyl chloride and benzoic anhydride, however, with benzoic anhydride producing somewhat more. The yield is significantly enhanced by the co-catalyst lithium perchlorate ($LiClO_4$) [20]. In the presence of an acylating agent, lithium perchlorate has been observed to generate a cationic species. In the presence of $Ln(OTf)_3$, $LiClO_4$ is projected to form such a cationic species, and it is predicted that the high reactivity of this cationic species will ensure successful acylation. Due to the solubility and stability of both $LiClO_4$ and $Ln(OTf)_3$ in aqueous environments, it is also anticipated that the $Ln(OTf)_3$-$LiClO_4$ catalytic system would be easily recovered by the aqueous workup of the reaction mixture.

Ar = $4\text{-}OMeC_6H_5$, $4\text{-}SMeC_6H_5$, $3,4\text{-}OMeC_6H_4$

Figure 10.5: $Sc(OTf)_3$-catalyzed Friedel-Crafts acylations.

10.3.4 Diels–Alder and related reactions

The Diels–Alder adduct (**13**) is produced in 91% yield when 10 mol% $Sc(OTf)_3$ is present in the reaction of methyl vinyl ketone (**11**) (MVK) with isoprene (**12**), whereas 10 mol% $Y(OTf)_3$ or $Yb(OTf)_3$ only produces a trace quantity of the adduct (Figure 10.6). Diels–Alder reactions catalyzed by [21] $Sc(OTf)_3$ have generally high yields and endo selectivities. Aqueous media can still experience the current Diels–Alder reaction. As a result, at room temperature, naphthoquinone and cyclopentadiene react to form the desired adduct in a high yield (100% *endo* product). $Sc(OTf)_3$ works well as a catalyst for Diels–Alder processes in supercritical CO_2 also [22].
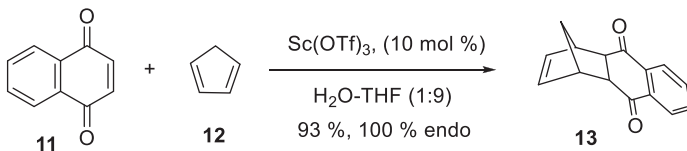

Figure 10.6: Diels–Alder reactions catalyzed by $Sc(OTf)_3$.

Azasugars and their derivatives, which usually exhibit distinctive physiochemical properties, are produced using the well-known aza-Diels–Alder reaction (Figure 10.7) [23]. The aza-Diels–Alder reaction is typically carried out in organic solvents with a Lewis acid present (ZnCl$_2$, BF$_3$, TiCl$_4$, etc.) [24]. Kitazume and his co-workers investigated the aza-Diels–Alder reaction of *N*-phenyl phenyl imine (**14**) with 1-methoxy-3-(trimethylsilyl)oxybuta-1,3-diene (**15**) in an ionic liquid (8-ethyl-1,8-diazabicyclo[5,4,0]-7-undecenium trifluoromethanesulfonate) [25]. The uncatalyzed process came to an abrupt end. A microencapsulated version of scandium trifluoromethanesulfonate (Lewis acid) is added, drastically increasing the yield to 75%. The current operations proceeded normally in an ionic liquid at room temperature.
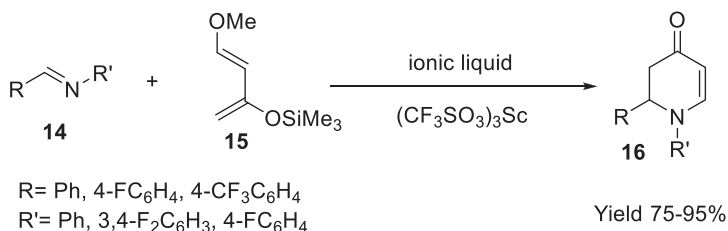

R= Ph, 4-FC$_6$H$_4$, 4-CF$_3$C$_6$H$_4$
R'= Ph, 3,4-F$_2$C$_6$H$_3$, 4-FC$_6$H$_4$

Yield 75-95%

Figure 10.7: Sc(OTf)$_3$-catalyzed aza-Diels–Alder reaction.

10.3.5 Miscellaneous reactions

Sc(OTf)$_3$ also catalyzes Meerwein–Ponndrof–Verley reductions [26], Tishchenko reductions [27], Baeyer–Villiger oxidations [28], acetalization reactions [29], acylal formation [30], β-selective glycosilation reactions with thioglycosides [31], chemoselective deprotection of silyl alkyl ethers [32], silyl ether protection of alcohols with allyl silanes [33], deprotection of benzylic poly(ethyleneglycol) ethers [34]. As a moderate Lewis acid for a variety of chemical transformations, scandium triflate has drawn a lot of attention [35]. Gibbs and his co-workers reported a quick technique for producing 2,3-dihydro-1 *H*-1,5-benzodiazepines (**19**) by condensation of *o*-phenylenediamine (**17**) with ketones (**18**) in the presence of catalytic amounts of Sc(OTf)$_3$ in a solvent-free environment (Figure 10.8) [36]. In terms of conversion and reaction rates, Sc(OTf)$_3$ was discovered to be the most efficient catalyst among the several metal triflates investigated for this reaction, including Cu(OTf)$_2$, La(OTf)$_3$, Lu(OTf), Nd(OTf), and Ce(OTf).

Fundamental procedures in organic chemistry include the esterification of carboxylic acids and the acylation of alcohols [37, 38]. In the presence of mineral or sulfonic acids, the Fischer esterification, which is a direct acylation of alcohols (20) with carboxylic acids (21), can be achieved as an atom-economic process [39]. Barrett and his co-workers described employing acetic acid to directly acylate primary, secondary, and tertiary alcohols in the presence of catalytic amounts of scandium(III) or lanthanide(III)
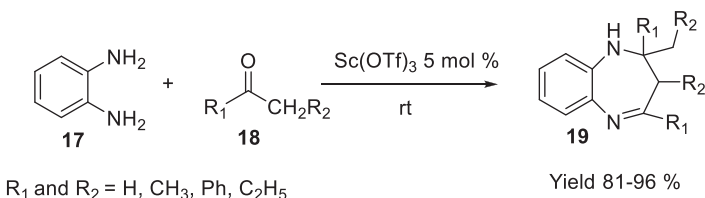
R_1 and R_2 = H, CH_3, Ph, C_2H_5

Yield 81–96 %

Figure 10.8: Sc(OTf)$_3$-catalyzed synthesis of 2,3-dihydro-1H-1,5-benzodiazepines.

triflates [40]. Both economically and environmentally, using acetic acid instead of acetic anhydride or acetyl chloride is preferable (Figure 10.9). In addition, the catalysts are easily reusable using a straightforward aqueous work-up.
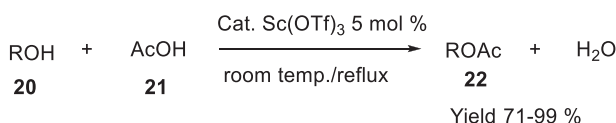

Figure 10.9: Acylation of alcohols using scandium(III) triflate.

The Lewis acid catalyzed synthesis of malonamides (**25**) has a new methodological approach. First, it has been developed to add coumarin-3-carboxylates (**23**) to a variety of nucleophiles, such as indoles (**24**), *N,N*-dimethyl-*m*-anisidine, 2-ethylpyrrole, and 2-methyl-allylsilane, to produce chromanone-carboxylates in high yields as a single diastereomer. Franz and his co-workers aimed to provide a generic approach for the Sc(III)-catalyzed addition of indoles (24), methallyltrimethylsilane, and *N,N*-dimethyl-*m*-anisidine to coumarin-3-carboxylates (**23**) as well as show that both esters can be used in further transformations that are advantageous for pharmaceutical molecules (Figure 10.10) [41]. As the Lewis acidity of a sequence of lanthanide catalysts, Sc > Y > La, decreased, less product is produced. No decarboxylation or loss of *tert*-butyl group is seen during the *tert*-butyl coumarin 3-carboxylate reaction under the reaction conditions.
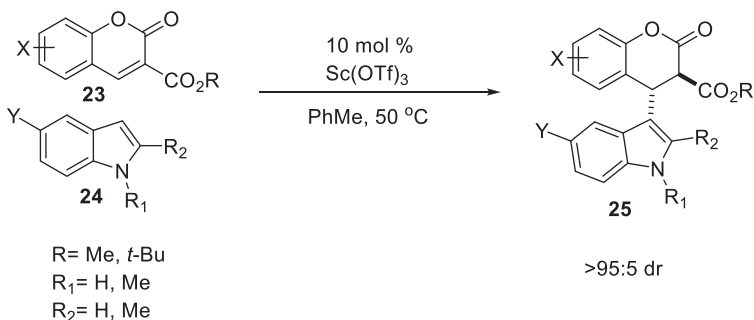

R= Me, *t*-Bu
R_1= H, Me
R_2= H, Me

>95:5 dr

Figure 10.10: Sc(III)-catalyzed synthesis of coumarin-3-carboxylates.

10.3.5.1 Carbon–carbon bond formation reaction

According to Park et al. Carbonyl compounds (**26**) were cyanosilylated with trimethyl-silyl cyanide (**27**) in an environmentally friendly and highly reactive method to produce the corresponding-(trimethylsilyloxy)carbonitriles (**28**) at ambient temperature in [bmim][SbF$_6$] (Figure 10.11). Furthermore, Sc(OTf)$_3$-containing ionic liquid was effectively recovered and utilized for a number of reaction cycles without suffering any catalytic activity loss [42]. A very efficient catalytic system for the cyanosilylation of carbonyl compounds might be produced with the right combination of metal triflate and ionic liquid. The anion exchange between Sc(OTf)$_3$ and [bmim][SbF$_6$] produced a more Lewis acidic catalyst, which is the cause of the increased catalytic activity of metal triflates in this compound.
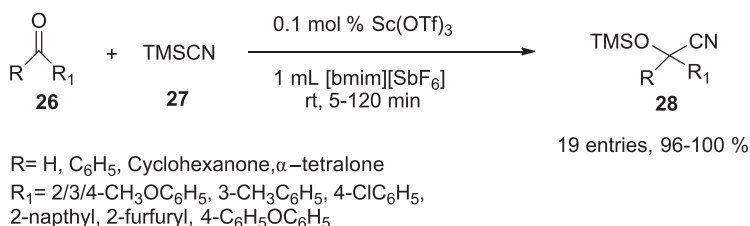

R= H, C$_6$H$_5$, Cyclohexanone,α–tetralone
R$_1$= 2/3/4-CH$_3$OC$_6$H$_5$, 3-CH$_3$C$_6$H$_5$, 4-ClC$_6$H$_5$,
2-napthyl, 2-furfuryl, 4-C$_6$H$_5$OC$_6$H$_5$

19 entries, 96-100 %

Figure 10.11: Sc(OTf)$_3$-catalyzed cyanosilylations of carbonyl compounds.

Sultana et al. created a straightforward procedure at room temperature in presence of scandium triflate catalyst, to create primary homoallylic alcohols (**31**) in this process from alkenes (**29**) and paraformaldehyde (**30**) (Figure 10.12) [43].

R$_1$= H, cyclohexyl
R= CH$_3$, C$_6$H$_5$, CH$_2$CH$_2$Br, 4-ClC$_6$H$_4$, 4-BrC$_6$H$_4$

10 entries, 55-85%
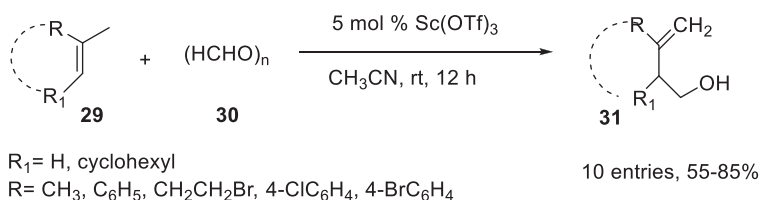
Figure 10.12: The synthesis of primary homoallylic alcohols using Sc(OTf)$_3$ catalyst.

There is currently a lot of scientific interest in lanthanide triflates, which are special Lewis acids. They are extremely oxophilic and form potent, but unstable, interactions with oxygen donor ligands. This property has frequently made it possible to use sub-stoichiometric amounts of the lanthanide Lewis acid to facilitate a number of reactions. In the presence of scandium triflate catalyst, Yadav et al. (Figure 10.13) reported a simple and effective alkylation reaction of indoles (**32**) with propargylic alcohols (**33**) in order to synthesize high yields of 3-propargylated indoles (**34**) in 1,2-dichloroethane

solvent at 80 °C temperature [44]. In an S_N2' reaction, the hydroxyl group of alcohol was simply substituted by indole.

Figure 10.13: The synthesis of different 3-propargylated indoles using Sc(OTf)$_3$ catalyst.
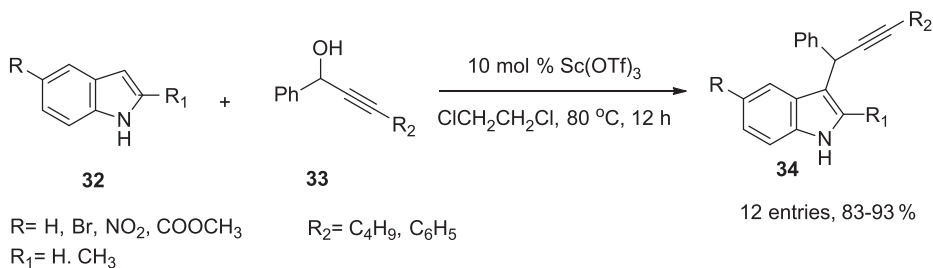
In order to synthesize good yields of resorcin[4]arene octaalkyl ethers (**37**), Morikawa et al. described a straightforward and easy-to-follow cyclocondensation of 1,3-dialkoxy-benzenes (**35**) with 1,3,5-trioxane (**36**) in acetonitrile solvent at 80 °C using catalytic amounts of Sc(OTf)$_3$ (Figure 10.14) [45].
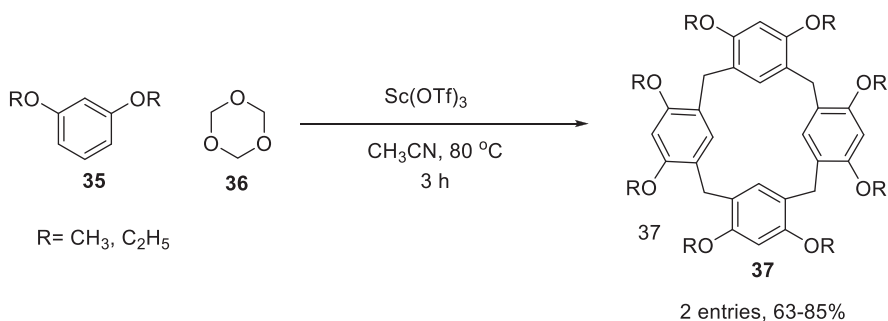
Figure 10.14: The synthesis of different resorcin[4]arene octaalkyl ethers using Sc(OTf)$_3$.

10.3.5.2 Carbon–nitrogen bond formation reaction

An efficient one-pot reaction of aldehydes (**38**) and hydroxylamine hydrochloride (**39**) to exert primary amides (**40**), Allam et al. [46] provided a flexible synthetic route to synthesize amides while there is microwave irradiation is present using Sc(OTf)$_3$ catalyst under aqueous phase (Figure 10.15).

Yadav et al. [47] described an amination reaction between arenes (**41**) and DEAD (diethyl azodicarboxylate) (**42**) through electrophilic pathway in DCM solvent at room temperature to produce the appropriate arylhydrazides (**43**) in regioselective manner with high yields (Figure 10.16).

Figure 10.15: Sc(OTf)₃-catalyzed synthesis of primary amides.

Figure 10.16: The amination reaction between arenes and diethyl azodicarboxylate using Sc(OTf)₃.

Coca et al. [48] synthesized several 5-substituted 1 *H*-tetrazoles (**46**) via the reaction between different nitriles (**44**) and sodium azide (**45**) through a [2 + 3] cyclo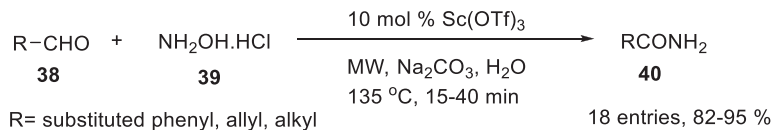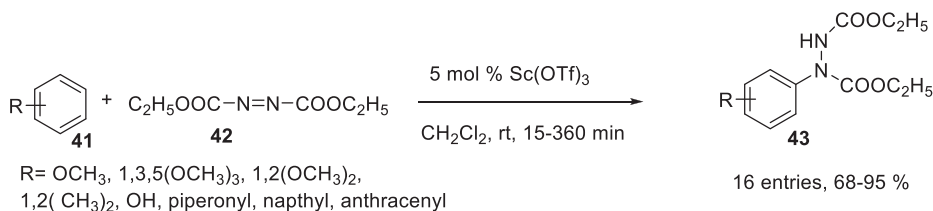addition pathway under microwave-assisted method at 160 °C in a 3:1 mixture of isopropanol/ water using Sc(OTf)₃ as catalyst (Figure 10.17).
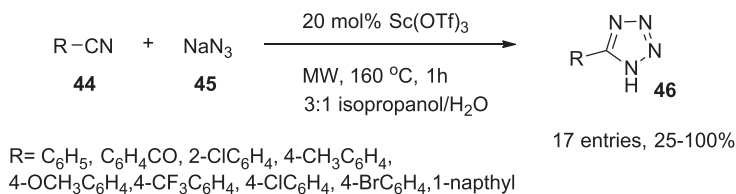
Figure 10.17: Sc(OTf)₃-catalyzed synthesis of 5-substituted 1*H*-tetrazoles.

Agrebi et al. [49] designed a straightforward and one-pot synthetic strategy for fluorescent compound imidazo[1,2-c]pyrazolo[3,4-e]pyridines (**49**) synthesis using aminopyrazolo[3,4-d]pyrimidine (**47**), aldehyde (**38**), and isocyanide (**48**) in the presence of Sc(OTf)₃ at 150 °C to obtain high yields of the desired product (Figure 10.18) [49].

According to Kumari et al. [50] the reaction of phenyl hydrazine (**50**), aldehydes (**38**), and ethyl acetoacetate (**51**) under neat conditions led to an effective, straightforward, easy-to-follow, microwave-irradiated, quick, and environmentally safe synthesis of functionalized pyrazoles (**52**) (Figure 10.19).

The two-component reaction of imines (**53**) with ethyl propiolate (**54**) to produce *N*-substituted 1,4- dihydropyridine derivatives (**55**), Kikuchi et al. [51] developed a simple and straightforward procedure when using catalytic amounts of scandium(III) triflate under toluene or benzotrifluoride solvent in reflux condition (Figure 10.20). The influence of various Lewis acids and the RE triflates (RE = Sc, Y, La, Ce, Pr, Nd, Sm, Yb)

Figure 10.18: Sc(OTf)$_3$-catalyzed synthesis of fluorescent imidazo[1,2-c]pyrazolo[3,4-e]pyridines.

R$_1$= H, CH$_3$
R$_2$= 4-OCH$_3$, 4-Cl, 3-NO$_2$
R$_3$= ^{t}Bu, cyclohexyl

8 entries, 61-78 %

R$_2$= CH$_2$CH$_3$, C$_6$H$_5$, 3-ClC$_6$H$_4$, 4-FC$_6$H$_4$, 4-BrC$_6$H$_4$, furfuryl,
4-OCH$_3$C$_6$H$_4$, 4-N(CH$_3$)$_2$C$_6$H$_4$,

14 entries, 74-92 %
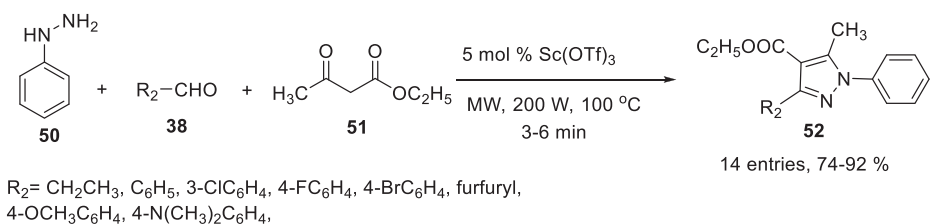
Figure 10.19: Sc(OTf)$_3$-catalyzed reaction of phenyl hydrazine, aldehydes and ethyl acetoacetate.

R$_1$= ^{t}Bu, C$_6$H$_5$, CH$_2$C$_6$H$_5$, CH(C$_6$H$_5$)$_2$, 4-OCH$_3$C$_6$H$_4$, 4-CH$_3$C$_6$H$_4$
R$_2$= C$_6$H$_5$, 4-CH$_3$C$_6$H$_4$, 4-FC$_6$H$_4$, 4-NO$_2$C$_6$H$_4$, 4-ClC$_6$H$_4$

9 entries, 18-78 %
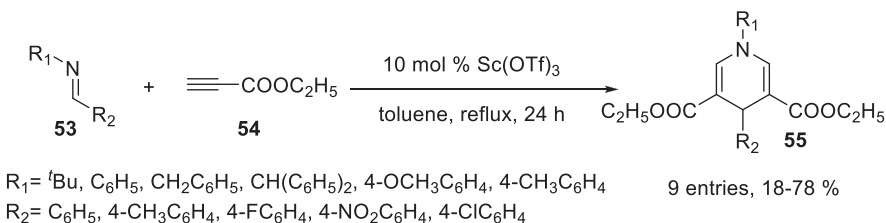
Figure 10.20: Sc(OTf)$_3$-catalyzed synthesis of N-substituted 1,4-dihydropyridine derivatives.

on the product yield in the reaction of imine with ethyl propiolate in toluene is investigated. The findings demonstrated that the best Lewis acid for this reaction is Sc(OTf)$_3$.

10.3.5.3 Carbon–oxygen bond formation reaction

Atkinson et al. [52] showed an efficient protocol for the production of esters (**57**) in presence of Sc(OTf)$_3$ catalyst from different primary amides (**56**) and alcohols (**20**) in n-heptane at 100 °C (Figure 10.21).
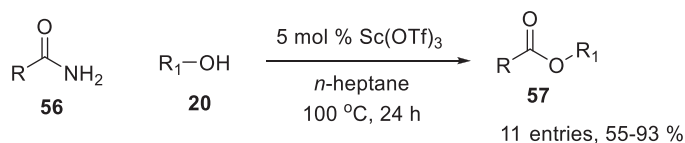
R= n-Pent, $C_6H_5CH_2$, C_6H_5CHCl
R_1= $C_6H_5CH_2$, 4-$ClC_6H_4CH_2$, 4-$NO_2C_6H_4CH_2$

Figure 10.21: Sc(OTf)$_3$-catalyzed synthesis of esters.

10.3.5.4 Sulfur–sulfur bond formation reaction

Liang et al. [53] showed that thiosulfonates (**60**) can be produced at room temperature in moderate to excellent yields by sulfenylating sodium sulfinates (**58**) with N-(organothio) succinimides (**59**) in a mixture of ionic liquids and water (Figure 10.22). Additionally, they were successful in recovering and reusing the remaining part of Sc(OTf)$_3$ without suffering a significant loss in catalytic activity [53]. Ionic liquids made of 1,3-dialkylimidazolium cations and their counter anions that are air- and moisture-stable at room temperature have become increasingly popular in recent years. These solvents allow polar or ionic catalysts to be immobilized without requiring further structural alteration, making it simple to separate the catalyst-containing ionic solutions from other reagents and products. In scandium triflate-catalyzed reactions, ionic liquids [bmim][X] function as potent media (or additives), in addition to aiding catalyst recovery, scandium triflate catalyzed processes significantly speed up the reaction rate and increase selectivity. Under the same reaction circumstances, all other lanthanide(III) triflates exhibited no activity. These outcomes can be attributed to Sc(OTf)$_3$'s higher Lewis acidity than lanthanide counterparts.
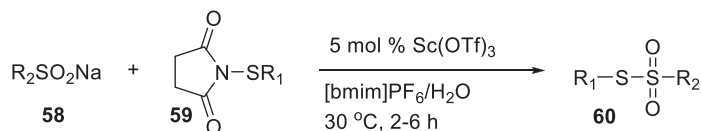
R_1= C_6H_5, 4-$CH_3C_6H_4$, 4-ClC_6H_4, 4-BrC_6H_4,
4-$NO_2C_6H_4$, $C_6H_5CH_2$
R_2= 4-$CH_3C_6H_4$, 2-$CH_3C_6H_4$, 4-ClC_6H_4, 4-BrC_6H_4, 4-$OCH_3C_6H_4$,
4-FC_6H_4, 4-$NO_2C_6H_4$, 4-$CF_3C_6H_4$

33 entries, 68-92 %

Figure 10.22: Sc(OTf)$_3$-catalyzed synthesis of thiosulfonates.

10.4 La(OTf)₃-catalyzed organic transformations

10.4.1 Aldol, Michael, and Diels–Alder reaction

As a Lewis acid catalyst the use of La(OTf)$_3$ has been demonstrated for Aldol condensation reaction between silyl enol ethers (**61**) and formaldehyde (**62**) in aqueous solutions (Figure 10.23) [11]. When silyl enol ethers (**64**) are added to α,β-unsaturated ketones (**6**) at room temperature in DCM, La(OTf)$_3$ can catalyze the reaction and produce the desired products in high yields. Other lanthanide triflates are also efficient in some of the instances tested, and as little as 1 mol percent of La(OTf)$_3$ is required. There are no 1,2-addition byproducts and enol silanes produced from ketones, thioesters, and esters are acceptable. La(OTf)$_3$ works well as a Diels–Alder cycloaddition catalyst for dienophiles that contain carbonyls and cyclopentadiene [54]. La(OTf)$_3$ is reusable and nearly fully recoverable after aqueous workup for all three of the catalytic methods discussed here [11].
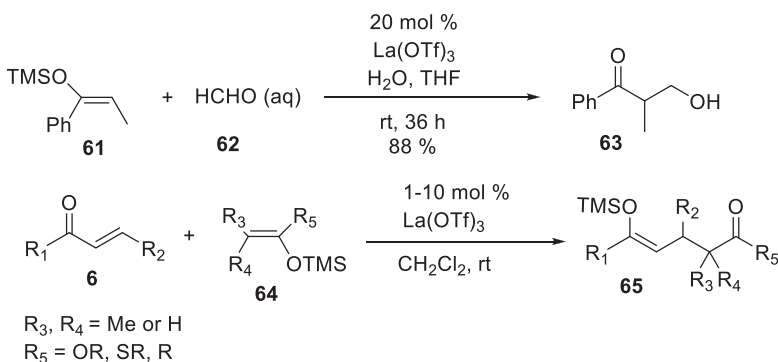
Figure 10.23: La(OTf)$_3$-catalyzed Aldol condensation reaction.

10.4.2 Synthesis of amidines

Primary amines (**66**) (2 equiv) react with nitriles (**67**) to produce *N,N*-disubstituted amidines (**68**) in good yields in the presence of 1 mol% of La(OTf)$_3$ (Figure 10.24); when primary diamines (**69**) (1 equiv) are used, cyclic amidines (**70**) are produced in good to exceptional yields [55]. When primary monoamines interact with organonitriles, an intermediate called N-substituted amidine (i) is produced. This intermediate then interacts with a second amine molecule to produce amidine (ii). In general, when the reactions were run at a 1:2 nitrile:amine mole ratio, the conversion of the nitrile to the disubstituted amidine was over 90%. Thus, this method presents a desirable, high yield alternative for the synthesis of *N,N'*-disubstituted amidines (Figure 10.25). Cyclic amidines are produced as a result of primary diamines and nitrile reactions.

These processes are comparable to those that involve primary monoamines. However, the hypothesized intermediate (ii) experiences quick intramolecular ring closure, which is undetectable by NMR. When equimolar concentrations of amine and nitrile are heated with 1 mol% Ln^{3+} over 24 h, these reactions are quite simple and essentially finished (isolated yields of 70–95%).
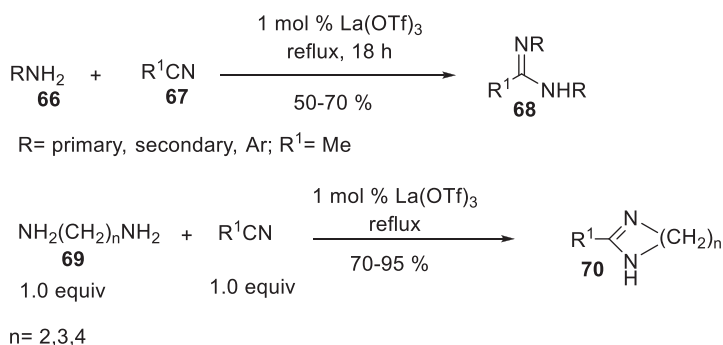
$$RNH_2 \; + \; R^1CN \xrightarrow[\substack{50\text{-}70\,\%}]{\substack{1\ mol\,\%\ La(OTf)_3 \\ reflux,\ 18\ h}} \underset{\textbf{68}}{R^1\!\!\overset{NR}{\underset{NHR}{\diagup\!\!\!\diagdown}}}$$

$$\underset{\textbf{66}}{RNH_2} \quad \underset{\textbf{67}}{R^1CN}$$

R= primary, secondary, Ar; R^1= Me

$$\underset{\substack{\textbf{69}\\ 1.0\ equiv}}{NH_2(CH_2)_nNH_2} \; + \; \underset{1.0\ equiv}{R^1CN} \xrightarrow[\substack{70\text{-}95\,\%}]{\substack{1\ mol\,\%\ La(OTf)_3 \\ reflux}} \underset{\textbf{70}}{R^1\!-\!\!\overset{N}{\underset{\underset{H}{N}}{\diagup\!\!\!\diagdown}}\!(CH_2)_n}$$

n= 2,3,4

Figure 10.24: La(OTf)$_3$-catalyzed synthesis of amidines.

$$RNH_2 + R^1CN \underset{}{\overset{Ln^{3+}}{\rightleftharpoons}} \underset{\textbf{(i)}}{R^1C\big(\!=\!NH\big)NHR} \xrightarrow{RNH_2} \underset{\textbf{68}}{R^1C\big(\!=\!NR\big)NHR} \; + \; NH_3$$

$$R^1CN + NH_2(CH_2)_nNH_2 \xrightarrow{Ln^{3+}} \underset{\textbf{(ii)}}{R^1C\big(\!=\!NH\big)NH(CH_2)nNH_2} \longrightarrow$$

$$\underset{\textbf{70}}{R^1\!-\!\!\overset{N}{\underset{\underset{H}{N}}{\diagup\!\!\!\diagdown}}\!(CH_2)_n} \; + \; NH_3$$
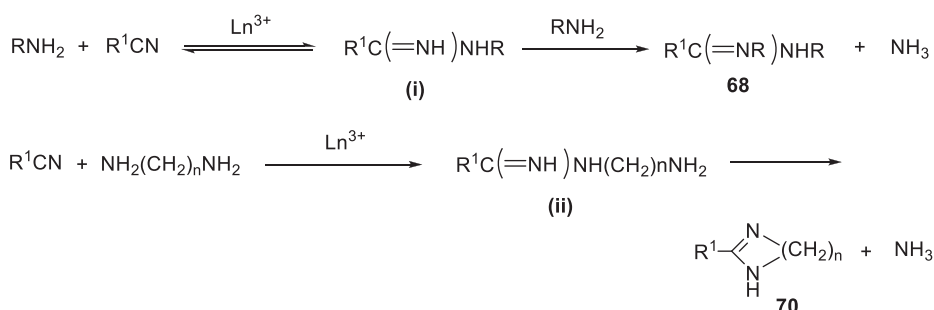
Figure 10.25: La(OTf)$_3$-catalyzed mechanism of the synthesis of disubstituted amidine and cyclic amidines.

10.4.3 Lewis acid catalyst for addition reactions to carbonyl derivatives

La(OTf)$_3$ catalyzes the reaction between silyl ketene acetals (**72**) and nitrones (**71**) to create, α,β-unsaturated esters (**73**) (Figure 10.26) [56]. La(OTf)$_3$ catalyzes the α-fluoroformylalkenylation (**75**) of aldehyde acetals using β-ethoxy-α-fluoro-α-(phenylselanyl) ethenes [57].
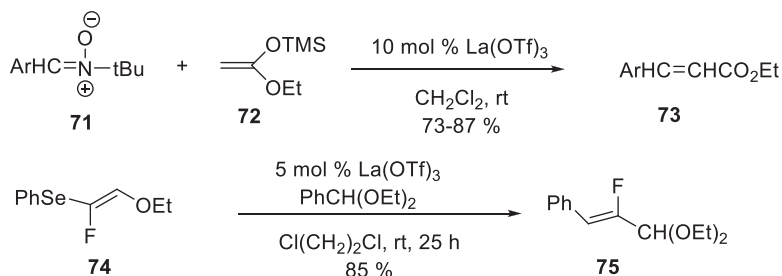
Figure 10.26: La(OTf)$_3$-catalyzed α-fluoroformyl alkenylation.

10.4.4 Lewis acid catalyst for protection/deprotection reactions

La(OTf)$_3$ catalyzes the PMB-protection (*para*-methoxybenzyl) of alcohols (**76**) *with PMBTCA* (trichloroacetimidate of para-methoxybenzyl alcohol) in moderate circumstances [58]. Alcohols that are susceptible to air can be safeguarded in these circumstances (Figure 10.27). La(OTf)$_3$ has been used to catalyze the biomimetic monoacylation of diols in water using methyl benzoyl phosphate [59–61]. 6-hydroxybicyclo[2.2.2]octan-2-ones are not epimerized during methanolysis of acetates when CH3ONa/La(OTf)3 is present [62–65].
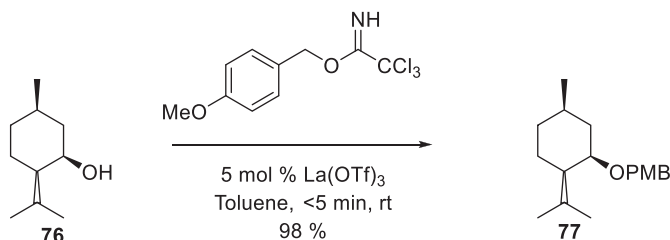

Figure 10.27: La(OTf)$_3$-catalyzed PMB protection of alcohols.

The importance of urea structures has led to the development of numerous synthetic techniques for their manufacture [66–67]. Kim and his co-worker reported the conversion of *N*-benzyloxycarbonyl (**78**), *N*-allyloxycarbonyl, and *N*-trichloroethoxycarbonyl protected amines into nonsymmetric ureas (**80**) by a unique lanthanum triflate mediated process (Figure 10.28) [68]. In this study, it was discovered that lanthanum triflate works well as a catalyst to produce several unsymmetrical ureas from protected amines. Diverse protected aromatic and aliphatic carbamates were observed in the presence of lanthanum triflate which rapidly interacted with different amines to produce the required ureas in high yields. This work showed that ureas prepared from Cbz, Alloc, and Troc carbamates using a unique lanthanum triflate catalyst can be used to create a variety of urea structures.
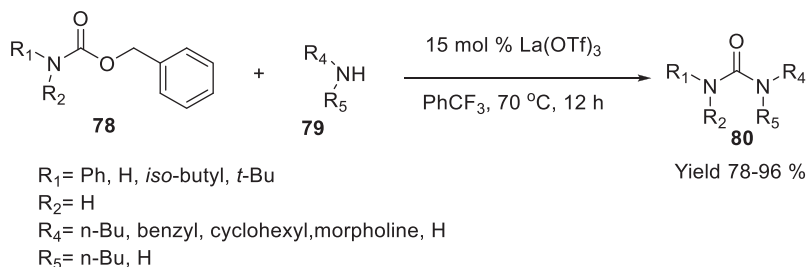
R$_1$= Ph, H, *iso*-butyl, *t*-Bu
R$_2$= H
R$_4$= n-Bu, benzyl, cyclohexyl,morpholine, H
R$_5$= n-Bu, H

Figure 10.28: Lanthanum triflate-catalyzed synthesis of *N*-trichloroethoxycarbonyl protected amines.

10.5 Conclusions

In aqueous media, rare earth metal triflates can act as Lewis acids. These triflates are able to successfully activate aldehydes in water solution, and demonstrated the first evidence of success of Lewis acid-promoted reactions in aqueous media. These reactions could be carried out directly using water-soluble aldehydes like formaldehyde and acetaldehyde. Furthermore, several different reactions could utilize the catalysts in organic solvents. In every instance, the catalyst was easily retrieved and reused once the reaction was finished, requiring just a catalytic amount of triflate. In industrial chemistry, Lewis acid-promoted reactions can take many different forms, and handling the acids in vast quantities that remain after the reactions has had negative effects on the environment. Rare earth metal triflates are anticipated to be novel forms of catalysts offering some solutions to these issues from the perspectives of their catalytic usage and reusability.

References

[1]   Molander, GA. Application of lanthanide reagents in organic synthesis. Chem Rev, 1992, 92, 29–68.
[2]   Imamaoto, T. Lanthanides in Organic Synthesis, London: Academic Press, 1994.
[3]   Marshmann, RW. Rare-earth triflates in organic-synthesis. Aldrichim Acta, 1995, 28, 77.
[4]   Kobayshi, S, Araki, M, Hachiya IA Chiral scandium catalyst for enantioselective Diels-Alder reactions. J Org Chem, 1994, 59, 3758–3759.
[5]   Aspinall, HC, Browning, AF, Greeves, N, Ravenscroft, P. Ytterbium trifluoromethanesulfonate [Yb(OTf)$_3$] as a novel catalyst for the allylation of aldehydes. Tetrahedron Lett, 1994, 35, 4639–4640.
[6]   Tsuchimoto, T, Tobita, K, Hiyama, T, Fukuzawa, SI. Scandium(III) triflate catalyzed friedel-crafts alkylation with benzyl and allyl alcohols. Synlett, 1996, 1996, 557–559.
[7]   Hachiya, I, Moriwaki, M,Kobayashi, S. Hafnium (IV) Trifluoromethanesulfonate, an efficient catalyst for the friedel–crafts acylation and alkylation reactions. Bull Chem Soc Jpn, 1995, 68, 2053–2060.
[8]   Kobayashi, S, Hachiya, I,Yasuda, M. Aldol reactions on solid phase. Sc(OTf)$_3$-Catalyzed aldol reactions of polymer-supported silyl enol ethers with aldehydes providing convenient methods for the

preparation of 1,3-diol, β-hydroxy carboxylic acid, and β-hydroxy aldehyde libraries. Tetrahedron Lett, 1996, 37, 5569–5572.

[9]   Kobayashi, S. Rare earth metal trifluoromethanesulfonates as water-tolerant lewis acid catalysts in organic synthesis. Synlett, 1994, 1994, 689–701.

[10] Thom, KF. US Patent 3615169, 1971, CA 1972, 76, 5436a.

[11] Kobayashi, S. Lanthanide trifluoromethanesulfonates as stable lewis acids in aqueous media. Yb $(OTf)_3$ catalyzed hydroxymethylation reaction of silyl enol ethers with commercial formaldehyde solution. Chem Lett, 1991, 20, 2187–2190.

[12] Collins, S, Hong, Y. Alkyl and aryllanthanum triflates: New reagents for the conversion of tertiary amides to ketones. Tetrahedron Lett, 1987, 28, 4391–4394.

[13] Kobayashi, S, Hachiya, I, Araki, M, Ishitani, H. Scandium trifluoromethanesulfonate $(Sc(OTf)_3)$. A novel reusable catalyst in the Diels-Alder reaction. Tetrahedron Lett, 1993, 34, 3755–3758.

[14] Smith, PH, Raymond, KN. A lanthanide-amine template synthesis. Preparation and molecular structures of $Ln(L)(CH_3CN)(CF_3SO_3)_3$ [L= 1,9-bis(2-aminoethyl)-1,4,6,9,12,14-hexaazacyclohexadecane; Ln = La, Yb] and $La(en)_4(CH_3CN)(CF_3SO_3)_3$. Inorg Chem, 1985, 24, 3469–3477.

[15] Forsberg, JH, Spaziano, VT, Balasubramanian, TM, Liu, GK, Kinsley, SA, Duckworth, CA, Poteruca, JJ, Brown, PS, Miller, JL. UseofLanthanide(III)IonsasCatalystsfortheReactionsofAmineswith Nitriles. J Org Chem, 1987, 52, 1017–1021.

[16] Castellani, CB, Carugo, O, Perotti, A, Sacchi, D, Invernizzi, AG, Vidari, G. Rare earth trifluoromethanesulphonates as catalysts in some meerwein-ponndorf-verley type reductions. J Mol Cat, 1993, 85, 65–74.

[17] Kobayashi, S, Hachiya, I, Ishitani, H, Araki, M. Scandium Trifluoromethanesulfonate $(Sc(OTf)_3)$ as a novel reusable lewis acid catalyst in aldol and michael reactions. Synlett, 1993, 1993, 472–474.

[18] Lipshtz, BH, Sclafani, JA, Takanami, T. Silyl cuprate couplings: Less silicon, accelerated, yet catalytic in copper. J Am Chem Soc, 1998, 120, 4021–4022.

[19] Kawada, A, Mitamura, S, Kobayashi, S. Scandium Trifluoromethanesulfonate. A Novel Catalyst for friedel-crafts acylation. Synlett, 1994, 1994, 545–546.

[20] Kawada, A, Mitamura, S, Kobayashi, S. $Ln(OTf)_3-LiClO_4$ as Reusable Catalyst System for Friedel-Crafts Acylation. Chem Commun, 1996, 183–184.

[21] Ishihara, K, Kubota, M, Kurihara, H, Yamamoto, H. Scandium Trifluoromethanesulfonate as an extremely active acylation catalyst. J Am Chem Soc, 1995, 11, 4413–4414.

[22] Oakes, RS, Heppenstall, TJ, Shezad, N, Clifford, AA, Rayner, CM. Use of scandium tris (trifluoromethanesulfonate) as a Lewis acid catalyst in supercritical carbon dioxide: Efficient Diels–Alder reactions and pressure dependent enhancement of endo: Exostereoselectivity. Chem Commun, 1999, 1459–1460.

[23] Legler, G. Glycoside hydrolases: Mechanistic information from studies with reversible and irreversible inhibitors. Adv Carbohydr Chem Biochem, 1990, 48, 319–384.

[24] Waldmann, H. Asymmetric Hetero Diels-Alder Reactions. Synthesis, 1994, 1994, 535–551.

[25] Zulfiqar, F, Kitazume, T. One-pot aza-Diels–Alder reactions in ionic liquids. Green Chem, 2000, 2, 137–139.

[26] Castellani, CB, Carugo, O, Perotti, A, Sacchi, D, Invernizzi, AG, Vidari, G. Rare earth trifluoromethanesulphonates as catalysts in some Meerwein-Ponndorf-Verley type reductions. J Mol Cat, 1993, 85, 65–74.

[27] Gillespie, KM, Munslow, IJ, Scott, P. Stereoselective catalytic Tishchenko reduction of β-hydroxyketones using scandium triflate. Tetrahedron Lett, 1999, 40, 9371–9374.

[28] Kotsuki, H, Arimura, K, Araki, T, Shinohara, T. $Sc(OTf)_3$- and TfOH-catalyzed baeyer-villiger oxidation of carbonyl compounds with m-chloroperbenzoic acid. Synlett, 1999, 1999, 462–464.

[29] Ishihara, K, Karumi, Y, Kubota, M, Yamamoto, H. Scandium trifluoromethanesulfonimide and scandium trifluoromethanesulfonate as extremely active acetalization catalysts. Synlett, 1996, 1996, 839–840.

[30] Aggarwal, VK, Fonquerna, S, Vennall, GP. Sc(OTf)$_3$, an efficient catalyst for formation and deprotection of geminal diacetates (Acylals): Chemoselective protection of aldehydes in presence of ketones. Synlett, 1998, 1998, 849–852.

[31] Fukase, K, Kinoshita, I, Kanoh, T, Nakai, Y, Hasuoka, A, Kusumoto, S. A novel method for stereoselective glycosidation with thioglycosides: Promotion by hypervalent iodine reagents prepared from PhIO and various acids. Tetrahedron, 1996, 52, 3897–3904.

[32] Oriyama, T, Kobayashi, Y, Noda, K. Chemoselective and Practical Deprotection of Alkyl Trialkylsilyl Ethers in the Presence of Aryl Trialkylsilyl Ethers by a Catalytic Amount of Sc(OTf)$_3$. Synlett, 1998, 1998, 1047–1048.

[33] Suzuki, T, Watahiki, T, Oriyama, T. A novel and efficient method for the silylation of alcohols with methallylsilanes catalyzed by Sc(OTf)$_3$. Tetrahedron Lett, 2000, 41, 8903–8906.

[34] Mehta, S, Whitfield, D. Beneficial participation of the polymer: Improvement in polymer-supported oligosaccharide synthesis. Tetrahedron Lett, 1998, 39, 5907–5910.

[35] Kobayashi, S, Siguira, M, Kitagawa, H, Lam WW. Rare-earth metal triflates in organic synthesis. Chem Rev, 2002, 102, 2227–2302.

[36] De, SK, Gibbs, RA. Scandium(III) triflate as an efficient and reusable catalyst for synthesis of 1,5-benzodiazepine derivatives. Tetrahedron Lett, 2005, 46, 1811–1813.

[37] Marzieh, S, Sohrab, T, Asghar, KA, Soleymani, JM. Esterification of carboxylic acids with alcohols under microwave irradiation in the presence of zinc triflate. J Chem Res, 2003, 3, 172–173.

[38] Mulzer, J. In: Comprehensive Organic Synthesis, Trost, BM, Fleming, I, ed., Pergamon Press, Oxford, 1991, vol. 6, 323.

[39] Trost, BM. Atom economy-a challenge for organic synthesis: homogeneous catalysis leads the way. Angew Chem Int Ed Engl, 1995, 34, 259–281.

[40] Barrett, AGM, Braddock, DC. Scandium(III) or lanthanide(III) triflates as recyclable catalysts for the direct acetylation of alcohols with acetic acid. Chem Commun, 1997, 351–352.

[41] Jennings, JJ, Bhatt, CP, Franz, AK. Lanthanum(III)-catalyzed three-component reaction of coumarin-3-carboxylates for the synthesis of indolylmalonamides and analysis of their photophysical properties. J Org Chem, 2016, 81, 6211–6222.

[42] Park, BY, Ryu, KY, Park, JH, Lee, S. A dream combination for catalysis: Highly reactive and recyclable scandium(iii) triflate-catalyzed cyanosilylations of carbonyl compounds in an ionic liquid. Green Chem, 2009, 11, 946–948.

[43] Sultana, S, Bondalapati, S, Indukuri, K,Gogoi, P, Saha, P, Saikia, AK. Scandium(III) triflate catalyzed synthesis of primary homoallylic alcohols via carbonyl-ene reaction. Tetrahedron Lett, 2013, 54, 1576–1578.

[44] Yadav, JS, Reddy, BVS, Rao, KVR,Narayana Kumar GGKS. Sc(OTf)3-catalyzed alkylation of indoles with propargyl alcohols: An expeditious synthesis of 3-substituted indoles. Tetrahedron Lett 2007, 48, 5573–5576.

[45] Morikawa, O,Nagamatsu, Y, Nishimura, A, Kobayashi, K, Konishi, H. Scandium triflate-catalyzed cyclocondensation of 1,3-dialkoxybenzenes with 1,3,5-trioxane. Formation of resorcin[4]arenes and confused resorcin[4]arenes. Tetrahedron Lett, 2006, 47, 3991-3994.

[46] Allam, BK, Singh, KN. Highly efficient one-pot synthesis of primary amides catalyzed by scandium (III) triflate under controlled MW. Tetrahedron Lett, 2011, 52, 5851–5854.

[47] Yadav, JS, Reddy, BVS, Veerendhar, G, Rao, RS, Nagaiah, K. Sc (OTf)3 Catalyzed Electrophilic Amination of Arenes: An Expeditious Synthesis of Aryl Hydrazides. Chem Lett, 2002, 31, 318–319.

[48] Coca, A,Turek, E,Feinn, L. Preparation of 5-Substituted 1H-tetrazoles catalyzed by scandium triflate in water. Synth Commun, 2015, 45, 218–225.

[49] Agrebi, A, Allouche, F, Chabchoub, F, El-Kaim, L, Alves, S,Baleizão, C, Farinha, JP. Sc(OTf)3 promoted multicomponent synthesis of fluorescent imidazo[1,2-c]pyrazolo[3,4-d]pyrimidine. Tetrahedron Lett, 2013, 54, 4781–4784.

[50] Kumari, K, Raghuvanshi, DS, Jouikov, V, Singh, KN. Sc(OTf)3-catalyzed, solvent-free domino synthesis of functionalized pyrazoles under controlled microwave irradiation. Tetrahedron Lett, 2012, 53, 1130–1133.

[51] Kikuchi, S, Iwai, M, Murayama, H,Fukuzawa, S. Catalytic synthesis of 1,4-dihydropyridine derivatives using scandium(III) triflate. Tetrahedron Lett, 2008, 49, 114–116.

[52] Atkinson, BN, Williams, JMJ. Scandium triflate catalyzed ester synthesis using primary amides. Tetrahedron Lett, 2014, 55, 6935–6938.

[53] Liang, G, Chen, J, Chen, J, Li, W, Chen, J, Wu, H. Sc(OTf)3-catalyzed synthesis of thiosulfonates in ionic liquid-water. Tetrahedron Lett, 2012, 53, 6768–6770.

[54] Kobayashi, S, Hachiya, I, Takahori, T, Araki, M, Ishitani, H. Lanthanide trifluoromethanesulfonates as reusable catalysts. Michael and Diels-Alder reactions. Tetrahedron Lett, 1992, 33, 6815–6818.

[55] Forsberg, JH, Spaziano, VT, Balasubramanian, TM, Liu, GK, Kinsley, SA, Duckworth, CA, Poteruca, JJ, Brown, PS, Miller, JL. Use of lanthanide(III) ions as catalysts for the reactions of amines with nitriles. J Org Chem 1987, 52, 1017–1021.

[56] Qian, C, Wang, L. Addition of silyl ketene acetals to nitrones catalyzed by lanthanide triflates. Tetrahedron, 2000, 56, 7193–7197.

[57] Hatanaka, F, Tsuchiya, M, Yoshimatsu, M. The first synthesis and reaction of β-ethoxy-α-fluoro-α-(phenyl-selanyl)ethene: scandium or lanthanum triflate catalyzed α-fluoroformylalkenylation of aldehydes. Synlett, 2005, 2005, 2191–2194.

[58] Rai, NA, Basu, A. An efficient method for para-methoxybenzyl ether formation with lanthanum triflate. Tetrahedron Lett, 2003, 44, 2267–2269.

[59] Cameron, LL, Wang, SC, Kluger, R. Biomimetic monoacylation of diols in water. Lanthanide-promoted reactions of methyl benzoyl phosphate. J Am Chem Soc, 2004, 126, 10721–10726.

[60] Kluger, R, Cameron, LL. Activation of acyl phosphate monoesters by lanthanide ions: enhanced reactivity of benzoyl methyl phosphate. J Am Chem Soc, 2002, 124, 3303–3308.

[61] Tsang, JSW,Neverov, AA, Brown, RS. La^{3+}-Catalyzed Methanolysis of Hydroxypropyl-p-nitrophenyl Phosphate as a Model for the RNA Transesterification Reaction. J Am Chem Soc, 2003, 125, 1559–1566.

[62] Stefano, SD, Leonelli, F, Garofalo, B, Mandolini, L, Bettolo, RM, Migneco, LM. Elusive 6-exo-Hydroxybicyclo[2.2.2]octan-2-ones from the Corresponding acetates by methanolysis in the Presence of CH3ONa/La(OTf)3. Org Lett, 2002, 4, 2783–2785.

[63] Brown, RS, Neverov, AA. Acyl and phosphoryl transfer to methanol promoted by metal ions. J Chem Soc Perkin Trans. 2, 2002, 1039–1049.

[64] Neverov, AA, McDonald, T, Gibson, G, Brown, RS. Catalysis of transesterification reactions by lanthanides – Unprecedented acceleration of methanolysis of aryl and alkyl esters promoted by La(OTf)3 at neutral sspH and ambient temperatures. Can J Chem, 2001, 79, 1704–1710.

[65] Neverov, AA, Montoya-Pelaez, PJ, Brown, RS. Catalysis of the Methanolysis of Activated Amides by Divalent and Trivalent Metal Ions. The Effect of Zn^{2+}, Co^{2+}, and La^{3+} on the Methanolysis of Acetylimidazole and Its (NH3)5CoIII Complex. J Am Chem Soc, 2001, 123, 210–217.

[66] Van Gool, M, Bartolomé, JM, Macdonald, GJ. An easy and versatile synthesis of ureas from 2-benzylaminopyrimidine. Tetrahedron Lett, 2008, 49, 7171–7173.

[67] Gallou, I. Unsymmetrical ureas. Synthetic methodologies and application in drug design. Org Prep Proced Int, 2007, 39, 355–383.

[68] Buia, TT, Kim, HK. Lanthanum(III) Trifluoromethanesulfonate Catalyzed Direct Synthesis of Ureas from N-Benzyloxycarbonyl-, N-Allyloxycarbonyl-, and N-2,2,2-Trichloroethoxycarbonyl-Protected Amines. Synlett 2020, 31, 997–1002.

Gyan Chandra Pariyar, Bijeta Mitra, Suvodip Mukherjee
and Pranab Ghosh[*]

11 Cerium (IV) ammonium nitrate (CAN)-catalyzed selective synthesis of *O*- and *S*-heterocycles

11.1 Introduction

Fifteen elements from atomic number 57–71 are termed "lanthanides." Cerium also belongs to this family. They are also known to be rare earth elements due to their minimal occurrence on the Earth's crust. Among these elements, cerium is considered to be the most abundant and it contributes nearly 0.0046% by weight of the coating of Earth. In reality, cerium should not be classified under rare elements, because its abundance is the same or more than other familiar elements such as cobalt, copper, zinc, bromine, tin, etc.

Among the lanthanides, cerium has a few properties that are unique as compared to other members of the group. Cerium can stay in double steady oxidation states of + 3 and + 4, having configurations as $[Xe]4f^1$ and $[Xe]4f^0$, respectively. The existence of unfilled f orbital imparts additional stabilization to the latter configuration as compared to the former, which gives its capability to take part in the single-electron transfer reactions. Ce(IV) has a high reduction potential of 1.61 V as compared to normal hydrogen electrode, and for this reason, it proves to be an excellent oxidizing reagent when compared to the other cations. Hence, cerium (IV) ammonium nitrate (CAN), which is easily available, has been widely explored as single-electron oxidizing agent [1]. In fact, when compared with manganese triacetate, the property to generate radicals in CAN is regarded to be superior [2].

CAN is a solid orange-colored inorganic compound that is easily soluble in water. The salt comprises of hexanitratocerate (IV) anion $[Ce(NO_3)_6]^{2-}$ and a pair of ammonium cations $[NH_4]^+$. In the structure of CAN, each nitrate group chelates the cerium atom in a bidentate manner (Figure 11.1). Being less toxic, having reasonable solubility

[*]**Corresponding author: Pranab Ghosh**, Department of Chemistry, University of North Bengal, Dist. Darjeeling, West Bengal, India, e-mail: pizy12@yahoo.com
Gyan Chandra Pariyar, Department of Food Technology, University of North Bengal, Dist. Darjeeling, West Bengal, India
Bijeta Mitra, Suvodip Mukherjee, Department of Chemistry, University of North Bengal, Dist. Darjeeling, West Bengal, India
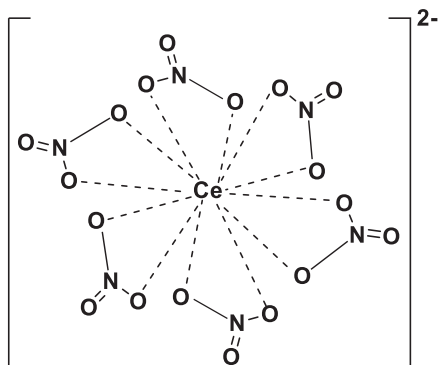
Figure 11.1: Structure of cerric ammonium nitrate (CAN).

in organic solvents, and being air-stable, inexpensive, and manageable are some of the additional properties of CAN that gives it an extra edge for its catalytic activities.

It was Heiba and Dessau [3] who first successfully employed Ce(IV)-generated radicals as an important tool for the synthesis of C-C bonds, after which it has been successfully employed for the construction of carbon-hetero bonds. From literature survey, it has been found that CAN is also useful in the formation of carbon-carbon [4] and carbon-hetero bond [5–13], as well as heterocyclic compounds such as tetrazole [14], benzimidazole [15], triazole [16], oxadiazole [17], pyrazole [18] 1,4-naphthoquinone [19], oxazole [20], triazoloquinazolinone [21], and many more [22–24].

Every person in this world will suffer from one disease or another. Hence, there is need to develop medicinal compounds that will help fight against various diseases. Researchers all around the world put in their best efforts to construct new compounds that will be helpful to treat and cure various diseases. In this regard, heterocyclic moieties are found to play an immense role in constructing biologically active compounds [25].

Sulfur-hetero compounds are regarded as one of the most important classes of heterocyclic compounds that have an immense utility in various fields of chemistry [26]. Several sulfur-containing structural fragments are found to exist in various natural bioactive compounds. [27]. In addition, due to the volatile nature and reactivity of sulfur compounds, they also have their use as flavoring agents in food products such as meat, vegetables, roasted products like coffee, peanuts, cocoa, etc. [28]. Sulfur-containing heterocyclic compounds have huge importance in pharmacology, due to its antiviral, anticancer, antimicrobial, anti-inflammatory, antitubercular activities, etc. The most important sulfur-containing heterocyclic compounds explored for drug designing are thiazole, thiophene, isothiazole, thiazoline, thiazepine, and thiopyran. Several drugs that are FDA approved possess sulfur heterocyclic compounds. Examples are Raloxifene [29], a famous drug used to treat breast cancer, Clopidogrel [30] used against artery disorder, Ritonavir [31], an important antiviral agent, Rosiglitazone [32] used against diabetes, and Thiabendazole [33], used for its antifungal activities.

Oxygen atom-containing heterocyclic compounds are another important class of heterocyclic compounds. They are extensively used as solvents, fragrances, and potent drugs. These compounds are found as key structural units in various natural products, biologically active compounds, and pharmaceuticals [34–36]. Various natural as well as semisynthetic oxygen-hetero compounds such as Taxol [37] used as an anticancer agent, Digoxin used for CHF treatment, Cyclosporine-A, used as immunosuppressant, and Lovastatin used as hypolipidemic, etc. are compounds known for their therapeutic values [38]. Some examples of oxygen-hetero and sulfur-hetero compounds are shown in Figure 11.2.
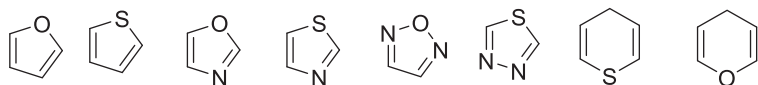

Figure 11.2: Some oxygen-hetero and sulfur-hetero compounds.

11.2 CAN-assisted synthesis of *O*-heterocycles

## 11.2.1 Solvent-free CAN-mediated synthesis

Kumar et al. [39] demonstrated one-pot three-component reaction between 2-naphthol **(1)**, aldehydes **(2)**, and 1.3-diketones **(3)** in the presence of CAN to produce libraries of benzoxanthenes **(4)** under solvent-free conditions (Figure 11.3). The effect of solvents was found to affect the efficiency of the reaction. The yield of the product was found to be better in more polar solvents as compared to less polar ones. However, the best results were reported under solvent-free conditions. Further, 14-phenyl-14 *H*-dibenzo[*a-j*]xanthene was obtained as a side product in all solution-phase reactions but the same was not formed under solvent-free conditions. The synthesized compounds were screened to evaluate their antiproliferative activities, and most of the compounds showed promising results.

They further extended their methodology by using malononitrile or ethyl cyanoacetate **(5)** along with 2-naphthol **(1)** and aldehydes **(2)** (Figure 11.4). In this CAN-mediated multicomponent reaction, good to excellent yield of benzochromes **(6)** were isolated. They also realized that in the absence of cyclic 1,3-diketone, CAN catalyzed the reaction between aldehydes and β-naphthol **(1)**, resulting in the synthesis of substituted-14 *H*-dibenzo[*a*, *j*]xanthene derivatives **(7)** under solvent-free conditions (Figure 11.5).
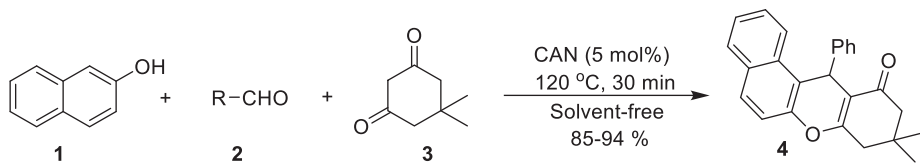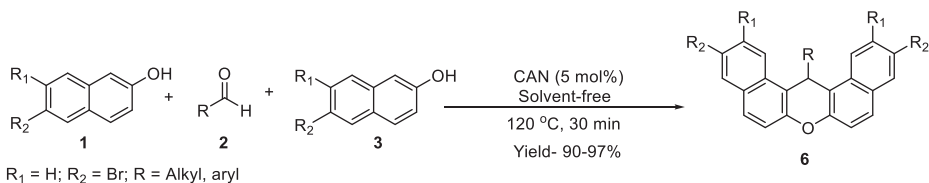
R = Aromatic, aliphatic, heterocyclic

Figure 11.3: One-pot three-component synthesis of benzoxanthenes.
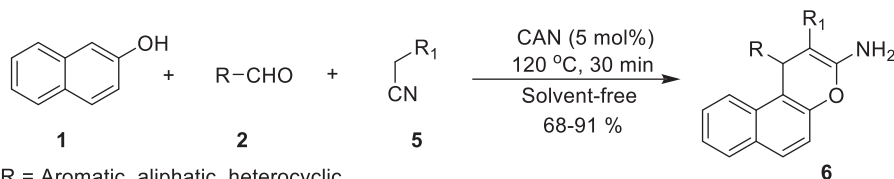
R = Aromatic, aliphatic, heterocyclic
R_1 = CN, COOEt

Figure 11.4: One-pot three-component synthesis of benzochromes.

R_1 = H; R_2 = Br; R = Alkyl, aryl

Figure 11.5: CAN-catalyzed synthesis of substituted-14 *H*-dibenzo[*a*, *j*]xanthene.

11.2.2 Microwave-assisted CAN-mediated synthesis

Jardosh et al. [40] depicted the preparation of 1 *H*-benzo[*b*]xanthenes **(10)** and 4 *H*-benzo [*g*]chromene **(11)** having *N*-allyl quinolone nucleus by using the microwave as a potential tool by the one-pot three-component reaction of *N*-allyl quinolone-3-carbaldehydes **(7)**, 2-hydroxy-1,4-naphthoquinone **(8),** and dimedone or malononitrile **(9),** respectively (Figure 11.6). This one-pot three-component reaction was catalyzed by 5 mol% CAN and the reaction was carried out under solvent-free conditions. The methodology allowed the construction of new biologically active molecules by incorporation of two bioactive moieties. Further, they found out on the basis of SAR analysis that the antimicrobial efficiencies of the products were dependent on the lipophilicity and electronic influence of the various groups present in the product. It was reported that compounds having benzo[*g*]chromene **(11)** nucleus were more promising than those containing benzo[*b*] xanthenes **(10)** nucleus.

Reddy et al. [41] were successful in synthesizing substituted coumarins (**13**) by means of Pechmann condensation, where phenols (**11**) and β-ketoesters (**12**) reacted together in solvent-free conditions (Figure 11.7). Both the conventional heating method and microwave irradiation were used in the methodology. Taking CAN as the catalyst, this simple and efficient methodology was reported to furnish good yield of the products in both the procedures.
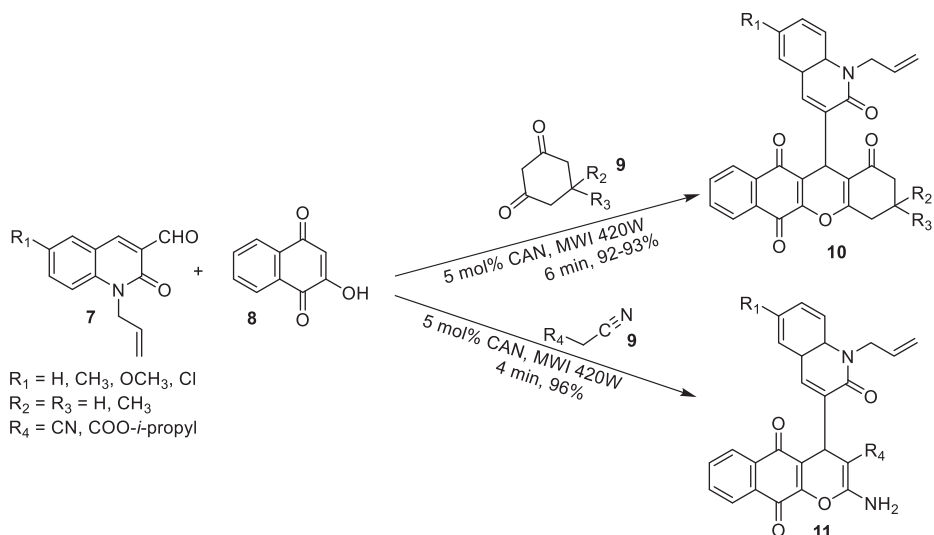

R_1 = H, CH$_3$, OCH$_3$, Cl
R_2 = R_3 = H, CH$_3$
R_4 = CN, COO-i-propyl

Figure 11.6: Microwave-induced CAN-promoted atom-economic synthesis of 1 *H*-benzo[*b*]xanthene and 4 *H*-benzo[*g*]chromene.

11
12
R = OH, CH$_3$, Ph
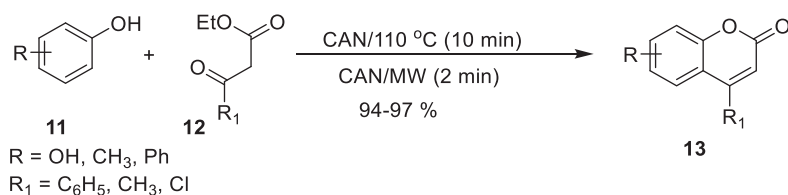R_1 = C$_6$H$_5$, CH$_3$, Cl

13

Figure 11.7: CAN-induced coumarin synthesis via Pechmann condensation using conventional heating and microwave irradiation.

11.2.3 Ultrasound-assisted CAN-mediated synthesis

Sudha et al. [42] proposed the use of ultrasound for the synthesis of tetrahydrobenzo[*c*]xanthene-11-ones (**15**). By using passive α-naphthol (**14**) and reacting with aromatic aldehydes (**2)** and dimedone (**3),** they were able to carry the synthesis of tetrahydrobenzo

[*c*]xanthene-11-ones using ultrasound in presence of catalytic amount of CAN (Figure 11.8). This energy efficient novel method was proposed by them to be both economical and environmentally friendly. Further according to them, they were able to overcome formation of by-products, high temperature, and low yield of the products by using the protocol.

Dandia et al. [43] introduced a facile and efficient method for the designing of a diverse array of 5-phenyl-5,6- dihydro-1 *H*-pyrano[2,3-*d*]pyrimidine-2,4,7(3 *H*)-trione (**17**) (Figure 11.9). In this one-pot multicomponent methodology, dimedone (**3**), aldehydes (**2**), and barbituric acid (**16**) were reacted employing CAN (10 mol%) as a catalyst, in the presence of ultrasonic irradiation using water as the medium. Various catalysts were scanned under the reaction condition, but they reported CAN to be the best one giving good to excellent results.
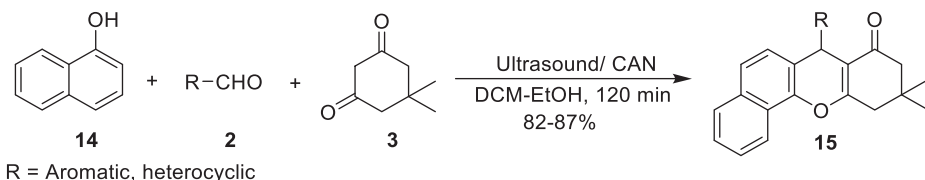

R = Aromatic, heterocyclic

Figure 11.8: CAN-mediated synthesis of tetrahydrobenzo[*c*]xanthene-11-ones in ultrasound.
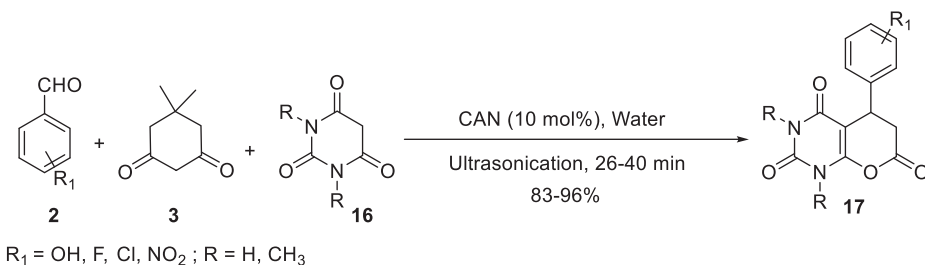

R₁ = OH, F, Cl, NO₂ ; R = H, CH₃

Figure 11.9: Preparation of 5-phenyl-5,6- dihydro-1 *H*-pyrano[2,3-*d*]pyrimidine-2,4,7(3 *H*)-trione derivatives using CAN.

11.2.4 CAN-mediated synthesis of *O*-heterocycles in various solvents

Baciocchi et al. [44], back in the year 1988, were able to synthesize 2-alkyl-3-acylfurans (**21**) or 2-alkyl-3-carboalkoxyfurans by a simple method involving the addition of carbonyl compounds and alkenes in the presence of CAN (Figure 11.10). During their research, they found that in the presence of CAN, when 1,3-dicarbonyl compound (**18**) was allowed to react with vinyl acetate (**19**), 5-acetoxy-4,5-dihydrofuran (**20**) was obtained. The 5-acetoxy-4,5-dihydrofurans (**20**) thus formed were then converted into furan derivatives in considerably good yield by simply refluxing in toluene in the

presence of pyridinium tosylate. However, during the course of their study, they also found that the yield of the product was low when the alkene used was propenyl acetate. According to them, the lower yield was due to the steric effect of methyl group present in the 2-position of vinyl acetate. One of the products that were synthesized by this methodology was the naturally occurring furano-monoterpene evodone.

Itoh et al. [45] reported the synthesis of isoxazole derivatives by the reaction of dipolarophiles with CAN, in the presence of acetone or acetophenone (Figure 11.11). They used several alkenes (**23**) and refluxed them in acetone with CAN(IV), where 3-acetyl-4,5-dihydroisoxazoles (**24**) were obtained, while heating with acetophenone (**22**) at 80 °C furnished 3-benzoyl-4,5-dihydroisoxazoles. When a similar reaction was tried using alkynes (**25**), the corresponding 3-acetylisoxazole and 3-benzoylisoxazoles (**26**) were the isolated products. Further attempts were made to elaborate the reaction when they found that better yield of the products was obtained by using CAN(III)-formic acid.
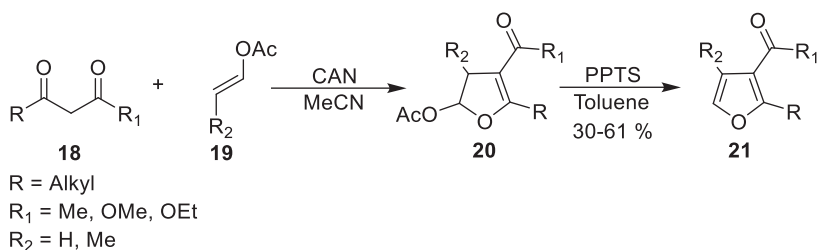

R = Alkyl
R$_1$ = Me, OMe, OEt
R$_2$ = H, Me

Figure 11.10: CAN-mediated synthesis of 2-alkyl-3-acylfurans.

R = Me, Ph
R$_1$ = C$_6$H$_{13}$, CH$_2$C$_6$H$_{11}$, CH$_2$Ph, CH$_2$CN
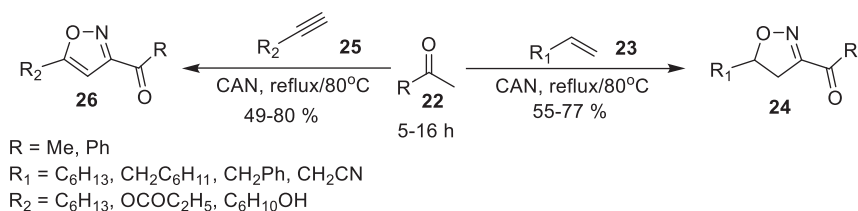R$_2$ = C$_6$H$_{13}$, OCOC$_2$H$_5$, C$_6$H$_{10}$OH

Figure 11.11: CAN-mediated one-pot synthesis of isoxazole derivatives.

They have also proposed the plausible mechanism for the reaction (Figure 11.12), where the reaction was said to have gone through furoxan as an intermediate. They confirmed the formation of furoxan as an intermediate, which proved that acetone was first converted into nitrile oxide via nitration of acetone by CAN(IV) or CAN(III). The nitrile oxide thus formed then underwent 1,3-dipolarcycloaddition with alkenes or alkynes to produce the isoxazole derivatives or dimerization to give furoxan.

Maiti et al. [46] published a robust procedure catalyzed by CAN for the 1,3-oxathioacetalisation of carbonyl compounds (Figure 11.13). When library of aldehydes
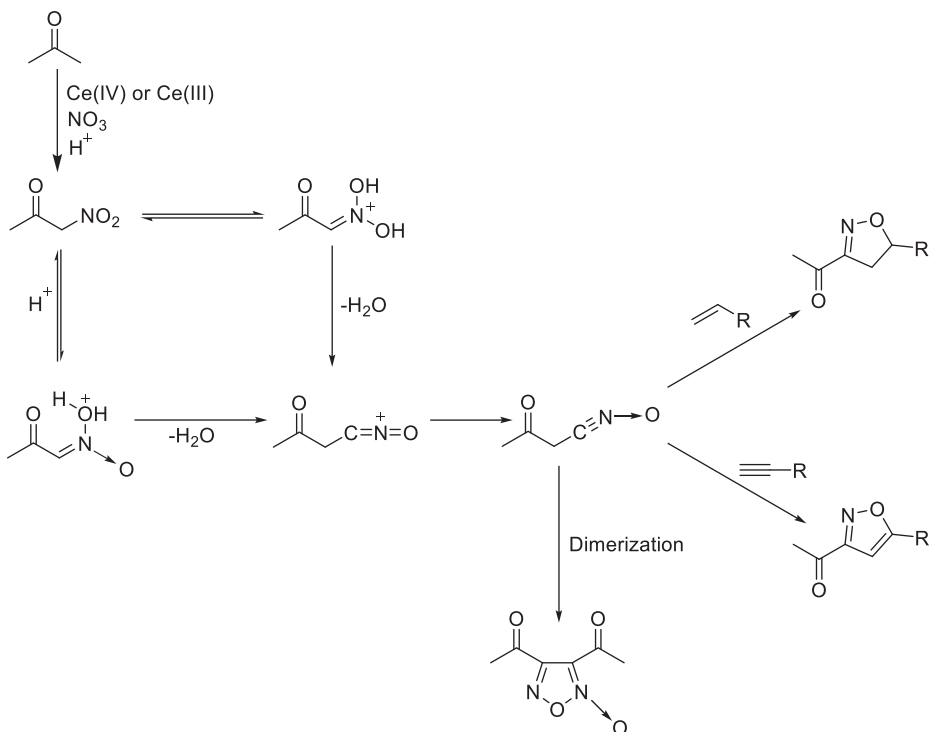
Figure 11.12: Reaction mechanism for one-pot synthesis of isoxazole derivatives.

and ketones **(27)** were treated with 2-mercaptoethanol **(28)** using acetonitrile as a solvent, good to excellent yield of oxathioacetals **(29)** was isolated at ambient temperature. A large variety of solvents were scanned but product formation in acetonitrile was found to give the best results. Most of the alkyl and aryl aldehydes and ketones gave good results but with diaryl and cyclic aryl ketones, no product was isolated even after carrying the results for 30 h.

Undeela et al. [47] published a simple synthetic procedure for the synthesis of furan derivatives **(32)**. This two-step oxidative cyclization involved condensation of aryl alkynes **(30)** and ketones **(31)**, furnishing a variety of substituted furans in the presence of a combination of CAN and potassium bromide as catalyst (Figure 11.14).

Sudha et al. [48] also did the comparative study on the reaction where the products obtained by using ultrasound were compared to those obtained without using them. They reported that during the silent conditions, 1,8-dioxo-dodecahydroxanthene **(33)** was found to be the predominating product (Figure 11.15), whereas under the ultrasonic conditions, tetrahydrobenzo[c]xanthene-11-one was the main product. Hence, they were able to highlight the importance of ultrasound in this reaction methodology.
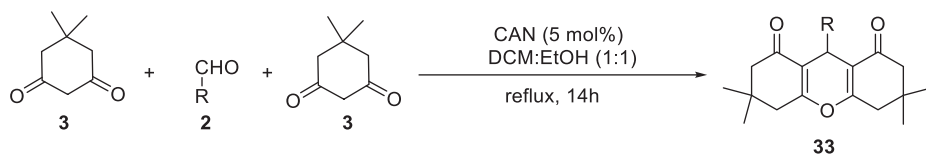
Figure 11.13: CAN-catalyzed synthesis of 1,3-oxathianes.
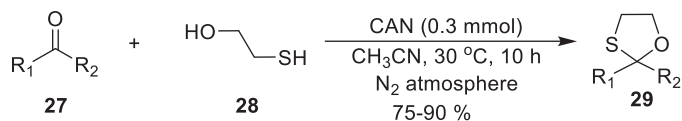
R_1 = Aromatic, aliphatic, heterocyclic
R_2 = H, CH_3
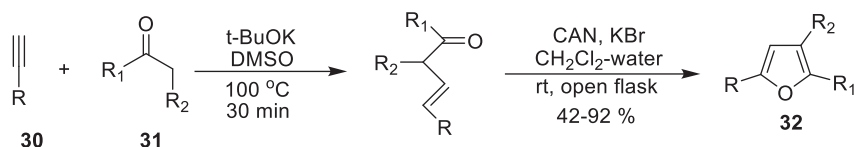
R = Aromatic
R_1 = Aromatic
R_2 = H, CH_3

Figure 11.14: Synthesis of substituted furans from aryl alkynes and ketones mediated by CAN.

R = Alkyl, aryl, heterocycles

Figure 11.15: Formation of 1,8-dioxo-dodecahydroxanthene under solvent-free silent condition.

Puligoundla et al. [49] demonstrated an efficient and cost-effective one-pot three-component protocol for the synthesis of tetrahydropyranoquinoline derivatives **(36 or 37)**. Aromatic amines **(34)**, aromatic aldehyde, and 3,4-dihydro-2 *H*-pyran **(35)** were condensed together in the presence of CAN as a catalyst for the synthesis of tetrahydropyranoquinoline derivatives (Figure 11.16).

Brahmachari et al. [50] published a facile one-pot synthesis of a library of 3,3′-(aryl-methylene)bis(4-hydroxy-2 *H*-chromen-2-one) **(39)** (Figure 11.17). By using a series of aromatic aldehydes **(2)** and 4-hydroxyl-coumarin **(38)**, this pseudo three-component reaction furnished 3,3′-(arylmethylene)bis(4-hydroxy-2 *H*-chromen-2-one) **(39)** in good to excellent yield. They used commercially available eco-friendly CAN as the catalyst and water as a medium in this reaction. Energy-efficiency, clean reaction profile, reusability, ease of purification, large synthetic applications, high atom economy, and being environmentally friendly were some of the advantages of the reaction, as proposed by them.
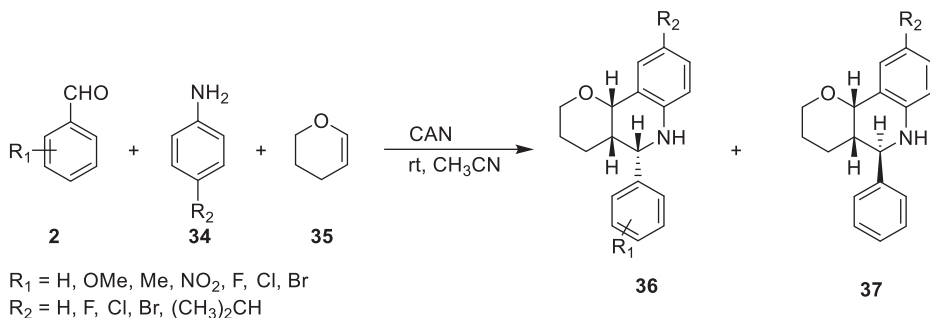
R$_1$ = H, OMe, Me, NO$_2$, F, Cl, Br
R$_2$ = H, F, Cl, Br, (CH$_3$)$_2$CH

Figure 11.16: Ceric ammonium nitrate–catalyzed preparation of tetrahydropyranoquinoline.

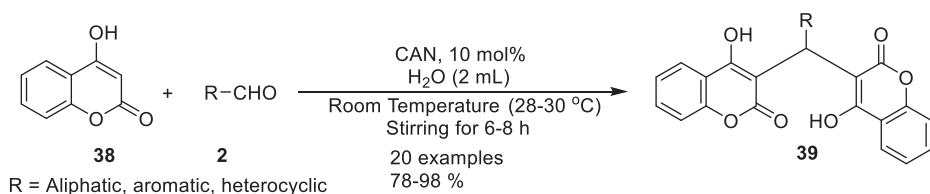
R = Aliphatic, aromatic, heterocyclic

Figure 11.17: CAN-assisted designing of diversely functionalized biscoumarins.

11.3 CAN-mediated synthesis of *S*-heterocycles

Al-Qalaf et al. [51] successfully used CAN for the first time for one-pot synthesis of 2-arylbenzothiazoles (Figure 11.18). They reported the reaction to be among the few where one-pot synthetic route for the synthesis of 2-arylbenzothiazoles **(41)** from aromatic aldehydes **(2)** and 2-aminothiophenol **(40)** was achieved under ambient condition.
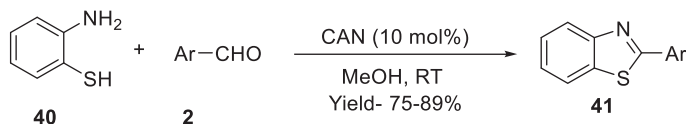

Figure 11.18: Synthesis of benzothiazoles using CAN.

11.4 Conclusions

In summary, we found that heterocyclic compounds have been extensively used as biologically active compounds. Most of the drugs designed to combat various illnesses in use today contain heterocyclic parts. A number of different methodologies have been

developed so far for the synthesis of heterocyclic compounds. Among the various catalysts used, CAN has emerged, so far, as a facile environmentally friendly catalyst for the synthesis of various sulfur-hetero as well as oxygen-hetero compounds. In addition, being less toxic, having reasonable solubility in organic solvents, being air-stable and inexpensive, and ease in management are some of the additional properties of CAN that give an extra edge, as compared to other catalysts.

References

[1]   Ho, TL. Ceric ion oxidation in organic chemistry. Synthesis, 1973, 347.

[2]   Nair, V, Mathew, J, Radhakrishnan, KV. Oxidative addition of 1,3-dicarbonyl compounds to alkenes mediated by cerium(IV) ammonium nitrate and manganese(III) acetate: A comparative study. J Chem Soc Perkin Trans, 1996, 1, 1487–1492.

[3]   Heiba, EI, Dessau, RM. Oxidation by metal salts. VII. Syntheses based on the selective oxidation of organic free radicals. J Am Chem Soc, 1971, 93, 524–527.

[4]   Brahmachari, G, Banerjee, B. Ceric ammonium nitrate (CAN): An efficient and eco-friendly catalyst for the one-pot synthesis of alkyl/aryl/heteroaryl-substituted bis(6- aminouracil-5-yl)methanes at room temperature. RSC Adv, 2015, 5, 39263–39269.

[5]   Shivaji, VM, Sastry, MNV, Yao, C-F. Cerium (IV) ammonium nitrate (CAN) as a catalyst in tap water: A simple, proficient and green approach for the synthesis of quinoxalines. Green Chem, 2006, 8, 91–95.

[6]   Shitolea, BV, Shitoleb, NV, Kakde, GK. A Simple, Proficient and green approach for the synthesis of 1,8-Dioxo-octahydroxanthenes catalyzed by cerium(IV) ammonium nitrate in aqueous media. Orbital: Electron J Chem, 2014, 6, 191–194.

[7]   Sangshetti, JN, Kokare, ND, Kotharkara, SA, Shinde, DB. Ceric ammonium nitrate catalysed three component one-pot efficient synthesis of 2,4,5-triaryl-1*H*-imidazoles. J Chem Sci, 2008, 120, 463–467.

[8]   Tapaswi, PK, Mukhopadhyay, C. Ceric ammonium nitrate (CAN) catalyzed one-pot synthesis of fully substituted new indeno[1,2-b]pyridines at room temperature by a multi-component reaction. Arkivoc. 2011, x, 287–298.

[9]   Dandia, A, Gupta, SL, Bhaskaran, S. Cerric ammonium nitrate (CAN) catalysed synthesis of pyrano [2,3-*d*]pyrimidine-2,4,7-triones in aqueous medium under sonication via one-pot three component reacton. Eur Chem Bull, 2013, 2, 836–841.

[10]   Kidwai, M, Bhatnagar, D. Ceric ammonium nitrate (CAN) catalyzed synthesis of N-substituted decahydroacridine-1,8-diones in PEG. Tetrahedron Lett, 2010, 51, 2700–2703.

[11]   Madabhushi, S, Vangipuram, VS, Mallu, KKR, Jillella, R, Kurva, S, Pamulaparthi, SR. Ceric (IV) ammonium nitrate (CAN) mediated synthesis of pyrrole-2,3,4,5-tetracarboxylates by reaction of dimethyl acetylene dicarboxylate with an amine. Tetrahedron Lett, 2013, 54, 6737–6739.

[12]   Sridharan, V, Maiti, S, Menéndez, JC. A Very Efficient Cerium(IV) ammonium nitrate catalyzed, four-component synthesis of tetrahydropyridines and its application in the concise generation of functionalized homoquinolizine frameworks. Eur J Chem, 2009, 15, 4565–4572.

[13]   Sridharan, V, Maiti, S, Menéndez, JC. Efficient generation of highly functionalized fused oxazepine frameworks based on a CAN-catalyzed four-component tetrahydropyridine synthesis/ring-closing metathesis sequence. J Org Chem, 2009, 74, 9365–9371.

[14]   Paramasivam, S, Kaliyan, B, Rangasamy, R, Appaswami, L. Synthesis of 5-substituted 1*H*-tetrazoles catalyzed by ceric ammonium nitrate supported HY-zeolite. Tetrahedron Lett, 2014, 55, 5683–5686.

[15]   Kamal, US, Fawzia, A-Q, Ramadan, AM, Mohamed, HE. Cerium (IV) ammonium nitrate-mediated reactions: Simple route to benzimidazole derivatives. Arab J Chem. 5, 2012, 2012, 63–66.

[16]   Mangarao, N, Ramu, T, Srinuvasarao, R, Prasanthi, S, Siddaiah, V. A simple and efficient synthesis of 3,4,5-Trisubstituted/N-Fused 1,2,4-Triazoles via ceric ammonium nitrate catalyzed oxidative cyclization of amidrazones with aldehydes using polyethylene glycol as a recyclable reaction medium. Synthesis, 2015, 47, 517–525.

[17]   Kidwai, M, Bhatnagar, D, Mishra, NK. Polyethylene glycol (PEG) mediated green synthesis of 2,5-disubstituted 1,3,4-oxadiazoles catalyzed by ceric ammonium nitrate (CAN). Green Chem Let Rev, 2010, 3, 55–59.

[18]   Devery, JJ, Mohanta, PK, Casey, BM, Flowers, RA. Facile route to tetrasubstituted pyrazoles utilizing ceric ammonium nitrate. Synlett, 2009, 2009, 1490–1494.

[19]   Huang, G, Zhao, H-R, Meng, -Q-Q, Zhou, W, Zhang, Q-J, Dong, J-Y, Cui, J-H, Li, -S-S. Cerium (IV) ammonium nitrate (CAN)-mediated regioselective synthesis and anticancer activity of 6-substituted 5,8-dimethoxy-1,4-naphthoquinone. Chin Chem Lett, 2017, 28, 1553–1558.

[20]   Béha, S, Giguère, D, Patnam, R, Roy, R. Formation of isoxazoles using cerium ammonium nitrate (CAN): A one-pot synthesis of glycomimetics. Synlett, 2006, 2006, 1739–1743.

[21]   Shaikh, KA, Chaudhar, UN. Novel synthesis of [1,2,4]-triazoloquinazolinone and pyrimidine derivatives mediated by ceric ammonium nitrate (CAN). Acta Chemica Iasi, 2021, 29, 15–30.

[22]   Ji, S-J, Wang, S-Y. Ultrasound-accelerated Michael Addition of Indole to α,β-Unsaturated Ketones Catalyzed by Ceric Ammonium Nitrate (CAN). Synlett, 2003, 2003, 2074–2076.

[23]   Pfister, JR. Rapid, high-yield oxidation of hantzsch-type 1,4-Dihydropyridines with ceric ammonium nitrate. Synthesis, 1990, 8, 689–690.

[24]   Chang, M-Y, Lin, C-Y, Wu, T-C. Aminohydroxylation and dihydroxylation of 4-aryl-1,2,5,6-tetrahydropyridines. Tetrahedron Lett, 2006, 47, 5445–5449.

[25]   Abdel-Wahab, BF, Shaaban, S, El-Hiti, GA. Synthesis of sulfur-containing heterocycles via ring enlargement. Mol Divers, 2018, 22, 517–542.

[26]   Dua, R, Shrivastava, S, Sonwane, S, Srivastava, S. Pharmacological significance of synthetic heterocycles scaffold: A review. Adv Biol Res, 2011, 5, 120–144.

[27]   Feng, M, Tang, B, Liang, SH, Jiang, X. Sulfur containing scaffolds in drugs: Synthesis and application in medicinal chemistry. Curr Top Med Chem, 2016, 16, 1200–1216.

[28]   Schutte, L, Teranishi, R. Precursors of sulfur-containing flavor compounds. Crit Rev Food Sci Nutr, 1974, 4, 457–505.

[29]   Kim, DE, Kim, Y, Cho, DH, Jeong, SY, Kim, SB, Suh, N, Lee, JS, Choi, EK, Koh, JY, Hwang, JJ. Raloxifene induces autophagy-dependent cell death in breast cancer cells via the activation of AMP-activated protein kinase. Mol Cell, 2015, 38, 138–144.

[30]   Nayak, KR, Cavendish, JJ. Risk reduction with clopidogrel in the management of peripheral arterial disease. Vasc Health Risk Manag, 2007, 3, 289–297.

[31]   Rawal, R, Murugesan, V, Katti, S. Structure-activity relationship studies on clinically relevant HIV-1 NNRTIs. Curr Med Chem, 2012, 19, 5364–5380.

[32]   Herdeiro, MT, Soares, S, Silva, T, Roque, F, Figueiras, A. Impact of rosiglitazone safety alerts on oral antidiabetic sales trends: A countrywide study in Portugal. Fundam Clin Pharmacol, 2016, 30, 440–449.

[33]   Seïde, M, Marion, M, Mateescu, MA, Averill-Bates, DA. The fungicide thia-bendazole causes apoptosis in rat hepatocytes. Toxicol In Vitro, 2016, 32, 232–239.

[34]   Kaur, P, Arora, R, Gill, NS. Review on oxygen heterocycles. Indo Am J Pharm Res, 2013, 3, 9067–9084.

[35]   Miyabe, H, Miyata, O, Naito, T. Pyran and its derivatives. In: Heterocycles in Natural Product Synthesis Majumdar, KC, Chattopadhyay, SK, eds., WILEY-VCH, Weinheim, Germany, 2011, 153–186.

[36]   Goel, A, Kumar, A, Raghuvanshi, A. Synthesis, stereochemistry, structural classification, and chemical reactivity of natural pterocarpans. Chem Rev, 2013, 113, 1614–1640.

[37] Kaur, P, Arora, R, Gill, NS. Review on oxygen heterocycles. Indo Am J Pharm Res, 2013, 3, 18.

[38] Cossy, J, Guérinot, A. Natural products containing oxygen heterocycles – Synthetic advances between 1990 and 2015. Adv Heterocyclic Chem, 2016, 119, 107–142.

[39] Kumar, A, Sharma, S, Maurya, RA, Sarkar, J. Diversity oriented synthesis of benzoxanthene and benzochromene libraries via one-pot, three-component reactions and their anti-proliferative activity. J Comb Chem, 2010, 12, 20–24.

[40] Jardosh, HH, Manish, PP. Microwave-induced CAN promoted atom-economic synthesis of 1*H*-benzo [*b*]xanthene and 4*H*-benzo[*g*]chromene derivatives of N-allyl quinolone and their antimicrobial activity. Med Chem Res, 2013, 22, 2954–2963.

[41] Reddy, YT, Sonar, VN, Crooks, PA, Dasari, PK, Reddy, PN, Rajitha, B. Ceric ammonium nitrate (CAN): An efficient catalyst for the coumarin synthesis via Pechmann condensation using conventional heating and microwave Irradiation. Synth Commun, 2008, 2082–2088.

[42] Sudha, S, Pasha, MA. Ultrasound assisted synthesis of tetrahydrobenzo[*c*]xanthene-11-ones using CAN as catalyst. Ultrason Sonochem, 2012, 19, 994–998.

[43] Dandia, A, Gupta, SL, Bhaskaran, S. Cerric ammonium nitrate (CAN) catalysed synthesis of pyrano [2,3-*d*]pyrimidine-2,4,7-triones in aqueous medium under sonication via one-pot three component reacton. Eur Chem Bull, 2013, 2, 836–841.

[44] Baciocchi, E, Ruzziconi, R. Synthesis of 3-acyl and 3-carboalkoxyfurans by the ceric ammonium nitrate promoted addition of 1,3-dicarbonyl compounds to vinylic acetates. Synth Commun, 1988, 18, 1841–1846.

[45] Itoh, K-I, Takahashi, S, Ueki., T, Sugiyama, T, Takahashic, T, Akira Horiuchia, CA. A novel one-pot synthesis of 3-acetyl- and 3-benzoylisoxazole derivatives using ammonium cerium nitrate (CAN). Tetrahedron Lett, 2002, 43, 7035–7037.

[46] Maiti, G, Roy, SC. Ceric ammonium nitrate as a convenient catalyst for protection of carbonyl compounds as 1,3-oxathianes. Synth Commun, 2002, 32, 2269–2273.

[47] Undeela, S, Ramchandra, JP, Menon, RS. A sequential synthesis of substituted furans from aryl alkynes and ketones involving a cerium(IV) ammonium nitrate (CAN)-mediated oxidative cyclization. Tetrahedron Lett, 2014, 55, 5667–5670.

[48] Sudha, S, Pasha, MA. Ultrasound assisted synthesis of tetrahydrobenzo[c]xanthene-11 ones using CANas catalyst. Ultrason Sonochem, 2012, 19, 994–998.

[49] Puligoundla, RG, Vulupala, HR, Kommu, N, Kondra, SB. Ceric ammonium nitrate (can) catalyzed efficient one-pot three component aza-diels-alder reactions for a facile synthesis of tetrahydropyranoquinoline derivatives. Synth Commun, 2015, 45, 494–502.

[50] Brahmachari, G, Begam, S. Ceric ammonium nitrate (CAN): An efficient and eco-friendly catalyst for one-pot synthesis of diversely functionalized biscoumarins in aqueous medium under ambient conditions. Chemi Select, 2019, 4, 5415–5420.

[51] Al-Qalaf, F, Mekheimer, RA, Sadek, KU. Cerium (IV) ammonium nitrate (CAN) catalyzed one-pot synthesis of 2-arylbenzothiazoles. Molecules, 2008, 13, 2908–2914.

K Ganesh Kadiyala, Vanipenta Yamini, Kommuru Goutham
and Naresh Kumar Katari*

12 Photocatalysis of rare earth complexes in organic synthesis

12.1 Introduction

A traditional photochemical reaction to excite the substrate or reagents uses high-energy UV light. These reactions are often unselective, highly difficult to control and involve special equipment to carry out the reaction. Visible light has emerged as an effective reagent in photocatalysis, an effective technique in organic synthesis that utilizes photons for excitation, paving the path for sustainable chemical reactions. In this field new reactions were developed that are mostly focused on a common photo redox cycle. In addition, recently a variety of new concepts and strategies have also emerged that involve the application of visible light with variable wavelengths and intensities that tune the properties of photocatalyst to control the reactivity of the organic compounds. Evidenced by volumes of reviews published in the last decade, many research groups have turned their interest in photocatalysis [1–8]. In general, iridium- and ruthenium-based photocatalysis dominates the chemical community till now, but recently rare earth metal complexes [9, 10] are also employed as photocatalysts for various organic transformations.

12.2 General mechanistic pathways involved in photocatalysis

Photocatalysts could initiate the organic transformations through various mechanistic manners. Particularly, visible light photoredox catalysis [11–15] is documented as an effective protocol in synthetic organic conversions. The various mechanistic cycles of photocatalysis are shown in Figure 12.1. Depending on the reagents and substrates present in the reaction mixture, an excited photocatalyst (PC*) may absorb or donate a single electron after being exposed to light, enabling oxidative or reductive quenching cycles. Occasionally, a coordinated proton transfer (proton-coupled electron transfer

---

*Corresponding author: Naresh Kumar Katari, Department of Chemistry, School of Science, GITAM Deemed to be University, Hyderabad, India, e-mail: nkatari@gitam.edu
K Ganesh Kadiyala, Depatment of Chemistry, Shri Vishnu Engineering College for Women, Bhimavaram, Andhra Pradesh, India
Vanipenta Yamini, Sri A. S. N. M. Govt. College (A), Palakollu, Andhra Pradesh, India
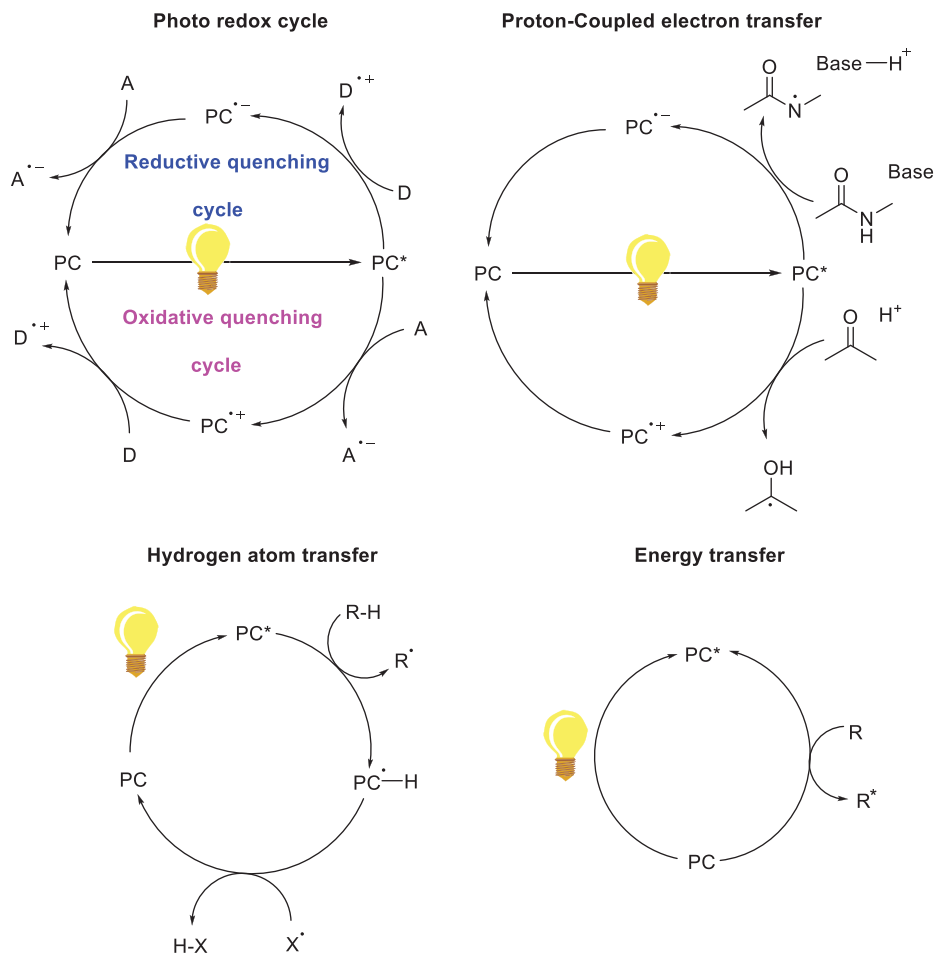Kommuru Goutham, Indian Institute of Chemical Technology, Hyderabad, Telangana, India

Figure 12.1: Distinct catalytic approaches of photocatalytic reactions.

[PCET]) could also work in tandem with the oxidative or reductive cycles. Contrarily, photocatalytic hydrogen atom transfer (HAT) occurs either following single electron transfer (SET) events or by the homolytic breakage of C–H bonds by the PC. Additionally, photocatalysts in their excited state can transfer their energy to reactants that are not capable of absorbing light to induce a chemical reaction.

12.3 Photosensitization

Zhang et al. [16] demonstrated the synthesis of Gd^{III} complexes that can serve as photosensitizer for singlet oxygen (Figure 12.2). These Gd^{III} complexes include porphyrin,
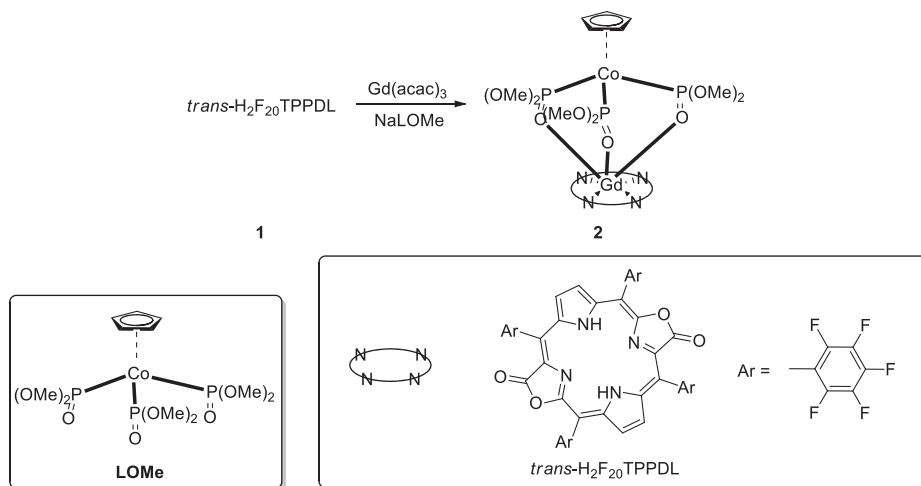
Figure 12.2: Synthesis of Gd^{III} *trans*-porphodilactone complex.

porpholactone, and *cis-* and *trans*-porphodilactone, which act as ligands that coordinate to Gd^{III} ion and alters its photosensitization efficiency. One of these ligands, *trans*-porphodilactone, produced singlet oxygen with high quantum yield when stimulated in the visible to near-infrared range (NIR). In addition to its photosensitization property, Gd(III) *trans*-porphodilactone complex (**2**) acts as effective catalyst for photooxidative C–H bond cleavage of secondary or tertiaryamines and also efficient in natural product cholesterol photo-oxygenation.

Schelter and coworkers [17] have developed luminescent Ce^{III} complexes with two complete mixed-ligand series (Figure 12.3). The general formula of Ce^{III} complexes is [N(SiMe$_3$)$_2$]$_{3-x}$Ce^{III}[(Me$_3$Si)$_2$NC(N^{i}Pr)$_2$]$_x$ ($x = 0$, **3 N**; $x = 1$, **4 N**, $x = 2$, **5 N**; $x = 3$, **6 N**) and (OAr)$_{3-x}$Ce^{III}[(Me$_3$Si)$_2$ NC(N^{i}Pr)$_2$]$_x$ ($x = 0$, 1-OAr; $x = 1$, 2-OAr, $x = 2$, 3-OAr; $x = 3$, 4) has lifetimes of 117(1) ns and quantum yields of photoluminescence up to 0.81(2). These Ce^{III} photosensitizers are extensively studied for their photocatalytic activity in C–C bond formation between benzene and 4-fluoroiodobenzene.

12.4 Photoreductions

Ce^{III} complexes have been extensively studied by Schelter et al. [18] for the photoreduction reactions of benzyl chloride (**7**) through single electron transfer mechanism (SET) to furnish homo-coupled products (**9**) (Figure 12.4). The reaction involves the formation of Ce^{IV}Cl complex which is a stronger absorber of light than Ce^{III} which leads to incomplete reaction. They anticipated that the addition of NaN(SiMe$_3$)$_2$ (**8**) might reduce Ce^{IV}Cl complex to Ce^{III} with NaCl precipitation, preventing the formation of Ce^{IV}Cl complex.
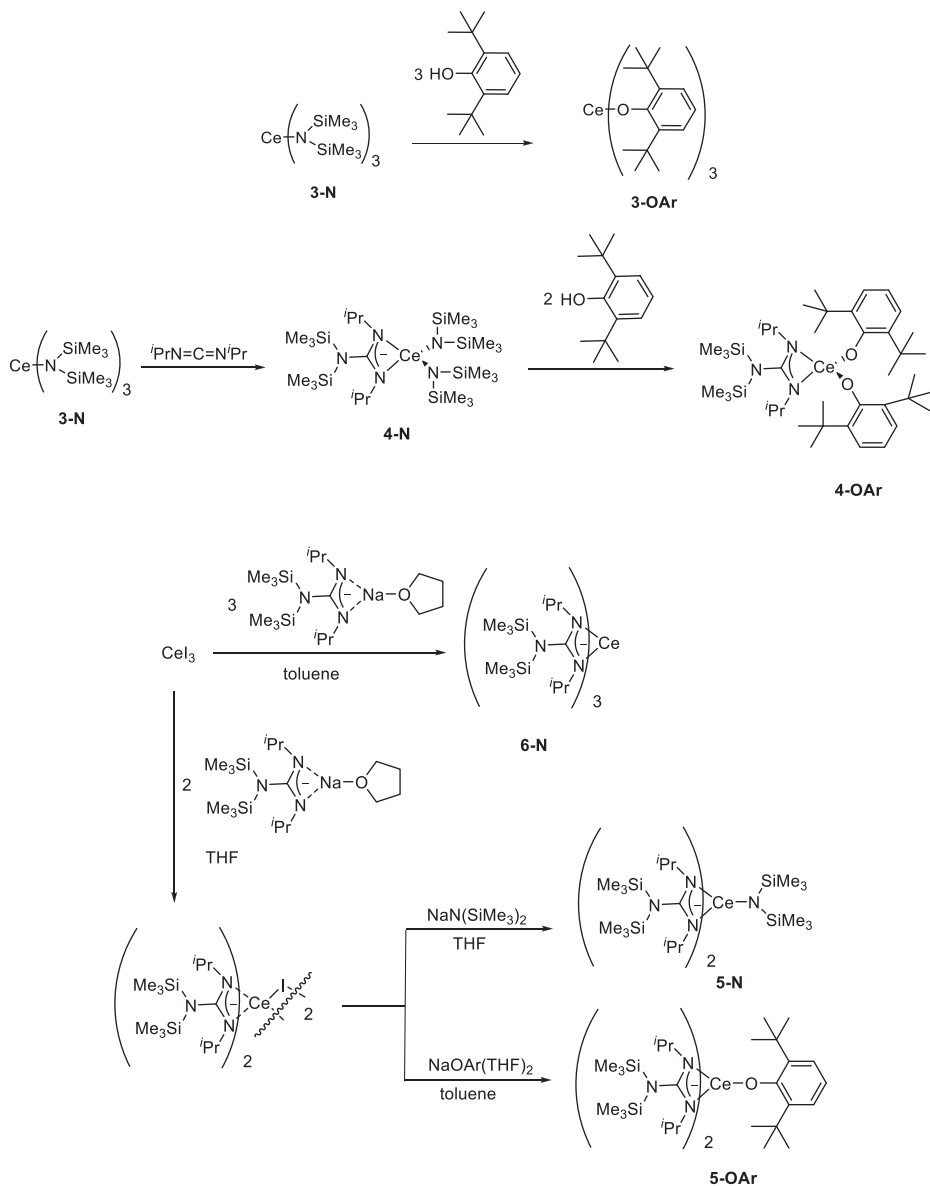
Figure 12.3: Synthesis of series of luminescent Ce^{III} complexes.

Pioneer in photocatalysis, Schelter and coworkers [19] revealed a robust method for the photo reduction of aryl chloride (**10**) to reduced aryl compounds (**11**) by using hexachlorocerate(III) $[Ce^{III}Cl_6]^{3-}$ (Figure 12.5). This complex is produced by in situ reaction of Et$_4$NCl and CeCl$_3$ in acetonitrile solutions (Figure 12.6). The main advantage
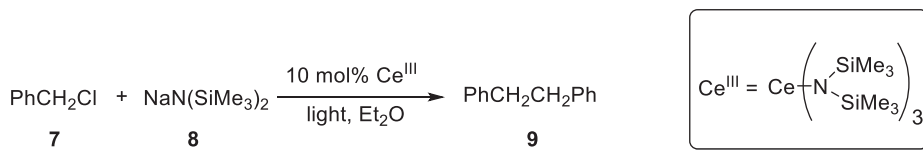
$$PhCH_2Cl + NaN(SiMe_3)_2 \xrightarrow[\text{light, Et}_2O]{\text{10 mol\% Ce}^{III}} PhCH_2CH_2Ph$$

7   **8**   **9**

$$Ce^{III} = Ce\left(N\begin{array}{c}SiMe_3\\SiMe_3\end{array}\right)_3$$

Figure 12.4: Photoreduction of benzyl chloride.

10, X = Cl or Br   **11**

20 examples
yield: 16-95%
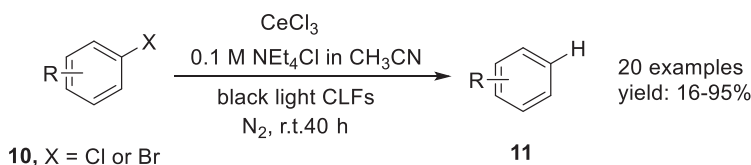
Figure 12.5: Photo reductive dehalogenation of aryl halides.

$$[NEt_4]_3[Ce^{III}Cl_6] \xrightarrow[\substack{\text{visible light CLFs}\\N_2, \text{r.t.}}]{\substack{\text{1 eq. NEt}_4Cl\\\text{toluene/CH}_3CN\ (1:4)}} [NEt_4]_3[Ce^{III}Cl_6]$$
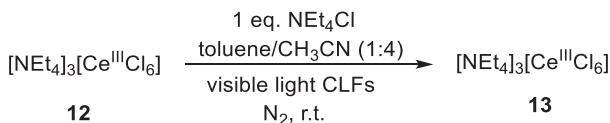
12   **13**

Figure 12.6: Synthesis of Ce^{III} complex.

of [Ce^{III}Cl$_6$]$^{3-}$ complex is the low photo reduction potentials and fast quenching kinetics which facilitates the dehalogenation of aryl chloride via aryl radical.

12.5 Photooxidations

Chen et al. [20] succeeded in developing an efficient protocol for the visible light driven photooxidation of diarylalkynes (**141**) to diketones (**15**) (Figure 12.7) and thioethers (**16**) to sulfoxides (**17**) (Figure 12.8). The team have prepared four isostructural lanthanides with same coordinated ligand 3,7-diamino-9,10-anthraquinone-2,6-disulfonatecomplexes via hydrothermal method. The complexes are [Er(H$_2$O)$_8$]•[Er(**L**)(H$_2$O)$_6$]•2 **L**•8H$_2$O (**Er-L**), [Tm(H$_2$O)$_8$]• [Tm(**L**)(H$_2$O)$_6$]•2 **L**•8.5H$_2$O (**Tm-L**), [Yb(H$_2$O)$_8$]•[Yb(**L**)(H$_2$O)$_6$]•2 **L**•9H$_2$O (**Yb-L**), [Lu(H$_2$O)$_8$] • [Lu(**L**)(H$_2$O)$_6$]•2 **L**•9H$_2$O (**Lu-L**), respectively. Based on single crystal X-ray analysis, the structure of these complexes is determined, and it also discloses the presence of free and coordinated ligand in the crystal structure. These complexes act as heterogeneous photooxidative catalysts. Among the four lanthanide complexes, the **Er-L** is superior over other complexes for visible light driven photooxidation. The advantage of **Er**-photocatalyst includes easy isolation of catalyst after the completion of photooxidation through simple filtration, and it can be used without activation for up to five catalytic cycles.
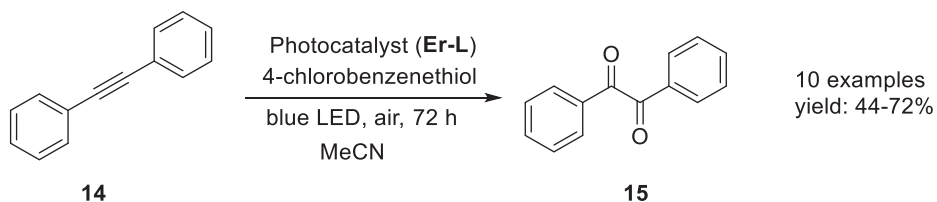
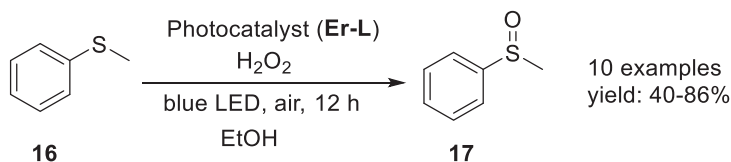**Figure 12.7:** Photooxidation of arylalkynes to diketones.

Figure 12.8: Photooxidation of thioethres to sulfoxides.

12.5.1 General procedure for the preparation of 3,7-diamino-9, 10-anthraquinone-2,6-disulfonic acid (H$_2$L)

2,6-Diamino-9,10-anthracenedione (4 g) was added gently to a stirring solution of 20 mL 20% oleum in 50 mL two-necked flask under cooling. To the reaction mixture H$_2$O$_2$ (30%, 0.5 mL) was added and run for 5 h at 100 °C. The resulting dark brown precipitate was filtered, washed cleanly with CH$_3$CN, and vacuum-dried to provide 5.4 g of product (a yield of 80%).

12.5.2 General procedure for the preparation [Er(H$_2$O)$_8$]•[Er(L)(H$_2$O)$_6$]•2L•8H$_2$O (Er-L)

A mixture of H$_2$L (19.8 mg, 0.05 mmol) and ErCl$_3$•6H$_2$O (38.2 mg, 0.1 mmol) was dissolved in a glass container into 3.0 mL water. The glass container was wrapped with a cap and heated to a temperature of 100 °C for 24 h. Then reaction mixture was gently cooled to room temperature to produce give reddish brown crystals, which were then filtered out, cleaned with CH$_3$COCH$_3$, and allowed to dry at ambient temperature. Yield: 65% according to H$_2$L.

12.6 Photocycloadditions

Anhua and coworkers [21] developed a robust [5 + 2] cycloaddition methodology upon reacting cycloalkonols (**18**) and electron deficient alkenes (**19**) by employing synergistic combination of a PET catalyst (photo-induced electron transfer catalyst–anthracene complex) and LMCT catalyst (cerium compound) for the construction of synthetically complex bridged lactones(**20**) (Figure 12.9). These bridged lactones are important scaffolds commonly found in natural products, such as hushinone [22], nepalactones [23], dendromonilisides [24], and tutin [25]. The process for the generation of alkoxy radical under SET mechanism is shown in Figure 12.10 by using photocatalyst anthracene complex. The reaction proceeds in a stepwise manner (Figure 12.11) in such a way that first the α-hydroxy C–C bond of alkoxy radical (**21**) could be selectively cleaved to give alkyl radical (**22**) and then undergo [5 + 2] cycloaddition with electron-deficient alkenes to give higher ring alcohol (**25**) followed by lactonization upon treatment with acid affording bridged lactones (**20**).
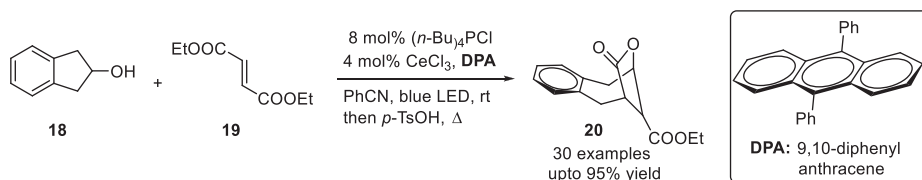

Figure 12.9: LMCT catalyst and PET catalyst-mediated photocycloaddition.
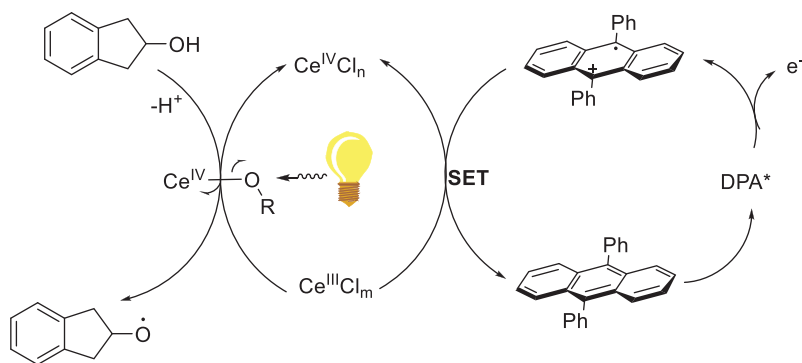
Figure 12.10: Generation of alkanol radical.

An efficient, mild and intermolecular [2 + 2] cycloaddition of indoles (**26**) with activated olefins (**27**) mediated by visible violet light-induced Gd(III) catalyst toward the construction of complex scaffolds cyclopenta[*b*]indoles (**28**) and indolines (**29**) (Figure 12.12) through one-pot, multistep fashion was developed by Glorious et al. [26]. The [2 + 2] cycloaddition takes place in an unusual head-to-head fashion rather than traditional head-to-tail

Figure 12.11: Photocycloaddition reaction mechanism.

Figure 12.12: Gd(OTf)$_3$-induced photocycloaddition of indoles with alkenes.
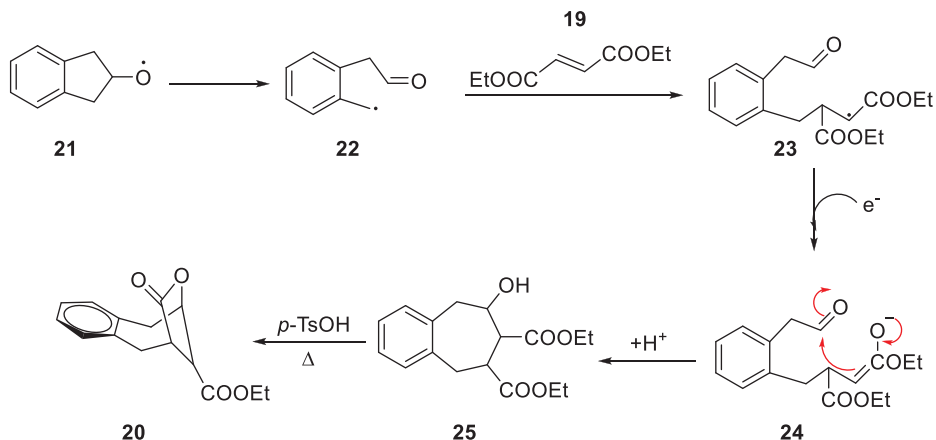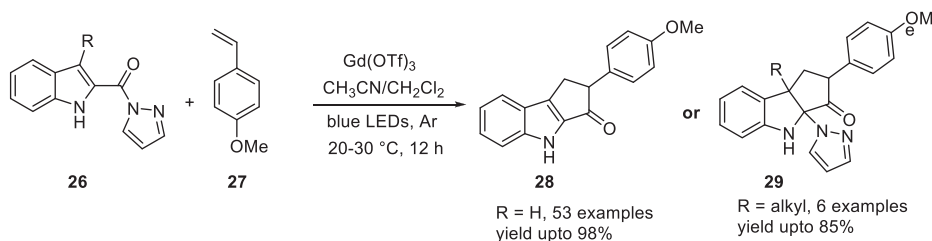
fashion. The tethered pyrazole moiety acts as directing group when there is no substituent present at 3-position leads to cyclopenta[*b*]indole derivatives, whereas presence of substituent at 3-position, pyrazole moiety acts as both masking amination reagent and a directing group leads to dearomative cyclopenta[*b*]indoline derivatives (Figure 12.13).

12.7 Photocatalytic C–C/C–heteroatom bond construction

Zuo and coworkers [27] have developed an excellent and efficient straightforward protocol for C–C bond construction by employing inexpensive cerium photocatalysis (Figure 12.14). The reaction involves generation of in situ alkyl radical (**42**) upon irradiation of simple alcohols (**41**) by dehydroxymethylation (loss of formaldehyde). The obtained alkyl radical undergoes various cross-couplings, including hydrogenation, alkenylation, amination, alkylation, and oxidation under mild reaction parameters.
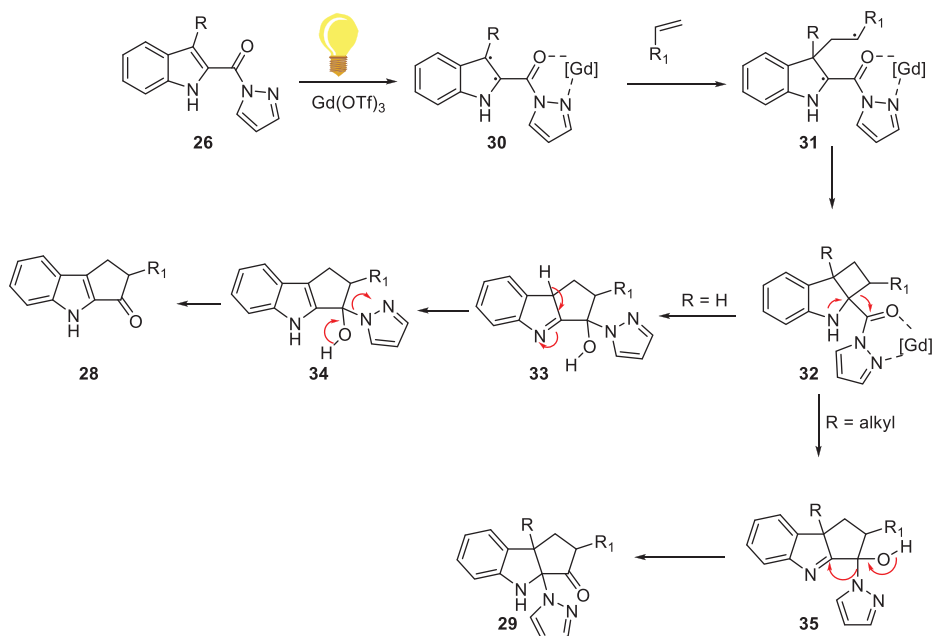
Figure 12.13: Mechanism of Gd(OTf)$_3$-induced photocycloaddition of indoles with alkenes.

Qiao et al. [28] achieved first-ever photo-induced Miyura borylation of sp^2 carbon by a rare earth photoreductant hexachlorocerate(III) anion (Ce^{III}Cl$_6$)$^{3-}$ (Figure 12.15). The developed photo-induced Miyura borylation was coupled with Suzuki–Miyura reaction resulting in the preparation of variety of biaryls from aryl chlorides.

Zuo et al. [29] developed a general protocol for δ C–H activation of primary alcohols (**52**) by employing inexpensive cerium photocatalysis (Figure 12.16). The advantage of this method is that it does not require prefunctionalization of primary alcohols for distal functionalization. This protocol involves LMCT (ligand-to-metal charge transfer) mechanism (Figure 12.17) for the direct activation of substrates containing heteroatom functionalities.

Inspired by the previous work, Zuo et al. [30] realized the photo-induced rare earth metal catalyzed HAT (hydrogen atom transfer) strategy for the activation of highly inert substrates methane, ethane, propane, and butane (**58**) to form C-heteroatom bonds (Figure 12.18). The reaction sequence involves excitation of alcohol to form alkoxy radical which in turn triggers the inert alkanes to produce an alkyl radical which was then reacted with array of electron deficient substrates to form desired C–C/C–heteroatom bonds.
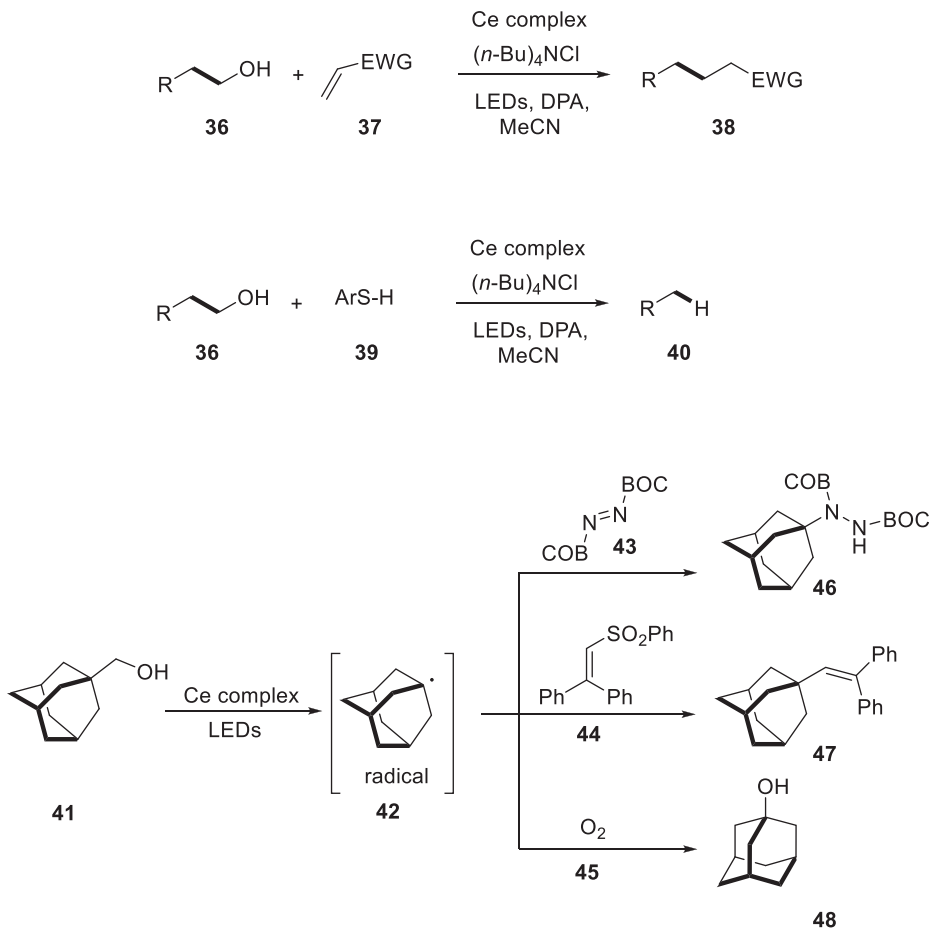
Figure 12.14: CeCl$_3$-induced photocatalytic C–H, C–C, and C–heteroatom bond-forming reaction.
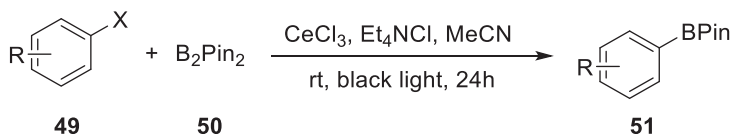
Figure 12.15: CeCl$_3$-induced photocatalytic C–B atom bond formation reaction.

12.8 Photocatalytic C–C bond cleavage

Guo and coworkers [31] demonstrated an efficient strategy for amination of cycloalkanols (**65**) by C–C bond cleavage through cerium complex catalyzed visible light-induced photoredox catalysis (Figure 12.19). This method is relevant to a wide array of
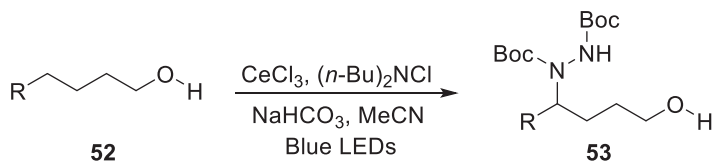
Figure 12.16: CeCl₃-induced photocatalytic δ C–H amination.
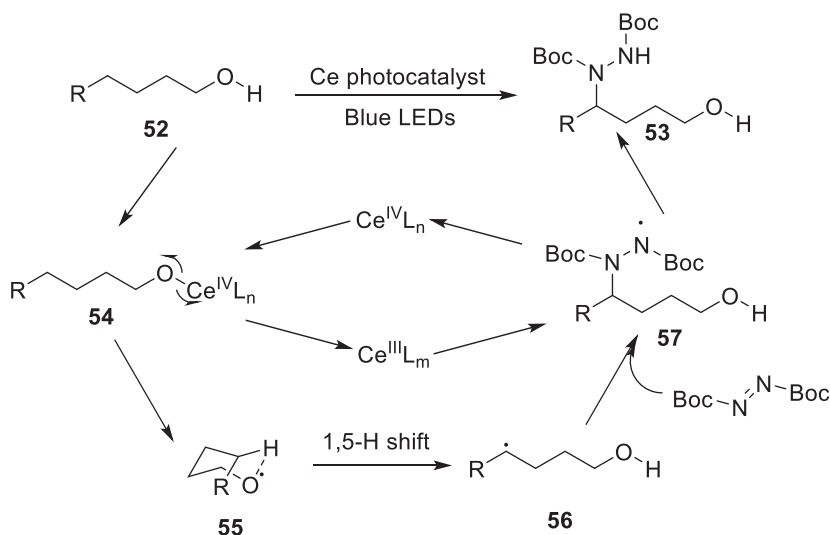
Figure 12.17: Mechanism of photocatalytic δ C–H amination.

secondary and tertiary cycloalkanols. The mechanism involves exposure of cerium chloride/alcohol complex (**67**) to radiation; the photo-excited state (**68**) is produced. The photo-excited Ce^{III} complex would result in a Ce^{IV} species (**69**) via a single electron transfer (SET) process with nitrogen radical intermediate (**71**). As anticipated, the extremely oxidized Ce^{IV} species (**69**) might facilitate the hard β-scission process to produce carbon radical (**70**). Then DBAD is coupled with extremely reactive radical species (**70**) to produce nitrogen-centered intermediate radical **71**, which subsequently produce the product through SET reduction (Figure 12.20).

Based on the previous C–C bond cleavage of cycloalkanols, the same group had continued the research on C–C bond scission of cyclic and acyclic ketones. They employed cooperative Lewis acid and cerium complex photocatalysis to selectively scission C–C bonds of different ketones by utilizing the ligand-to-metal charge transfer (LMCT) excitation method (Figure 12.21) [32]. This C–C bond scission reaction serves as an alternate to Norrish type l reaction. Many acyclic and cyclic ketones, ranging from straightforward, strained cyclobutanone (**72**) to intricate, less strained androsterone
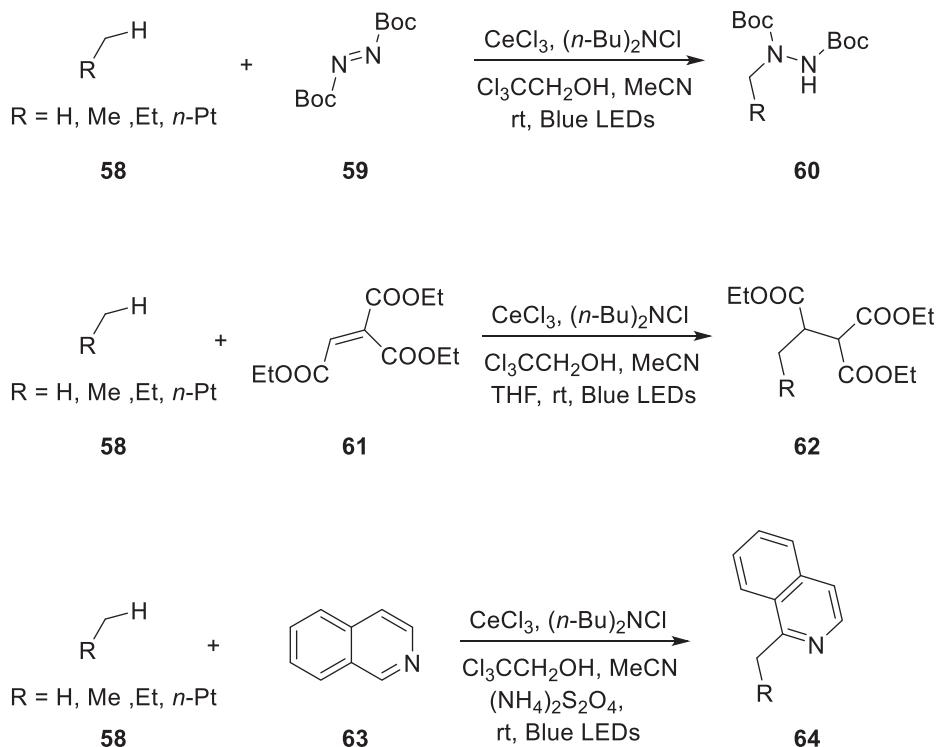
Figure 12.18: CeCl$_3$-induced photocatalytic inert sp^3 C–H amination, alkylation, and arylation.
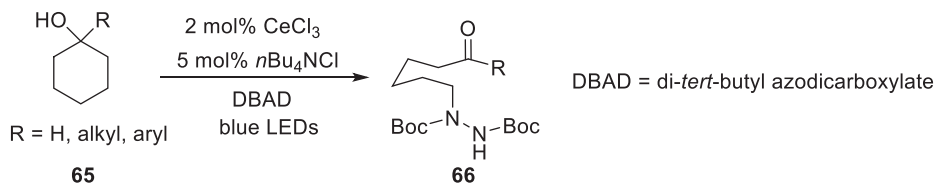
Figure 12.19: CeCl$_3$ Photo mediated C–C bond scission and amination.

(cyclopentanone) (**75**), could successfully undergo C–C bond scission and converted into useful chemical feed stocks. The obtained substrate from strained ketones was easily converted to desired lactams (**77**). The substrates from unstrained ketones (cyclohexanone), the C–C bond scission would result in the production of ω-aminated acyl cyanide (**76**), which would yield a carboxylic ester upon alcohol hydrolysis with a wide range of synthetic applications.

Coming over to linear ketone compounds (**77**), C–C bond scission was accomplished successfully, installing carboxylic ester (**78**) and hydrazine derivatives (**79**) at altered carbon fragments without any intervention of Norrish type II reaction (Figure 12.22). In
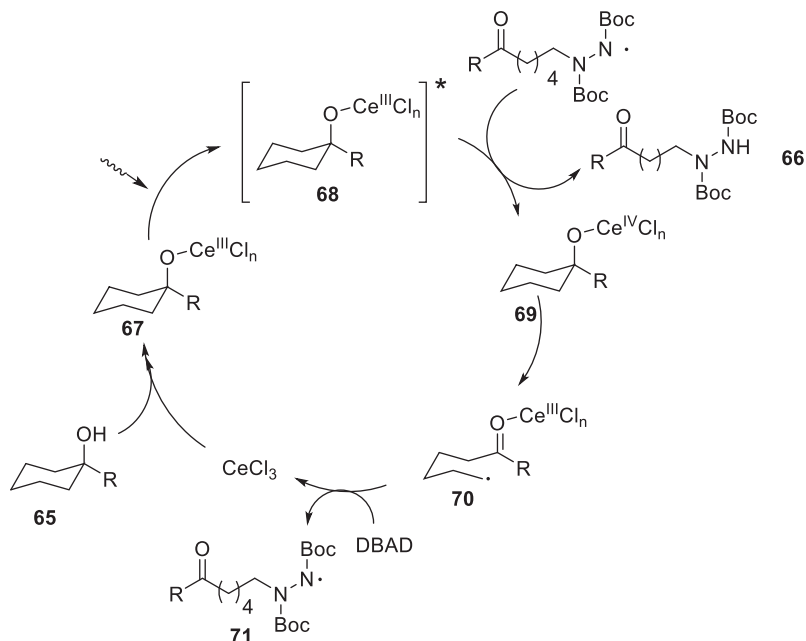
Figure 12.20: Proposed reaction mechanism of C–C bond scission and amination.
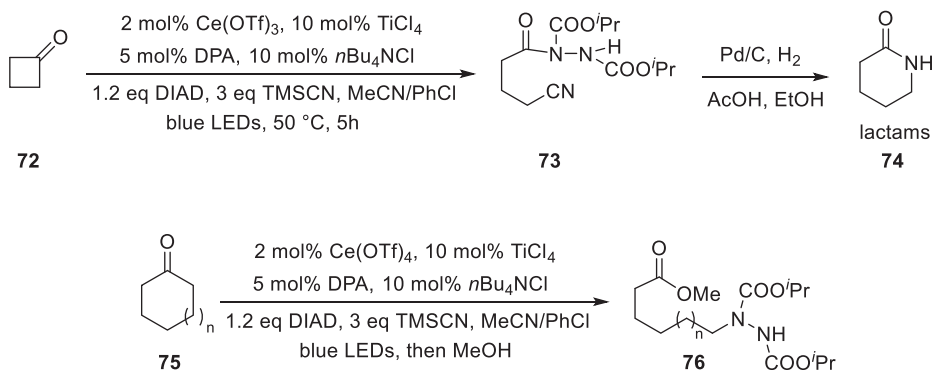
Figure 12.21: Cerium photocatalyzed C–C bond cleavage of strained ketones, unstrained.
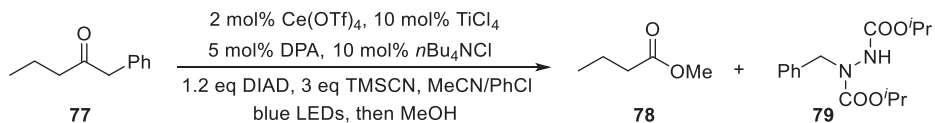
Figure 12.22: Cerium photocatalyzed C–C bond scission of acyclic ketones.

unsymmetrical linear ketones, more substituted α-C–C bond with greater stabilized radical could cleave precisely to furnish corresponding products.

Xiao et al. [33] published first report of cyanation of strained cyclopropylketones (**80**) via C–C cleavage by combining photoredox catalysis with Lewis acid catalysis (triple catalysis) and copper catalysis for the preparation of γ-cyanoketones (**82**) (Figure 12.23). The synthetic application of the present protocol has been showcased through the preparation of piperidine scaffolds (**84**) and (**85**) (Figure 12.24).
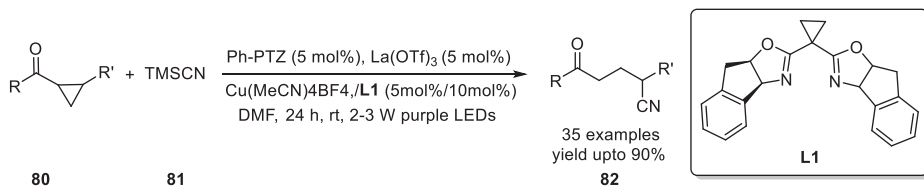
Figure 12.23: C–C bond scission of cyclopropylketones by triple catalysis.
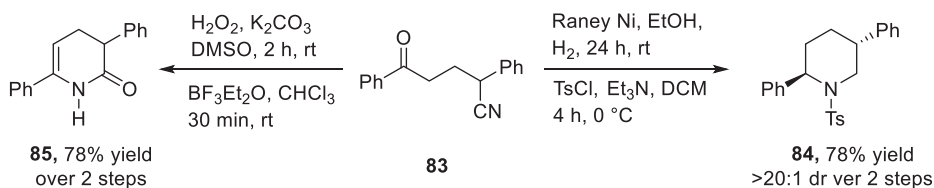
Figure 12.24: Synthetic utility of triple catalysis for the construction of piperidines.

12.9 Conclusions

In conclusion, rare earth metal complexes can act as redox-neutral Lewis acids as well as redox-active centers in photochemical reactions. The redox properties of rare earth complexes trigger the activation of halogen compounds, carboxylic acid derivatives, alcohols, unsaturated systems, and chalcogens, while switching to Lewis acid character they are able to activate a plethora of compounds containing carbonyl functionality. There is plethora of queries still unanswered with respect to mechanism of lanthanide photocatalysis.

References

[1]   Skubi, KL, Blum, TR, Yoon, TP. Dual catalysis strategies in photochemical synthesis. Chem Rev, 2016, 116, 10035–10074.

[2]   Shaw, MH, Twilton, J, MacMillan, DWC. Photoredox catalysis in organic chemistry. J Org Chem, 2016, 81, 6898–6926.

[3]   Romero, NA, Nicewicz, DA. Organic photoredox catalysis. Chem Rev, 2016, 116, 1007–10166.

[4]   Matsui, JK, Lang, SB, Heitz, DR, Molander, GA. Photoredox-mediated routes to radicals: The value of catalytic radical generation in synthetic methods development. ACS Catal, 2017, 7, 2563–2575.

[5]   McAtee, RC, McClain, EJ, Stephenson, CRJ. Illuminating photoredox catalysis. Trends Chem, 2019, 1, 111–125.

[6]   Tsui, E, Wang, H, Knowles, RR. Catalytic generation of alkoxy radicals from unfunctionalized alcohols. Chem Sci, 2020, 11, 11124–11141.

[7]   Amos, SGE, Garreau, M, Buzzetti, L, Waser, J. Photocatalysis with organicdyes: Facile access to reactive intermediates for synthesis. Beilstein J Org Chem, 2020, 16, 1163–1187.

[8]   Lee, Y, Kwon, MS. Emerging organic photoredox catalysts for organictransformations. Eur J Org Chem, 2020, 2020, 6028–6043.

[9]   Bünzli, JC. Chapter 287-Lanthanide luminescence: From a mystery torationalization, understanding and applications. In: Handbook on the Physics and Chemistry of Rare Earths, 2016, vol 50, 141–176.

[10]   Werts, MHV. Making sense of lanthanide luminescence. Sci Prog, 2005, 88(Pt 2), 101–131.

[11]   Pitre, SP, Overman, LE. Strategic use of visible-light photoredox catalysis in natural product synthesis. Chem Rev, 2022, 122, 1717–1751.

[12]   Marzo, L, Pagire, SK, Reiser, O, König, B. Visible-light photocatalysis: Does it make a difference in organic synthesis? Angew Chem Int Ed, 2018, 57, 10034–10072.

[13]   Prier, CK, Rankic, DA, MacMillan, DWC. Visible light photoredox catalysis withtransition metal complexes: Applications in organic synthesis. Chem Rev, 2013, 113, 5322–5363.

[14]   Narayanama, JMR, Stephenson, CRJ. Visible light photoredox catalysis: Applications in organic synthesis. Chem Soc Rev, 2011, 40, 102–113.

[15]   Xuan, J, Xiao, WJ. Visible-light photoredox catalysis. Angew Chem Int Ed, 2012, 51, 6828–6838.

[16]   Ke, XS, Ning, Y, Tang, J, Hu, JY, Yin, HY, Wang, GX, Yang, ZS, Jie, J, Liu, K, Meng, ZS, Zhang, Z, Su, S, Shu, C, Zhang, JL. Gadolinium(III) pharpholactones as efficient and robust singlet oxygen photosensitizers. Chem Eur J, 2016, 22, 9676–9686.

[17]   Yin, H, Carroll, PJ, Manor, BC, Anna, JM, Schelter, EJ. cerium photosensitizers: Structure–function relationships and applications in photocatalyticaryl coupling reactions. J Am Chem Soc, 2016, 138, 5984–5993.

[18]   Yin, H, Carroll, PJ, Anna, JM, Schelter, EJ. Luminescent Ce(III) complexes as stoichiometric and catalytic photoreductants for halogen atom abstraction reactions. J Am Chem Soc, 2015, 137, 9234–9237.

[19]   Yin, H, Jin, Y, Hertzog, JE, Mullane, KC, Carroll, PJ, Manor, BC, Anna, JM, Schelter, EJ. The hexachlorocerate(III) anion: A potent, benchtop stable, and readily available ultraviolet a photosensitizer for aryl chlorides. J Am ChemSoc, 2016, 138, 16266–16273.

[20]   Zhu, TT, Tao, YT, Sun, Y, Wang, X, Zhang, XW, Chai, JL, Han, J, Zhao, XL, Chen, XD. Lanthanide complexes based on an anthraquinone derivative ligand and applications as photocatalysts for visible-light driving photooxidation reactions. JMolStruct, 2021, 1236, 130289–130293.

[21]   Hu, A, Chen, Y, Guo, JJ, Yu, N, An, Q, Zuo, Z. Cerium-catalyzed formalcycloaddition of cycloalkanols with alkenes through dual photoexcitation. J Am Chem Soc, 2018, 140, 13580–13585.

[22]   Klika, KD, Demirci, B, Salminen, JP, Ovcharenko, VV, Vuorela, S, CanBaşer, KH, Pihlaja, K. New sesquiterpenoid-type bicyclic compounds from the buds of betulapubescens − ring-contracted products of β-Caryophyllene?. Eur J Org Chem, 2004, 2004, 2627–2635.

[23] Wang, Y, Tian, J, Zhang, C, Luo, B, Gao, J. Picrotoxane sesquiterpene glycosides and a coumarin derivative from coriaria nepalensis and their neurotrophic activity. Molecules, 2016, 21, 1344–1352.

[24] Zhao, C, Liu, Q, Halaweish, F, Shao, B, Ye, Y, Zhao, W. Copacamphane, picrotoxane, and alloaromadendrane sesquiterpene glycosides and phenolic glycosides from Dendrobium moniliforme. J Nat Prod, 2003, 66, 1140–1143.

[25] Easterfield, TH, Aston, BC. XI. Tutu. Part I. Tutin and coriamyrtin. J Chem Soc Trans, 1901, 79, 120–126.

[26] Ma, J, Schäfers, F, Daniliuc, C, Bergander, K, Strassert, CA, Glorius, F. Gadolinium photocatalysis: Dearomative [2+2] Cycloaddition/Ring-Expansion sequence with indoles. Angew Chem Intd Ed, 2020, 59, 9639–9645.

[27] Zhang, K, Chang, L, An, Q, Wang, X, Zuo, Z. Dehydroxymethylation of alcohols enabled by cerium photocatalysis. J Am Chem Soc, 2019, 141, 10556–10564.

[28] Qiao, Y, Yang, Q, Schelter, EJ. Photoinduced miyaura borylation by a rare-earth-metal photoreductant: The hexachlorocerate(III) Anion. Angew Chem Intd Ed, 2018, 57, 10999–11003.

[29] Hu, A, Guo, JJ, Pan, H, Tang, H, Gao, Z, Zuo, Z. δ-Selective functionalization of alkanols enabled by visible-light-induced ligand-to-metal charge transfer. J Am Chem Soc, 2018, 140, 1612–1616.

[30] Hu, A, Guo, JJ, Pan, H, Zuo, Z. Selective functionalization of methane, ethane,and higher alkanes by cerium photocatalysis. Science, 2018, 361, 668–672.

[31] Guo, JJ, Hu, A, Chen, Y, Sun, J, Tang, H, Zuo, Z. Photocatalytic C-C bondcleavage and amination of cycloalkanols by Cerium(III) chloride complex. Angew Chem Intd Ed, 2016, 55, 15319–15322.

[32] Chen, Y, Du, J, Zuo, Z. Selective C-C bond scission of ketones via visible-lightmediated cerium catalysis. Chem, 2020, 6, 266–279.

[33] Liu, J, Liu, XP, Wu, H, Wei, Y, Lu, FD, Guo, KR, Cheng, Y, Xiao, WJ. Visible-light-induced triple catalysis for a ring-opening cyanationofcyclopropyl ketones. Chem Commun (Camb.), 2020, 56, 11508–11511.

Hosam M. Saleh* and Amal I. Hassan

13 Innovative techniques utilized for bioremediation of rare earth elements to attain a sustainable world

13.1 Introduction

Rare earth elements (RREs) are referred to be "rare" because they are not found in commercially accessible deposits. These metals are increasingly being employed in high-intensity magnets, lasers, and colorful phosphors [1]. Color determination, high thermal stability, outstanding performance, high luminous intensity, low energy consumption, and longevity, for example, make phosphors indispensable in lighting [2]. REEs are becoming crucial components of sustainable energy technologies because of their unique physical and chemical features, including wind generators, electronic mobility, rising illumination, batteries, and H_2 fuel [3].

REEs play an important role in current electronics and green technology items such as computers, cell phones, lights, hybrid and electric cars, wind turbines, and solar cells. They are also used as catalysts in glass polishing powders, optical glass, and petroleum refining [4]. The lanthanide family and yttrium and scandium, are all chemically related metallic elements. Although these elements are not very scarce, obtaining them in sufficient amounts is difficult [5]. REEs are crucial metals due to their importance in rising innovative trends and sustainable sources. RE is plentiful and extensively dispersed in the earth's mantle, but unlike other metals, it is seldom concentrated in mining, making it economically viable to utilize [6]. To fulfill the expanding worldwide demand, REEs are now mined quite often in China, which provides over 85% of the world's REEs [7]. The integration of renewable energy sources has grown substantially in recent decades, putting a great strain on the current RE supply system. Mining activities have expanded because of the continued demand, resulting in the production of RE into the soil, particularly in mining zones, posing a risk to humans and the environment. Currently, typical hydrometallurgical separation of REE is performed at high temperatures under severe acidic and basic circumstances, resulting in huge volumes of hazardous and radioactive waste released [8]. Consequently, the removal rate is reliant on ores with substantial REE levels, which limits recovery [9]. The use of RE hyperaccumulating plants in phytoremediation (i.e., phytoextraction) looks to be a unique method that might aid in the reduction of high RE levels in soils (Figure 13.1). In contrast, the introduction of bacteria

*Corresponding author: Hosam M. Saleh, Radioisotope Department, Nuclear Research Center, Egyptian Atomic Energy Authority, Cairo, Egypt, e-mail: hosam.saleh@eaea.org.eg
Amal I. Hassan, Radioisotope Department, Nuclear Research Center, Egyptian Atomic Energy Authority, Cairo, Egypt

capable of mobilizing RE and/or supporting plant growth may augment the amount of REEs recovered by the flora and optimize bioconversion efficiency. The combination of bioaugmentation and phytostabilization may provide an appealing alternative to traditional methods in terms of cost-effectiveness and environmental friendliness [9]. No investigation integrating bioaugmentation and phytoremediation for the treatment of RE has been carried out.

Rare earth elements play a significant role in our daily lives since they are used in a variety of goods. Such items include those that may significantly contribute to considerably improve energy efficiency and combat climate change, both of which are emerging increasingly important on a global basis [10]. Rare earth mining and processing, on the other hand, have environmental and economic consequences. While extracting any ore body generates vast amounts of waste, the presence of radioactive components uranium and thorium in REEs waste has caused the most worry in terms of environmental and health concerns [11].
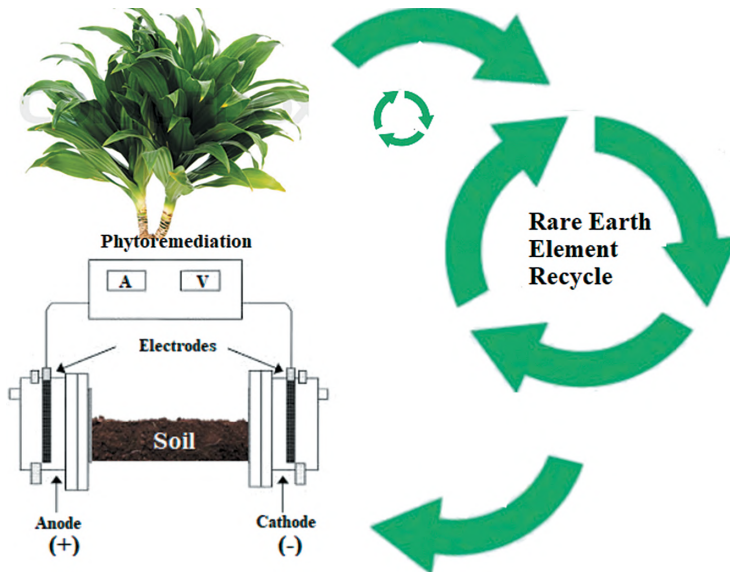
Figure 13.1: Phytoremediation and electrokinetics for REE remediation (modified from [12]).

Soil contamination is a critical issue because it endangers public health, the food supply, and groundwater [13]. Contamination of soil can occur at any point of the REE life span, including mineral exploration, manufacturing of products, distribution, and disposal. It is believed that contaminated soil contains REE that may be recovered and reused [3]. Because rare earth elements are often present at tiny levels in soils, extraction costs may be an impediment to REE recovery. Traditional REE extraction and purification procedures are both energy and chemical-intensive intense [14].

13.2 Methods of separation

The hunt for REE began around the 1800s. The first element found was yttrium, while promethium was discovered 150 years later. Promethium can only be produced intentionally and does not occur naturally [15]. While the metals and alloys used to manufacture rare earth magnetic materials are among the most common rare earth materials, REEs are utilized to make a variety of materials for consumers, industrial, and military applications. REEs offer steel and aluminum unique characteristics and have enabled glass improvements [16]. The creation of rare-earth-infrequent glasses, for example, has permitted various improvements in the composition of both marketable and novel functional glasses. REEs have recently sparked substantial interest because of their potential use in sustainability technologies that might assist humanity in transitioning away from dependency on fossil fuels [17]. REEs are used to generate red (EU and Y) and blue (EU) phosphors for energy-efficient light-emitting diodes (LEDs), which can provide more power than incandescent and fluorescent lighting. Conventional lighting systems use two orders of magnitude smaller than LEDs [17].

The isolation of REEs from ore is a hot topic, because of the intricacy of the processes required (due to the similar chemical properties of REEs) and because of the health, environmental and human influences attributed to the reagents and tailings [18]. According to a recent assessment of REEs containing minerals, the principal beneficiation methods include gravitational, electromagnetic, and flotation separation techniques. Surprisingly, the authors noticed that the available research on the physical refinement of RE minerals focuses mostly on two significant rare earth element mineral resources floating extraction procedures. Surprisingly, the authors discovered that most research on the physical refining of rare earth element mineral resources concentrates on two significant rare earth element mineral deposits [19]. As a result, when it comes to the technical components of RE durability, using high-performance and clean renewable energy technologies, as well as improving recycling and waste reclamation, is clearly crucial. Improvements in extraction and processing, as well as the development of low-impact substitutes, are also crucial for the future.

The worldwide REE output is 130,000 metric tons of rare earth oxide (REO) equivalent annually, with the 2014 REE industry valued at US $2051 million, while it is presently uncertain how recycling may affect the REE market due to the tiny level of recycling of these materials [20]. World consumption of these elements has steadily increased, and prices have remained constant following a significant jump caused by the enforcement and subsequent lifting of Chinese trade restrictions, which resulted in an overstock of certain REEs [20].

According to current research (e.g., according to current research (e.g., Geological Survey Of USA, Mineral Commodity Reports) [21], the estimated REE distributions by end-use include catalyst (75%), ceramics (6%), metallurgical applications (4%), glass polishing (5%), and other (10%), as seen in Figure 13.2.

A recent study indicates that landfills contain large levels of REEs [21]. According to UN estimates, the world generates 50 million tons of e-waste (old televisions, processors, displays, and smartphones) annually, costing more than $50 billion, with just 20% of it recycled. They forecasted that massive worldwide e-waste would be greater than a hundred million tons by 2050. The preceding study has also discovered that platinum group metal concentrations (e.g., palladium, ruthenium, osmium, platinum, and rhodium), Au, and Ag in landfill e-waste dumps are comparable to significant ore deposits now accessible from traditional mines.

Previously, several procedures (such as adsorption, ion, and precipitation flotation) were employed to extract and pre-concentrate REEs [22]. Soares et al. [23] explored innovative procedures for recovering REEs such as Neodymium (Nd) and Dysprosium (Dy) using the solid phase partial extraction method and discovered that this treatment was very successful in the extraction process for liquid REEs due to its durability and simplicity of processing.

Hosseinzadegan et al. [24] utilized a microwave to pre-concentrate REEs after dissolving leaf samples (tealeaf) in water with coated bio-particles and an ionic solvent.
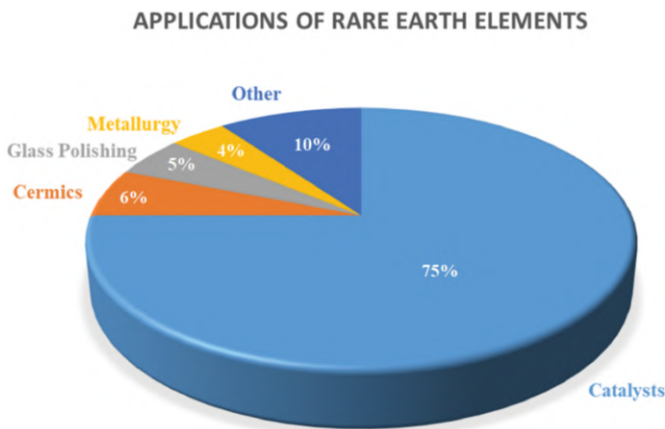
Figure 13.2: Application of REEs (modified from the USA Geological Survey Mineral Commodity (GSMC) 2020).

REEs are essential components of a wide range of industrial, commercial, and household items, as well as the growing electrifying of transportation in the industrialized world. Despite the fact that REEs are only used at tiny levels, they can provide performance or lifespan benefits to some goods relying on and making them difficult to substitute [26]. Lerner et al. [27] have confirmed the effectiveness of the Soares method by studying the use of chemically modified silica gel as an ion exchange resin for REEs by pre-concentrates. [27]. Wilfong et al. [28] explored the recovery of Dy and Yb from the water phase using amine sorbents (Table 13.1). According to their findings, the adsorbed

Table 13.1: REEs and their ubiquitous utilization (adapted from [25]).

Element	Applications
Lanthanum (La)	Optics, batteries, catalysis
Cerium (Ce)	Chemical applications, coloring, catalysis
Praseodymium (Pr)	Magnets, lighting, optics
Neodymium (Nd)	Magnets, lighting, lasers, optics
Samarium (Sm)	Magnets, lasers, masers
Europium (Eu)	Lasers, color TV, lighting, medical applications
Scandium (Sc)	Alloys in aerospace engineering, lighting
Gadolinium (Gd)	Magnets, glassware, lasers, X-ray generation, computer applications, medical applications
Terbium (Tb)	Lasers, lighting
Dysprosium (Dy),	Magnets, lasers
Holmium (Ho)	Lasers
Erbium (Er)	Lasers, steelmaking
Thulium (Tm)	X-ray generation
Ytterbium (Yb)	Lasers, chemical industry applications
Lutetium (Lu)	Medical applications, chemical industry applications
Yttrium (Y)	Lasers, superconductors, microwave filters, lighting

material may be used to pre-concentrate 7.6 percent/wt of REEs in fluid, which is higher than the US Department of Energy's REE pre-concentration objectives. This achievement demonstrates that the sorbent may be used to pre-concentrate REEs from real-world waste streams [28]. Alshameri et al. [29] have provided more information on REEs extraction/pre-concentration processes. Many research used various procedures for REEs decontamination and purification (e.g., evaporation, minimizing percolation, and membranes electroplating. El Afifi et al. [30] studied the effective expulsion of radioactive elements and ferrous in REE fluids from monazite and discovered that when a sulfate or sulfide (0.058/0.04 mol/L) admixture was employed, the average percent removal of unwanted species reached 96%. The average percent elimination of contaminants was 99% when a potassium iodate (KIO_3) of 0.155 mol/L was employed. They deduced that iodate is an effective and promising agent for removing radium isotopes, lead (Pb-210), Th (IV), and Fe(III) from rare earth chloride liquor with no loss of lanthanides and that these ingredients nullify the human hazards connected with radionuclides while generating higher-purity REEs from monazite ore. Silva et al. [31] had successfully undertaken an experimental investigation of various neutralizing reagents on the removal of various

pollutants in REE sulfuric liquor and concluded that the wisest purifying criterion was accomplished when the pH of limestone pulp was first increased to 3.5, then the lime pulp was added to the mixture to achieve a pH of 5.0. Pereao et al. [32] revealed that when polymer adsorbents were utilized, they could separate roughly 95% REEs. The recovery and separation of 99% for La, 100% for Y, and 100% for Gd from wasted glass material containing La-oxide, Y-oxide, and gadolinium oxide were achieved using sodium hydroxide, accompanied by hydrochloric acid flushing of the remaining particles [32]. Abhilash [33] also covered numerous REE separation strategies as well as several feedstocks to consider [33]. Da Costa et al. [34] explored the bioabsorption of RE metals from liquid solutions using non-traditional materials.

Hydrometallurgical procedures require the capacity to extract and separate RE components in a variety of ways by varying pH and acid/base ratios. Because of its simplicity of use, flexibility to a wide range of concentration ranges, and product purity, solvent extraction has become a popular technology [35]. Alternative procedures using supercritical fluids like CO_2 have also been thoroughly researched. Furthermore, microbial or other biological or enzymatic approaches for RE extraction are gaining favor because of their promise of reduced processing intensity and less environmental emissions [36]. Several key studies examining developments in the recovery of RE by recycling low-value waste flows such as bauxite residue, phosphogypsum, waste water, slag, and mine tailings have recently been published. Other writers have focused on the waste generated by RE [37].

13.3 Rare earth elements by sustainable approaches (phytoextraction)

Biological approaches have remained popular because of their minimal price, sustainability, and environmental friendliness. Bioleaching, biosorption, bioaccumulation, biomineralization, and bioprecipitation are examples of REE microbial activities. Biological procedures including bacteria, fungi, algae, and plants are another strategic emphasis for extracting REEs from samples collected and impurities [38].

Plants have long been used to clean polluted water and soil. Plant-based technologies such as rhizofiltration (i.e., the uptake of contaminants in the solution surrounding the root zone), phytoextraction, phytotransformation, phytostimulation, and phytostabilization are used to remove a variety of contaminants from polluted settings [39]. Plants use rhizofiltration (adsorption of REEs in the plant root system), phytoextraction (i.e. absorption of REEs within plants), and phytostabilization (deactivation and/or precipitation of REEs in the root system and surrounding soil) to remove REEs (Figure 13.3). The chemical properties of the soil and water environment in which the REE is located also influence its transport, whereas cation exchange aids in regulating REE transport in that specific environment [40]. The transfer of REE from soil to plants is influenced by particular parameters such as pH, soil clay concentration, soil organic matter content,

and redox potential, all of which make REE available to plants. Some plant species, such as *Taraxacum officinale* prevalent in urban environments, can be utilized as a bio-marker of trace elements and REE [41]. When exposed to harmful substances, these plants exhibit unusual traits such as decreased leaf thickness and less structured paren-chyma palisade tissue. Some of the elements have even been discovered to improve plant development. When exposed to harmful substances, these plants exhibit unusual traits such as decreased leaf thickness and less structured parenchyma palisade tissue. Some of the ingredients have been discovered to improve plant development. For instance, when exposed to 100 mM praseodymium (Pr), *Salvia miltiorrhiza* demonstrated improved growth and greater secondary metabolite content in plant sections [42].
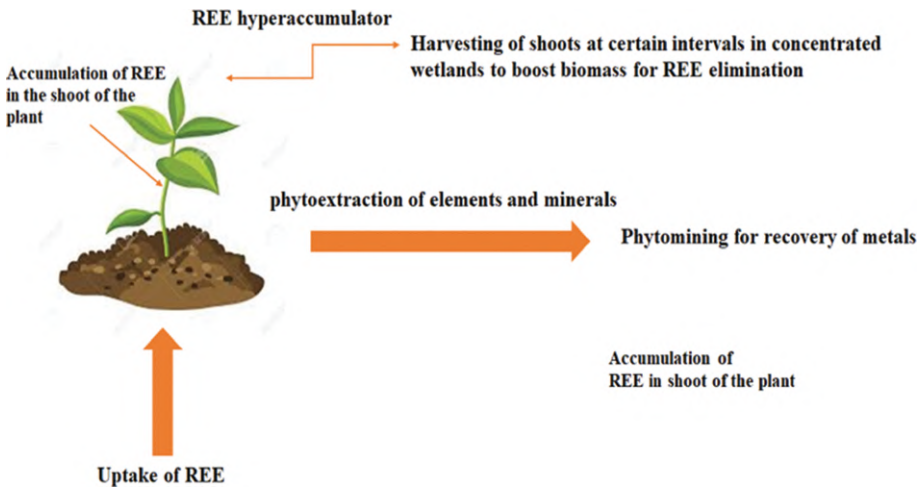

REE hyperaccumulator

Harvesting of shoots at certain intervals in concentrated wetlands to boost biomass for REE elimination

Accumulation of REE in the shoot of the plant

phytoextraction of elements and minerals

Phytomining for recovery of metals

Accumulation of REE in shoot of the plant

Uptake of REE

Figure 13.3: The phytoremediation of REEs.

When traditional mines are no longer feasible, the notion of phytomanagement offers a viable option, to just not to mention all of the ecological benefits supplied by flora [43]. The phytoremediation process enables the separation and retrieval of RE from agricultural lands or wastes of different industries (for example, phosphogypsum is a waste by-product of the processing of phosphate rock in facilities generating phosphoric acid and phosphate fertilizers) with the potential for commercial added value [43]. Recently, 20 bioaccumulation plant species (nearly ferns like *Dicranopteris dicthotoma*) have been found to collect large quantities of RE, particularly in their aerial portions [44]. While the possible functions of regional bacteria in mobilizing RE from ores are still being studied, those of plant growth boosting rhizosphere bacteria (PGBR) are far less well understood [45]. PGBR can mobilize metals and drive plant growth in order to improve the quantity of RE extracted by the plant, resulting in a greater phytoextraction efficiency [45]. The number of studies leading to novel methods for RE recovering from various sources, such as mining, industrial, and electronic wastes is quickly increasing.

Despite this, recycling remains exceedingly complex, costly, and restricted, accounting for just around 1% of total RE production in 2011 [45]. This resulted in the creation of techniques that are both commercially viable and ecologically beneficial. On the contrary, phytoremediation appears to be a unique alternative for lowering high RE-level sites by the utilization of RE uptake plants [46]. Because there is insufficient data on the consequences of liming and fertilization on plant absorption of specific REEs, relevant knowledge on the effects of soil modifications on trace element uptake from the soil should be expanded. Liming, like the other treatments, has an influence on the chemical composition of the soil solution due to the unique characteristics of the plant species and the behavior of each of the components investigated.

Nissen et al. [47] discovered that liming decreased the phytoextraction of certain elements such as chromium (Cr), lead (Pb), copper (Cu), and arsenic (As) in Zea mays, arsenic (As) in *Lupinus albus* (*L. albus*), and arsenic (As) and lead (Pb) in *Brassica napus* (*B. napus*). This might be owing to PTE immobilization caused by the formation of insoluble metal complexes and metal precipitation, which affects the bio-accessibility of these elements to *Z. mays* [48]. The increase in Cu, Cr, and Pb phytoextraction by *L. albus* [49] and Cu and Cr by *B. napus* [50, 51] may be due to organic acid (OA) efflux by the root systems, which ensures microorganism bioactivity [52,53]. Organic acids boost the accessibility of phosphorus in the rhizospheres and act as carbon sources for the bacteria in the soil, which can produce chemicals that improve iron availability for plant absorption. It is not unexpected, however, that comparable patterns were identified in phytoextraction of P, Fe, and Cu in *L. albus* and *B. napus* after liming [54]. Reduced total REE phytoextraction may be related to a rise in soil pH to alkaline conditions since REEs' bioavailability in soil solution increases with soil acidity [54].

Biosorption is the quickest biological technique, and the interaction of REEs with functional clusters on the microorganisms leads to their retention inside the biomass [55]. REEs can be transferred from the microbial surface to the interstitial space, detoxified, decreased, and stored inside vacuoles [55]. In comparison to the other techniques, this bioaccumulation of REEs happens to a lesser level. Bioprecipitation can occur directly because of the microbial activity or indirectly because of the generation of reagents, which precipitate REE and changes in environmental conditions. In several cases when microbiological treatment of REEs is required, a confluence of these techniques results in 100% removal and recovery of REEs [56].

Combining bioaugmentation and phytoextraction could be a viable alternative to traditional procedures, resulting in a cost-effective and ecologically friendly option [56]. Phytotechnologies are a viable option for in-situ depollution because they allow soil qualities to be preserved, allowing soils to reclaim their role in food production and for plantings [57]. Phytotechnologies go further than the simple role of plants in risk management, encompassing all of the benefits that plants may bring to humans [57], which encompass all of the advantages that plants may provide to humans. All geochemistry cycles of trace metals, including RE, are mediated by microorganisms. Lanthanum is known as "super calcium" because it substitutes calcium (Ca) and hinders numerous

plant enzymes and other functioning proteins [58]. When REEs replace "Ca" at extrinsic binding sites, the release of extracellular and intracellular calcium is prevented, which has a detrimental impact on plant development and vitality [59]. Scientists have long considered RE inert due to their low solubility in the environment. REs such as cerium and lanthanum (Ce^{3+} and La^{3+}, respectively) have been revealed to be essential for the function of the methanol (Me) dehydrogenase enzyme, which is employed by certain bacteria to oxidize Me for carbon and energy since eleven years [60]. As a result, several types of research have been conducted to get a better knowledge of the interconnections between microflora and RE via metabolic processes and RE sequestration from liquids by biomass sorption [61]. Microorganisms mobilize TE from all solid matrices, such as those containing RE, via three methods. (i) proton-induced acidolysis with the removal of RE via chelated agent clearance, (ii) ligand-induced solubilization (complexolysis), and (iii) oxidation/reduction processes (redoxolysis) [61]. This mobility is affected by a combination of variables, including pH, oxidizing circumstances, the availability and type of inorganic and organic colloids, and the existence and activities of microbial organisms. This is because various microorganisms have varying optimal pH that favors the synthesis of the most helpful microbial agents for RE leaching. A fungus isolated from cementation has been revealed to mobilize Ce and Eu from dolomite at pH less than seven, whereas *Arthrobacter sp.* leads to the mobilization of all the RE from hornblende between pH 6.5 and 7.5. In some other cases, it has been demonstrated that at low pH of media (less than two), *Aspergillus niger* generates mostly citric acid ($C_6H_8O_7$), but at higher pH (greater than four) it produces pentahydroxy caproic ($C_6H_{12}O_7$) and oxalic acids ($C_2H_2O_4$) [62].

As the majority of REEs are present in oxidation state III, it is easily absorbed by a broad array of soil hauling phases, such as metallic oxides and hydroxides [63]. Manganese alloys (Mn (III) and (IV)) absorb trivalent RE, particularly somewhat more readily than Pr and La, and oxidize to Ce (IV) [63]. The organic matter concentration and ligand competition will also affect these adsorption and oxidation-reduction processes. Once mobilized, bacterium interactions with RE alter their activity and transport into the environment. Lui et al. [64] reported that the sorption process of Ce by *P. fluorescens* in Ce (III) form prevented future oxidation to Ce (IV) by manganese oxides, modifying its transmission. Microbial exogenous polysaccharides can enhance RE dispersion by chelation of the ions in the solution, decreasing the latter's saturation level. Kraemer et al. [65] showed that siderophores had a high affinity for Ce (IV). Andrès et al. [66] observed the development of RE Lanthanum, Scandium, and Yttrium-siderophore complexes in *Mycobacterium smegmatis*. The rhizosphere includes ten to a hundred of folding more microorganisms/gram of agricultural soil than non-rhizospheric soil due to the inclusion of carbon and nitrogen molecules from rhizodeposits [67]. Thus, plants interact closely with rhizosphere microorganisms, some of which can boost plant growth and development by enhancing nutrient uptake and resistance to telluric diseases and other stressors [67].

Yuan et al. [68] investigated the fragmentation distribution of REE in soil uptake to plant and root-to-shoot transport processes in *Phytolacca americana* growing in REEs mining zones. They also looked at the capacity of *P. americana*, which grows naturally in the mining region, to accumulate REEs. According to Wen et al. [69], the concentration of REE collected was in the sequence of roots, stem, leaves, and grains. La and Ce pollution harmed germination in *D. canadense* and *S. lycopersium*, whereas Ce harmed *A. syriaca, S. lycopersicum, R. sativus, and P. virgatum*. A negative effect was detected for D. canadense at a high dosage in yttrium soils (102.8 mg/kg of soil) and for *A. syriaca* at a low pH cerium soil (70.9 mg Ce/kg of soil) [70]. Plants may absorb Ce, penetrate their tissues, and cause toxicity.

13.4 Rare earth bionanoparticles

REEs can also be recovered by using organisms that produce rare earth element nanoparticles (REE-NPS). REEs have recently become an essential component of sophisticated industries. However, the industry faces REE material deficit, owing mostly to a lack of robust recovery solutions associated with long-term REE removal. Scientists employed nanotechnology to create nanocellulose that can successfully recover REE uniquely and sustainably. Adsorbents such as silica, clay, nanotubes, and chitosan have already been employed in several investigations for REE recovery. However, cellulose is the most cost-effective and plentiful raw material that has seldom been employed as an adsorbent for REEs extraction [71]. Nd is a critical component of magnets NdFeB, which are among the most powerful ferromagnetic material. NdFeB magnets are widely employed in a variety of sectors such as electrical gadgets, manufacturing engines, and magnetic resonance imaging scanners (MRIS) [72]. These magnets are also used in green energy industries such as wind turbine turbines and solar panels. As these sectors progress, the need for Nd has increased substantially; 400% rise in the last two decades. Approximately 81% of REEs, including Nd, are mined and processed in China, the world's largest exporter [72]. Anionic hairy nanocellulose is a technique that can remove neodymium ions (Nd^{3+}) from aqueous solutions. The hairy nanoparticles have been negatively charged to attract and bind with positively charged neodymium ions (Nd^{3+}) [71]. This agglomeration of nanoparticles and NB leads to bigger pieces that can be easily recycled and reused. Dicarboxylated cellulose (DCC) chains and cellulose nanocrystals are entirely solubilized in anionic hairy nanocellulose technology (CNC). When compared to traditional CNC, DCC hairs have a higher charge density, almost one order of magnitude higher. Polyanionic hairs in this method can remove 264 milligrams of Nd^{3+} from nano adsorbents in seconds. When the starting Nd^{3+} concentration was changed from 140 ppm to 1000 ppm, the Nd^{3+} clearance capability *vs* equilibrium Nd^{3+} concentration was shown. Because unsaturated adsorbents stay stable in solution, one of the persistent issues with nanostructures element separation is the lack of colloidal agglomeration at

low adsorbate-to-adsorbent ratios. In these circumstances, adsorption occurs, but the adsorptive species do not undergo phase separation [71]. Nd^{3+} cannot be eliminated from solution at low doses (C0 100 ppm, COO^-: Nd^{3+} 4.4 mol:1 mol), because charged AHNC-Nd aggregates persist. Wamea et al. [71] used calcium ions + as a supplementary cation to help in AHNC saturating and the removal of AHNC-Nd aggregates after Nd^{3+} adsorption. When AHNC is added to the Nd^{3+} solution initially, the carboxylate groups first interact with Nd ions, and the residual groups are bridged with calcium ions afterward, with no effect on COO^- and Nd^{3+} binding. These findings suggest that AHNC is a feasible long-term resource for Nd^{3+} removal from solutions, which might assist neodymium recycling from secondary sources such as e-waste and NdFeB permanently magnets, as well as aid in the resolution of neodymium-related environmental and supply risk concerns [71].

Until now, REE-NPs have been synthesized virtually entirely from plant biomass. Ce-NPs, for example, have been created utilizing a variety of plant extracts. An extract of *Petroselinum crispum* has been proven to produce CeO_2 nano- and microparticles. *Acalypha indica* leaf extract may also be used to make cerium oxide nanoparticles. The antibacterial efficacy of these biosynthesized CeO_2 NPs against Gram-positive and Gram-negative bacteria (GNB) was shown. An eco-acceptable approach for the manufacture of dysprosium oxide NPs was developed using clove bud extract (*Syzygium aromaticum*). When tested against *Staphylococcus aureus* (*S. aureus*) and *Escherichia coli*, these NPs seemed innocuous and showed no inhibition of GNB. They were evaluated as a non-toxic method of detecting picric acid, an organic pollutant [73]. La-NPs have also been synthesized using *Mutingia calabura* leaves extract [74]. These La-NPs demonstrated antioxidant action and mild antibacterial activity against a variety of bacterial species.

Terbium oxide NPs were synthesized by incubating Tb_4O_7 in the presence of the fungus species *Fusarium oxysporum*. The NPs developed thus demonstrated good biocompatibility and prevented the proliferation of osteo-cancerous cells while causing no harm to normal osteoblasts even at relatively high concentrations [75]. A recent study used hybrid *E. coli*-expressing protease enzyme called "phytochelatin synthase" and metallothionein (heavy-metal-binding proteins (HMBPs), to synthesize *Europium selenide* (EuSe) NPS. According to the authors, the cationic precursors of the EuSe-NPS bind to the HMBPs surfaces and aggregate into NPs via electrostatic forces [74]. The revelation of bacterial regulatory proteins in REE transfer and biocontacts with REE, like lanmodulin, may pave the way for the discovery of thermophilic bacteria that biosynthesize REE-NPS [74]. Furthermore, unlike most other metalloproteins, LM has metal-binding capabilities and structural stability. LM sustains REE affinity below pH 2.5, and LM-REE complexes can tolerate high temperatures (greater than 90 °C), repetitive acid procedures, and higher to molar quantities of competing for non-REE metal ions (such as Ca, Mg, Cu, and Zn), enabling the protein to be used in severe chemical processes.

Microbial NPs manufacturing offers the benefit of creating more stable metallic nanoparticles (MeNPs) with a lower agglomeration propensity. This enhanced stability is generally triggered by microbial proteins and other biomolecules capping the NP

surface [76]. These capped proteins (CP) attach to MeNPs via their amine and cysteine clusters, neutralizing the particles' overall surface charges and blocking clustering, which would result in the scarcity of their distinguishing characteristics. Surfactants are frequently employed to boost the stability of chemically generated NPs; however, these substances are generally poisonous, limiting their biological uses.

Protein-enabled biosynthesized NP stability is non-toxic, ecologically benign, and generally safer. Moreover, MeNP synthesis by microorganisms provides better management of the process parameters, which is important pH of medium utilized, light, metal ion concentration, and temperature may all influence the form, volume, and manufacturing adequacy of MeNPs. As a result, extremophilic microorganisms (EXMs) that have evolved to exist in harsh environments are particularly important to MeNPs biosynthesis [77]. Numerous EXMs have particular characteristics for mitigating toxicity of metal stresses, and some of them thrive at extremely high metal ion concentrations, like those observed in hydrothermal vents or magma zones, depositing sites for metallurgical wastes from processed ores, in which mesophilic microorganisms essentially cannot sustain life [78, 79]. *Deinococcus radiodurans* is a notable example of an extremophile's use in MeNPs production. This polyextremophile bacterium is exceptionally radio-, thermos-, psychro-, and acid-tolerant, and it has been found to make CP spherical silver NPs.

13.5 Conclusions

Globally, most REEs are used for catalysts, magnets, ceramics, glass, and polishing. REEs have been utilized in agriculture to boost plant growth, productivity, and stress tolerance, with no apparent deleterious impacts on human and animal consumption.

Physicochemical or biological techniques may be used to extract REE from solid materials. Dissolution, electrochemical technology, fractional crystallization, and solvent extraction are examples of traditional physicochemical procedures for REE extraction and separation. Because of concerns about environmental sustainability and raw material extraction, investigations on improving ecologically sound extraction of these components from the soil for resource recovery and remediation are recommended. There is great interest in these elements and great future prospects that bacteria producing rare earth organisms (REE-NPs) may expose to biomineralization of these valuable and expensive minerals, especially bacterial biosynthesis of REE-NPs.

References

[1] Opare, EO, Struhs, E, Mirkouei, A. A comparative state-of-technology review and future directions for rare earth element separation. Renew Sustain Energy Rev, 2021, 143, 110917.

[2] Xia, M, Wu, X, Zhong, Y, Hintzen, HTB, Zhou, Z, Wang, J. Photoluminescence properties and energy transfer in a novel Sr_8 ZnY (PO 4) 7: Tb^{3+}, Eu^{3+} phosphor with high thermal stability and its great potential for application in warm white light emitting diodes. J Mater Chem C, 2019, 7, 2927–2935.

[3] Omodara, L, Pitkäaho, S, Turpeinen, E-M, Saavalainen, P, Oravisjärvi, K, Keiski, RL. Recycling and substitution of light rare earth elements, cerium, lanthanum, neodymium, and praseodymium from end-of-life applications-A review. J Clean Prod, 2019, 236, 117573.

[4] Sola, ABC, Parhi, PK, Thenepalli, T, Jyothi, RK. Introduction of rare earth metal recovery for green and clean energy technologies. In: Rare-Earth Metal Recovery for Green Technologies, Springer, 2020, 1–8.

[5] Massari, S, Ruberti, M. Rare earth elements as critical raw materials: Focus on international markets and future strategies. Resour Policy, 2013, 38, 36–43.

[6] Balaram, V. Rare earth elements: A review of applications, occurrence, exploration, analysis, recycling, and environmental impact. Geosci Front, 2019, 10, 1285–1303.

[7] Zhang S, Ding Y, Liu B, Chang C. Supply and demand of some critical metals and present status of their recycling in WEEE. Waste Manag, 2017, 65, 113–127.

[8] Deblonde, GJ-P, Mattocks, JA, Park, DM, Reed, DW, Cotruvo, JJA, Jiao, Y. Selective and efficient biomacromolecular extraction of rare-earth elements using lanmodulin. Inorg Chem, 2020, 59, 11855–11867.

[9] Dong, Z, Mattocks, JA, Deblonde, GJ-P, Hu, D, Jiao, Y, Cotruvo, JJA, Park, DM. Bridging hydrometallurgy and biochemistry: A protein-based process for recovery and separation of rare earth elements. ACS Cent Sci, 2021, 7, 1798–1808.

[10] Tursi, A, Mastropietro, TF, Bruno, R, Baratta, M, Ferrando-Soria, J, Mashin, AI, Nicoletta, FP, Pardo, E, De Filpo, G, Armentano, D. Synthesis and enhanced capture properties of a new bioMOF@ SWCNT-BP: Recovery of the endangered rare-earth elements from aqueous systems. Adv Mater Interfaces, 2021, 8, 2100730.

[11] Talan, D, Huang, Q. A review of environmental aspect of rare earth element extraction processes and solution purification techniques. Miner Eng, 2022, 179, 107430.

[12] Lima, AT, Ottosen, L. Recovering rare earth elements from contaminated soils: Critical overview of current remediation technologies. Chemosphere, 2021, 265, 129163.

[13] Nalbantcilar, MT, Pinarkara, SY. Public health risk assessment of groundwater contamination in Batman, Turkey. J Water Health, 2016, 14, 650–661.

[14] Wintzheimer, S, Reichstein, J, Groppe, P, Wolf, A, Fett, B, Zhou, H, Pujales-Paradela, R, Miller, F, Müssig, S, Wenderoth, S. Supraparticles for sustainability. Adv Funct Mater, 2021, 31, 2011089.

[15] Zhang, C. Retracted article: Detection of rare earth elements in groundwater based on SAR imaging algorithm and fatigue intervention of dance training. Arab J Geosci, 2021, 14, 1–15.

[16] Stopic, S, Friedrich, B. Advances in understanding of the application of unit operations in metallurgy of rare earth elements. Metals (Basel), 2021, 11, 978.

[17] Hossain, MK, Hossain, S, Ahmed, MH, Khan, MI, Haque, N, Raihan, GA. A review on optical applications, prospects, and challenges of rare-earth oxides. ACS Appl Electron Mater, 2021, 3, 3715–3746.

[18] Malhotra, N, Hsu, H-S, Liang, S-T, Roldan, MJM, Lee, J-S, Ger, T-R, Hsiao, C-D. An updated review of toxicity effect of the rare earth elements (REEs) on aquatic organisms. Animals, 2020, 10, 1663.

[19] Vrbický, T, Přikryl, R. Recovery of some critical raw materials from processing waste of feldspar ore related to hydrothermally altered granite: laboratory-scale beneficiation. Minerals, 2021, 11, 455.

[20] Chowdhury, NA, Deng, S, Jin, H, Prodius, D, Sutherland, JW, Nlebedim, IC. Sustainable recycling of rare-earth elements from NdFeB Magnet Swarf: Techno-economic and environmental perspectives. ACS Sustain Chem Eng, 2021, 9, 15915–15924.

[21] Herrington, R. Mining our green future. Nat Rev Mater, 2021, 6, 456–458.

[22] Zuma, MC, Lakkakula, J, Mketo, N. Recent trends in sample preparation methods and plasma-based spectrometric techniques for the determination of rare earth elements in geological and fossil fuel samples. Appl Spectrosc Rev, 2020, 1–25.

[23] Soares, KL, Barbosa, SC, Primel, EG, Fillmann, G, Diaz-Cruz, MS. Analytical methods for antifouling booster biocides determination in environmental matrices: A review. Trends Environ Anal Chem, 2021, 29, e00108.

[24] Hosseinzadegan, S, Nischkauer, W, Bica, K, Limbeck, A. Bioparticles coated with an ionic liquid for the pre-concentration of rare earth elements from microwave-digested tea samples and the subsequent quantification by ETV-ICP-OES. Anal Methods, 2016, 8, 7808–7815.

[25] Weng, Z, Jowitt, SM, Mudd, GM, Haque, N. A detailed assessment of global rare earth element resources: Opportunities and challenges. Econ Geol, 2015, 110, 1925–1952.

[26] Barrett, CB. Overcoming global food security challenges through science and solidarity. Am J Agric Econ, 2021, 103, 422–447.

[27] Lerner, N, Meyerstein, D, Shamir, D, Marks, V, Shamish, Z, Ohaion-Raz, T, Maimon, E. A chemically modified silica-gel as an ion exchange resin for pre-concentration of actinides and lanthanides. Inorganica Chim Acta, 2019, 486, 642–647.

[28] Wilfong, WC, Kail, BW, Wang, Q, Shi, F, Shipley, G, Tarka, TJ, Gray, ML. Stable immobilized amine sorbents for heavy metal and REE removal from industrial wastewaters. Environ Sci: Water Res Technol, 2020, 6, 1286–1299.

[29] Alshameri, A, He, H, Xin, C, Zhu, J, Xinghu, W, Zhu, R, Wang, H. Understanding the role of natural clay minerals as effective adsorbents and alternative source of rare earth elements: Adsorption operative parameters. Hydrometallurgy, 2019, 185, 149–161.

[30] El Afifi, EM, Borai, EH, Shahr El-Din, AM. New approaches for efficient removal of some radionuclides and iron from rare earth liquor of monazite processing. Int J Environ Sci Technol, 2019, 16, 7735–7746.

[31] de Fátima da Silva, M, de Sousa Oliveira, MR, Dos Santos, ID, Radino-Rouse, P, Mansur, MB. Iron precipitation strategies from nickel laterite ore sulfuric acid leach liquor. Miner Process Extr Metall Rev, 2022, 43, 28–39.

[32] Pereao, O, Bode-Aluko, C, Fatoba, O, Laatikainen, K, Petrik, L. Rare earth elements removal techniques from water/wastewater: A review. Desalin Water Treat, 2018, 130, 71–86.

[33] Meshram, P, Abhilash. Recovery and recycling of cerium from primary and secondary resources-a critical review. Miner Process Extr Metall Rev, 2020, 41, 279–310.

[34] da Costa, TB, da Silva, MGC, Vieira, MGA. Recovery of rare-earth metals from aqueous solutions by bio/adsorption using non-conventional materials: A review with recent studies and promising approaches in column applications. J Rare Earths, 2020, 38, 339–355.

[35] Mattocks, JA, Cotruvo, JA. Biological, biomolecular, and bio-inspired strategies for detection, extraction, and separations of lanthanides and actinides. Chem Soc Rev, 2020, 49, 8315–8334.

[36] Vollmer, I, Jenks, MJF, Roelands, MCP, White, RJ, van Harmelen, T, de Wild, P, van Der Laan, GP, Meirer, F, Keurentjes, JTF, Weckhuysen, BM. Beyond mechanical recycling: Giving new life to plastic waste. Angew Chem Int Ed, 2020, 59, 15402–15423.

[37] Meshram, P, Pandey, BD. Perspective of availability and sustainable recycling prospects of metals in rechargeable batteries–a resource overview. Resour Policy, 2019, 60, 9–22.

[38] Karim S, Ting Y-P. Recycling pathways for platinum group metals from spent automotive catalyst: A review on conventional approaches and bio-processes. Resour Conserv Recycl, 2021, 170, 105588.

[39] Vijgen, J, de Borst, B, Weber, R, Stobiecki, T, Forter, M. HCH and lindane contaminated sites: European and global need for a permanent solution for a long-time neglected issue. Environ Pollut, 2019, 248, 696–705.

[40] Liu, C, Liu, W, Huot, H, Yang, Y, Guo, M, Morel, JL, Tang, Y, Qiu, R. Responses of ramie (Boehmeria nivea L.) to increasing rare earth element (REE) concentrations in a hydroponic system. J Rare Earths. 2021. https://doi.org/10.1016/j.jre.2021.04.002.

[41] Skrynetska, I, Karcz, J, Barczyk, G, Kandziora-ciupa, M, Ciepa, R. Using Plantago major and Plantago lanceolata in environmental pollution research in an urban area of Southern Poland. 2019, 23359–23371

[42] Fan, Z, Zhang, K, Wang, F, Zhao, X, Bai, R, Liu, B. Effects of rare earth elements on growth and determination of secondary metabolites under in vitro conditions in salvia miltiorrhiza. Hort Sci, 2020, 55, 310–316–2020 v.55 no.3. https://doi.org/10.21273/HORTSCI14661-19.

[43] Zine, H, Midhat, L, Hakkou, R, El, M. Guidelines for a phytomanagement plan by the phytostabilization of mining wastes Guidelines for a phytomanagement plan by the phytostabilization of mining wastes. Sci Afr, 2020, 10, e00654. https://doi.org/10.1016/j.sciaf.2020.e00654.

[44] Yang, L, Huang, Y, Lima, LV, Sun, Z, Liu, M, Wang, J, Liu, N, Ren, H. Rethinking the ecosystem functions of dicranopteris, a widespread genus of ferns. Front Plant Sci, 2021, 11, 581513. https://doi.org/10.3389/fpls.2020.581513.

[45] Jalali, J, Lebeau, T. The role of microorganisms in mobilization and phytoextraction of rare earth elements: A review. 2021, 9, 1–19. https://doi.org/10.3389/fenvs.2021.688430.

[46] Land, M, Ghosh, S, Chen, Z. Phytoremediation: A promising approach for revegetation of heavy. 2020, 11, 1–15. https://doi.org/10.3389/fpls.2020.00359.

[47] Nissen, LR, Lepp, NW, Edwards, R. Synthetic zeolites as amendments for sewage sludge-based compost. Chemosphere, 2000, 41, 265–269.

[48] Hamid, Y, Tang, L, Wang, X, Hussain, B, Yaseen, M, Aziz, MZ, Yang, X. Immobilization of cadmium and lead in contaminated paddy field using inorganic and organic additives. Sci Rep, 2018, 8, 1–10.

[49] Tyler, G, Olsson, T. Plant uptake of major and minor mineral elements as influenced by soil acidity and liming. Plant Soil, 2001, 230, 307–321.

[50] Chaignon, V, Quesnoit, M, Hinsinger, P. Copper availability and bioavailability are controlled by rhizosphere pH in rape grown in an acidic Cu-contaminated soil. Environ Pollut, 2009, 157, 3363–3369.

[51] Akhtar, N, Ilyas, N, Yasmin, H, Sayyed, RZ, Hasnain, Z, Elsayed E, A, Enshasy HA, E. Role of Bacillus cereus in improving the growth and phytoextractability of Brassica nigra (L.) K. Koch in chromium contaminated soil. Molecules, 2021, 26, 1569.

[52] Delorme, TA, Gagliardi, JV, Angle, JS, Chaney, RL. Influence of the zinc hyperaccumulator Thlaspi caerulescens J. & C. Presl. and the nonmetal accumulator Trifolium pratense L. on soil microbial populations. Can J Microbiol, 2001, 47, 773–776.

[53] Wachendorf, C. Effects of liming and mineral N on initial decomposition of soil organic matter and post harvest root residues of poplar. Geoderma, 2015, 259, 243–250.

[54] Okoroafor, PU, Kunisch, N, Epede, MN, Ogunkunle, CO, Heilmeier, H, Wiche, O. Phytoextraction of rare earth elements, germanium and other trace elements as affected by fertilization and liming. Environ Technol Innovation, 2022, 102607.

[55] Fathollahi, A, Khasteganan, N, Coupe, SJ, Newman, AP. A meta-analysis of metal biosorption by suspended bacteria from three phyla. Chemosphere, 2021, 268, 129290. https://doi.org/https://doi.org/10.1016/j.chemosphere.2020.129290.

[56] Jurkowski, W, Paper, M, Brück, TB. Isolation and investigation of natural rare earth metal chelating agents from calothrix brevissima – a step towards unraveling the mechanisms of metal biosorption. 2022, 10, 1–10. https://doi.org/10.3389/fbioe.2022.833122.

[57] Mourinha, C, Alexandre, C, Cruz, N, Rodrigues, M, Alvarenga, P. Potentially toxic elements' contamination of soils affected by mining activities in the portuguese sector of the iberian pyrite belt and optional remediation actions: A review. Environments, 2022, 9, 11. https://doi.org/10.3390/environments9010011.

[58] Rather, RA, Wani, AW, Mumtaz, S, Padder, SA, Khan, AH, Almohana, AI, Almojil, SF, Alam, SS, Baba, TR. Bioenergy: A foundation to environmental sustainability in a changing global climate scenario. J King Saud Univ – Sci, 2022, 34, 101734. https://doi.org/https://doi.org/10.1016/j.jksus.2021.101734.

[59] Valdespino-Castillo, PM, Hu, P, Merino-Ibarra, M, López-Gómez, LM, Cerqueda-García, D, González-De Zayas, R, Pi-Puig, T, Lestayo, JA, Holman, H-Y, Falcón, LI. Exploring biogeochemistry and microbial diversity of extant microbialites in Mexico and Cuba. Front Microbiol, 2018, 9, https://doi.org/10.3389/fmicb.2018.00510.

[60] Kruco, T. Lanthanide-Dependent Methanol Metabolism of a Proteobacteria-Dominated Community in a Light Lanthanide-Rich Deep Environment, 2022.

[61] Fomina, M, Skorochod, I. Microbial Interaction with clay minerals and its environmental and biotechnological implications. Miner, 2020, 10.

[62] Jalali, J, Lebeau, T. The role of microorganisms in mobilization and phytoextraction of rare earth elements: A review. Front Environ Sci, 2021, 9, https://doi.org/10.3389/fenvs.2021.688430.

[63] Dinali, GS, Root, RA, Amistadi, MK, Chorover, J, Lopes, G, Guilherme, LRG. Rare earth elements (REY) sorption on soils of contrasting mineralogy and texture. Environ Int, 2019, 128, 279–291. https://doi.org/https://doi.org/10.1016/j.envint.2019.04.022.

[64] Liu, H, Guo, H, Pourret, O, Chen, Y, Yuan, R. Role of manganese oxyhydroxides in the transport of rare earth elements along a groundwater flow path. Int J Environ Res Public Heal, 2019, 16.

[65] Kraemer, D, Tepe, N, Pourret, O, Bau, M. Negative cerium anomalies in manganese (hydr)oxide precipitates due to cerium oxidation in the presence of dissolved siderophores. Geochim Cosmochim Acta, 2016, https://doi.org/10.1016/j.gca.2016.09.018.

[66] Andrès, Y, Thouand, G, Boualam, M, Mergeay, M. Factors influencing the biosorption of gadolinium by micro-organisms and its mobilisation from sand. Appl Microbiol Biotechnol, 2000, 54, 262–267. https://doi.org/10.1007/s002530000368.

[67] Li, J, Luo, Z, Zhang, C, Qu, X, Chen, M, Song, T, Yuan, J. Seasonal Variation in the Rhizosphere and Non-Rhizosphere Microbial Community Structures and Functions of Camellia yuhsienensis Hu. Microorganisms, 2020, 8, 1385. https://doi.org/10.3390/microorganisms8091385.

[68] Yuan, M, Liu, C, Liu, W-S, Guo, M-N, Morel, JL, Huot, H, Yu, H-J, Tang, Y-T, Qiu, R-L. Accumulation and fractionation of rare earth elements (REEs) in the naturally grown Phytolacca americana L. in southern China. Int J Phytorem, 2018, 20, 415–423. https://doi.org/10.1080/15226514.2017.1365336.

[69] Wen, B, Yuan, D, Shan, X, Li, F, Zhang, S. The influence of rare earth element fertilizer application on the distribution and bioaccumulation of rare earth elements in plants under field. 2015, https://doi.org/10.3184/095422901783726825.

[70] Thomas, PJ, Carpenter, D, Boutin, C, Allison, JE. Rare earth elements (REEs): Effects on germination and growth of selected crop and native plant species. Chemosphere, 2014, 96, 57–66. https://doi.org/https://doi.org/10.1016/j.chemosphere.2013.07.020.

[71] Wamea, P, Pitcher, ML, Muthami, J, Sheikhi, A. Nanoengineering cellulose for the selective removal of neodymium: Towards sustainable rare earth element recovery. Chem Eng J, 2022, 428, 131086.

[72] Bonfante, MC, Raspini, JP, Fernandes, IB, Fernandes, S, Campos, LMS, Alarcon, OE. Achieving Sustainable Development Goals in rare earth magnets production: A review on state of the art and SWOT analysis. Renew Sustain Energy Rev, 2021, 137, 110616.

[73] Jain, A, Sharma, A, Gupta, P, Wadhawan, S, Mehta, SK. Biosynthesis driven dysprosium oxide nanoparticles as a sensor for picric acid. Curr Res Green Sustain Chem, 2021, 4, 100080.

[74] Atalah, J, Espina, G, Blamey, L, Muñoz-Ibacache, SA, Blamey, JM. Advantages of using extremophilic bacteria for the biosynthesis of metallic nanoparticles and its potential for rare earth element recovery. Front Microbiol, 2022, 13, 855077.

[75] Eivazzadeh-Keihan, R, Bahojb Noruzi, E, Khanmohammadi Chenab, K, Jafari, A, Radinekiyan, F, Hashemi, SM, Ahmadpour, F, Behboudi, A, Mosafer, J, Mokhtarzadeh, A. Metal-based nanoparticles for bone tissue engineering. J Tissue Eng Regener Med, 2020, 14, 1687–1714.

[76] Borgheti-Cardoso, LN, San Anselmo, M, Lantero, E, Lancelot, A, Serrano, JL, Hernández-Ainsa, S, Fernandez-Busquets, X, Sierra, T. Promising nanomaterials in the fight against malaria. J Mater Chem B, 2020, 8, 9428–9448.

[77] Chauhan, G, González-González, RB, Iqbal, HMN. Bioremediation and decontamination potentials of metallic nanoparticles loaded nanohybrid matrices–A review. Environ Res, 2022, 204, 112407.

[78] Beeler, E, Singh, OV. Extremophiles as sources of inorganic bio-nanoparticles. World J Microbiol Biotechnol, 2016, 32, 1–11.

[79] Ovais, M, Khalil, AT, Ayaz, M, Ahmad, I, Nethi, SK, Mukherjee, S. Biosynthesis of metal nanoparticles via microbial enzymes: A mechanistic approach. Int J Mol Sci, 2018, 19, 4100. https://doi.org/10.3390/ijms19124100.

Mausumi Ganguly* and Sangeeta Agarwal

14 Recent advances in the biomedical applications of rare earth elements

14.1 Introduction

Rare earth elements (REEs) are a set of 17 silvery-white soft heavy metals which consist of scandium, yttrium, and 15 f-block elements of the lanthanoid series. Scandium and yttrium are referred to as REEs though their electronic and magnetic properties are quite different from the lanthanoids. This is because they exhibit chemical properties similar to the lanthanoids, and are found in the same ore deposits as the lanthanoids [1]. REEs are not as rare as suggested by their designation. For example, cerium is the 25th most abundant element on earth. The word "Earth" is the old name of oxides and has been used in the title because the rare earth elements were first identified in the form of oxides [2]. The word "Rare" was used because these earthy oxides are rare compared to the other abundant oxides such as lime.

Rare earth elements are calcium analogs in biological systems and have unique magnetic, optical, and electrical properties that have attracted the attention of the science community toward their application in the biomedical field. Their unique chemical and physical properties have made them vital for high technology applications. These elements are called "the vitamins of modern industries" and find applications as high-performance permanent magnets, magnetic resonance image (MRI) contrast enhancers, superconductors, etc. [1]. Though REEs have been used since a long time in the biomedical field, the recent emerging technologies have increased scope of their applications in this field. Some recent advancements in the biomedical applications of REEs are discussed in this chapter.

14.2 Biomedical applications of rare earth elements

14.2.1 Applications in bioimaging

14.2.1.1 REEs as contrast agents in magnetic resonance imaging (MRI)

Magnetic resonance imaging (MRI) is a medical imaging technique that uses a strong magnetic field and computer-generated radio waves to produce three-dimensional

*Corresponding author: Mausumi Ganguly, Department of Chemistry, Cotton University, Guwahati, 781001, Assam, India, e-mail: ganguly_mausumi@rediffmail.com
Sangeeta Agarwal, Department of Chemistry, Cotton University, Guwahati, 781001, Assam, India

images of the internal organs and soft tissues of the human body. This technique does not use X-rays or any ionic radiation, and is helpful in the detection, diagnosis and follow- up treatment of several diseases. The working of the MRI technique is based on the principle of NMR. Hydrogen atoms (protons) are abundant in the human body and other biological organisms in the form of water and fats. In MRI, powerful magnets are used to generate a strong magnetic field. When a particular organ of the patient's body is exposed to the external magnetic field, the hydrogen nuclei of water in tissues are oriented in the direction of the magnetic field. When an appropriate radiofrequency current is pulsed through the tissues, the protons are excited and the resultant signal (spin polarization) is detected by a receiving coil (RF coil). There are random molecular oscillations with matching frequency that help the excited nuclear spins to return to their equilibrium state either by spin-lattice (longitudinal) or spin-spin (transverse) relaxation mechanism. Water protons in different tissues have different relaxation times that form the main source of contrast in MR images. Though the imaging of the anatomical structures or blood flow by MRI does not require any contrast agent due to the varying properties of the tissues or blood which provide natural contrast, yet some specific types of imaging require chemical compounds as contrast agents in order to improve the visibility of the internal body organs. Oral or intravenous administration of these contrast agents may alter the relaxation time of the hydrogen nuclei within the body tissues, thereby improving the contrast in the images [3].

The presence of paramagnetic species with unpaired electrons in the contrast agents is observed to shorten the longitudinal relaxation time T1 of water protons under a powerful and uniform external magnetic field after a resonant radiofrequency excitation and consequently, these species increase the contrast of the magnetic resonance images. Some rare earth ions like Gd^{3+} have the highest magnetic moment with seven unpaired electrons. As a result, they help in reducing the longitudinal relaxation time (T1) and produce bright images. Gadolinium is the most common MRI contrast agent due to the higher availability and chemical stability. As free Gd ions are toxic, the chelated form of the metal is used as an MRI contrast agent. About 40% of all magnetic resonance imaging (MRI) examinations and about 60% of neuro MRI exams use Gadolinium (III)-based chelating agents. After the approval of Gd-DTPA in 1988, the growth of Gd-based MRI contrast agents with enhanced imaging quality are growing so rapidly that the yearly administration of Gd in this field is almost 50 tons worldwide [2, 4]. Structures of some clinically approved Gd^{3+}-based chelates [5], which are commercially available contrast agents, are shown in Figure 14.1.

Gadolinium(III)-based contrast agents have been extensively used worldwide because the essential diagnostic information provided by these compounds cannot be obtained using other noninvasive techniques. Gd(III)-based contrast agents have been reported to detect blood brain barrier disruption, breast cancer, blockages in blood vessels, etc. [4].

Recently, publications related to paramagnetic contrast agents utilizing rare earth ions, other than gadolinium (III), have also been increasing. In 2006, Bottrill et al. [5] have reported the involvement of europium(II) chelates and dysprosium(III) complexes along
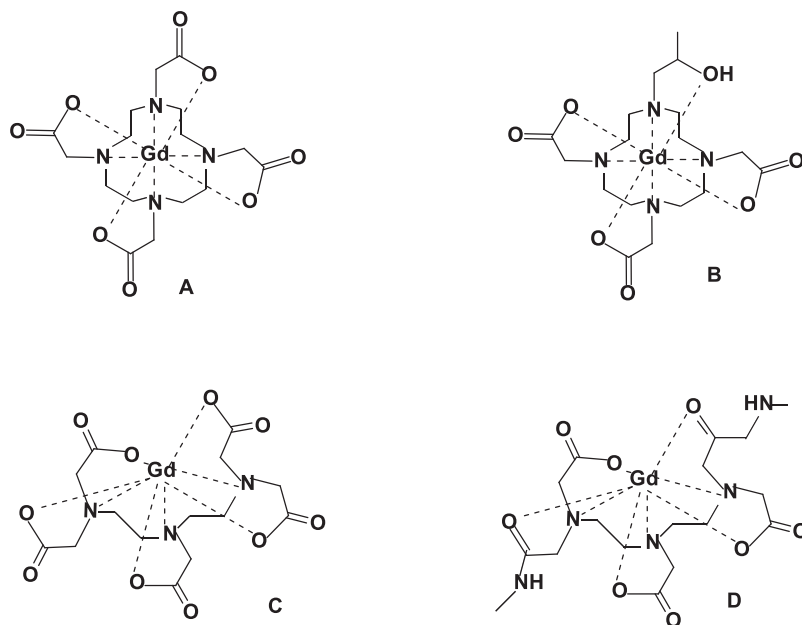
Figure 14.1: Structures of gadolinium (III)-based contrast agents [A =Gd(DOTA)⁻, B =Gd(HDO₃A), C =Gd (DTPA)$^{2-}$ and D = Gd(DTPA-BMA), which are commercially available.

with Gd(III) chelates as MRI contrast agents. Eu(II) is isoelectronic with Gd(III), with seven unpaired electrons. Moreover, as the ionic radius of Eu(II) falls in between that of Ca(II) and Sr(II), it can act as calcium(II) analogue in biological systems. In order to control the thermodynamic and redox stability of Eu(II), macrocyclic ligands with an optimum cavity size were proposed. High redox stability has been reported for an Eu(II)-based MRI active 10-coordinated complex, formed with the cryptand 2.2.2 (4,7,13,16,21,24-hexaoxa-1,10-diaza-bicyclo[8.8.8]hexacosane) (Figure 14.2) [5]. Ekanger et al. [6] have recently reported Eu(II) containing cryptates as a redox sensor in MRI imaging of living tissues. This is the first report on in vivo contrast enhancement by Eu(II)-based cryptates.
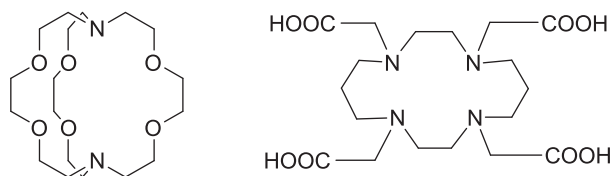
Figure 14.2: Structure of cryptand 2.2.2 and TETA used to develop Eu(II)-based contrast agents showing redox response.

Dysprosium(III) complexes have also been reported as high-field MRI contrast agents. These are considered better than the commercial Gd(III)-based contrast agents, which exhibit poor water relaxivity at high magnetic fields. The interest in Dy(III)-based negative contrast agents have been increasing due to efficient transverse relaxivity of Dy-based complexes at high magnetic fields [7]. One of the examples of such Dy-based complexes is given in Figure 14.3.
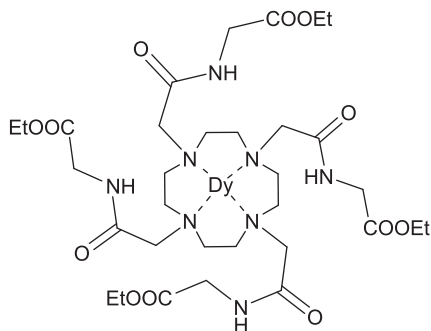
Figure 14.3: The structure of Dy-DOTA-4AmCE (negative contrast agent).

Elst et al. [7] studied and reported several Dy-(DTPA)$^{2-}$ and Dy-DTPA bisamide derivatives as negative contrast agents at high magnetic fields.

Eu(III) is a poor relaxation agent compared to Eu(II). However, it can be used as a structural probe for corresponding Gd(III) analogues because of its efficient luminescence properties. Like Eu(III) ions, Terbium(III) ions are also used for luminescence studies as they show emission in the visible region.

Some smart contrast agents have also been designed based on Eu(III)/Eu(II) redox pairs, whose relaxivity changes with changing physiological surrounding conditions, like pH, partial pressure of oxygen, metal ion concentration, etc. [5]. In 2005, To'th et al. [8] reported water-soluble fullerene derivatives of Gadolinium, Gd@C$_{60}$(OH)$_x$, and Gd@C$_{60}$[C(COOH)$_2$]$_{10}$, which may be used as pH-responsive MRI contrast agents.

Kalaivani et al. [9] explored the biomedical application of rare earth ion-doped yttria (Y$_2$O$_3$). Dy^{3+}- and Yb^{3+}-substituted Y$_2$O$_3$ showed computed tomography (CT) imaging features. Dy^{3+}-, Tb^{3+}-, and Nd^{3+}-doped Y$_2$O$_3$ was suitable for T2 MRI contrast and Gd^{3+}-doped Y$_2$O$_3$ exhibited both T1 and T2 MRI features.

A new class of multimodal contrast agents has been recommended based on REE metal organic frameworks in order to avoid chances of toxicity in traditional Gd-based contrast agents. These new materials can increase T1 and T2 relaxation rates of proton spin simultaneously and improve the image quality in MRI [10]. Wang et al. [11] recently reported a series of ultrathin rare earth element-based metal organic framework (MOF) nanosheets, with unique properties of quenching fluorescence for two-color intracellular adenosine imaging in living cells.

14.2.1.2 REE -based nanomaterials as contrast agents in magnetic resonance imaging (MRI)

The development of rare-earth-based nanoparticles has become a very active field of research nowadays. The rare earth-based nanoparticles can be used as MRI contrast agents, with additional specific properties like unique optical properties, low cytotoxicity, high photostability, absence of blinking, long lifetime, etc. [12]. There are three reasons for replacing the existing REE-based MRI contrast agents by the REE-based nanoparticles.

1. The large surface-area-to-volume ratio of REE-based nanoparticles enable specificity to a target area.
2. The size of the nanoparticle improves the relaxivity by slowing down the tumbling rate of the contrast agent.
3. Compared to a 'lone' paramagnetic chelate, the supported REE- based nanoparticles enable a large amount of paramagnetic reagent to reach the target site, generating much larger relaxivity [5].

For the past two decades, efforts are being made in employing rare earth nanomaterials for increasing the sensitivity of contrast agents and recording better quality MR images [4]. As the surface modifications of the nanoscale materials are much easier than that of their bulk forms, various interestingly engineered nano REEs are reported, which act as better MRI contrast agents. In 2017, Ertas [13] reported the synthesis of oxide-free core-shell Gd metal nanocrystals with high values of transverse proton relaxivity (r2) per Gd atom and per-particle relaxivity, which proves that these Gd-based nanocrystals are better MRI contrast agents. An adequate coating on the nanoparticles leads to longer blood circulation times, minimizing the leaching of Gd^{3+} ions to a great extent.

Yue et al. [14] reported carbon-coated ultra small Gd_2O_3 core-shell nanoparticles having excellent colloidal stability and photoluminescence in the visible region, which may be applied as T1 MRI contrast agent.

Luminescent hybrid core-shell nanoparticles (with a paramagnetic Gd_2O_3 core and polysiloxane shell) carrying organic fluorophores and carboxylated PEG covalently tethered to the inorganic network (Figure 14.4) have been reported by Bridot et al. [15] for use as MRI contrast agent as well as in vivo fluorescence contrast agents. The longitudinal proton relaxivities of these nanoparticles are found to be higher than the clinically used positive contrast agent Gd-DOTA. Moreover, these nano particles circulate in the blood vessels without being accumulated in the lungs and liver.

Hifumi et al. [16] have designed and reported the dextran-coated gadolinium phosphate nanoparticles for higher magnetic resonance tumor imaging resolution. These nanosized particles can be retained in tumor cells, and the biocompatible dextran coating prevents its rapid elimination from the blood stream.
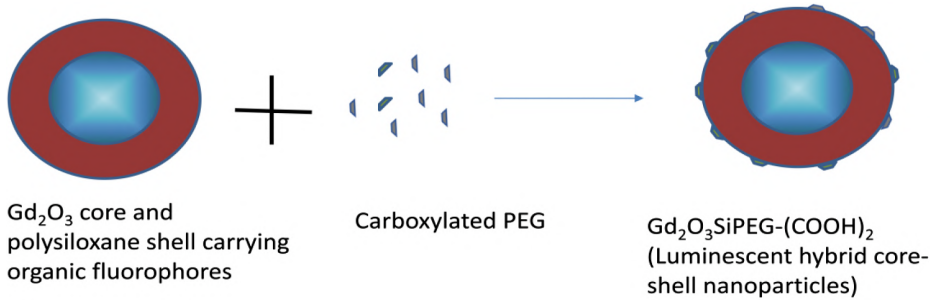
Gd_2O_3 core and
polysiloxane shell carrying
organic fluorophores

Carboxylated PEG

$Gd_2O_3SiPEG-(COOH)_2$
(Luminescent hybrid core-
shell nanoparticles)

Figure 14.4: Surface-modified luminescent core-shell nanoparticles.

Chen et al. [17] have reported a novel synthesis of glycine-coated Gd_2O_3 nanoparticles (size 25 nm) using sonication method and the outstanding stability of their MRI signal.

The properties of REEs have been enhanced for their use in MRI technique by doping these elements in hydroxyapatite. Pure hydroxyapatite nanoparticles do not possess luminescent properties but these materials may serve as promising host materials for doping rare earth elements and can provide novel fluorescent properties in bio-imaging [18]. Tesch et al. [19] have combined the photoluminescence property of Eu (III) and the high magnetic moment property of Dy (III) by doping these two elements together in hydroxyapatite for multimodal imaging.

14.2.1.3 REEs in scintillating materials

Rare earth elements are used to develop luminescent materials because some of them emit light very efficiently on excitation with different sources. These elements are therefore very useful in the field of scintillators. The scintillating materials activated with Ln^{3+} ions emit strong light from the UV to near IR region on excitation with some ionizing radiation like X-rays or γ-rays. This emitted light can be detected by simple photo-detectors. These types of materials find extensive applications in medical diagnostics and imaging. Modern imaging techniques such as Computed Tomography (CT) and Positron Emission Tomography (PET), which are applicable in cancer diagnostics, use these types of materials [2].

14.2.1.4 REEs as super magnets for MRI instrumentation

REEs are not only used as contrast agents but they find applications as supermagnets in biomedical imaging equipment. For example, neodymium permanent magnets offer the maximum polarization and can be used as a strong magnet in medical

diagnostic techniques – MRI or CT – to generate powerful magnetic fields, and hence high resolution and accuracy [20].

14.2.2 Applications in drug delivery

Rare earth elements have contributed significantly in drug delivery methods. Although organic molecules containing drugs are still making contributions to clinical practice, it is difficult to monitor and control them after administration. The nanoscale surface-engineered REEs that possess unique optical properties play a vital role for this purpose [21, 22]. In drug delivery, mesoporous materials and polymeric micelles, which can load large amounts of drug efficiently, are used as vehicles or carriers. When REE nanoparticles are doped into these carriers, not only is the drug loading capacity increased but the pathway of the drug transport in the body can also be tracked by bioimaging due to the luminescence property of the REEs. The drug delivery system is made responsive to endogenous and exogenous factors like pH, light, temperature etc., enabling them to provide important information for clinical diagnosis. The pH-responsive drug delivery systems can deliver the drug without leakage, absorption, or corrosion in the surrounding physiological environment and thus improve the utilization of the drug. Similarly, light-responsive drug delivery systems help in the controlled release of the drug to the targeted area. Accordingly, scientists are trying to design drug delivery systems of superior quality [23].

In 2018, Yang et al. [24] designed a pH-responsive drug delivery system by doping Nd^{3+} in $GdPO_4$. The system had egg yolk-shell structure, and it was loaded with anticancer drug doxorubicin (DOX). The drug delivery study revealed pH-responsive controlled release of the DOX in tumor cells. The biodistribution and real-time tracking of $GdPO_4:Nd^{3+}$ spheres were also demonstrated in living mice.

Recently Saha et al. [25] reported Eu-doped Gd_2O_3-based paramagnetic nanoplates with triangular shapes, which were coated with polyacrylate and attached to folic acid. Modified drug molecules were linked to these surface-engineered nanoparticles, producing a drug delivery system that could load both hydrophilic drug daunorubicin (~69% loading) and hydrophobic drug curcumin (~75% loading) efficiently, and exhibited strong red emission. The high drug loading capacity and targeted pH-responsive delivery of the two drugs makes it a potent drug delivery system.

Zhou et al. [26] reported the synthesis of Eu-doped mesoporous gadolinium oxide nanorods (MS-Gd_2O_3: Eu@PEG) coated with silica layer. The in vitro cytotoxicity test, drug loading, and drug delivery experiments revealed that these nanorods had good biocompatibility, effective drug loading capacity, pH-sensitive drug release behavior, and the ability for multimodal imaging, which make them an ideal drug delivery vehicle for cancer therapy.

In 2019, Li et al. [27] reported a bifunctional drug delivery system based on multi rare earth ions by combining magnetic nanoparticles and fluorophore. They designed

the drug system by binding Aspirin with rare earth ions terbium (Tb) and gadolinium (Gd), and incorporated them into chitosan microspheres with magnetic nanoparticles, Fe_3O_4. This drug system, $Tb_xGd_{1-x}(Aspirin)_3 \cdot 2H_2O$ (x = 0.25, 0.5, 0.75), showed excellent fluorescent and magnetic properties. Multiple rare earth ions instead of a single ion were used in designing this complex in order to achieve superior fluorescent intensity.

Light-responsive drug delivery systems have also been reported for the controlled release of drugs. In 2020, Liu et al. [28] loaded anticancer drug DOX in silica-coated $NaYF_4$:Tm/Yb@$NaYF_4$ nanoparticle carrier, and modified it with azo-benzene molecules for light-responsive drug release behavior. The amount of the drug (DOX) released in the Hela cells could be controlled by adjusting the intensity or time of the near-infrared (NIR) light irradiation.

The drug delivery systems based on rare earth doped-up conversion nanoparticles (UCNP) have received significant attention over the past 10 years. UCNPs are actually the rare-earth-doped nanocrystals that have emerged as an appealing candidate for the application of NIR light [29]. UCNPs absorb two or more incident photons of relatively low energy and emit one photon with higher energy. A rare-earth-doped UCNP consists of a host matrix, a sensitizer, and an activator doped with trivalent lanthanide ions. The sensitizer gets excited after absorbing 980 nm photons and transfers energy to the neighboring activators, which in turn are also excited, emitting light of shorter wavelength. REE-doped UCNPs can be excited with NIR light, and they emit visible light. The NIR light penetrates the biological materials to more depth and cuts the generation of strong auto-fluorescence [29].

A light-responsive drug system based on up-conversion nanoparticles (UCNPs), $NaYF_4$: Yb^{3+}, Er^{3+} was reported by Zhao et al. [30]. They fabricated caspase-3–responsive functionalized up-conversion nanoparticles (CFUNs) for near-infrared (NIR)-triggered Photo Dynamic Therapy (PDT), along with the activation and release of caspase-3 and cascade chemotherapeutic activation. In order to formulate CFUNs, DEVD peptide was tethered to caspase-3-responsive doxorubicin (DOX) prodrug. A self-assembly of DEVD-DOX, up-conversion nanoparticles (UCNP), a photosensitizer (pyropheophorbide-a methyl ester, MPPa), and tumor-targeting ligand cRGD-PEG-DSPE, was formed to produce multifunctional CFUNs, MPPa/UCNP-DEVD-DOX/cRGD. Reactive oxygen species (ROS) for photodynamic therapy (PDT) were produced when the cellular uptake and NIR irradiation of UCNP emit visible light and excite MPPa. The caspase-3 was also activated to cleave DEVD peptide and release DOX within tumor cells, achieving NIR-triggered photo dynamic therapy, and cascade chemotherapy [23].

Yan et al. [31] used continuous-wave diode NIR laser to disrupt the block copolymer (BCP) micelles and triggered drug release. They encapsulated $NaYF_4$:TmYb UCNPs inside the micelles of poly (ethylene oxide)-block-poly(4,5-dimethoxy-2-nitrobenzyl methacrylate). When the micellar solution was exposed to 980 nm light, UCNPs released photons in the UV region, which were absorbed by *o*-nitrobenzyl groups on the micelle core-forming block. This process activated the photo-cleavage reaction and led to the dissociation of BCP micelles, releasing the co-loaded hydrophobic species.

This approach of using UCNPs as an internal UV light source, when excited with NIR light, can be used for many photosensitive polymeric materials.

14.2.3 Applications in biosensing

Biosensing in biomedical field is one of the areas where REE-based materials have noticeable applications. The low background fluorescence and high sensitivity of rare earth materials can be used to design biosensors for different areas like pH sensing, metal ion sensor, temperature sensor, reactive oxygen species (ROS) detection, and even bacteria detection [21, 32–34]. During the outbreak of COVID19, simple and rapid methods were urgently needed to identify COVID positive cases. In 2020, Chen et al. [35] reported a rapid and sensitive lateral flow immunoassay (LFIA) that used REE-doped polystyrene nanoparticles in order to detect anti-SARS-CoV-2 IgG in human serum. The REE-based biosensors developed for applications in biomedical field may be categorized as follows.

14.2.3.1 Biomolecule sensors

Tian et al. [36] reported highly sensitive and robust peroxidase-like activity of porous ceria nanorods (PN-Ceria) in detecting the breast cancer antigen CA15-3, with a detection limit higher than that of horseradish peroxidase system, which is a natural enzyme.

Highly sensitive cerium metal organic frameworks (Ce-MOFs)-based aptasensor and Zn^{2+}-dependent DNAzyme-assisted recycling was reported by Shen et al. [37] as dual amplification strategy for the electrochemical detection of lipopolysaccharide (LPS). LPS is responsible for fever reaction, septic shock, and disseminated intravascular coagulation. Ce-MOFs could catalyze the ascorbic acid oxidation for signal intensification in aptasensor construction. LPS detection was accomplished by introducing Zn^{2+}-dependent DNAzyme, following aptamer technology, which managed the shortage of protein enzyme. The proposed aptasensor was highly sensitive to LPS detection and can be efficiently used in diagnostics [33].

Recently, Yilmaz et al. [38] reported a novel fluorescent Eriochrome Black T (EBT)−Eu^{3+} complex, which can detect dipicolinic acid (DPA) with high selectivity. UV−vis titrations changed the blue solution of EBT to magenta in the presence of Eu^{3+} ions. When DPA was added to this solution, the magenta color changed to blue immediately due to the characteristic fluorescence emission from DPA−Eu^{3+} complex. DPA is a major constituent of bacterial spores. So, this ratiometric and colorimetric biosensor may detect the pathogenic bacterial spores very sensitively.

In 2018, Ou et al. [39] reported a highly stable and specific X-ray luminescence-based immune assay for the detection of α-fetoprotein(AFP) using $NaGdF_4$:Tb@$NaYF_4$

nanoparticles. AFP is a serum biomarker of hepatocellular carcinoma whose serum levels increase during liver cancer, chronic active hepatitis, carbon tetrachloride intoxication, and other health disorders. This immunoassay produced no auto fluorescence under X-ray excitation. Applications of this type of biosensors may be extended for multiplexing sensing and medical diagnosis.

Ren et al. [40] reported the sensitive detection of liver specific Micro RNA 122 (miR-122) by designing fluorescence resonance energy transfer (FRET)-based DNA-functionalized core-shell UCNPs.

In 2020, Peng et al. [41] fabricated a biosensor based on "turn-on" luminescence from chromophore-modified UCNPs (Cy7-PEI-UCNPs) for rapid and sensitive detection of peroxy nitrite ions $ONOO^-$, which indicates hepatotoxicity caused by overdose of drugs like paracetamol. This type of UCNP-based materials may serve as an appropriate assay kit for screening hepatotoxicity from modified UCNP drug molecules.

A novel Eu^{3+}@MOF composite has also been reported by He et al. [42] as a fluorescence sensor for specific detection of urinary 1-hydroxypyrene, which is a metabolite of polycyclic aromatic hydrocarbons (PAH) inhaled in the human body.

The abnormal levels of small biomolecules, like thiols, lactic acid, adenosine triphosphate (ATP), H_2O_2, *etc.* in the human body may cause health problems. Early detection and regular monitoring of these biomolecules in body may help in the treatment of some diseases like dementia, psoriasis, liver problems, leukemia, cancer, AIDS, heart failure, myocardial ischemia, *etc.* [33]. Liu and coworkers [43] broke the limit of signal-to-background ratio (SBR) of up-conversion probes by fabricating UC nanoprobes using an organic dye as a target-modulated sensitizing switch. This biosensor could detect glutathione (GSH) with an improved SBR of ~30. Zhao et al. [44] reported a synthetic DNA nanodevice, which, on activation with NIR-light, can detect ATP molecules in cells through the integration of aptamer-based lock design. This UCNP nanodevice can help in ATP imaging, on NIR-excitation. Sardesai et al. [45] reported the synthesis of platinum-doped ceria and lactate-oxidase-based enzymatic biosensors in order to measure lactate levels during hypoxia conditions in vitro and in vivo. Liu et al. [46] reported Er^{3+}-sensitized $NaErF_4$: Ho@$NaYF_4$ UCNPs, with both excitation (1,530 nm) and emission (1,180 nm) in the NIR-II window (Figure 14.5). This biosensor could detect H_2O_2 molecules.

14.2.3.2 Metal ion sensors

Metal ions like calcium, magnesium, copper, chromium, iron, manganese, molybdenum, zinc, sodium, and potassium play important roles in biology by serving as essential cofactors in the life processes like respiration, gene transcription, growth, cell proliferation, and immune function. These metals are required in very small amounts in the body, as the excess accumulation or the deficiency of some metal ions like Fe^{3+}, Zn^{2+}, Cu^{2+} can cause diseases like pernicious anemia, growth retardation, heart diseases, etc. Excess accumulation of Al^{3+} in the human body causes Alzheimer's disease.
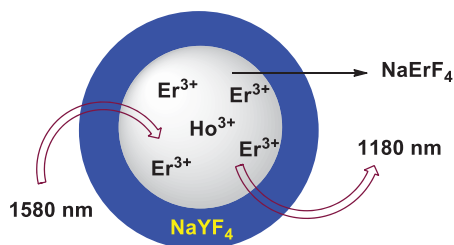
Figure 14.5: NaErF$_4$: Ho@NaYF$_4$ Core-Shell UCNPs biosensor.

An early detection of the excess or deficit levels of metal ion in body is therefore important for diagnostic purposes. REE-based highly selective and sensitive sensors have been developed by the science community for this purpose.

Chang and coworkers [47] reported the synthesis of a Zn^{2+} fluorescent-based probe by assembling polyacrylic acid-modified lanthanide-doped multilayer UCNPs (1-PAA-UCNPs) with chromophores. A FRET process with NaYF$_4$: Yb/Tm@NaYF$_4$ as the energy donor and Zn^{2+}-responsive 1-PAA-UCNPs as the acceptor was constructed. The formation of Zn complex with 1-PAA-UCNPs inhibited FRET, which made possible the quantitative monitoring of Zn^{2+} ions. Isaac et al. [48] also reported a biosensor based on a zinc finger peptide functionalized by a Tb(III)-DOTA monoamide complex in order to selectively detect Zn^{2+} ions.

Wang et al. [49] synthesized Eu(III) complex-based luminescent probe, BPED-BHHCT-Eu^{3+}-BPT, by conjugating the Cu^{2+}-binding N,N-bis(2-pyridylmethyl)ethanediamine (BPED) to a tetradentate β-diketone ligand 4,4′-*bis*(1,1,1,2,2,3,3-heptafluoro-4,6-hexanedione-6-yl) chlorosulfo-o-terphenyl (BHHCT) and coordinating with a co-ligand 2-(N,N-diethylanilin-4-yl)-4,6-bis(pyrazol-1-yl)-1,3,5-triazine) (BPT) (Figure 14.6). This probe could detect Cu^{2+} ions and H$_2$S molecules in living cells, on excitation with visible light. The luminescence of BPED-BHHCT-Eu^{3+}-BPT was proficiently quenched on its co-ordination with Cu^{2+} ions, and could be restored by the addition of H$_2$S. The "on-off-on"-type luminescence behavior of this biosensor could detect Cu^{2+} and H$_2$S simultaneously, with high sensitivity and selectivity.

Zhou et al. [50] fabricated a luminescent Eu^{3+} post functionalized nanosized Metal Organic Framework (MOF) by doping Eu^{3+} ions in the pores of MIL-53–COOH (Al) nanocrystals. The cation exchange between Fe^{3+} and Al^{3+} in MIL-53–COOH (Al) quenched the luminescence from Eu^{3+} ions in MOF, detecting Fe^{3+} ions in aqueous solutions. This shows great potential of this biosensor for intracellular detection and the imaging of Fe^{3+} ions.

Xu et al. [51] reported highly sensitive and selective detection of Al^{3+} ions by designing a recyclable luminescent Eu^{3+}-based MOF sensor. Some scientists also developed sensors to detect toxic metal ions in the body. For example, the accumulation of methylmercury ion (MeHg$^+$) in organs can cause prenatal nervous system and visceral damage. Liu et al. [52] developed a hydrophobic heptamethine cyanine dye (hCy7), modified by two long alkyl moieties and amphiphilic polymer (P-PEG)-modified nanophosphors (hCy7- UCNPs) water-soluble probe for UC luminescence monitoring and
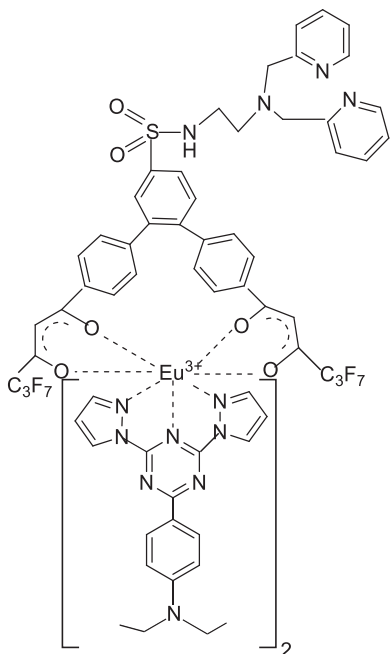
Figure 14.6: Structure of Eu(III)-based luminescent probe, BPED-BHHCT-Eu^{3+}-BPT.

imaging of MeHg$^+$ ions in a mouse model. Recently, dual-emitting REE-MOF-based ratiometric fluorescent sensors are also attracting the attention of scientists [53].

14.2.3.3 Temperature sensors

Temperature monitoring in physiological processes taking place in human body may help in the accurate diagnosis and treatment of certain diseases. Temperature measurement of cells is quite a difficult task. REE-based nanomaterials are the most adaptable thermal probes used in luminescent nanothermometers. Capobianco and coworkers [54] designed a nanothermometer that could measure the temperature of even an individual cancer cell. This nanothermometer was based on the temperature-sensitive fluorescence of NaYF$_4$:Er^{3+} and Yb^{3+} nanostructures. The intensity ratio of the green fluorescence bands of the Er^{3+} dopant ions changed with temperature in this sensor. These fluorescent nanothermometers could measure the internal temperature of the living HeLa cervical cancer cell from 25 °C to 45 °C.

Cadiau et al. [55] prepared nanorods of MOF Tb$_{0.99}$Eu$_{0.01}$(BDC)$_{1.5}$(H$_2$O)$_2$ (BDC = 1-4-benzendicarboxylate) by the reverse microemulsion technique. Aqueous suspensions of these nanorods performed excellently as luminescent nanothermometers in the physiological temperature range 300 K to 320 K.

Zhao et al. [56] fabricated a near-infrared luminescent MOF, $Nd_{0.866}Yb_{0.134}BTB$ as a self-calibrated thermometer, which showed outstanding temperature dependence of the photoluminescent properties in 303 K to 333 K range. The geometry and shorter spatial distance of Nd^{3+}-Yb^{3+} centers promoted the sensitization effect of this sensor, showing maximum relative sensitivity of 4.755% K^{-1}, which was higher than that of its contemporary temperature sensors. This sensor can, therefore, be used for intracellular thermal sensing.

An interesting temperature sensing probe was reported by Zhang's group [57]. It was a dual-emissive phosphorescent polymer probe, which consisted of Ir(III) complexes as a temperature-sensitive unit with phosphorescence lifetime of ~500 ns and Eu(III) complexes as reference unit with a lifetime of ~400 µs. Ratiometric detection of temperature using this probe was possible because of the higher luminescence intensity obtained from the Ir(III) complexes with increasing temperature, while there was no change in that of Eu(III) complexes. The emission lifetime was made longer by introducing Eu(III) complex in the polymer thermometer.

14.2.3.4 pH sensors

Intracellular pH monitoring plays an important role in biological processes. The unique optical properties of REE are helpful in developing the luminescence-based pH sensors. Zhang et al. [58] synthesized and reported new fluorescent pH probes, based on Eu(III)-Eu(TTA)$_2$-DSQ and Eu(TTA)$_3$-DR1 (where HDSQ is 5-(dimethylamino)-N-(4-(2-((8-hydroxyquinolin-2-yl)methylene)hydrazinecarbonyl)phenyl)naphthalene-1-sulfonamide, DR1 is N1-(4-(dimethylamino)-benzylidene)-N2-(rhodamine-6 G) lactamethylene-diamine, and TTA = thiophentrifluoroacetone). High pH sensitivity of the probe was demonstrated by them in HeLa cells and zebra fish.

Chu et al. [59] synthesized the pH sensors by doping Europium in one-dimensional silicon nanorods (Eu@SiNRs). These sensors could measure the pH in live cells. In order to reveal important information regarding pH fluctuations, they employed Eu@SiNRs for the visualization of cytoplasmic alkalization process, arbitrated by nigericin in living cells.

Ma et al. [60] have also reported Tm^{3+}-doped UCNPs, with their surface functionalized with xylenol orange, for intracellular pH sensing under continuous-wave excitation at 980 nm by quenching and recovering of UCL at 450 nm from UCNPs.

14.2.4 Applications in tissue engineering

The accidental loss of an organ and tissue damage is the most distressing problems in human health. Tissue engineering can provide functional substitutes in order to restore and maintain the damaged tissue by applying the principles of engineering and life sciences. The biocompatibility, fluorescence UC, antimicrobial, and antioxidant

properties of RE materials make them suitable biomaterials to be used in tissue engineering [61]. These elements in their 3^+ oxidation state have close resemblance with Ca^{2+}, which is a biologically very important ion. Having a higher charge, rare earth ions (in 3+ oxidation state) are more attractive to Ca^{2+} site. This strategy makes the rare earth element suitable candidate for bone tissue engineering [62]. REEs have diverse applications in bio-active scaffolds and bone regeneration. Some of the recent applications reported by scientists can draw the attention of researchers.

Bioactive glasses containing Ce_2O_3 and Ga_2O_3 have shown significant versatility in bonding with different types of tissues [63]. Recently, Mesoporous Bioactive Glasses (MBGs) have been widely explored for applications in tissue engineering [64]. In order to upgrade the properties of MBGs, Shruti et al. [65] designed 3-D macro mesoporous bioactive glass scaffolds containing Ce, Ga and Zn therapeutic ions for applications in bone tissue engineering. These fabricated scaffolds contained large pores (pores>400 µm) interconnected with each other, and could be used for vascular growth and proliferation of cells.

Modified hydroxyapatite has been extensively used in bone tissue engineering and dental applications, considering its superior biocompatibility and excellent osteoconductive characteristics [18, 66]. Madhumathi et al. [67] reported the ability of chitosan hydrogel–Hydroxyapatite composite membranes for use in tissue engineering field. Li and Chen [68] fabricated Yb^{3+}, Ho^{3+} co-doped fluorapatite (FA:Yb^{3+}/Ho^{3+}), and hydroxyapatite (HA:Yb^{3+}/Ho^{3+}) particles in order to differentiate the implanted material from the bone tissue. Upon NIR excitation under 980 nm, FA:Yb^{3+}/Ho^{3+} particles showed green luminescence, while HA:Yb^{3+}/Ho^{3+} particles exhibited red emission. These UC apatite particles showed good biocompatibility and superiority in labeling implanted material for fluorescence tracking, and exploring bone reconstruction with time. Recently, Prabhakaran et al. [69] have reported the fabrication of REE-based hydroxyapatite/aloevera composite-coated titanium plate for bone tissue regeneration, following a rat bone defect model.

Liu et al. [70] carried out a study on the toxicity of Gd_2O_3:Eu^{3+} nanotubes and its distribution in mice after oral administration. Gd_2O_3:Eu^{3+} nanotubes could successfully enhance the bone mineral density and bone biomechanics in the mice.

Lack of appropriate cell proliferation and angiogenesis are the main problems associated with the success of in situ tissue engineering, as observed during in vivo studies. Augustine et al. [71] fabricated polycaprolactone (PCL) scaffolds, loaded with Y_2O_3 nanoparticles, using electrospinning technique. In vitro cell culture studies, in vivo angiogenesis assay, and in vivo implantation studies revealed that Y_2O_3 nanoparticles at optimum concentrations (0.5–2% w/w) can induce angiogenesis and cell proliferation in biomaterial scaffolds, and hence are suitable for in situ tissue engineering.

Liu et al. [72] designed self-assembled terbium-cysteine nanoparticles, which efficiently promote bone repair. They further found that this form of metal-amino acid combinations could be served as model for reasonable assessment of the long-term biosafety of tissues.

Recently Weng et al. [73] reported that alloying of REEs with clinically used Mg alloys might assist in the development of advanced alloys, which could serve as biodegradable orthopedic implants and cardiovascular stents.

14.2.5 Applications in cancer diagnosis and therapies

According to World Health Organization's definition, cancer is a large group of diseases that can start in any organ or tissue of the body with abnormal growth of cells. The adjoining parts of the body may also be invaded, spreading the disease to other organs. Cancer is the second leading cause of death in the world. This disease exerts intense physical, emotional, and financial strain on the affected individuals and the health systems. Timely quality diagnosis and treatment can improve the survival rate of cancer patients. Therefore, modern-day cancer diagnostic and therapeutic methods have been evolving rapidly. Metals are used widely in cancer diagnosis and therapies. REEs occupy an ideal position in this field. The first study on the connection of rare earth elements with cancer was published in 1945. Since then, the applications of rare earth elements in cancer diagnosis and treatment have been significantly increasing. Recently, in 2022, Wang and Li [74] reported the evidence mapping and scientometric analysis of published reports on the applications of rare earth elements in cancer. REEs have not only been used as cytotoxic agents, but every aspect of cancer treatment, starting from diagnosis to therapies, involves REEs because of their unique magnetic and optical properties [75]. The top 10 rare earth elements used in cancer detection and treatment are gadolinium, lanthanum, yttrium, cerium, holmium, lutetium, europium, neodymium, thulium, and ytterbium [74]. Some latest applications that can help to explore the prospects of REEs in cancer diagnosis and treatment are listed here.

14.2.5.1 REEs as cytotoxic agents

REE (III)-based anticancer agents have been reported with a wide range of ligands. Kostova et al. [76] reported two lanthanum(III) complexes of bis-coumarins, which exhibited in vitro cytotoxic effects in micromolar concentrations. Liu et al. [77] synthesized mononuclear and iso-structural lanthanide (Sm/Eu/Tb/Dy) complexes with 5,7-dibromo-8-quinolinol, which interacted with DNA more strongly than free quinolinoline, showing good cytotoxicity. Wei et al. [78] fabricated water-soluble oxoglaucine-Y(III), Dy(III) complexes possessing in vitro and in vivo anticancer activities by triggering DNA damage. Yang et al. [79] reported novel quinoline-based Ir(III) complexes exhibiting high antitumor activity in vitro and in vivo.

In addition to small rare earth complexes, rare earth-based nanomaterials have also been reported to show excellent cytotoxicity. Wason and Zhao [80] reviewed the

potential applications of cerium oxide nanoparticles in cancer treatment. According to their study, cerium oxide nanoparticles are not only toxic to cancer cells but can also inhibit invasion and sensitize cancer cells to radiation therapy. The antioxidant capabilities of cerium oxide nanoparticles, which enable radiation protection, can also treat other diseases characterized by ROS accumulation, like diabetes and macular degeneration. Wang et al. [81] compared the cytotoxicity of nano-CeO_2crystals with different morphologies in human hepatocellular carcinoma cells (HepG2 cells) and found that due to larger specific surface area compared with cube-like and octahedron-like nano-CeO_2, the rod-like nano-CeO_2 showed lowest toxicity to HepG2 cells.

A cytotoxic agent should be selective i.e., it should only target cancer cells while leaving the nearby normal cells unaffected. As RE complexes and nanoparticles suffer from this limitation, REEs are reported to be conjugated with proteins or nucleic acids in order to bring specificity. Chan et al. [82] synthesized two morphologically different and Plk1(polo-like kinase1) specific peptide-conjugated RE-doped UCNPs in order to investigate their photophysical properties, cellular uptake efficiencies, and selective inhibitory effects on cancer and normal cell lines. They found that spherical β-$NaGdF_4$@SiO_2-P1 are the best candidates in in vitro imaging, G2 phase cell arrest and inhibit cell cycle. Chan's group [83] also reported the surface functionalization of nanoscale REEs with cyclin D-specific peptides to prepare bifunctional REE-based UCNPs for the inhibition of cyclin D.

14.2.5.2 RE-containing materials for cancer therapies

14.2.5.2.1 Photodynamic therapy (PDT)

Photodynamic therapy (PDT) is a cancer treatment in which light energy with a specific wavelength activates a drug (photosensitizer) and helps it in destroying cancerous cells. Upon light irradiation, the photosensitizer produces ROS, which kills the tumor cells directly. Rare-earth-doped nanoparticles are proper candidates as photosensitizers because they exhibit long-lived luminescence, large antenna-generated Stokes or anti-Stokes shifts, narrow emission bands, high resistance to photo bleaching, and low toxicity [84]. Specifically rare-earth-doped UCNPs have emerged as promising photosensitizers for NIR-triggered PDT. Kalluru et al. [85] reported multifunctional Eu/Gd oxide-doped mesoporous silica frameworks, which could sensitize the formation of $^1O_2$, when irradiated with a low power of NIR light, thereby helping in dual-modal fluorescence, MRI, and PDT. Moreover, these frameworks could load drugs like DOX for safe delivery to the target organ. Yao et al. [86] developed H_2O_2-activatable/O_2-evolving hollow UC cerium oxide, which acted as a biophotocatalyst for highly efficient PDT and chemotherapy for overcoming hypoxia cancer. Park et al. [87] reported dual-modal in vivo tumor imaging and PDT using hexagonal $NaYF_4$: Yb, Er/$NaGdF_4$ core-shell UCNPs, combined with a photosensitizer and chlorin e6. They also demonstrated in vivo photodynamic therapy under irradiation (980 nm) by systemic administrations.

14.2.5.2.2 Photothermal therapy (PTT)

Photothermal therapy (PTT) has attracted much attention for cancer treatment due to its high specificity to tumor tissue and negligible side effects to the cancer patient. During this process, photoabsorbent converts excitation light energy into heat, leading to the death of cancer cells. Rare earth oxides are identified as good candidates for PTT. de Rosal et al. [88] reported ultra-small (2.4 nm) stoichiometric $NdVO_4$ nanoparticles having superior light-to-heat conversion efficiency, which was the consequence of large absorption cross-section at 808 nm and ultra-small size of $NdVO_4$. These photothermal agents behave like the traditional metallic, organic or carbon-based nanoparticles. Kolesnikov et al. [89] reported multifunctional $YVO_4:Nd^{3+}$ nanoparticles acting both as nanoheaters and nanothermometers under single beam excitation. They demonstrated the potential application of neodymium-doped yttrium vanadate nanoparticles ($YVO_4:Nd^{3+}$) for deep tissue fluorescence bioimaging and controlled photothermal therapies. Yu et al. [90] reported core shell nanocomplex with extremely improved photothermal conversion efficiency. These nanocomplexes were fabricated by coating Prussian blue on $NaNdF_4$ nanoparticles and generating new cross relaxation pathways between the ladder-like energy levels of Nd^{3+} ions and the continuous energy band of Prussian blue. In order to improve the photothermal conversion capabilities of RE oxides and using these kinds of materials for photothermal therapy, Yu et al. [91] in 2020, reported Au/Sm_2O_3 composites with ultra-broad emission range in the near-infrared region. Paul et al. [92] used a simple physicochemical route to synthesize gadolinium oxide nanoparticles. These nanoscale (<10 nm) particles could be used for hyperthermia application due to their Brownian relaxation.

14.2.5.2.3 Radiation therapy (RT)

Radiation therapy is one of the cancer treatments that uses high doses of radiation to kill cancer cells and shrink tumors. This therapy takes time – weeks or months – to damage the DNA completely and cure cancer. This therapy is of two types – external beam radiation therapy and internal radioisotope radiation therapy. In external beam radiation, high intensity radiation beams are directly focused at the tumor site, which causes serious side effects to nearby healthy tissues. REEs, having high atomic numbers, may serve as radio sensitizing agents with minimal side effects. In internal radioisotope therapy, radioisotopes of elements are directly targeted to the tumor site. RE radioisotopes that are reported to be used in internal therapy for cancer treatment are ^{90}Y, [153]Sm, [166]Ho, ^{177}Lu, and some isotopic complexes, like ^{90}Y microspheres, [153]Sm ethylene diamine tetramethylene phosphonate,[177]Lu-Dotatate, etc. [93] [165]Ho possesses a large cross-section for capturing thermal neutrons. Kim et al. [94] irradiated Ho-containing mesoporous carbon nanoparticles with a neutron flux. [166]Ho was produced along with β-particles and γ-photons, and it could kill the human ovarian cancer cell. Other groups have also reported radioactive [166]Ho microspheres as safe and effective for the treatment of oral, head, and neck squamous cell carcinoma in

human beings [95]. Ehlerding et al. [96] have demonstrated the potential of the isotope pair, [86]Y and ^{90}Y for targeted imaging and angiogenesis therapy in murine breast cancer models using a chimeric anti-CD105 antibody, TRC105. They also reported dual tumor-mitochondria-targeted theragnostic porphyrin polyethylene glycol nanocomplexes, whose stable coordination with ^{177}Lu could integrate fluorescence imaging and PDT with positron emission tomography (PET) imaging and internal radiotherapy (RT).

Wason et al. [97] reported that cerium oxide nanoparticle pre-treatment of acidic human pancreatic cancer cells enhanced radiation-induced ROS production and sensitized the cells prior to RT. This could potentiate the cancer cell apoptosis in tumors and inhibit pancreatic tumor growth without harming the normal tissues. Zhong et al. [98] reported cerium (Ce)-doped $NaCeF_4$:Gd, Tb scintillating nanoparticle in which Ce ions sensitized Tb ions to emit fluorescence under X-ray irradiation. Both Ce and Tb ions absorbed the energy of the secondary electrons generated by X-ray to produce ROS for RT. The REE-based materials are increasingly being used in RT.

There are reports of using properties of REEs in antioxidant therapy. CeO_2 nanoparticles have been used as imitator natural enzyme with many active sites for antioxidant applications because cerium may reversibly be converted from +3 to +4 oxidation state. This couple can scavenge ROS efficiently to reduce oxidative stress in vitro and in vivo [33].

14.2.5.3 REE-based anticancer drug delivery

Rare earth oxide-based nanomaterials have been widely used for targeted and visualized drug delivery in cancer diagnosis and treatment. Zhang et al. [99] synthesized ultrathin Eu-doped Sm_2O_3 and Gd_2O_3 nanosheets loaded with anticancer drug5-Fluorouracil. Their studies revealed that these photoluminescent RE-based nanosheets exhibit promising pH-controlled anticancer drug-delivery behavior. Shen et al. [100] demonstrated how REE-doped UCNPs help in image-guided targeted drug delivery in the treatment of cancer and other diseases. The surrounding environment of tumor cells is usually acidic, having pH of endosomes and lysosome between 4 and 6. Recently, pH-responsive drug-loaded NPs are more emphasized for tumor treatment [23].

In 2019, Tawfik et al. [101] designed a stable and biocompatible NIR, NaLuGdF4: Yb, Er, Cr NPs (Ex ¼ 980 nm), modified with Al-NH-PEG-NHFA polymers, which could successfully encapsulate and release anticancer drugs like doxorubicin (DOX).

Luo et al. [102] have fabricated the porous gadolinium oxide nanosheets that could help in pH-responsive drug release in cancer chemotherapy.

14.2.5.4 REE-based biosensors in cancer treatment

Sensitive and selective bio detection is necessary for early cancer diagnosis and therapeutics. REE-based biosensors are the new generation of luminescent nanoprobes that have been employed for emission-based as well as mass spectrometry-based bioassays. Rare earth (III) ion-doped UCNPs have been identified as suitable candidates for bio detection and bioimaging [103]. Zhou et al. [104] demonstrated the use of antibody conjugated single band UCNPs in multiplexed simultaneous in situ bio detection of biomarkers in breast cancer cells and tissue specimens. Zhang et al. [105] fabricated a mixed crystal, Tb/Eu zeolite-like metal-organic framework, which could be used as a fluorescent Indicator for lysophosphatidic acid (a cancer biomarker). RE nanoparticles have also been identified as suitable fluorescence resonance energy transfer (FRET) donors for homogeneous emission-based bioassays. Wang et al. [106] reported a homogeneous biosensor, based on FRET, from upconversion phosphors to carbon nanoparticles for selective determination of matrix metalloproteinase-2, a very important biomarker in human blood. Several other literatures are available on this topic.

REE and mass spectrometry-based techniques are used to detect various nucleic acid and protein cancer biomarkers. These techniques are still in their infancy. One of the reports includes the fabrication of lanthanide ([165]Ho, [159]Tb, and [169]Tm)-labeled DNA probes for the detection of microRNA biomarker on membranes using laser ablation by inductively coupled plasma mass spectrometry (LA-ICPMS) by De Bang et al. [107].

In addition, rare earth elements can also be used for screening ligand−protein interactions, finding target sites for cancer drug delivery, and assisting in drug designing [75, 108].

14.2.5.5 REEs-based bioimaging for cancer diagnosis and treatment

Bioimaging plays a vital role in the early diagnosis and treatment of diseases like cancer. REEs are widely used as bioimaging agents in different imaging techniques because of their unique intrinsic properties.

Gd(III) is the most ideal ion for bioimaging but due to toxicity of free Gd^{3+}ion, chelated forms of Gd(III) are being used as MRI contrast agents. Gd complexes, including gadopentetic acid, gadoteric acid, and Gd^{3+} doped inorganic nanostructures like silica, CaF_2, hydroxyapatite, carbon nanomaterials (carbon nanotubes, carbon nanodots, fullerene), semiconductor nanocrystals (TiO_2, ZnS, ZnO, CdSe, CdTe), and other Ln^{3+}-based nanoparticles have been used in bioimaging as T1-weighted MRI contrast agents. Other REE ions such as Tb^{3+}, Ho^{3+}, Tm^{3+}, Yb^{3+}, Eu^{3+}, Dy^{3+} and Er^{3+} have also been explored as contrast agents in T2-weighted MRI because of their large magnetic moments.

The properties of Gd_2O_3 nanoparticles that make them suitable for multimodal contrast and as therapeutic agents were first evaluated by McDonald and Watkin in 2003

[109]. Since then, this rare earth oxide has become the prototype of Gd-based inorganic nanoparticulate T1 contrast agents. In order to enhance the MRI contrast, Gd_2O_3 nanostructures with insufficient relaxivity were subjected to surface modification. For example, Cho et al. [110] synthesized Gd_2O_3 nanoplates by the thermal decomposition method with core diameter in the 2 nm to 22 nm range and thickness in the range of 1 to 2 nm. They coated these nanoplates with either an oleic acid bilayer or an octylamine-modified polyacrylic acid polymer layer. These polymer-coated Gd_2O_3 nanoplates exhibited ten times increase in longitudinal relaxivity over the commercially available Gd-based contrast agents. Gd_2O_3 nanoparticles were made suitable for optical imaging and dual mode imaging agents by doping Ln^{3+} ions (Eu^{3+}, Tb^{3+}, Tm^{3+}) or other materials with fluorescent properties in it. The size and shape of the nanoparticles determines their relaxivity. Not only oxides but the fluorides, hydroxides, and oxysalts of gadolinium have also been reported as contrast agents in bioimaging [111]. Recently, layered rare earth hydroxides, with the general composition, $RE_2(OH)_{5X}\cdot nH_2O$ (where RE = rare earth and X = anions), have been reported by Stefanakis et al. [112] as new age materials, which are a class of anionic clays. They synthesized $Gd_2(OH)_5NO_3$ nanosheets, with an average size of 80 nm, could enhance the MRI contrast. These nanosheets could also be used for PDT, when modified with rose Bengal. Gupta et al. [113] fabricated mesoporous silica nanoparticles, encapsulating Gd_2O_3 and horseradish peroxidase together. The entrapped enzyme was used to convert a benign pro-drug, indole-3-acetic acid into a toxic oxidized product, which could kill cancer cells.

The multimodal biomedical imaging could be developed by the surface engineering of nanomaterials with multiple discrete function-related components, integrated in one nanoparticle. UCNPs, which can emit high-energy photons, when excited with NIR light, are applied as novel optical nanoprobes in biomedical imaging [114]. NIR excitation-based imaging improves the quality of images, as reported by Park et al. [87]. Some of the recent applications of UCNPs have already been explained sections on drug delivery and biosensing.

14.2.6 Miscellaneous applications

14.2.6.1 Dentistry

Cerium oxide (ceria) nanomaterials possess exceptional ROS scavenging properties, due to which they can protect human dental stem cells from oxidative stress through intracellular or extracellular actions [115]. Ceria (CeO_2) and yttria (Y_2O_3) contribute as stabilizers in dental biomaterials like zirconia [116]. In order to achieve the color effect of natural teeth, currently the REEs – Ce, Pr, Er, Nd, etc. are being applied to dental coloring. REEs-based magnets, Sm-Co and Nd-Fe-B, are reported to be used in orthodontics [117].

14.2.6.2 Antimicrobial agents

CeO_2/TiO_2 composite and other cerium oxide-based nanomaterials can weaken the harmful effects of microbes such as *S. aureus* and *S. Typhimurium* by releasing ROS and targeting the cell membrane of the pathogen [118–120].

14.2.6.3 Cell tracking and labeling

Nauplii, dosed with yttrium (Y_2O_3)/dysprosium (Dy_2O_3), was used as a digestibility marker for fecal solids [121]. Glassy carbon electrodes modified with Sm_2O_3 nanoparticles are reported to be used for the sensitive detection of neurotransmitters (dopamine) in human blood serum and urine samples [122]. Dy_2O_3 nanoparticle-decorated reduced graphene oxide nanocomposite-based electrochemical sensor is reported for the detection of injury and disease [123].

14.2.6.4 Theragnostic

In the theragnostic method of treating diseases, therapeutics and diagnostics are combined for targeting the specific diseased cells or tissues, together. Gd-based layered double hydroxides and graphene oxide nano-carriers have been reported for simultaneous high contrast MRI and anticancer drug delivery [124].

Sayour et al. [125] fabricated ultrafine yttrium oxide nanoparticles (size 7–8 nm) with a functional polymer layer on its surface. These surface-modified nanoparticles were followed by the grafting of a co-polymer made of acrylic acid (AA) and ethylene glycol in order to exhibit theragnostic capabilities.

14.2.6.5 Reduction of oxidative stress

RE oxides such as ionic liquid mediated samarium oxide nanoparticles possess strong anti-oxidant and anti-inflammatory activities, which can make them alternative candidates to existing antioxidant compounds such as vitamin C [126]. Mitra et al. [127] reported astonishing antioxidant benefits using Y_2O_3 nanoparticles, which could prevent photoreceptor death in a light-damage model of retinal degeneration.

14.3 Environmental impact

14.3.1 Risk of toxic pollution caused by the widespread applications of REE

The use of REEs in different industries, agriculture, and health sector is alarmingly increasing worldwide, resulting in a constant rise in the concentrations of these elements in the environment, which would not only affect the aquatic system but also the plant and soil ecosystem, leading to several health issues.

Recently, several studies have indicated that the use of rare earth metals has huge implications in terms of toxic pollution. The mining of these metals not only causes carbon spewing into the atmosphere, but also releases toxins into the ground. Moreover, as it is difficult and not economic to recover the REEs from waste, there is a tendency to dump the waste without any attempt to recycle the REEs.

Gadolinium is one of the most frequently used REEs. This is mostly applied in biomedical field as a contrast agent in magnetic resonance imaging (MRI). Many articles reported that gadolinium complexes may cause nephrogenic system fibrosis (NSF) in patients suffering from kidney failure [128]. Gd shows toxicity when present as free positively charged ions Gd^{3+}. Due to its similarity with calcium, free gadolinium ions can block many voltage-gated Ca^{2+} channels, causing alterations in the cellular processes [129]. Moreover, it can hamper physiological processes, which depend upon calcium influx, lowering the contraction of smooth, skeletal, and cardiac muscles. The ever-increasing use of this element enhances the potential risk of its release into the environment, particularly into rivers and lakes through industrial wastewaters.

A number of studies have already reported the adverse health effects of REEs on aquatic and terrestrial organisms [130–132]. However, there is a need for more comprehensive toxicological studies as the mechanism of the harmful effects to species or to ecosystems is still not clearly understood [131].

In an in vivo experiment aimed at investigating the effects of exposure to lanthanoids (Ln) on the immune response and liver function, mice were orally exposed to La, Ce, and Nd salts for 30 days. The results showed that exposure to Lanthanoids affected the cell and humoral immunity, also disturbing the liver function in mice. The results also suggested that long-term exposure to Ln can lead to histopathological changes in liver, kidney, and heart [133]. Once the rare earth elements enter the liver, they bind with many proteins and other molecules in the cells, thereby lowering the activities of enzymes and interfering in the physiological functions of the liver [134].

With rare earth metals becoming increasingly scarce and their supply being controlled by several geographical, economic, and political factors, the manufacturers and consumers of REE-based technological devices need to take a more responsible approach in producing, using, and disposing the REE-based materials.

14.4 Conclusions

The importance of rare earth elements in health is well established. These elements have now become indispensable in diagnostic imaging techniques. Moreover, many routine procedures in biology laboratories nowadays use rare earth elements. Using rare earth elements leads to a colossal improvement of existing methods because of the photostability, low or absence of cytotoxicity, and coupling of magnetic and luminescent properties of REEs. From the present review of the applications of REEs in biology and medicine, which clearly indicate that these elements will be increasingly relevant in the near future, it can be anticipated that the ever-increasing demand for REEs will soon exceed their supply. This calls for innovative research to design processes to recycle and reuse these elements, and to find efficient methods to control the distribution of REE in the environment. Though there are no reports on the immediate harmful effects of the REEs, the effects of prolonged exposure to REEs should be evaluated. Till now, there are only some fragmentary reports on the occupational health problems of the workers associated with mining and transportation of the REEs. There is a need for investigations on long-term exposures to rare earth elements for the sustainable growth of RE industries.

References

[1]   Balaram, V. Rare earth elements: A review of applications, occurrence, exploration, analysis, recycling, and environmental impact. Geosci Front, 2019, 10, 1285–1303.

[2]   Ascenzi, P, Bettinelli, M, Boffi, A, Botta, M, De Simone, G, Luchinat, C, Marengo, E, Mei, H, Aime, S. Rare earth elements (REE) in biology and medicine. Rend Fis Acc Lincei, 2020, 31, 821–833.

[3]   McRobbie, DW, Moore, EA, Graves, MJ, Prince, MR. MRI from Picture to Proton, Cambridge, New York: Cambridge University Press, 2007, 42–44.

[4]   Wahsner, J, Gale, EM, Rodríguez-Rodríguez, A, Caravan, P. Chemistry of MRI contrast agents: Current challenges and new frontiers. Chem Rev, 2019, 119, 957–1057.

[5]   Bottrill, M, Kwok, L, Long, NJ. Lanthanides in magnetic resonance imaging. Chem Soc Rev, 2006, 35, 557–571.

[6]   Ekanger, LA, Polin, LA, Shen, Y, Haacke, EM, Martin, PD, Allen, MJA. Eu(II)-containing cryptate as a redox sensor in magnetic resonance imaging of living tissue. Angew Chem Int Ed Eng, 2015, 54, 14398–14401.

[7]   Elst, LV, Roch, A, Gillis, P, Laurent, S, Botteman, F, Bulte, JWM, Muller, RN. Dy-DTPA derivatives as relaxation agents for very high field MRI: The beneficial effect of slow water exchange on the transverse relaxivities. Magn Reson Med, 2002, 47, 1121–1130.

[8]   Tóth, E, Bolskar, RD, Borel, A, González, G, Helm, L, Merbach, AE, Sitharaman, B, Wilso, LJ. Water-soluble gadofullerenes: Toward high-relaxivity, pH-responsive MRI contrast agents. J Am Chem Soc, 2005, 127, 799–805.

[9]   Kalaivani, S, Guleria, A, Kumar, D, Kannan, S. Bulk Yttria as a host for lanthanides in biomedical applications: Influence of concentration gradients on structural, mechanical, optical, and in vitro imaging behavior. ACS Appl Bio Mater, 2019, 2, 4634–4647.

[10]   Younis, SA, Bhardwaj, N, Bhardwaj, SK, Kim, KH, Deep, A. Rare earth metal–organic frameworks (RE-MOFs): Synthesis, properties, and biomedical applications. Coord Chem Rev, 2021, 429, 213620.

[11]   Wang, HS, Li, J, Li, JY, Wang, K, Ding, Y, Xia, XH. Lanthanide-based metal-organic framework nanosheets with unique fluorescence quenching properties for two-color intracellular adenosine imaging in living cells. NPG Asia Mater, 2017, 9, e–354.

[12]   Bouzigues, C, Gacoin, T, Alexandrou, A. Biological applications of rare-earth based nanoparticles. ACS Nano, 2011, 5, 8488–8505.

[13]   Ertas, YN. Oxide-Free Gadolinium Nanoparticles as MRI Contrast Agents. UCLA Electronic Theses and Dissertations, 2017, 29–39.

[14]   Yue, H, Marasini, S, Ahmad, MY, Ho, SL, Cha, H, Liu, S, Jang, YJ, Tegafaw, T, Ghazanfari, A, Miao, X, Chae, KS, Chang, Y, Lee, GH. Carbon-coated ultrasmall gadolinium oxide (Gd_2O_3@C) nanoparticles: application to magnetic resonance imaging and fluorescence properties. Colloids Surf A Physicochem Eng Asp, 2020, 586, 124261.

[15]   Bridot, JL, Faure, AC, Laurent, S, Rivière, C, Billotey, C, Hiba, B, Janier, M, Josserand, V, Coll, JL, Elst, L, Vander, Muller, R, Roux, S, Perriat, P, Tillement, O. Hybrid gadolinium oxide nanoparticles: Multimodal contrast agents for in vivo imaging. J Am Chem Soc, 2007, 129, 5076–5084.

[16]   Hifumi, H, Yamaoka, S, Tanimoto, A, Akatsu, T, Shindo, Y, Honda, A, Citterio, D, Oka, K, Kuribayashi, S, Suzuki, K. Dextran coated gadolinium phosphate nanoparticles for magnetic resonance tumor imaging. J Mater Chem, 2009, 19, 6393–6399.

[17]   Chen, C, Fang, J, Xu, C. Ultrasonication mediated fabrication of glycine coated gadolinium oxide nanoparticles as MRI contrast agents. J Clust Sci, 2021, 32, 773–778.

[18]   Neacsu, IA, Stoica, AE, Vasile, BS, Andronescu, E. Luminescent hydroxyapatite doped with rare earth elements for biomedical applications. Nanomaterials, 2019, 9, 239.

[19]   Tesch, A, Wenisch, C, Herrmann, KH, Reichenbach, JR, Warncke, P, Fischer, D, Müller, FA. Luminomagnetic Eu^{3+} – And Dy^{3+} -Doped hydroxyapatite for multimodal imaging. Mater Sci Eng C, 2017, 81, 422–431.

[20]   Jha, AR. Rare Earth Materials: Properties and Applications, Boca Raton: Taylor & Francis group: CRC press, 2014, 81–98.

[21]   Hossain, MK, Khan, MI, El-Denglawey, A. A review on biomedical applications, prospects, and challenges of rare earth oxides. Appl Mater Today, 2021, 24, 101104.

[22]   Chawda, NR, Mahapatra, SK, Banerjee, I. Surface-modified lanthanide nanomaterials for drug delivery. In: Surface Modification of Nanoparticles for Targeted Drug Delivery. Pathak, YV, ed., Switzerland AG, Springer Nature, 2019, 431–449.

[23]   Fan, Q, Cui, X, Guo, H, Xu, Y, Zhang, G, Peng, B. Application of rare earth-doped nanoparticles in biological imaging and tumor treatment. J Biomater Appl, 2020, 35, 237–263.

[24]   Yang, Q, Li, X, Xue, Z, Li, Y, Jiang, M, Zeng, S. Short-wave near-infrared emissive $GdPO_4$: Nd^{3+}Theranostic probe for: In Vivo Bioimaging beyond 1300 nm. RSC Adv, 2018, 8, 12832–12840.

[25]   Saha, A, Mohanta, SC, Deka, K, Deb, P, Devi, PS. Surface-engineered multifunctional eu: Gd_2O_3Nanoplates for targeted and PH-responsive drug delivery and imaging applications. ACS Appl Mater Interfaces, 2017, 9, 4126–4141.

[26]   Zhou, C, Wu, H, Huang, C, Wang, M, Jia, N. Facile synthesis of single-phase mesoporous Gd_2O_3: Eu Nanorods and their application for drug delivery and multimodal imaging. Part Part Syst Charact, 2014, 31, 675–684.

[27]   Li, P, Song, Y, Niu, X, Li, K, Fan, Y. Drug delivery system with multiple rare earth ions fluorescent-labeling drugs and magnetic nanoparticles. J Nano Sci Nanotechnol, 2019, 19, 3288–3292.

[28]   Liu, J, Bu, W, Pan, L, Shi, J. NIR-triggered anticancer drug delivery by upconverting nanoparticles with integrated azobenzene-modified mesoporous silica. Angew Chem – Int Ed Engl, 2013, 52, 4375–4379.

[29] Gorris, HH, Wolfbeis, OS. Photon-upconverting nanoparticles for optical encoding and multiplexing of cells, biomolecules, and microspheres. Angew Chem – Int Ed, 2013, 52, 3584–3600.

[30] Zhao, N, Wu, B, Hu, X, Xing, D. NIR-triggered high-efficient photodynamic and chemo-cascade therapy using caspase-3 responsive functionalized upconversion nanoparticles. Biomaterials, 2017, 141, 40–49.

[31] Yan, B, Boyer, JC, Branda, NR, Zhao, Y. Near-infrared light-triggered dissociation of block copolymer micelles using upconverting nanoparticles. J Am Chem Soc, 2011, 133, 19714–19717.

[32] Zhang, Q, O'brien, S, Grimm, J. Biomedical applications of lanthanide nanomaterials, for imaging, sensing and therapy. Nanotheranostics, 2022, 6, 184–194.

[33] Lei, P, Feng, J, Zhang, H. Emerging biomaterials: Taking full advantage of the intrinsic properties of rare earth elements. Nano Today, 2020, 35, 100952.

[34] Li, B, Yu, Q, Duan, Y. Fluorescent labels in biosensors for pathogen detection. Crit Rev Biotechnol, 2015, 35, 82–93.

[35] Chen, Z, Zhang, Z, Zhai, X, Li, Y, Lin, L, Zhao, H, Bian, L, Li, P, Yu, L, Wu, Y, Lin, G. Rapid and sensitive detection of anti-SARS-CoV-2 IgG, using lanthanide-doped nanoparticles-based lateral flow immunoassay. Anal Chem, 2020, 92, 7226–7231.

[36] Tian, Z, Li, J, Zhang, Z, Gao, W, Zhou, X, Qu, Y. Highly sensitive and robust peroxidase-like activity of porous nanorods of ceria and their application for breast cancer detection. Biomaterials, 2015, 59, 116–124.

[37] Shen, WJ, Zhuo, Y, Chai, YQ, Yuan, R. Ce-Based Metal-Organic Frameworks and DNAzyme-Assisted Recycling as Dual Signal Amplifiers for Sensitive Electrochemical Detection of Lipopolysaccharide. Biosens Bioelectron, 2016, 83, 287–292.

[38] Yilmaz, MD, Oktem, HA. Eriochrome black T-Eu^{3+} complex as a ratiometric colorimetric and fluorescent probe for the detection of dipicolinic acid, a biomarker of bacterial spores. Anal Chem, 2018, 90, 4221–4225.

[39] Ou, XY, Guo, T, Song, L, Liang, HY, Zhang, QZ, Liao, JQ, Li, JY, Li, J, Yang, HH. Autofluorescence-free immunoassay using X-ray scintillating nanotags. Anal Chem, 2018, 90, 6992–6997.

[40] Ren, H, Long, Z, Shen, X, Zhang, Y, Sun, J, Ouyang, J, Na, N. Sandwich DNA hybridization fluorescence resonance energy-transfer strategy for MiR-122 detection by core-shell upconversion nanoparticles. ACS Appl Mater Interfaces, 2018, 10, 25621–25628.

[41] Peng, J, Samanta, A, Zeng, X, Han, S, Wang, L, Su, D, Loong, DTB, Kang, NY, Park, SJ, All, AH, Jiang, W, Yuan, L, Liu, X, Chang, YT. Real-time in vivo hepatotoxicity monitoring through chromophore-conjugated photon-upconverting nanoprobes. Angew Chem – Int Ed, 2017, 56, 4165–4169.

[42] He, R, Wang, YL, Ma, HF, Yin, SG, Liu, QY. Eu^{3+}-functionalized metal-organic framework composite as ratiometric fluorescent sensor for highly selective detecting urinary 1-hydroxypyrene. Dye Pigm, 2018, 151, 342–347.

[43] Liang, T, Li, Z, Wang, P, Zhao, F, Liu, J, Liu, Z. Breaking through the signal-to-background limit of upconversion nanoprobes using a target-modulated sensitizing switch. J Am Chem Soc, 2018, 140, 14696–14703.

[44] Zhao, J, Gao, J, Xue, W, Di, Z, Xing, H, Lu, Y, Li, L. Upconversion luminescence-activated DNA nanodevice for ATP sensing in living cells. J Am Chem Soc, 2018, 140, 578–581.

[45] Sardesai, NP, Ganesana, M, Karimi, A, Leiter, JC, Andreescu, S. Platinum-doped ceria based biosensor for in vitro and in vivo monitoring of lactate during hypoxia. Anal Chem, 2015, 87, 2996–3003.

[46] Liu, L, Wang, S, Zhao, B, Pei, P, Fan, Y, Li, X, Zhang, F. Er^{3+} sensitized 1530 nm to 1180 Nm second near-infrared window upconversion nanocrystals for in vivo biosensing. Angew Chem – Int Ed, 2018, 57, 7518–7522.

[47]   Peng, J, Xu, W, Teoh, CL, Han, S, Kim, B, Samanta, A, Er, JC, Wang, L, Yuan, L, Liu, X, Chang, YT. High-efficiency in vitro and in vivo detection of Zn^{2+} by dye-assembled upconversion nanoparticles. J Am Chem Soc, 2015, 137, 2336–2342.

[48]   Isaac, M, Pallier, A, Szeremeta, F, Bayle, PA, Barantin, L, Bonnet, CS, Sénèque, O. MRI and luminescence detection of Zn^{2+} with a lanthanide complex-zinc finger peptide conjugate. Chem Commun, 2018, 54, 7350–7353.

[49]   Wang, Y, Wang, H, Yang, M, Yuan, J, Wu, J, Visible-Light-Excited Europium(III, A. Complex-based luminescent probe for visualizing copper ions and hydrogen sulfide in living cells. Opt Mater, 2018, 75, 243–251.

[50]   Zhou, Y, Chen, HH, Yan, B. An Eu^{3+} post-functionalized nanosized metal-organic framework for cation exchange-based Fe^{3+}-sensing in an aqueous environment. J Mater Chem A, 2014, 2, 13691–13697.

[51]   Xu, H, Fang, M, Cao, CS, Qiao, WZ, Zhao, B. Unique (3,4,10)-connected lanthanide-organic framework as a recyclable chemical sensor for detecting Al3+. Inorg Chem, 2016, 55, 4790–4794.

[52]   Liu, Y, Chen, M, Cao, T, Sun, Y, Li, C, Liu, Q, Yang, T, Yao, L, Feng, W, Li, F, Cyanine-Modified, A. Nanosystem for in vivo upconversion luminescence bioimaging of methylmercury. J Am Chem Soc, 2013, 135, 9869–9876.

[53]   Sun, T, Gao, Y, Du, Y, Zhou, L, Chen, X. Recent advances in developing lanthanide metal–organic frameworks for ratiometric fluorescent sensing. Front Chem, 2021, 8, 624592.

[54]   Vetrone, F, Naccache, R, Zamarrón, A, De La Fuente, AJ, Sanz-Rodríguez, F, Maestro, LM, Rodriguez, EM, Jaque, D, Sole, JG, Capobianco, JA. Temperature sensing using fluorescent nanothermometers. ACS Nano, 2010, 4, 3254–3258.

[55]   Cadiau, A, Brites, CDS, Costa, PMFJ, Ferreira, RAS, Rocha, J, Carlos, LD. Ratiometric nanothermometer based on an emissive Ln^{3+}-organic framework. ACS Nano, 2013, 7, 7213–7218.

[56]   Zhao, D, Zhang, J, Yue, D, Lian, X, Cui, Y, Yang, Y, Qian, A. A highly sensitive near-infrared luminescent metal-organic framework thermometer in the physiological range. Chem Commun, 2016, 52, 8259–8262.

[57]   Zhang, H, Jiang, J, Gao, P, Yang, T, Zhang, KY, Chen, Z, Liu, S, Huang, W, Zhao, Q. Dual-emissive phosphorescent polymer probe for accurate temperature sensing in living cells and zebrafish using ratiometric and phosphorescence lifetime imaging microscopy. ACS Appl Mater Interfaces, 2018, 10, 17542–17550.

[58]   Zhang, X, Jiao, Y, Jing, X, Wu, H, He, G, Duan, C. pH-sensitive fluorescent sensors based on Europium (III) complexes. Dalt Trans, 2011, 40, 2522–2527.

[59]   Chu, B, Song, B, Ji, X, Su, Y, Wang, H, He, Y. Fluorescent silicon nanorods-based ratiometric sensors for long-term and real-time measurements of intracellular PH in live cells. Anal Chem, 2017, 89, 12152–12159.

[60]   Ma, T, Ma, Y, Liu, S, Zhang, L, Yang, T, Yang, HR, Lv, W, Yu, Q, Xu, W, Zhao, Q, Huang, W. Dye-conjugated upconversion nanoparticles for ratiometric imaging of intracellular pH values. J Mater Chem C, 2015, 3, 6616–6620.

[61]   Natarajan, D, Ye, Z, Wang, L, Ge, L, Pathak, JL. Rare earth smart nanomaterials for bone tissue engineering and implantology: Advances, challenges, and prospects. Bio EngTransl Med, 2022, 7, e10262.

[62]   Gao, J, Liang Feng, L, Chen, B, Fu, B, Zhu, M. The role of rare earth elements in bone tissue engineering scaffolds – A review. Compos Part B: Eng, 2022, 235, 109758.

[63]   Deliormanlı, AM. Synthesis and characterization of cerium- and gallium-containing borate bioactive glass scaffolds for bone tissue engineering. J Mater Sci Mater Med, 2015, 26, 67.

[64]   Salinas, AJ, Vallet-Regí, M. Glasses in bone regeneration: A multiscale issue. J Non Cryst Solids, 2016, 432, 9–14.

[65]   Shruti, S, Salinas, AJ, Lusvardi, G, Malavasi, G, Menabue, L, Vallet-Regi, M. Mesoporous bioactive scaffolds prepared with cerium-, gallium- and zinc-containing glasses. Acta Biomater, 2013, 9, 4836–4844.

[66]   Coelho, J, Hussain, NS, Gomes, PS, Garcia, MP, Lopes, MA, Fernandes, MH, Santos, JD. Development and characterization of lanthanides doped hydroxyapatite composites for bone tissue application. Curr Trends Glas Ceram Mater, 2012, 4, 87–115.

[67]   Madhumathi, K, Shalumon, KT, Divya Rani, VV, Tamura, H, Furuike, T, Selvamurugan, N, Nair, SV, Jayakumar, R. Wet chemical synthesis of chitosan hydrogel-hydroxyapatite composite membranes for tissue engineering applications. Int J Biol Macromol, 2009, 45, 12–15.

[68]   Li, X, Chen, H. Yb^{3+}/Ho^{3+} Co-doped apatite upconversion nanoparticles to distinguish implanted material from bone tissue. ACS Appl Mater Interfaces, 2016, 8, 27458–27464.

[69]   Prabakaran, S, Rajan, M, Lv, C, Meng, G. Lanthanides-substituted hydroxyapatite/Aloe vera composite coated titanium plate for bone tissue regeneration. Int J Nanomed, 2020, 15, 8261–8279.

[70]   Liu, H, Jin, Y, Ge, K, Jia, G, Li, Z, Yang, X, Chen, S, Ge, M, Sun, W, Liu, D, Zhang, J. Europium-doped Gd_2O_3 nanotubes increase bone mineral density in vivo and promote mineralization in vitro. ACS Appl Mater Interfaces, 2017, 9, 5784–5792.

[71]   Augustine, R, Dalvi, YB, Yadu Nath, VK, Varghese, R, Raghuveeran, V, Hasan, A, Thomas, S, Sandhyarani, N. Yttrium oxide nanoparticle loaded scaffolds with enhanced cell adhesion and vascularization for tissue engineering applications. Mater Sci Eng C Mater Boil Appl, 2019, 103, 109801.

[72]   Liu, Z, Yu, Y, Kang, W, Chen, F, Yan, F, Ma, B, Ge, S. Self-assembled terbium-amino acid nanoparticles as a model for terbium biosafety and bone repair ability assessment. Compos B Eng, 2022, 244, 110186.

[73]   Weng, W, Biesiekierski, A, Li, Y, Dargusch, M, Wen, C. A review of the physiological impact of rare earth elements and their uses in biomedical Mg alloys. Acta Biomater, 2021, 130, 80–97.

[74]   Wang, J, Li, S. Applications of rare earth elements in cancer: Evidence mapping and scientometric analysis. Front Med, 2022, 9, 94610.

[75]   Teo, RD, Termini, J, Gray, HB. Lanthanides: Applications in cancer diagnosis and therapy. J Med Chem, 2016, 59, 6012–6024.

[76]   Kostova, I, Momekov, G, Tzanova, T, Karaivanova, M. Synthesis, characterization, and cytotoxic activity of new lanthanum(III) complexes of bis-coumarins. Bioinorg Chem Appl, 2006, 2006, 25651.

[77]   Liu, YC, Chen, ZF, Song, XY, Peng, Y, Qin, QP, Liang, H. Synthesis, crystal structure, cytotoxicity and DNA interaction of 5,7-dibromo-8-quinolinolato-lanthanides. Eur J Med Chem, 2013, 59, 168–175.

[78]   Wei, JH, Chen, ZF, Qin, JL, et al. Water-soluble oxoglaucine-Y(III), Dy(III) complexes: In vitro and in vivo anticancer activities by triggering DNA damage, leading to S phase arrest and apoptosis. Dalton Trans, 2015, 44, 11408–11419.

[79]   Yang, Y, Bin, YD, Qin, QP, Luo, XJ, Zou, BQ, Zhang, HX. Novel quinoline-based Ir(III) complexes exhibit high antitumor activity in vitro and in vivo. ACS Med Chem Lett, 2019, 10, 1614–1619.

[80]   Wason, MS, Zhao, J. Cerium oxide nanoparticles: Potential applications for cancer and other diseases. Am J Transl Res, 2013, 5, 126–131.

[81]   Wang, L, Ai, W, Zhai, Y, Li, H, Zhou, K, Chen, H. Effects of nano-CeO_2 with different nanocrystal morphologies on cytotoxicity in hepG2 cells. Int J Environ Res Public Health, 2015, 12, 10806–10819.

[82]   Chan, CF, Xie, C, Tsang, MK, Lear, S, Dai, L, Zhou, Y, Cicho, J, Karbowiak, M, Hreniak, D, Lan, R, Cobb, SL, Lam, MHW, Hao, J, Wong, KL. The effects of morphology and linker length on the properties of peptide-lanthanide upconversion nanomaterials as G2 phase cell cycle inhibitors. Eur J InorgChem, 2015, 2015, 4539–4545.

[83]   Chan, CF, Tsang, MK, Li, H, Lan, R, Chadbourne, FL, Chan, WL, Law, GL, Cobb, SL, Hao, J, Wong, WT, Wong, KL. Bifunctional up-converting lanthanide nanoparticles for selective in vitro imaging and inhibition of cyclin D as anti-cancer agents. J Mater Chem B, 2014, 2, 84–91.

[84] Dong, H, Du, SR, Zheng, XY, Lyu, GM, Sun, LD, Li, LD, Zhang, PZ, Zhang, C, Yan, CH. Lanthanide nanoparticles: From design toward bioimaging and therapy. Chem Rev, 2015, 115, 10725–10815.

[85] Kalluru, P, Vankayala, R, Chiang, CS, Hwang, KC. Unprecedented "All-in-One" Lanthanide-doped mesoporous silica frameworks for fluorescence/MR imaging and combination of NIR light triggered chemo-photodynamic therapy of tumors. Adv Funct Mater, 2016, 26, 7908–7920.

[86] Yao, C, Wang, W, Wang, P, Zhao, M, Li, X, Zhang, F. Near-infrared upconversion mesoporous cerium oxide hollow biophotocatalyst for concurrent pH-/H_2O_2-Responsive O_2-evolving synergetic cancer therapy. Adv Mater, 2018, 30, 1704833.

[87] Park, YI, Kim, HM, Kim, JH, Moon, KC, Yoo, B, Lee, KT, Lee, N, Choi, Y, Park, W, Ling, D, Na, K, Moon, WK, Choi, SH, Park, HS, Yoon, SY, Suh, YD, Lee, SH, Hyeon, T. Theranostic probe based on lanthanide-doped nanoparticles for simultaneous in vivo dual-modal imaging and photodynamic therapy. Adv Mater, 2012, 24, 5755–5761.

[88] del Rosal, B, Pérez-Delgado, A, Carrasco, E, Jovanović, DJ, Dramićanin, MD, Dražić, G, de la Fuente, ÁJ, Sanz-Rodriguez, F, Jaque, D. Neodymium-based stoichiometric ultrasmall nanoparticles for multifunctional deep-tissue photothermal therapy. Adv Opt Mater, 2016, 4, 782–789.

[89] Kolesnikov, IE, Golyeva, EV, Kalinichev, AA, Kurochkin, MA, Lähderanta, E, Mikhailov, MD. Nd^{3+} Single Doped YVO_4 nanoparticles for sub-tissue heating and thermal sensing in the second biological window. Sens Actuators B Chem, 2017, 243, 338–345.

[90] Yu, Z, Hu, W, Zhao, H, Miao, X, Guan, Y, Cai, W, Zeng, Z, Fan, Q, Tan, TTY. Generating new cross-relaxation pathways by coating prussian blue on $NaNdF_4$ to fabricate enhanced photothermal agents. Angew Chem – Int Ed, 2019, 58, 8536–8540.

[91] Yu, Y, Xu, S, Gao, Y, Jiang, M, Li, X, Zhang, J, Zhang, X, Chen, B. Enhanced photothermal conversion performances with ultra-broad plasmon absorption of Au in Au/Sm_2O_3 composites. J Am Ceram Soc, 2020, 103, 4420–4428.

[92] Paul, N, Borah, JP, Mohanta, D. Temperature responsive gadolinium oxide nanoparticles for hyperthermia application. AIP Conf Proc, 2017, 1832, 1–4.

[93] Song, G, Cheng, L, Chao, Y, Yang, K, Liu, Z. Emerging nanotechnology and advanced materials for cancer radiation therapy. Adv Mater, 2017, 29, 1–26.

[94] Kim, J, Luo, ZX, Wu, Y, Lu, X, Jay, M. In-situ formation of holmium oxide in pores of mesoporous carbon nanoparticles as substrates for neutron-activatable radiotherapeutics. Carbon N Y, 2017, 117, 92–99.

[95] Van Nimwegen, SA, Bakker, RC, Kirpensteijn, J, van Es, RJJ, Koole, R, Lam, MGEH, Hesselink, JW, Nijsen, JFW. Intratumoral injection of radioactive holmium ([166]Ho) microspheres for treatment of oral squamous cell carcinoma in cats. Vet Comp Oncol, 2018, 16, 114–124.

[96] Ehlerding, EB, Ferreira, CA, Aluicio-Sarduy, E, Jiang, D, Lee, HJ, Theuer, CP, Engle, JW, Cai, W. [86/90]Y-Based theranostics targeting angiogenesis in a murine breast cancer model. Mol Pharm, 2018, 15, 2606–2613.

[97] Wason, MS, Colon, J, Das, S, Seal, S, Turkson, J, Zhao, J, Baker, CH. Sensitization of pancreatic cancer cells to radiation by cerium oxide nanoparticle-induced ROS production. Nanomedicine, 2013, 9, 558–569.

[98] Zhong, X, Wang, X, Zhan, G, Tang, Y, Yao, Y, Dong, Z, Hou, L, Zhao, H, Zeng, S, Hu, J, Cheng, L, Yang, X. $NaCeF_4$:Gd,Tb Scintillator as an X-Ray responsive photosensitizer for multimodal imaging-guided synchronous radio/radiodynamic therapy. Nano Lett, 2019, 19, 8234–8244.

[99] Zhang, X, Ge, J, Xue, Y, Lei, B, Yan, D, Li, N, Liu, Z, Du, Y, Cai, R. Controlled synthesis of ultrathin lanthanide oxide nanosheets and their promising pH-controlled anticancer drug delivery. Chem – A Eur J, 2015, 21, 11954–11960.

[100] Shen, J, Zhao, L, Han, G. Lanthanide-doped upconverting luminescent nanoparticle platforms for optical imaging-guided drug delivery and therapy. Adv Drug Deliv Rev, 2013, 65, 744–755.

[101] Tawfik, SM, Sharipov, M, Huy, BT, Gerelkhuu, Z, Speziale, DB, Lee, YI. Naturally modified nonionic alginate functionalized upconversion nanoparticles for the highly efficient targeted pH-responsive drug delivery and enhancement of NIR-imaging. J Ind Eng Chem, 2018, 57, 424–435.

[102] Luo, M, Xu, L, Xia, J, Zhao, H, Du, Y, Lei, B. Synthesis of porous gadolinium oxide nanosheets for cancer therapy and magnetic resonance imaging. Mater Lett, 2020, 265, 127375.

[103] Tu, D, Zheng, W, Liu, Y, Zhu, H, Chen, X. Luminescent biodetection based on lanthanide-doped inorganic nanoprobes. Coord Chem Rev, 2014, 273, 13–29.

[104] Zhou, L, Wang, R, Yao, C, Li, X, Wang, C, Zhang, X, Xu, C, Zeng, A, Zhao, D, Zhang, F. Single-band upconversion nanoprobes for multiplexed simultaneous in situ molecular mapping of cancer biomarkers. Nat Commun, 2015, 6, 6938.

[105] Zhang, SY, Shi, W, Cheng, P, Zaworotko, MJ. A Mixed-Crystal Lanthanide Zeolite-like metal-organic framework as a fluorescent indicator for lysophosphatidic acid, a cancer biomarker. J Am Chem Soc, 2015, 137, 12203–12206.

[106] Wang, Y, Shen, P, Li, C, Wang, Y, Liu, Z. Upconversion fluorescence resonance energy transfer based biosensor for ultrasensitive detection of matrix metalloproteinase-2 in blood. Anal Chem, 2012, 84, 1466–1473.

[107] De Bang, TC, Shah, P, Cho, SK, Yang, SW, Husted, S. Multiplexed MicroRNA detection using lanthanide-labeled DNA probes and laser ablation inductively coupled plasma mass spectrometry. Anal Chem, 2014, 86, 6823–6826.

[108] Canales, Á, Mallagaray, Á, Berbís, MÁ, Navarro-Vázquez, A, Domínguez, G, Cañada, FJ, André, S, Gabius, HJ, Pérez-Castells, J, Jiménez-Barbero, J. Lanthanide-chelating carbohydrate conjugates are useful tools to characterize carbohydrate conformation in solution and sensitive sensors to detect carbohydrate-protein interactions. J AmChem Soc, 2014, 136, 8011–8017.

[109] McDonald, MA, Watkin, KL. Small particulate gadolinium oxide and gadolinium oxide albumin microspheres as multimodal contrast and therapeutic agents. Invest Radiol, 2003, 38, 305–310.

[110] Cho, M, Sethi, R, Ananta Narayanan, JS, Lee, SS, Benoit, DN, Taheri, N, Decuzzi, P, Colvin, VL. Gadolinium oxide nanoplates with high longitudinal relaxivity for magnetic resonance imaging. Nanoscale, 2014, 6, 13637–13645.

[111] Dong, H, Du, SR, Zheng, XY, Lyu, GM, Sun, LD, Li, LD, Zhang, PZ, Zhang, C, Yan, CH. Lanthanide nanoparticles: From design toward bioimaging and therapy. Chem Rev, 2015, 115, 10725–10815.

[112] Stefanakis, D, Seimenis, I, Ghanotakis, D. Synthesis and characterization of gadolinium nanosheets with bound rose bengal: Potential use in photodynamic therapy and MRI. J Nanopart Res, 2014, 16, 2694.

[113] Gupta, N, Shrivastava, A, Sharma, RK. Silica nanoparticles coencapsulating gadolinium oxide and horseradish peroxidase for imaging and therapeutic applications. Int J Nanomed, 2012, 7, 5491–5500.

[114] Wang, F, Banerjee, D, Liu, Y, Chen, X, Liu, X. Upconversion nanoparticles in biological labeling, imaging, and therapy. Analyst, 2010, 135, 1839–1854.

[115] Mahapatra, C, Singh, RK, Lee, JH, Jung, J, Hyun, JK, Kim, HW. Nano-shape varied cerium oxide nanomaterials rescue human dental stem cells from oxidative insult through intracellular or extracellular actions. Acta Biomater, 2017, 50, 142–153.

[116] Bona, AD, Pecho, OE, Alessandretti, R. Zirconia as a dental biomaterial. Materials (Basel), 2015, 8, 4978–4991.

[117] Noar, JH, Evans, RD. Rare earth magnets in orthodontics: An overview. Br J Orthod, 1999, 26, 29–37.

[118] Hassan, MS, Amna, T, Al-Deyab, SS, Kim, HC, Oh, TH, Khil, MS. Toxicity of Ce_2O_3/TiO_2 composite nanofibers against S. Aureus and S. Typhimurium: A novel electrospun material for disinfection of food pathogens. Colloids Surf A Physicochem Eng Asp, 2012, 415, 268–273.

[119] Kumar, KM, Mahendhiran, M, Diaz, MC, Hernandez-Como, N, Hernandez-Eligio, A, Torres-Torres, G, Godavarthi, S, Gomez, LM. Green synthesis of Ce^{3+} Rich CeO_2 nanoparticles and its antimicrobial studies. Mater Lett, 2018, 214, 15–19.

[120] Abou Hammad, AB, Hemdan, BA, El Nahrawy, AM. Facile synthesis and potential application of $Ni_{0.6}Zn_{0.4}Fe_2O_4$ and $Ni_{0.6}Zn_{0.2}Ce_{0.2}Fe_2O_4$ magnetic nanocubes as a new strategy in sewage treatment. J Environ Manage, 2020, 270, 110816.

[121] Johnson, RB, Cook, MA, Nicklason, PM, Rust, MB. Determination of apparent protein digestibility of live artemia and a microparticulate diet in 8-week-old atlantic cod gadus morhua larvae. Aquaculture, 2009, 288, 290–298.

[122] Tamilalagan, E, Chen, TW, Chen, SM, Akilarasan, M, Huang, YC, Rwei, SP. An efficient electrocatalyst for the nano-level detection of neurotransmitter (Dopamine) in Biologic Matrices based on Samarium (III) Oxide Nanoparticles; An Electrochemical Approaches. Int J Electrochem Sci, 2020, 15, 6981–6990.

[123] Manavalan, S, Rajaji, U, Chen, SM, Steplin Paul Selvin, S, Govindasamy, M, Chen, TW, Ajmal Ali, M, Al-Hemaid, FMA, Elshikh, MS. Determination of 8-Hydroxy-2′-Deoxyguanosine oxidative stress biomarker using dysprosium oxide nanoparticles@reduced graphene oxide. Inorg Chem Front, 2018, 5(11), 2885–2892.

[124] Usman, MS, Hussein, MZ, Fakurazi, S, Ahmad Saad, FF. Gadolinium-based layered double hydroxide and graphene oxide nano-carriers for magnetic resonance imaging and drug delivery. Chem Cent J, 2017, 11, 47.

[125] Sayour, H, Kassem, S, Canfarotta, F, Czulak, J, Mohamed, M, Piletsky, S. Biocompatibility and biodistribution of surface-modified yttrium oxide nanoparticles for potential theranostic applications. Environ Sci Pollut Res, 2020, 27, 19095–19107.

[126] Muthulakshmi, V, Balaji, M, Sundrarajan, M. Biomedical applications of ionic liquid mediated samarium oxide nanoparticles by andrographis paniculata leaves extract. Mater Chem Phys, 2020, 242, 122483.

[127] Mitra, RN, Merwin, MJ, Han, Z, Conley, SM, Al-Ubaidi, MR, Naash, MI. Yttrium oxide nanoparticles prevent photoreceptor death in a light-damage model of retinal degeneration. Free Radic Biol Med, 2014, 75, 140–148.

[128] Cheng, J, Cheng, Z, Hu, R, Cui, Y, Cai, J, Li, N, Gui, S, Sang, X, Sun, Q, Wang, L, Hong, F. Immune dysfunction and liver damage of mice following exposure to lanthanoids. © 2011 Wiley Periodicals. Inc Environ Toxicol, 2014, 29, 64–73.

[129] Rogosnitzky, M, Branch, S. Gadolinium-based contrast agent toxicity: A review of known and proposed mechanisms. Biometals, 2016, 29, 365–376.

[130] Tyler, G. Rare earth elements in soil and plant systems – A review. Plant Soil, 2004, 267, 191–206.

[131] Feng, LX, Xiao, H, He, X, Li, Z, Li, F, Liu, N, Zhao, Y, Huang, Y, Zhang, Z, Chai, Z. Neurotoxicological consequence of long-term exposure to lanthanum. Toxicol Lett, 2006, 165, 112–120.

[132] Perrat, E, Parant, M, Py, JS, Rosin, C, Cossu-Leguille, C. Bioaccumulation of gadolinium in freshwater bivalves. Environ Sci Pollut Res Int, 2017, 24, 12405–12415.

[133] Cheng, J, Li, N, Cai, J, Cheng, Z, Hu, R, Zhang, Q, Wan, F, Sun, Q, Gui, S, Sang, X, Wang, L, Hong, F. Organ histopathological changes and its function damage in mice following long-term exposure to lanthanides chloride. Biol Trace ElemRes, 2012, 145, 361–368.

[134] Zhu, W, Xu, S, Shao, P, Zhang, H, Wu, D, Yang, W, Feng, J, Feng, L. Investigation on liver function among population in high background of rare earth area in South China. Biol Trace Elem Res, 2005, 104, 1–8.

Manish Taunk

15 Recovery of rare earth elements from electronic waste

15.1 Introduction

Rare earth elements (REE) are extensively used materials in consumer products, especially in the electrical and electronics industry due to their unique and extraordinary physical and chemical properties. In the periodic table, fifteen elements from Lanthanum (La, Z = 57) to Lutetium (Lu, Z = 71), such as cerium (Ce), praseodymium (Pr), neodymium (Nd), promethium (Pm), samarium (Sm), Europium (Eu), gadolinium (Gd), terbium (Tb), dysprosium (Dy), holmium (Ho), erbium(Er), thulium (Tm), and ytterbium (Yb) are commonly known as lanthanides and are also considered REE [1, 2]. In addition, two other d-transition metals, namely, Scandium (Sc, Z = 21) and Yttrium (Y, Z = 39) with properties similar to those of lanthanides are also termed REE. The electronic configuration of their outermost shell is the same for all while 4f orbitals, in particular, are progressively filled with increasing atomic numbers from La to Lu. Thus, screening of 4f orbitals leads to extremely similar physiochemical properties. Also, a regular decrease in the ionic radii from La^{3+} (1.06 Å) to Lu^{3+} (0.85 Å), known as lanthanide contraction, is a related consequence [3, 4].

All these REEs are found in nature in an impure form as their ores, except Pm. Pm, being the rarest, is found in trace quantities naturally due to the absence of its stable isotopes. These REEs are mostly found in trivalent oxidation states, while Eu can also be found in divalent state and Ce is found in tetravalent state [5]. These seventeen materials are a special category of elements that play a key role in contemporary life, with a variety of uses and applications in the fabrication of various sophisticated devices, such as smart phones, high-performance permanent magnets, light emitting diodes, displays, rechargeable batteries, integrated chips, tablets, laptops, solar panels, fiber optics, superconductors, hydrogen storage applications, etc., as shown in Figure 15.1. In short, REEs are vital to our modern and futuristic technologies for high tech applications and are, therefore, termed "The vitamins of modern industry." The human population on earth is rising day by day and is expected to reach 8.5 billion by the year 2030. With the

***Corresponding author: Manish Taunk,** Department of Physics, Maharaja Agrasen University, Baddi 174103, Himachal Pradesh, India, e-mail: manishphy@gmail.com

rising population, use of tech-enabled gadgets and devices is also increasing exponentially, leading to the consumption of natural resources at a higher rate [6]. Annually, 1.3 billion tons of electrical and electronic waste is being generated worldwide, and it is expected that it will triple by 2025 [7].
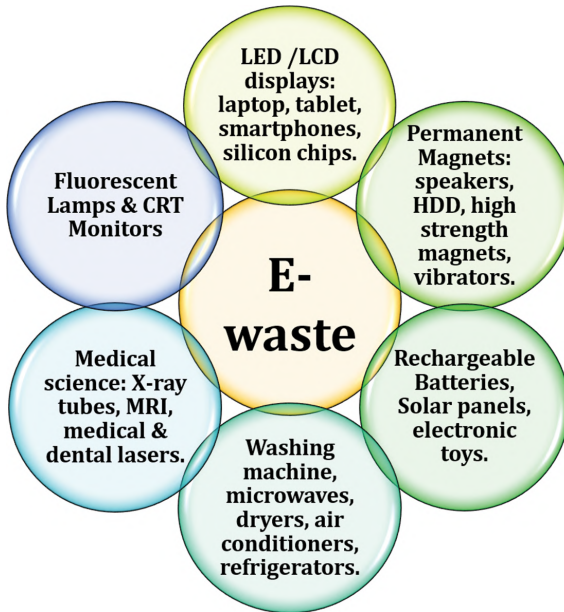
Figure 15.1: Electronic and electrical waste.

The main concerns about REE are their limited supplies and increased cost due to restricted trade. It is not possible to match the rising demand for REE from the limited resources that are available only in a few countries (China, Brazil, Vietnam, Russia, and India), and it is creating an imbalance between supply and demand. China is reported to be the major source of rare earth metals in the global market and has gradually reduced rare earth mineral mining and exports due to newly implemented internal policies, since 2010 [8]. Furthermore, the extraction of REE through mining is linked to various challenges like low concentration extraction, pollution or adverse effect on our environment, and also the generation of chemically reactive and radioactive waste material as by-products. The huge amount of electrical and electronic waste (e-waste) generated at the global level is the fastest-growing waste stream and has attracted human attention to the environmental aspects [5, 9]. Moreover, REE concentration present in electrical and electronic waste is much higher than that obtained by the mining process from natural or primary resources, which are an advantage and a potential secondary source of REEs. Hence, it is reasonable to treat the e-waste using suitable scientific methods and generate wealth with proper recycling and extraction

techniques. In this way, huge piles of e-waste can be utilized for recycling to recover REE, and this can also lead to a circular mineral economy.

15.2 Recycling and recovery process

Considering these factors, i.e., environmental impact and resource availability, secondary resource processing, i.e., manufacturing-generated waste and used devices containing REE are eventual and alternative resources to meet the requirements. A great deal of research work has been carried out by researchers worldwide to develop extraction methods, but commercially a very small portion of REE – approximately 1% – is recycled from end-of-life products [10, 11]. The reasons observed for the low recovery are inhomogeneity of feedstock, inefficient collection, immature technologies, high recycling costs, and lack of incentives. However, in a few categories, efficient collections and categorical separation of e-waste have increased the recycling rate to a slightly higher value [12]. These situations have prompted researchers to innovate unique processes for efficient recycling and recovery. Hence, there is a need to develop cost-effective and eco-friendly methods to recover REE from various end-of-life products or e-waste.

Figure 15.2: Recycling and recovery process.

The end-of-life products are normally discarded as a whole by the consumers and are later termed e-waste. The recycling and recovery process is generally divided into four parts, i.e., collection, dismantling, separation, and processing, as shown in Figure 15.2. The processing part continues mostly with chemical leaching, solution concentration, purification, and finally, metal recovery. The process of REE retrieval from end-of-life products starts with the collection of e-waste for post-processing at the recycling facility. Thereafter, the dismantling of the e-waste products takes place. Dismantling is a very complex process, and its complexity increases with the smaller size and integrated approach of

internal components. Different types of dismantling processes – automatic, manual, and semi-automatic are performed on these used products [13]. After dismantling of e-waste, physical separation is performed for different kinds of materials like plastic housing, glass, metallic parts, cables, screws, printed circuit boards, and REE-containing materials and components. Separation is an important process, and effective separation, preferably with 100% efficiency of the dismantled parts, has the potential to increase the purity and rate of recovery of the final material including REE. The recovery (%) of REE from end-of-life products is shown in Table 15.1.

Table 15.1: The % (w/w) of recoverable REE from end-of-life products [15].

End-of-life product	Y (%)	Ce (%)	Sm (%)	Eu (%)	Nd (%)	Pr (%)	La (%)	Dy (%)	Gd (%)
CRT monitors	58	87	90	90	–	–	–	–	–
LEDs	20.8	16.2	–	–	–	–	–	–	–
LCDs	99	90	–	95	–	26	91	–	–
Permanent magnets	–	–		–	63	56	–	22	–
Fluorescent lamps	90	–	–	81	–	–	–	–	40
NiMH batteries	–	45–85	–	–	46–90	57–86	41–85	–	–

Also, effective separation can maintain component integrity for potential reuse and prevent accidental destruction of a good component. To reduce electrical and electronic waste, it is also imperative to design the internal components in such a way that after dismantling, the end-of-life product reusable parts can be easily extracted without damage. Reuse of the undamaged internal parts is also a favorable, environment-friendly, and economical approach to the recycling process. Printed circuit boards (PCBs) also contain metals such as copper, nickel, indium, tin, and precious metals like gold, silver, and palladium. These valuable metals, including REE, can be recovered using suitable techniques. The concentration of these metals in discarded PCBs is higher than in the natural deposits. A typical manual recovery process for precious metals from printed circuit boards can reach up to 95%, before sending them into a shredder [14].

The majority of the recycling or recovery work is limited to fluorescent lamps, permanent magnets, and nickel metal hydride (NiMH) batteries, because it is difficult to separate strongly bonded REE-containing components from other small electronic products. In this chapter, REE recovery from fluorescent lamps, permanent magnets, and NiMH batteries has been discussed. Phosphor is an essential and imperative material in fluorescent lamps and contains REE, especially Y (75%), Eu (4%), and Tb (2%). Different proportions of these REE are used to generate red, green, and blue phosphor. The permanent magnets are also an integral part of various speakers, containing 22–40%, 25–30%, 0.07–13%, and 0.07–4.2% of Sm, Nd, Pr, and Dy, respectively. Similarly, nickel metal hydride batteries contain REE, namely, Ce, Nd, La, Pr, and Y – 6–10%, 2.4%, 20.2%, 1%, and 0.7–0.9%, respectively [15].

15.3 Leaching methods

Numerous studies have focused on the extraction of REE using pyro metallurgical, hydrometallurgical, or a combination of both methods from various primary and secondary sources. Both methods have their own advantages and disadvantages. The pyro metallurgical method involves metal extraction by heating at high temperatures in a plasma arc or blast furnace. Involvement of high temperature and high energy processing steps made this process energy-consuming, costly, and with high environmental impacts. On the other side, the hydrometallurgical process involves the extraction of valuable metals into the liquid medium by leaching at room temperature or, sometimes, moderate temperature (~100 °C) for processing and could be considered more environmentally friendly as compared to the pyrometallurgical method [16]. The hydrometallurgical process is a well-developed promising technology for the extraction of REEs from REE-carrying substances such as natural ores and other secondary sources [17]. Mainly, it contains three steps: leaching, solution purification, and precipitation for recovery of the target metal. In the chemical leaching process, the REEs are separated from REE-carrying discarded e-waste, using chemical reagents in an aqueous solution. The leaching process involves acid leaching using H_2SO_4, HCl, and HNO_3 as well as combined base and acid leaching for the dissolution of separated e-waste [18]. A general leaching reaction of RE oxides with sulfuric acid can be represented as

$$RE_2O_3 + nH^+ = nRE^3 + nH_2O \tag{15.1}$$

$$n\,RE^3 + n\,SO_4^{2-} + n\,H_2O = RE_2(SO_4)_n \cdot n\,H_2O \tag{15.2}$$
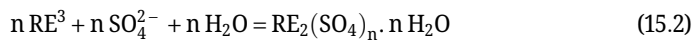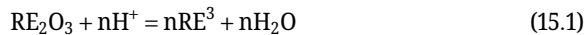
Similarly, a leaching reaction using hydrochloric acid can be represented as

$$RE_2O_3 + nHCl = nRECl_3 + nH_2O \tag{15.3}$$
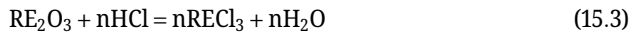
Various chemical and physiochemical approaches like acid dissolution, electro-slag refining, direct melting, liquid media extraction, glass slag methods, and gas phase extraction have been employed for the detachment of REE from source materials. As mentioned above, these processes mostly have high operational costs, environmental impacts, and poor recovery of the final product. Also, in most of the reported studies, the extraction of REE is achieved using harsh acidic and or alkaline conditions at high temperatures, releasing toxic and radioactive wastes. Biological recovery methods such as bioleaching, biosorption, and siderophores offer a greener and environmentally friendly alternative to classical approaches, when implemented properly [19]. These processing methods generally occur at low temperatures, normal temperature and pressure, and also without the use of expensive and aggressive reagents.

Bioleaching is a biologically based method and an effective technique of metal retrieval from primary as well as secondary sources with little environmental footprint of recycling. It uses microorganisms like extremophiles, moderately thermophilic bacteria,

and mesophiles. It has been effectively used in the recovery of various precious metals at low concentrations [20]. When bioleaching extraction results are compared to other processes like hydro metallurgy and pyro metallurgy, bio recovery was reported to be the more environmentally friendly and cost-effective technique for the extraction of valuable metals. The microorganisms can be used to solubilize REE, particularly from secondary sources [15]. The selection of microorganisms (autotrophic or heterotrophic) depends upon the type of mineral and REE to be extracted. The extraction of REE, such as Sc, from minerals containing polymetallic sulfides has been done using autotrophic microorganisms, whereas, heterotrophic bacteria are primarily used for minerals containing a rich amount of phosphate and carbonates. Mostly, heterotrophs are used for REE extraction with some external supplements to provide electron donors and carbon sources keeping in mind the high value of obtained products. The heterotrophic-assisted extraction process produces organic acids like acetic, oxalic, formic, citric, and malic acids that lower pH and help in the leaching of REE. Also, the metal-binding molecules produced during the extraction process act as chelating agents to isolate the target species from the solution [21]. The field of bioleaching is in its infancy and is growing day by day with new discoveries.

Biosorption has emerged as the modern biological method for the recovery of REE from e-waste due to several advantages, such as high recovery efficiency for metals in low concentration, fast kinetics, simple process, and minimum sludge production. Biosorption, in simple terms, is the separation of target substances such as metals, metalloid species, compounds, and particulates from liquid media through biological methods. It is a physio-chemical process that includes absorption, adsorption, surface complexation, ion exchange, and precipitation [22]. The process is also cost-effective and can be easily integrated with other extraction processes. Recovery efficiency in biosorption is also affected by temperature, pH, agitation rate, contact period, and initial metal concentration [15, 23]. Extensive studies have been carried out by researchers using bacteria, fungi, and algae as biosorption material from e-waste [24, 25]. They used Sargassum biomass, Agrobacterium species, and Pseudomonas species as adsorbent for the recovery of La, whereas, for the recovery of Nd, Monoraphidium species, Penicillium species, *Saccharomyces cerevisiae*, *Candida colliculus*, and baker's yeast were used [20].

Siderophores are low-molecular-weight, high-affinity iron-chelating compounds secreted by microorganisms like bacteria, fungi, and grasses. Siderophores concentration in the environment typically lies in the μM-mM range. They form complexes with a diverse range of metals including REE [20]. The recovery of REE using siderophores is cost-effective, reversible, rapid, and eco-friendly, compared to traditional methods. It is reported that the highest removal efficiency achieved for Sm, La, and Ce were 66.7%, 51%, and 50%, respectively when the siderophore, *Aspergillus niger*, was used [26, 27]. Siderophores have high stability to enhance recovery of REE from e-waste and in the future, they have great potential in effective separation technology.

15.4 REE recovery from phosphor

Electrical and electronic devices for lighting purposes are an essential part of human civilization. Incandescent lamps have been used for lighting purposes for many years. Florescent lamps and light-emitting diodes (LED) have taken the place of incandescent lamps due to their higher efficiency, better energy-saving ability, and longer life as compared to incandescent lamps. In the last 15 years, the replacement of incandescent lamps with fluorescent lamps and LEDs has taken place rapidly, leading to an almost-complete phase-out of incandescent lamps in modern lighting. REE-based phosphors are luminescent materials and are an essential part of florescent lamps, backlight of flat panel displays (LCD & LED), cathode ray tube (CRT) monitors, X-ray screens, etc.

Fluorescent lamps use phosphors as the main ingredient, and it was reported that all of Eu, 85.2% of Tb, 76.7% of the Y, and small quantities of La (1.6%) and Ce (2%) were used for the production of lamp phosphors [8]. The composition of lamp phosphor is shown in Figure 15.3. Florescent lamps are generally made up of 88% glassy material, 5% metallic parts, 4% plastics, 3% lamp phosphor in the form of powder, and a tiny amount (0.005%) of mercury, by mass [28]. Therefore, the lamp phosphors contain a considerable amount of REE, which could be collected, separated, and recycled effectively. Fluorescent lamps contain different kinds of phosphors that show different reactivities toward strong acids and other chemicals.

Generally, three different methods are employed for recycling lamp phosphors: [12]
i.   Direct use of lamp phosphor collected from end-of-life lamps, in new lamps.
ii.   Separation of mixed phosphor into its constituent components (halo phosphor, red phosphor, green phosphor, and blue phosphor) for reuse in new lamps, where the red phosphor is mainly an oxide structure and the blue and green are mostly complex aluminate structures.
iii. Chemical processing of collected phosphor powder to recover various rare earth metals or oxides. Chemical methods are more suitable for the extraction of high-purity REE.
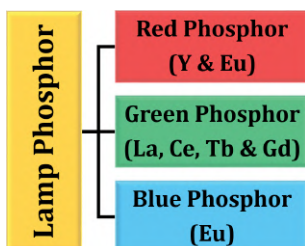
Figure 15.3: Presence of various REEs in lamp phosphor.

In the last three decades, CRT displays were extensively employed in computer monitors and television screens. With the advancement in technology, CRT monitors have been replaced by LCD or LED displays. Thus, large numbers of discarded CRT monitors

are available for REE recovery. The display glass of these CRT monitors is covered with a proportionate blend of blue, green, and red phosphors depending upon different manufacturing brands. Among these, red phosphor contains Y and Eu as REE. Normally, a CRT monitor contains 0.37–0.5 g of Y and 0.03–0.05 g of Eu, which is much higher as compared to primary or natural ore concentration. A backlit LCD monitor has around 20 mg and a LED monitor has 5 mg of REE, which is much less compared to the content available in CRT monitors [28].

In LCDs, REEs are present as doping elements to improve the quality and intensity of RGB colors. Recently, Astrid et al. have reported ultrasound-assisted leaching followed by magnetic separation as an efficient method for recovery of REE from LCD screen wastes. In this method sonochemistry, being a simple and environmentally friendly technique, is used to intensify the metal leaching process. The LCD screen waste contains Er (477 mg/kg), Gd (93 mg/kg), Sn (835 mg/kg), and In (2422 mg/kg), and by this method, 72–99% metals were selectively recovered after only 2 h of leaching [7].

Chemical leaching of phosphor is achieved by complete or selective dissolution of phosphor in an acidic medium. Halo phosphor easily dissolves in dilute acids, red phosphor in slightly strong acids, and green phosphor in very strong acids at high temperatures (~800 °C), whereas, blue phosphor shows resistance toward acids and dissolves in strongly alkaline conditions. Y and Eu in red phosphor can be easily leached because of their oxide form, which dissolves easily in the acid medium. Green phosphor requires a strongly acidic medium because tetravalent Ce and Tb oxides in it are difficult to dissolve. A comparative analysis of REE extraction from phosphor obtained from the fluorescent lamp and fluorescent tube light was carried out by Shukla et al. in 2022. They performed acid leaching using 2 M HCl at 80 °C for one hour. They reported that 86.5% Y and 69% Eu were extracted after acid leaching and 100% La, 60% Tb, and 20.6% Eu after alkali baking with 97% purity. They found alkali baking results in better REE extraction from both phosphors [29]. After the leaching process, the recovery of REE is either done by solvent extraction or by precipitation method, forming REE oxalates or carbonates.

15.5 REE recovery from permanent magnets

Permanent magnets, being an essential part of various electrical and electronic devices, constitute a major part of e-waste and contain nearly 20–30% REE with other elements such as iron, cobalt, boron, etc. It is expected that consumption of REE for magnets will increase in the near future because of the boosted demand for electric motors to be used in electric vehicles. Generally, four types of permanent magnets are in demand, namely neodymium-iron-boron ($Nd_2Fe_{14}B$), samarium-cobalt (SmCo) magnets, ferrite magnets, and alnico magnets. Out of these, only the first two categories contain REE, where Nd and Sm are the main REE constituents in the range of 22–31%

and 22–40%, respectively [16]. More precisely, neodymium-iron-boron permanent magnets commonly referred to as NdFeB magnets are preferred over others, because of their high volume minimization and Curie temperature. Nd, being the major constituent of these magnets, is present in the tetragonal crystalline structure. Dy, Tb, and Pr are also added to these magnets to improve the anisotropy, chemical, and high-temperature stability. The addition of Gd improves the temperature coefficient [30].

Nd magnets have the highest strength among other magnets, so they are frequently used in the making of hard disc drives, speakers, vibrators, etc. NdFeB magnets are used in computer hard disc drives with about 10–20 g of magnet per hard disc drive, leading to annual consumption of NdFeB alloy of approximately 12,000 tons [31]. Thus, discarded magnets from end-of-life products can be used as the secondary source with a much higher concentration (~25%) of REE available as compared to natural ores (maximum 2%). Sm magnets are primarily alloys of samarium, cobalt, and iron. Sm magnets are typically prepared for operation at high temperatures or conditions where temperature stability is vital. The common application areas of these magnets are hard disc drives, sensors, satellite systems, medical devices, and high-performance motors. These magnets are found in different shapes, and their weight may vary from one gram to as much as 2,000 kg.

At present, shredding is mostly performed without dismantling the permanent magnet-containing small electronic items such as hard disc drives, mobile phones, speakers, etc., and then the shredded material is separated into ferrous and nonferrous scraps. The ferrous scrap is then used to extract Nd, Dy, Pr, Tb, and Sm, and other small traces of REEs. In the case of hard disc drives, the results demonstrated that the REE is completely lost in shredding-based processing. Shredding of hard disc drives is necessarily carried out for data security purposes, and it increases the complexity of recovery of REE from the mixed scrap. To recover REE from such scrap, they are treated separately. Proceeding further, the separated magnetic residues after grinding and screening go through the thermal demagnetization process. It has been reported that for all the REEs in the collected residues of less than one millimeter in diameter, a recovery rate of 95% has been achieved [32].

The leaching process is always the first step in dissolving REE present in the magnetic scrap. Complete leaching, as well as selective leaching of magnetic scrap, are the two preferred routes for rare earth recovery. The leaching of REE can be achieved efficiently with both organic (acetic and oxalic acid) and inorganic (HCl, H_2SO_4 & HNO_3) acids. The reported results have shown that inorganic acids, especially HCl and H_2SO_4, were more promising as leaching agents, because experiments can be completed at room temperature under mild conditions and for a shorter duration, generally less than 3 h. Layman and Palmer developed the method of complete leaching in 1993 [33]. All components in NdFeB magnets are dissolved in H_2SO_4, and Nd precipitates can be separated in the form of oxides and fluorides. Bandara et al. developed a new leaching process in 2016, in which demagnetized particles are dissolved in a 4 M hydrochloric acid solution for 24 h at normal temperature. The main advantage of

this method is that the steel and copper particulates remain unreacted completely. The leach solution is then treated with oxalic acid to precipitate REE as oxalates. By this processing method, 82% REE recovery has been reported, with a product purity of 99.8% REE oxalates [5].

Tanaka et al. [34] reported a selective leaching method for the extraction of Nd metal through roasting followed by leaching. They developed an aqueous process to isolate Nd metal from scrap NdFeB magnets by using a 2 M H_2SO_4 solution for dissolution. In this process, the pH value is maintained at a low level to inhibit the precipitation of iron during the entire duration. Double salts of Nd are formed by keeping the pH at 1.5 or lower to convert into neodymium fluoride by leaching in an HF solution. This acid-leaching process is an effective way, but it takes a lot of time, which was later improved by using the ultrasonic method during the leaching process [35]. Researchers have proposed demagnetization as a mandatory process to avoid sticking of magnetic material in the metallic parts of the reactor during the leaching process. In addition, the milling process with reduced particle size improves the efficiency of leaching in permanent magnets. However, the milling of NdFeB magnets is challenging due to the rapid corrosion of these magnets. Recently, Tanvar et al. [31] used microwave-assisted recovery of REE in a short process and reported a purity of more than 98%. They found that after microwave exposure of only 1.2 min significant oxidation at high temperatures was achieved. Then, the REE recovery was carried out by the process of leaching and precipitation. This short microwave exposure process yields 56% recovery of Nd and Dy oxides, with a purity of more than 98%.

15.6 REE recovery from NiMH batteries

Rechargeable batteries, especially NiMH (nickel metal hydride) batteries, are a portable source of energy for electronic devices with an average lifetime of about 3–5 years, depending upon their usage. They have been extensively used to power mobile phones, video recorders, notebook computers, etc., due to their high energy density, high specific volume, resistance to overcharge, and no electrolyte consumption during charging and discharging cycles [36]. Many electric vehicles also use NiMH batteries. The discarded NiMH batteries pose an environmental hazard that can be solved through effective management. NiMH batteries consist of nickel oxyhydroxide (NiOOH) as the cathode and misch metal as the anode. The end-of-life batteries have 8–10% misch metal to improve the hydrogen storage capacity of the battery. Misch metal is an alloy of about 50% Ce, 25% La, 15% Nd, and 10% other REEs and iron [5, 12]. REE extraction from spent NiMH batteries is generally performed in three major steps – chemical leaching, solvent extraction, and precipitation. In the chemical leaching process, HCl, H_2SO_4, and HNO_3 acids are generally used, followed by a mixture of separation procedures. It is reported that using

acidic conditions, Nd, Sm, Pr, and Ce were recovered in high concentrations at 99.1%, 98.4%, 95.54%, and 89%, respectively [37].

The use of waste acid for leaching is also considered an environmentally favorable process to utilize the acids produced during etching and cleaning processes in the semiconductor industry. Recently phosphoric acid is being successfully used to recover La selectively [38]. Continuing the approach of the utilization of waste acid, selective recovery of REE from NiMH batteries was investigated using a two-stage acid leaching followed by precipitation. In the first stage, conventional leaching was performed using phosphoric acid at room temperature for 60 min and it converted more than 90% REE into insoluble phosphate precipitates. Simultaneously, the other metals were also leached out during the first stage. In the second stage, leaching was performed using subcritical water extraction with 1 M sulfuric acid to dissolve the precipitate of REE phosphates. The recovery of REE was conducted by adjusting the low pH of the leaching solution. The leaching efficiency of REE was reported to be increased by increasing acid concentration, and 100% efficiency for REE was achieved using 1 M sulfuric acid. By lowering the pH value to 1, 82.59% of La, 90.75% of Ce, and 85.97% of Nd were recovered in the form of hexagonal rod crystals [39].

Recently in 2022, Zhi et al. [40] developed an innovative extraction precipitation approach using dibenzyl phosphate, diphenyl phosphate, and triphenyl phosphate without using organic solvents during the extraction and precipitation procedure. They reported that dibenzyl phosphate has resulted in high precipitation efficiencies that can reach up to 97.84%, 100%, 100%, and 99.77% for La^{3+}, Ce^{3+}, $Pr^{3+,}$ and Nd^{3+}, respectively. Considering the advantage of low chemical consumption, this method can be effectively applied for the separation of REE from discarded NiMH batteries. In recent years, ammonium compounds were also successfully employed as leaching agents for the extraction of REEs. Weshahy et al. [41] have performed REE extraction using ammonium sulfate as a leaching agent and reported nearly complete leaching of REEs. They optimized the conditions for complete dissolution (~99.98%) of REEs by using 300 g/L ammonium sulfate concentration, after a leaching time of 3 h. Also, the study was focused on the individual separation of Ce ions from the total REE cake, using 10% of HCl at pH 3.5 for 40 min at room temperature.

15.7 Conclusions

The demand for REE is growing and essential for the development of high-tech industries all over the world. In addition to the exploitation of natural resources, REE recovery from e-waste or secondary sources is an effective measure for promoting the sustainable use of resources and reducing environmental hazards. The REE content and purity in discarded products are much higher than those available in natural minerals. Consequently, to have a clean and green world, it is necessary to implement

REE extraction from secondary sources using environment-friendly methods. It is also observed that a single metallurgical technique cannot be fruitful for the efficient or complete recovery of all REEs from e-waste, so a combinational approach with the intention of green methods may pave the path for better recovery of REEs. Due to increasing global efforts in this direction, it is expected that, in the near future, better industrial processes will be developed for the recycling and recovery of REEs.

References

[1] Fathollahzadeh, H, Eksteen, JJ, Kaksonen, AH, Watkin, ELJ. Role of microorganisms in bioleaching of rare earth elements from primary and secondary resources. Appl Microbiol Biotechnol, 2019, 103, 1043–1057.

[2] Chen, Z, Li, Z, Chen, J, Kallem, P, Banat, F, Qiu, H. Recent advances in selective separation technologies of rare earth elements: A review. J Environ Chem Eng, 2022, 10, 107104.

[3] Balaram, V. Rare earth elements: A review of applications, occurrence, exploration, analysis, recycling, and environmental impact. Geosci Front, 2019, 10, 1285–1303.

[4] Cardoso, CED, Almeida, JC, Lopes, CB, Trindade, T, Vale, C, Pereira, E. Recovery of rare earth elements by carbon-based nanomaterials – A review. Nanomaterials, 2019, 9, 1–35.

[5] Dushyantha, N, Batapola, N, Ilankoon, IMSK, Rohitha, S, Premasiri, R, Abeysinghe, B, Ratnayake, N, Dissanayake, K. The story of rare earth elements (REEs): Occurrences, global distribution, genesis, geology, mineralogy and global production. Ore Geol Rev, 2020, 122, 103521.

[6] Diaz, LA, Lister, TE, Parkman, JA, Clark, GG. Comprehensive process for the recovery of value and critical materials from electronic waste. J Cleaner Prod, 2016, 125, 236–244.

[7] Toache-Pérez, AD, Lapidus, GT, Bolarín-Miró, AM, Jesús, FS. De selective leaching and recovery of Er, Gd, Sn, and in from liquid crystal display screen waste by sono-leaching assisted by magnetic separation. ACS Omega, 2022, 7, 31897–31904.

[8] Tan, Q, Li, J. Rare earth metal recovery from typical e-waste. In: Waste Electrical and Electronic Equipment (WEEE) Handbook, Woodhead Publishing Series in Electronic and Optical Materials Elsevier, 2019, 393–421.

[9] Li, Z, Diaz, LA, Yang, Z, Jin, H, Lister, TE, Vahidi, E, Zhao, F. Comparative life cycle analysis for value recovery of precious metals and rare earth elements from electronic waste. Resour Conserv Recycl, 2019, 149, 20–30.

[10] Jyothi, RK, Thenepalli, T, Ahn, JW, Parhi, PK, Chung, KW, Lee, JY. Review of rare earth elements recovery from secondary resources for clean energy technologies: Grand opportunities to create wealth from waste. J Cleaner Prod, 2020, 267, 122048.

[11] Traore, M, Gong, A, Wang, Y, Qiu, L, Bai, Y, Zhao, W, Liu, Y, Chen, Y, Liu, Y, Wu, H, Li, S, You, Y. Research progress of rare earth separation methods and technologies. J Rare Earths press, 2022. 10.1016/j.jre.2022.04.009.

[12] Mudali, UK, Patil, M, Saravanabhavan, R, Saraswat, VK. Review on E-waste Recycling: Part II – Technologies for Recovery of Rare Earth Metals. Trans Indian Natl Acad Eng, 2021, 6, 613–631.

[13] Sethurajan, M, Hullebusch, E, Fontana, D, Akcil, A, Deveci, H, Batinic, B, Leal, JP, Gasche, TA, Ali Kucuker, M, Kuchta, K, Neto, IFF, Soares, HMVM, Chmielarz, A. Recent advances on hydrometallurgical recovery of critical and precious elements from end of life electronic wastes – A review. Crit Rev Environ Sci Technol, 2019, 49, 212–275.

[14] Ruiz-Mercado, GJ, Gonzalez, MA, Smith, RL, Meyer, DE. A conceptual chemical process for the recycling of Ce, Eu, and Y from LED flat panel displays. Resour Conserv Recycl, 2017, 126, 42–49.

[15] Dev, S, Sachan, A, Dehghani, F, Ghosh, T, Briggs, BR, Aggarwal, S. Mechanisms of biological recovery of rare-earth elements from industrial and electronic wastes: A review. Chem Eng J, 2020, 397, 124596.

[16] Papagianni, S, Moschovi, AM, Sakkas, KM, Chalaris, M, Yakoumis, I. Preprocessing and leaching methods for extraction of REE from permanent magnets: A scoping review. Appl Chem, 2022, 2, 199–212.

[17] Elbashier, E, Mussa, A, Hafiz, MA, Hawari, AH. Recovery of rare earth elements from waste streams using membrane processes: An overview. Hydrometallurgy, 2021, 204, 105706.

[18] Belfqueh, S, Seron, A, Chapron, S, Arrachart, G, Menad, N. Evaluating organic acids as alternative leaching reagents for rare earth elements recovery from NdFeB magnets. J Rare Earths, 2022, in press. DOI: 10.1016/j.jre.2022.04.027.

[19] Castro, L, Blázquez, ML, González, F, Muñoz, JÁ. Biohydrometallurgy for rare earth elements recovery from industrial wastes. Molecules, 2021, 26, 6200.

[20] Ambaye, TG, Vaccari, M, Castro, FD, Prasad, S, Rtimi, S. Emerging technologies for the recovery of rare earth elements (REEs) from the end-of-life electronic wastes: A review on progress, challenges, and perspectives. Environ Sci Pollut Res, 2020, 27, 36052–36074.

[21] Mowafy, AM. Biological leaching of rare earth elements. World J Microbiol Biotechnol, 2020, 36, 61.

[22] Gadd, GM. Biosorption: Critical review of scientific rationale, environmental importance and significance for pollution treatment. J Chem Technol Biotechnol, 2009, 84, 13–28.

[23] Andrès, Y, Gérente, C. Removal of rare earth elements and precious metal species by biosorption. In: Microbial Biosorption of Metals, 2011, 179–196.

[24] Binnemans, K, Jones, PT, Blanpain, B, Van Gerven, T, Yang, Y, Walton, A, Buchert, M. Recycling of rare earths: A critical review. J Cleaner Prod, 2013, 51, 1–22.

[25] Marra, A, Cesaro, A, Rene, ER, Belgiorno, V, Lens, PNL. Bioleaching of metals from WEEE shredding dust. J Environ Manage, 2018, 210, 180–190.

[26] Osman, Y, Gebreil, A, Mowafy, AM, Anan, TI, Hamed, SM. Characterization of Aspergillus niger siderophore that mediates bioleaching of rare earth elements from phosphorites. World J Microbiol Biotechnol, 2019, 35, 1–10.

[27] Williamson, AJ, Folens, K, Matthijs, S, Paz Cortes, Y, Varia, J, Du Laing, G, Boon, N, Hennebel, T. Selective metal extraction by biologically produced siderophores during bioleaching from low-grade primary and secondary mineral resources. Miner Eng, 2021, 163, 106774.

[28] Giese, EC. E-waste mining and the transition toward a bio-based economy: The case of lamp phosphor powder. MRS Energy Sustainability, 2022, 9, 494–500.

[29] Shukla, N, Dhawan, N. Comparison of processing routes for recovery of rare earth elements from discarded fluorescent lamp phosphors. Miner Eng, 2022, 187, 107759.

[30] Magrini, C, Jagodzińska, K. Can bioleaching of NIB magnets be an answer to the criticality of rare earths? An ex-ante life cycle assessment and material flow cost accounting. J Cleaner Prod, 2022, 365, 132672.

[31] Tanvar, H, Kumar, S, Dhawan, N. Microwave exposure of discarded hard disc drive magnets for recovery of rare earth values. JOM, 2019, 71, 2345–2352.

[32] Yang, Y, Walton, A, Sheridan, R, Güth, K, Gauß, R, Gutfleisch, O, Buchert, M, Steenari, BM, Van Gerven, T, Jones, PT, Binnemans, K. REE recovery from end-of-life NdFeB permanent magnet scrap: A critical review. J Sustainable Metall, 2017, 3, 122–149.

[33] Lyman, JW, Palmer, GR. Recycling of rare earths and iron from NdFeB magnet scrap. High Temp Mater Process, 1993, 11, 175–188.

[34] Tanaka, M, Oki, T, Koyama, K, Narita, H, Oishi, T. Recycling of rare earths from scrap. In: Handbook on the Physics and Chemistry of Rare Earths. 2013, vol 43, 159–211.

[35] Jha, MK, Kumari, A, Panda, R, Rajesh Kumar, J, Yoo, K, Lee, JY. Review on hydrometallurgical recovery of rare earth metals. Hydrometallurgy, 2016, 165, 2–26.

[36] Jha, MK, Choubey, PK, Dinkar, OS, Panda, R, Jyothi, RK, Yoo, K, Park, I. Recovery of rare earth metals (REMs) from nickel metal hydride batteries of electric vehicles. Minerals, 2022, 12, 34.

[37] Meshram, P, Pandey, BD, Mankhand, TR. Process optimization and kinetics for leaching of rare earth metals from the spent Ni–metal hydride batteries. Waste Manag, 2016, 51, 196–203.

[38] Onoda, H, Yoneda, Y. Selective formation of lanthanum phosphate from lanthanum–copper solutions. J Environ Chem Eng, 2018, 6, 1760–1763.

[39] Lie, J, Liu, JC. Selective recovery of rare earth elements (REEs) from spent NiMH batteries by two-stage acid leaching. J Environ Chem Eng, 2021, 9, 106084.

[40] Zhi, H, Ni, S, Su, X, Xie, W, Zhang, H, Sun, X. Separation and recovery of rare earth from waste nickel-metal hydride batteries by phosphate based extraction-precipitation. J Rare Earths, 2022, 40, 974–980.

[41] Weshahy, AR, Gouda, AA, Atia, BM, Sakr, AK, Al-otaibi, JS, Almuqrin, A, Hanfi, MY, Sayyed, MI, Sheikh, R, Radwan, HA, Hassen, FS, Gado, MA, Sheikh, R, Radwan, HA, Hassen, FS, Gado, MA. Efficient recovery of rare earth elements and zinc from spent Ni–metal hydride batteries: Statistical studies. Nanomaterials, 2022, 12, 2305.

Index